issn 0424-7116
An open-access journal by the German Quaternary Association
Editor-in-chief: Christopher Lüthgens

E&G

Quaternary Science Journal

Eiszeitalter und Gegenwart

Volume 70
No. 1 & 2
2021

An open-access journal of the German Quaternary Association

Copernicus Publications
The Innovative Open Access Publisher

E&G Quaternary Science Journal

An open-access journal of the German Quaternary Association

E&G Quaternary Science Journal (EGQSJ) is an interdisciplinary open-access journal, which publishes peer-reviewed articles and express reports, and retrospectives, as well as thesis abstracts related to Quaternary geology, paleo-environments, paleo-ecology, soil science, paleo-climatology, geomorphology, geochronology, archaeology, geoarchaeology, and now also encompassing methodological advances and aspects of the societal relevance of Quaternary research. EGQSJ is a non-profit, community-based effort: It is run by Quaternary scientists, financed by Quaternary scientists, and supporting Quaternary scientists, because any revenue generated is only used to support publications in the journal.

Copernicus Publications
The Innovative Open Access Publisher

Copernicus Publications
Bahnhofsallee 1e
37081 Göttingen
Germany

Phone: +49 551 90 03 39 0
Fax: +49 551 90 03 39 70

publications@copernicus.org
https://publications.copernicus.org

Printed in Germany.
Schaltungsdienst Lange o.H.G.

ISSN 0424-7116

Published by Copernicus GmbH (Copernicus Publications) on behalf of the
German Quaternary Association (DEUQUA).

Image credit:
Caption: Decorated block of so-called Sed-festival hall in the Temple of Bastet at ancient Bubastis.
Southeastern Nile Delta, by Eva Lange-Athinodorou (2018).

E&G Quaternary Science Journal
An open-access journal of the German Quaternary Association
https://www.eg-quaternary-science-journal.net/

E&G Quaternary Science Journal
An open-access journal of the German Quaternary Association
https://www.eg-quaternary-science-journal.net/

E&G Quaternary Science Journal
An open-access journal of the German Quaternary Association
https://www.eg-quaternary-science-journal.net/

Advisory board

E&G Quaternary Science Journal
An open-access journal of the German Quaternary Association
https://www.eg-quaternary-science-journal.net/

Grußwort des Editor-in-chief

Liebe Leser:innen,
Liebe DEUQUA Mitglieder,

wenn Sie diese Druckausgabe des 70. Jahrgangs von E&G Quaternary Science Journal (E&G QSJ) in den Händen halten und diese Zeilen lesen, merken Sie sicher bereits am Gewicht und an der Länge dieses Bandes, dass sich die Zeitschrift in den letzten Jahren sehr positiv entwickelt hat und die Anzahl der Einreichungen und Veröffentlichungen deutlich gestiegen ist. Im Sommer des Jahres 2021 wurde E&G QSJ bei Clarivate Analytics in den Emerging Sources Citation Index (ESCI) aufgenommen, ein weiterer Meilenstein in der Entwicklung der Zeitschrift, der ihre steigende internationale und nationale Beachtung widerspiegelt. Diese sehr positive Entwicklung brachte aber auch gleichzeitig neue Herausforderungen mit sich. Die gestiegene Seitenzahl führte dementsprechend zu einer Erhöhung der Druckkosten. Aus ökonomischen aber auch aus ökologischen Gründen sah sich die DEUQUA deshalb veranlasst, die Zeitschrift nicht mehr automatisch an alle DEUQUA Mitglieder zu versenden, aber natürlich weiterhin die Möglichkeit zu erhalten, die Zeitschrift in gedruckter Form zu beziehen. Diese Entscheidung wurde von Ihnen, den DEUQUA Mitgliedern, überaus positiv aufgenommen und ich möchte mich an dieser Stelle im Namen des DEUQUA Vorstandes für die vielen freundlichen und unterstützenden Rückmeldungen bedanken.

Mit dem Band, den Sie hiermit in den Händen halten, begeht E&G QSJ seinen 70. Geburtstag und aus diesem Anlass finden Sie ab der Seite 205 insgesamt zwölf Beiträge, die anlässlich dieses Jubiläums in Form des Sonderbandes „Celebrating 70 years of E&G: tributes“ publiziert wurden. Die Gastherausgeber:innen Frank Preusser, Markus Fuchs und Christine Thiel stellen diesen Sonderband in ihrem Vorwort ab Seite 201 im Detail vor. Das Besondere an diesem Band: Es handelt sich um einen Tandem-Band, der in Zusammenarbeit mit DEUQUA Special Publications (DEUQUASP) entstanden ist. Die DEUQUASP-Ausgabe enthält Nachdrucke einer Sammlung klassischer E&G QSJ-Forschungsartikel, die ins Englische übersetzt wurden, um sie einem breiteren internationalen Publikum zugänglich zu machen. Die begleitende E&G QSJ-Ausgabe bietet dagegen einen detaillierten Einblick in die Bedeutung jedes dieser Meilensteine der Quartärforschung in Form von Retrospektiven, die von internationalen Expert:innen verfasst wurden und die den wegweisenden Beitrag der jeweiligen Veröffentlichungen zur Quartärwissenschaft kritisch bewerten. Weiterhin enthält der Jubiläumsband auch die abschließenden Beiträge des äußerst erfolgreichen Sonderbandes „Geoarchaeology of the Nile Delta“, der von Julia Meister, Eva Lange-Athinodorou und Tobias Ullmann als Gastherausgeber:innen betreut wurde; das Vorwort zu diesem Sonderband finden Sie ab Seite 187.

Ein ganz herzliches Dankeschön geht deshalb an die Teams von Gastherausgeber:innen sowie natürlich auch an das Team des gesamten Editorial Boards von E&G QSJ für ihren unermüdlichen Einsatz für die Zeitschrift. Ein ebenso großes Dankeschön geht natürlich auch an alle Autor:innen, die mit ihren Einreichungen die Zeitschrift zu dem gemacht haben, was sie heute ist: ein internationales, lebendiges Forum für Wissenschaftler:innen aus allen Disziplinen der Quartärforschung.

Mit den allerbesten Grüßen im Namen des gesamten Editorial Boards

Christopher Lüthgens
(Editor-in-chief)

E&G Quaternary Science Journal
An open-access journal of the German Quaternary Association
https://www.eg-quaternary-science-journal.net/

Greetings from the Editor-in-chief

Dear readers,
Dear DEUQUA members,

If you are holding this print edition of the 70th volume of E&G Quaternary Science Journal (E&G QSJ) in your hands and you are reading these lines, you will certainly already notice from the weight and length of this volume that the journal has developed very positively in recent years and that the number of submissions and publications has increased significantly. In the summer of 2021, E&G QSJ was included in the Emerging Sources Citation Index (ESCI) at Clarivate Analytics, another milestone in the journal's development reflecting its increasing international and national attention. However, this very positive development also brought new challenges at the same time. The rising number of pages resulted in a corresponding increase in printing costs. For economic as well as ecological reasons, DEUQUA therefore felt compelled to stop sending the journal automatically to all DEUQUA members, but of course to continue to offer the possibility of receiving the journal in printed form. You, the DEUQUA members, received this decision extremely positively and I would like to take this opportunity to thank you on behalf of the DEUQUA Board for the many kind and supportive responses.

With the volume you are holding in your hands, E&G QSJ is celebrating its 70th birthday and on this occasion you will find a total of 12 contributions published in the form of the special issue "Celebrating 70 years of E&G: tributes" starting on page 205. The guest editors Frank Preusser, Markus Fuchs and Christine Thiel present this special volume in detail in their preface starting on page 201. What is special about this volume is that it is a tandem volume produced in cooperation with DEUQUA Special Publications (DEUQUASP). The DEUQUASP special issue contains reprints of a collection of classic E&G QSJ research articles translated into English to make them accessible to a wider international audience. The accompanying E&G QSJ edition, on the other hand, provides a detailed insight into the significance of each of these milestones of Quaternary research in the form of retrospectives written by international experts who critically assess the seminal contribution of each publication to Quaternary science. Furthermore, the anniversary volume also contains the final contributions of the highly successful special issue "Geoarchaeology of the Nile Delta", which was guest edited by Julia Meister, Eva Lange-Athinodorou and Tobias Ullmann; the preface to this special issue can be found on page 187.

A very big thank you therefore goes to the teams of guest editors and, of course, to the entire editorial board of E&G QSJ for their tireless commitment to the journal. An equally big thank you goes to all authors whose submissions have made the journal what it is today: an international, lively forum for scientists from all disciplines of Quaternary research.

With best regards on behalf of the entire Editorial Board

Christopher Lüthgens
(Editor-in-chief)

E&G Quaternary Sci. J., 70, 1–17, 2021
https://doi.org/10.5194/egqsj-70-1-2021

Open Access E&G Quaternary Science Journal

Research article

Towards timing and stratigraphy of the Bronze Age burial mound royal tomb (Königsgrab) of Seddin (Brandenburg, northeastern Germany)

Moritz Nykamp[1], **Jacob Hardt**[1], **Philipp Hoelzmann**[1], **Jens May**[2], **and Tony Reimann**[3,4]

[1]Institute of Geographical Sciences, Freie Universität Berlin, Berlin, Germany
[2]Brandenburgisches Landesamt für Denkmalpflege und Archäologisches Landesmuseum, OT Wünsdorf, Zossen, Germany
[3]Soil Geography and Landscape group & Netherlands Centre for Luminescence dating, Wageningen University, Wageningen, the Netherlands
[4]Institute of Geography, University of Cologne, Cologne, Germany

Correspondence: Moritz Nykamp (m.nykamp@fu-berlin.de)

Relevant dates: Received: 15 April 2020 – Revised: 13 November 2020 – Accepted: 26 November 2020 – Published: 12 January 2021

How to cite: Nykamp, M., Hardt, J., Hoelzmann, P., May, J., and Reimann, T.: Towards timing and stratigraphy of the Bronze Age burial mound royal tomb (Königsgrab) of Seddin (Brandenburg, northeastern Germany), E&G Quaternary Sci. J., 70, 1–17, https://doi.org/10.5194/egqsj-70-1-2021, 2021.

Abstract: This study uses an integrated multi-method geoarcheological and geochronological approach to contribute to the understanding of the timing and stratigraphy of the monumental burial mound royal tomb (Königsgrab) of Seddin. We show that the hitherto established radiocarbon-based terminus post quem time frame for the construction of the burial mound of 910–800 BCE is supported by optically stimulated luminescence (OSL) dating. The radiocarbon samples were obtained from a substrate directly underneath the burial mound which supposedly represents the late glacial/Holocene soil that was buried below the structure. We use sedimentological (grain-size analyses) and geochemical analyses (element analyses, carbon, pH, and electric conductivity determinations) to reassess and confirm this hypothesis. In addition to the burial age associated with the last anthropogenic reworking during construction of the burial mound, the OSL dating results provide new insights into the primary deposition history of the original substrates used for the structure. In combination with regional information about the middle and late Quaternary development of the environment, our data allow us to provide a synoptic genetic model of the landscape development and the multiphase stratigraphy of the royal tomb of Seddin within the Late Bronze Age cultural group "Seddiner Gruppe" of northern Germany. Based on our initial experiences with OSL dating applied to the sediments of a burial mound – to the best of our knowledge the first attempt in Europe – we propose a minimal invasive approach to obtain datable material from burial mounds and discuss related opportunities and challenges.

Kurzfassung: Diese Studie nutzt einen integrativen geoarchäologisch-geochronologischen Ansatz, um einen Beitrag zum Verständnis der Chronologie und Stratigraphie des monumentalen Grabhügels „Königsgrab" von Seddin zu leisten. Wir zeigen, dass der bislang etablierte, auf Radiokarbondaten basierende, post quem Zeitrahmen von 910–800 BCE für die Errichtung des Grabhügels durch optisch-stimulierte Lumineszenz (OSL) Alter unterstützt wird. Die Proben für die Radiokarbondatierung stammen aus einem Substrat unterhalb des Grabhügels, das den vermeintlich begrabenen spätglazialen/holozänen Boden repräsentiert. Wir nutzen sedimentologische (Korngrößenanalysen) und geochemische Analysen (Elementanalyse, Kohlenstoffbestimmung, pH- und elektrische Leitfähigkeitsmessung), um diese Annahme zu evaluieren und zu bestätigen. Ergänzend zu dem Alter der Überdeckung des spätglazialen/holozänen Bodens, das mit der letzten anthropogenen Materialumlagerung während der Konstruktion des Grabhügels assoziiert wird, geben die Ergebnisse der OSL-Datierungen einen Einblick in die ursprüngliche Ablagerungsgeschichte des Ausgangssubstrates, das für die Errichtung des Grabhügels verwendet wurde. In Kombination mit Informationen zur regionalen mittel- bis spätquartären Landschaftsgenese, lässt sich aus unseren Daten ein genetisches Übersichtsmodell der Landschaftsentwicklung und der mehrphasigen Stratigraphie des „Königsgrabes" von Seddin als Teil der spätbronzezeitlichen Kulturgruppe „Seddiner Gruppe" von Norddeutschland ableiten. Auf Grundlage unserer ersten Erfahrungen mit der OSL-Datierung von Sedimenten eines Grabhügels, nach unserem Wissen der erste Versuch in Europa, schlagen wir einen minimalinvasiven Ansatz vor, um datierbares Material aus Grabhügeln zu gewinnen und diskutieren damit verbundene Möglichkeiten und Herausforderungen.

1 Introduction

Burial mounds form part of the most important monuments of European prehistory, and many thousands of these architectural elements are still visible in the landscapes of Europe (Doorenbosch, 2013). Furthermore, new technologies such as high-resolution lidar-derived digital elevation models that are more and more available will likely increase the number of newly discovered monuments significantly.

Generally, burial mounds are an important form of burial practice as they serve as a permanent marker of a dead person, keeping them in the memory of those who live on (Harding, 2012). In northern Central Europe, they occur from the Neolithic to the Slavic period/Viking age.

Although archeologists from the different European regions and specialists for certain cultural epochs are usually able to date newly discovered burial mounds based on their external appearance, numerical age control is often still required to reliably relate a burial mound to a specific cultural epoch. This mostly requires excavation for either archeological artifacts or macroscopic remains of organic matter suitable for ^{14}C dating – the former is undesirable in many cases for the purposes of cultural heritage preservation and the latter is often difficult to obtain (Kristiansen et al., 2003). Kristiansen et al. (2003), therefore, propose an approach with minimal disturbance to obtain samples for ^{14}C analysis of soil organic matter fractions. They demonstrate that augering through the mound can provide suitable samples from former surface soils buried by the mound and that ^{14}C dating of soil organic matter fractions can yield good results. Their results show that the humic acid fractions in 7 out of 10 mounds are in good agreement with the reference ages (Kristiansen et al., 2003). Relying on the presence of a buried organic-rich topsoil horizon alone can, however, be problematic: it might be lacking as a consequence of soil erosion after vegetation clearance or surface leveling prior to the construction of the mound. Sand-sized quartz grains suitable for optically stimulated luminescence (OSL) dating, in contrast, can be regarded as ubiquitous in most (if not all) burial mounds located along the European sand belt. However, to the best of our knowledge, OSL dating has not yet been performed on burial mounds in Europe, unlike examples from archeological mound structures (e.g., tells and burial mounds) in the USA, Israel, and Jordan (e.g., Feathers, 1997; Porat et al., 2012; Pluckhahn et al., 2015; al Khasawneh et al., 2020).

A precisely dated burial mound and thus an ideal test object for OSL dating of mound sediments is the royal tomb (Königsgrab) of Seddin (federal state of Brandenburg, northeastern Germany). It dates to the 9th century BCE and is considered one of the most important tombs of the Nordic Bronze Age and an excellent example of an elite or chief tomb (May, 2018). The mound was piled up in layers consisting of alternating strata of erratic boulders and sand (May and Hauptmann, 2012; May, 2018). A stone pavement followed by a sand layer form the lowermost layers. The construction continues with a second stone pavement and another sand layer. A third stone pavement forms the uppermost deposit. During archeological excavations, at several locations a layer of either dark substrate or pale solidified sand was identified directly underneath the basal stone pavement, i.e., in stratigraphically identical positions. The dark material was interpreted as a paleosol that was buried during the initial construction phase by the boulders of the first stone pavement (May, 2018). However, geoscientific analyses to support the interpretation of a buried paleosol underneath the royal tomb including the pedological horizon designation of the dark substrate and the pale sand are currently lacking. The additional information can provide important insights into the conditions and processes immediately preceding the initial construction phase of the burial mound, e.g., potential erosion by water or wind of the organic-rich topsoil horizon after vegetation clearance or possible leveling of the foundation soil. The pedological characterization of the buried soil horizons also helps to assess their potential for additional paleoenvironmental studies such as pollen analyses from fossil organic-rich topsoil horizons (e.g., Kaiser et al., 2020).

Radiocarbon ages obtained from pieces of charred wood from the dark layer provide a rather precise terminus post quem time frame for the construction of the burial mound ranging from 910 to 800 BCE (May and Hauptmann, 2012; May, 2018). These ages provide a maximum age estimate for the construction of the burial mound but are completely decoupled from the construction process (cf. Pluckhahn et al., 2015). Thus, even though the age range is precise, independent numerical age control obtained by a dating technique that is capable of recording the construction process itself such as OSL dating is useful.

Therefore, the aims of this contribution are to provide (i) independent numerical age estimates to verify the terminus post quem time frame of the construction period by applying OSL dating to capture the construction process and (ii) sedimentological and geochemical analyses to further investigate and classify the suggested buried paleosol.

We present a compilation of radiocarbon and OSL ages and thereby contribute to the chronology of the royal tomb of Seddin by applying two dating methods that are independent of each other. Moreover, our OSL datings also provide important insights into the Quaternary history of the construction material itself. We combine the local chronological and sediment/soil data with regional information on the middle and late Quaternary environmental history to set up a genetic model of the landscape development and possible construction phases of the royal tomb of Seddin. Furthermore, we discuss opportunities and challenges of a minimally invasive approach – following Kristiansen et al. (2003) – in combination with luminescence dating techniques to provide initial numerical age estimates for newly discovered burial mounds.

2 Regional setting and archeological background

2.1 Regional setting

The royal tomb (Königsgrab) of Seddin is located in the Prignitz region approximately 2 km southwest of the village of Seddin, in the northwest of the federal state of Brandenburg, northeast Germany (Fig. 1).

The monumental burial mound is situated in the middle reaches of the Stepenitz river, a smaller lowland tributary of the Elbe river discharging into the North Sea. The area is part of the old morainic glacial landscape that was initially formed by the Scandinavian Ice Sheet (SIS) during the penultimate Saalian glaciation (∼ late MIS 6, marine isotope stage; Ehlers et al., 2011; Lippstreu et al., 2015) and afterwards altered by periglacial processes during the last Weichselian ice age (mainly MIS 4 and MIS 2).

The late Saalian deposits in the vicinity of the burial mound comprise till, as well as glaciofluvial sand and gravel

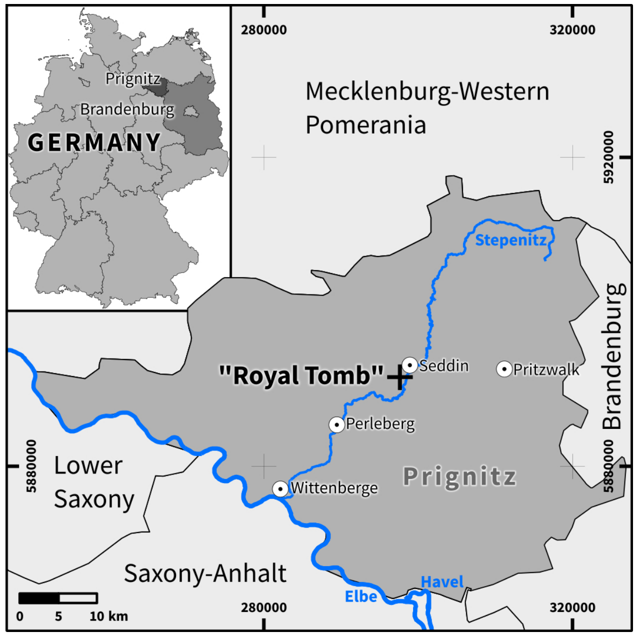

Figure 1. Overview map showing the Prignitz region in northwest Brandenburg (northeast Germany) and the location of the royal tomb of Seddin (reference system: WGS84; projection: UTM33N; data sources: Naturalearthdata, 2020; Offenedaten, 2020; Geofabrik, 2020).

(Fig. 2a). The smoothly undulating topography of the area is a result of periglacial reworking processes, e.g., gelisolifluction, and coversand formation. This landscape type is characterized as old morainic landscape (Lippstreu et al., 1997; Nagel et al., 2003; Lippstreu et al., 2015). Direct numerical ages of the late Saalian sediments are generally rare in the region and are lacking for the wider surroundings of the burial mound. OSL ages of Saalian glaciofluvial deposits from the south of Brandenburg (Beelitz, ca. 120 km southeast of Seddin) yielded an age range of 150–130 kyr (Lüthgens et al., 2010). This is in agreement with previous age estimates that were based on stratigraphic and morphostratigraphic correlations (Litt et al., 2007; Böse et al., 2012). Coversand formation probably took place starting at the end of the Weichselian Pleniglacial, as was shown at different sites within the European sand belt (Kasse, 2002; Koster, 2005; Kaiser et al., 2009). Coversands at Beelitz were dated to ∼ 15 ka by means of OSL (Lüthgens et al., 2010).

“Fahlerde” or “Braunerde-Fahlerde” (according to Ad-Hoc-AG Boden, 2005, and MLUV, 2005), i.e., Luvisols (according to IUSS Working Group WRB, 2006), have developed in the sandy to loamy-sandy substrates (Fig. 2). These soils form one of the typical soils in the Prignitz region (MLUV, 2005; GeoBasis-DE/LGB, 2012) and are predominant in the surroundings of the royal tomb (Fig. 2b).

The onset of soil formation in the region was in the Late Glacial, as shown by micromorphological analyses (Kühn,

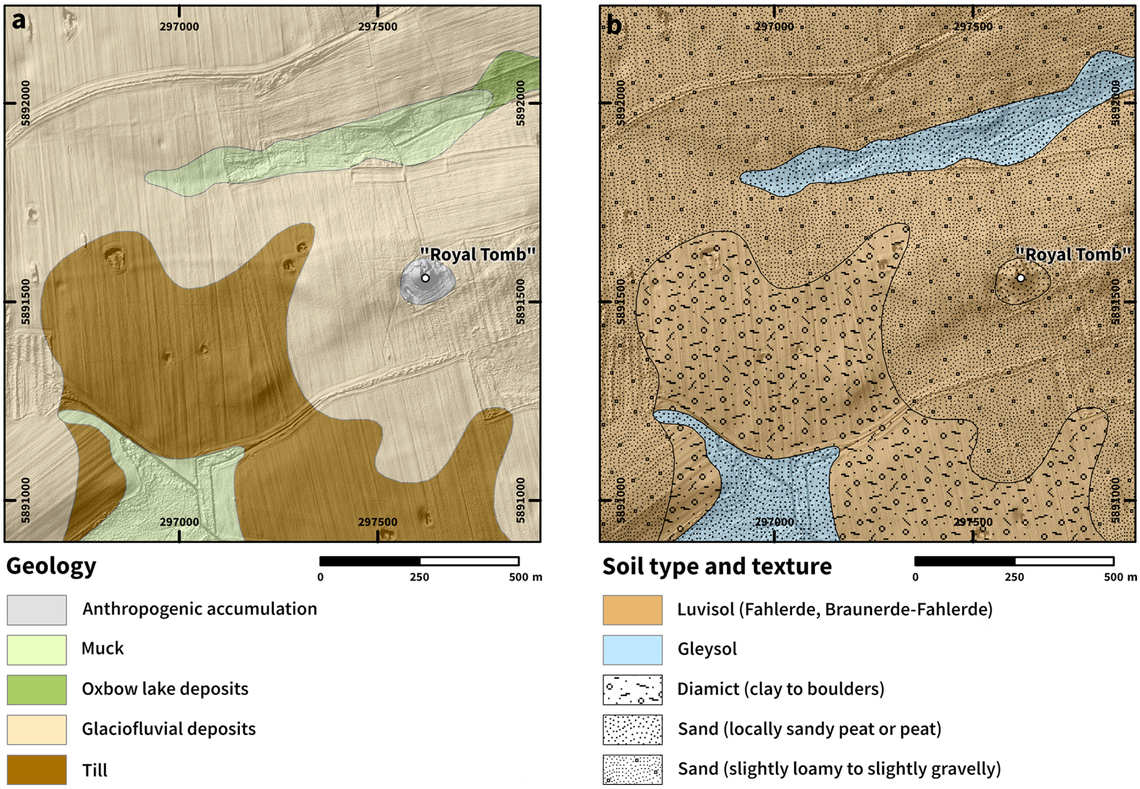

Figure 2. Simplified overview maps showing **(a)** the geology and **(b)** the dominating soil types and textures in the surroundings of the royal tomb (reference system: WGS84; projection: UTM33N; data sources: Schulte and Wahnschaffe, 1905; GeoBasis-DE/LGB, 2012; LBGR Brandenburg, 2020).

2003) and a review of available geochronological data on soil formation in northeast Germany (Kappler et al., 2019).

Palynological evidence from different archives in Brandenburg show a simultaneous increase in human activity in the Late Bronze Age compared to the Early and Middle Bronze Age. Increasing frequencies of cereal-type pollen and secondary anthropogenic indicators document the strong human impact on the vegetation; strongly decreasing arboreal pollen points to large-scale clearings of woodland (Jahns, 2015, 2018). The pollen diagram from the Bergsoll, i.e., a small wetland area ca. 7.2 km northeast of the royal tomb, provides evidence for extensive deforestation in ca. 800 BCE (Jahns, 2018). Also, a distinct decline of *Quercus* pollen at the Sacrower See lake in ca. 800 BCE suggests the intensive use of oak lumber that resulted in a shift of the forest composition (Jahns, 2015). These results from archives in Brandenburg are in agreement with results of pollen and charcoal analyses from fossil soils in south Mecklenburg-Western Pomerania indicating the first human impacts on the vegetation during the Neolithic and an intensification during the Bronze Age; fire events started to increase roughly around the transition from the Bronze Age to the Iron Age (Kaiser et al., 2020). The present-day land cover in the surroundings of the royal tomb is dominated by arable land, pastures, and forests (European Environment Agency, 2020).

The study site is located at the transition from a temperate oceanic climate in the west to a humid continental climate in the east (i.e., west–east transition from Cfb to Dfb according to the Köppen–Geiger classification; Beck et al., 2018). The weather station Marnitz (German Meteorological Service, DWD; station ID: 3196) is located ca. 20 km north of the study area at an elevation of 81.0 m above sea level. This station recorded a mean annual air temperature of 8.2 °C (range: 7.1–9.9 °C) and a mean annual precipitation of 660 mm a^{-1} (range: 460–816 mm a^{-1}) for the period 1961–1990 (DWD Climate Data Center, 2020a, b).

2.2 Archeological background

The locality of the royal tomb of Seddin was eponymous for the cultural group “Seddiner Gruppe” in southwest Mecklenburg and northwest Brandenburg (May and Hauptmann, 2012) in the Late Bronze Age (1100 to 530 BCE). It is considered one of the most important tombs of the 9th century BCE in northern Central Europe and an excellent example of an elite or chief tomb at the transition from the Late Bronze Age to the Iron Age (May and Hauptmann, 2012). Its isolated position, as well as the presence of other richly equipped graves in the area, indicates the existence of an elite during the Late Bronze Age at the southern margin of the Nordic Bronze Age cultural groups (May, 2018).

The burial mound has a diameter of ca. 61.5 m, and its original height was ca. 9 m. Erratic boulders form a circle around the foot of the grave mound. This circle has a circumference of ca. 193.5 m surrounding an area of ca. 3000 m^2 (May, 2018). It is likely that the stone ring was built before the mound was erected. The mound itself was built of alternating strata of stones and sand, and it was piled up in layers. Due to its monumental dimensions it was visible from all directions over several kilometers, at least during periods of sparse vegetation (May, 2018). Palynological analyses at the Bergsoll near Seddin point to widespread deforestation in the area during the Bronze Age, and thereby it seems likely that the burial mound represented a landmark at this time (Jahns, 2018). In combination with the surrounding grave mounds and grave mound fields, it exemplifies the ritual use and reorganization of the area (May, 2018).

A large burial chamber made of stones is located inside the mound. This chamber is situated ca. 9 m to the southeast of the center of the stone circle and was built on level ground (May, 2018). The chamber contained painted clay plasters and rich burial equipment consisting of 41 objects and the cremated remains of three individuals. A 30–40-year-old man was buried together with two presumably younger women (Kiekebusch, 1928; May and Hauptmann, 2005, 2011).

The royal tomb of Seddin was initially dated based on the archeological findings from the burial chamber. Researchers agree that the youngest objects of the burial equipment date to period V based on Montelius (1885). Period V is, according to Montelius (1885), one out of six (I–VI) relative chronological periods for the Nordic Bronze Age. Stratigraphy, typology, and coincident findings (*geschlossene Funde*), such as all objects obtained from a grave or hoard for which a coincident laying down is assumed, form the basis for the relative chronological periodization of the archeological findings. Therefore, the exact timing and duration of the periods is controversial among archeologists. In the case of the royal tomb of Seddin, it is agreed upon that the burials belong to Montelius' period V, but there is no consensus regarding its placement within this period. While Wüstemann (1974) dates the burial equipment to an early phase of period V, Kossinna (1910) argues that the equipment rather points to a late phase of period V, i.e., dating to ca. 800 BCE. Thus, both ends of the temporal assignment of the burial equipment within period V are covered by these opinions. Owing to numerical dating techniques, e.g., radiocarbon dating, the timing and duration of the periods become more precise. One of the most recent advances in providing accurate numerical dates of coincident findings is the radiocarbon dating of cremated human remains. Such an example is provided by Hornstrup et al. (2012) who radiocarbon dated cremated human remains from Danish graves and thereby suggest that period V covers the time span from 950/920 to 800 BCE.

In the course of archeological investigations, four radiocarbon dates were obtained from charcoal fragments recovered from four different trenches in close proximity to the inner side of the stone ring of the burial mound of Seddin (Fig. 3). Each of these radiocarbon samples originates from a substrate which most likely corresponds to layer 3 of profile SD17P1 (Fig. 4). Three of the obtained charcoal pieces were dated to 910–800 BCE (at 2σ range; Table 2). This agrees well with the abovementioned estimation of the duration of period V. These ages also provide a terminus post quem for the construction of the burial mound since the construction of the burial mound rests directly on layer 3 (Fig. 4). The fourth radiocarbon sample (MAMS 35030; Fig. 3) was obtained from a stratigraphic position that is identical with layer 3 of profile SD17P1 (Fig. 4). However, while layer 3 of profile SD17P1 consists of dark organic-rich material (see below), sample MAMS 35030 (*Fagus* charcoal) was taken from a layer consisting of white, strongly solidified sand and is dated to 1740–1620 BCE (at 2σ range; Table 2). This age is roughly 790 years older than the oldest dating of the grave. At the current state of research, it remains unclear whether this indicates a previous use of the area where the burial mound was erected later on or if the sample is affected by the "old wood effect" as is the case for other radiocarbon samples obtained from locations close by (May, 2018).

3 Material and methods

3.1 Field work

Profile SD17P1 (5891584 N, 297601 E; UTM 33N) was recorded in August 2017 during archeological excavations on the northwestern slope of the Bronze Age burial mound (Fig. 3). The profile was excavated in three ca. 1 m deep sections separated by ca. 1 m wide steps. It was cleaned and documented by photographs (Fig. 4a) before the sediment succession was described and sampled. The macroscopic sediment description was carried out according to the German manual for soil mapping (KA 5; Ad-Hoc-AG Boden, 2005) and includes texture, humus content, redoximorphic features, layer boundaries, and signs of pedogenic processes. The English terminology follows Schoeneberger et al. (2012). Colors were recorded using the Munsell soil color charts and converted to RGB values to allow realistic colorization of the profile drawing. A total of 39 sediment samples were extracted for more detailed particle size and geochemical analyses (Sect. 3.2). Additionally, three samples for luminescence dating and bulk samples for gamma spectrometry measurements were obtained; OSL samples were extracted with metal tubes (25 cm length, Ø 5 cm) that were covered with aluminum foil and plastic caps (Sect. 3.3).

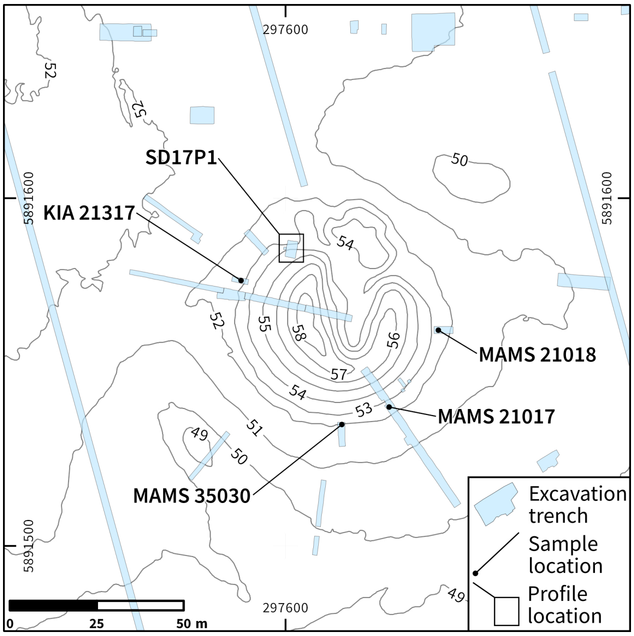

Figure 3. Topographic plan of the close vicinity of the royal tomb of Seddin (in the center) showing the locations of the excavation trenches, the radiocarbon-dated charcoal fragments (Table 2), and profile SD17P1 (reference system: WGS84; projection: UTM33N; contour lines were derived from lidar-based 1 m elevation data; GeoBasis-DE/LGB, 2020).

3.2 Sediment analyses

Sediment analyses comprise particle size analyses, pH, electric conductivity, and total carbon (TC) measurements, and Fe, Al, and Si determinations to characterize the sediments and to identify potential paleosurfaces within the profile. Sample preparation included drying at 105 °C in a drying cabinet, crushing aggregates, separation of coarse components with a 2 mm sieve, and homogenizing the <2 mm subsamples in a vibrating disk mill for carbon and p-ED-XRF (portable energy-dispersive X-ray fluorescence) analyses.

The grain size distributions were determined for the fraction ≤ 1 mm using a laser diffraction particle size analyzer; particle size classes are defined according to Ad-Hoc-AG Boden (2005).

Total carbon (TC) contents were determined using a CHN analyzer. All samples were tested negatively for inorganic carbon using 10 % HCl and therefore the TC contents are regarded as presenting total organic carbon (TOC) contents.

A wide range of chemical elements were measured with a portable energy-dispersive X-ray fluorescence spectrometer. Selected elements (Al, Si, Fe) are used after quality control to characterize the sediments of the burial mound.

Further details on analytical steps and quality control are included in the Supplement.

3.3 OSL dating

OSL dating was used to determine the time of burial of three sand-sized quartz samples from profile SD17P1. The analyses were carried out at the Netherlands Centre for Luminescence dating at Wageningen University. To calculate an OSL age, two quantities need to be measured: (i) the paleodose (in Gy), which is the amount of dose that was received by the sample since it was last exposed to sunlight, and (ii) the amount of ionizing radiation that the sample is exposed to during burial, which is termed the dose rate (in Gy kyr^{-1}).

Purified quartz-rich extracts of 212–250 µm grain size were used for paleodose determination. For equivalent dose measurements, the SAR protocol of Murray and Wintle (2003) was applied to small 1 mm aliquots (∼ 15–50 grains per aliquot). The most light-sensitive OSL signal of quartz grains is selected using the early background approach (Cunningham and Wallinga, 2010). The performance and heat treatment of this protocol was tested by dedicated dose recovery experiments. The most optimal dose recovery ratio (1.01 ± 0.05, $n = 13$) was obtained with a combination of 220, 200, and 230 °C for preheat, cut-heat, and hot-bleach, respectively. To obtain meaningful single-aliquot equivalent dose (D_e) distributions, we measured 96 aliquots per sample with around 50 % of the aliquots providing a sufficient OSL signal. The D_e distributions derived from the acceptable single-aliquot D_e values revealed significantly more scatter than we would expect for a well-bleached and unmixed sample. To obtain the paleodose that can be associated with the youngest single-aliquot population, the bootstrap version of the minimum age model (bootMAM; Galbraith et al., 1999; Cunningham et al., 2012) was applied. This model was run with a sigma_b input parameter of 15 ± 5 % (van der Meij et al., 2019).

To obtain the activity concentration associated with the decay of ^{40}K and the uranium and thorium decay chains, we performed high-resolution gamma spectrometry measurements on dry bulk sediment samples. Activity concentrations were converted to beta and gamma dose rates using the conversion factors of Guérin et al. (2011). Grain size, water, and organic matter attenuation effects were incorporated using the equations provided by Mejdahl (1979) and Aitken (1985). The moisture content of the sample's surroundings was estimated to be 6 ± 3 %, associated with relatively well-sorted and well-drained sandy deposits. The corresponding cosmic dose rate of a sample was calculated according to Prescott and Hutton (1994).

4 Results

4.1 Sediment description

The recorded profile SD17P1 reaches a total depth of 314 cm below the present-day surface of the burial mound and consists of 25 macroscopically distinguishable layers (Fig. 4).

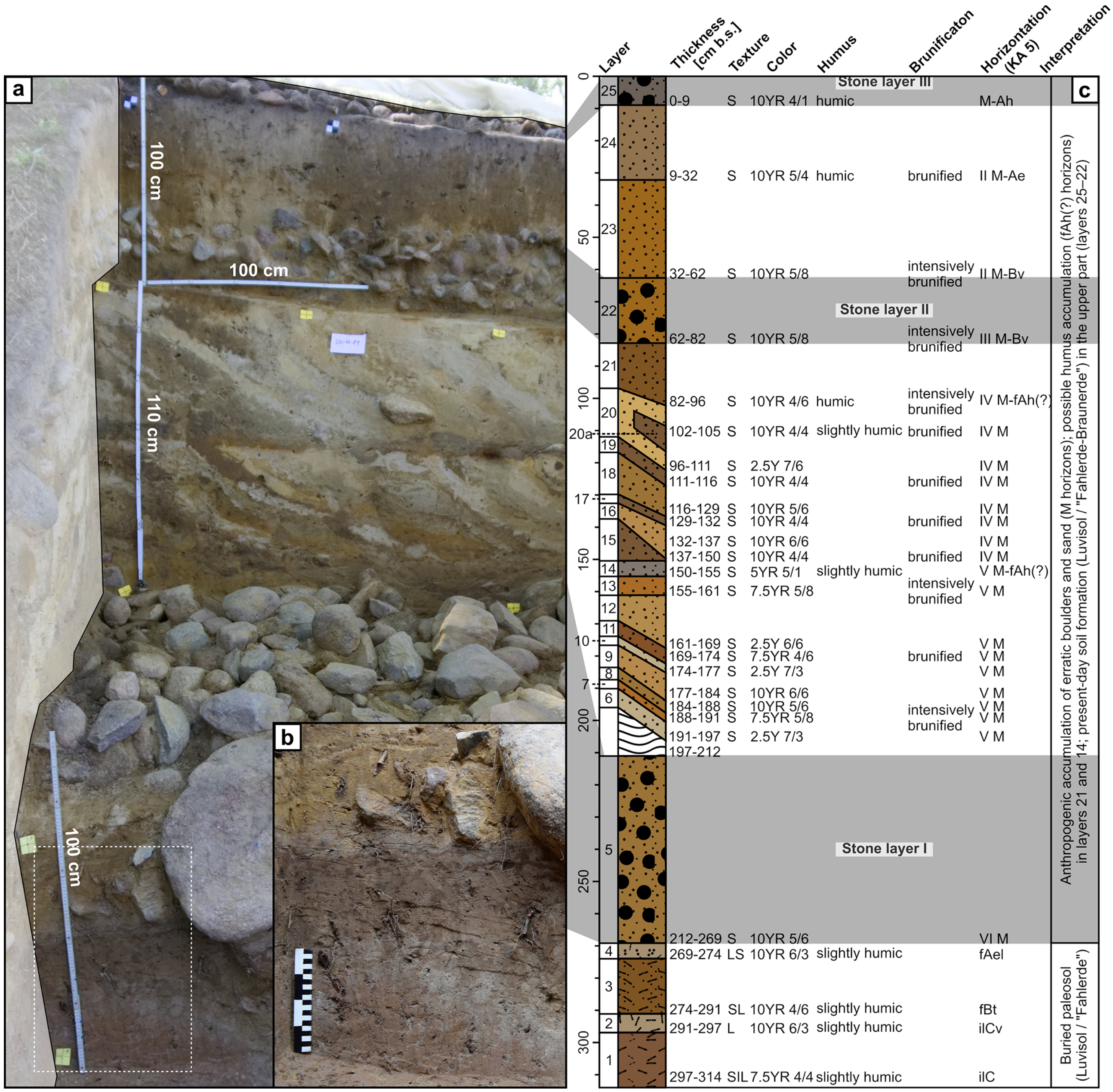

Figure 4. Composite illustration of **(a)** photograph of profile SD17P1 after cleaning (the white box in **a** marks the approximate extent of **b**); **(b)** detailed photograph of the lowest part of the profile; and **(c)** schematic drawing according to the field description, including summarized sediment characteristics (texture: S is sand, LS is loamy sand, SL is sandy loam, L is loam, SIL is silty loam) and pedological horizon designation according to KA 5 (Ad-Hoc-AG Boden, 2005). Designation of soil horizons includes the naming of the horizons (A is topsoil horizon, B is subsoil horizon, C is parent material, M is anthropogenic accumulation; prefixes: f is fossil, i is siliceous, l is loose; suffixes: e is leached-out, h is humus rich, l is depleted in clay, t is enriched in clay, v is weathered, brunified) and the counting of the main sand and stone strata (roman numerals are main strata of the anthropogenic accumulation). The gray shaded areas in **(c)** represent the three stone layers that structure the profile. For reference to the texture symbology, see Fig. 5.

The section is characterized by three artificial stone layers at 0–9, 62–82, and 212–269 cm b.s. (below surface) that consist of glacial boulders with up to 80 cm edge length. According to May (2018), the three stone layers are numbered I to III from the bottom to the top. The indication below surface refers to the surface of the burial mound at the location of the excavation trench, and the layers are counted from 1 to 25 (including the stone layers) from bottom to top. Between the stone layers, loose, sandy material was deposited during the construction of the burial mound (May, 2018). The upper 21 layers, between 0 and 269 cm b.s., represent material that was piled up during the construction of the burial mound.

Layer 25 (0–9 cm b.s.) represents the uppermost stone layer (III) that covers the burial mound. The stones are embedded in a dark gray (10YR 4/1) humic matrix consisting of sand. Layers 24 (9–32 cm b.s.) and 23 (32–62 cm b.s.) between stone layer III and II consist of sand and show gradual to diffuse layer boundaries. The color is yellowish brown with an increasing chroma towards the bottom (layer 24 is 10YR5/4; layer 23 is 10YR 5/8). The humus content decreases with depth, while brunification increases. Layer 22 (62–82 cm b.s.) represents stone layer II. The stones are embedded in brunified, yellowish brown (10YR 5/8) sand. Between stone layer II and stone layer I (82–212 cm b.s.), two packages of inclined layers (layers 21–15 and layers 12–6) are present. These two packages are separated by two horizontally running layers (layers 14 and 13). The inclined and the horizontal layers between stone layers II and I consist of sand, show varying humus contents and brunification intensities, and mostly have clearly defined layer boundaries. Layer 5 (212–269 cm b.s.) represents stone layer I. The stones, mostly cobble to stone size and partly up to boulder size, are embedded in slightly brunified yellowish brown (10YR 5/6) sand.

Layer 4 (269–274 cm b.s.) consists of pale brown (10YR 6/3) loamy sand with occasional fine gravels and horizontal dark yellowish brown (10YR 3/4) bands; the boundaries with layers 5 and 3 are abrupt. Layer 3 (274–291 cm b.s.) is characterized by dark yellowish brown (10YR 4/6), slightly mottled sandy loam and shows a clear to gradual wavy boundary with layer 2 (291–297 cm b.s.), which consists of pale brown (10YR 6/3) loam. The boundary of layers 2 and 1 is gradual and wavy, and the lowermost layer 1 (297–314 cm b.s.) is composed of brown (7.5YR 4/4) silt loam.

Based on this detailed description, profile SD17P1 is subdivided into the base representing the remnants of a buried paleosol developed from glaciofluvial loamy sand (layers 4 and 3) above till (layers 2 and 1) and alternating layers of anthropogenically heaped up stones and sand (layers 5–25) forming the upper part of the sequence (Fig. 4c).

4.2 Grain size distributions and geochemical characteristics

The grain size distributions of the upper 21 layers are rather uniform, ranging between 79.6 vol % and 98.5 vol % sand ($\bar{x} = 90.9$ vol %; $\sigma = 5.1$ vol %; $n = 34$) with only minor silt and clay contents (Fig. 5). In these sediments, medium sand is the major grain size fraction. The material below becomes increasingly fine. Layers 4 and 3 show decreasing sand ($\bar{x} = 69.7$ vol %; $\sigma = 8.4$ vol %; $n = 3$) and increasing silt and clay contents. The loamy material of the two lowermost sections (2 and 1) show the lowest sand ($\bar{x} = 36.9$ vol %; $\sigma = 4.6$ vol %; $n = 2$) and the highest silt and clay contents.

The sediments of layer 25 (0–9 cm b.s.) show the highest concentration of total carbon (TC = 2.14 mass %), intermediate electrical conductivity (EC = 71 µS cm^{-1}) values, and strong acidity (pH = 3.2). With depth, the TC and EC concentrations decrease towards the bottom of layer 22 (62–82 cm b.s.; TC = 0.23 mass %; EC = 24 µS cm^{-1}), while the pH values markedly increase to 4.5. At the top of layer 21 (82–96 cm b.s.), the TC concentrations (0.82 mass %) and, to a lesser extent, the EC values (52 µS cm^{-1}) increase abruptly, and the pH values show a slight decrease to 4.3. Between 96 and 150 cm depth (layers 20–15), the TC concentrations and the EC values show little variation; the pH values vary slightly more. The sediments of layers 14 (150–155 cm b.s.) and 13 (155–161 cm b.s.) show slightly increased TC concentrations ($\bar{x} = 0.44$ mass %) compared to the layers above and below. The EC shows a strong increase in layer 13 (111 µS cm^{-1}), whereas the pH value decreases to 3.8. Between layers 12 (161–169 cm b.s.) and 5 (212–269 cm b.s.), the TC contents slightly vary in the lower range of values; the EC values slightly decrease and then slightly increase with depth, and the pH values slightly vary around 4.3. The sediments of the lowermost layers 4 to 1 (269–314 cm b.s.) show slightly increased TC concentrations compared to the layers above. This part of the profile shows markedly increasing EC values (54 µS cm^{-1} at 271.5 cm depth), reaching the highest values (126 µS cm^{-1} at 303.5 cm depth) in the lowermost layer 1 (297–314 cm b.s.) and showing a distinct decrease in the pH values to 3.0, which is comparably acidic to layer 25.

The concentrations of the elements Al, Si, and Fe generally show minor variation in the upper part of the profile (between layers 25 and 5) and major shifts in the lower part. The upper part of the profile is characterized by low Fe ($\bar{x} = 0.5$ mass %; $\sigma = 0.1$ mass %; $n = 34$) and Al ($\bar{x} = 1.7$ mass %; $\sigma = 0.2$ mass %; $n = 34$) contents, while the Si contents are high ($\bar{x} = 43.8$ mass %; $\sigma = 0.8$ mass %; $n = 34$). The Si concentration starts to slightly decrease at the bottom of layer 5 and shows strongly decreased contents in layers 2 and 1 ($\bar{x} = 29.7$ mass %; $\sigma = 0.7$ mass %; $n = 2$). Generally, the Al and Fe contents of the lower profile show the opposite course of the Si concentrations; the highest values are reached in layers 2 and 1 (Al: $\bar{x} = 6.1$ mass %; $\sigma =$

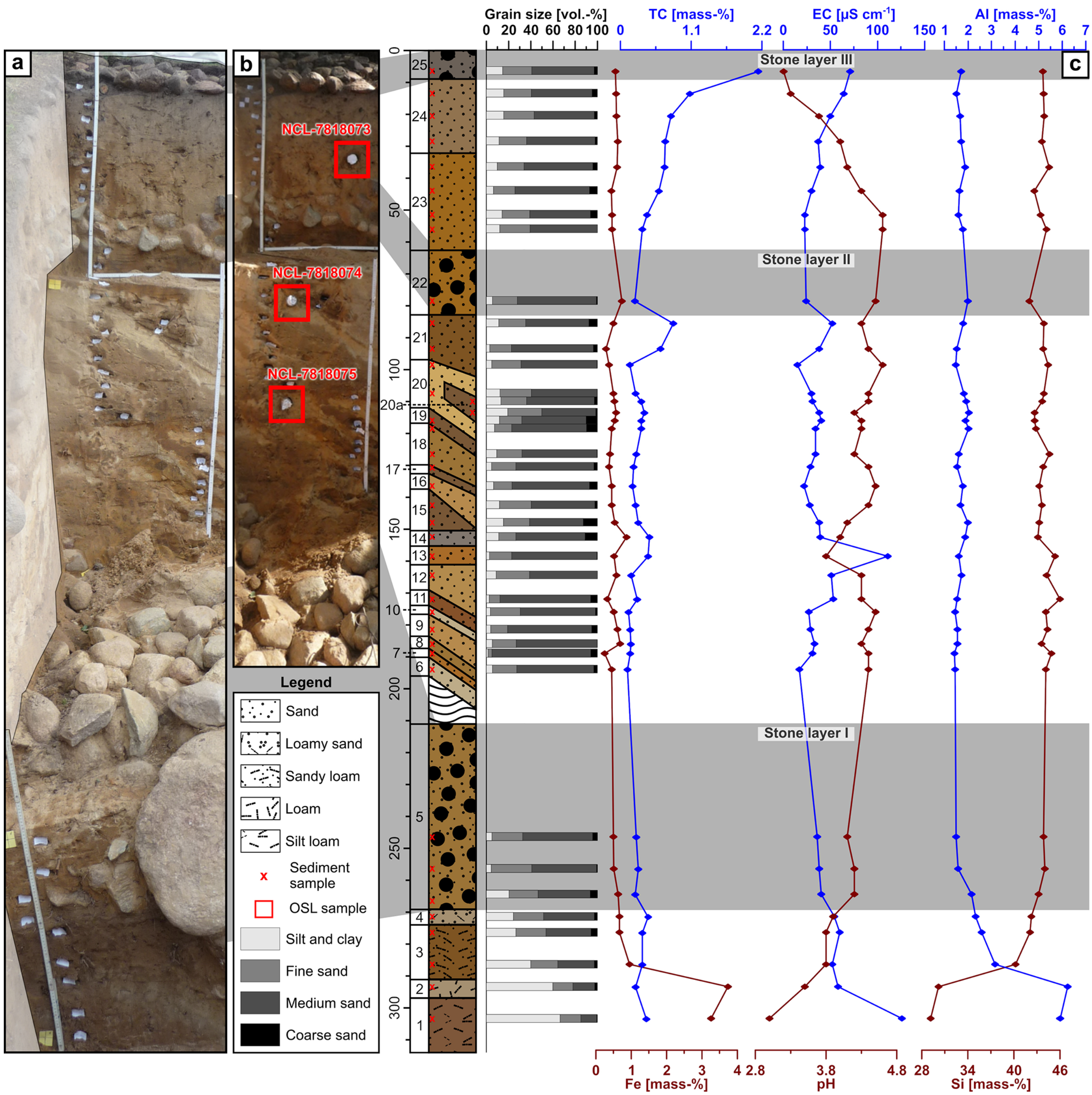

Figure 5. Composite illustration of **(a)** photograph of profile SD17P1 after description and sampling (the white labels in the photograph show the sampling spots); **(b)** profile photograph of the upper profile part highlighting the OSL sampling locations and sample IDs; and **(c)** schematic drawing with grain size composition and geochemical sediment parameters (TC is total carbon contents, EC is electrical conductivity, Al is aluminum, Fe is iron, Si is silicon).

0.2 mass %; $n = 2$; Fe: $\bar{x} = 3.5$ mass %; $\sigma = 0.3$ mass %; $n = 2$).

4.3 OSL ages

The results of paleodose and dose rate determination are listed in Table 1. The dose rates of the three samples vary between $1.11 \pm 0.04\,\mathrm{Gy\,kyr^{-1}}$ to $1.30 \pm 0.05\,\mathrm{Gy\,kyr^{-1}}$, which is in the normal range for this kind of sediment. The paleodose of samples NCL-781873 and NCL-7818075 are significantly smaller than of NCL-781874. This suggests that the former two samples contain sand grains that can be associated with recent, thus most likely anthropogenic, reworking while sample NCL-78118074 shows a large paleodose (and thus age) that is most likely associated with the primary deposition of the sediments.

The corresponding ages indicate for the uppermost and the lowermost samples that the anthropogenic reworking occurred between 4.5 ± 1.0 and 3.1 ± 0.7 kyr ago. The errors associated with both samples are relatively large because the youngest dose population modeled by the bootMAM only represents a fraction of the total D_e distribution (see distributions in Fig. 6). It should be noted that OSL ages are reported with their 1σ uncertainty and range between 3520 and 420 BCE. Based on the 2σ confidence interval, the youngest age components of NCL-78118073 and NCL-7818075 that are again most likely associated with anthropogenic reworking range between 4520 BCE and 320 CE.

5 Discussion

5.1 Chronological framework

The sediment layers bracketed by the stone pavements contain sand-sized quartz well suited for OSL dating. With OSL dating, we ideally determine the time when these sediments were last reworked (presumably by humans). The idea is that during this anthropogenic reworking some grains were exposed to light. Using OSL dating we are able to determine the burial age associated with this last reworking event (e.g., van der Meij et al., 2019). OSL samples NCL-7818073 and NCL-7818075 (layer 23 and layer 12, respectively) show large variations in their corresponding small aliquot D_e distributions (Fig. 6) with (i) large D_e values likely representing the original deposition of glaciofluvial or coversand deposits and (ii) very small D_e values (of <10 Gy) most likely being associated with anthropogenic reworking. It should be noted at this point that our 1 mm aliquots are regarded, at least in this sedimentary setting, as reliable proxies for genuine single-grain OSL analyses (e.g., Lüthgens et al., 2011; Reimann et al., 2012). Therefore, the calculated bootMAM ages derived from the youngest D_e population of samples NCL-7818073 and NCL-7818075 point at an anthropogenic reworking age of 2.4–5.5 ka (1σ confidence interval). This age range is in good agreement with the radiocarbon ages and the archeological evidence, i.e., the suggested time span for period V (Hornstrup et al., 2012). Additionally, the three radiocarbon ages from the fossil soil layer below the basal stone layer I yield a similar age range and a terminus post quem time frame for the construction of the burial mound of 910–800 BCE (Table 2).

The age error that we had to assign to both ages is relatively large (~ 22 %) compared to OSL ages from well-bleached and unmixed samples that typically show smaller age errors between 5 to 10 %. These large errors reflect the complexity of the corresponding D_e distributions of samples NCL-7818073 and NCL-7818075, more precisely the small fraction of D_e values that were used to calculate the paleodose associated with the anthropogenic reworking. However, it should be noted that the youngest age components in the uppermost and lowest samples both fall into the radiometric age of the construction site even though the OSL ages reflect rather large error bars. We assume that the construction of the sediment packages between the stone pavements was done within a rather short time frame and material was taken from continuously used pits. However, based on the OSL ages and due to non-calculable factors such as the number of individuals involved in the construction or the equipment they used, it is not possible to provide a time estimate for the duration of the construction process.

Sample NCL-7818074 (layer 20) contains no young grains in its D_e distribution, suggesting that during anthropogenic reworking no or too few sand grains were surfaced, and thus this reworking event was not able to leave an imprint on the corresponding D_e distribution.

Interestingly, anthropogenic reworking of the sediment packages only produced incompletely mixed samples presumably linked to the corresponding construction technique. While we can use the paleodose of the youngest dose population to estimate the timing of the anthropogenic disturbance (outlined above), we can use the number of aliquots in this population, which is assumed to be proportional to mixing intensity (Reimann et al., 2017), as a fingerprint of the construction technique that produced the disturbance. From the D_e distribution shown in Fig. 6, it appears that the uppermost sample NCL-7818073 (at ~ 0.52 m depth) contains more grains in the younger population than that of the lowest sample NCL-7818075 (at ~ 1.68 m depth). This may point to a different way of constructing the upper part of the section presumably characterized by more intensive grain surfacing. Alternatively, this observation might be linked to subsequent soil formation and thus grain surfacing through bioturbation.

Looking at the older population of the complex D_e distributions (Fig. 6), we can also learn something about the primary deposition(s) of the sandy material (e.g., Huisman et al., 2019). The middle sample NCL-7818074 (~ 1.22 m depth) is dominated by aliquots with D_e values well above 100 Gy which can be associated with the deposition of glaciofluvial sand during the late Saalian. Furthermore, we can observe younger aliquots below 100 Gy, pos-

Table 1. OSL dating results (n/a is no answer). See Sects. 3.3 and 4.3 for details.

NCL Code	Sample ID	Depth (m)	Paleodose (Gy)	Dose rate (Gy kyr^{-1})	Age (ka)	Date (BCE)	Systematic	Random	Reliability	Comments
NCL-7818073	SD17P1 53	0.52	4.1 ± 0.9	1.29 ± 0.05	3.1 ± 0.7	1120 ± 700	0.12	0.67	Likely OK	
NCL-7818074	SD17P1 125	1.22	153 ± 11	1.11 ± 0.04	138 ± 11	n/a	5.29	10.09	Inaccurate	Not bleached
NCL-7818075	SD17P1 170	1.68	5.9 ± 1.3	1.30 ± 0.05	4.5 ± 1.0	2520 ± 1000	0.17	1.04	Questionable	Too few young aliquots

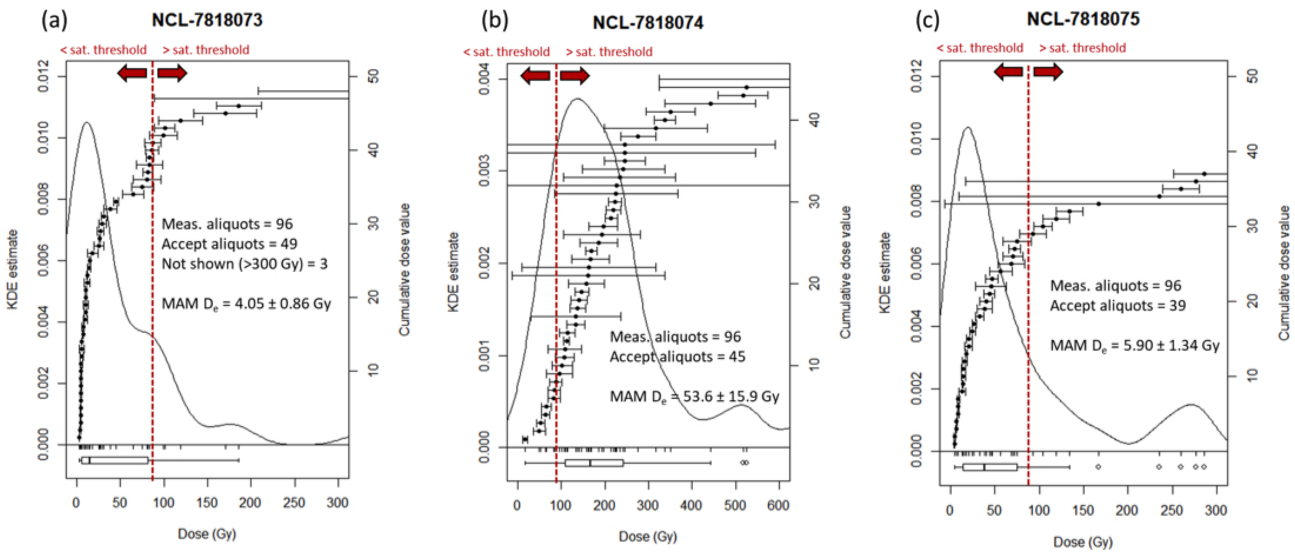

Figure 6. **(a)** to **(c)** D_e distribution of the three OSL samples shown as kernel density plots (KDEs). Dashed red line represents the average lower threshold of OSL signal saturation (2D0 value is sat. threshold) which was estimated based on the dose response curves to ~ 90 Gy. For D_e values to the right of this dashed line, it is not possible to calculate an accurate age. Although the face value of these large D_e values needs to be taken with caution, they provide insights into (i) the approximate age and (ii) the fraction of grains that have not been surfaced since approximately the early Weichselian. Note that the x axis for **(b)** is different from **(a)** and **(c)**.

sibly associated with the reworking of the sediment package during the early to middle Weichselian related to either periglacial processes (cryoturbation) or soil mixing (bioturbation) during interstadials. The uppermost and the lowermost samples (NCL-7818073, NCL-7818075) also seem to recover the late Saalian and Weichselian aliquot populations.

5.2 Interpretation of the site and landscape context

Our results are in good agreement with previous studies regarding the prevailing substrates and their middle to late Quaternary history of deposition and reworking. The silty loam and loam deposits of layers 2 and 1 have substantially reduced sand contents in favor of increased silt and clay contents. This is also supported by the substantially increased Fe and Al contents, together with the considerably decreased Si values within these layers compared to the top layers that generally show minor variations for these elements (Fig. 5c). These layers are regarded as presenting late Saalian till deposits (Fig. 7a) that form part of the slightly undulating till plains in the old morainic area of the Prignitz region (Lippstreu et al., 1997; Nagel et al., 2003; Lippstreu et al., 2015; Fig. 2a). Next to the till plains, late Saalian glaciofluvial sand plains (Fig. 7a) form a major landscape component in the surroundings of the royal tomb (Königsgrab) of Seddin, and the overlying layers 3 and 4 correspond to the sandy to loamy-sandy deposits that commonly cover the till deposits (GeoBasis-DE/LGB, 2012; Fig. 2a). Periglacial reworking of these deposits and coversand formation occurred during the Weichselian (Kasse, 2002; Nagel et al., 2003; Koster, 2005; Kaiser et al., 2009; Lüthgens et al., 2010; Fig. 7b) and soil formation, in conjunction with the development of the vegetation cover, during the late glacial and Holocene (Kühn, 2003; Kappler et al., 2019; Fig. 7c).

During the Bronze Age, the landscape in Brandenburg opened substantially due to large-scale woodland clearings especially during the Late Bronze Age (Jahns, 2015, 2018).

Table 2. Comparison of ^{14}C and OSL ages.

Laboratory ID	Material	^{14}C age (years BP)	Uncertainty (years)	Age (2σ; from–to cal. a BP)	Age (2σ; from–to BCE)	Reference
KIA 21317[a]	*Salix*/*Populus*/*Quercus*	2694	31	2851–2754	902–805	May (2018)
MAMS 35030[a]	*Fagus*	3375	22	3688–3570	1739–1621	This study
MAMS 21017[a]	*Pinus*	2719	19	2855–2769	906–820	May (2018)
MAMS 21018[a]	*Corylus*	2725	19	2859–2773	910–824	May (2018)
		Paleodose (Gy)	Dose rate (Gy kyr^{-1})	Age (1σ; ka)	Age (1σ; BCE)	
NCL-7818073[b]	Purified quartz-rich extracts (212–250 µm)	4.1 ± 0.9	1.29 ± 0.05	2400–3800	420–1820	This study
NCL-7818075[b]	Purified quartz-rich extracts (212–250 µm)	5.9 ± 1.3	1.30 ± 0.05	3500–5500	1520–3520	This study

[a] Radiocarbon ages were obtained from charcoal pieces recovered from layers that stratigraphically correspond to layer 23 of profile SD17P1 yielding the terminus post quem time frame for the construction of the burial mound; [b] OSL ages from the deposits of the burial mound providing direct age estimates for the construction phases.

The charcoals obtained from the substrate below the burial mound (Table 2) suggest that the local forest composition at the construction site prior to the initial construction phase in the Late Bronze Age included pine (*Pinus*), hazel (*Corylus*), and either willow (*Salix*), poplar (*Populus*), or oak (*Quercus*).

A comparison of the grain size distributions of the layers that form the burial mound (layers 5–25) and the geological, soil type, and texture maps (Fig. 2) indicate that the mound most likely was exclusively constructed from glaciofluvial sand – except for the erratic boulders forming the three stone layers. The first stone pavement is regarded as representing the first material that was deposited during the initial construction phase of the alternating stone and sand strata, and May (2018) suggests that the substrate below stone layer I represents a fossil soil that was buried during this initial construction phase (Fig. 7d). The dark material that was recorded during several archeological excavations underneath stone layer I (May, 2018) stratigraphically corresponds to layer 3 in profile SD17P1. Our geochemical sediment analyses support the assumption of May (2018) as the TC values very slightly increase below layer 5, the pH values are reduced in layers 4 and 3 compared to layer 5, and the electric conductivity is concurrently increased (Fig. 5c). However, the increased EC values might result from a grain-size effect as the texture becomes finer towards the base of the profile. As these characteristics roughly resemble the horizon characteristics of a typical Fahlerde or Braunerde-Fahlerde in this part of the Prignitz–Brandenburg region (MLUV, 2005), we interpret layer 4 as the fAel horizon and layer 3 as the fBt horizon (according to Ad-Hoc-AG Boden, 2005). According to the soil classification system of the IUSS Working Group WRB (2006), this corresponds to a Luvisol with layer 4 being the fossil albic horizon and layer 3 being the underlying fossil argic horizon. This soil horizon designation also suggests that the soil profile is truncated and that a fAh horizon is missing below stone layer I. The missing fossil, organic-rich topsoil horizon (fAh horizon) was already recorded at several locations below the mound; it was pointed out that either a "dark substrate" or a "pale solidified sand" occurs directly underneath the lowermost stone pavement, i.e., in stratigraphically identical positions (May, 2018). Based on the present results, we assume that the "dark substrate" from the archeological descriptions represents the fBt horizon and the "pale solidified sand" the fAel horizon showing an irregular occurrence below stone layer I. On the one hand, the absence of the fAh horizon and partially also of the fAel horizon may be the result of soil erosion by water or wind after the surface of the construction site was cleared of vegetation; the sandy material of the fAh and fAel horizons is more susceptible to erosion compared to the loamy material of the fBt horizon below. On the other hand, intentional leveling of the construction ground after vegetation clearance but before the deposition of stone layer I might have caused the removal of the topsoil horizon(s). Both scenarios are supported by the archeological observation that pieces of charcoal and ceramic are incorporated into the fAel and the fBt horizons below the mound, indicating that the soil surface was disturbed during the Late Bronze Age construction of the burial mound. It seems very likely that the erosion or removal of the topsoil horizon(s) occurred closely before the initial construction phase of the royal tomb, but at present, we have no evidence to favor either of these scenarios.

At a Bronze Age burial mound site in Denmark (Lejrskov), Holst et al. (1998) also describe a buried soil beneath the mound structure. The fossil A horizon at their site has a little more than 0.5 % of organic matter. They argue that the organic matter content could have been higher but might be subjected to decomposition since burial.

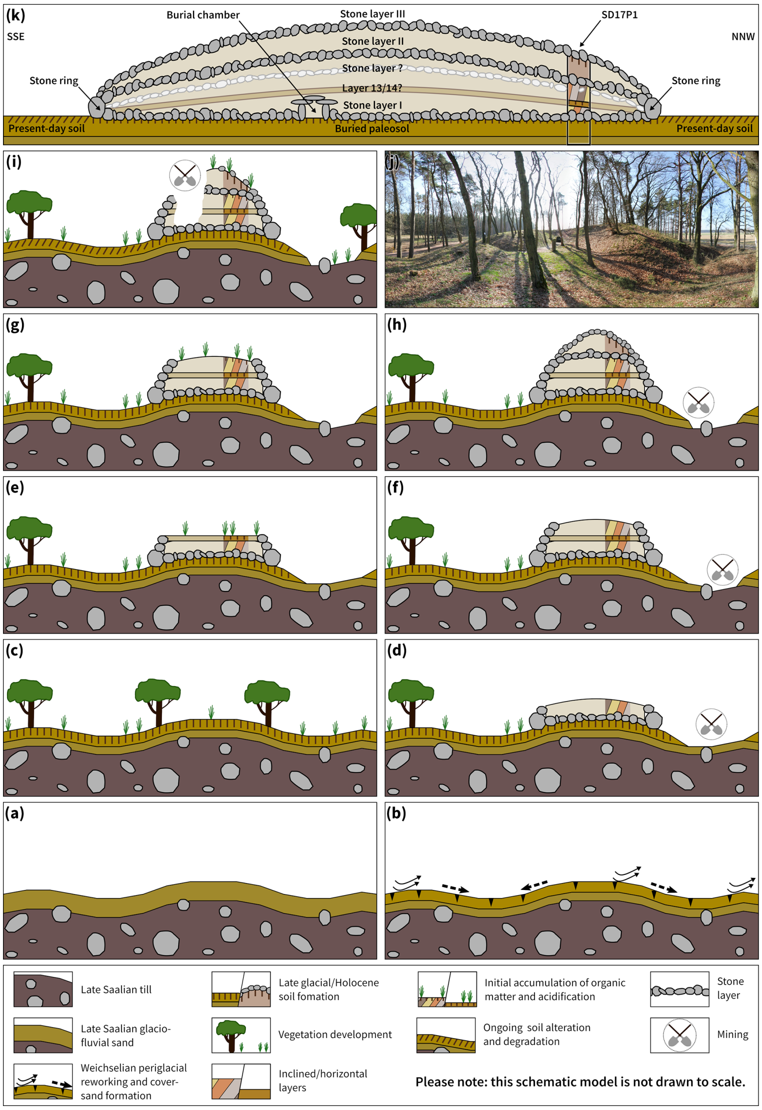

Figure 7. Schematic genetic model of the late Saalian to Holocene landscape development, possible construction phases of the burial mound, and its present-day schematic concept according to the state of the art (cf. locations of the excavation trenches in Fig. 3). During the late Saalian, till was deposited and partly covered by glaciofluvial deposits **(a)**. Periglacial reworking and cover sand formation occurred during the Weichselian **(b)**. During the late glacial and Early Holocene, a denser vegetation cover developed, and soil formation occurred **(c)**. With the start of the construction of the burial mound, the soil was truncated, and its remaining fAel and fBt horizons were buried underneath the first stone pavement; the overlying sand packages show late Saalian and Weichselian, as well as Holocene, OSL ages, the latter being linked to anthropogenic reworking **(d)**. After the first construction phase, weedage may have occurred that would allow for the initial accumulation of organic matter **(e)**. The sand package of the second construction phase solely shows a late Saalian OSL age **(f)**. Weedage and initial accumulation of organic matter may also have occurred after the second construction phase **(g)**. The second stone pavement, the uppermost sand package, and the surface-covering stone pavement were presumably deposited during a third construction phase; the sand packages show late Saalian and Holocene OSL ages **(h)**. The paleosol recorded underneath the burial mound is not preserved in the area around, but soil development continued, and the soil was modified and degraded by land use such as plowing and sediment extraction. Gravel mining in the late 19th century partially destroyed the burial mound **(i)**, but heritage protection measures preserved the archeological remains until the present day **(j)**. The presented schematic genetic model **(d–i)** is based on the results of profile SD17P1 and is simplified compared to the schematic concept according to the state of the art **(k)**. The manifestation of particular characteristics such as the two packages of inclined layers or the two horizontal layers in between vary locally. Also, some of the excavation trenches yielded indications for an additional stone layer between stone layers I and II **(k)**. Please note that the location(s) of the sand pit(s) that were exploited to construct the burial mound have not been identified and are presented idealized here.

Other studies carried out in the context of Bronze Age burial mounds focused on paleosols as a proxy for paleoenvironmental conditions during the times of usage of the mounds. At a site in northern Germany (Bornhöved), Dreibrodt et al. (2009) suggest that the surrounding area was probably forested during the time. In contrast, at a burial mound site in southern Sweden (Bjäre peninsula), a significant decrease in forest coverage was reconstructed for the respective time of usage (Hannon et al., 2008).

The particular geochemical properties as described above (i.e., layers with increased TC contents, high electric conductivity values, and decreased pH values) also occur in layers 14–13, 21, and 25–24. These characteristics may point to phases when humic acids, together with a higher availability of soluble salts, may have occurred in conjunction with humus accumulation. This interpretation is supported by the particular signature of the values, i.e., the TC values decrease with increasing depth, which is a typical feature of soil development. The results of Haburaj et al. (2020) support this interpretation, too. They study the upper part of the same excavation trench and combine data from RGB and multispectral cameras, visible and near-infrared hyperspectral data, and geochemical data. Their image classifications show that soil organic carbon is mainly increased in layers 24, 21, and 14 (according to the layer counting presented here) and that these layers run more or less horizontally along the entire width of the excavation trench (Haburaj et al., 2020). Even though these arguments support the interpretation of initial in situ accumulation of organic matter, inherited sediment properties from reworked material cannot be excluded.

These characteristics occur three times in our profile (Fig. 5). First, it (Fig. 7e) occurs in the horizontally bedded layers 14 and 13 that overly the lowermost package of inclined layers (12–6). The upper package of inclined layers (15–21) bury the two horizontal layers (Fig. 7f). Within the sediments of layer 21, which represents the final stage of sand accumulation below stone layer II (Fig. 7g), the initial accumulation of organic matter, increasing acidity, and higher availability of soluble salts occur again. We interpret this as an indication for phases when the construction works possibly were interrupted for a short, yet not further definable, period of time. Such an interruption of the construction process likely would have allowed the development of an initial vegetation cover due to weedage and as a consequence the accumulation of organic matter. The inclined structure of layers 12–6 and 21–15 are clearly visible in section SD17P1. This is not necessarily the case throughout the entire burial mound as other sections that were opened did not display this structure so distinctly. Such locally varying characteristics are also documented for other burial mounds (e.g., Holst and Rasmussen, 2015). These sediments are buried by the second stone pavement, the uppermost sand package (layers 23–24), and stone layer III (Fig. 7h). The properties of layers 25–23 presumably represent the result of ongoing soil formation processes that started from the completion of the Late Bronze Age burial mound, also as a consequence of post-Bronze-Age vegetation development on top of the burial mound. Intensive exploitation of rock and sand in the course of the late 19th century led to the partial destruction of the burial mound (Fig. 7i) and ultimately to its discovery in the year 1899 (May, 2018). Restoration and the planting of trees started at the beginning of the 20th century (May, 2018), preserving the remains of the monumental burial mound royal tomb (Königsgrab) of Seddin (Fig. 7j).

5.3 Opportunities and challenges of a minimal invasive approach for OSL dating of burial mounds

As shown by Kristiansen et al. (2003), augering through burial mounds can yield material from buried organic-rich topsoil horizons suitable for the ^{14}C analysis of soil organic matter fractions. An absent or fragmentarily preserved organic-rich topsoil horizon below the mound – as is the case for the profile presented here – would cause problems. Sand-sized quartz grains, in contrast, are ubiquitous in the European sand belt, and probably most, if not all, burial mounds contain it as a fraction of their construction material. Therefore, we propose to modify the approach of Kristiansen et al. (2003) and suggest to rather use engine-driven vibracoring techniques instead of augering to obtain undisturbed sediment cores from the body of the burial mound and the (possibly) underlying buried soil in plastic tubes. In doing so, datable material for ^{14}C analysis from a possibly present buried organic-rich topsoil horizon and sand-sized quartz grains from the burial mound itself suitable for OSL dating can be obtained. It has been shown that samples for OSL dating can be obtained from plastic liners that were driven into the subsurface by means of steel probes (e.g., Reimann et al., 2010, 2012).

Our first attempt to use OSL dating of sand-sized quartz grains to determine the construction period of a burial mound generally shows good applicability of this approach but also reveals challenges (cf. also Porat et al., 2012; Pluckhahn et al., 2015; al Khasawneh et al., 2020). One of the main challenges is the relatively large error of ca. 22 % compared to errors of 5 %–10 % that are typical for well-bleached and unmixed samples. Therefore, the clear temporal association of a burial mound to a specific cultural epoch can be problematic. One solution to reduce this error and thus possibly date newly discovered burial mounds more accurately would be the use of single-grain feldspar luminescence instead. Sand-sized feldspar grains typically occur in various Quaternary deposits along the European sand belt (e.g., Füchtbauer and Elrod, 1971; Saye and Pye, 2006; Kalińska-Nartiša et al., 2015; Kalinìska et al., 2019), and Reimann et al. (2017) have shown that this novel method holds important advantages over quartz single-grain OSL in settings with a complex history of reworking. In a burial mound setting as presented in this study, it might be possible to reduce the age error to 6 %–7 % using single-grain feldspar luminescence.

6 Conclusions

Our OSL chronology – on account of its much larger age range – matches the radiocarbon-based terminus post quem time frame of 910–800 BCE for the construction period of the monumental burial mound royal tomb (Königsgrab) of Seddin and therewith supports its chronological affiliation to the transition from the Late Bronze Age to the Iron Age now with process-based datings. Beyond this temporal correspondence with the construction period, our OSL ages also provide new temporal insights into the initial deposition of late Saalian glaciofluvial sand and its Weichselian periglacial reworking. Our initial experiences with the OSL dating of sediments from a burial mound have revealed its generally good applicability but also related challenges. Based on our experiences, we have proposed a minimal invasive approach to obtain samples for ^{14}C and OSL dating that can be tested on well-studied burial mounds and may help to provide initial numerical age control for newly discovered ones.

The presented results of the sedimentological and geochemical analyses prove the existence of a truncated paleosol underneath the lowermost stone pavement of the tomb. The two identified fossil horizons are interpreted as fAel and fBt horizons of a Fahlerde or Braunerde-Fahlerde, i.e., fossil albic and fossil argic horizons of a Luvisol, which is a typical soil in this part of the Prignitz region. At three locations of the upper part of the profile (layers 14–13, 21, and 25–24), increased TC and electric conductivity values and decreased pH values occur. This may point to the in situ enrichment of humus, soluble salts, and humic acids as a consequence of possible phases when the construction works were likely interrupted and weedage occurred.

Data availability. Additional information on the applied methods, quality control measures, and the sedimentological and geochemical data are provided in the Supplement.

Supplement. The supplement related to this article is available online at: https://doi.org/10.5194/egqsj-70-1-2021-supplement.

Author contributions. This study was designed by MN, PH, and JM who also carried out field work. Luminescence dating was done by TR. MN wrote the paper; JH, PH, JM, and TR provided contributions. All authors read, commented on, and approved the paper and the revised version.

Competing interests. The authors declare that they have no conflict of interest.

Acknowledgements. This study is funded by the Excellence Cluster (EXC 264) Topoi – The Formation and Transformation of Space and Knowledge in Ancient Civilizations. We acknowledge support from the open-access publication fund of Freie Universität Berlin. The authors very much appreciate the technical support from Erna Voskuilen during the OSL analyses and Lena Schimmel and Vincent Haburaj during field work. We express our sincere thanks to Knut Kaiser and an anonymous reviewer for thoroughly evaluating our paper. Their constructive comments and criticisms helped to critically reflect and clarify some aspects of this study; detailed suggestions enhanced its value. Markus Fuchs is acknowledged for handling our paper as associate editor.

Financial support. This research has been supported by the Deutsche Forschungsgemeinschaft (DFG) (grant no. 39235742).

We acknowledge support from the open-access publication initiative of Freie Universität Berlin.

Review statement. This paper was edited by Markus Fuchs and reviewed by Dr. Knut Kaiser and one anonymous referee.

References

Ad-Hoc-AG Boden: Bodenkundliche Kartieranleitung, Schweizerbart, Stuttgart, 2005 (in German).

Aitken, M. J.: Thermoluminescence Dating, Academic Press Inc. Ltd, London, 1985.

al Khasawneh, S., Murray, A., Kafafi, Z., and Petit, L.: Luminescence Dating of the Iron Age Deposits from Tell Damiyah in the Jordan Valley, Radiocarbon, 62, 1–12, 2020.

Beck, H. E., Zimmermann, N. E., McVicar, T. R., Vergopolan, N., Berg, A., and Wood, E. F.: Present and future Köppen-Geiger climate classification maps at 1-km resolution, Scientific Data, 5, 180214, https://doi.org/10.1038/sdata.2018.214, 2018.

Böse, M., Lüthgens, C., Lee, J. R., and Rose, J.: Quaternary glaciations of northern Europe, Quatern. Sci. Rev., 44, 1–25, 2012.

Cunningham, A. C. and Wallinga, J.: Selection of integration time intervals for quartz OSL decay curves, Quat. Geochronol., 5, 657–666, 2010.

Cunningham, A. C., DeVries, D. J., and Schaart, D. R.: Experimental and computational simulation of beta-dose heterogeneity in sediment, Radiat. Meas., 47, 1060–1067, 2012.

Doorenbosch, M.: Ancestral heaths: reconstructing the barrow landscape in the Central and Southern Netherlands, Sidestone Press, Leiden, the Netherlands, 2013.

Dreibrodt, S., Nelle, O., Lütjens, I., Mitusov, A., Clausen, I., and Bork, H.-R.: Investigations on buried soils and colluvial layers around Bronze Age burial mounds at Bornhöved (northern Germany): an approach to test the hypothesis of "landscape openness" by the incidence of colluviation, Holocene, 19, 487–497, 2009.

DWD Climate Data Center: Annual mean of Station observations of air temperature at 2 m above ground in °C for Germany, version v19.3., available at: https://cdc.dwd.de/portal/ (last access: 15 July 2020), 2020a.

DWD Climate Data Center: Annual station observations of precipitation in mm for Germany, version v19.3., available at: https://cdc.dwd.de/portal/ (last access: 15 July 2020), 2020b.

Ehlers, J., Grube, A., Stephan, H.-J., and Wansa, S.: Pleistocene Glaciations of North Germany–New Results, in: Quaternary Glaciations – Extent and Chronology. A Closer Look, Developments in Quaternary Science, 15, edited by: Ehlers, J., Gibbard, P. L., and Hughes, P. D., Elsevier, Amsterdam, the Netherlands, 149–162, 2011.

European Environment Agency: Corine Land Cover (CLC) 2018, Version 2020_20u1, available at: https://land.copernicus.eu/pan-european/corine-land-cover/clc2018, last access: 15 July 2020.

Feathers, J. K.: Luminescence dating of early mounds in Northeast Louisiana, Quaternary Sci. Rev., 16, 333–340, 1997.

Füchtbauer, H. and Elrod, J. M.: Different sources contributing to a beach sand, southeastern Bornholm (Denmark), Sedimentology, 17, 69–79, 1971.

Galbraith, R. F., Roberts, R. G., Laslett, G. M., Yoshida, H., and Olley, J. M.: Optical dating of single and multiple grains of quartz from Jinmium rock shelter, Northern Australia: part 1, experimental details and statistical models, Archaeometry, 41, 339–364, 1999.

GeoBasis-DE/LGB: Bodenübersichtskarte des Landes Brandenburg 1:300 000, available at: http://www.geo.brandenburg.de/boden/ (last access: 21 April 2020), 2012 (in German).

GeoBasis-DE/LGB: Digitales Geländemodell, available at: https://data.geobasis-bb.de/geobasis/daten/dgm/xyz/, last access: 21 April 2020 (in German).

Geofabrik: Brandenburg (mit Berlin), available at: http://download.geofabrik.de/europe/germany.html, last access: 21 April 2020.

Guérin, G., Mercier, N., and Adamiec, G.: Dose rate conversion factors: update, Ancient TL, 29, 5–8, 2011.

Haburaj, V., Nykamp, M., May, J., Hoelzmann, P., and Schütt, B.: On-Site VIS-NIR Spectral Reflectance and Colour Measurements–A Fast and Inexpensive Alternative for Delineating Sediment Layers Quantitatively? A Case Study from a Monumental Bronze Age Burial Mound (Seddin, Germany), Heritage, 3, 528–548, 2020.

Hannon, G. E., Bradshaw, R. H. W., Nord, J., and Gustafsson, M.: The Bronze Age landscape of the Bjäre peninsula, southern Sweden, and its relationship to burial mounds, J. Archaeol. Sci., 35, 623–632, 2008.

Harding, A.: The Tumulus in European Prehistory: Covering the Body, Housing the Soul, in: Ancestral Landscape. Burial mounds in the Copper and Bronze Ages, Proceedings of the International Conference, Udine, Italy, 15–18 May 2008, 21–30, 2012.

Holst, M. K. and Rasmussen, M.: Skelhøj and the Bronze Age barrows of southern Scandinavia, Jut. Arch. Soc. Pub., 78, Aarhus University Press, Aarhus, Denmark, 2015.

Holst, M. K., Breuning-Madsen, H., and Olsson, M.: Soil Forming Processes in and below a Bronze Age Burial Mound at Lejrskov, Southern Jutland, Geogr. Tidsskr., 98, 46–55, 1998.

Hornstrup, K. M., Olsen, J., Heinemeier, J., Thrane, H., and Bennike, P.: A new absolute Danish Bronze Age chronology as based on radiocarbon dating of cremated bone samples from burials, Acta Archaeol., 83, 5–53, 2012.

Huisman, H., de Kort, J.-W., Ketterer, M. E., Reimann, T., Schoorl, J. M., van der Heiden, M., van Soest, M., and van Egmond, F.: Erosion of archaeological sites: Quantifying the threat using optically stimulated luminescence and fallout isotopes, Geoarchaeology, 34, 478–494, 2019.

IUSS Working Group WRB: World Reference Base for Soil Resources 2006, World Soil Resources Reports No. 103, FAO, Rome, Italy, 2006.

Jahns, S.: Bronze Age settlements reflected in pollen diagrams from Brandenburg, Eastern Germany, in: The third food revolution? Setting the Bronze Age table: common trends in economic and subsistance strategies in Bronze Age Europe, edited by: Kneisel, J., Dal Corso, M., Kirleis, W., Scholz, H., Taylor, N., and Tiedtke, V., Habelt, Bonn, Germany, 237–248, 2015.

Jahns, S.: Pollenanalytische Untersuchungen zur Bronzezeit am Bergsoll bei Helle, Lkr. Prignitz, in: Der Grabhügel von Seddin im norddeutschen und südskandinavischen Kontext, Arbeitsberichte zur Bodendenkmalpflege in Brandenburg, 33, edited by: Hansen, S. and Schopper, F., Brandenburgisches Landesamt für Denkmalpflege und Archäologisches Landesmuseum, Wünsdorf, Germany, 85–90, 2018 (in German).

Kaiser, K., Hilgers, A., Schlaak, N., Jankowski, M., Kühn, P., Bussemer, S., and Przegiętka, K.: Palaeopedological marker horizons in northern central Europe: characteristics of Lateglacial Usselo and Finow soils, Boreas, 38, 591–609, 2009.

Kaiser, K., Schneider, T., Küster, M., Dietze, E., Fülling, A., Heinrich, S., Kappler, C., Nelle, O., Schult, M., Theuerkauf, M., Vogel, S., de Boer, A. M., Börner, A., Preusser, F., Schwabe, M., Ulrich, J., Wirner, M., and Bens, O.: Palaeosols and their cover sediments of a glacial landscape in northern central Europe: Spatial distribution, pedostratigraphy and evidence on landscape evolution, Catena, 193, 104647, https://doi.org/10.1016/j.catena.2020.104647, 2020.

Kalinìska, E., Hang, T., JoÞeleht, A., Olo, S., Nartišs, M., and Adamiec, G.: Macro- and micro-scale study and chronology of Late Weichselian aeolian sediments in Estonia, north-eastern European Sand Belt, Int. J. Earth Sci., 108, 2021–2035, 2019.

Kalinìska-Nartiša, E., Thiel, C., Nartišs, M., Buylaert, J.-P., and Murray, A. S.: Age and sedimentary record of inland eolian sediments in Lithuania, NE European Sand Belt, Quaternary Res., 84, 82–95, 2015.

Kappler, C., Kaiser, K., Küster, M., Nicolay, A., Fülling, A., Bens, O., and Raab, T.: Late Pleistocene and Holocene terrestrial geomorphodynamics and soil formation in northeastern Germany: a review of geochronological data, Phys. Geogr., 40, 405–423, 2019.

Kasse, C.: Sandy aeolian deposits and environments and their relation to climate during the Last Glacial Maximum and Lateglacial in northwest and central Europe, Prog. Phys. Geog., 26, 507–532, 2002.

Kiekebusch, A.: Das Königsgrab von Seddin, Führer zur Urgeschichte, Benno Filser, Augsburg, Germany, 1928 (in German).

Kossinna, G.: Ansprache über die "Kulturgeschichtliche Stellung der Prignitz in der Vorzeit", Mannus Zeitschrift für Vorgeschichte, 2, 234–240, 1910 (in German).

Koster, E. A.: Recent Advances in Luminescence Dating of Late Pleistocene (Cold-Climate) Aeolian and Loess Deposits in Western Europe, Permafrost Periglac., 16, 131–143, 2005.

Kristiansen, S. M., Dalsgaard, K., Holst, M. K., Aaby, B., and Heinemeier, J.: Dating of prehistoric burial mounds by ^{14}C analysis of soil organic matter fractions, Radiocarbon, 45, 101–112, 2003.

Kühn, P.: Micromorphology and Late Glacial/Holocene genesis of Luvisols in Mecklenburg-Vorpommern (NE-Germany), Catena, 54, 537–555, 2003.

LBGR Brandenburg: Geologische Karte 1:25.000, available at: http://www.geo.brandenburg.de/gk25, last access: 16 July 2020 (in German).

Lippstreu, L., Hermsdorf, N., and Sonntag, A.: Geologische Übersichtskarte des Landes Brandenburg 1:300 000, Landesamt für Geowissenschaften und Rohstoffe Brandenburg, Potsdam, Germany, 1997 (in German).

Lippstreu, L., Hermsdorf, N., Sonntag, A., and Strahl, J.: Pleistozän, in: Geologie von Brandenburg, edited by: Stackebrandt, W. and Franke, D., Schweizerbart'sche Verlagsbuchhandlung, Stuttgart, Germany, 333–419, 2015 (in German).

Litt, T., Behre, K.-E., Meyer, K.-D., Stephan, H.-J., and Wansa, S.: Stratigraphical Terms for the Quaternary of the North German Glaciation Area, E G Quaternary Sci. J., 56, 7–65, 2007.

Lüthgens, C., Böse, M., and Krbetschek, M.: On the age of the young morainic morphology in the area ascribed to the maximum extent of the Weichselian glaciation in north-eastern Germany, Quatern. Int., 222, 72–79, 2010.

Lüthgens, C., Böse, M., and Preusser, F.: Age of the Pomeranian ice marginal position in north-eastern Germany determined by Optically Stimulated Luminescence (OSL) dating of glaciofluvial (sandur) sediments, Boreas, 40, 598–615, 2011.

May, J.: Neue Forschungen am "Königsgrab" von Seddin, in: Der Grabhügel von Seddin im norddeutschen und südskandinavischen Kontext, Arbeitsberichte zur Bodendenkmalpflege in Brandenburg, 33, edited by: Hansen, S. and Schopper, F., Brandenburgisches Landesamt für Denkmalpflege und Archäologisches Landesmuseum, Wünsdorf, Germany, 9–35, 2018 (in German).

May, J. and Hauptmann, T.: Seddin, in: Reallexikon der Germanischen Altertumskunde, 28, edited by: Beck, H., Steuer, H., and Timpe, D., De Gruyter, Berlin, Germany, 1–6, 2005 (in German).

May, J. and Hauptmann, T.: Warum befindet sich das "Königsgrab" von Seddin am Mittellauf der Stepenitz?, Wasserwege und archäologische Sachkultur der jüngeren Bronzezeit in der Prignitz, Siedlungs- und Küstenforschung im südlichen Nordseegebiet, Verlag Marie Leidorf GmbH, Rahden/Westfalen, Germany, 34, 129–150, 2011 (in German).

May, J. and Hauptmann, T.: Das "Könisggrab" von Seddin und sein engeres Umfeld im Spiegel neuer Feldforschungen, in: Gräberlandschaften der Bronzezeit, Bodenaltertümer Westfalens, 51, edited by: Bérenger, D., Philipp von Zabern, Darmstadt, Germany 77–104, 2012 (in German).

Mejdahl, V.: Thermoluminescence dating: beta-dose attenuation in quartz grains, Archaeometry, 21, 61–72, 1979.

MLUV (Ministerium für Ländliche Entwicklung, Umwelt und Verbraucherschutz): Braunerde-Fahlerde. Steckbriefe Brandenburger Böden, available at: https://mluk.brandenburg.de/Steckbriefe-BB-Boeden/SB-5-3-Braunerde-Fahlerde.pdf, last access: 31 January 2020, 2005 (in German).

Montelius, O.: Om tidsbestämning inom bronzeålderen med särskildt afseende på Skandinavien, in: Kungl. Vitterhets historie och antikvitets akademiens handlingar, 30, Akademiens Förlag, Stockholm, Sweden, 1885 (in Swedish).

Murray, A. S. and Wintle, A. G.: The single aliquot regenerative dose protocol: potential for improvements in reliability, Radiat. Meas., 37, 377–381, 2003.

Nagel, D., Hermsdorf, N., Lippstreu, L., and Martiklos, G.: Geologische Übersichtskarte 1:200 000, Bundesanstalt für Geowissenschaften und Rohstoffe (BGR), Hannover, Blatt: CC 3134 Wittenberge, 2003 (in German).

Naturalearthdata: Internal administrative boundaries, available at: https://www.naturalearthdata.com/downloads/10m-cultural-vectors/, last access: 21 April 2020.

Offenedaten: Brandenburg Landkreise, available at: https://offenedaten.de/dataset/landkreise-brandenburg, last access: 21 April 2020.

Pluckhahn, T. J., Hodson, A. D., Rink, W. J., Thomson, V. D., Hendricks, R. R., Doran, G., Farr, G., Cherkinsky, A., and Norman, S. P.: Radiocarbon and Luminescence Age Determinations on Mounds at Crystal River and Roberts Island, Florida, USA, Geoarchaeology, 30, 238–260, 2015.

Porat, N., Duller, G. A. T., Roberts, H. M., Piasetzky, E., and Finkelstein, I.: OSL dating in multi-strata Tel: Megiddo (Israel) as a case study, Quat. Geochronol., 10, 359–366, 2012.

Prescott, J. R. and Hutton, J. T.: Cosmic ray distributions to dose rates for luminescence and ESR dating: large depths and long-term variations, Radiat. Meas., 23, 497–500, 1994.

Reimann, T., Naumann, M., Tsukamoto, S., and Frechen, M.: Luminescence dating of coastal sediments from the Baltic Sea coastal barrier-spit Darss-Zingst, NE Germany, Geomorphology, 122, 264–273, 2010.

Reimann, T., Lindhorst, S., Thomas, K. J., Murray, A. S., and Frechen, M.: OSL dating of mixed coastal sediment (Sylt, German Bight, North Sea), Quat. Geochronol., 11, 52–67, 2012.

Reimann, T., Román-Sánchez, A., Vanwalleghem, T., and Wallinga, J.: Getting a grip on soil reworking–Single-grain feldspar luminescence as a novel tool to quantify soil reworking rates, Quat. Geochronol., 42, 1–14, 2017.

Saye, S. E. and Pye, K.: Variations in chemical composition and particle size of dune sediments along the west coast of Jutland, Denmark, Sediment. Geol., 183, 217–242, 2006.

Schoeneberger, P. J., Wysocki, D. A., and Benham, E. C.: Field book for describing and sampling soils, Version 3.0., Natural Resources Conservation Service, National Soil Survey Center, Lincoln, NE, USA, 2012.

Schulte, L. and Wahnschaffe, F.: Geognostisch Agronomische Karte 1:25,000, Königliche Preussische Geologische Landesanstalt, Berlin, Blatt: 2837 Bäk (1900–1901), 1905.

van der Meij, W. M., Reimann, T., Vornehm, V. K., Temme, A. J. A. M., Wallinga, J., van Beek, R., and Sommer, M.: Reconstructing rates and patterns of colluvial soil redistribution in agrarian (hummocky) landscapes, Earth Surf. Proc. Land., 44, 2408–2422, 2019.

Wüstemann, H.: Zur Sozialstruktur im Seddiner Kulturgebiet, Z. Archäol., 8, 67–107, 1974 (in German).

E&G Quaternary Sci. J., 70, 19–27, 2021
https://doi.org/10.5194/egqsj-70-19-2021

Open Access E&G Quaternary Science Journal

Research article

Nomes of Lower Egypt in the early Fifth Dynasty

Mohamed Ismail Khaled

Ministry of Antiquities, University of Würzburg, Würzburg, Germany

Correspondence: Mohamed Ismail Khaled (mohamed.khaled@uni-wuerzburg.de)

Relevant dates: Received: 8 July 2020 – Revised: 4 November 2020 – Accepted: 17 November 2020 – Published: 15 January 2021

How to cite: Khaled, M. I.: Nomes of Lower Egypt in the early Fifth Dynasty, E&G Quaternary Sci. J., 70, 19–27, https://doi.org/10.5194/egqsj-70-19-2021, 2021.

Abstract: Having control over the landscape played an important role in the geography and economy of Egypt from the predynastic period onwards. Especially from the beginning of the Old Kingdom, we have evidence that kings created new places (funerary domains) called *ḥw.t* (centers) and *njw.t* (*Ezbah*) for the equipment of the building projects of the royal tomb and the funerary cult of the king, as well as to ensure the eternal life of both kings and individuals. Kings used these localities in order to do so, and they oftentimes expanded the border of an existing nome and created new establishments. Consequently, these establishments were united or divided into new nomes. The paper discusses the geography of Lower Egypt and the associated royal domains in the early Fifth Dynasty based on the new discoveries from the causeway of Sahura at Abusir.

Kurzfassung: Die geographische Unterteilung des Landes als Voraussetzung des Zugriff auf die Ressourcen des Landes spielte für die Wirtschaft Ägyptens und königliche Bauprojekte seit der prädynastischen Zeit eine wichtige Rolle. Um die landwirtschaftliche Nutzung des Landes auszuweiten und diesen Zugriff gleichzeitig zu sichern, begründeten die ägyptischen Könige Wirtschaftsanlagen (Grabdomänen) an schon bestehenden oder neu geschaffenen Siedlungen. Da sich der größte Teil der agrarisch nutzbaren Fläche im Delta befand, wurde im Laufe der Zeit auch das bestehende Gausystem dieses Gebietes mehrfach verändert. Das Papier erörtert die Geographie des Deltas in der frühen fünften Dynastie auf der Grundlage neuer Entdeckungen vom Aufweg des Pyramidenbezirkes des Sahure in Abusir (*Abstract was translated by Eva Lange-Athinodorou.*).

1 Introduction

The term nome is a territorial division in ancient Egypt; it comes from the ancient Greek word νομός, nomós. The term was used when the Greek language was common in Egypt, and this made the Greek historian adapt the term nome to identify the large lists of depictions of nomes with its divisions that are depicted in the late Greco-Roman temples. They usually take the shape of personified male or female figures, and they sometimes carry offerings; above their head is the sign of the nome that they represent, which is depicted on a standard.

In 1907–1908, Ludwig Borchardt carried out the principal exploration of the pyramid complex of Sahura, the second king of the Fifth Dynasty (2490–2475 BCE). Here, he discovered a large number of decorated wall reliefs which until today are considered the most complete example of a decorative program of a royal pyramid complex from the Old Kingdom. His publication still remains the most important source of information about the monument (Borchardt, 1910, 1913).

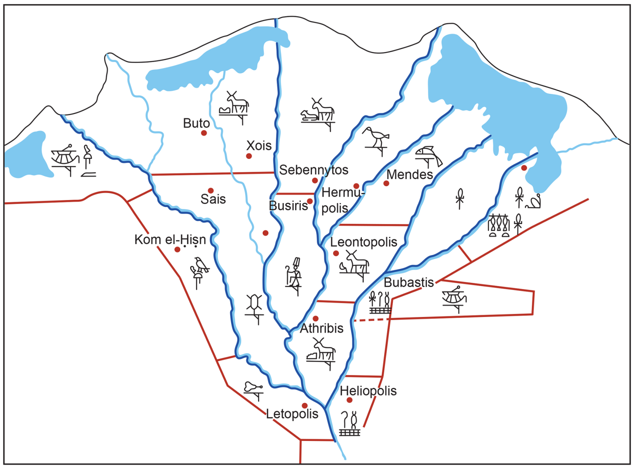

Figure 1. The map of the delta showing the distribution of nomes during the Fifth Dynasty based on the work of Helck (1974), redrawn by Svenja Dirksen based on Helck (1974).

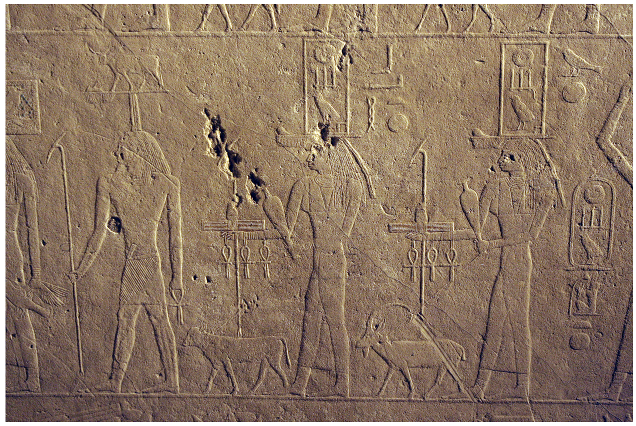

Figure 2. Depiction of the 10th nome of Lower Egypt from a newly discovered block from the causeway of Sahura (photo by Martin Frouz).

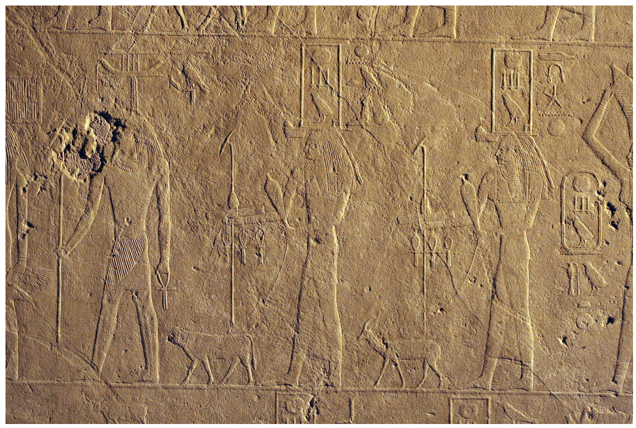

Figure 3. Depiction of the western part of the seventh nome of Lower Egypt from a newly discovered block from the causeway of Sahura (photo by Martin Frouz).

The decoration of the south wall of the southern portico of the side entrance to the king's pyramid temple shows different nomes from Lower Egypt in the form of a procession of the personifications of nomes and funerary domains of Sahura. Reflecting the physical geography of Egypt, the scene is divided symmetrically into a southern and a northern section. Unfortunately, only fragments depicting female personifications (most probably from Upper Egypt) were found by Borchardt (1913, 45–46, 106–109, plate 28).

On the opposite north wall of the side entrance, the personifications of Lower Egypt are depicted (Borchardt, 1913, 46, 109–111, plate 31). The scene shows two male and one female bearer of the nomes. The males wear a long wig, necklace and false beard tied to the long wig by means of straps. They also wear a short kilt. Their right hand holds a *w3ś* scepter, while the loosely hanging left hand carries an *ʿnḫ* sign. On a fragment published by Borchardt (1913, 42, 105, plate 26), the symbol of the first nome can be seen on the head of the male figure; a complete relief depicting the 10th and 11th nomes of Lower Egypt was also found by Borchardt (1913, 41, 105, plate 31). The female nome personification wears a long wig with a lappet falling over her left shoulder, which hangs down to the top of her long tight-fitting dress held up by shoulder straps that expose her right breast. She wears a broad collar consisting of several layers of beads and a tight choker necklace, bracelets and anklets. Her right hand holds a *w3ś* scepter, while the loosely hanging left hand carries an *ʿnḫ* sign. On the head of the female figure is the symbol of the 16th nome of Lower Egypt. Two female bearers of the *ḥwt* type, representing the centers that the king created in each Egyptian nome, follow each of these figures.

The recent excavation by the Supreme Council of Antiquities (SCA) along the upper part of the north wall of Sahura's causeway revealed the most complete example of an Old Kingdom procession of funerary domains. The domains are represented as both the *ḥwt* and *niwt* types. However, the majority are of the *niwt* type, and there are only six figures of the *ḥwt* type. In addition to the domains, the 10th nome and western part of the seventh nome of Lower Egypt are represented (Khaled, 2008, 101, 131–132). The procession of the funerary domains of Sahura's causeway ends with an additional section which shows a group of fecundity figures in four registers with each register containing three figures. This list represents the northern borders (subdivision) of the nomes depicted in the procession, representing what is called the pehou (*pḥww*) list, i.e., a list of the names of the backwaters of each nome (Khaled, 2018, 235–42).

The depiction of the nome as a male figure occurs for the first time in the pyramid temple of Sahura, and, as in the case of Userkaf, only the standard of the nome is attested (Labrousse and Lauer, 2000, 85–86, Fig. 133a, b). Afterwards, this method of depiction became standard in the royal

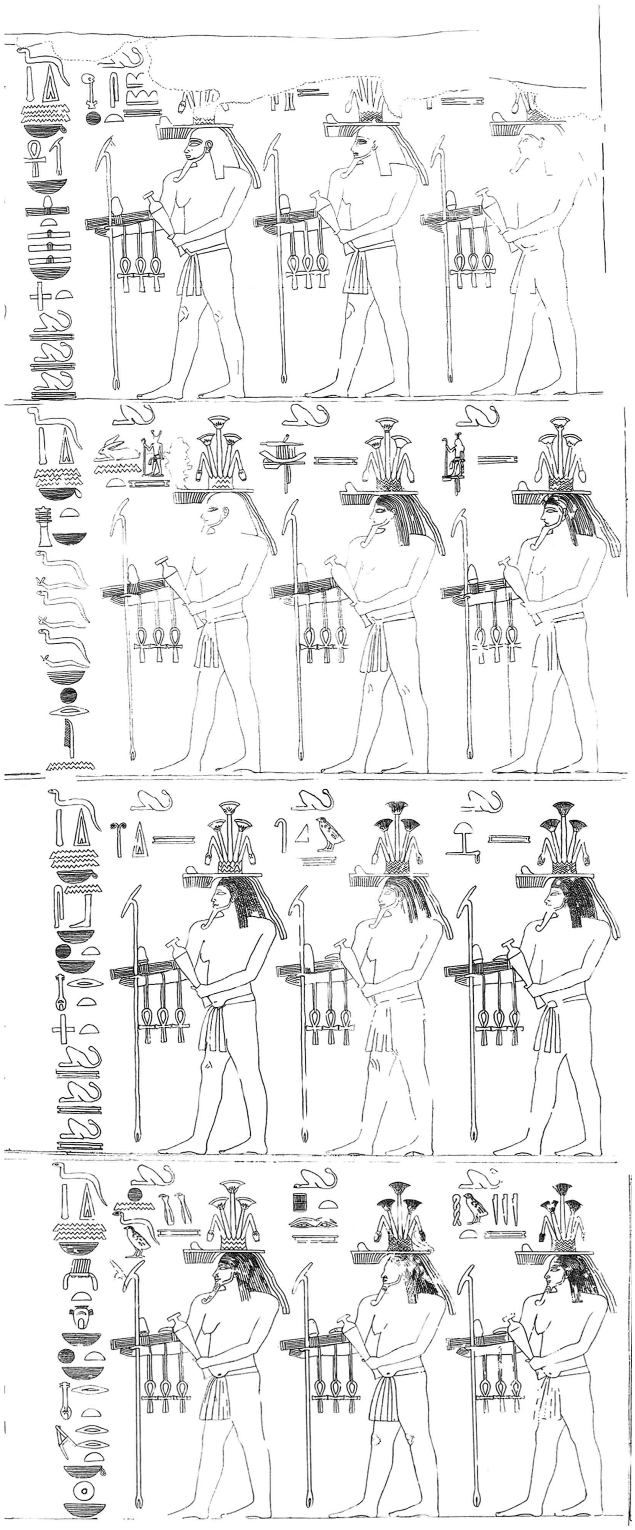

Figure 4. The earliest list of pehou from a newly discovered block from the causeway of Sahura drawn by Jolana Malátková based on the photo of Martin Frouz.

decorative programs of Sahura's successors. What remains unclear is the depiction of a female personification of a nome in the same scenes, which opens a new debate on the attestation of nomes in the form of males and females. Of course, this leads to the suggestion that the depiction of these figures is found only in scenes from the pyramid temple as female personifications as nomes have not yet been discovered in the recently excavated scenes from the causeway. Future exploration of the remaining blocks should clarify this unresolved dilemma.

Additional scenes of nomes are attested on an alabaster altar in the open courtyard on which offerings were presented to the deceased king. These scenes consist of the personifications of male and female figures representing the nomes of Egypt (Megahed, 2014, 58).

1.1 Nomes of Lower Egypt in the Old Kingdom

The late Greco-Roman temples introduced Egyptology to the list of nomes with their division by *mr*, "canal", *ww*, "farmland", and *pḥw.w*, "swamp" (Gauthier, 1935; Helck, 1974; Leitz, 2014, 69–126, plate 1b). They usually take the shape of personified male or female figures, and they sometimes carry offerings. Above their head is the sign of the nome that they represent, which is depicted on a standard.

Jacquet-Gordon (1962, 113) believed that the lists of the nomes from the Old Kingdom to the New Kingdom are different in several aspects from the standard list of later periods. She added that the reasons behind such changes are vague, and they were perhaps due to some administrative requirements.

The new discovery from the northern wall of the causeway of Sahura presents two more nomes of Lower Egypt in addition to the already known Lower Egyptian nomes depicted on the walls of the pyramid temple. Furthermore, the abovementioned so-called pehou list, which brings up the rear of the procession of the funerary domains of Sahura, represents the northern border of the Lower Egyptian nomes. It is the only example of the listing of pehou areas from the Old Kingdom.

Comprehensive information regarding the nomes of Lower Egypt during the Old Kingdom can be derived from different sources. First, there are the royal monuments, such as pyramid complexes belonging to Snefru, Userkaf and Sahura, or the solar temple of Niuserra where nearly complete lists of Lower Egyptian nomes are attested (von Bissing, 1955, 319–38; Kees, 1956, 33–40; Nuzzolo, 2018, 188–198; Seyfried, 2019, 39–42, plates 1–3). Second, there are non-royal tombs where several other nomes from the delta also occur. Nevertheless, only the symbol of the nomes was depicted on a standard. These are usually portrayed within the procession of the funerary domains, referring to the location of the domains that follow. Most of them are incorporated with a royal name. However, in a few cases, nomes also are attested with some private names in the non-royal tombs, such as the tomb of Nikaura (L.G. 87; G 8158), which is attributed to the reign of Khafra (Jacquet-Gordon, 1962, 219–221), and the tombs of Akhethotep and Ptahhotep II (D 64), which are attributed to the reign of Djedkara (Griffith and Davies, 1900, 8–9, plate 13; Baer, 1960, 75 [161]; Strudwick, 1985, 88 [50]; Harpur, 1987, 274 [400]). The tomb of Kairer is attributed to the reign of Unas and Teti (Jacquet-Gordon, 1962, 428–429). The tomb of Sabu/Ibebi (E1, 2+ H3) dates back to the reign of Teti (Baer, 1960, 118 [402]; Strudwick, 1985, 128 [113]; Harpur, 1987, 216–217; El-Khadragy, 2005, 169–199, plates 16–19). The tomb of Khnumenti (G 2374) was created in the reign of Teti (Jacquet-Gordon, 1962, 310–312; Brovarski, 2001, 122–123, plate 92, Fig. 87a). The tomb of Hesi is attributed to the reign of Pepi I (Kanawati and Abder-Raziq, 1999, 13:42, plate 62); however, Silverman (2000, 1–13; Kloth, 2002, 25–26) attributed it to the reign of Teti. Correspondingly, the tomb of Mehou dates to the reign of Pepi I (Baer, 1960, 83 [202]; Strudwick, 1985, 101–102 [69]; Harpur, 1987, 274 [424]), while Altenmüller (1998, 202–205), on the other hand, dates the tomb to the reign of Teti.

Furthermore, nomes are sometimes attested in the autobiography and the titles of the high officials who were in charge of such nomes in the delta; for example, in the biographical inscription of Metjen (tomb: L.S. 6) (Goedicke, 1966, 1–71) and Pehernefer (Junker, 1939, 63–84).

In addition to the nomes attested in the royal annals on the Palermo stone, the Abusir Papyri and other written documents are useful here as will be shown in the following survey.

1.1.1 The first nome 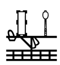

Royal complexes: the first nome of Lower Egypt has been attested in the pyramid complex of Sahura (Borchardt, 1913, 42, 105, plate 26). A possible likeness of the same depiction was found in the "room of the seasons" in the solar temple of Niuserra at Abu Ghurab.

However, it is not clear since it does not appear on top of a standard like the other nomes (von Bissing, 1955, 321, plates 3, 4; Nuzzolo, 2018, 188–198; Seyfried, 2019, plate 3).

Administrative titles, royal annals, etc.: the first nome has appeared in the royal annals of Sahura on the Palermo stone (Wilkinson, 2000, 160–161).

Non-royal tombs: the first nome has appeared in the tomb of Akhethotep (D 64) with a private domain incorporated with his name; however, the nome is not depicted on a standard.

1.1.2 The second nome 

Royal complexes: the second nome of Lower Egypt has been depicted in the pyramid complex of Userkaf (Labrousse and Lauer, 2000, 88, Doc. 62, Fig. 134a–b).

Administrative titles, royal annals, etc.: the second nome has been attested in the biographical inscription of Metjen. Also, it occurs in the Abusir Papyri in an administrative title (Posener-Kriéger, 1976, 595).

Non-royal tombs: the second nome appears in the tombs of Akhethotep (D 64) on a standard in front of two Hwt centers incorporated with the name of king Isesi, of Ptahhotep II with a private name of a domain, of Sabu/Ibebi with a domain with the name of king Teti, of Khnumenti with the names of both kings Unas and Teti, and of Hesi with the name of king Teti.

1.1.3 The third nome 

Royal complexes: the third nome of Lower Egypt has been attested in the "room of the seasons" in the solar temple of Niuserra at Abu Ghurab.

Administrative titles, royal annals, etc.: the third nome can be found in the biographical inscription of Metjen.

Non-royal tombs: the third nome occurs in the procession of the funerary domains of the tombs of Akhethotep (D 64) on a standard followed by two domains incorporated with the name of Isesi and his queen Setibhor (Megahed, 2011, 616–634; Megahed et al. 2019, 44), of Ptahhotep II and also incorporated with the name of queen Setibhor, of Kairer with the name of Teti, of Sabu/Ibebi with the name of Teti, of Khnumenti with the name of Teti, of Hesi with the name of Teti, and of Mehou incorporated with the names of Isesi, Unas and Teti in addition to a private domain incorporated with his name.

1.1.4 The fourth and fifth nomes 

Royal complex: both the fourth and fifth nomes of Lower Egypt have been attested in the pyramid complex of Niuserra (Jacquet-Gordon, 1962, 155), as well as in the "room of the seasons" in the solar temple of Niuserra at Abu Ghurab.

Administrative titles, royal annals, etc.: the fourth and fifth nomes have occurred in the biographical inscription of Metjen. Also, they have been attested in an administrative title in the Abusir Papyri of the Fifth Dynasty (Posener-Kriéger, 1976, 594).

Non-royal tombs: the fourth and fifth nomes have appeared in the tomb of Khnumenti preceding a domain incorporated with the name of Teti. Also, they can be found in the tomb of Hesi above a name of a domain incorporated with the name of Teti.

1.1.5 The sixth nome

Royal complex: the sixth nome of Lower Egypt has been attested in the pyramid complex of Userkaf (Labrousse and Lauer, 2000, 87–88, DOC. 61 A–C, Fig. 133a, b). Another depiction can be seen in the “room of the seasons” in the solar temple of Niuserra at Abu Ghurab in addition to the last available attestation of this nome in the time of the Old Kingdom in the pyramid complex of Unas (Labrousse and Moussa, 2002, 97–98 Doc. 107, Fig. 139, plate 19a.).
Administrative titles, royal annals, etc.: the sixth nome has occurred in the biographical inscription of Metjen.
Non-royal tombs: the sixth nome has appeared in the tomb of Hesi above a name of a domain incorporated with the name of Teti.

1.1.6 The seventh nome (west)

Royal complex: the seventh nome of Lower Egypt has been attested on the newly discovered blocks from the northern side of the causeway of Sahura. Also, it has appeared in the pyramid complex of Unas, but it is worth noting that Jacquet-Gordon marked it as the 11th nome of Lower Egypt (Jacquet-Gordon, 1962, 173). Labrousse and Moussa (2002, 98–99 Doc. 108, Fig. 140), on the other hand, believed that this nome is the eighth Lower Egyptian nome. However, based on our new list, we can conclude now that the seventh nome (west) is the best candidate since the same nome is attested in the procession of domains in the non-royal tombs incorporated with the name of Unas. In contrast, the eighth nome with the name of Unas never occurs.
Non-royal tombs: the seventh nome (west) appears in the tomb of Akhethotep (D 64) on a standard followed by eight domains, two of which are in the form of Hwt incorporated with the name of Niuserra, while the rest are depicted in the form of *nìwt* incorporated with the name of Userkaf (once, possibly twice through reconstruction) and Isesi (four times). It is also noteworthy that the writing of the name in the tomb shows a different writing for the sign for the west, Z 11 in Gardiner’s sign list (Gardiner, 1957). Also, the name has been attested in the tomb of Kairer preceding the name of two domains incorporating the names of Unas and Teti. In the tomb of Khnumenti, it appears incorporated with the name of Teti and, in the tomb of Hesi, with the name of Teti. Finally, it can be seen in the tomb of Mehou incorporated with the birth names of Niuserra (Ini), Unas and Teti.

1.1.7 The seventh/eighth nome (harpoon)

Royal complex: the seventh and eighth nome of Lower Egypt has been attested in the “room of the seasons” in the solar temple of Niuserra at Abu Ghurab.
Administrative titles, royal annals, etc.: the name of the seventh/eighth nome has appeared in the biographical inscription of Metjen. The name of the harpoon nome is also attested on Ostracon Leiden J 427 (Goedicke, 1968, 27).
Non-royal tombs: the name of the seventh/eighth nome has been attested three times in the tomb of Ptahhotep II (D 64) incorporated with the name of Sahura followed by a domain in the form of Hwt and with the names of Ikauhor and Isesi, followed by domains in the form of *nìwt*.

1.1.8 The eighth nome

Royal complex: the eighth nome of Lower Egypt has been attested in the pyramid complex of Pepi II as a sign on a standard preceding two domains in the form of Hwt (Jéquier, 1940, plate 25).
Non-royal tombs: the name of the eighth nome has been attested in the tomb of Mehou incorporated with the name of Isesi.

1.1.9 The ninth nome

Royal complex: the ninth nome of Lower Egypt has never been attested in any royal complexes of the Old Kingdom; however, it appeared as a name of a pehou from the newly discovered blocks from the causeway of Sahura (Khaled, 2018, 238–239, Fig. 1).
Administrative titles, royal annals, etc.: the name of the ninth nome has been attested in the biographical inscription of Pehernefer (Junker, 1939, 68 Nr. 24). Also, it occurred in the royal annals of Sahura on the Palermo stone (Wilkinson, 2000, 160–161).
Non-royal tombs: the ninth nome has been attested twice in the procession of the funerary domains in the tomb of Ptahhotep II (D 64) incorporated with the names of Userkaf and the sanctuary of Nekhen Osiris. It also appeared in the tomb of Kairer with the name of Teti preceding a domain in the form of Hwt and in the tomb of Hesi incorporated with the names of Unas and Teti. Finally, it can be found in the tomb of Mehou incorporated with the name of Teti.

1.1.10 The 10th nome

Royal complex: the 10th nome of Lower Egypt has been attested in the pyramid complex of Sahura (Borchardt, 1913, 42, 105, plate 31), as well as in the newly discovered blocks from the northern side of the causeway of Sahura. The same depiction can be found in the “room of the seasons” in the solar temple of Niuserra at Abu Ghurab.
Administrative titles, royal annals, etc.: the name of the 10th nome has occurred in the royal annals of Sahura on the Palermo stone (Wilkinson, 2000, 160–161).
Non-royal tombs: The 10th nome has occurred twice in the procession of the funerary domains in the tomb of Ptahhotep II (D 64) incorporated with the names of Snefru and the birth

name of Neferirkara (Kakai); unfortunately, the nome sign is destroyed so that only the rear part of the bull can still be seen. Jacquet-Gordon (1962, 401, 13) reconstructed this nome as the 12th nome; however, based on this present study, it is apparent that this nome is either the 10th or 11th Lower Egyptian nome. Also, the name of the 10th nome has been attested in the tomb of Hesi incorporated with the name of Unas and Teti. Moreover, the same depiction of the bull alone on a standard is depicted in the tomb of Mehou with two domains incorporated with the name of Teti. Jacquet-Gordon (1962, 424, 25) reconstructed this nome as the 12th nome. At any rate, it is far more likely that this depiction also shows the 10th nome since the name of the domain is similar to the name of the domain in the tomb of Hesi.

1.1.11 The 11th nome 

Royal complex: the attestation of the 11th nome of Lower Egypt has occurred in the pyramid complex of Sahura (Borchardt, 1913, 42, 105, plate 31). The nome has also been attested in the pyramid complex of Niuserra (Borchardt, 1907, plate 14), as well as in the "room of the seasons" in the solar temple of Niuserra at Abu Ghurab.
Administrative titles, royal annals, etc.: the 11th nome has occurred in an administrative title in the Abusir Papyri (Posener-Kriéger, 1976, 594).
Non-royal tombs: the 11th nome has been attested in the tomb of Akhethotep (D 64) incorporated with the name of Djedfra, as well as in the tomb of Ptahhotep II with the name of Isesi. This depiction also occurred in the tomb of Sabu/Ibebi with the name of Teti. Jacquet-Gordon (1962, 417, 2) was confused because the bull was depicted alone on a standard, and she preferred to identify it as the 12th nome. Correspondingly, the recent publication by El-Khadragy followed Jacquet-Gordon, Still, the current study shows that this is in fact the 11th Lower Egyptian nome as a recent publication of the tomb of Hesi shows a similar name for the domain of Teti located in the 11th nome.

1.1.12 The 12th nome 

Non-royal complex: the 12th nome of Lower Egypt has been attested in the royal complexes, namely in the "room of the seasons" in the solar temple of Niuserra at Abu Ghurab.
Administrative titles, royal annals, etc.: the name of the 12th nome has occurred in the biographical inscription of Pehernefer (Junker, 1939, 6).
Non-royal tombs: the 12th nome has been attested in the tomb of Ptahhotep II with a domain incorporated with the name of Isesi. Furthermore, the name of the 12th nome has also been attested in the tomb of Hesi incorporated with the name of Teti.

1.1.13 The 13th nome 

The depiction of the 13th nome has not been attested in any royal complex from the Old Kingdom. The 13th and 14th nomes were both most probably united until the end of the Fifth Dynasty; consequently, both of them were split into two separate nomes after that time (Fischer, 1959, 129–142; Jacquet-Gordon, 1962, 110; Altenmüller, 1998, 124).
Non-royal tombs: the 13th nome has been attested in the tomb of Sabu/Ibebi incorporated with the name of Teti. The same nome has occurred in the tomb of Hesi with the name of Teti, as well as in the tomb of Mehou with the names of Unas and Teti, which could serve as proof that the nome was divided during the reign of Unas as this is the oldest attestation.

1.1.14 The 13th/14th nome (east nome) 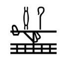

Royal complex: the two nomes have been attested before the division in the pyramid complex of Snefru (Fakhry, 1961, 50. Fig. 24); they are also depicted on the alabaster altar of Niuserra (Borchardt, 1907, plate 14).
Administrative titles, royal annals, etc.: the nome has been documented in the autobiography of the official Nesutnefer (Junker, 1938, 172–175, Abb. 27).
Non-royal tombs: the two nomes have occurred before their division in the tomb of Sabu//Ibebi in the procession of his funerary domains incorporated with the names of Khafra and Isesi. This also serves as proof that, until the time of the Isesi, there was no splitting up of the 13th and 14th nomes.

1.1.15 The 14th nome 

Royal complex: the 14th nome of Lower Egypt has been attested in the pyramid complex of Sahura (Borchardt, 1913, 42, 105, plate 26). Another possible depiction comes from the pyramid complex of Niuserra (von Bissing, 1955, 321, plates 3, 4).
Non-royal tombs: the 14th nome has occurred in the tomb of Khnumenti with the name of Teti. Also, it occurred in the tomb of Hesi with the name of Teti. This could serve as proof that the division was already completed during the reign of Teti.

1.1.16 The 15th nome 

Royal complex: the 15th nome of Lower Egypt has been attested in the "room of the seasons" in the solar temple of Niuserra at Abu Ghurab.
Administrative titles, royal annals, etc.: the nome has also been documented in the autobiography of the official Sehetepu, however, in opposition to Montet (1946, 219–220) who reads it as a name of the god Thoth.

Non-royal tombs: the 15th nome has occurred in the tomb of Kairer with the names of Unas and Teti, as well as in the tomb of Sabu/Ibebi with the names of Unas and Teti. Finally, in the tomb of Mehou, the nome precedes a number of domains of Kaki, Isesi, Unas, queen Seshseshet and Teti in addition to the name of prince Ptahshepses.

1.1.17 The 16th nome 

Royal complex: the 16th nome of Lower Egypt has been attested in the royal complexes in the pyramid complex of Sahura (Borchardt, 1913, 42, 105, plate 31).
Administrative titles, royal annals, etc.: the nome has also been documented in the autobiography of the official Metjen.
Non-royal tombs: the 16th nome has occurred in the tomb of Nikaura with the name of Khafra, as well as in the tomb of Khnumenti with the name of Teti. Finally, in the tomb of Mehou the name is attested with the name of Teti and the royal mother Seshseshet.

2 Conclusions

From the current study, it is apparent that, during the reign of Niuserra, Lower Egypt had its complete division and number of nomes; in addition, the changes in the administration of high regional officials outside the Memphite region serve as other evidence of expanding the land of the delta (Willems, 2014, 20–23). As Helck mentioned, the delta contained 16 nomes by the Fifth Dynasty (Helck, 1974, 199–203). On the other hand, one can observe that the delta had only 12 nomes in the time of Sahura at the beginning of the Fifth Dynasty. Some are attested in his pyramid temple and causeway, while the others are mentioned in the non-royal tombs. Other nomes already occur prior to Sahura's reign, such as the nomes of the delta mentioned in the autobiography of Metjen and also those attested with the names of Snefru, Khafra and Userkaf.

According to Helck, the fourth and fifth nomes of Lower Egypt were counted as one nome in the Old Kingdom (Helck, 1974, 158–163). Therefore, this paper proposes that the existing nomes of Lower Egypt in the time of Sahura were only 12 in number and include the 1st, 2nd, 3rd, 4th/5th and 6th and the west of the 7th, 8th, 9th, 10th, 11th, 13th/14th and 16th nomes. The new discovery of the pehou list from the causeway of Sahura somewhat confirms this number.

Scholars have already observed that the order of the nomes is not consistent, especially in the list of Niuserra in which the ninth nome is followed by the 12th and then the 11th and 10th nomes. Therefore, based on this observation, it is logical to accept variation in the names and their locations within the lists, which do not necessarily follow the numerical order of our modern view. However, it seems impossible to know the exact number of nomes, especially during the Old Kingdom, because these numbers were created according to later lists.

For example, the geographical location of the 16th nome of Lower Egypt depicted in the pyramid temple of Sahura is unknown, and this nome might have occupied the 12th position at the time of this king.

An important observation can be made, however, on the basis of the new data: the organization of the nomes was fluid in a way that the territory assigned to them and their borders was altered from time to time by the requirements of ancient Egyptian administration. The new reliefs from the causeway of Sahura at Abusir show how the kings were concerned about the geography of the country besides the important information that can be generated from the scenes that the territory of the delta was growing and expanding very quickly. Kings used to expand the borders of an existing nome and to create new establishments. Consequently, these establishments were united or divided into new nomes. (See above the division of the 13th and 14th nomes.) This could also serve as evidence for the changes in the names of the list of nomes. Of course, future excavation and discoveries will add more new information to the subject.

Data availability. All data relevant for this contribution are presented within the article itself (see Sects. 1 and 2).

Competing interests. The author declares that there is no conflict of interest.

Special issue statement. This article is part of the special issue "Geoarchaeology of the Nile Delta". It is a result of the workshop "Geoarchaeology of the Nile Delta: Current Research and Future Prospects", Würzburg, Germany, 29–30 November 2019.

Acknowledgements. This article was completed within the framework of the DFG project ID 389349558 (see https://gepris.dfg.de/gepris/projekt/389349558, last access: 8 July 2020). "Archäologie des ägyptischen Staates und seiner Wirtschaft im 3. Jahrtausend v. Chr.: eine neue Untersuchung des Sahurê-Aufwegs in Abusir".

Financial support. This open-access publication was funded by Julius-Maximilians-Universität Würzburg.

Review statement. This paper was edited by Eva Lange-Athinodorou and reviewed by two anonymous referees.

References

Altenmüller, H.: Die Wanddarstellungen Im Grab Des Mehu in Saqqara, Archäologische Veröffentlichungen 42, Mainz am Rhein, von Zabern, 1998.

Baer, K.: Rank and Title in the Old Kingdom: The Structure of the Egyptian Administration in the Fifth and Sixth Dynasties, Chicago: University of Chicago Press, 1960.

Borchardt, L.: Das Grabdenkmal Des Königs Ne-User-Re', Leipzig, Hinrichs'sche Buchhandlung, 1907.

Borchardt, L.: Das Grabdenkmal Des Königs S'ahu-Re. Leipzig: J. C. Hinrichs, 1910.

Borchardt, L.: Das Grabdenkmal Des Königs Sahu-Re: Abbildungsblätter, Leipzig: Hinrichs'sche Buchhandlung, 1913.

Brovarski, E.: The Senedjemib Complex. Pt. 1, [Ill.]: The Mastabas of Senedjemib Inti (G2370), Khnumenti (G2374), and Senedjemib Mehi (G2378), Giza Mastabas 7, Boston, Art of the Ancient World, Museum of Fine Arts, Boston, 2001.

Fakhry, A.: The Monuments of Sneferu at Dahshur II. The Valley Temple, Part I. The Temple Reliefs, Cairo: General Organization for Government Printing Offices, 1961.

Fischer, H. G.: Some Notes on the Easternmost Nomes of the Delta in the Old and Middle Kingdoms, in: Journal of Near Eastern Studies, 18, 129–42, 1959.

Gardiner, A. H.: Egyptian Grammar: Being an Introduction to the Study of Hieroglyphs, Third revised edition, London, Oxford University Press, 1957.

Gauthier, H.: Les Nomes d'Égypte Depuis Hérodote Jusqu'à La Conquête Arabe, Vol. 25. Mémoires de l'Institut d'Égypte, Le Caire: Imprimerie de l'Institut français d'archéologie orientale, 1935.

Goedicke, H.: Die Laufbahn Des MTn: in: Mitteilungen Des Deutschen Archäologischen Instituts, Abteilung Kairo, 21, 1–71, 1966.

Goedicke, H.: Four Hieratic Ostraca of the Old Kingdom, J. Egypt. Archaeol., 54, 23–30, 1968.

Griffith, F. Ll. and Davies, N. de G.: The Mastaba of Ptahhetep and Akhethetep at Saqqareh, Vol. 8–9. 2 vols. Archaeological Survey of Egypt, London, Egypt Exploration Fund, 1900.

Harpur, Y.: Decoration in Egyptian Tombs of the Old Kingdom: Studies in Orientation and Scene Content, Studies in Egyptology, London; New York: New York, NY, USA: KPI; Distributed by Methuen, Routledge & Kegan Paul, 1987.

Helck, W.: Die Altägyptischen Gaue, TAVO, B/5, Wiesbaden: Dr. Ludwig Reichert, 1974.

Jacquet-Gordon, H.: Les Noms Des Domaines Funéraires Sous l'Ancien Empire Égyptien. BdÈ 34, Caire: Institut Français d'Archéologie Orientale, 1962.

Jéquier, G.: Le Monument Funéraire de Pepi II: Tome 3. Les Approches Du Temple. Fouilles à Saqqarah, Le Caire: l'Institut francais d'archeologie orientale, 1940.

Junker, H.: Giza III: Bericht Über Die von Der Akademie Der Wissenschaften in Wien Auf Gemeinsame Kosten Mit Dr. Wilhelm Pelizaeus Unternommenen Grabungen Auf Dem Friedhof Des Alten Reiches Bei Den Pyramiden von Giza. Band III, Die Mastabas Der Vorgeschrittenen V. Dynastie Auf Dem Westfriedhof, Wien – Leipzig: Hölder-Pichler-Tempsky, 1938.

Junker, H.: PHrnfr, in: Zeitschrift Für Ägyptische Sprache Und Altertumskunde, 75, 63–84, 1939.

Kanawati, N. and Abder-Raziq, M.: The Teti Cemetery at Saqqara. Volume V: The Tomb of Hesi. Vol. 13. Australian Centre for Egyptology: Reports, Warminster: Aris & Phillips, 1999.

Kees, H.: Zu Den Gaulisten Im Sonnenheiligtum Des Neuserrê, in: Zeitschrift Für Ägyptische Sprache Und Altertumskunde, 81, 33–40, 1956.

El-Khadragy, M.: The Offering Niche of Sabu/Ibebi in the Cairo Museum, in: Studien Zur Altägyptischen Kultur, 33, 169–99, 2005.

Khaled, M. I.: The Old Kingdom Royal Funerary Domains: New Evidence from the Causeway of the Pyramid Complex of Sahure, PhD thesis, Prague: Charles University in Prague (PhD dissertation), 2008.

Khaled, M. I.: The Earliest Attested Pehou List in the Old Kingdom, in: The Art of Describing: The World of Tomb Decoration as Visual Culture of the Old Kingdom. Studies in Honour of Yvonne Harpur, edited by: Peter Jánosi and Hana Vymazalová, Prague: Charles University, Faculty of Arts, 235–247, 2018.

Kloth, N.: Die (Auto-) Biographischen Inschriften Des Ägyptischen Alten Reiches: Untersuchungen Zur Phraseolohgie Ung Entwicklung, SAK 8, Hamburg: Buske, 2002.

Labrousse, A. and Lauer, J. P.: Les Complexes Funéraires d'Ouserkaf et de Néferthétepès. BdE 130, Le Caire, Institut français d'archéologie orientale, 2000.

Labrousse, A. and Moussa, A. M.: La Chaussée Du Complexe Funéraire Du Roi Ounas. BdE 134, Le Caire: Institut francais d'archéologie orientale, 2002.

Leitz, C.: Geographische Soubassementtexte Aus Griechisch-Römischer Zeit Eine Hauptquelle Altägyptischer Kulttopographie, in: Altägyptische Enzyklopädien, Die Soubassements in Den Tempeln Der Griechisch-Römischen Zeit, Studien Zur Spätägyptischen Religion 7, Wiesbaden, I, 69–126, 2014.

Megahed, M.: The Pyramid Complex of Djedkare's Queen' in South Saqqara Preliminary Report 2010, in: Abusir and Saqqara in the Year 2010, edited by: Bárta, M., Coppens, F., and Krejčí, J., Prague, Czech Institute of Egyptology Faculty of Arts, Charles University in Prague, 616–634, 2011.

Megahed, M.: The Altar of Djedkare's Funerary Temple, from South Saqqara, in: Cult and Belief in Ancient Egypt: Proceedings of the Fourth International Congress for Young Egyptologists, 25–27 September 2012, Sofia, edited by: Lekov, T. and Buzov, E., Sofia: Bulgarian Institute of Egyptology, New Bulgarian University, 56–62, 2014.

Megahed, M., Hashesh, Z., Jánosi, P., and Vymazalová, H.: Djedkare-Isesis Pyramidenkomplex: Grabungskampagnen 2018, in: Sokar 38, 24–49, 2019.

Montet, P.: Tombeaux de La Ière et de La IVe Dynasties à Abou-Roach: Deuxième Partie, Inventaire Des Objets, in: Kêmi, 8, 157–227, 1946.

Nuzzolo, M.: The Fifth Dynasty Sun Temples: Kingship, Architecture and Religion in Third Millenium BC Egypt, Prague: Charles University Faculty of Arts, 2018.

Posener-Kriéger, P.: Les Archives Du Temple Funéraire de Néferirkare-Kakai (Les Papyrus d'Abousir): Traduction et Commentaire I-II. BdÈ 65, Caire: Institut Français d'Archéologie Orientale, 1976.

Seyfried, K. J.: Jahreszeitenreliefs Aus Dem Sonnenheiligtum Des Koenigs Ne-User-Re, 1st edition, Boston, MA, De Gruyter, 2019.

Silverman, D.: The Threat Formula and Biographical Text in the Tomb of Hezi at Saqqara, in: Journal of the American Research Center in Egypt, 37, 1–13, 2000.

Strudwick, N.: The Administration of Egypt in the Old Kingdom: The Highest Titles and Their Holders, Studies in Egyptology, London, KPI, 1985.

von Bissing, F. W.: La Chambre Des Trois Saisons Du Sanctuaire Solaire Du Roi Rathourès (Ve Dynastie) à Abousir, in: Annales Du Service Des Antiquités de l'Égypte, 53, 319–38, 1955.

Wilkinson, T.: Royal Annals of Ancient Egypt: The Palermo Stone and Its Associated Fragments, Studies in Egyptology, London, Kegan Paul International, 2000.

Willems, H.: Historical and Archaeological Aspects of Egyptian Funerary Culture: Religious Ideas and Ritual Practice in Middle Kingdom Elite Cemeteries, Culture and History of the Ancient Near East, volume 73, Leiden, Boston, Brill, 2014.

E&G Quaternary Sci. J., 70, 29–38, 2021
https://doi.org/10.5194/egqsj-70-29-2021

Open Access E&G Quaternary Science Journal

Research article

A new look at the Butic Canal, Egypt

Robert Schiestl

Institute of Ancient History, Ludwig-Maximilians-University Munich, 80539 Munich, Germany

Correspondence: Robert Schiestl (robert.schiestl@lmu.de)

Relevant dates: Received: 24 August 2020 – Accepted: 2 November 2020 – Published: 26 January 2021

How to cite: Schiestl, R.: A new look at the Butic Canal, Egypt, E&G Quaternary Sci. J., 70, 29–38, https://doi.org/10.5194/egqsj-70-29-2021, 2021.

Abstract: The Butic Canal – a Roman period transversal route across the northern Nile Delta – was the longest artificial watercourse in the Nile Delta, yet it remains very poorly understood. To date, the canal has not yet been verified by archeological excavations. The route of the eastern section of the canal has been indirectly identified based on a linear elevated feature most likely representing earth from the excavation of the canal. This study combines the analysis of historical sources and remote sensing data, such as satellite imagery and the TanDEM-X digital elevation model, in order to discuss its date of construction, route, and functions. Based on the data of the digital elevation model, new constructional features are visible in the eastern delta providing the first detailed route of a Roman-era artificial watercourse in Egypt. It is suggested that the canal's construction is placed in the context of imperial investments in the infrastructure of the eastern part of the Roman empire.

Kurzfassung: Der Butische Kanal war eine römerzeitliche Querverbindung durch das nördliche Nildelta. Obwohl er die längste künstliche Wasserstraße des Deltas darstellt, ist unsere Kenntnislage über diesen Kanal sehr gering. Bis heute ist der Kanal nicht durch archäologische Ausgrabungen verifiziert. Der Verlauf eines Abschnitts des Kanals im östlichen Nildelta wurde indirekt durch eine lineare Struktur identifiziert, die höchstwahrscheinlich den Aushub des Kanals repräsentiert. Dieser Artikel kombiniert die Analyse historischer Quellen und Fernerkundungsdaten, wie Satellitenbilder und das TanDEM-X Digitale Höhemodell, um die Datierung, die Route und die Funktionen des Kanals zu diskutieren. Auf der Grundlage der Daten des Digitalen Höhenmodells sind im östlichen Delta bestimmte bauliche Merkmale des Kanals erstmals genauer erkennbar. Dadurch kann die erste detaillierte Route eines Abschnittes einer römerzeitlichen künstlichen Wasserstraße in Ägypten rekonstruiert werden. Es wird vorgeschlagen, die Errichtung des Kanals im Zusammenhang mit imperialen Infrastrukturprojekten in der Osthälfte des römischen Reiches zu verstehen.

1 Introduction

The *Boutikos potamos*, the Butic Canal, is named and described only in one ancient source, a 2nd century CE geographic treatise written in Greek by Ptolemy (Klaudios Ptolemaios, 4, 5, 44; Stückelberger and Graßhoff, 2006). The term *potamos* can refer to both natural and artificial watercourses (Bonneau, 1993). Here it is clearly an artificial watercourse spanning the Egyptian Nile Delta from west to east with a reconstructed length of about 185 to 200 km. Thus, it constitutes the longest man-made ancient watercourse in the delta, distinctly longer than the other major ancient delta canal which connected the Nile to the Red Sea (Cooper, 2009). Despite its size and unique route, very little is known about this canal. Recent discussions of the canal have addressed it in a wider delta perspective, looking at it in the context of trans-delta networks (Redon, 2018) but also including the course in a regional setting in the eastern delta (Blouin, 2014). To date, however, it has never been the topic of a specialized study. This holds true for the field of Egyptology, but also within the wider scope of ancient water technology (Wikander, 2000; Grewe, 2009) and Roman imperial construction, this watercourse finds no mention. While the Butic Canal does appear on maps of the Nile Delta (Ball, 1942; Bietak, 1975; Talbert, 2000; Wittke et al., 2007), the course is largely conjectural, attempting to place Ptolemy's description of the canal in the landscape. Its precise course, its date of construction, its period of activity, and its purpose(s) remain in discussion (Ball, 1942; Bietak, 1975; Yoyotte, 1987; Blouin, 2014; Redon, 2018) as does the question of its influence on the traffic, development, and economy of the delta. The background to this study is a survey which was conducted in the northwestern delta in the region of Buto (Tell el-Fara'in; Schiestl, 2012). For the surveyed area, see the yellow rectangle in Fig. 1. Traditionally, reconstructions of the course of the Butic Canal show it passing close to Buto and crossing the area surveyed. As the survey pursued, inter alia, a landscape archeological angle, the ancient land- and waterscapes were investigated using historic maps, satellite images, auger core drillings, and a digital elevation model (DEM). While this has resulted in much new information on the ancient water courses of the region (Ginau et al., 2019), no features were discerned which suggest themselves as a regional segment of the Butic Canal. Empirical evidence for this canal in the western delta remains elusive. In contrast, in the eastern delta, a linear elevated feature, still in parts extant between Mendes/Thmuis and Tanis (red rectangle on Figs. 1, 2a–c), has long been considered as evidence of the remains of the excavated earth of the Butic Canal. New data from the TanDEM-X digital elevation model provide new details of this feature which will be discussed in the following Sect. 4 in the context of the reconstruction of the route. This will be preceded by a discussion of the textual sources for the canal (Sect. 2) and the chronology (Sect. 3) and will be followed by an analysis of the functions of the canal (Sect. 5) and a summary of the main results (Sect. 6). Methodologically, this investigation combines ancient historical textual sources, archeological sources, and remote sensing information.

2 Textual evidence

There are two main textual sources describing a Roman period (30 BCE–7th century CE) transversal delta canal which are frequently considered as referring to the same system. The earlier one is an indirect reference in Flavius Josephus' History of the Jewish War (Jos. BI, IV, 11, 5). In 70 CE, during the reign of Vespasian, his son Titus moved troops from Alexandria to Judea in order to quell the Jewish uprising. Josephus describes how this was done: marching from Alexandria east to Nikopolis, the troops boarded ships there. They then sailed to the Mendesian nome as far as Thmuis. Here the army disembarked and continued on foot, the assumption being that the canal had ended at this point. No name for this west–east canal is, however, given, and geographic details for the course are lacking. The first leg of the journey was undertaken on a canal linking Nikopolis to Schedia on the Canopic branch of the Nile. While this canal's course has also not yet been archeologically verified, textual evidence exists which also provides a name, Agathos Daimon. In year 7 of Titus' reign (80/81), 14 stelae were erected along the Agathos Daimon canal documenting its repair (Zimmermann, 2003; Scheuble, 2009; Jördens, 2009). The name Agathos Daimon was later transferred to the Canopic branch, as evidenced by Ptolemy (5, 42–43). Further names, such as the Sebastos canal and the Philagrian canal, refer to the same or other canals linking the Canopic branch and Alexandria; they represent potential alternative routes taken by Titus and his soldiers (Jördens, 2009; Hairy and Senounne, 2011). Whether the canal used by Titus and his soldiers is an early, partial version of the Butic Canal (Ball, 1942; Bietak, 1975) or an entirely separate construction (Redon, 2018) is a matter of debate. The second source is the Geography by Ptolemy from the mid-2nd century CE (4, 5, 44; Stückelberger and Graßhoff, 2006). It is only here that the canal is actually named *Boutikos potamos*, and its course spans the entire width of the delta, running "parallel to the coast of the Mediterranean" and connecting the Canopic (= Agathodaemon) branch with the Thermuthiakos, Athribikos, Busiritikos, and Bubastikos branches.

3 Chronology

The two halves of the trans-delta canal, the western half from the Agathodaemon/Canopic branch to Thmuis and the eastern half from Thmuis to Pelusium, have individual biographies and are best analyzed separately. While the eastern half was not functional in Vespasian's time, there are textual and archeological arguments for the existence of earlier, pre-Roman versions (Blouin, 2014; Redon, 2018). A biographical inscription on the backpillar of a statue of the Ptolemaic official Pamerih from Tanis (Cairo, CG 687) from the 2nd century BCE references a journey from the region of Busiris in the central delta to Tanis in the eastern delta which is assumed to have been conducted on a canal (Zivie-Coche, 2004). Bietak (1975) proposed that the Butic Canal on this stretch replaced an earlier land route. A series of important towns in the eastern delta are aligned along roughly the same latitude, ca. 30° 57′, which suggests they were linked by a road or an earlier canal. The foundations of these towns range from the Predynastic Period at Mendes (late 4th millennium BCE), the New Kingdom at Baqlia/Hermopolis (mid-2nd

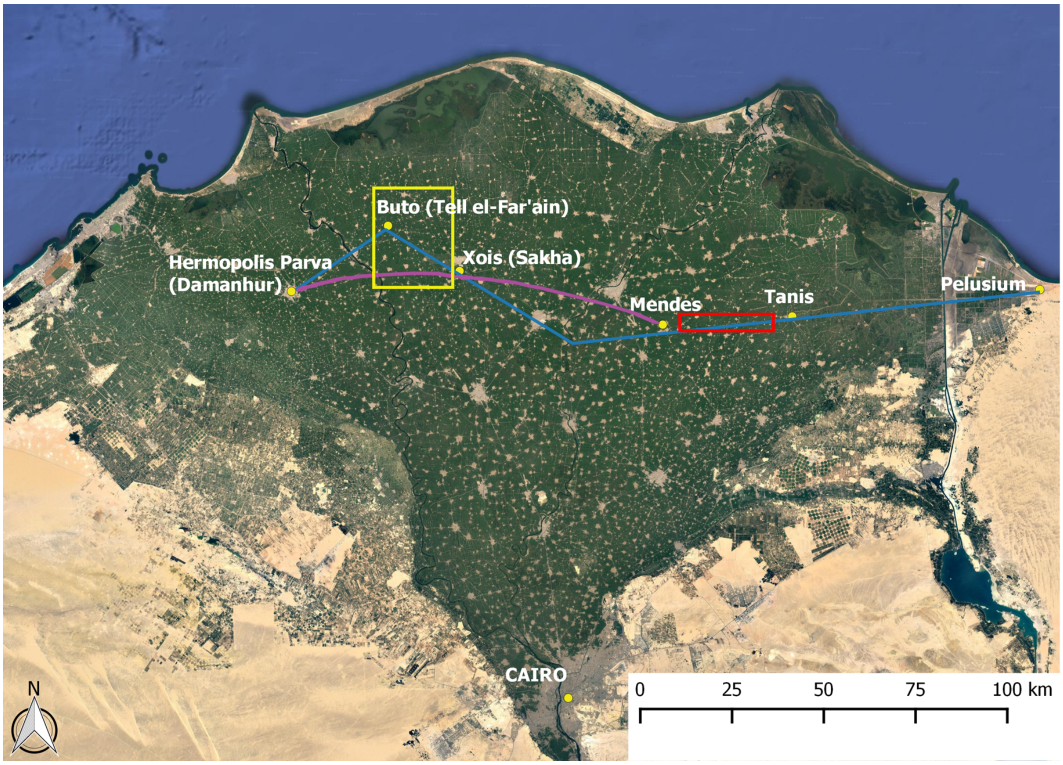

Figure 1. Nile delta, © Google Earth image. The blue line is the reconstruction of the Butic Canal by Talbert (2000), and the purple line is the reconstruction of the Butic Canal by Ball (1942). The rectangle outlined in red is the area enlarged in Fig. 2a–c, and the rectangle outlined in yellow is the area surveyed by the author.

millennium BCE), and the Third Intermediate Period at Tanis (11th century BCE), indicating a long tradition of trans-delta connections. This point is reinforced when we add a series of smaller, less well-known sites also located directly on this route (see Fig. 2c): Tell el-Dab^{c}a (EES 172, formerly known as Tell Qanan; Ball, 1942) was founded in the Predynastic Period, and Deir el-Hamra (EES 169) and El Tell el-Ahmar (EES 349) were founded in the Ptolemaic period. As few of these sites have been thoroughly investigated and published to date, in some cases the dating of their foundation may turn out to be earlier (dating information summarized on the Delta Survey web page: https://www.ees.ac.uk/delta-survey, last access: 3 August 2020). The eastern half thus seems to be older than the western but had fallen out of use by the later 1st century CE when Titus marched east. The western route used by Titus and his soldiers most likely made use of pre-existing canals which linked Nikopolis to the Canopic branch of the Nile and from that point on continued on a presumably new canal connecting the Canopic branch to the Mendesian branch. By the mid-2nd century CE, the eastern section, linking Mendes to Pelusium, had been reactivated or constructed anew, thus completing the trans-delta route and forming Ptolemy's Butic Canal. The date of construction is not known but probably falls between 70 CE and the mid-2nd century CE. This is a period of large-scale investment in Egyptian and Near-Eastern infrastructure (Sidebotham et al., 2000; Brun, 2018; Young, 2001), encompassing both the construction of public buildings, temples, canals, and roads and the foundation of a town (Antinoopolis), and it is suggested that the construction of the Butic Canal is to be placed in the context of such imperial building projects. A more detailed discussion of the chronology follows below in Sect. 5.

4 The route

A series of European maps from the late 16th century (Mercator, 1578, 1584; Ortelius, 1584, 1592; see Silotti, 1998) show the Butic Canal as a straight line crossing through the delta. These maps, however, are not the results of observations based on actual visits to Egypt but attempts at implementing Ptolemy's description. In some respects, this generation of maps is a step back in the accuracy of representing topographic realities as compared to earlier medieval maps (Haguet, 2018). Standard modern editions of historic maps show somewhat different routes while still also following Ptolemy's description. The route shown in blue in Fig. 1 follows that of Talbert's Barrington Atlas of the Greek and Roman World (Talbert, 2000) and the route shown in purple that of Ball (1942). Again, the eastern section and the western section are best discussed separately. The course in the

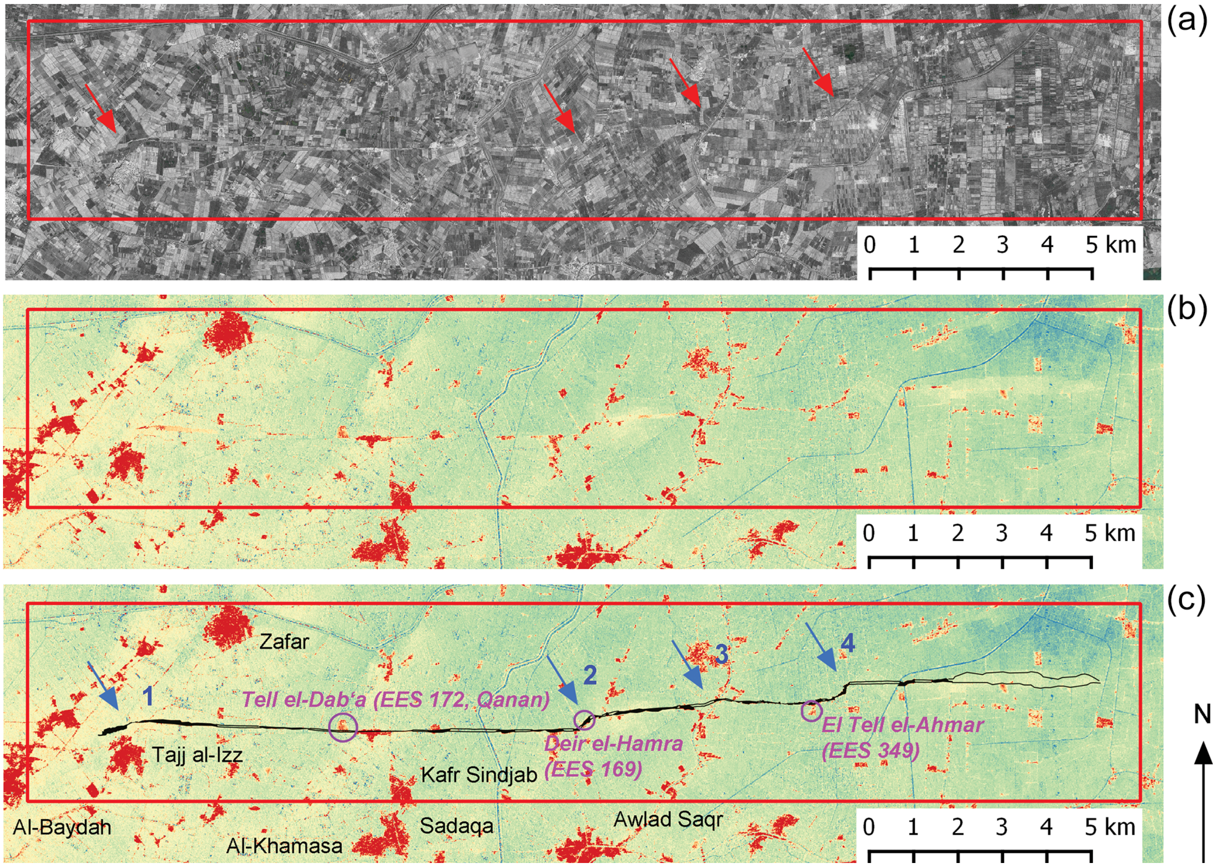

Figure 2. **(a)** Corona satellite image, 18 November 1968 (Corona Atlas of the Middle East, https://corona.cast.uark.edu, last access: 5 June 2020). **(b)** TanDEM-X digital elevation model of the area of investigation. TanDEM-X DEM courtesy of the German Aerospace Center (DLR). **(c)** TanDEM-X digital elevation model with the reconstructed course of the canal. TanDEM-X DEM courtesy of the German Aerospace Center (DLR). Names of ancient settlements shown in purple and modern names in black.

eastern part is based on an elevated feature which remains in parts still extant today. Compared to historic maps and older satellite imagery, such as the Corona image from 1968 (Fig. 2a), some details have been lost, but new data based on a digital elevation model (Fig. 2b) also provide new levels of detail in some areas. The information has been combined in Fig. 2c. This earthen linear feature, about 22 km long and of varying widths reaching a maximum of 140 m, is widely assumed to represent the excavated material from the canal (Bietak, 1975). As the canal itself has not been detected, its relationship to the elevated feature is a matter of debate; it has been suggested that the watercourse originally ran north (Holz et al., 1980) or south (Bietak, 1975) of this feature. A position in the middle seems to be suggested by some Corona satellite imagery and fits the common pattern of canals with dikes on both sides.

For the route of the western half, however, there is to date no archeological evidence. Neither historic maps, satellite images, nor the new digital elevation model provide comparable data to those in the eastern delta. Historic maps show some short stretches of west–east features south of Buto, which also find themselves reflected in the digital elevation model, but we lack any information on dating and function. These segments are not paired by the elevated features as in the eastern delta. The reasons for the very different data, or better lack thereof, in the western delta remain unclear. At this point, it cannot be stated whether the difference is caused by varying formation processes of the canals, lengths of use, or natural or man-made transformation processes post-abandonment. With the increased use of remote sensing data, the interruption or disappearance of hydrological features in the delta landscape has already been observed for various natural features (Ginau et al., 2019).

Talbert (2000; similar to Wittke et al., 2007) shows the western segment of the canal emerging from the Canopic branch at the town of Hermopolis Parva/Mikra, modern Damanhur, and turning northeast in order to reach Buto (Fig. 1, blue line). This is based on the assumption that, due to its name, it must have passed the city of Buto. From Buto, the course then turns in a southeastern direction reaching the area of Sebennytos, which lies roughly on the same latitude as Mendes/Thmuis and Tanis. This requires the canal to flow from a lower-lying region to a higher region. Based on the modern surface, the canal would have flowed from a region of currently about 2 m a.s.l. (meters above sea level), past the region of Xois, modern Sakha, at around 5–6 m a.s.l., to a region of about 6–7 m a.s.l. at Sebennytos, modern Samannud. All in all, the difference in height would have been around 5 m. We are missing, however, one fundamental piece of information: in which direction did the canal flow? The assumption west–east is suggested by the initial northeastern direction when branching off from the Canopic arm. The physical evidence in the eastern delta points in the same direction in that the canal displays a slightly northern shift moving east (Figs. 1 and 2, and discussion below). If the direction were reversed, that is from east to west, the canal would, following the blue route via Buto as shown in Fig. 1, be confronted with the same dilemma of having to flow uphill, albeit on a shorter stretch, namely from Buto to Hermopolis Parva/Damanhur. Overcoming differences in elevation in canals was technically possible in antiquity (Bockius, 2014). There is, however, a substantial effort involved, which begs the question of why such a route would be chosen. Was Roman Buto so significant it warranted such a detour? This seems unlikely, as Buto was neither a strategic, economic, or religious center of preeminent importance in this period. The region, however, was flourishing in Roman times. Two alternative scenarios emerge: firstly, the canal changes its direction of flow. In this scheme, in the western delta, the canal would flow from the west and from the east, in order to meet in Buto, where the water may have been redirected to northern distributaries. If this were the case, it would place Buto at the crucial junction and may explain naming the canal after this town. Secondly, a more southern course, minus the Buto detour, was chosen. If the town of Buto is no longer connected to the Butic Canal, how can the designation of Butic Canal then be explained? Butic does not necessarily refer to the town alone but is also applied to a larger region, the "land of Wadjet (Buto)", which we find outlined in the Satrap Stela of the late 4th century BCE (Schäfer, 2011). Redon (2018) has recently added further Roman examples for the descriptor *Butikos* applied to different topographic features or goods which are located or produced on a regional level. For example, Strabo mentions a Butic lake (XVII, 1, 18) which most likely refers to the northern lagoon, the later Lake Burullus. Butic linen is mentioned by Pliny (HN, XIX, II, 14) as a product of the district. In short, the canal may have been named Butic for crossing the region of Buto without actually passing the town, as was recently also suggested by Redon (2018). Such a southern route would avoid the above-discussed problems of flowing "uphill". Taking Ptolemy's description of the canal "parallel to the coast line" literally, a curved shape would seem the most likely, as was already proposed by Ball (1942; see Fig. 1, purple route). In this way, the canal could remain on the same elevation while flowing west–east. For the eastern delta, new data are available in the form of a digital elevation model (DEM) which provides a greater level of detail (Fig. 2b and c). The DEM, based on the German satellite pair TanDEM-X, was acquired in cooperation with the German Aerospace Center in order to investigate the landscape in the survey area (Ginau et al., 2019). Due to the high resolution of the elevation information, it has been possible to use these data very successfully for the region north of Buto in order to reconstruct ancient watercourses based on the traces of elevated levees. No features, however, were detected which suggest themselves as being part of a west–east delta transversal route. In the eastern delta, the elevated linear feature appears clearly, and some new details emerge, which will be discussed in the following.

On the segment between Mendes/Thmuis and Tanis (Fig. 2c), four sharp bends, or "steps", are detectable. They are designated, from west to east, steps 1–4. In such a step, the canal turns sharply in a northeastern direction and, after a length of between 480 and 843 m, turns right again in order to continue due east in a linear fashion. The distance between these steps is between 2.3 and 10.5 km. In this way, the canal is incrementally shifting slightly north: over the distance of 22 km, about 1 km. In steps 1, 2, and possibly 3, the steps coincide with an intersection with an elevated feature, most likely an ancient branch. These steps possibly served to support the crossing of branches, feeding them in and out of the canal. In Bietak's reconstruction (1975), there are small branches crossing the canal in the area of steps 1 and 3. Between steps 1 and 2, east of Tell el-Dab^{c}a (EES 172), there is also an elevated feature crossing the canal, but there is no evidence for a step. This was possibly the levee of an old waterway which was no longer active. A similar stepped feature, albeit on a much smaller scale, was archeologically investigated in the middle of the Fossa Corbulonis, a 1st century CE Roman canal in the Netherlands (de Kort and Razczynski-Henk, 2014). This canal, which on average has a width of 12–15 m, narrows here to 4 m. The feature was interpreted as a portage, an area where the ship had to be taken out of the water and dragged over land, before being placed back in the canal. In the case of the Fossa Corbulonis, it was a measure to balance different levels of water. This does, upon first impression, not seem to be the case in the Butic Canal, but the definite function remains unclear. As the settlements are directly attached to the canal, these stepped features possibly served the purpose of redirecting the canal closer to some settlements. In between the steps, the canal runs along a mostly linear course. Notably, between steps 1 and 2, there is a slight southward shift of around 286 m between the top of step 1 and the base of step 2. With step 2, the course returns to its northward direction. This stretch of the canal provides the first detailed evidence of a Roman period artificial watercourse in the delta. Targeted archeological investigations and comparisons with other Roman period canals could supply crucial further understanding.

5 The function(s) of the canal

Apart from Josephus' description of the movement of troops on the "Titus Canal", the sources remain silent on the uses of the trans-delta route. The military purpose of the Titus Canal has been projected onto the later Butic Canal, comparing its construction to that of "Hitler's and Mussolini's highways" (Carrez-Maratray, 1999). Taking this analogy as a cue, it should be noted that current analysis of the program of the construction of highways by National Socialist Germany discusses them as tools of propaganda, embodying numerous ideas far more varied than those purely focused on strategic military deployment. A recent discussion shows how 1930s *Autobahnen* were conceived as a tool of healing a perceived rupture between landscape and technology. *Autobahnen* were deeply embedded in evolving concepts of landscape and in turn had a massive effect on the landscape (Zeller, 2007). Josephus' account itself raises questions for the strategic value of this route. Titus' journey was undertaken in three parts of distinctly different lengths: part 1, by ship from Nikopolis to Thmuis and continuing on land from Thmuis to Tanis, covered almost 200 km and was by far the longest; part 2, on land from Tanis to Herakleopolis Parva (Tell Belim), was about 28 km long; and part 3, from Herakleopolis Parva to Pelusium, was about 37 km long. Josephus writes that after arriving at Pelusium, the soldiers rested for 2 d (BI IV, 11, 5). Evidently reaching Jerusalem as fast as possible was not the main concern. It has been suggested that the journey by Titus was undertaken to test the strategic efficiency of the canal (Carrez-Maratray, 1999). The basic question remains: why bother creating such a watercourse parallel to the Mediterranean, in particular when the point of departure lay on the coast? One reason may have been the seasonality of sea travel, which due to weather conditions in the Mediterranean all but ceased in the winter. Between October, at the latest November, and March or April, large ships avoided traveling in the Mediterranean Sea. Additionally, entering and leaving Nile mouths presented challenges which made circumventing them attractive (Cooper, 2014). During this period, the transportation of goods switched to land routes or had to wait until spring. Titus' journey did indeed take place in winter. While the emperor Vespasian stayed in Alexandria and postponed his return to Rome until winter was over, Titus and his troops were sent off in the direction of Judea, with the siege of Jerusalem taking place in spring shortly before Passover (Jos. BI, IV, 11, 5; V, 3, 1; Schäfer, 2003). Thus, the canal created the strategic advantage of allowing transport by ship also in the winter. The Butic Canal itself, however, fell into the category of seasonal canals which were not operational year-round. Once the Nile was very low, they were dammed off and the dams were opened only after the peak of the flood. Such canals were active from September to the end of December/early January (Cooper, 2014). While the data on this are late antique, medieval, and modern, it seems likely that the same system was in place in Roman times. The period of activity falls into the period with no or only very dangerous sea travel, reducing this period to January to March and thus underscoring the value of an alternative provided by an artificial waterway. While the ancient sources remain silent on the Butic Canal's purpose, in other cases they supply an intriguing variety of reasons for the construction of waterways. The Fossa Corbulonis, connecting the Rhine and the Meuse in the Netherlands and being ca. 30 km in length, was built in the mid-1st century CE and has only recently been identified archeologically (de Kort and Raczinsky-Henk, 2014). According to Tacitus, it was built to keep troops busy and to provide a route to circumvent the dangers of the North Sea (Ann. XI, 18–20), while Cassius Dio (Hist Rom LXI 30, 4–6) provides another reason, namely that it could serve as a water management system. Seemingly inconsistent, these different purposes may reflect a blend of concepts, original functions, and eventual uses. In canals with long and complex biographies, primary purposes and later functions may vary fundamentally (Salomon et al., 2014). The Red Sea Canal, verifiably completed in the Persian period, certainly served the political purpose of binding Egypt, now a Persian province, closer to the Persian heartland. After the Persian domination over Egypt ended, the canal was rebuilt in the Ptolemaic period and later again in the Roman period with different functions, such as providing commercial links to the Red Sea, Arabia, and southern India, as well as a strategic role in Trajan's Parthian wars (Sijpesteijn, 1963; Reddé, 1986; Cooper, 2009). The canal also generated settlement development, with the foundation of a Ptolemaic harbor settlement adjoining the canal, and an opportunity to set up stelae extolling royal accomplishments along its path. While only Persian and Ptolemaic examples of such stelae survive from the Red Sea Canal, the erection of Roman stelae is very likely. If Titus had 14 stelae set up for the, in comparison, minor Agathos Daimon canal, discussed above in Sect. 2, the Roman Red Sea Canal and the Butic Canal provided greater opportunities for imperial self-presentations. That a canal was actually only re-excavated or repaired and not built from scratch is notably mentioned in Titus' stelae but not in the Persian or Ptolemaic stelae along the Red Sea Canal. Young (2001) considers the construction of the Red Sea Canal less an act "of economic policy and more as an act of euergetism". Roman roads – and canals by inference – are, as Kolb summed it up recently, "instrument and symbol of Roman rule" (Kolb, 2019). Imperial connectivity, in particular in the eastern part of the Roman empire, was greatly enhanced in the 2nd century CE. Such infrastructure measures also served travelers beyond the borders of the empire, as evidenced in Lucian's description of a journey of a young man in 170 CE sailing from Alexandria to Clysma thanks to the Red Sea Canal and continuing to India (Young, 2001). The Butic Canal was most likely also used for strategic purposes and provided a seasonal alternative to sea travel. Troops stationed in Egypt were moved to assist in eastern conflicts even prior to the Jewish uprising in 70 CE, for which the Titus Canal may have been built. Starting with an Armenian war of succession against Nero in 58–63, a pattern emerges during the 1st and 2nd centuries CE in which entire Egyptian legions or parts of them were involved in numerous conflicts in the east. The two main theaters of conflict were the wars with the Parthians and the Jewish uprisings in Judea. Movements of troops went in both directions, with the contingents leaving Nikopolis and eventually returning; occasionally other troops were shifted around (Mor, 2016). The Egyptian III legion, *Cyrenaica*, participated in Trajan's Parthian wars (Gilliam, 1966), and a vexillation of this legion was stationed in Jerusalem in 116 (Cotton, 2000, 353). For the suppression of the Jewish revolts in Egypt in 115–117 CE, troops were moved there to replace losses of soldiers (Gilliam, 1966). In the 130s CE, during the Bar Kokhba revolt, it is quite likely that the Egyptian XXII legion, *Deiotoriana*, was transferred to Judea (Millar, 1993; Eck, 1999). In this period, there was massive investment in road construction in the eastern provinces, particularly in Judea, which provided a military corridor between Egypt, Arabia, and Syria (Schäfer, 1990). However, the Judean road constructions under Hadrian took place in the years 120 and 129/30 CE prior to the Bar Kokhba revolt (Isaac, 1990). The building activities are thus not a strategic reaction to the unrest but are likely linked to the emperor's journey to Judea. Hadrian's visit to Egypt in 130–131 CE took him from Pelusium to Alexandria (Vita Hadriani, 14, 4; Cassius Dio, Hist Rom LXIX, 11.1; Sijpesteijn, 1969), but no information is provided on how this trip was undertaken (Halfmann, 1986; Birley, 2003). The Butic Canal possibly formed part of an imperial construction program linked to Hadrian's journey. It has been argued that Hadrian's visit to Egypt in 130 was his second, preceded by a visit in 117 shortly after his accession (Capponi, 2010). As in the trip of 130, Hadrian's entry to Egypt is suggested to have been from the east and continuing to Alexandria. This journey possibly fostered the plans to build an imperial canal, which may have been inaugurated on his second journey. Hadrian's visit(s) to Egypt were accompanied by the restoration of buildings and temples which formed part of an "imperial image campaign" (Capponi, 2010). The canal must have also had a major effect on the water system of the delta (Ball, 1942; Bietak, 1975; Blouin, 2008). The crossing branches of the Nile fed the canal, reducing the flow of water in these branches. It could, thus, have served as a sort of valve to regulate and distribute the Nile flood and may have been harnessed for irrigation purposes. The earthen dikes of the canal built across the delta plain would also have served to regulate the flood, as suggested by Bietak (1975). During Trajan's and Hadrian's reigns, low Nile floods are attested (Sijpesteijn, 1969; Pfeiffer, 2010) which may have been the reason for improvements to the canal-system undertaken during their reigns. The Butic Canal was possibly part of this scheme. Just as the date of the canal's opening remains unclear, so does the date of its demise. The very substantial elevated linear feature in the eastern half is probably the result of continued dredging over a longer time period, with the deposited earth thus creating a higher levee. Much of this may, however, have already accumulated during the canal's Pharaonic and Ptolemaic existence prior to the completion of the Roman Butic Canal. The lack of any trace of such a feature in the western section may reflect that part's shorter life use. By the early 4th century CE, the Butic Canal no longer seems to have been in use. The detailed travel log of Theophanes (Matthews, 2006), who in 320 CE traveled from Hermopolis in Middle Egypt to Antioch in Syria, crossed the delta from Thmuis to Tanis, and continued to Herakleopolis and to Pelusium on exactly the route covered by the Butic Canal. He did not, however, go by ship but on land, most likely in a horse drawn carriage. As he traveled in mid-March, this may have been due to seasonal reasons, when the low Nile made travel on canals all but impossible. The road traveled was likely on the dike of the Butic Canal. These elevated features provided the traditional placement for roads secure from the floods. In the eastern segment, from Thmuis to Pelusium, the route of a road crossing the delta shown on the tabula Peutingeriana (Talbert, 2010) concurs with that of the Butic Canal. The tabula Peutingeriana is a medieval copy of a map compiled in the late Roman period from mixed sources, some of which date to the early Roman period (Arnaud, 1990). It is very likely that this road was erected on the dike of the Butic Canal. On the stretch from Tanis to Pelusium, the remains of the Butic Canal may be depicted on the tabula Peutingeriana, with the road shown running parallel to a west–east watercourse (Redon, 2018). The full length of the Butic Canal most likely was not in existence very long. In contrast to other imperial prestige projects, canals required intense yearly maintenance lest they fall into disuse. The canal possibly fell apart into segments again, with an eastern part remaining in function and providing a local transportation route.

6 Conclusions

The Butic Canal was most likely created by reactivating existing canals: a Flavian section in the western delta and a possibly Pharaonic route in the eastern delta. Its route did not pass by the town of Buto but ran further south, crossing the region of Buto. Based on a digital elevation model, new features are clearly discernible in the eastern section of the canal. Four sharp bends, or steps, shift its course slightly north. These features possibly served to feed crossing watercourses in and out of the canal. The greatest artificial watercourse of Egypt was completed sometime between 70 CE and the mid-2nd century CE. It may have been built in connection with Hadrian's visit to Egypt and thus be considered less a strategic necessity than a representation of imperial rule. When traveling east from Alexandria by ship, the canal did provide a seasonal alternative to the Mediterranean route, which was to be avoided in the winter. It must have had a substantial impact on the waterscape of the delta and may have been an attempt at creating a new water management system. Whether this was entirely beneficial remains unclear, but the yearly maintenance required possibly outweighed the benefits and led to the abandonment of this cross-delta route. The canal's last traces may be found on the tabula Peutingeriana on which in the eastern delta a road is shown running parallel to a watercourse, quite likely on the dike of the Butic Canal. This study demonstrates the usefulness of new data, such as the TanDEM-X digital elevation model, used in combination with newly available data, such as the Corona satellite imagery, for the fields of archeology, landscape archeology, and geoarcheology of the Nile Delta.

Data availability. The TanDEM-X digital elevation model is used with the permission of the German Aerospace Center (DLR) and is based on the data requested via the proposal (DEM_HYDR1426) by Andreas Ginau, Robert Schiestl, Jürgen Wunderlich, Eva Lange-Athinodorou, and Tobias Ullmann. The TanDEM-X data are used within the framework of the agreement with the German Aerospace Center (DLR) and are not freely accessible.

Competing interests. The author declares that there is no conflict of interest.

Special issue statement. This article is part of the special issue "Geoarchaeology of the Nile Delta". It is a result of the workshop "Geoarchaeology of the Nile Delta: Current Research and Future Prospects", Würzburg, Germany, 29–30 November 2019.

Acknowledgements. I am grateful for the assistance of Andrea Squitieri in preparing the maps and for Henry Heitmann-Gordon and Janice Schiestl for helpful comments and for correcting my English. I am also grateful to the two anonymous reviewers for their valuable comments and suggestions.

Review statement. This paper was edited by Tobias Ullmann and reviewed by two anonymous referees, one of whom requested to be thanked anonymously in the Acknowledgements.

References

Arnaud, P.: L'origine, la date de rédaction et la diffusion de l'archétype de la Table de Peutinger, Bulletin de la Société Nationale des Antiquaires de France, 1988, 302–321, https://doi.org/10.3406/bsnaf.1990.9424, 1990 (in French).

Ball, J.: Egypt in the Classical Geographers, Survey of Egypt, Government Press, Cairo, Egypt, 1942.

Bietak, M.: Tell el-Dab^{c}a II. Der Fundort im Rahmen einer archäologisch-geographischen Untersuchung über das ägyptische Ostdelta, Untersuchungen der Zweigstelle Kairo des Österreichischen Archäologischen Instituts 1, Denkschriften der Gesamtakademie der Österreichischen Akademie der Wissenschaften 4, Austrian Academy of Sciences, Vienna, Austria, 1975 (in German).

Birley, A. R.: Hadrian's Travels, in: The Representation and Perception of Roman Imperial Power. Proceedings of the Third Workshop of the International Network Impact of Empire (Roman Empire, c. 200 B.C.–A.D. 476), Netherlands Institue in Rome, March 20–23, 2002, edited by: de Blois, L., Erdkamp, P., Hekster, O., de Kleijn, G., and Mols, S., J. C. Gieben, Amsterdam, 425–438, 2003.

Blouin, K.: De Mendès à Thmouis: hydrographie mobile, société mobile?, in: L'eau comme patrimoine−−de la Méditerranée à l'Amérique du Nord, edited by: Hermon, E., Presses de l'Université Laval, Québec, Canada, 107–128, 2008 (in French).

Blouin, K.: Triangular Landscapes. Environment, Society, and the State in the Nile Delta under Roman Rule, Oxford University Press, Oxford, United Kingdom, https://doi.org/10.1093/acprof:oso/9780199688722.001.0001, 2014.

Bockius, R.: Künstliche Schifffahrtswege. Wasserbau und hydrotechnische Einrichtungen im Altertum, in: Großbaustelle 793. Das Kanalprojekt Karls des Großen zwischen Rhein und Donau. Mosaiksteine. Forschungen am RGZM 11, edited by: Ettel, P., Daim, F., Berg-Hobohm, S., Werther, L., and Zielhofer, C., Verlag des Röm.-German. Zentralmuseums, Mainz, Germany, 87–94, 2014 (in German).

Bonneau, D.: Le régime administratif de l'eau du Nil dans l'Égypte grecque, romaine et byzantine, Probleme der Ägyptologie 8, Brill, Leiden, The Netherlands, 1993 (in French).

Brun, J.-P.: Chronology of the Forts of the Routes to Myos Hormos and Berenike during the Graeco-Roman Period, in: The Eastern Desert of Egypt during the Greco-Roman Period: Archaeological Reports, Paris: Collège de France, https://doi.org/10.4000/books.cdf.5239, 2018.

Capponi, L.: Hadrian in Jerusalem and Alexandria in 117, Athenaeum, 98, 489–501, 2010.

Carrez-Maratray, J.-Y.: Péluse et l'angle oriental du Delta égyptien aux époques grecque, romaine et byzantine ‚Bibliothèque d'étude 124, Institut Français d'Archéologie Orientale, Cairo, Egypt, 403–404, 1999 (in French).

Cooper, J. P.: Egypt's Nile-Red Sea Canals: Chronology, Location, Seasonality and Function, in: Connected Hinterlands. Proceedings of the Red Sea Project IV Held at the University of Southampton September 2008, Society for Arabian Studies Monographs No. 8, BAR International Series 2052, edited by: Blue, L., Cooper, J. P., Thomas, R., and Whitewright, J., Archaeopress, Oxford, United Kingdom, 195–210, 2009.

Cooper, J.P.: The Medieval Nile: Route, Navigation, and Landscape in Islamic Egypt, American University in Cairo Press, Cairo, Egypt, 2014.

Cotton, H.: The Legio VI Ferrata, in: Les légions de Rome sous le Haut-Empire I, edited by: Le Bohec, Y., de Boccard, Lyon, France, 351–357, 2000.

De Kort, J.-W. and Raczynski-Henk, Y.: The Fossa Corbulonis between the Rhine and Meuse estuaries in the Western Netherlands, in: Roman canal studies, Water History 6/1, edited by: Salomon, F., Purdue, L., Goiran, J.-P., and Berger, J.-F., Springer, Berlin, Heidelberg, Germany, 51–71, https://doi.org/10.1007/s12685-014-0097-3, 2014.

Gilliam, J. F.: An Egyptian Cohort in A.D. 117, in: Bonner Historia Augusta-Colloquium 1964/1965, Bonn, 91–97, 1966.

Eck, W.: The Bar-Kokhba Revolt: The Roman Point of View, Journal of Roman Studies, 89, 76–89, 1999.

Ginau, A., Schiestl, R., and Wunderlich, J.: Integrative geoarchaeological research on settlement patterns in the dynamic landscape of the northwestern Nile delta, QI, 511, 51–67, https://doi.org/10.1016/j.quaint.2018.04.047, 2019.

Grewe, K.: Tunnels and Canals, in: The Oxford Handbook of Engineering and Technology in the Classical World, edited by: Oleson, J. P., Oxford University Press, Oxford, United Kingdom, 319–336, https://doi.org/10.1093/oxfordhb/9780199734856.013.0013, 2009.

Haguet, L.: Egypt and Maps, Or: What Early Modern Maps Are (Not) Telling Us about the History of Egyptology in Europe, in: Mapping Ancient Identities. Methodisch – kritische Reflexionen zu Kartierungspraktiken, Berlin Studies of the Ancient World 55, edited by: Grunwald, S., Hofmann, K. P., Werning, D. A., and Wiedemann, F., Edition Topoi, Berlin, Germany, 91–113, https://doi.org/10.17171/3-55, 2018.

Hairy, I. and Sennoune, O.: Le canal d'Alexandrie: la course au Nil, in: Du Nil à Alexandrie: histoires d'eaux, edited by: Hairy, I., Céntre d'Études Alexandrines, De Boccard, Alexandrie, 140–161, 2011 (in French).

Halfmann, H.: Itinera Principum. Geschichte und Typologie der Kaiserreisen im Römischen Reich, F. Steiner Verlag, Stuttgart, Germany, 1986 (in German).

Holz, R. K., Stieglitz, D., Hansen, D. P., and Ochsenschlager, E.: Mendes I, American Research Center in Egypt, Cairo, Egypt, 1980.

Isaac, B.: The Limits of Empire. The Roman Army in the East, Clarendon Press, Oxford, United Kingdom, 1990.

Jördens, A.: Statthalterliche Verwaltung in der römischen Kaiserzeit, Studien zum praefectus Aegypti, Historia Einzelschriften 175, Steiner, Stuttgart, Germany, 2009 (in German).

Kolb, A.: Via ducta – Roman Road Building: An Introduction to Its Significance, the Sources and the State of Research, in: Roman Roads. New Evidence - New Perspectives, edited by: Kolb, A., de Gruyter, Berlin, Boston, 3–21, https://doi.org/10.1515/9783110638332-002, 2019.

Matthews, J.: The journey of Theophanes. Travel, Business, and Daily Life in the Roman East, Yale University Press, New Haven, USA, 2006.

Millar, F.: The Roman Near East, 31 BC–AD 337, Harvard University Press, Cambridge, MA, USA, 1993.

Mor, M.: The Second Jewish Revolt. The Bar Kokhba War, 132–136 CE, The Brill Reference Library of Judaism 50, Brill, Leiden, The Netherlands, 2016.

Pfeiffer, S.: Der römische Kaiser und das Land am Nil. Kaiserverehrung und Kaiserkult in Alexandria und Ägypten von Augustus bis Caracalla (30 v.Chr.–217 n.Chr.), Historia Einzelschrift 212, Steiner, Wiesbaden, Germany, 2010 (in German).

Reddé, M.: Mare nostrum. Les infrastructures, le dispositive et l'histoire de la marine militaire sous l'Empire romain, École française de Rome, Rome, Italy, 1986 (in French).

Redon, B.: Les circulations transversales dans le Delta égyptien – entre adaptation au paysage et nécessités pratiques, in: Landscape Archaeology, Egypt and the Mediterranean World, Proceedings of the Cairo Conference, Bibliothèque d'étude 169, edited by: Tristant, Y. and Ghilardi, M., Institut Français d'Archéologie Orientale, Cairo, Egypt, 151–172, 2018 (in French).

Salomon, F., Purdue, L., Goiran, J.-P., and Berger, J.-F.: Introduction to the special issue: Roman canal studies – Main research aims, Water History, Springer, Berlin, Germany, 1–9, 2014.

Schäfer, D.: Makedonische Pharaonen und hieroglyphische Stelen. Historische Untersuchungen zur Satrapenstele und verwandten Denkmälern, Studia Hellenistica 50, Peeters, Leuven, Belgium, 2011 (in German).

Schäfer, P.: Hadrian's policy in Judaea and the Bar Kokhba revolt: a reassessment, in A Tribute to Geza Vermes. Essays on Jewish and Christian Literature and History, Journal for the Study of the Old Testament Supplement Series 100, edited by: Davies, P. R. and White, R. T., JSOT Press, Sheffield, United Kingdom, 281–303, 1990.

Schäfer, P.: The History of the Jews in the Greco-Roman world, Routledge, London, United Kingdom, 2003.

Scheuble, S.: Inschriften aus Schedia, Chiron, 39, 463–503, 2009 (in German).

Schiestl, R.: Field Boundaries and Ancient Settlement Sites: Observations from the Regional Survey around Buto, Western Delta, in: Mitteilungen des Deutschen Archäologischen Instituts, Abteilung Kairo, 68, 175–190, 2012.

Sidebotham, S. E., Zitterkopf, R. E., and Helms, C. C., Survey of the Via Hadriana: The 1998 Season, J. Am. Res. Center Egypt, 37, 115–126, 2000.

Sijpesteijn, P. J.: Der ΠΟΤΑΜΟΣ ΤΡΑΙΑΝΟΣ, Aegyptus, 43, No. 1/2, 70–83, 1963.

Sijpesteijn, P. J.: A New Document concerning Hadrian's Visit to Egypt, Historia, 18, 109–118, 1969.

Silotti, A.: The Discovery of Ancient Egypt, Edizione White Star, Vercelli, Italy, 1998.

Stückelberger, A. and Graßhoff, G. (Eds.): Klaudios Ptolemaios. Handbuch der Geographie: griechisch-deutsch; Einleitung, Text und Übersetzung, Index/1: Einleitung und Buch 1–4, Schwabe, Basel, Switzerland, 2006 (in German).

Talbert, R. J. A.: Barrington Atlas of the Greek and Roman World, Princeton University Press, Princeton, USA, 2000.

Talbert, R. J. A.: Rome's World: The Peutinger Map Reconsidered, Cambridge University Press, Cambridge, United Kingdom, 2010.

Wikander, C.: Canals, in: Handbook of Ancient Water Technology, Technology and Change in History, Vol. 2, edited by: Wikander, Ö., Brill, Leiden, The Netherlands, 321–330, 2000.

Wittke, A.-M., Olshausen, E., Szydlak, R.: Historischer Atlas der antiken Welt, Der Neue Pauly, Supplemente, J. B. Metzler Verlag, Stuttgart, Germany, 2007.

Young, G.: Rome's Eastern Trade. International commerce and imperial policy, 31 BC–AD 305, Routledge, London, United Kingdom, 2001.

Yoyotte, J.: Tells oubliés de la region de Sân, in: Cahiers de Tanis I, Éditions Recherche sur les Civilisations, Paris, 107–112, 1987 (in French).

Zeller, T.: Driving Germany. The landscape of the German Autobahn, 1930-1970, Studies in German History 5, Berghahn Books, New York, USA, 2007.

Zimmermann, M.: Der Kaiser als Nil, in: Propaganda-Selbstdarstellung – Repräsentation im römischen Kaiserreiche des 1. Jhs. n. Chr., Historia Einzelschriften 164, edited by: Weber G., and Zimmermann, M., Steiner, Stuttgart, Germany, 317–348, 2003 (in German).

Zivie-Coche, C.: Statues et autobiographies de dignitaires, Tanis à l'époque Ptolémaique, Tanis, Travaux récents sur le Tell San El-Hagar, mission française des fouilles de Tanis 3, Éd. Noesis, Paris, France, 2004 (in French).

E&G Quaternary Sci. J., 70, 39–52, 2021
https://doi.org/10.5194/egqsj-70-39-2021

Open Access E&G Quaternary Science Journal

Research article

Western Mareotis lake(s) during the Late Holocene (4th century BCE–8th century CE): diachronic evolution in the western margin of the Nile Delta and evidence for the digging of a canal complex during the early Roman period

Maël Crépy[1] **and Marie-Françoise Boussac**[2]

[1]UMR5133 Archéorient and UMR5189 HiSoMA, Maison de l'Orient et de la Méditerranée, CNRS, Lyon 69007, France
[2]UMR7041 ArScAn, Université Paris Nanterre, 21 allée de l'Université, 92023 Nanterre, France

Correspondence: Maël Crépy (crepy.mc@gmail.com)

Relevant dates: Received: 25 September 2020 – Revised: 7 December 2020 – Accepted: 17 December 2020 – Published: 28 January 2021

How to cite: Crépy, M. and Boussac, M.-F.: Western Mareotis lake(s) during the Late Holocene (4th century BCE–8th century CE): diachronic evolution in the western margin of the Nile Delta and evidence for the digging of a canal complex during the early Roman period, E&G Quaternary Sci. J., 70, 39–52, https://doi.org/10.5194/egqsj-70-39-2021, 2021.

Abstract: Lake Mareotis (modern Mariut), located near the Mediterranean coast of Egypt west of the Nile Delta, is bordered by ancient sites dating from the New Kingdom (end of the 2nd millennium BCE) to the Medieval period (8th century CE), the most famous one being Alexandria. In its western part (wadi Mariut), several sites are equipped with harbour structures, but they also have structures contemporaneous with them that are not compatible with the lake level required for the operation of the harbour. Between the 1990s and 2010, several sedimentological studies tried to solve this paradox without completely succeeding. To go further, this study is based on the reassessment of geoarchaeological data and on the analysis of early scholars' accounts (1800–1945), maps (1807–1958) and satellite photographs (Corona). It allows us to reconstruct the extension of the lake(s) at different periods in wadi Mariut. During the 1st millennium BCE, the Mariut lagoon experienced a drawdown in its western part, and several distinct lakes formed, followed by building operations in some emerged areas during the Hellenistic period (332–30 BCE). During the early Roman period (30 BCE–284 CE), the digging of several canals in the 2nd century CE to connect the sites of the wadi Mariut to the eastern part of the Mariut basin reconfigured the lake(s).

Kurzfassung: Der Mareotis-See (mod. Mariut), nahe der ägyptischen Mittelmeerküste, westlich des Nildeltas, liegt an antiken Siedlungen, die vom Neuen Reich (Ende des zweiten Jt. v. Chr.) bis ins Mittelalter (8. Jh. n. Chr.) datieren; die berühmteste ist Alexandria. In seinem westlichen Teil (Wadi Mariut) sind mehrere Siedlungen mit Hafenanlagen angelegt, enthalten aber auch zeitgenössische Gebäude, die mit dem Seespiegel unvereinbar sind und die für das Funktionieren der Häfen in Betracht gezogen werden müssen. Zwischen den 1990er Jahren und 2010 wurden mehrere Studien, die sich auf die Sedimentologie stützten, auf diese Frage angewandt, ohne dieses Paradox vollständig zu lösen. Um noch einen Schritt weiter zu gehen, stützt sich diese Studie auf die Neubewertung geoarchäologischer Daten, und zwar auf Analyse von Berichten früher Gelehrter (1800–1945), Karten (1807–1958) und Satellitenfotos (Corona). Sie ermöglicht es, die Ausdehnung des Sees/der Seen zu verschiedenen Zeiten im Wadi Mariut zu rekonstruieren. Während des ersten Jt. v. Chr. erlebte die Lagune in ihrem westlichen Teil eine Absenkung, gefolgt von Bauarbeiten in neu entstandenen Gebieten während der hellenistischen Periode (332–30 v. Chr.). Durch das Graben mehrerer Kanäle im 2. Jh. n. Chr., um die Siedlungen mit dem östlichen Teil des Mariut-Beckens zu verbinden, wurden der See bzw. die Seen neu gestaltet.

1 Introduction and objectives

Lake Mariut, ancient Mareotis (Fig. 1), is a lagoon that polarised the human occupation of Egypt's north-western margins during antiquity. The region developed mainly after the foundation of Alexandria in 332 BCE (Fraser, 1972), although earlier occupation is archaeologically evidenced since the New Kingdom at Plinthine (Boussac et al., 2015; Boussac and Redon, 2021) and Kom Bahig (Empereur, 2018). Agricultural lands and towns, such as Taposiris on the north shore (Boussac, 2015) and Marea (Pichot, 2012) on the southern one, flourished until the Arab-Muslim conquest, which was followed in the 7–8th centuries CE by a reconfiguration of the territory and the abandonment of many settlements (Décobert, 2002). During all periods, the human occupation of the region has been closely linked to the lake (Blue and Khalil, 2011).

Strabo (∼ 60 BCE–∼ 20 CE) mentions a very large lake (Strabo, 2015:17, 14) of major economic importance (Strabo, 2015:17, 7). Later, accounts by travellers from the 6th century CE to 1798 (Sennoune, 2015), maps (Awad, 2010) and sedimentological data (Flaux, 2011) indicate significant fluctuations of the lake levels and positions (including phases of desiccation). At the beginning of the French expedition to Egypt (1798–1801), the lake area was dry (Le Père, 1825).

If one focuses on the wadi Mariut (western part of the Mariut basin; Fig. 1), the presence at some Hellenistic and/or Roman sites of harbour structures close to remains that are incompatible with the vicinity of a lake (e.g. amphora workshops) and dating back to the same periods constitutes a geoarchaeological paradox. How can this paradox be solved? Did the lake levels shift at high frequency during this period? Have several independent lakes of small extent coexisted in the Mariut basin? Should a major water engineering work be considered?

This geoarchaeological study, undertaken within the French mission at Taposiris Magna and Plinthine (dir. M.-F. Boussac and then B. Redon), aims to assess, through a composite method, the western extension of the Mareotis lake(s) in wadi Mariut from the 4th century BCE to the 8th century CE.

2 General settings and previous studies

2.1 Geomorphic settings

Lake Mariut lies at the interface between three geomorphological systems: the Mediterranean littoral, the Nile Delta and the Libyan desert. During the Holocene, distinct morphogenetic processes have influenced its evolution: climate change and the evolution of the Nile floods (Macklin et al., 2015), sea level rise (Dalongeville and Fouache, 2005), wind erosion (Woronko, 2012; Crépy, 2021), subsidence (Pennington et al., 2017), and neotectonics (Stanley, 2003), to which must be added the impact of human activities (Flaux et al., 2012).

The lagoon, whose water level is currently controlled by means of pumps and a canal to the Mediterranean Sea located at Al Max (in the vicinity of Alexandria), occupies parts of a depression, some areas of which are below mean sea level. This depression consists of two distinct areas (Fig. 1). To the east, its edges slope gently, and no significant topographical features separate it from the now-drained Abukir lagoon to the north-east, the delta to the east, the desert to the west and the agricultural lands of Al Buhayrah to the south. In the western part, often called wadi Mariut or Mariut valley, the depression stretches from east to west and is bordered by two steeply sloping calcarenite ridges separating it from the Mediterranean Sea in the north and from another depression in the south.

2.2 Archaeological and historic settings (∼ 1000 BCE–∼ 1000 CE)

The archaeology of the western part of Lake Mareotis (wadi Mariut) has been investigated since the beginning of the 20th century (e.g. De Cosson, 1935). From the beginning of the 1st millennium BCE to the end of the 1st millennium CE, the following dynamics of occupation have been demonstrated: from the New Kingdom (∼ 1580–∼ 1077 BCE), occupation on high points on the northern and southern banks of the valley (Boussac et al., 2015; Empereur, 2018; Nenna et al., 2020); from the Saite Period (664–525 BCE) at the latest, agricultural development (wine) attested to in Plinthine on the northern bank (Redon et al., 2017); during the Hellenistic period (332–30 BCE), urban development in sectors located lower down on both banks and on Mariut island (Blue and Khalil, 2011; Boussac, 2015); and from the early Roman

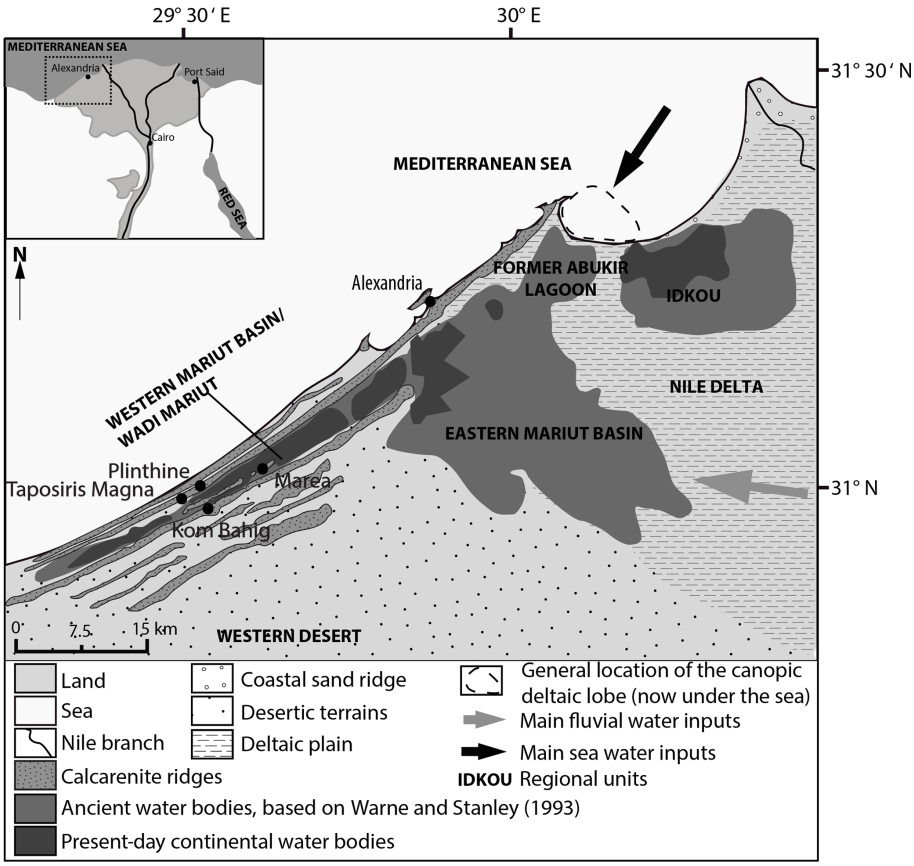

Figure 1. Main geomorphic units in the Mariut area, based on Flaux (2011).

period (30 BCE–284 CE) to the Arab-Islamic conquest (mid-7th century CE), increasing harbour and economic development (including wine export) (Décobert, 2002; Blue and Khalil, 2011; Boussac and El-Amouri, 2010; Dzierzbicka, 2018; Pichot and Simony, 2021). The Hellenistic and Roman periods are characterised by structures occupying areas that are very close to the current shores of the lake (or even in the present lake) and located at altitudes much lower than the remains of other periods, suggesting that the lake levels were lower during these periods or that the geometry of the lake was different. This has been demonstrated at Taposiris and on Mariut island (Blue and Khalil, 2011; Flaux, 2012).

2.3 Previous geomorphological and geoarchaeological studies

2.3.1 Holocene history of the Mariut lagoon

The calcarenite ridge separating the Mariut depression and the Mediterranean Sea, as well as the ridge delimiting the wadi Mariut to the south, predate the Holocene (El Asmar and Wood, 2000) and have durably limited the extension of the lagoon. The Holocene shifts of the lagoon were therefore mainly conditioned by the balance between sea level variations, subsidence, and the Nile's liquid and solid inputs, the latter being determined by climatic conditions and human activities in its watershed.

During the Holocene, the evolution of the Mariut region (Table 1) has been established by the work of Clément Flaux mainly thanks to data from the eastern part of the Mariut but also from Taposiris and from the southern bank of the wadi Mariut (Flaux et al., 2011; Flaux, 2011, 2012). From the early Roman period (30 BCE–284 CE), the evolution of the lagoon has been linked to the filling in of the Canopic branch (Fig. 1; Bernand, 1970; Hairy and Sennoune, 2009) and to the sinking of its deltaic lobe below sea level around the 8th century CE (Stanley et al., 2001).

2.3.2 A geoarchaeological paradox

This general environmental pattern cannot be directly applied to the wadi Mariut; on the one hand, subsidence is strong in the eastern part of the Mariut depression but very weak in wadi Mariut (Pennington et al., 2017), and on the other hand, marine and Nilotic water inputs both originate from the east (Fig. 1). Moreover, in wadi Mariut, Pleistocene outcrops are not uncommon and the Pleistocene–Holocene boundary is generally close to the topographic surface, so less sedimentation occurred during the Holocene (Flaux, 2012).

Table 1. Holocene evolution of the Mariut region based on Flaux et al. (2011) and Flaux (2011, 2012).

Period	Status	Main causes
∼ 9000–∼ 7000 BCE	Coastal deltaic plain periodically flooded by the Nile	Nile Delta progradation
∼ 6000–∼ 5500 BCE	Lagoon sedimentation	Holocene marine transgression
∼ 5500–∼ 2800 BCE	Lagoon closed to marine influences	Nile Delta progradation
∼ 2800–∼ 1200 BCE	Marine influence and hydrological instability	Climatic aridification and reduced Nile flow
∼ 1000 BCE–∼ 200 CE	Lagoon more subject to the Nilotic influence than to the maritime one and anthropogenic disturbances	Canopic branch defluviation and anthropogenic activities
∼ 200–∼ 800 CE	Brackish lagoon dominated by nilotic inputs	To be determined
∼ 800–∼ 1200 CE	Sebkha	Nile defluviation and canal siltation

Sedimentological and physico-chemical analyses have been interpreted as evidence of a large extension of the Mariut lagoon westward between ∼ 4000 BCE and ∼ 1200 CE even beyond the present limits of the lake (Warne and Stanley, 1993). A generally high water level in antiquity has also been assumed for Taposiris (Tronchère, 2010; Tronchère et al., 2014).

A lot of ancient harbour infrastructure has been prospected (Blue and Khalil, 2011) but also Hellenistic and Roman remains submerged or located close to the current shores of the lagoon, including amphora workshops (Empereur and Picon, 1998; Flaux, 2012). Their underground kilns make them incompatible with their proximity to the lake and high water levels. However, the operation of the few ports and sites bordering the lake studied in more detail implies relatively high water levels, for the Roman period at least, for example at Taposiris (Boussac and El Amouri, 2010) or on Mariut island (Flaux, 2012).

The archaeological remains and the environmental data from wadi Mariut thus present a geoarchaeological paradox to be solved. Not only do the environmental and archaeological data not converge, but even the archaeological data seem to contradict each other unless we consider a variability in water levels of high frequency, several independent lakes or water engineering on the scale of the wadi Mariut, whose remains have not yet been highlighted.

2.3.3 Illustration of the geoarchaeological paradox: Taposiris harbour

The lake complex of Taposiris (Fig. 2), investigated since 1998 by the French mission at Taposiris Magna and Plinthine, consists of a dug or deepened canal bordered to the south by an artificial sedimentary levee on which warehouses are lined up and to the north, at its eastern end, by dredging material. A bridge that connects the bank to the artificial levee is dated to early Roman times, more specifically to the 2nd century CE (Boussac and El Amouri, 2010). The artificial levee and the dredged material cover Hellenistic remains (2nd–1st century BCE), part of which is below the present water surface (Boussac and El-Amouri, 2010). To the east, a stone pier from the late Roman period (4th century CE) closes the port complex. The swamp located to the north, which could suggest a harbour basin, was already a swamp during antiquity (Flaux, 2012).

The chronological sequence is as follows (Boussac and El-Amouri, 2010; Boussac, 2015):

- urban development during the 2nd–1st century BCE;
- building of an artificial levee during the 2nd century CE;
- raising of the artificial levee after the 4th century CE;
- installation of the eastern pier around the 4th century CE;
- abandonment of the area after the 7th century CE.

3 Material and methods

Carrying out a geoarchaeological study in wadi Mariut is complex due to the lack of analysis equipment and to Egyptian legislation prohibiting the export of samples. Moreover, urbanisation and agricultural development in the region in the 20th century has considerably altered the topography and sedimentary formations of the region (quarries, salt ponds, etc.). We therefore used a combination of methods to overcome these obstacles.

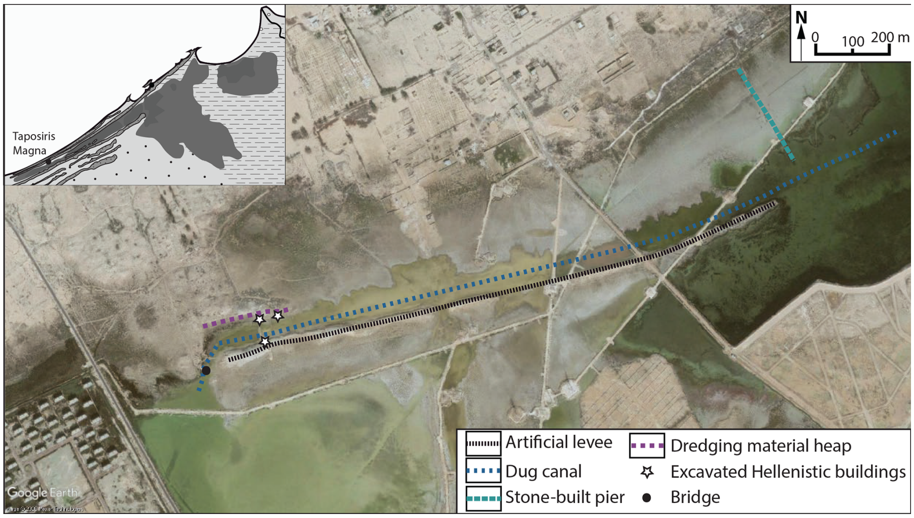

Figure 2. Harbour of Taposiris. Base map image: © Google Earth Pro November 2009.

3.1 Reassessment of geoarchaeological data

We reassessed and crossed three types of data that led researchers to reconstruct a large extension of Lake Mareotis in wadi Mariut:

- sedimentological, biological and physico-chemical data (available in Tronchère, 2010; Tronchère et al., 2014; Warne and Stanley, 1993);

- archaeological data, in particular the distribution of sites (from Blue and Khalil, 2011 and Boussac, 2015);

- historical data, through an analysis of two sources frequently used in the study of the region (Strabo, 2015:17; Jacotin, 1818).

3.2 Early scholars' accounts (1800–1945)

A total of 11 early western scholars' contributions (Chabrol and Lancret, 1829; De Cosson, 1935; El Falaki, 1872; Le Père, 1823, 1825, 1829; Jacotin, 1824; Oliver, 1945; Reclus, 1885; Rennell, 1800; St John, 1849) have been selected and studied to recover data erased over time. They describe a period during which human activities were less developed than today and provide additional elements on archaeology, completing the data concerning the distribution of the sites and the topography.

3.3 Maps (1807–1958)

Eight maps (Table 2) have been analysed to identify the topography of the lands currently flooded and the vanished archaeological sites and to characterise the recent evolution of the extension of the lake.

3.4 Corona photographs

Three declassified satellite photographs from the Corona programme (Table 3) were acquired free of charge on EarthExplorer (https://earthexplorer.usgs.gov/, last access: 22 January 2021).

They allow us to evaluate the topography of the now-flooded areas and to observe the region before its current development. Moreover, they help us to escape the subjectivity of early scholars and the bias of cartographic surveys in swampy areas and to observe the terrain from the sky to identify macrostructures.

4 Results and interpretation

4.1 Reassessment of geoarchaeological data

4.1.1 Sedimentological data: playa, lake or lakes?

Two studies led to the reconstruction of a large extension of Lake Mareotis in its western part: Warne and Stanley (1993) at the regional scale and Tronchère (2010) and Tronchère et al. (2014) around Taposiris. The first study (Warne and Stanley, 1993) was based on the analysis of sedimentary cores and revealed the presence of a lagoon dominated by fluvial inputs throughout wadi Mariut and up to Taposiris in the west $\sim$ 2500–$\sim$ 2000 years ago. If only the regional scale and major trends are considered, these conclusions are correct, although a reassessment is needed at the local scale and is made possible by the rigour of Warne and Stanley (1993) in presenting their data. At the scale of wadi Mariut, the data highlight three points:

- on several isopleth maps (Fig. 3), the Nilotic influence does not appear (verdine/glauconite) or appears very slightly (mica, heavy minerals) in the western part of wadi Mariut, and other parameters strongly differentiate it (gypsum, foraminifera);

- the Holocene sedimentary column represents less than 2.5 m in most of wadi Mariut;

- in the western part of wadi Mariut, the only facies that can be linked to a lagoon are "lagoon margin mud" facies whose composition could just as well correspond to playa or semi-playa deposits (as described by Embabi, 2004, and by Crépy, 2016).

The continuity of the lagoon up to Taposiris is therefore not established by Warne and Stanley's data (1993) which show, in contrast, that at least one basin has undergone a specific evolution (Fig. 3).

Data from Tronchère (2010) and Tronchère et al. (2014) at local scale led to the reconstruction of a lake or lagoon reaching Taposiris during the whole Holocene (the alteration layer of the calcarenite substratum was dated to 40 254–38 032 cal BCE[1]). However, the very small quantity of ostracods found (some samples were totally free of them) and the granulometric data do not go in this direction. The laser granulometry curves are all multimodal, which Tronchère (2010) attributed to a sampling bias. The presence of recurrent aeolian modes (loess: 10–20 µm; dune sand: 100–200 µm; according to Tsoar and Pye, 1987) mixed with other modes would rather indicate a palustrine environment influenced by desert dynamics (e.g. playa or sebkha margin). To sum up, the sedimentological data are more likely to correspond to marshy or immersed areas disconnected from the Mariut lagoon.

4.1.2 Historical data: some necessary precautions

Strabo's Book 17 (Strabo, 2015:17) and Jacotin's map (1818) are often used to study Lake Mareotis' extension during antiquity. According to the ancient geographer, the lake measured, in his time, 150 stadia (~ 27.75 km) or more in width and less than 300 stadia (~ 55.5 km) in length (Strabo, 2015:17, 14). These measurements have generally been interpreted in light of the current state of the lake, and the orientation has often been used as follows: 300 stadia from the north-east to south-west and 150 stadia from the north-west to south-east. However, there is no indication of this orientation in Strabo's text, and data on the Holocene evolution of the Nile Delta and on subsidence in the eastern Mariut basin would rather fit with an opposite orientation, especially if one takes into account a Nilotic influence.

Jacotin's map (1818) has sometimes been used as a reference state of ancient Mariut (e.g. Tronchère et al., 2014) even if the limits of the lake have been drawn after a British military operation, as mentioned on the map, "Cuts made by the English to flood Lake Mareotis (19 Germinal An 9–19 April 1801)". The lake on the map corresponds to a state when it was directly connected to the Aboukir lagoon, itself open to the sea, and therefore at a much higher level than the maxima during most of the studied period (4th century BCE–8th century CE) when the Canopic deltaic lobe used to be an obstacle to links with the Mediterranean Sea (Stanley et al., 2001).

4.1.3 Archaeological data

The spatio-temporal distribution of the sites could seem relevant to draw the ancient shores of the lake. However, two obstacles prevent the proper exploitation of the survey results (e.g. Blue and Khalil, 2011; Picon and Empereur, 1998). In the absence of underwater surveys, the distribution of sites is incomplete and draws a shoreline corresponding to the limit of the lake at the time of the survey (even if Blue and Khalil, 2011, also mentioned some underwater remains, they saw from the land), and surface surveys are not sufficient to give an exhaustive chronology of the sites. However, the following observations can be made thanks to the Hellenistic and Roman amphora workshops of Mariut island and Borg el Arab (surveyed by Empereur and Picon, 1998, and Blue and Khalil, 2011; Fig. 4). The altitude of their kilns shows that the lake must have been located within more restricted limits or at a lower level than today in this part of wadi Mariut. The kilns of this area are indeed located below the top of the phreatic water table induced by the current lake. Similar levels inferred for antiquity would thus hinder their use. Likewise, the Hellenistic quarter of the lower town of Taposiris is incompatible with the present level of the lagoon (Flaux, 2012)

4.2 Early scholars' accounts (1800–1945)

4.2.1 Limits of the lake(s)

Before the flooding in 1801, low areas of the Mariut depression could fill with water after rainfall (Chabrol and Lancret, 1829; Le Père, 1825) and form small independent lakes, for example southwest of Taposiris (St John, 1849). At the peak of the flood, the western limit of the water would have been located at the level of the so-called Arabs' tower (Jacotin, 1824) or 1000 m east of Taposiris (Le Père, 1829) or about 500 m east of the Arabs' tower (Fig. 5). W. G. Browne, at the end of the 18th century, saw no reason to consider a lake that would have been more than 1 or 1.5 leagues (~ 4.83 or ~ 7.25 km) from Alexandria in the past based on the observation of the ground and the topography (Rennell, 1800).

4.2.2 Data on archaeological remains

Early scholars mention remains that have now disappeared, such as walls and canals in wadi Mariut (Chabrol and Lancret, 1829), as well as levees or small dikes (now under wa-

[1] Calibration by M. Crépy with OxCal using IntCal20 calibration curve based on raw data from Tronchère et al. (2014).

Table 2. Maps used in this study.

Date	Author	Link
1807	Arrowsmith	https://gallica.bnf.fr/ark:/12148/btv1b530669569/ (last access: 22 January 2021)
1818	Jacotin	https://gallica.bnf.fr/ark:/12148/btv1b531569998/ (last access: 22 January 2021)
1827	Coste	https://gallica.bnf.fr/ark:/12148/btv1b8491814n/ (last access: 22 January 2021)
1850	St John	https://gallica.bnf.fr/ark:/12148/btv1b53136219p/ (last access: 22 January 2021)
1866	El Falaki	https://gallica.bnf.fr/ark:/12148/btv1b10101071m/ (last access: 22 January 2021)
1910	Survey of Egypt	https://www.davidrumsey.com/luna/servlet/detail/ RUMSEY~8~1~317305~90086593:Sheet-47-Bahig (last access: 22 January 2021)
1942	AMS	http://legacy.lib.utexas.edu/maps/ams/egypt/ txu-pclmaps-oclc-6559596-el-hammam.jpg (last access: 22 January 2021)
1958	AMS	http://legacy.lib.utexas.edu/maps/ams/north_africa/ txu-oclc-6949452-nh35-8.jpg (last access: 22 January 2021)

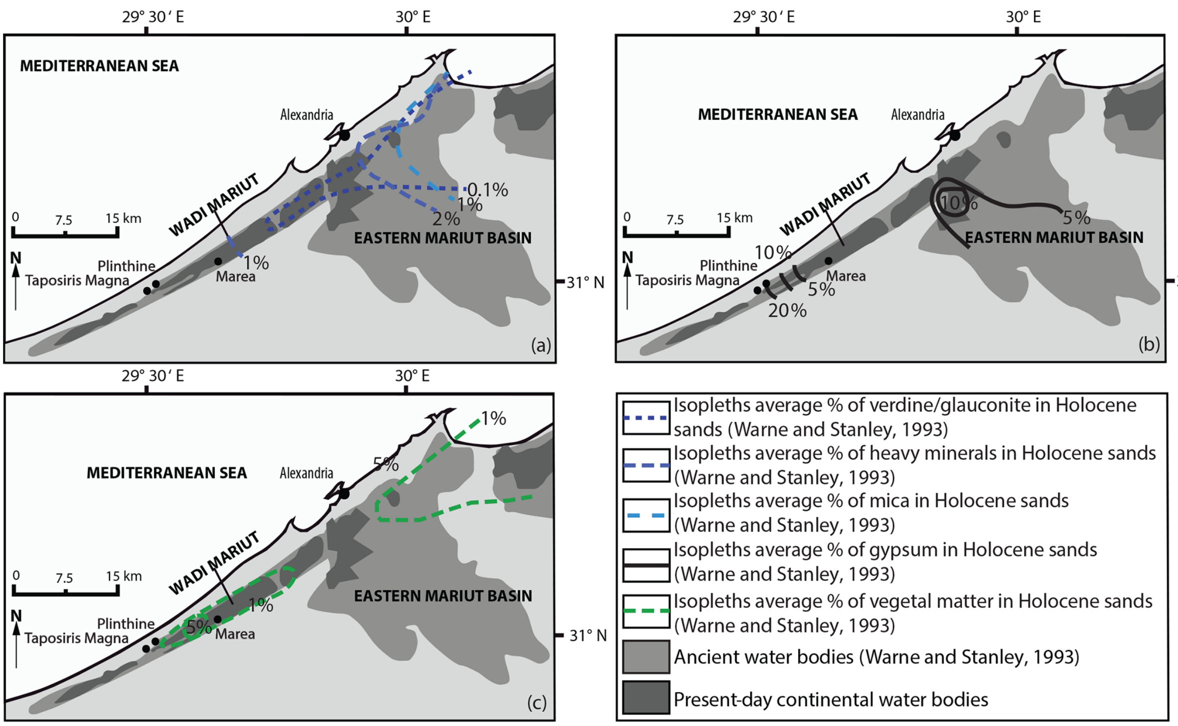

Figure 3. **(a)** Isopleths (based on Warne and Stanley, 1993) recording the Nile's influence on the Mariut basin. **(b)** Isopleths (based on Warne and Stanley, 1993) indicating high evaporation processes during the Holocene in the western part of wadi Mariut. **(c)** Isopleths (based on Warne and Stanley, 1993) emphasising specific local dynamics in wadi Mariut.

Figure 4. Amphora workshops in the area (base map image: © Google Earth Pro).

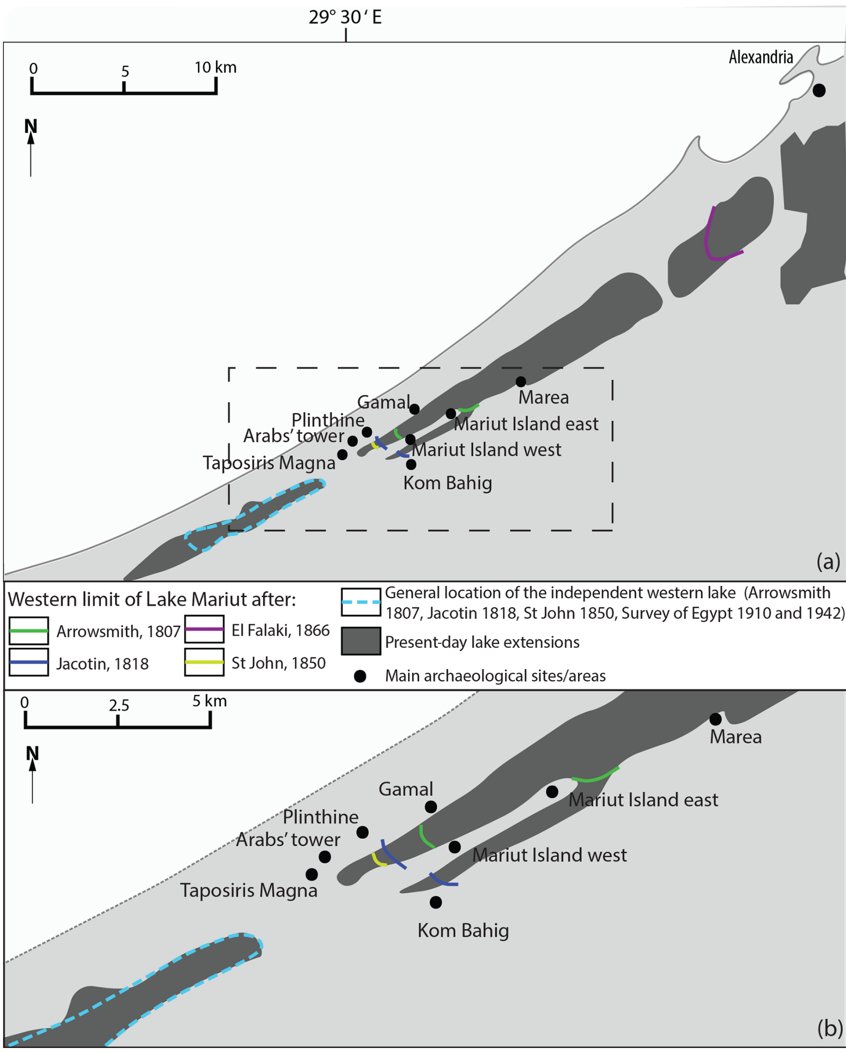

Figure 5. Limit of the lakes according to old maps. **(a)** Regional scale. **(b)** More local scale.

Table 3. Corona photographs used in this study.

Corona ID	Acquisition (mm/yyyy)
DS1016-2088DF007	01/1965
DS1109-2171DF010	03/1970
DS1111-2167DA024	08/1970

ter) which were spanned by small bridges and crossed the wadi Mariut (Le Père, 1823). El Falaki (1872) even mentions entire sites (destroyed by modern construction) extending over 9 km north-east of Taposiris, thus offering a counterpart on the north bank to the succession of sites still visible on the south bank (Blue and Khalil, 2011; Pichot and Simony, 2021). Because of the presence of underwater remains, some early scholars speculated that the lake was completely or partially desiccated during part of antiquity without specifying a precise period (e.g. Reclus, 1885).

4.2.3 Data on Taposiris artificial levee

Some early scholars described the harbour complex of Taposiris, bringing two pieces of information that have now been erased. The west–east artificial levee of Taposiris was doubled by an ancient causeway (De Cosson, 1935), and a second canal dug across the wadi Mariut from north to south linked Taposiris harbour to a dock on the south side of the valley and was doubled with a causeway located on the sedimentary levee forming the west bank of the canal (Oliver, 1945).

4.3 Maps (1807–1958)

4.3.1 Extension of the lake(s)

For all but one (St John, 1850) of the studied maps, the lake did not reach the Arabs' tower even in the periods following the flood of 1801 (Fig. 5). Wadi Mariut is often depicted as being occupied exclusively by marshes (El Falaki, 1866; on a smaller area, Survey of Egypt, 1910, 1942) or being completely dry (AMS, 1958). The boundaries of the lake, whether dried up (Coste, 1827) or in water (Arrowsmith, 1807; Jacotin, 1818), extend farther to the east-south-east in its eastern part than to the west in wadi Mariut, which is in favour of a reinterpretation of the measurements given by Strabo (cf. Sect. 4.1.2). Finally, a small independent lake or marsh is drawn to the west of Taposiris (Fig. 5) in five out of six maps covering this sector (Arrowsmith, 1807; Jacotin, 1818; St John, 1850; Survey of Egypt, 1910, 1942).

4.3.2 Subaquatic topography

One map (AMS, 1958) gives an insight into the now-flooded topography of the bottom of wadi Mariut; the western part of wadi Mariut includes several closed basins whose elevations are below mean sea level and are separated by topographic thresholds and higher areas.

4.3.3 Mention of ruins and remains

The ruins are numerous on both banks of wadi Mariut, as well as on islands and even in the marshy part at its bottom (El Falaki, 1866). To the south of Taposiris and near Kom Bahig, a map (St John, 1850) shows the remains of catacombs and an excavation on the opposite bank. Many dikes, causeways or bridges are also indicated (Jacotin, 1818); there is one causeway between Marea and Sidi Kirayr and a second between Gamal and Mariut island, and elements of dikes or causeways are represented at Taposiris. Finally, the dug canal of the port of Taposiris appears clearly on two maps; El Falaki (1866) indicates in addition to this canal, which he extends to the west, a second canal towards the south in accordance with the descriptions of Oliver (1945; cf. Sect. 4.2.3), and Arrowsmith (1807) roughly draws the shape of the west–east canal and designates it as "Remains of an ancient canal from the Nile". Unfortunately, travellers' descriptions do not make it possible to assess precisely the dating of the remains, but the low occupation of the area from the end of the 7th century CE (Décobert, 2002) until at least the end of the 18th century (Hairy and Sennoune, 2009) makes an ancient dating very likely. Moreover, concerning the canals, neither the books of Coste (1878) and Linant de Bellefonds (1873), who worked on agricultural projects in the region, nor the topographical maps of the 20th century mention the canals, which confirms that they were not made in the 19th or 20th centuries.

4.4 Corona photographs: canals in wadi Mariut

In the photographs used, the levels and extent of the lake are lower than they are today as the agricultural projects that now bring in large amounts of surplus irrigation water were still in their initial stages. In the photograph of August 1970 in particular, the level is very low because of summer evaporation and scarce rainfall, whereas it is higher in the two other ones (March 1970 and January 1965). In the photographs, it appears that in the western part of wadi Mariut, several of the closed basins are linked by two large canals or channels (the longest being more than 12 km) joined to the west of Gamal. From there, a unique canal extends discontinuously up to the artificial levee of Taposiris and further south-west and then west from the Roman bridge of Taposiris where it ends in the small lake mentioned in maps and accounts (Fig. 6). The maximal width of the two joint canals is around 80 m. They border some depressions which could have been harbour basins as they are located close to sites including ancient piers (Fig. 6). The north–south canal (reported by El Falaki, 1866; Oliver, 1945) is also visible.

Some shorter, narrow canals branch to the two main ones and join sites to the south. It is difficult to determine whether

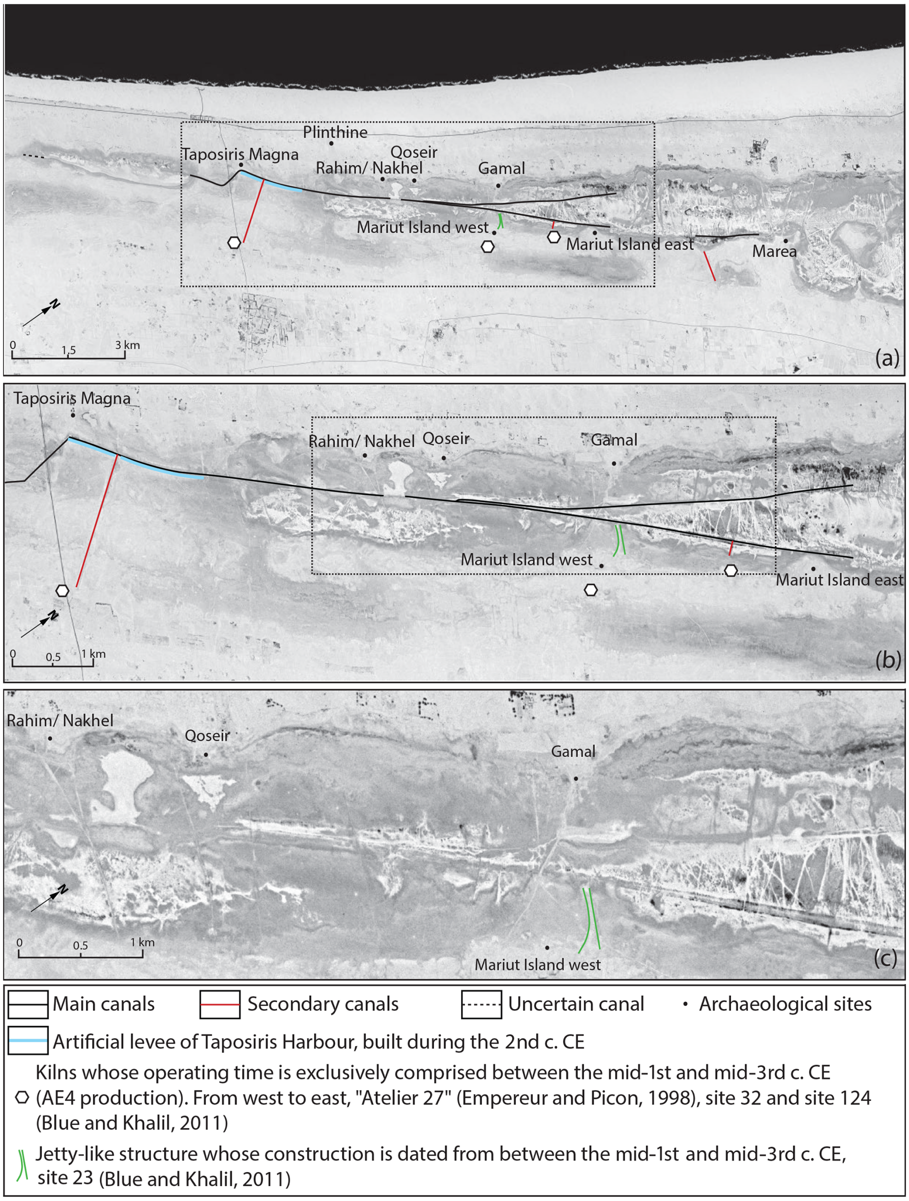

Figure 6. Corona photograph DS1111-2167DA024 (USGS). **(a)** Canal from Marea to the west of Taposiris. **(b)** Focus on the central area. **(c)** Details of the canals.

these canals were deepened channels in flooded areas or if they were canals dug in dry or marshy areas. However, the shapes of the banks of rubble along some parts of the two main canals indicate digging in an environment dry enough for the rubble to remain despite the high proportions of silt and clay at the bottom of wadi Mariut.

5 Discussion

5.1 Solving the paradox: lakes and canals

The combination of all these elements shows that for certain periods of the Holocene, there was not a unique Mariut lake but several lakes occupying closed depressions (cf. Sects. 4.1, 4.2, 4.3.2, 4.4) which could be filled by rainfall. The creation of canals (cf. Sect. 4.4) made it possible to connect them by crossing the topographic thresholds (cf. Sect. 4.3.2). In this way, it was possible to have harbour infrastructures without a continuous stretch of water. These canals are connected to the Taposiris harbour canal, whose digging is firmly dated to the 2nd century CE, and they border several sites that were occupied during the same period, including three amphora kilns whose construction is dated between the mid-1st and the mid-3rd centuries CE (Fig. 6). It is therefore probable that the canals were built during the

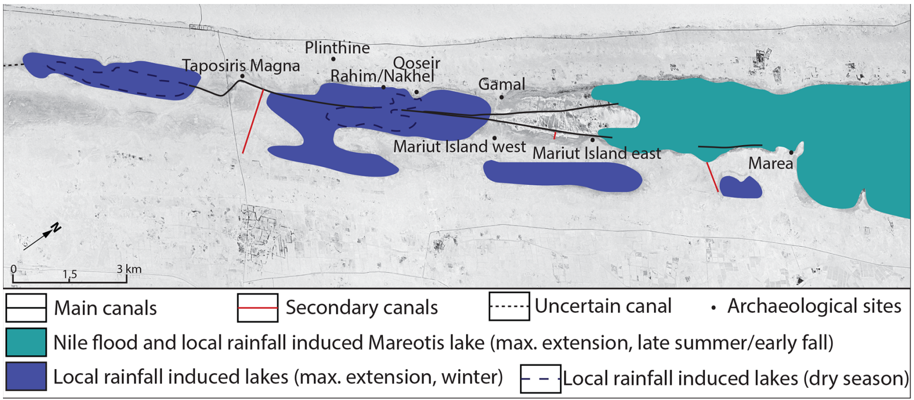

Figure 7. Corona photograph DS1111-2167DA024 (USGS). Proposed extension of the lakes in wadi Mariut during the Hellenistic and early Roman period. Coloured patches correspond to maximum extensions.

Roman period as a harbour complex including several sites (including Taposiris, Mariut island, Marea, etc.). Under these conditions, it becomes easier to understand how Roman harbours could have been in the direct vicinity of Roman amphora kilns; it was not an extensive lake with a highly developed underground water table but smaller basins connected to each other by canals. This interpretation pattern is fully consistent with previously published sedimentological data (e.g. Warne and Stanley, 1993; Tronchère, 2010; Tronchère et al., 2014; Flaux, 2012). Obviously, the chronology will have to be refined by fieldwork at the scale of the wadi Mariut. The magnitude of the works raises a question: for what reasons were canals and at least one bridge built? This article alone cannot provide a complete answer, but it is likely that in an Egyptian climatic context dominated by hyper aridity, the agricultural opportunities offered by the Mediterranean winter rainfall and the natural concentration of surface water in wadi Mariut justified the efforts in connection with the export of local agricultural productions (e.g. wine).

5.2 New hypothesis on Mareotis lake(s) evolution

During the first part of the period under study (first half of the 1st millennium BCE), the archaeological remains were mainly found in high areas, which could lead to the assumption of high lake levels compatible with the palaeoenvironmental data (from Flaux, 2012), but the lack of archaeological excavations calls for caution. In contrast, it is clear that during the Hellenistic and early Roman periods, the water levels were lower, and the extension of the water was smaller (Fig. 7) thanks to the presence of numerous sites incompatible with a single large lake. This reduction can be explained both by the progradation of the Canopic lobe closing off the Bay of Aboukir and the connection to the sea (Flaux, 2012) and by the canal of Alexandria, depriving the lake of part of the Nile flood to the benefit of the city's water supply. The urban and agricultural development of this period could therefore partly explain the ruins mentioned by the early scholars and the maps at the bottom of the wadi Mariut, which are located in some of the topographic threshold areas separating the closed depressions. However, flooding during intense rainfall or an exceptional Nile flood cannot be excluded.

During the Roman period, the digging of the canal artificially re-established the connectivity between the lakes of the wadi Mariut and linked all the sites to Lake Mareotis proper in the east and thus to Alexandria, the Nile and the Mediterranean, contributing to the economic growth of the region. Finally, the construction of the stone jetty at Taposiris after the 4th century CE, which includes a fish pond, as well as the raising of the levee after the 4th century CE (Boussac and El Amouri, 2010), seems to indicate a rise in the water level which could be linked to the gradual subsidence of the Canopic branch (Stanley et al., 2001) or greater Nile floods. This rise has also been demonstrated near Marea (Pichot and Flaux, 2015). Our study does not allow us to know more, but that of Flaux (2011) indicates a severe drying up as early as the 9th century CE.

6 Conclusion and perspectives

This article returns to a subject already addressed by classical sedimentological methods of geoarchaeology. This type of data alone, although obviously necessary to study past environments, was not sufficient to solve the paradox of the wadi Mariut. Combining it with geohistorical sources (Corona photographs, maps, accounts of early scholars) allows for new interpretations. They provide a complementary vision of the spatial organisation, landscapes and environmental dynamics prior to the profound changes in this region since the 1980s.

They allow for the development of a model of the evolution of the wadi Mariut from the beginning of the Hellenistic period (late 4th century BCE) to the beginning of the Medieval period (8th century CE). The lake first experienced a period of drying up followed by urban and agricultural development, including in some sectors of the bottom of the wadi Mariut. During the Roman period in the 2nd century CE, a system composed of large canals was set up, linking independent basins to each other and to the large Lake Mareotis (the lake actually described by Strabo) in the east. After the 4th century CE, higher water levels are likely, before drying up in the 9th century CE (Flaux, 2012). Refining and completing this chronology and this model, as well as studying the canals in detail (possible locks, variability of water levels, etc.) now requires us to go back to the field and start new coring and excavations. It is also a starting point for a new analysis of regional economy and history.

Data availability. The reassessed sedimentological datasets are available in the articles cited in the paper. All the maps are available free of charge on online platforms (last access: 22 January 2021): http://legacy.lib.utexas.edu/maps/ams/egypt/txu-pclmaps-oclc-6559596-el-hammam.jpg (AMS, 1942), http://legacy.lib.utexas.edu/maps/ams/north_africa/txu-oclc-6949452-nh35-8.jpg (AMS, 1958), https://gallica.bnf.fr/ark:/12148/btv1b530669569/ (Arrowsmith 1807), https://gallica.bnf.fr/ark:/12148/btv1b8491814n/ (Coste, 1827), https://gallica.bnf.fr/ark:/12148/btv1b10101071m (El Falaki, 1866), https://gallica.bnf.fr/ark:/12148/btv1b531569998/f42.item (Jacotin, 1818), https://gallica.bnf.fr/ark:/12148/btv1b53136219p/ (St John, 1850), https://www.davidrumsey.com/luna/servlet/detail/RUMSEY~8~1~317305~90086593:Sheet-47-Bahig (Survey of Egypt 1910). These URLs are also indicated in the References. Most of the traveller or early scholar accounts used in this paper are available free of charge on online platforms (last access: 22 January 2021): https://gallica.bnf.fr/ark:/12148/bpt6k28016p/f1.item.r=descriptiondel{'}egypte (Chabrol and Lancret, 1829; Le Père, 1829), https://books.google.fr/books?id=yWo3AQAAMAAJ&printsec=frontcover&hl=fr#v=onepage&q&f=false (Coste, 1878), https://gallica.bnf.fr/ark:/12148/bpt6k280140.r=descriptionel{'}egypte (Jacotin, 1824), https://gallica.bnf.fr/ark:/12148/bpt6k2991761/f9.item.r=dictionnaire%20des%20d%C3%A9couvertes%20mou%20-%20pat (Le Père, 1823), https://gallica.bnf.fr/ark:/12148/bpt6k28013n.r=descriptiondel{'}egypte (Le Père, 1825), https://books.google.de/books?id=tepYAAAAYAAJ&printsec=frontcover&hl=fr#v=onepage&q&f=false (Linant de Bellefonds, 1873), https://archive.org/details/geographicalsys00renn/page/n7/mode/2up (Rennell, 1800), https://archive.org/details/adventuresinliby00stjo/page/n7/mode/2up (St John, 1849). These URLs are also indicated in the References. Corona photographs are available free of charge at https://earthexplorer.usgs.gov/ (USGS, 2021) using the following Corona ID (also provided in Table 3): DS1016-2088DF007, DS1109-2171DF010, DS1111-2167DA024.

Author contributions. MC carried out the reassessment of sedimentological, archaeological and historical data, as well as the collection and analysis of maps, early scholars' accounts, and Corona photographs. MFB contributed to the reassessment of the archaeological and historical data, as well as to the collection of maps and early scholars' accounts. MC took charge of the writing of the paper, MFB amended and approved it.

Competing interests. The authors declare that they have no conflict of interest.

Special issue statement. This article is part of the special issue "Geoarchaeology of the Nile Delta". It is a result of the workshop "Geoarchaeology of the Nile Delta: Current Research and Future Prospects", Würzburg, Germany, 29–30 November 2019.

Acknowledgements. This study has been done as part of the French mission at Taposiris Magna and Plinthine with the kind authorisation of the Egyptian Ministry of Antiquities. We thank Bérangère Redon and Ninon Blond for their suggestions. We thank the anonymous referee and Judith Bunbury for their reviewing works. We warmly thank the editors of this special issue and the organisers of the workshop "Geoarchaeology of the Nile Delta: Current Research and Future Prospects".

Financial support. This research was funded by the French Institute of Oriental Archaeology (IFAO), HiSoMA (MOM) and the French Ministry of Foreign Affairs. The open-access publication was partly funded by DEUQUA and partly by the Shelby White and Leon Levy Program for Archaeological Publications.

Review statement. This paper was edited by Julia Meister and reviewed by Judith Bunbury and one anonymous referee.

References

AMS: El Hammam 88/42, available at: http://legacy.lib.utexas.edu/maps/ams/egypt/txu-pclmaps-oclc-6559596-el-hammam.jpg (last access: 22 January 2021), 1942.

AMS: Burg El Arab, Serie P-502, available at: http://legacy.lib.utexas.edu/maps/ams/north_africa/txu-oclc-6949452-nh35-8.jpg (last access: 22 January 2021), NH35-8, 1958.

Arrowsmith, A.: Map of Lower Egypt, available at: https://gallica.bnf.fr/ark:/12148/btv1b530669569/ (last access: 22 January 2021), 1807.

Awad, I.: A Study of the Evolution of the Maryut Lake through Maps, in: Lake Mareotis Conference: Reconstructing the past, Universities of Southampton and Alexandria, Alexandria, Egypt, 2008, edited by: Blue, L. and Khalil, E., Archaeopress, Oxford, UK, 11–33, 2010.

Bernand, A.: Le Delta égyptien d'après les textes grecs. 1 – les confins libyques, IFAO, Le Caire, 1970 (in French).

Blue, L. K. and Khalil, E.: A multidisciplinary approach to Alexandria's economic past: The Lake Mareotis research project, Archaeopress, Oxford, UK, 2011.

Boussac, M.-F.: Recent works at Taposiris and Plinthine, Bulletin de la Société archéologique d'Alexandrie, 49, 189–217, 2015.

Boussac, M.-F. and El-Amouri, M.: The lake structures at Taposiris, in: Lake Mareotis Conference: Reconstructing the past, Universities of Southampton and Alexandria, Alexandria, Egypt, 2008, edited by: Blue, L. and Khalil, E., 87–105, Archaeopress, Oxford, UK, 2010.

Boussac, M.-F. and Redon, B.: L'intégration des confins nord-ouest de l'Égypte du Nouvel Empire à l'époque ptolémaïque. À propos des découvertes archéologiques récentes à Plinthine et Taposiris Magna (côte méditerranéenne, région du lac Mariout), in: Western borders and margins of Egypt from Antiquity to the Middle Ages, edited by: Boussac, M.-F., Dhennin, S., Redon, B., Somaglino, C., and Tallet, G., IFAO press, in press, 2021 (in French).

Boussac, M.-F., Dhennin, S., and Redon, B.: Plinthine et la Maréotide Pharaonique, BIFAO, 115, 15–35, 2015 (in French).

Chabrol, G. and Lancret, M. A.: Notice topographique sur la partie de l'Egypte comprise entre Rahmanyeh et Alexandrie, et sur les environs du lac Mareotis, available at: https://gallica.bnf.fr/ark:/12148/bpt6k28016p/f1.item.r=descriptiondel'egypte (last access: 22 January 2021), in: Description de l'Égypte, C.L.F. Pancoucke, Paris, France, 18, 2, 3–28, 1829 (in French).

Coste, P.-X.: Carte de la Basse-Égypte dédiée à Mohammed Aly Pacha, available at: https://gallica.bnf.fr/ark:/12148/btv1b8491814n/ (last access: 22 January 2021), vice Roi, 1827.

Coste, P.-X.: Mémoires d'un artiste. Notes et Souvenirs de voyages (1817–1877), available at: https://books.google.fr/books?id=yWo3AQAAMAAJ&printsec=frontcover&hl=fr#v=onepage&q&f=false (last access: 22 January 2021), Marseille, Cayer et Cie, Marseille, France, 1878 (in French).

Crépy, M.: Géomorphologie et environnement du site de la nécropole de Plinthine, in: La nécropole hellénistique de Plinthine, IFAO press, Le Caire, in press, 2021 (in French).

Crépy, M.: Les Paysages du vent: géohistoire et géoarchéologie de la dépression de Kharga (désert Libyque, Égypte) du cinquième siècle avant notre ère à nos jours, PhD thesis, Université Lumière Lyon 2, France, Université de Lyon, 2 December 2016, available at: https://hal.archives-ouvertes.fr/tel-01490559/document (last access: 23 March 2017), 2016 (in French).

Dalongeville, R. and Fouache, E.: Les variations de la ligne de rivage en mer Méditerranée orientale du Pléistocène supérieur et de l'Holocène récent: réflexions, Paleo, 31, 27–38, https://doi.org/10.3406/paleo.2005.4781, 2005 (in French).

De Cosson, A.: Mareotis, Country Life Ltd., London, UK, 1935.

Décobert, C.: Maréotide médiévale. Des Bédouins et des chrétiens, Alexandrie Médiévale, 2, 139–148, 2002 (in French).

Dzierzbicka, D.: Oinos, Production and import of wine in Graeco-roman Egypt, JJP Suppl. 31, University of Warsaw, Warsaw, Poland, 2018.

El-Asmar, H. M. and Wood, P.: Quaternary shoreline development: the northwestern coast of Egypt, Quaternary Sci. Rev., 19, 1137–1149, https://doi.org/10.1016/S0277-3791(99)00097-9, 2000.

El-Falaki, M. B.: Carte des environs d'Alexandrie, available at: https://gallica.bnf.fr/ark:/12148/btv1b10101071m (last access: 22 January 2021), Erhard, Paris, France, 1866.

El-Falaki, M. B.: Mémoire sur l'antique Alexandrie, Bianco-Luno, F.-S. Mulhe, Copenhague, Denmark, 1872 (in French).

Embabi, N. S.: The geomorphology of Egypt: landforms and evolution, 1st Ed., Egyptian Geographical Society, Cairo, Egypt, 2004.

Empereur, J.-Y.: New data concerning the foundation of Alexandria, in: Hellenistic Alexandria, edited by: Zerefos, C. and Vardinoyannis, M., Archaeopress, Athens, Greece, 3–12, 2018.

Empereur, J.-Y. and Picon, M.: Les ateliers d'amphores du lac Mariout, Bulletin de Correspondance Hellénique, 33, 75–79, 1998 (in French).

Flaux, C.: Connexion de la région lagunaire d'Alexandrie au Nil depuis 2 000 ans: entre contrôle anthropique et forçage naturel, Méditerranée, 117, 73–79, https://doi.org/10.4000/mediterranee.5935, 2011 (in French).

Flaux, C.: Paléo-environnements littoraux Holocène du lac Maryut, nord-ouest du delta du Nil, Égypte, PhD thesis, Aix-Marseille, France, 2012 (in French).

Flaux, C., Morhange, C., Marriner, N., and Rouchy, J.-M.: Bilan hydrologique et biosédimentaire de la lagune du Maryût (delta du Nil, Egypte) entre 8 000 et 3 200 ans cal. B.P., Geomorphologie, 17, 261–278, https://doi.org/10.4000/geomorphologie.9474, 2011.

Fraser, P.M.: Ptolemaic Alexandria, Clarendon Press, Oxford, UK, 1972.

Flaux, C., El-Assal, M., Marriner, N., Morhange, C., Rouchy, J.-M., Soulié-Märsche, I., and Torab, M.: Environmental changes in the Maryut lagoon (northwestern Nile delta) during the last $\sim$2000 years, J. Archaeol. Sci., 39, 3493–3504, https://doi.org/10.1016/j.jas.2012.06.010, 2012.

Hairy, I. and Sennoune, O.: Le canal d'Alexandrie: la course au Nil, in Du Nil à Alexandrie: Histoire d'eaux, edited by: Hairy, I., Harpocrates Publishing, Alexandria, Egypt, 2009.

Jacotin, P.: Carte topographique de l'Égypte et de plusieurs parties des pays limitrophes, available at: https://gallica.bnf.fr/ark:/12148/btv1b531569998/f42.item (last access: 22 January 2021), Dépôt général de la Guerre, Paris, France, 1818.

Jacotin, P.: Mémoire sur la construction de la carte de l'Egypte, available at: https://gallica.bnf.fr/ark:/12148/bpt6k280140.r=descriptionel'egypte (last access: 22 January 2021), in: Description de l'Egypte, 17, 437–652, C.L.F. Pancoucke, Paris, France, 1824 (in French).

Le Père, G.: Nome Maréotique, in: Dictionnaire des Découvertes, available at: https://gallica.bnf.fr/ark:/12148/bpt6k2991761/f9.item.r=dictionnaire%20des%20d%C3%A9couvertes%20mou%20-%20pat (last access: 22 January 2021), 12, Louis Colas, Paris, France, 214–222, 1823 (in French).

Le Père, G.: Extrait d'un Mémoire sur les lacs et les déserts de la Basse Egypte, available at: https://gallica.bnf.fr/ark:/12148/bpt6k28013n.r=descriptiondel'egypte (last access: 22 January 2021), in: Description de l'Egypte, 16, 199–227, Panckoucke, Paris, France, 1825 (in French).

Le Père, G.: Mémoire sur la partie occidentale de la province de Bahyreh, connue anciennement sous le nom de nome maréotique, available at: https://gallica.bnf.fr/ark:/12148/bpt6k28016p/f1.item.r=descriptiondel'egypte (last access: 22 January 2021), in: Description de l'Egypte, 18, 29–57, Panckoucke, Paris, France, 1829 (in French).

Linant de Bellefonds, L. M. A.: Mémoires sur les principaux travaux d'utilité publique exécutés en Egypte, available at: https://books.google.de/books?id=tepYAAAAYAAJ&printsec=frontcover&hl=fr#v=onepage&q&f=false (last access: 22 January 2021), Arthus Bertrand, Paris, France, 1873 (in French).

Macklin, M. G., Toonen, W. H. J., Woodward, J. C., Williams, M. A. J., Flaux, C., Marriner, N., Nicoll, K., Verstraeten, G., Spencer, N., and Welsby, D.: A new model of river dynamics, hydroclimatic change and human settlement in the Nile Valley derived from meta-analysis of the Holocene fluvial archive, Quaternary Sci. Rev., 130, 109–123, https://doi.org/10.1016/j.quascirev.2015.09.024, 2015.

Nenna, M. D., Simony, A., Machinek, K., Soukiassian, G., Pichot, V., Awad, I., Séguier, R., Abdelaziz, M., Elsayed, M., Hairy, I., and Soubias, P.: Alexandrie (actions du Centre d'études alexandrines), Bulletin archéologique des Écoles françaises à l'étranger, Égypte, https://doi.org/10.4000/baefe.1094, 2020 (in French).

Oliver, F. W.: Dust-Storms in Egypt and Their Relation to the War Period, as Noted in Maryut, 1939–45, Geogr. J., 106, 26, https://doi.org/10.2307/1790101, 1945.

Pennington, B. T., Sturt, F., Wilson, P., Rowland, J., and Brown, A. G.: The fluvial evolution of the Holocene Nile Delta, Quaternary Sci. Rev., 170, 212–231, https://doi.org/10.1016/j.quascirev.2017.06.017, 2017.

Pichot, V.: La Maréotide: région fertile de la chôra d'Alexandrie, carrefour du commerce, in Quartiers artisanaux en Grèce ancienne, Une perspective méditerranéenne, edited by Esposito, A. and Sanidas, G., Presses Universitaires du Septentrion, Lille, France, 81–104, 2012 (in French).

Pichot, V. and Flaux, C.: Les fours à amphores du Haut-Empire du site d'Akadémia (Maréotide): campagne de fouille et carottages 2014, BCE 25, 259–276, 2015 (in French).

Pichot, V. and Simony, A.: An archaeological map of the Mareotid: initial results regarding the evolution of occupation in the region, in: Western borders and margins of Egypt from Antiquity to the Middle Ages, edited by: Boussac, M.-F., Dhennin, S., Redon, B., Somaglino, C., and Tallet, G., IFAO press, in press, 2021.

Reclus, E.: L'Afrique Septentrionale. Le Bassin du Nil, Hachette et cie, Paris, France, 1885 (in French).

Redon, B., Vanpeene, M., and Pesenti, M.: "La vigne a été inventée dans la ville égyptienne de Plinthine". À propos de la découverte d'un fouloir saïte à Kôm el-Nogous (Maréotide), Bulletin de l'Institut français d'archéologie orientale, 116, 303–323, https://doi.org/10.4000/bifao.440, 2017 (in French).

Rennell, J.: The Geographical System of Herodotus, available at: https://archive.org/details/geographicalsys00renn/page/n7/mode/2up (last access: 22 January 2021), W. Bulmer, London, UK, 1800.

Sennoune, O.: Alexandrie dans les récits de voyage, VIe–XVIIIe siècles, L'Harmattan, Paris, France, 2015 (in French).

Stanley, J.-D.: Nile delta margin: failed and fluidized deposits concentrated along distributary channels / La marge du delta du Nil: concentration de dépôts fracturés et fluidisés le long des paléochenaux fluviatiles, Geomorphology, 9, 211–226, https://doi.org/10.3406/morfo.2003.1186, 2003.

Stanley, J.-D., Goddio, F., and Schnepp, G.: Nile flooding sank two ancient cities, Nature, 412, 293–294, https://doi.org/10.1038/35085628, 2001.

St John, B.: Adventures in the Libyan Desert, available at: https://archive.org/details/adventuresinliby00stjo/page/n7/mode/2up (last access: 22 January 2021), Putnam-John Murray, New York-London, 1849.

St John, B.: Map to Illustrate a Journey from Alexandria (Egypt) to The Oasis of Siwah, available at: https://gallica.bnf.fr/ark:/12148/btv1b53136219p/ (last access: 22 January 2021) Housselin, Paris, France, 1850.

Strabo: Géographie, Livre XVII, 1re partie: l'Égypte et l'Éthiopie nilotique, text edited and translated by Laudenbach, B., Les Belles Lettres, Paris, France, 2015.

Survey of Egypt: Mudiriyet El-Beheira, available at: https://www.davidrumsey.com/luna/servlet/detail/RUMSEY~8~1~317305~90086593:Sheet-47-Bahig (last access: 22 January 2021), Sheet of the 1:50,000 series, Bahîg V-VI N.W., 1910.

Tronchère, H.: Approche paléoenvironnementale de deux sites archéologiques dans le delta du Nil: Avaris et la branche Pélusiaque, Taposiris et le lac Mariout, PhD thesis, Lumière Lyon 2, Lyon, France, 2010 (in French).

Tronchère, H., Millet, B., Goiran, J.-P., Carbonel, P., Djerbi, H., Vera, R., Torab, M., Elassal, M., and Callot, Y.: Geoarchaeological results from the harbor of Taposiris and implications concerning the construction of the harbor, AEundL, 22–23, 383–394, https://doi.org/10.1553/s383, 2014.

Tsoar, H. and Pye, K.: Dust transport and the question of desert loess formation, Sedimentology, 34, 139–153, https://doi.org/10.1111/j.1365-3091.1987.tb00566.x, 1987.

US Geological Survey (USGS): EarthExplorer, available at: https://earthexplorer.usgs.gov/, last access: 22 January 2021.

Warne, A. and Stanley, J.-D.: Late Quaternary Evolution of the Northwest Nile Delta and Adjacent Coast in the Alexandria Region, Egypt, J. Coastal Res., 9, 26–64, 1993.

Woronko, B.: Late-Holocene dust accumulation within the ancient town of Marea (coastal zone of the South Mediterranean Sea, N Egypt), Quaternary Int., 266, 4–13, https://doi.org/10.1016/j.quaint.2011.09.010, 2012.

E&G Quaternary Sci. J., 70, 53–71, 2021
https://doi.org/10.5194/egqsj-70-53-2021

Open Access E&G Quaternary Science Journal

Research article

A comparison of polymineral and K-feldspar post-infrared infrared stimulated luminescence ages of loess from Franconia, southern Germany

Neda Rahimzadeh[1], Tobias Sprafke[2], Christine Thiel[3], Birgit Terhorst[4], and Manfred Frechen[1]

[1]S3 Geochronology, Leibniz Institute for Applied Geophysics, Hannover, 30655, Germany
[2]Institute of Geography, University of Bern, Bern, 3012, Switzerland
[3]Federal Seismological Survey, Federal Institute for Geosciences and Natural Resources, Hannover, 30655, Germany
[4]Institute of Geography and Geology, Julius-Maximilians University of Würzburg, Würzburg, 97074, Germany

Correspondence: Neda Rahimzadeh (neda.rahimzadeh@leibniz-liag.de)

Relevant dates: Received: 22 July 2020 – Revised: 24 November 2020 – Accepted: 26 November 2020 – Published: 8 February 2021

How to cite: Rahimzadeh, N., Sprafke, T., Thiel, C., Terhorst, B., and Frechen, M.: A comparison of polymineral and K-feldspar post-infrared infrared stimulated luminescence ages of loess from Franconia, southern Germany, E&G Quaternary Sci. J., 70, 53–71, https://doi.org/10.5194/egqsj-70-53-2021, 2021.

Abstract: Loess-paleosol sequences (LPSs) are essential records for reconstructing Quaternary paleoenvironments. No previous study has provided numerical chronologies of loess in Lower Franconia, southern Germany; their chronostratigraphic assumptions have relied mainly on German (pedo)stratigraphic schemes. In this study, we provide for the first time a chronology for LPSs in Lower Franconia based on optically stimulated luminescence (OSL) dating using quartz and a comparison of K-feldspar (63–100 µm) and the polymineral fraction (4–11 µm). Our results show that all obtained ages are in stratigraphic order, ranging from Holocene to late Pleistocene, and in general confirm the former stratigraphical interpretations. A good agreement of the obtained ages is observed between both feldspar grain size fractions; they also agree well with the quartz OSL ages up to ~ 50 ka. However, a marked difference between the growth pattern of the dose response curves and consequently different saturation characteristics of fine and coarse grains is found. Even though in our samples the discrepancy in ages is not very significant, we suggest the use of coarse-grained K-feldspar whenever possible in order to not be confronted with unknowns such as the mineral composition of the polymineral fraction.

Kurzfassung: Löss-Paläoboden-Sequenzen sind wichtige Archive zur Rekonstruktion der quartären Umwelt. Bisher hat sich noch keine Arbeit mit der numerischen Chronologie mainfränkischer Lösse befasst; die bisherigen chronostratigraphischen Einordnungen haben ihren Ursprung in deutschen (pedo)stratigraphischen Schemata. In der vorliegenden Arbeit stellen wir erstmals eine auf optisch stimulierter Lumineszenz (OSL) basierende Chronologie für Löss-Paläoboden-Sequenzen in Mainfranken vor. Hierzu wurden Quarz und in vergleichender Weise sowohl K-Feldspat (63–100 µm) als auch die polymineralische Feinkornfraktion (4–11 µm) verwendet. Unsere Ergebnisse zeigen, dass alle gewonnenen Alter in stratigraphischer Reihenfolge sind, vom Holozän bis zum Spätpleistozän, und generell die früher angenommenen stratigraphischen Interpretationen stützen. Eine gute Altersübereinstimmung liegt für die beiden Feldspatfraktionen vor; die Alter stimmen weiterhin mit den Quarz-OSL-Altern bis 50 ka überein. Im Vergleich von Feldspat-Grobkorn und Feinkorn (polymineralische Fraktion) zeigt sich bei jedoch ein stark voneinander abweichendes Verhalten in den Wachstumsverläufen der Dose Response Curves und ein sich daraus ergebendes unterschiedliches Sättigungsverhalten. Auch wenn die Unterschiede für die hier vorliegenden Proben nicht übermäßig groß sind, so empfehlen wir, wenn immer möglich, die Verwendung von grobkörnigem K-Feldspat für die Datierung, um nicht mit möglichen Unbekannten, wie der Mineralzusammensetzung von polymineralischen Extrakten konfrontiert zu sein.

1 Introduction

Loess-paleosol sequences (LPSs) are complex terrestrial archives of Quaternary landscape evolution that are widely distributed in the temperate zone, allowing for regionalization of past climatic changes and providing information of paleo-geoecological responses to paleoclimatic shifts (Sprafke, 2016). Despite its wide distribution and well-differentiated profiles, loess in Lower Franconia (Germany; Fig. 1) remains poorly studied (Brunnacker, 1956; Semmel and Stäblein, 1971; Skowronek, 1982; Rösner, 1990). Accessible LPSs have been untouched from systematic investigation for 3 decades, and numerical ages are lacking. Current chronological assumptions are only possible by correlating previously identified pedostratigraphic units with the German loess (pedo)stratigraphic scheme (Schönhals et al., 1964; Semmel, 1968) and related chronostratigraphies recently updated by Lehmkuhl et al. (2016); the first well-developed Bt horizon below the present day soil is supposed to represent the Eemian (128–115 ka) paleosol affected by periglacial reworking. One to three early glacial (EG; 115–72 ka) humic horizons (Mosbach Humuszones, MHZs) are superimposed by lower Pleniglacial (LPG; 60–72 ka) colluvial deposits (Niedereschbach Zone, NEZ) and loess. The middle Pleniglacial (MPG; 60–32 ka) is mainly represented by weak to moderate paleosols (Lohne soil, LS, on the top) alternating with loess. The upper Pleniglacial (UPG; 32–15 ka), sometimes characterized by reworked horizons at the base, contains the thickest loess deposits with intercalated tundra gley soils (Erbenheim soils, En), in which the late glacial (LG; 15–11 ka) to Holocene (< 11 ka) pedogenesis took place.

To test the validity of pedostratigraphic and thus the preliminary chronostratigraphic assumptions in the area of investigation from the 1970s to late 1980s (e.g., Semmel and Stäblein, 1971; Rösner, 1990), numerical geochronological methods are crucial. Our study provides the first optically stimulated luminescence (OSL) ages of loess from Lower Franconia (NW Bavaria, Germany). OSL dating enables the determination of the time elapsed since the last exposure of sediment to sunlight (Aitken, 1998), and it has been successfully applied for determining the depositional age of eolian deposits, such as loess (e.g., Roberts, 2008). However, in the case of (paleo)soils, OSL dating helps us to understand the timing and rates of soil mixing. Quartz and potassium feldspar are the two most widely used minerals in OSL dating. Although quartz has been found to be a robust and accurate dosimeter (Murray and Olley, 2002), its application is commonly limited to the last 100–150 kyr (Wintle and Murray, 2006). In the quest for extending this limitation, feldspar infrared stimulated luminescence (IRSL) has been suggested. However, the use of feldspar as a dosimeter has major drawbacks including signal loss of IRSL during burial, known as anomalous fading (Spooner, 1994), which can lead to age underestimation. This problem can be accounted for by using IR signals less affected by fading, the so-called post-IR IRSL (hereafter pIRIR) (Thomsen et al., 2008), and post-measurement fading correction models (Huntley and Lamothe, 2001; Kars et al., 2008).

The majority of luminescence dating studies on loess deposition in Europe is based on quartz OSL signals and different IRSL signals from fine-grained (4–11 µm) samples (e.g., Austria: Thiel et al., 2011a, b; Hungary: Novothny et al., 2011; Croatia: Wacha et al., 2011; Germany: Schmidt et al., 2011; Zens et al., 2018; Poland: Moska et al., 2018; Serbia: Fuchs et al., 2008; Schmidt et al., 2010; Romania: Vasiliniuc et al., 2012, 2013; Belgium: Frechen et al., 2001). In contrast, many OSL dating studies of Chinese loess deposits have focused on sand-sized K-rich feldspar extracts (Li and Li, 2012; Buylaert et al., 2015; Yi et al., 2015, 2016; Stevens et al., 2018). Recent comparative studies on the quartz OSL signal from different grain size fractions indicate different saturation characteristics and subsequently different growth pattern of the dose response curve for different fractions and consequently age discrepancies (Timar-Gabor et al., 2011, 2015; Timar-Gabor and Wintle, 2013; Constantin et al., 2015). Using the multi-elevated temperature post-IR IRSL (MET-pIRIR) protocol, Fu et al. (2012) showed consistent results between polymineral fine-grain (FG) and K-feldspar coarse-grain (CG) MET-pIRIR ages for Chinese loess samples. However, there is a lack of direct comparison of obtained IRSL ages for two different grain size fractions extracted from Central European loess. There are few comparative studies about the characteristics of the IRSL signal from polymineral FGs and polymineral, K-feldspar and Na-feldspar CGs (Tsukamoto et al., 2012; Zhang and

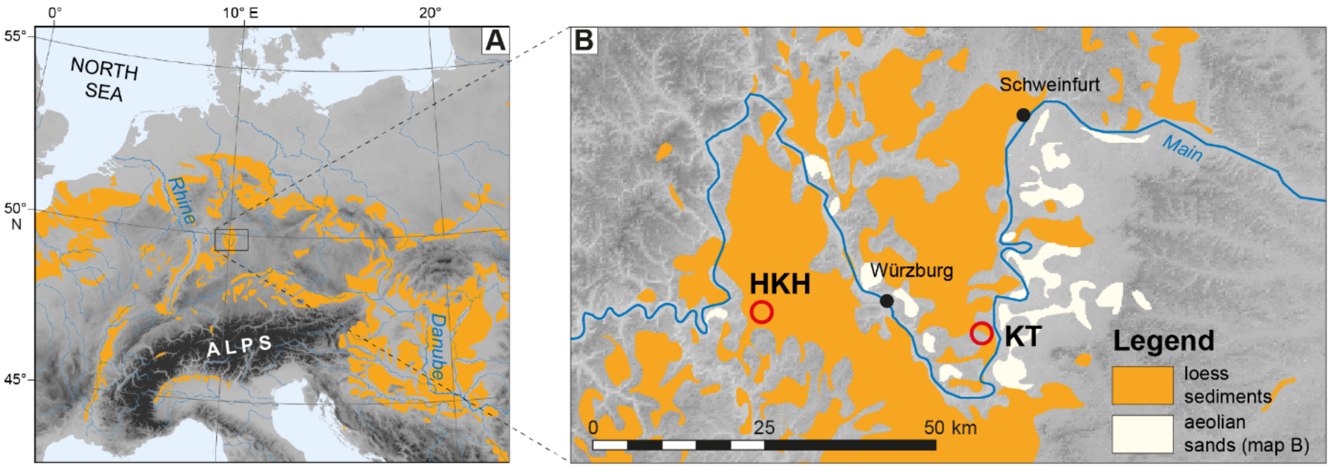

Figure 1. (a) Distribution of loess and loess derivates (loess sediments) in Central Europe modified according to Haase et al. (2007) and Sprafke (2016); **(b)** studied sections (red circles) of Holzkirchhausen (HKH) and Kitzingen (KT) in the Lower Franconian loess region. Loess sediments and eolian sands distribution modified from Lehmkuhl et al. (2018).

Li, 2019). Tsukamoto et al. (2012) demonstrate that in both blue and UV detection windows, IRSL and pIRIR signals in polymineral FGs mainly originate from Na-feldspar grains when a lower preheat temperature (260–300 °C) is being used. However, Zhang and Li (2019) showed that the standardized growth curves (SGCs) of the K-feldspar, plagioclase and polymineral CGs are very similar in shape and are distinctly different in shape from the polymineral FG SGCs.

In this paper, we aim to present a robust luminescence chronology of Lower Franconian LPSs using pIRIR stimulated at 225 °C (hereafter $pIRIR_{225}$) for different grain size fractions and test the reliability of both FG and CG $pIRIR_{225}$ ages. When possible, the fast component quartz OSL ages were determined to assess which $pIRIR_{225}$ ages from different grain size fractions are more accurate. Based on our results of luminescence dating, we then investigate the validity of chronostratigraphic assumptions based on the use of German loess (pedo)stratigraphic schemes.

2 Study area context and logging

The studied sections are located on the Mainfranken plateau, an undulating to hilly plain 220 to 400 m a.s.l. (above sea level) made up of Middle Triassic limestones, marls and claystones with a few intercalated sandstone layers. The plateau is incised by the Main river and its tributaries flowing with large deviations in its course from E to W (220 m to 140 m a.s.l., respectively; Fig. 1). Shielded from Atlantic moisture by the highland chain of Odenwald, Spessart and Rhön (400–900 m a.s.l.), annual precipitation is < 600 mm. Loess sediments of a few decimeters to more than 10 m thickness cover the plateau. Only a very few profiles investigated during the last century (Rösner, 1990) are accessible; among these, we studied the well-resolved, presumably Late Pleistocene profiles of Kitzingen (KT; ca. 20 km SE of Würzburg) and Holzkirchhausen (HKH; ca. 20 km W of Würzburg) (Fig. 2). Our reconnaissance surveys revealed the presence of most of the stratigraphic units previously reported in the literature.

The LPS KT (Fig. 2a, d, e and f) is exposed at the former Pavel and Becker loam pit 2.5 km west of Kitzingen city on the northern side of the road to Kaltensondheim (236 m a.s.l.; profile KTM, 49°44′7.98″ N, 10°7′43.51″ E). The road follows the bottom of the asymmetric valley of the Eherieder Bach, a small tributary to the Main river (Fig. 2a). The valley cuts Middle Triassic claystones, marls (lower Keuper) and limestone (Muschelkalk). Old maps show that the loam extraction has advanced since the investigations of Semmel and Stäblein (1971) and Rösner (1990). Only the upper 4 to 5 m of the up to 12 m thick LPS are available due to the partial filling of the pit (Fig. 2d and e). Sketches of the former outcrop by Semmel and Stäblein (1971) and Rösner (1990) testify to the large lateral variability of stratigraphic units (Fig. 2d). The presumably Eemian paleosol formed in over 5 m thick, weakly differentiated penultimate glacial loess. Up to two MHZs separated by a clayey, greenish colluvial layer of local material (Keuperfliesserde; KFE) are present in the central part of the SW-facing outcrop. An erosive colluvial phase led to the erosion of a major part of the MHZs and even the last interglacial Bt horizon in the W part of the outcrop, leaving a reddish-brown colluvial layer (NEZ) there. A few decimeters of loess and a moderately developed paleosol, referred to as LS, are superimposed (Rösner, 1990; Semmel and Stäblein, 1971). Thick UPG loess is found in a paleo-depression which is incised into the early glacial sequence in the E part of the outcrop. In total, three profiles were excavated in the outcrop (Fig. 2d and f). KTE (3 m thick) exposes the youngest loess deposits in the paleo-depression of the eastern part of the outcrop, whereas KTM ca. 35 m fur-

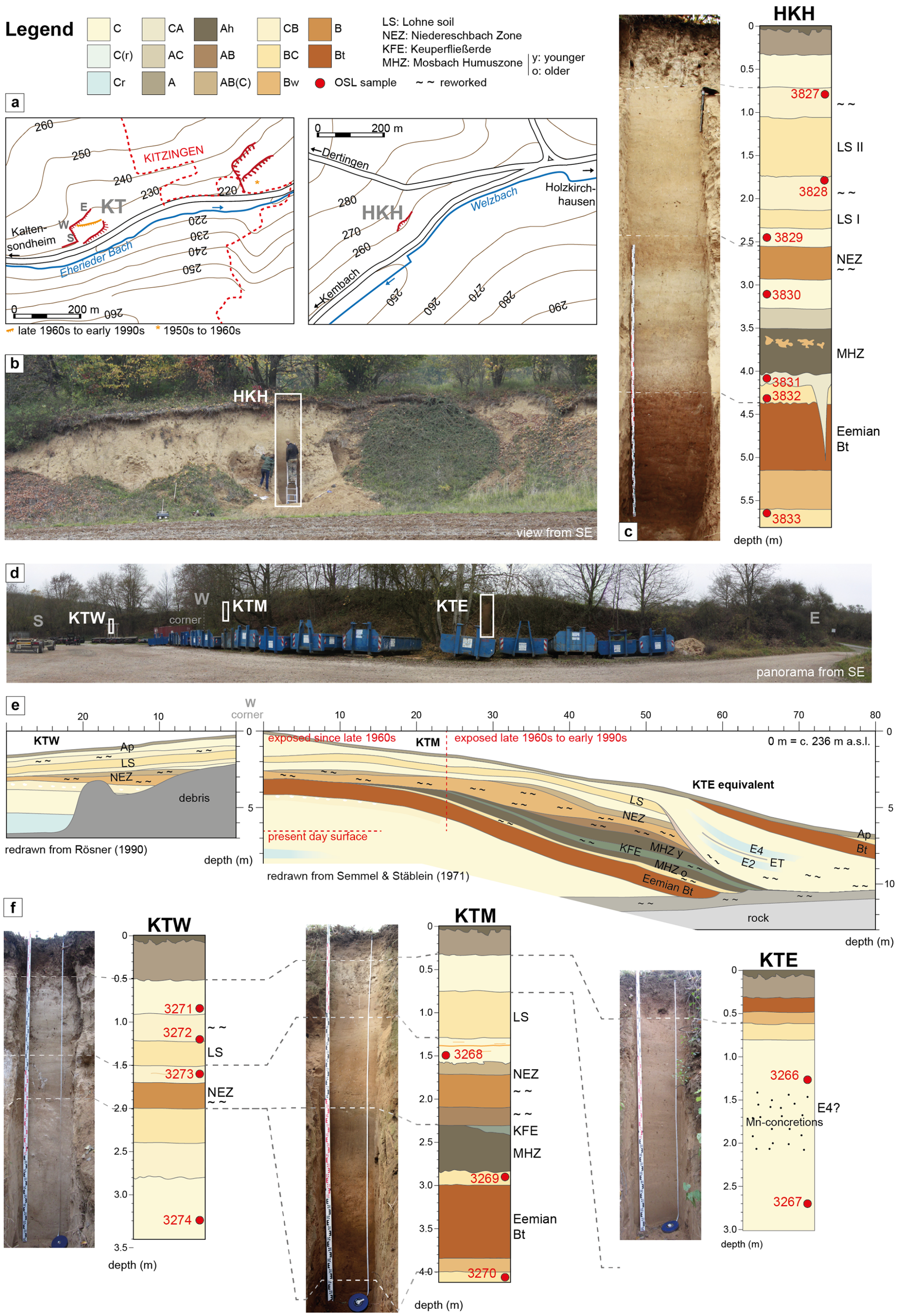

Figure 2. Profiles and sample locations. **(a)** Local topography of KT and HKH. Note for KT the location of the old brickyard studied by Brunnacker (1959) and the location of the outcrop wall studied by Semmel and Stäblein (1971). **(b)** Overview photo of HKH outcrop. **(c)** Photo and HKH profile sketch with position of OSL samples and laboratory codes. **(d)** KT today with the locations of three studied profiles: KTE, -M and -W. **(e)** Outcrop sketches of the exposed E wall (Rösner, 1990) and the exposed S wall (Semmel and Stäblein, 1971); the latter shifted further north in the 1990s (Fig. 2a). **(f)** Photos and sketches of the studied KT profiles with the position of OSL samples with laboratory codes.

ther west (4.2 m thick) allows access to all major units of the standard stratigraphy (i.e., LS, NEZ, MHZs, Eemian Bt) down to the penultimate glacial loess. KTW (3.5 m thick) is situated in the exposed E outcrop wall with a major hiatus between the NEZ and the penultimate glacial loess according to Rösner (1990).

The LPS HKH (Fig. 2a–c; Holzkirchhausen II according to Rösner, 1990) is located in a small former loam pit 1.5 km west of the village of Holzkirchhausen at 265 m a.s.l. (49°45′31.89″ N, 9°38′50.01″ E). It is situated on a SE-facing smooth slope ca. 70 m north of the road to Kembach, which is located downstream of the Kembach valley (Fig. 2a). The local geology is made up of Lower Triassic red claystone covered by loess sediments of varying thickness. The outcrop is ca. 10 m wide and shows little lateral variation, with the lower horizons dipping slightly towards the west (Fig. 2b). According to Skowronek (1982), the strongly developed basal paleosol of HKH overlies the local claystone, but in our profile, this paleosol developed in loess sediments. Rösner (1990) provides a detailed description of the profile (her Holzkirchhausen II profile). The pedostratigraphic designations follow the standard nomenclature of SW and central Germany (Schönhals et al., 1964; Semmel, 1968) outlined above and marked in Fig. 2c. The main features of the HKH profile are the Eemian Bt horizon at the bottom, one MHZ separated from the NEZ by loess and a twofold LS. There is no indication of thick upper Pleniglacial loess at this location.

All four profiles were thoroughly cleaned and described in the field based on color, grain size and structural properties using pedological horizon designations by the FAO (2006) in the way suggested by Sprafke (2016). At both sites, the previously defined pedostratigraphic units could be unambiguously traced except for the Erbenheim soils in the paleodepression in the E part of the KT outcrop. Pedostratigraphic units by Semmel and Stäblein (1971) and Rösner (1990), as well as sample locations including laboratory codes, are shown in Fig. 2f.

3 Luminescence dating

3.1 Sampling, sample preparation and analytical facilities

Luminescence samples were taken from selected stratigraphic units (Fig. 2c and f) by hammering 15–20 cm long steel tubes into freshly cleaned outcrop walls. For paleosol horizons, samples were taken from loess units above and below the well-developed soil horizon (Bt horizon), providing an upper and lower age limit of the soil formation.

Sample preparation for luminescence measurements was carried out under subdued red light at the Leibniz Institute for Applied Geophysics (LIAG), Hannover. The outer ~ 2 cm at the ends of the tubes was removed, and the inner material was treated with hydrochloric acid (HCl; 10 %) to remove carbonate, with sodium oxalate (0.1 N) to dissolve aggregates and with hydrogen peroxide (H_2O_2, 30 %) to remove organic matter. It should be noted that the chemical treatment was done for each grain size fraction separately, i.e., two sediment subsamples were prepared. For the polymineral FG fractions, the 4–11 µm grain size fraction was separated by repeated settling and washing using a centrifuge (cf. Frechen et al., 1996). For the coarse-grain fractions, the 63–100 µm grain size fraction was isolated by wet sieving. Quartz and potassium-rich feldspar grains were then separated using a heavy liquid solution (sodium polytungstate; quartz: $\rho \geq 2.62\,\mathrm{g\,cm^{-3}}$; K-feldspar: $\rho \leq 2.58\,\mathrm{g\,cm^{-3}}$). The quartz fraction was further treated with concentrated hydrofluoric acid (40 %) for 1 h to remove any remaining feldspar and the alpha-irradiated outer layer. Subsequently, the purified quartz was treated with HCl (20 %) for about 1 h to dissolve any fluorides which might have built up during HF etching.

For luminescence measurements, the quartz and K-feldspar extracts were mounted as aliquots 2.5 mm in diameter on stainless steel disks using silicone spray as adhesive. The polymineral fraction was settled from deionized water to aluminum disks. All equivalent dose (D_e) measurements and relevant tests were performed on automated luminescence readers (Risø TL/OSL DA-20; Thomsen et al., 2006) equipped with arrays of blue (470 ± 30 nm) and infrared (870 ± 40 nm) LEDs and calibrated ^{90}Sr/^{90}Y beta sources. The beta sources of the readers were calibrated for both coarse and fine grains. The luminescence signal from quartz grains was detected through a 7.5 mm Hoya U-340 filter and the K-feldspar and polymineral (post-IR) IRSL signals through a combination of Schott BG-39/Corning 7-59 filters (blue-violet light spectrum between 320 and 450 nm).

3.2 Dose rate determination

The supplementary material taken from the direct surrounding of each sample was dried, crushed for homogenization, filled into 50 g N-type beakers, sealed and stored for at least 4 weeks to ensure equilibrium between radon and its daughter nuclides. The radionuclide concentrations (^{238}U, ^{232}Th and ^{40}K) were subsequently measured by high-resolution gamma spectrometry; the results are summarized in Table 1. The dose rate conversion factors of Guerin et al. (2011) and beta attenuation factors of Mejdahl (1979) were used for dose rate calculation. A small cosmic dose rate of ~ 0.1–$0.2\,\mathrm{Gy\,kyr^{-1}}$ was calculated based on Prescott and Hutton (1994) and Prescott and Stephan (1982). Water content was assumed to be 20 ± 5 % for samples collected from the well-developed pedocomplexes and loess below (i.e., LUM 3269, 3270, 3274, 3831, 3832 and 3833) and 15 ± 5 % for all other samples. These values are in accordance with loess studies from the Neckar region ca. 100 km southwest of our study area with comparable physicogeographical conditions (e.g., Zens et al., 2018). The large error in this estimate is used to account for the possible alterations in water content over geological time. It should also be noted that some of the dose rate uncertainties originate from the difficulty in cosmic dose rate and water content estimation due to variable thickness of overburden sediments over burial time and climatic conditions over that period, respectively. For the coarse-grained feldspar extracts, an additional internal beta dose rate was calculated based on an internal potassium content of 12.5 ± 0.5 % (Huntley and Baril, 1997) and a rubidium content of 400 ± 100 ppm (parts per million; Huntley and Hancock, 2001). As the outer layer of the coarse-grained quartz was removed by HF etching, the contribution of alpha radiation was not taken into account. An a value of 0.08 ± 0.02 (Rees-Jones, 1995) and 0.11 ± 0.02 (Kreutzer et al., 2014) was applied for FG polymineral and CG K-feldspar grains, respectively.

3.3 Equivalent dose measurement

3.3.1 Post-IR IRSL measurements

A single aliquot regenerative (SAR) post-IR IRSL measurement procedure was employed for the D_e determination of K-feldspar CG and polymineral FG samples. The procedure uses a preheat of 250 °C for 60 s and a first IR stimulation at 50 °C for 100 s (IR_{50} signal), followed by a second IR stimulation at 225 °C for 100 s ($pIRIR_{225}$ signal; Buylaert et al., 2009). The test dose was ∼ 50 and ∼ 250 Gy for young and old samples, respectively. In order to reduce the effect of recuperation, an IR illumination at 290 °C for 40 s was applied at the end of each measurement cycle. The first ∼ 3 s of stimulation minus a background from the last ∼ 10 s was used to construct the dose response curves (DRCs). Dose response curves were fitted using a single exponential function. Full DRCs were obtained from one aliquot per sample (Fig. 3). The dose response and decay curves of the $pIRIR_{225}$ signals of both the CG K-feldspar and FG polymineral for two representative samples (LUM 3266 and LUM 3270; uppermost and lowermost sample) are shown in Fig. 3.

To determine the equivalent doses, six aliquots per sample (both for CG K-feldspar and FG polymineral) were measured. The mean recycling ratios generated from CG K-feldspar and FG polymineral were 1.001 ± 0.004 and 1.005 ± 0.004, respectively, and recuperation was below 2 %, therefore well within the acceptable range (Murray and Wintle, 2003).

The reliability of the $pIRIR_{225}$ protocol was checked by means of dose recovery tests for each sample using six aliquots previously bleached for 4 h in a Hönle SOL2 solar simulator. To test whether a given dose could be accurately recovered, three bleached aliquots were then given a dose similar to the natural equivalent dose, and subsequently the $pIRIR_{225}$ measurement procedure described above was applied. The other bleached aliquots were used for the measurement of the residual dose after bleaching in the solar simulator. Figure 4a and b shows a summary histogram of the measured-to-given dose ratio, with a mean of 0.94 ± 0.01 for CG K-feldspar and 0.96 ± 0.01 for FG polymineral, which is within the suggested range of 0.9–1.1 (Wintle and Murray, 2006). All the measured residual doses were negligible (≤ 6 Gy) with respect to the measured D_e values; they were not subtracted from the measured D_e values for the final age calculation.

To test the athermal stability of the feldspar signals, fading experiments following Auclair et al. (2003) were run on the aliquots previously used for dose recovery tests. The fading rate is expressed by the g value, where g is the percentage signal loss per decade of time (Aitken, 1985). We applied two fading correction models. The Huntley and Lamothe (2001) fading correction model was used for samples for which the luminescence ages are < 50 ka and correspond to the linear part of DRC (Huntley and Lamothe, 2001). The fading correction for samples with ages up to field saturation was performed using the Kars et al. (2008) fading correction model, which is known to correct anomalous fading for older samples with ages in the nonlinear part of the DRC (Li et al., 2019).

3.3.2 Blue OSL measurements

First, the purity of quartz samples was checked by examining the IR depletion ratio (Duller, 2003), which was for all samples within 10 % of unity, indicating that there is no significant feldspar contribution to the OSL signal.

The quartz D_e values were obtained using a SAR protocol (Murray and Wintle, 2000, 2003). In order to select the most appropriate thermal treatment, preheat plateaus were measured on two representative samples (LUM 3266, KT; LUM 3827, HKH). The temperatures were set to 160–280 °C with an interval of 20 °C; the cut heat was 20 °C lower than the preheat temperature. A preheat of 260 °C (10 s) and a cut heat of 240 °C (0 s) was selected for the final D_e measurements, which were then conducted on 12 aliquots per sample. The test dose used for all samples was ∼ 10 Gy. At the end of each SAR cycle, a high-temperature blue light illumination (280 °C for 60 s) was carried out.

For D_e calculations, the signal integrated over the initial ∼ 0.4 s minus the immediate ∼ 0.5–1.5 s (early background subtraction; Cunningham and Wallinga, 2010) was used, and the DRC were fitted using a single saturating exponential function (Fig. 6). The characteristic saturation dose (D_0) of ∼ 80 Gy suggests that the upper dose limit for quartz signal is about 160 Gy. Since most of the samples were found to be in saturation ($D_e > 2D_0$; Wintle and Murray, 2006; Fig. 6b), the quartz ages were obtained for six samples only, all of which are expected to be in the datable range according to the field stratigraphy. For all samples, recycling was < 10 %, and recuperation was < 5 %. The suitability of the protocol was tested by means of dose recovery tests on three aliquots per sample. Prior to measurements, the aliquots were bleached in the luminescence reader using two blue stimulations for 1000 s separated by a 10 000 s pause. The aliquots were then

Table 1. Summary of the present burial depths, radionuclide concentrations, and calculated quartz (Qz), K-feldspar CGs (K-fsp) and polymineral FGs (poly.) dose rates.

LUM no.	Site	Depth (m)	U (ppm)	Th (ppm)	K (%)	Total dose rate Qz (Gy kyr^{-1})	Total dose rate K-fsp (Gy kyr^{-1})	Total dose rate poly. (Gy kyr^{-1})
3266	KT	1.30	3.6 ± 0.2	11.8 ± 0.7	1.6 ± 0.1	2.96 ± 0.21	3.88 ± 0.17	4.00 ± 0.24
3267		2.70	3.6 ± 0.2	12.2 ± 0.7	1.6 ± 0.1	2.94 ± 0.20	3.86 ± 0.17	3.40 ± 0.24
3268		1.50	3.2 ± 0.2	11.9 ± 0.7	1.7 ± 0.1	2.97 ± 0.20	3.87 ± 0.17	3.96 ± 0.24
3269		2.90	3.8 ± 0.2	14.6 ± 0.9	1.8 ± 0.1	3.12 ± 0.20	4.04 ± 0.16	4.25 ± 0.25
3270		4.05	3.1 ± 0.2	11.8 ± 0.7	1.8 ± 0.1	2.85 ± 0.20	3.74 ± 0.16	3.77 ± 0.22
3271		0.85	3.2 ± 0.2	10.7 ± 0.6	1.5 ± 0.1	2.68 ± 0.19	3.58 ± 0.16	3.62 ± 0.23
3272		1.20	3.3 ± 0.2	11.0 ± 0.6	1.4 ± 0.1	2.67 ± 0.19	3.57 ± 0.16	3.62 ± 0.23
3273		1.60	3.5 ± 0.2	12.7 ± 0.7	1.6 ± 0.1	3.01 ± 0.21	3.93 ± 0.17	4.08 ± 0.25
3274		3.30	3.1 ± 0.2	11.2 ± 0.7	1.7 ± 0.1	2.69 ± 0.20	3.57 ± 0.16	3.58 ± 0.22
3827	HKH	0.80	3.5 ± 0.2	13.1 ± 0.7	1.5 ± 0.1	2.92 ± 0.20	3.84 ± 0.17	4.00 ± 0.25
3828		1.80	3.5 ± 0.2	12.6 ± 0.7	1.4 ± 0.1	2.77 ± 0.19	3.69 ± 0.17	3.83 ± 0.24
3829		2.45	3.1 ± 0.2	12.2 ± 0.7	1.5 ± 0.1	2.74 ± 0.19	3.63 ± 0.16	3.72 ± 0.23
3830		3.10	3.0 ± 0.2	10.8 ± 0.6	1.4 ± 0.1	2.51 ± 0.18	3.39 ± 0.16	3.41 ± 0.22
3831		4.05	3.8 ± 0.2	14.5 ± 0.8	1.6 ± 0.0	2.93 ± 0.20	3.86 ± 0.16	4.05 ± 0.25
3832		4.30	3.4 ± 0.2	14.2 ± 0.8	1.9 ± 0.1	3.06 ± 0.21	3.97 ± 0.17	4.12 ± 0.24
3833		5.65	3.7 ± 0.2	15.2 ± 0.8	2.1 ± 0.1	3.33 ± 0.23	4.25 ± 0.17	4.47 ± 0.25

given a dose close to the expected D_e value and measured using the same SAR protocol. For all samples, the dose recovery ratio falls within 10 % of unity (Fig. 5b).

4 Results and discussion

4.1 CG K-feldspar and FG polymineral D_e and apparent pIRIR ages

The D_e values of 16 samples from two different sections were measured using the $pIRIR_{225}$ protocol for FG polymineral and CG K-feldspar multi-grain aliquots, and the measurement results and calculated ages are listed in Table 2. The non-fading-corrected final $pIRIR_{225}$ D_e values for FG polymineral samples range between 72 ± 1 and 393 ± 12 Gy (KT) and 124 ± 1 and 431 ± 12 Gy (HKH), with corresponding ages ranging from 18 ± 1 to 110 ± 7 ka (KT) and 31 ± 2 to 97 ± 6 ka (HKH). The non-fading-corrected final $pIRIR_{225}$ D_e values determined for CG K-feldspar samples range between 59 ± 1 and 357 ± 10 Gy and 111 ± 1 and 379 ± 11 Gy, with corresponding ages ranging from 15 ± 1 to 100 ± 5 ka and 29 ± 1 to 89 ± 4 ka, for KT and HKH, respectively.

4.2 Fading correction

Fading measurements indicate significantly different fading behavior between the $pIRIR_{225}$ and the corresponding $IRSL_{50}$ signals with a mean $g_{2\,d}$ value of 4.0 ± 0.2 % for the $IRSL_{50}$ signals and a mean $g_{2\,d}$ value of 1.9 ± 0.10 % for the $pIRIR_{225}$ signals (Fig. 7a, d). It is interesting to note that the fading rates of FG polymineral samples, both IR_{50} and $pIRIR_{225}$, are slightly lower than the fading rates of CG K-feldspar samples (Fig. 7d, e and f), which implies a higher athermal stability of the FG polymineral luminescence signals. The observed difference in fading rate may originate from the Na-feldspar grains in the mineralogical composition of the FG extracts which tend to have lower fading rates (Huntley et al., 2007; Huot and Lamothe, 2012); however, it has to be noted that none of the associated papers report the detection window that was used in their study. For the $pIRIR_{225}$ signals of the FG polymineral samples, the mean $g_{2\,d}$ value is 1.8 ± 0.1 % per decade (Fig. 7b), which is lower than the $g_{2\,d}$ value of the $pIRIR_{225}$ signal for CG K-feldspar samples (2.2 ± 0.1 % per decade; Fig. 7c).

The Huntley and Lamothe (2001) fading correction model was applied to all samples for which the non-fading-corrected $pIRIR_{225}$ ages are < 40 ka (Table 2). The fading-corrected CG K-feldspar $pIRIR_{225}$ ages vary from 18 ± 1 to 26 ± 2 ka (KT) and 34 ± 2 to 39 ± 3 ka (HKH), while the fading-corrected FG polymineral $pIRIR_{225}$ ages are between 21 ± 2 and 30 ± 3 ka (KT) and 31 ± 2 and 39 ± 3 ka (HKH) (Table 2).

The Kars et al. (2008) fading correction model was applied to the other samples. The final corrected $pIRIR_{225}$ ages range from 67 ± 7 to 160 ± 17 ka (KT) and from 61 ± 7 to 144 ± 14 ka (HKH) for CG K-feldspar samples and from 70 ± 7 to 163 ± 21 ka (KT) and from 68 ± 13 to 165 ± 21 ka (HKH) for FG polymineral samples (Table 2).

4.3 Dose response curves and saturation characteristics of different grain size fractions

Based on the age calculation for both FG polymineral and CG K-feldspar, all calculated ages are stratigraphically consistent within errors, which allows us to have a reasonable

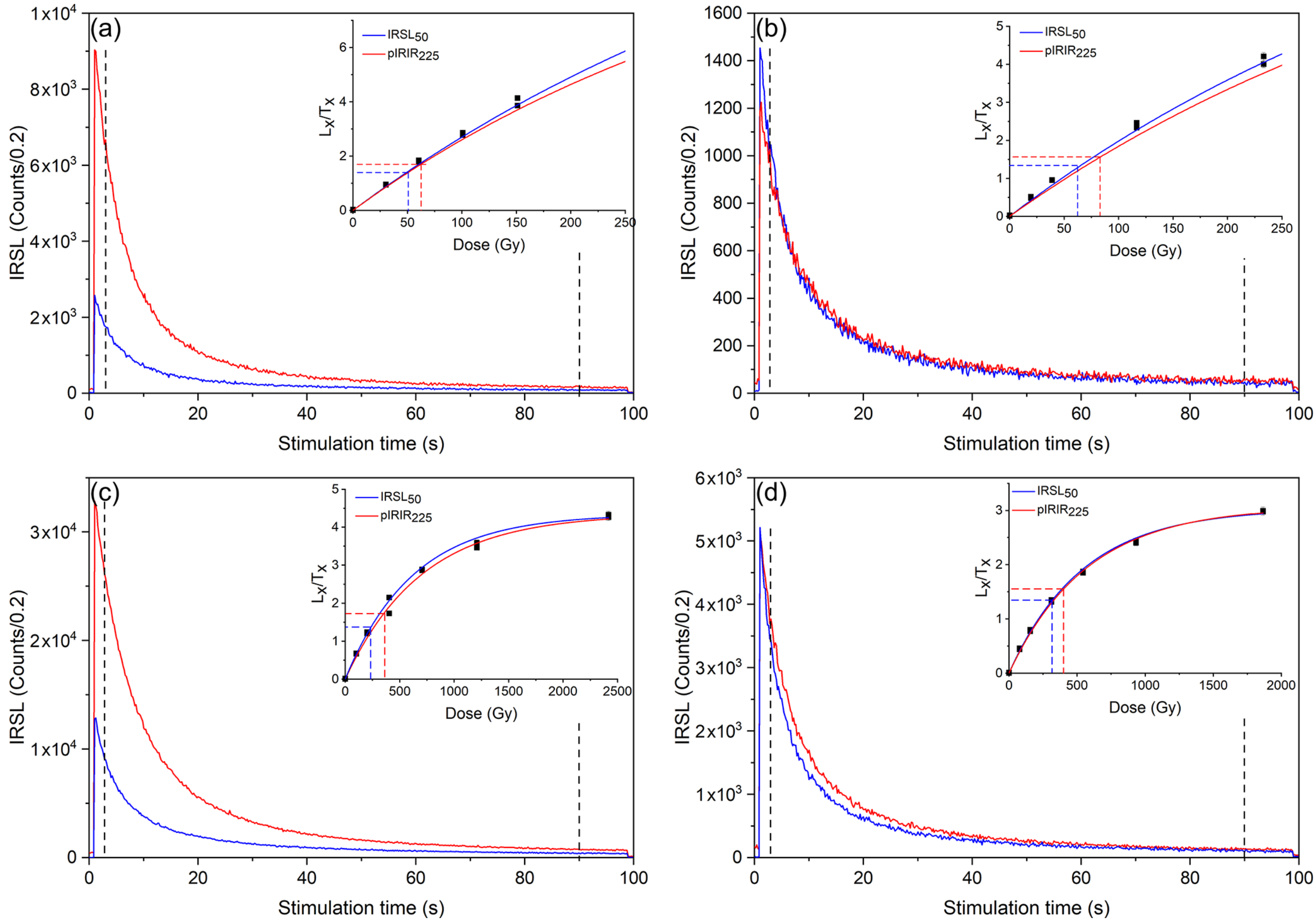

Figure 3. Example of **(a, c)** CG K-feldspar and **(b, d)** FG polymineral natural IRSL decay curves for $pIRIR_{225}$ (in red) and its associated IR_{50} (in blue) signals, with the corresponding dose response curve in the inset, for the representative samples (**a, b**: LUM 3266 and **c, d**: LUM 3270). The integration intervals are denoted by the dashed black line.

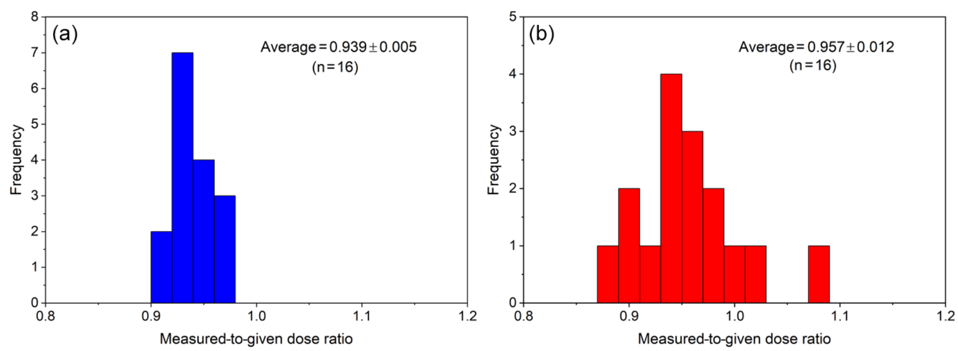

Figure 4. Summary of measured-to-given dose ratios for **(a)** the K-feldspar CG and for **(b)** the polymineral FG $pIRIR_{225}$ signals.

degree of confidence in these ages. The fading-corrected FG polymineral and CG K-feldspar $pIRIR_{225}$ ages agree within uncertainty (1σ) for all of the samples (Fig. 8, Table 2).

The comparison of the natural DRCs of FGs and CGs for the lowermost samples (LUM 3270 and 3833, KT and HKH, respectively; Fig. 9c, d) shows different saturation characteristics of the fine-grained fraction compared to coarse-grain DRCs and a large divergence in shape and growth of DRCs which may cause the age discrepancy. Although the DRCs of the two grain sizes investigated also have the different shape for the youngest samples (LUM 3266 and 3828, KT and HKH, respectively; Fig. 9a, b), this discordance is less

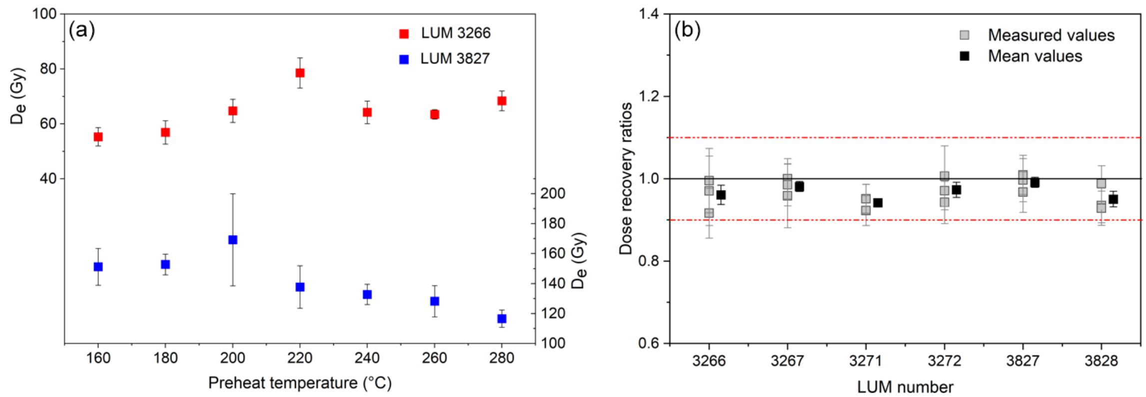

Figure 5. **(a)** Preheat plateau using varying preheat temperatures conducted on two representative samples (LUM 3266, 3827); **(b)** dose recovery test conducted on all measured quartz samples.

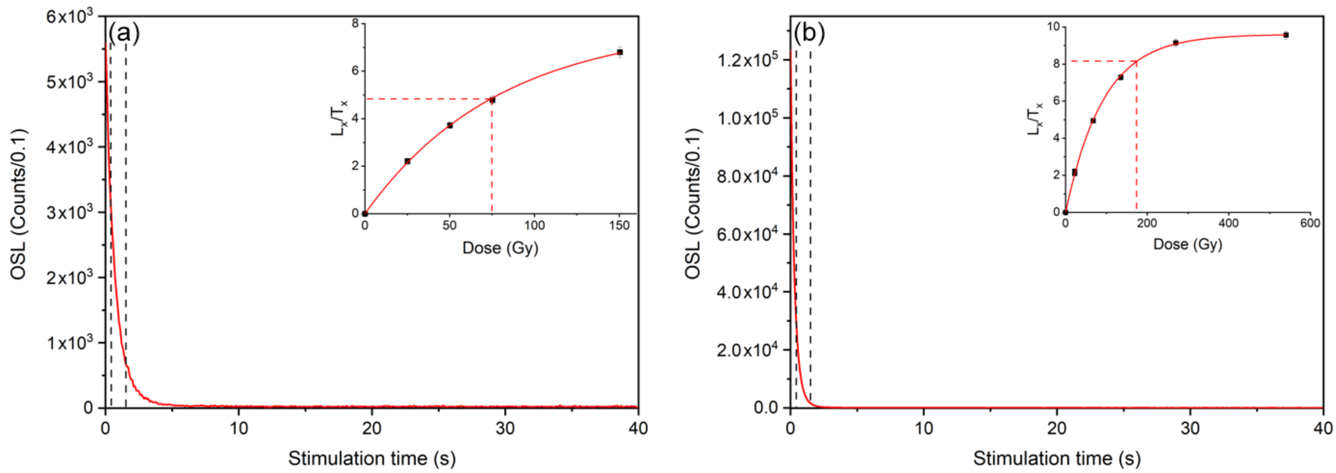

Figure 6. Natural blue OSL decay curve and dose response curve (inset) for representative young and old samples, respectively (**a**: LUM 3266 and **b**: LUM 3268 with quartz OSL signal in saturation). The integration intervals are denoted by the dashed black line.

problematic as the obtained D_e values lie in the linear region of the DRCs. Furthermore, different D_0 values of FG and CG samples were observed (Fig. S1 in the Supplement). In particular, the K-feldspar CG fractions yield much larger D_0 values than the polymineral FG fractions for most of the samples except for the four youngest samples of KT (LUM 3266, 3267, 3271, 3272), which is consistent with previous observations (Li et al., 2019; Zhang and Li, 2019). These observations suggest that the pIRIR signals from CG K-feldspar may allow for the dating of even older samples compared to FG; this, however, has not been systematically tested. Zhang and Li (2019) attributed this discordance between the FG and CG SGCs to either the difference in alpha irradiation received in nature – as the grain size decreases, the surface / volume ratio increases, and so more alpha irradiation will be received – or the removal of the alpha irradiated outer layer of CGs using HF. Interestingly, Timar-Gabor et al. (2017) reported negative correlations between D_0 values of DRCs of quartz and grain size.

4.4 Quartz OSL ages: age comparison

The robustness of derived luminescence ages from FG polymineral and CG K-feldspar measurements remains uncertain and would need additional supporting chronological data to be validated. For studied samples without independent age control, reliable fast component quartz OSL ages can be obtained at least up to 40–50 ka (maximum D_e of about 120–150 Gy; Buylaert et al., 2007). Since most of the quartz samples are close to or beyond saturation (Fig. 6b), quartz ages are only presented for those samples for which $D_e < 2D_0$ ($\sim$ 160 Gy) (Wintle and Murray, 2006). The OSL ages of these samples are then considered the most reliable age estimates available to evaluate the accuracy of both FG polymineral and CG K-feldspar pIRIR_{225} dating.

Quartz OSL ages are available for the six youngest samples; the ages range from 22 ± 2 ka (LUM 3266; KT) to 43 ± 4 ka (LUM 3828; HKH) (Table 2). In Fig. 10, a comparison of quartz OSL ages with FG and CG pIRIR_{225} ages is shown. There is a similar trend for both sets of pIRIR ages; most of

Table 2. Equivalent doses (Gy) and ages (ka) for quartz OSL, K-feldspar CG (K-fsp) and polymineral FG (poly.) pIRIR$_{225}$. The corrected CG pIRIR$_{225}$ ages are being used for discussion. For details see text.

LUM no.	D_e OSL (Gy)	D_e pIRIR225 (K-fsp) (Gy)	D_e pIRIR225 (poly.) (Gy)	pIRIR$_{225}$ age (ka) uncorr. (K-fsp)	pIRIR$_{225}$ age (ka) uncorr. (poly.)	Quartz age (ka)	pIRIR$_{225}$ age (ka) corr. (K-fsp)	pIRIR$_{225}$ age (ka) corr. (poly.)
3266	64.5 ± 2.6	58.7 ± 0.5	71.6 ± 1.0	15.1 ± 0.7	17.9 ± 1.1	21.8 ± 1.8	18.2 ± 1.3	20.5 ± 1.7
3267	78.7 ± 3.3	69.5 ± 1.7	83.1 ± 2.1	18.0 ± 0.9	20.8 ± 1.4	26.8 ± 2.2	20.1 ± 1.5	23.7 ± 2.2
3268	166.4 ± 19.4	173.4 ± 3.6	196.0 ± 6.0	44.8 ± 2.2	49.5 ± 3.4	> 56*	66.7 ± 6.7	69.8 ± 7.3
3269	–	281.6 ± 11.5	294.7 ± 41.4	69.6 ± 4.0	69.4 ± 10.5	–	110 ± 13	102 ± 20.8
3270	–	352.6 ± 12.7	388.9 ± 11.2	94.4 ± 5.3	103 ± 7	–	160 ± 17	154 ± 18
3271	66.5 ± 5.3	68.0 ± 0.8	81.8 ± 1.0	19.0 ± 0.9	22.6 ± 1.5	24.8 ± 2.7	22.6 ± 1.6	27.5 ± 2.4
3272	84.0 ± 6.1	79.5 ± 1.1	97.6 ± 1.3	22.3 ± 1.1	26.9 ± 1.8	31.5 ± 3.2	26.0 ± 1.9	30.1 ± 2.7
3273	163.3 ± 12.1	166.1 ± 5.0	203.5 ± 6.0	42.3 ± 2.2	50.0 ± 3.3	> 55*	59.7 ± 7.7	69.5 ± 8.7
3274	–	356.8 ± 10.1	392.9 ± 11.6	99.8 ± 5.2	110 ± 7	–	149 ± 16	163 ± 21
3827	119.0 ± 5.4	110.8 ± 1.3	124.4 ± 1.2	28.9 ± 1.3	31.1 ± 1.9	40.8 ± 3.3	34.2 ± 2.4	31.2 ± 2.2
3828	119.2 ± 5.6	116.7 ± 1.4	130.2 ± 2.9	31.7 ± 1.5	34.0 ± 2.3	43.0 ± 3.6	39.0 ± 2.7	38.8 ± 3.3
3829	184.2 ± 1.9	171.3 ± 3.5	202.1 ± 6.9	47.2 ± 2.3	54.3 ± 3.9	> 68*	61.1 ± 6.5	68.1 ± 12.9
3830	–	157.1 ± 4.2	190.2 ± 7.0	46.3 ± 2.5	55.7 ± 4.2	–	64.6 ± 6.9	73.0 ± 8.6
3831	–	236.0 ± 8.5	286.7 ± 8.8	61.4 ± 3.4	70.8 ± 4.8	–	93.0 ± 10.4	97.5 ± 12.6
3832	–	301.7 ± 10.5	365.2 ± 9.8	76.1 ± 4.1	88.6 ± 5.8	–	107 ± 12	129 ± 14
3833	–	378.8 ± 10.5	431.2 ± 11.6	89.0 ± 4.4	96.5 ± 6.1	–	144 ± 14	165 ± 21

* Minimum ages due to saturation of the quartz OSL signal.

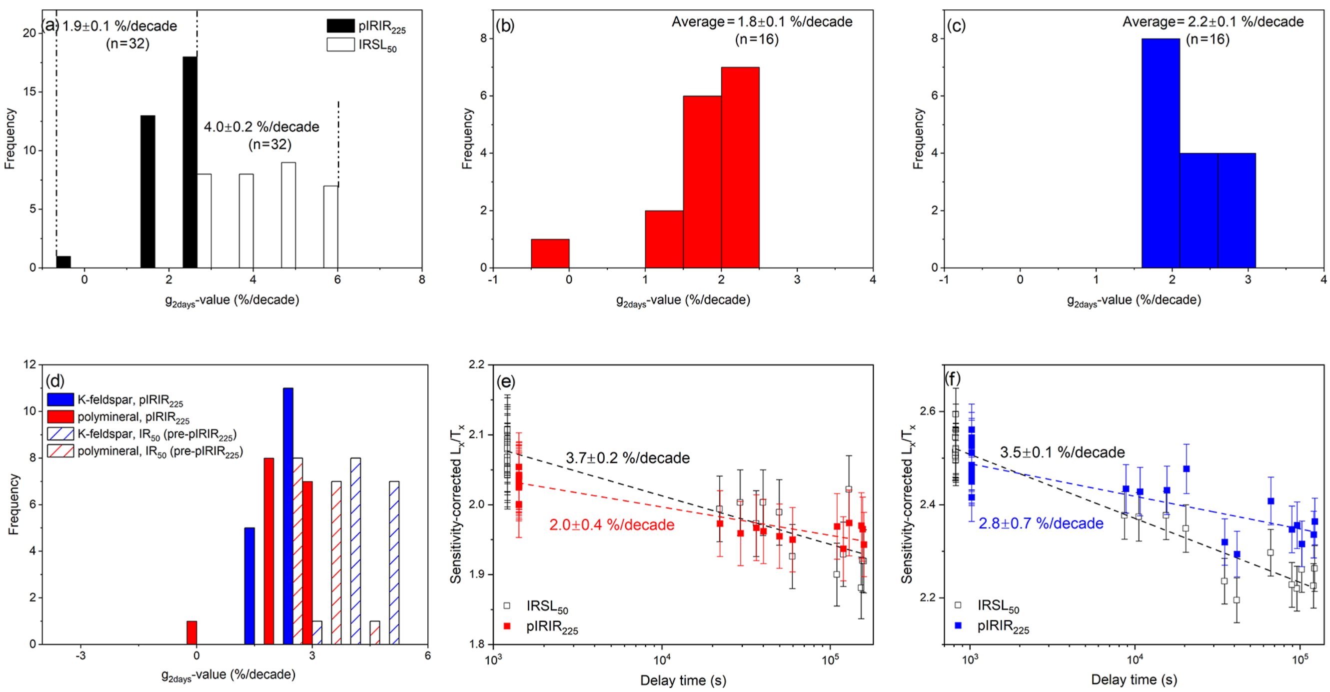

Figure 7. Histogram summarizing average fading rates of **(a)** IR$_{50}$ and pIRIR$_{225}$, **(b)** FG polymineral of pIRIR$_{225}$, **(c)** CG K-feldspar of pIRIR$_{225}$, and **(d)** anomalous fading of IR$_{50}$ (pre-pIR$_{225}$) and pIRIR$_{225}$ signals of both grain size fractions for all samples; fitting of luminescence sensitivity and delay time of IR$_{50}$ and pIRIR$_{225}$ for **(e)** FG polymineral and **(f)** CG K-feldspar for sample LUM 3270.

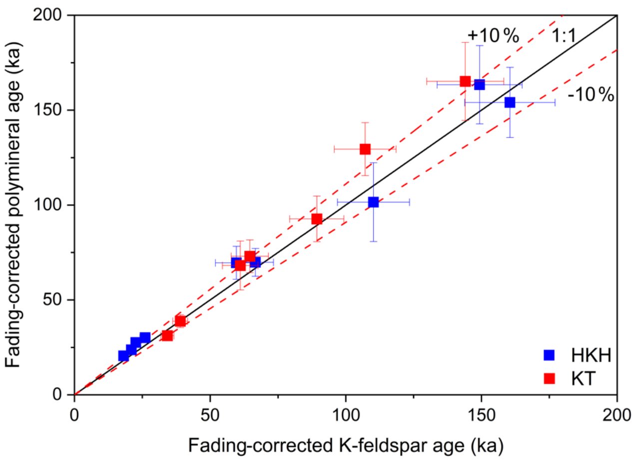

Figure 8. Comparison of CG K-feldspar $pIRIR_{225}$ ages with FG polymineral $pIRIR_{225}$ ages for KT (in red) and HKH (in blue). The solid line is the 1 : 1 line, and the dotted red lines represent ±10 %.

the pIRIR ages agree with corresponding quartz OSL ages within 1σ uncertainty except one CG sample (LUM 3267) and one FG sample (LUM 3271) which both agree within 2σ uncertainty. These observations are in agreement with the results of Fu et al. (2012). They used the MET-pIRIR protocol for Late Pleistocene Chinese loess samples and indicated that the MET-pIRIR ages of FG polymineral samples are consistent with the CG K-feldspar MET-pIRIR ages, quartz OSL ages and stratigraphic ages. Moreover, the comparison of ages derived from quartz OSL and pIRIR signals further verifies the fully bleached $pIRIR_{225}$ signals, considering that the quartz OSL signal bleaches much faster than any IRSL signal; the post-IR IRSL signal bleaches more slowly than the $IRSL_{50}$ signal (Buylaert et al., 2012; Murray et al., 2012; Colarossi et al., 2015; Möller and Murray, 2015). Frouin et al. (2017) compared the FG polymineral ages with CG K-feldspar ages and quartz OSL ages (Guérin et al., 2015) in order to evaluate bleaching and thus distinguish the depositional processes. Their results showed that the FG $pIRIR_{290}$, CG $pIRIR_{290}$ and quartz OSL ages agree for most of the samples except for two samples which are attributed to colluvium deposits and for which CG ages significantly overestimate the FG and quartz ages. For those two layers, the consistency between their FG $pIRIR_{290}$ ages and CG $pIRIR_{160}$ ages suggested that the fine grains may have been sufficiently exposed to sunlight, considering that the bleachability of the IRSL signals decrease with increasing stimulation temperature (Poolton et al., 2002; Buylaert et al., 2012; Colarossi et al., 2015; Tsukamoto et al., 2017).

4.5 Thermoluminescence experiments: origin of the signals

It has consistently been reported that the intensity of elevated temperature pIRIR signals of K-feldspar is much higher than the prior IRSL signal at low temperature (Thomsen et al., 2008; Buylaert et al., 2009). However, the intensity of the $pIRIR_{225}$ signals of polymineral fine grains is similar to or lower than that of the prior $IRSL_{50}$ signal (Fig. 3a, c) which was also observed by Wacha and Frechen (2011) and Thiel et al. (2011b) for loess from Croatia and Austria, respectively, but is in contrast to other studies (e.g., Thiel et al., 2011a). Tsukamoto et al. (2012) suggested that the effect of stimulation temperature might be different between K-feldspar and polymineral fine grains resulting in different signal intensities. One possible explanation might be related to different luminescence properties for feldspar in different grain size fractions and mineral compositions as the IRSL signal of the FG polymineral fraction is mainly derived from Na-rich feldspar (Tsukamoto et al., 2012). We therefore examined the thermoluminescence (TL) glow curves and loss of TL signal after IR stimulation in order to explore the origin of the IRSL and pIRIR signals and investigate the relationship between IRSL and TL signals (Duller, 1995; Murray et al., 2009; Tsukamoto et al., 2012). An aliquot of two representative samples (LUM 3270 and 3833) was mounted as loose grains in stainless steel cups and sensitized through repeated cycles of irradiation and annealing. The TL response to a ∼ 40 Gy regenerative dose was then measured in four sets of experiments: after a preheat of 60 s at 250 °C (set 1), IR stimulation at 50 °C for 100 s (set 2), hold temperature at 225 °C for 200 s (set 3) and pIRIR stimulation at 225 °C for 200 s (set 4). TL glow curves up to 500 °C with a heating rate of 5 °C s^{-1} were measured and the background signal measured during a second heating was subtracted. The lost TL resulting from IR and pIRIR stimulations was obtained by the difference between two TL glow curves, i.e., one measured without and one measured with IR stimulation (TL set 1/set 3 – TL set 2/set 4; Tsukamoto et al., 2012).

Figure 11 shows the TL signals from a CG K-feldspar and FG polymineral sample (LUM 3833) following various IRSL and pIRIR stimulations. The TL glow curves are shown in Fig. 11a and b and the loss of TL due to IRSL and pIRIR stimulations in Fig. 11c and d. Similar results were also observed for sample LUM 3270. The regenerated TL signal after a preheat with no IR stimulation shows a peak centered at ∼ 350 °C for both grain size fractions. However, a tail of the higher temperature was observed in the FG polymineral sample. The IR stimulation at 50 °C clearly depletes the main peak at ∼ 350 °C while simultaneously optically transferring charge into low-temperature TL peaks. The TL peak position after IR stimulation at 50 °C in FG polymineral samples shifted slightly to the higher temperature region (i.e., ∼ 380 °C). The holding of the sample at 225 °C for 200 s resulted in a small reduction in the peak intensity at the lower temperature side. The TL peak after IR stimulation at 225 °C remains unaffected in the CG K-feldspar sample. However, a small reduction in the TL peak at the lower temperature region was observed in the FG polymineral sample. In general, the FG polymineral sample shows an asymmetrical peak

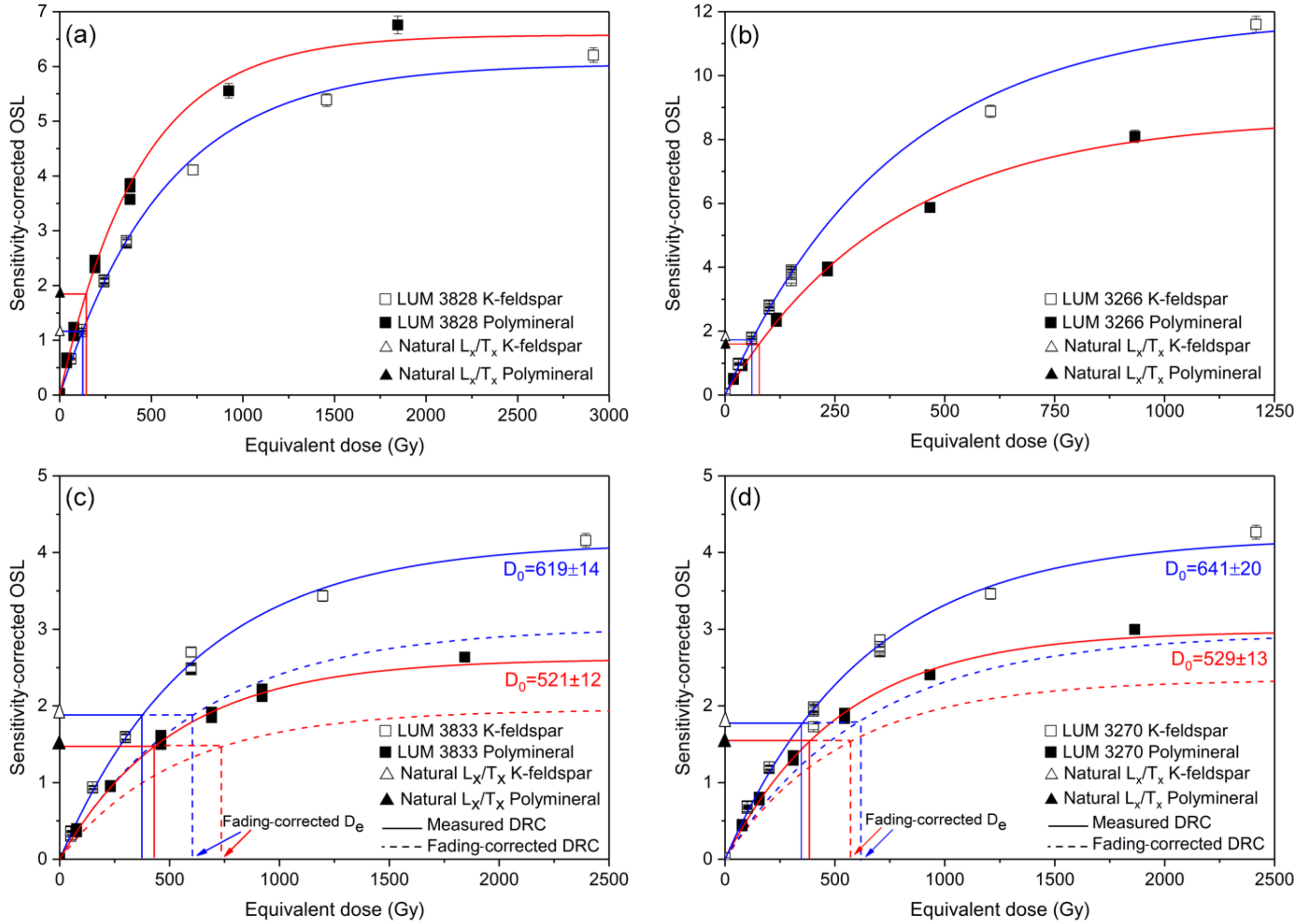

Figure 9. Dose response curves of **(a, b)** uppermost samples and **(c, d)** lowermost samples from HKH and KT, respectively. The fading-corrected DRCs for the two lowermost samples **(c, d)** was constructed following Kars et al. (2008), and fading-corrected D_e values were determined by interpolating the natural intensity onto the fading-corrected DRCs.

at ∼ 380 °C with the shoulder on the higher temperature and a tail spreading up to 500 °C. In contrast, the CG K-feldspar sample shows a narrower TL peak than FG polymineral samples at ∼ 350 °C, with an absence of a higher temperature shoulder. The lost TL curves (Fig. 11c, d) further show which regions of the glow curve are reduced by the IR and pIRIR stimulations. A peak centered at ∼ 340–350 °C was obtained, indicating the TL component at ∼ 350 °C is the most IR sensitive and is the main source of IR-bleachable TL peaks, which is in agreement with conclusions of Li and Li (2011) and Wang et al. (2014). Tsukamoto et al. (2012) observed a double TL loss peak at 320 and 410 °C after IRSL with a preheat at 250 °C for K-feldspar samples but with the complete absence of the 410 °C peak for the polymineral sample. Murray et al. (2009) demonstrated that the main source of the IRSL signal following a preheat at both 320 and 250 °C is an IR-bleachable TL peak at 410 °C in K-feldspar, which is not observed in our sample. A negative TL peak at low temperature, which is a reflection of phototransfer, indicates the recharging of electron traps during IR stimulation. The phototransfer of charge into low temperature TL peaks located between 100 and 300 °C during IR stimulation has also been reported by others (Duller, 1995; Murray et al., 2009; Li and Li, 2011). The main depletion in TL due to pIRIR occurs at ∼ 320 °C for FG polymineral, slightly higher than that of CG K-feldspar (∼ 310 °C). Tsukamoto et al. (2012) showed that the main TL loss peaks during pIRIR stimulation at 225 °C are situated at lower temperature for Na-feldspar and polymineral samples (∼ 320 °C) but at higher temperature for K-feldspar samples (∼ 410 °C). They therefore concluded that IRSL and pIRIR signals in polymineral FGs originate mainly from Na-feldspar grains. However, our results showed the similarity in TL loss peak temperature (∼ 320 °C) for both FG polymineral and CG K-feldspar samples.

It should be remembered that feldspars are chemically and structurally complex and display a broad range of compositions, which caused a broad range of thermoluminescence

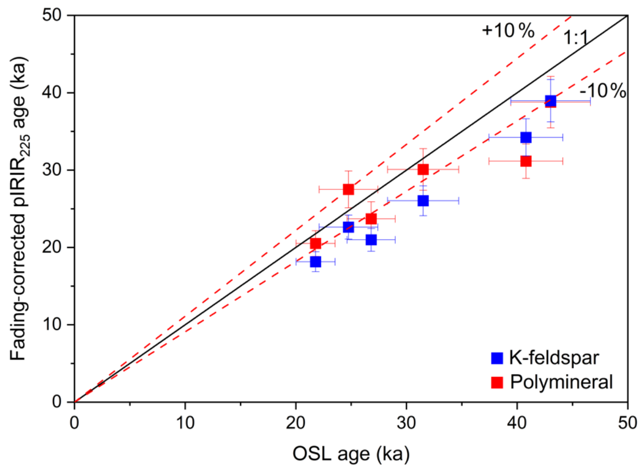

Figure 10. Comparison of quartz OSL ages with CG K-feldspar (in blue) and FG polymineral (in red) $pIRIR_{225}$ ages. The solid line is 1 : 1 line, and the red dotted lines represent ±10 %.

peaks and luminescence behavior (Duller, 1997). Duller (1995) showed that the TL signal loss during IR stimulation for 6000 s increased from high potassium to high sodium contents, and so physical separation of the different types of the feldspar is necessary. The standard approach to isolate a restricted range of mineralogies is density separation using heavy liquid (Wintle, 1997). K-feldspar minerals (2.53–2.56 $g\,cm^{-3}$) are separated by heavy liquid (of density < 2.58 $g\,cm^{-3}$) since they are lighter than plagioclase (> 2.61 $g\,cm^{-3}$) and Na-feldspar (2.58–2.62 $g\,cm^{-3}$). However, it should be noted that other studies (i.e., scanning electron microscopy with energy dispersive X-ray spectroscopy, SEM-EDX; X-ray diffractometry, XRD; and inductively coupled plasma optical emission spectroscopy, ICP-OES) have indicated that Na-feldspar grain contamination in the K-rich fraction and vice versa is possible (Huot and Lamothe, 2012; Tsukamoto et al., 2012; Sohbati et al., 2013; Thiel et al., 2015). Therefore, investigating the mineral composition in more detail, e.g., SEM-EDX, may be a powerful approach to assess the OSL behavior of the samples. If carrying out an assessment of the mineral composition is not possible, the use of a high temperature preheat, i.e., $pIRIR_{290}$, is suggested since similar behavior and stability of the same signal from the different types of feldspar were observed (Tsukamoto et al., 2012). However, because of bleaching problems resulting in large residuals (either in nature or as laboratory artifacts) and additionally a poor dose recovery of the $pIRIR_{290}$ signal (Tsukamoto et al., 2017), the $pIRIR_{290}$ protocol has to be used cautiously.

As the agreement with quartz OSL is equally satisfactory for the younger samples, it is difficult to judge which fraction gives the most reliable ages in the higher dose region. Since the FG polymineral fraction contains different components and therefore its signal might include contributions from other minerals of which luminescence properties are poorly known (Feathers et al., 2012), preference should be given to CG K-feldspar as a dosimeter. It is acknowledged that in our study the obtained ages from different grain size fractions are in agreement and thus seem equally reliable, but to facilitate reading, we exclusively use CG K-feldspar $pIRIR_{225}$ ages in the following discussion.

4.6 Relation between pedostratigraphy and luminescence chronology

Figure 12 summarizes the obtained numerical ages from the investigated loess sections with their pedostratigraphic designations used by Rösner (1990) and compares these to the German loess stratigraphic scheme, including the chronology suggested by Lehmkuhl et al. (2016) and Zens et al. (2018). It should be noted that all OSL ages from the studied profiles are in stratigraphical order, ranging from 18(±1) to 160(±17) ka for KT and 34(±2) to 144(±14) ka for HKH. This confirms the pedostratigraphic interpretation of Semmel and Stäblein (1971) and Rösner (1990) that both LPSs mainly represent the Late Pleistocene to Holocene.

The three profiles in Kitzingen capture distinct parts of the laterally variable outcrop. The youngest OSL samples were obtained from KTE, exposing loess sediments deposited in a paleo-depression younger than the LS (Semmel and Stäblein, 1971). The samples (LUM 3266 and 3267) gave an age of 18.2 ± 1.3 and 20.1 ± 1.5 ka, respectively, suggesting loess accumulation during the UPG, specifically during and after the last glacial maximum (LGM). The UPG is known as the period with the highest accumulation rate of dust in Europe during the last glacial (Frechen et al., 2003). Tundra gleys or the Eltville Tephra (ET) reported from a profile wall 20–30 m further south (Semmel and Stäblein, 1971; cf. Fig. 2a) were not clearly visible in the studied profile. Due to the absence of clear stratigraphic markers, we are unable to evaluate the reliability of the luminescence ages in more detail.

According to Semmel and Stäblein (1971), KTM contains the main elements of the Late Pleistocene pedostratigraphy between PUG loess at the bottom and a thin package of UPG loess with remnants of the surface soil at the top. The uppermost sample (LUM 3268) is taken from a ca. 30 cm thick loess package between the LS and NEZ. The location is below a ca. 1 cm thick brown clayey band of unclear origin in the middle of this loess layer. The age of 66.7 ± 6.7 ka agrees with pedostratigraphic reasoning that this unit represents LPG (60–72 ka) loess that formed directly after the NEZ (Lehmkuhl et al., 2016; Zens et al., 2018). Sample LUM 3269 between the MHZs of the EG period and a well-developed Bt horizon attributed to the Eemian was dated to 110 ± 13 ka. This agrees with the stratigraphic assumption that this horizon represents post-Eemian colluvial deposits (Semmel and Stäblein, 1971). The loess deposits from the bottom of KTM, just below the thick Bt horizon assigned to the Eemian in previous works, yielded an age of 160 ± 17 ka (sample LUM 3270) corresponding to the PUG.

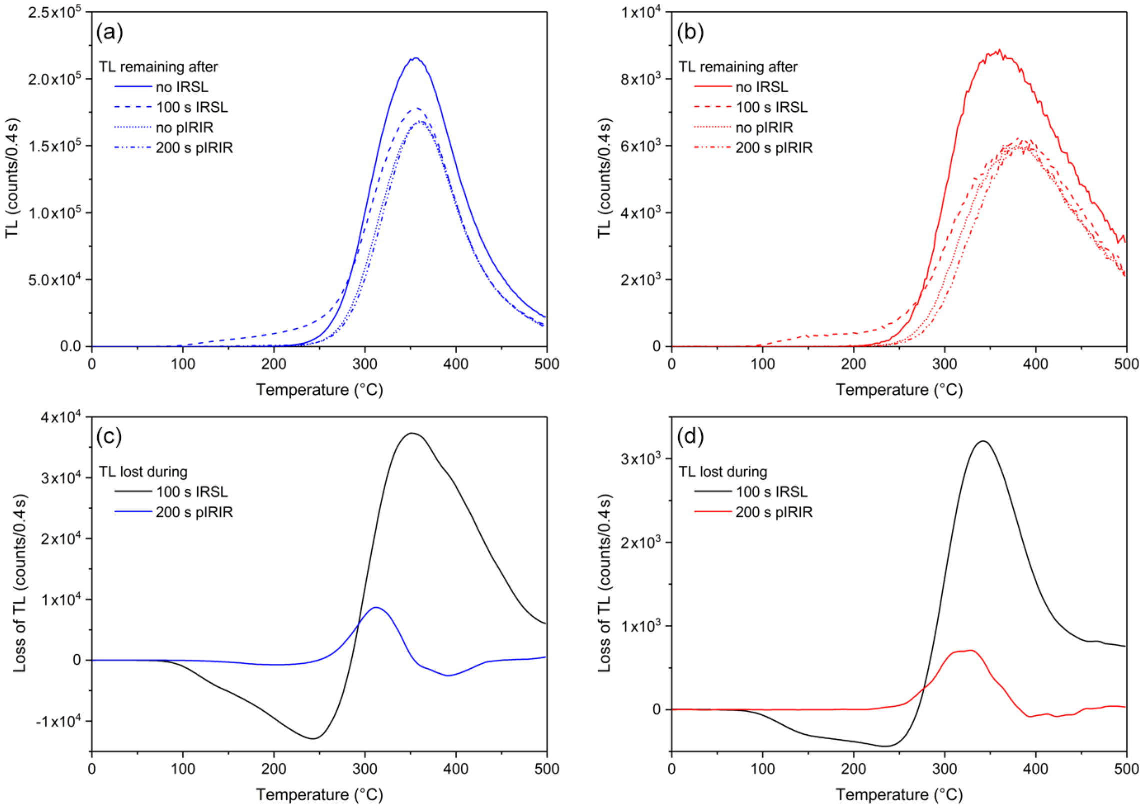

Figure 11. **(a, b)** TL glow curve from **(a)** CG K-feldspar and **(b)** FG polymineral sample LUM 3833 after various IR stimulation; **(c, d)** lost TL as a result of IRSL and pIRIR stimulations for **(c)** CG K-feldspar and **(d)** FG polymineral sample LUM 3833.

According to Rösner (1990), the KTW section is comparable to parts of KTM with a large erosional gap between the NEZ and the PUG loess. The uppermost sample (LUM 3271) dates to 22.6 ± 1.6 ka, which is in accordance with dating results from UPG loess just below the recent soil in profile KTE. Sample LUM 3272 from reworked deposits just above the LS dates to 26.0 ± 1.9 ka, whereas LUM 3273 below the LS has an age of 59.7 ± 7.7 ka. It is unlikely that the weakly developed LS at Kitzingen represents over 30 kyr of landscape stability. More likely it is the result of polygenesis including phases of erosion. The end of LS formation has been discussed controversially (Terhorst et al., 2015; Sauer et al., 2016), which is due to chronological insecurities and geographic differences (e.g., paleoclimate, sedimentation rates, paleotopographic position) in landscape response to climatic deterioration at the MPG–UPG boundary. At the Central European high-resolution reference LPS Nussloch, this transition dates to ca. 34 ka (Moine et al., 2017), which is older than our age. In this context, the resolution and available data from Kitzingen are insufficient to reconstruct the local response to suborbital paleoclimatic oscillations that occurred during the MPG and early UPG (Frechen and Schirmer, 2011; Lehmkuhl et al., 2016). The loess deposits at the bottom of KTW (LUM 3274) date to 149±16 ka, corresponding to the PUG. This confirms the absence of the nearby exposed (KTM) Eemian and EG pedocomplexes most likely due to extensive erosion in the LPG, as stated by Rösner (1990).

At HKH, there is no indication of considerable UPG loess. The uppermost OSL sample (LUM 3827) yields an age of 34.2 ± 2.4 ka above pale brown horizons interpreted as LS II by Rösner (1990). Sample LUM 3828 between LS II and LS I is only slightly older (39.0 ± 2.7 ka) but agrees within error. The age of LS II at HKH agrees well with the LS at the LPS Nussloch (Moine et al., 2017), an assignment that was not possible at Kitzingen. The loess below LS (LUM 3829) is dated to 61.1 ± 6.5 ka, which is the LPG–MPG transition. It is unlikely that LS I represents 20 kyr of stable environments as other Central European LPSs record more intensively developed soils and/or soils higher in number (Lehmkuhl et al., 2016). Erosion apparently reduced the early to middle MPG record of HKH.

LUM 3829 and LUM 3830 (64.6±6.9 ka) enclose the NEZ layer, which agrees with the pedostratigraphic assignment of this colluvial horizon to the LPG (Lehmkuhl et al., 2016). Similar to the obtained age of early glacial deposits from the KTM profile, which is enclosed by MHZs and the Eemian Bt horizon, the samples LUM 3831 and 3832 yield ages of 93.0 ± 10.4 and 107 ± 12 ka, respectively, and thus can be assigned to the EG period. The upper of these two ages is

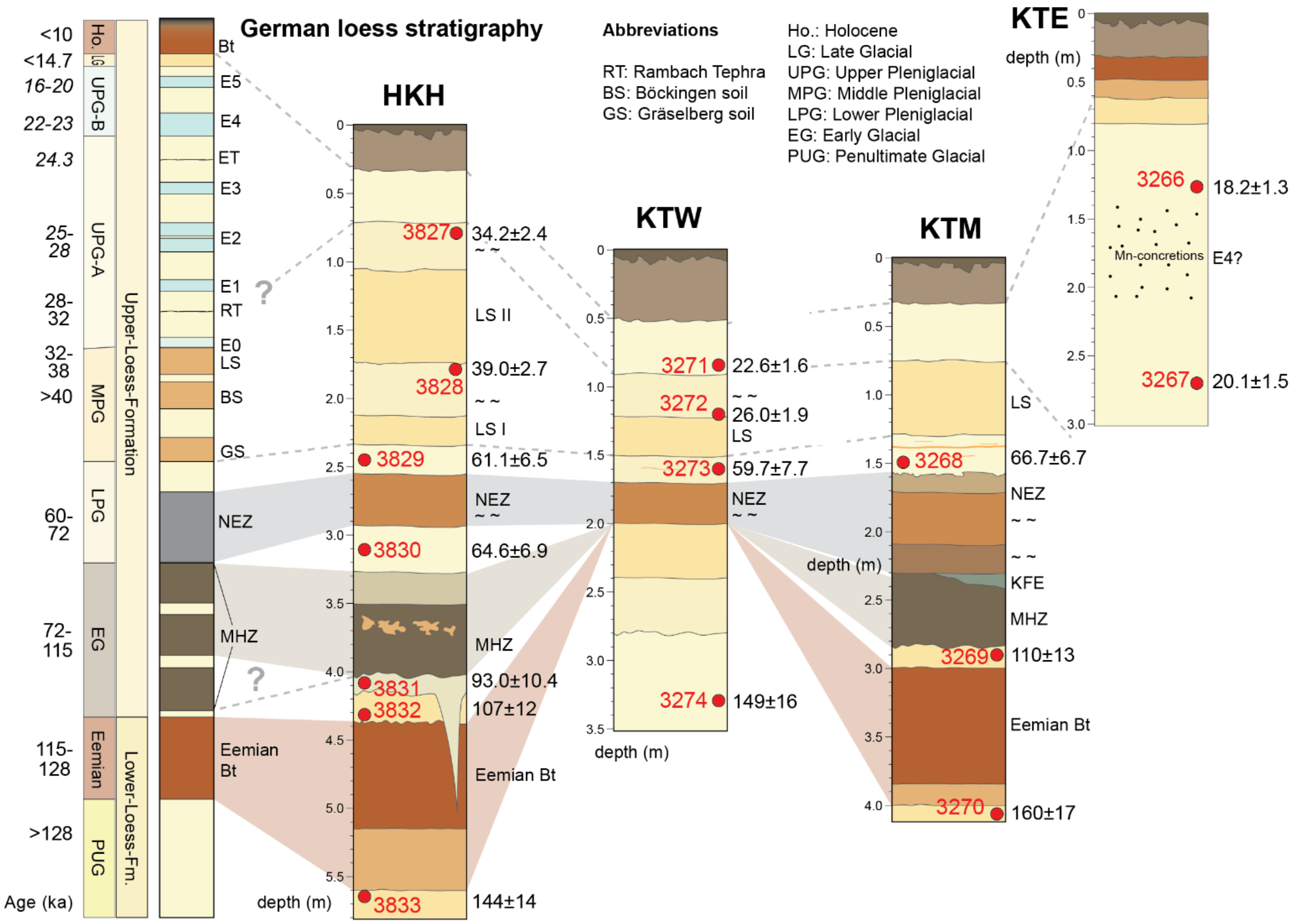

Figure 12. Fading-corrected CG pIRIR$_{225}$ ages and correlation of the studied profiles in comparison to German loess stratigraphy and approximate ages (Lehmkuhl et al., 2016) with partly updated ages by Zens et al. (2018) in italics. For a legend and further abbreviations, the reader is referred to Fig. 2.

outside the range of the post-Eemian colluvial layer; therefore, we tentatively correlate the MHZ at HKH to the middle MHZ of the German pedostratigraphy. The lowermost sample of HKH (LUM 3833) from loess sediments below the well-developed Eemian Bt horizon dates the PUG period and therefore confirms the chronostratigraphic assumptions based on German loess stratigraphy (Rösner, 1990). Nevertheless, numerical age determinations are of uppermost importance in LPS studies as there may be significant differences between pedostratigraphic assumptions and ages obtained (e.g., Steup and Fuchs, 2017; Stevens et al., 2018).

5 Conclusions

The main aim of this study was to test the application of both FG polymineral and CG K-feldspar pIRIR$_{225}$ dating to LPSs in Lower Franconia, southern Germany. Chronostratigraphic schemes from these sites relied entirely on pedostratigraphic assumptions based on the German loess stratigraphic scheme. This study provides the first OSL ages from LPS in Lower Franconia, which are in stratigraphic order and agree well with previous chronostratigraphic designations. The good agreement of the obtained ages from two different grain size fractions increases our confidence in the reliability of the derived ages, as further confirmed by comparison with some quartz blue OSL ages. Although the obtained ages from both grain size fractions are consistent, the different growth pattern of DRCs and correspondingly different saturation characteristics of fine and coarse grains are observed. Based on these results, we suggest caution in dating samples with equivalent doses in the nonlinear part of the DRC.

On the basis of the results obtained from TL experiments, the IRSL in FG polymineral and CG K-feldspar behaves similarly and hence likely shares most of their luminescence characteristics. However, the different luminescence behavior among FG and CG samples due to the different mineral composition is possible. We therefore give preference to using CG K-feldspar extracts, which mostly have particular minerals with well-known luminescence properties. In the absence of coarse fractions, the mineralogical composition of polymineral fine fractions would need to be investigated in order to identify different components and subsequently select the most appropriate protocol, e.g., high temperature preheat for an FG sample which is dominated by Na-feldspar grains.

Data availability. Most of the OSL data underlying this study are presented in the article, and OSL raw data can be obtained on request.

Supplement. The supplement related to this article is available online at: https://doi.org/10.5194/egqsj-70-53-2021-supplement.

Author contributions. TS, BT and CT designed the study. NR, TS and CT drafted the paper with final contributions from BT and MF.

Competing interests. The authors declare that they have no conflict of interest.

Acknowledgements. We thank Michael Menke, Simon Meyer-Heintze, Jan Grunau, Alexander Bauer, Peter Zwosta, Johannes Väth and the University of Würzburg and University of Bern field course students for help during fieldwork and critical discussions. We are grateful to the technicians from the LIAG for the laboratory responsibilities, Sonja Riemenschneider and Sabine Mogwitz for preparation of the luminescence samples, and Petra Posimowski for gamma spectrometry measurements. We are also thankful to Sumiko Tsukamoto for scientific discussions. We are indebted to Hofmann Transporte GmbH Kitzingen and to the Verwaltungsgemeinschaft Helmstadt for permission to repeatedly access the outcrops KT and HKH, respectively. We are especially grateful to Ludwig Zöller and Tony Reimann for their constructive reviews and comments.

Review statement. This paper was edited by Markus Fuchs and reviewed by Tony Reimann and Ludwig Zöller.

References

Aitken, M. J.: Thermoluminescence Dating, Academic Press, London, 1985.

Aitken, M. J.: An introduction to optical dating, Oxford University Press, Oxford, 1998.

Auclair, M., Lamothe, M., and Huot, S.: Measurement of anomalous fading for feldspar IRSL using SAR, Radiat. Meas., 37, 487–492, https://doi.org/10.1016/S1350-4487(03)00018-0, 2003.

Brunnacker, K.: Regionale Bodendifferenzierungen während der Würmeiszeit, Eiszeitalter and Gegenwart, 7, 43–48, 1965.

Buylaert, J. P., Vandenberghe, D., Murray, A. S., Huot, S., De Corte, F., and Van den haute, P.: Luminescence dating of old (> 70 ka) Chinese loess: a comparison of single-aliquot OSL and IRSL techniques, Quat. Geochronol., 5, 9–14, https://doi.org/10.1016/j.quageo.2006.05.028, 2007.

Buylaert, J. P., Murray, A. S., Thomsen, K. J., and Jain, M.: Testing the potential of an elevated temperature IRSL signal from K-feldspar, Radiat. Meas., 44, 560–565, https://doi.org/10.1016/j.radmeas.2009.02.007, 2009.

Buylaert, J. P., Jain, M., Murray, A. S., Thomsen, K. J., Thiel, C., and Sohbati, R.: A robust feldspar luminescence dating method for Middle and Late Pleistocene sediments, Boreas, 41, 435–451, https://doi.org/10.1111/j.1502-3885.2012.00248.x, 2012.

Buylaert, J. P., Yeo, E. Y., Thiel, C., Yi, S., Stevens, T., Thompson, W., Frechen, M., Murray, A. S., and Lu, H.: A detailed post-IR IRSL chronology for the last interglacial soil at the Jinbian loess site (northern China), Quat. Geochronol., 30, 194–199, https://doi.org/10.1016/j.quageo.2015.02.022, 2015.

Colarossi, D., Duller, G. A. T., Roberts, H. M., Tooth, S., and Lyons, R.: Comparison of paired quartz and feldspar post-IR IRSL dose distributions in poorly bleached fluvial sediments from South Africa, Quat. Geochronol., 30, 233–238, https://doi.org/10.1016/j.quageo.2015.02.015, 2015.

Constantin, D., Jain, M., Murray, A. S., Buylaert, J. P., and Timar-Gabor, A.: Quartz luminescence response to a mixed alpha-beta field: investigations on Romanian loess, Radiat. Meas., 81, 110–115, https://doi.org/10.1016/j.radmeas.2015.01.001, 2015.

Cunningham, A. S. and Wallinga, J.: Selection of integration time intervals for quartz OSL decay curves, Quat. Geochronol., 5, 657–666, https://doi.org/10.1016/j.quageo.2010.08.004, 2010.

Duller, G. A. T.: Infrared bleaching of the thermoluminescence of four feldspars, J. Phys. D Appl. Phys., 28, 1244–1258, https://doi.org/10.1088/0022-3727/28/6/030, 1995.

Duller, G. A. T.: Behavioral studies of stimulated luminescence from feldspars, Radiat. Meas., 27, 663–694, https://doi.org/10.1016/S1350-4487(97)00216-3, 1997.

Duller, G. A. T.: Distinguishing quartz and feldspar in single grain luminescence measurements, Radiat. Meas., 37, 161–165, https://doi.org/10.1016/S1350-4487(02)00170-1, 2003.

FAO: Guidelines for soil description. Food and Agriculture Organization of the United Nations, 4th edn., Roma, Italy, 2006.

Feathers, J. K., Casson, M. A., Schmidt, A. H., and Chithambo, M. L.: Application of pulsed OSL to polymineral fine-grained samples, Radiat. Meas., 47, 201–209, https://doi.org/10.1016/j.radmeas.2012.01.003, 2012.

Frechen M. and Schirmer, W.: Luminescence chronology of the Schwalbenberg II loess in the middle Rhine valley, E&G – Quaternary Science Journal, 60, 78–89, https://doi.org/10.23689/fidgeo-965, 2011.

Frechen, M., Schweitzer, U., and Zander, A.: Improvements in sample preparation for the fine grain technique, Ancient TL, 14, 15–17, 1996.

Frechen, M., van Vliet-Lanoë, B., and Van Den Haute, P.: The Upper Pleistocene loess record at Harmignies/Belgium – high resolution terrestrial archive of climate forcing, Palaeogeogr. Palaeocl., 173, 175–195, https://doi.org/10.1016/S0031-0182(01)00319-4, 2001.

Frechen, M., Oches, E. A., and Kohfeld, K. E.: Loess in Europe–mass accumulation rates during the Last Glacial Period, Loess and the Dust Indicators and Records of Terrestrial and Marine Palaeoenvironments (DIRTMAP) database, Quaternary Sci. Rev., 22, 1835–1857, https://doi.org/10.1016/S0277-3791(03)00183-5, 2003.

Frouin, M., Guérin, G., Lahaye, C., Mercier, N., Huot, S., Aldeias, V., Bruxelles, L., Chiotti, L., Dibble, H. L., Goldberg, P., Madelaine, S., McPherron, S. J. P., Sandgathe, D., Steele, T. E., and Turq, A.: New luminescence dating results based on polymineral fine grains from the Middle and Upper Palaeolithic site of La Ferrassie (Dordogne, SW France), Quat. Geochronol., 39, 131–141, https://doi.org/10.1016/j.quageo.2017.02.009, 2017.

Fu, X., Li, B., and Li, S. H.: Testing a multi-step post-IR IRSL dating method using polymineral fine grains from Chinese loess, Quat. Geochronol., 10, 8–15, https://doi.org/10.1016/j.quageo.2011.12.004, 2012.

Fuchs, M., Rousseau, D.-D., Antoine, P., Hatté, C., Gauthier, C., Marković, S., and Zoeller, L.: Chronology of the last climatic cycle (upper Pleistocene) of the Surduk loess sequence, Vojvodina, Serbia, Boreas, 37, 66–73, https://doi.org/10.1111/j.1502-3885.2007.00012.x, 2008.

Guérin, G., Mercier, N., and Adamiec, G.: Dose-rate conversion factors: update, Ancient TL, 29, 5–8, 2011.

Guérin, G., Frouin, M., Talamo, S., Aldeias, V., Chiotti, L., Dibble, H., Goldberg, P., Hublin, J. J., Jain, M., Lahaye, C., Madelaine, S., Maureille, B., McPherron, S., Mercier, N., Murray, A. S., Sandgathe, D., Steele, T. E., Thomsen, K., and Turq, A.: A multi-method luminescence dating of the paleolithic sequence of La Ferrassie based on new excavations adjacent to the La Ferrassie 1 and 2 skeletons, J. Archaeol. Sci., 58, 147–166, https://doi.org/10.1016/j.jas.2015.01.019, 2015.

Haase, D., Fink, J., Haase, G., Ruske, R., Pécsi, M., Richter, H., Altermann, M., and Jäger, K. D.: Loess in Europe-its spatial distribution based on a European loess map, scale $1:2,500,000$, Quaternary Sci. Rev., 26, 1301–1312, https://doi.org/10.1016/j.quascirev.2007.02.003, 2007.

Huntley, D. J. and Baril, M. R.: The K content of the K-feldspar being measured in optical dating or in thermoluminescence dating, Ancient TL, 15, 11–13, 1997.

Huntley, D. J. and Hancock, R. G. V.: The Rb contents of K-feldspar grains being measured in optical dating, Ancient TL, 19, 43–46, 2001.

Huntley, D. J. and Lamothe, M.: Ubiquity of anomalous fading in K-feldspars and the measurement and correction for it in optical dating, Can. J. Earth Sci., 38, 1093–1106, https://doi.org/10.1139/e01-013, 2001.

Huntley, D. J., Baril, M. R., and Haidar, S.: Tunnelling in plagioclase feldspars, J. Phys. D Appl. Phys., 40, 900–906, https://doi.org/10.1088/0022-3727/40/3/031, 2007.

Huot, S. and Lamothe, M.: The implication of sodium-rich plagioclase minerals contaminating K-rich feldspars aliquots in luminescence dating, Quat. Geochronol., 10, 334–339, https://doi.org/10.1016/j.quageo.2012.03.003, 2012.

Kars, R. H., Wallinga, J., and Cohen, K. M.: A new approach towards anomalous fading correction for feldspar IRSL dating – tests on samples in field saturation, Radiat. Meas., 43, 786–790, https://doi.org/10.1016/j.radmeas.2008.01.021, 2008.

Kreutzer, S., Schmidt, C., DeWitt, R., and Fuchs, M.: The a-value of polymineral fine grain samples measured with the post-IR IRSL protocol, Radiat. Meas., 69, 18–29, https://doi.org/10.1016/j.radmeas.2014.04.027, 2014.

Lehmkuhl, F., Zens, J., Krauß, L., Schulte, P., and Kels, H.: Loess-paleosol sequences at the northern European loess belt in Germany: distribution, geomorphology and stratigraphy, Quaternary Sci. Rev., 153, 11–30, https://doi.org/10.1016/j.quascirev.2016.10.008, 2016.

Lehmkuhl, F., Pötter, S., Pauligk, A., and Bösken, J.: Loess and other Quaternary sediments in Germany, J. Maps, 14, 330–340, https://doi.org/10.1080/17445647.2018.1473817, 2018.

Li, B. and Li, S. H.: Thermal stability of infrared stimulated luminescence of sedimentary K-feldspar, Radiat. Meas., 46, 29–36, https://doi.org/10.1016/j.radmeas.2010.10.002, 2011.

Li, B. and Li, S. H.: Luminescence dating of Chinese loess beyond 130 ka using the non-fading signal from K-feldspar, Quat. Geochronol., 10, 24–31, https://doi.org/10.1016/j.quageo.2011.12.005, 2012.

Li, Y., Tsukamoto, S., Shang, Z., Tamura, T., Wang, H., and Frechen, M.: Constraining the transgression history in the Bohai Coast China since the Middle Pleistocene by luminescence dating, Mar. Geol., 416, 105980, https://doi.org/10.1016/j.margeo.2019.105980, 2019.

Mejdahl, V.: Thermoluminescence dating: beta-dose attenuation in quartz grains, Archaeometry, 21, 61–72, https://doi.org/10.1111/j.1475-4754.1979.tb00241.x, 1979.

Moine, O., Antonie, P., Hatté, C., Landais, A., Mathieu, J., Prud'homme, C., and Rousseau, D.-D.: The impact of Last Glacial climate variability in west-European loess revealed by radiocarbon dating of fossil earthworm granules, P. Natl. Acad. Sci. USA, 114, 6209–6214, https://doi.org/10.1073/pnas.1614751114, 2017.

Möller, P. and Murray, A. S.: Drumlinised glaciofluvial and glaciolacustrine sediments on the Småland peneplain, South Sweden- new information on the growth and decay history of the Fennoscandian Ice Sheets during MIS 3, Quaternary Sci. Rev., 122, 1–29, https://doi.org/10.1016/j.quascirev.2015.04.025, 2015.

Moska, P., Adamiec, G., Jary, Z., Bluszcz, A., Poręba, G., Piotrowska, N., Krawczyk, M., and Skurzyński, J.: Luminescence chronostratigraphy for the loess deposits in Złota, Poland, Geochronometria, 45, 44–55, https://doi.org/10.1515/geochr-2015-0073, 2018.

Murray, A. S. and Olley, J. M.: Precision and accuracy in the optically stimulated luminescence dating of sedimentary quartz: a status review, Geochronometria, 21, 1–16, 2002.

Murray, A. S. and Wintle, A. G.: Luminescence dating of quartz using an improved single-aliquot regenerative-dose protocol, Radiat. Meas., 32, 57–73, https://doi.org/10.1016/S1350-4487(99)00253-X, 2000.

Murray, A. S. and Wintle, A. G.: The single aliquot regenerative dose protocol: potential for improvements in reliability, Radiat. Meas., 37, 377–381, https://doi.org/10.1016/S1350-4487(03)00053-2, 2003.

Murray, A. S., Buylaert, J. P., Thomsen, K. J., and Jain, M.: The effect of preheating on the IRSL signal from feldspar, Radiat. Meas., 44, 554–559, https://doi.org/10.1016/j.radmeas.2009.02.004, 2009.

Murray, A. S., Thomsen, K. J., Masuda, N., Buylaert, J. P., and Jain, M.: Identifying well-bleached quartz using the different bleaching rates of quartz and feldspar luminescence signals, Radiat. Meas., 47, 688–695, https://doi.org/10.1016/j.radmeas.2012.05.006, 2012.

Novothny, A., Frechen, M., Horváth, E., Wacha, L., and Rolf, C.: Investigating the penultimate and last glacial cycles of the Süttö loess section (Hungary) using luminescence dating, high-resolution grain size, and magnetic susceptibility data, Quatern. Int., 234, 75–85, https://doi.org/10.1016/j.quaint.2010.08.002, 2011.

Poolton, N. R. J., Ozanyan, K. B., Wallinga, J., Murray, A. S., and Bøtter-Jensen, L.: Electrons in feldspar II: a consideration of the influence of conduction band-tail states on luminescence processes, Phys. Chem. Miner., 29, 217–225, https://doi.org/10.1007/s00269-001-0218-2, 2002.

Prescott, J. R. and Hutton, J. T.: Cosmic ray contributions to dose rates for luminescence and ESR dating: large depths and long term variations, Radiat. Meas., 23, 497–500, https://doi.org/10.1016/1350-4487(94)90086-8, 1994.

Prescott, J. R. and Stephan, L. G.: The contribution of cosmic radiation to the environmental dose for thermoluminescent dating – latitude, altitude and depth dependences, PACT, 6, 17–25, 1982.

Rees-Jones, J.: Optical dating of young sediments using fine-grain quartz, Ancient TL, 13, 9–14, 1995.

Roberts, H. M.: The development and application of luminescence dating to loess deposits: a perspective on the past, present and future, Boreas, 37, 483–507, https://doi.org/10.1111/j.1502-3885.2008.00057.x, 2008.

Rösner, U.: Die Mainfränkische Lößprovinz, Mitteilungen der Fränkischen Geographischen Gesellschaft Erlangen, Bd. 37, 290 pp., 1990.

Sauer, D., Kadereit, A., Kühn, P., Kösel, M., Miller, C. E., Shinonaga, T., Kreutzer, S., Herrmann, L., Fleck, W., Starkovich, B. M., and Stahr, K.: The loess-palaeosol sequence of Datthausen, SW Germany: characteristics, chronology, and implications for the use of the Lohne Soil as a marker soil, Catena, 146, 10–29, https://doi.org/10.1016/j.catena.2016.06.024, 2016.

Schmidt, E. D., Machalett, B., Marković, S. B., Tsukamoto, S., and Frechen, M.: Luminescence chronolgy of the upper part of the Stari Slankamen loess sequence (Vojvodina, Serbia), Quat. Geochronol., 5, 137–142, https://doi.org/10.1016/j.quageo.2009.09.006, 2010.

Schmidt, E. D., Frechen, M., Murray, A. S., Tsukamoto, S., and Bittmann, F.: Luminescence chronology of the loess record from the Tönchesberg section: A comparison of using quartz and feldspar as dosimeter to extend the age range beyond the Eemian, Quatern. Int., 234, 10–22, https://doi.org/10.1016/j.quaint.2010.07.012, 2011.

Schönhals, E., Rohdenburg, H., and Semmel, A.: Ergebnisse neuerer Untersuchungen zur Würmlöß-Gliederung in Hessen, E&G – Quaternary Science Journal, 15, 199–206, https://doi.org/10.23689/fidgeo-1507, 1964.

Semmel, A.: Studien über den Verlauf jungpleistozäner Formung in Hessen, Frankfurter Geographische Hefte, Hefte 45, 133 pp., 1968.

Semmel, A. and Stäblein, G.: Zur Entwicklung quartärer Hohlformen in Franken, Eiszeitalter u. Gegenwart, 22, 23–34, https://doi.org/10.23689/fidgeo-1443, 1971.

Skowronek, A.: Paläoböden und Lösse in Mainfranken vor ihrem landschaftsgeschichtlichen Hintergrund, Würzburger Geographische Arbeiten, 57, 89–107, 1982.

Sohbati, R., Murray, A. S., Jain, M., Thomsen, K., Hong, S., Yi, K., and Choi, J.: Na-rich feldspar as a luminescence dosimeter in infrared stimulated luminescence (IRSL) dating, Radiat. Meas., 51–52, 67–82, https://doi.org/10.1016/j.radmeas.2012.12.011, 2013.

Spooner, N. A.: The anomalous fading of infrared-stimulated luminescence from feldspars, Radiat. Meas., 23, 625–632, https://doi.org/10.1016/1350-4487(94)90111-2, 1994.

Sprafke, T.: Löss in Niederösterreich – Archiv quartärer Klima- und Landschaftsveränderungen, Würzburg University Press, Würzburg, E-book version, 272 pp., available at: https://opus.bibliothek.uni-wuerzburg.de/files/12778/978-3-95826-039-9_Sprafke_Tobias_OPUS_12778.pdf (last access: 29 January 2021), 2016.

Steup, R. and Fuchs, M.: The loess sequence at Münzenberg (Wetterau/Germany): A reinterpretation based on new luminescence dating results, Z. Geomorphol., 61, 101–120, https://doi.org/10.1127/zfg_suppl/2016/0408, 2017.

Stevens, T., Buylaert, J. P., Thiel, C., Újvári, G., Yi, S., Murray, A. S., Frechen, M., and Lu, H.: Ice-volume-forced erosion of the Chinese Loess Plateau global Quaternary stratotype site, Nat. Commun., 9, 983, https://doi.org/10.1038/s41467-018-03329-2, 2018.

Terhorst, B., Sedov, S., Sprafke, T., Peticzka, R., Meyer-Heintze, S., Kühn, P., and Solleiro Rebolledo, E.: Austrian MIS 3/2 loess-palaeosol records – key sites along a west-east transect, Palaeogeogr. Palaeocl., 418, 43–56, https://doi.org/10.1016/j.palaeo.2014.10.020, 2015.

Thiel, C., Buylaert, J. P., Murray, A. S., Terhorst, B., Hofer, I., Tsukamoto, S., and Frechen, M.: Luminescence dating of the Stratzing loess profile (Austria) – testing the potential of an elevated temperature post-IR IRSL protocol, Quatern. Int., 234, 23–31, https://doi.org/10.1016/j.quaint.2010.05.018, 2011a.

Thiel, C., Buylaert, J.-P., Murray, A. S., Terhorst, B., Tsukamoto, S., Frechen, M., and Sprafke, T.: Investigating the chronostratigraphy of prominent palaeosols in Lower Austria using post-IR IRSL dating, E&G Quaternary Sci. J., 60, 11, https://doi.org/10.3285/eg.60.1.10, 2011b.

Thiel, C., Tsukamoto, S., Kayoko, T., Buylaert, J. P., Murray, A. S., Tanaka, K., and Shirai, M.: Testing the application of quartz and feldspar luminescence dating to MIS 5 Japanese marine deposits, Quat. Geochronol., 29, 16–29, https://doi.org/10.1016/j.quageo.2015.05.008, 2015.

Thomsen, K. J., Bøtter-Jensen, L., Denby, P. M., Moska, P., and Murray, A. S.: Developments in luminescence measurement techniques, Radiat. Meas., 41, 768–773, https://doi.org/10.1016/j.radmeas.2006.06.010, 2006.

Thomsen, K. J., Murray, A. S., Jain, M., and Bøtter-Jensen, L.: Laboratory fading rates of various luminescence signals from feldspar-rich sediment extracts, Radiat. Meas., 43, 1474–1486, https://doi.org/10.1016/j.radmeas.2008.06.002, 2008.

Timar-Gabor, A. and Wintle, A. G.: On natural and laboratory generated dose response curves for quartz of different grain sizes from Romanian loess, Quat. Geochronol., 18, 34–40, https://doi.org/10.1016/j.quageo.2013.08.001, 2013.

Timar-Gabor, A., Vandenberghe, D. A. G., Vasiliniuc, S., Panaiotu, C. E., Panaiotu, C. G., Dimofte, D., and Cosma, C.: Optical dating of Romania loess: a comparison between sand-sized and silt-sized quartz, Quatern. Int., 240, 62–70, https://doi.org/10.1016/j.quaint.2010.10.007, 2011.

Timar-Gabor, A., Constantin, D., Marković, S. B., and Jain, M.: Extending the area of investigation of fine versus coarse quartz optical ages from the Lower Danube to the Carpathian Basin, Quatern. Int., 388, 168–176, https://doi.org/10.1016/j.quaint.2014.09.065, 2015.

Timar-Gabor, A., Buylaert, J.-P., Guralnik, B., Trandafir-Antohi, O., Constantin, D., Anechitei-Deacu, V., Jain, M., Murray, A. S., Porat, N., Hao, Q., and Wintle, A. G.: On the importance of grain size in luminescence dating using quartz, Radiat. Meas., 106, 464–471, https://doi.org/10.1016/j.radmeas.2017.01.009, 2017.

Tsukamoto, S., Jain, M., Murray, A. S., Thiel, C., Schmidt, E., Wacha, L., Dohrmann, R., and Frechen, M.: A comparative study of the luminescence characteristics of polymineral fine grains and coarse-grained K- and Na-rich feldspars, Radiat. Meas., 47, 903–908, https://doi.org/10.1016/j.radmeas.2012.02.017, 2012.

Tsukamoto, S., Kondo, R., Lauer, T., and Jain, M.: Pulsed IRSL: A stable and fast bleaching luminescence signal from feldspar for dating Quaternary sediments, Quat. Geochronol., 41, 26–36, https://doi.org/10.1016/j.quageo.2017.05.004, 2017.

Vasiliniuc, Ş., Vandenberghe, D. A. G., Timar-Gabor, A., Panaiotu, C., Cosma, C., and Van Den haute, P.: Testing the potential of elevated temperature post-IR-IRSL signals for dating Romanian loess, Quat. Geochronol., 10, 75–80, https://doi.org/10.1016/j.quageo.2012.02.014, 2012.

Vasiliniuc, Ş., Vandenberghe, D. A. G., Timar-Gabor, A., Cosma, C., and Van Den haute, P.: Combined IRSL and POST-IR OSL dating of Romanian loess using single aliquots of polymineral fine grains, Quatern. Int., 293, 15–22, https://doi.org/10.1016/j.quaint.2012.01.002, 2013.

Wacha, L. and Frechen, M.: The geochronology of the "Gorjanović loess section" in Vukovar, Croatia, Quatern. Int., 240, 87–99, https://doi.org/10.1016/j.quaint.2011.04.010, 2011.

Wacha, L., Mikulčić Pavlaković, S., Novothny, Á., Crnjaković, M., and Frechen, M.: Luminescence dating of upper Pleistocene loess from the island of Susak in Croatia, Quatern. Int., 34, 50–61, https://doi.org/10.1016/j.quaint.2009.12.017, 2011.

Wang, X. L., Wintle, A. G., and Adamiec, G.: Post-IR IRSL production in perthitic feldspar, Radiat. Meas., 64, 1–8, https://doi.org/10.1016/j.radmeas.2014.03.006, 2014.

Wintle, A. G.: Luminescence dating: laboratory procedures and protocols, Radiat. Meas., 27, 769–817, https://doi.org/10.1016/S1350-4487(97)00220-5, 1997.

Wintle, A. G. and Murray, A. S.: A review of quartz optically stimulated luminescence characteristics and their relevance in single-aliquot regeneration dating protocols, Radiat. Meas., 41, 369–391, https://doi.org/10.1016/j.radmeas.2005.11.001, 2006.

Yi, S., Buylaert, J. P., Murray, A. S., Thiel, C., Zeng, L., and Lu, H.: High resolution OSL and post-IR IRSL dating of the last interglacial-glacial cycle at the Sanbahuo loess site (northeastern China), Quat. Geochronol., 30, 200–206, https://doi.org/10.1016/j.quageo.2015.02.013, 2015.

Yi, S., Buylaert, J. P., Murray, A. S., Lu, H., Thiel, C., and Zeng, L.: A detailed post-IR IRSL dating study of the Niuyangzigou loess site in northeastern China, Boreas, 45, 644–657, https://doi.org/10.1111/bor.12185, 2016.

Zens, J., Schulte, P., Klasen, N., Krauß, L., Pirson, S., Burow, C., Brill, D., Eckmeier, E., Kels, H., Zeeden, C., Spagna, P., and Lehmkuhl, F.: OSL chronologies of paleoenvironmental dynamics recorded by loess-paleosol sequences from Europe: case studies from the Rhine-Meuse area and the Neckar Basin, Palaeogeogr. Palaeocl., 509, 105–125, https://doi.org/10.1016/j.palaeo.2017.07.019, 2018.

Zhang, J. and Li, S. H.: Constructions of standarised growth curves (SGCs) for IRSL signals from K-feldspar, plagioclase and polymineral fractions, Quat. Geochronol., 49, 8–15, https://doi.org/10.1016/j.quageo.2018.05.015, 2019.

E&G Quaternary Sci. J., 70, 73–82, 2021
https://doi.org/10.5194/egqsj-70-73-2021

Open Access E&G Quaternary Science Journal

Research article

Implications of geoarchaeological investigations for the contextualization of sacred landscapes in the Nile Delta

Eva Lange-Athinodorou

Lehrstuhl für Ägyptologie, Julius-Maximilians-Universität Würzburg, Würzburg, 97070, Germany

Correspondence: Eva Lange-Athinodorou (eva.lange@uni-wuerzburg.de)

Relevant dates: Received: 2 July 2020 – Revised: 30 September 2020 – Accepted: 9 October 2020 – Published: 12 February 2021

How to cite: Lange-Athinodorou, E.: Implications of geoarchaeological investigations for the contextualization of sacred landscapes in the Nile Delta, E&G Quaternary Sci. J., 70, 73–82, https://doi.org/10.5194/egqsj-70-73-2021, 2021.

Abstract: Key elements of sacred landscapes of the Nile Delta were lakes, canals and artificial basins connected to temples, which were built on elevated terrain. In the case of temples of goddesses of an ambivalent, even dangerous, nature, i.e. lioness goddesses and all female deities who could appear as such, the purpose of sacred lakes and canals exceeded their function as a water resource for basic practical and religious needs. Their pleasing coolness was believed to calm the goddess' fiery nature, and during important religious festivals, the barques of the goddesses were rowed on those waters. As archaeological evidence was very rare in the past, the study of those sacred waters was mainly confined to textual sources. Recently applied geoarchaeological methods, however, have changed this situation dramatically: they allow in-depth investigations and reconstructions of these deltaic sacred landscapes. Exploring these newly available data, the paper presented here focuses on the sites of Buto, Sais and Bubastis, by investigating the characteristics of their sacred lakes, canals and marshes with respect to their hydrogeographical and geomorphological context and to their role in ancient Egyptian religion and mythology as well.

Kurzfassung: Heilige Gewässer verschiedener Art, d.h. Seen, Kanäle und künstliche Becken, verbunden mit auf erhöhtem Gelände befindlichen Tempelgebäuden, sind als Schlüsselelemente sakraler Landschaften des Nildeltas anzusehen. Im Falle von Tempeln von Göttinnen ambivalenter, ja gefährlicher Natur, wie Löwengöttinnen und allen anderen weiblichen Gottheiten, die als solche erscheinen konnten, ging die Funktion heiliger Seen und Kanäle über ihren Zweck als Wasserressource für grundlegende praktische und religiöse Bedürfnisse hinaus. Man glaubte, dass ihre angenehme Kühle die feurige Natur der Göttin beruhigte; auf den Gewässern fuhren auch die heiligen Barken, in denen die Göttinnen bei wichtigen religiösen Festen gerudert wurden. Da man bis vor relativ kurzer Zeit kaum über archäologische Belege verfügte, beschränkte sich das Studium dieser heiligen Gewässer hauptsächlich auf Textquellen. Die in neuerer Zeit verstärkt angewandten geoarchäologischen Methoden haben diese Situation jedoch dramatisch verändert und ermöglichen nun eingehende Untersuchungen und Rekonstruktionen dieser heiligen Landschaften des Nildeltas. Unter Einbeziehung dieser neu verfügbaren Daten konzentriert sich die hier vorgelegte Arbeit auf die heilige Landschaft von Buto, Sais und Bubastis, indem sie die Merkmale ihrer heiligen Seen, Kanäle und Sümpfe im Hinblick auf ihren hydrogeographischen und geomorphologischen Kontext sowie auf ihre Rolle in der altägyptischen Religion und Mythologie untersucht.

1 Introduction

Investigations of sacred landscapes occur at the very intersection of geomorphology and archaeology, where the methods and aims of both disciplines truly come together. The recent increase in geoarchaeological studies at several sites in the Nile Delta allows the reconstruction of important features of their respective palaeo-landscapes. In archaeology, the investigation of landscapes and their impact on human cultural history is well established (David and Thomas, 2016; on the different concepts of landscape in geoarchaeology cf. also Cordoba, 2020, p. 50).

The study of sacred landscapes represents a special branch of landscape archaeology, since sacred landscapes are essentially landscapes that are marked and mapped with mythological references and explanations. They were sometimes changed due to human activities or by additions of human material culture. In Egyptology, the term "sacred landscape" is oftentimes used for temple complexes and their nearby surroundings. Sometimes also waterways or land routes come into play, as they could connect two or more temples, thus widening the sacred landscape. For important Egyptian religious celebrations such as the so-called Opet festival as a well-known example, it was essential that the cult image of the god Amun travelled on his sacred barque from his main temple at Karnak to Luxor around 3 km to the south (Darnell, 2010). These travels took place on natural as well as on artificial waterways and land routes. These were the Nile and the canals connecting the temples to their surroundings and also their paved stone paths (dromoi) leading to their entrances (Geßler-Löhr, 1983, pp. 144–145; Boreik et al., 2017). Here and elsewhere, we can observe a most interesting process: at first, existing natural topographical features were exploited to conduct religious ceremonies. Subsequently, their requirements could then initiate the addition of artificial structures and perhaps even the changing of the natural landscape.

Turning now from the Nile Valley to the Nile Delta, what were the main constituents of a sacred landscape there? In the delta, temples and cemeteries were set on top of natural elevations (van den Brink, 1986, p. 12). In the eastern delta, these were the remains of deeply eroded massive Pleistocene sediments, accumulated by the vigorous Pre-Nile, the so-called *geziras* (Said, 1981, 1993). In the western delta, temples were built on elevations as well, which seem to be the result of different geomorphological processes, as became clear in the case of Buto (Wunderlich, 1989). Regardless of their geomorphological origin, *geziras* were the dominant feature of the vast alluvial plain of the delta. Other distinctive characteristics of this landscape were the manifold watercourses and marshlands with their stagnant waters. Therefore, a body of water, whether in the shape of a stream, canal, lake or pool, connected to an elevated temple formed the basic elements of a deltaic sacred landscape.

In the past, knowledge of the existence of sacred lakes or canals attached to or surrounding temple buildings was mainly based on religious texts with little additional archaeological evidence. The previously available record pointed to the existence of deltaic sacred landscapes at a number of sites. Of them, Buto (Geßler-Löhr, 1983, pp. 403–404) and Sais (Geßler-Löhr, 1983, pp. 233–240; Wilson, 2006, 2019, pp. 5, 17) in the western delta, Busiris in the central delta (Geßler-Löhr, 1983, pp. 437–438), and Tanis (Montet, 1966; Leclère, 2008, pp. 442–443) and Bubastis (Lange-Athinodorou et al., 2019) in the eastern delta were especially well known. At any rate, comparative studies of sacred lakes are still rare (Yoyotte, 1962; Sauneron, 1964; Geßler-Löhr, 1983; Tillier, 2010); in particular, studies on sacred lakes as elements of deltaic sacred landscapes do not exist at all.

Nowadays, evidence comes from a much wider variety of sources. In addition to textual and archaeological records, we have access to results of sedimentological analysis from core drillings, as well as from geoelectric and geomagnetic investigations. These now allow the investigation of the location, shape or course of sacred waters at temple sites. To date however, such comprehensive, multi-methodological approaches have only been applied to a relatively small number of delta sites with well-known large-temple districts. At present, Buto, Sais and Bubastis are the main sites that provide us with sufficient textual, archaeological and geoarchaeological material for a comparative analysis. Therefore, they represent the topics of the following case study, which will focus on the landscape surrounding the large temples of these cities. Moreover, the local main deities of these cities all belonged to the canon of the so-called dangerous goddesses; i.e. they all shared specific qualities, which influenced certain elements of their cults, temple buildings and their surroundings as well.

2 Buto

At Buto in the northwestern delta the sacred landscape refers to the temple of the goddess Wadjet, the main deity of the city, who also embodied the red crown of Lower Egypt. In this capacity, Wadjet was the northern counterpart to the goddess Nekhbet, the goddess of the white crown of Upper Egypt (Leclère, 2008, p. 198, remark no. 5).

2.1 Textual sources

A statue dating to the Middle Kingdom from Meidum mentions the goddess Wadjet with the epithet "lady of the *Isheru*" (Geßler-Löhr, 1983, p. 403). The Egyptian term *Isheru* usually designates horseshoe-shaped lakes or canals connected to or surrounding temples of goddesses, who were believed to display not only benevolent but also dangerous qualities (Sauneron, 1964, pp. 50–57; Geßler-Löhr, 1983, pp. 47, 401). To capture this ambivalent character, these Egyptian goddesses were imagined to appear as lionesses, primarily Sekhmet, Bastet, Shesemtet and other genuinely feline goddesses. In addition others, e.g. Hathor, Mut, Neith, Nekhbet and Wadjet, who usually appeared in a different, either anthropomorphic or zoomorphic, form (Tillier, 2010, pp. 167, 171–172; Lange-Athinodorou, 2019, pp. 554–561, 580–581) could also be imagined as lionesses. According to their predatory nature, lionesses were feared as wild and fiery. Possibly based on wildlife observations at natural water places were lions would rest, canals or lakes close to temples of lioness goddesses were believed to please the goddesses' wild nature. Therefore, locations surrounded by lakes or canals were considered the ideal setting for their cult.

Still, that the inscription on the above-mentioned statue really referred to a sacred lake or canal of the temple of Wadjet at Buto is not beyond all doubt. The reason for that uncertainty is that several temples all over Egypt had lakes called *Isheru* where Wadjet and other goddesses obtained subsidiary cults. The most famous *Isheru* lake was the horseshoe-shaped one at the temple of Mut at Karnak. However, the earliest attestations of the *Isheru* of the temple of Mut at Karnak date back to the 18th dynasty (ca. 1460 BCE). They are therefore much younger than the earliest records of the term *Isheru* (Yoyotte, 1962, pp. 101–103, 106; Geßler-Löhr, 1983, p. 412); one proof comes from a list of deities of Egypt receiving offerings from the king. Each deity is not only listed by name but also further specified by its cult place. There, the lioness goddess Sekhmet bears the epithet "Sekhmet in *Isheru*", with the name of the sacred water used as a toponym of its own (Mariette, 1869, T. I. Pl. 44.9). As the text comes from the temple of Seti I at Abydos one would date it to the New Kingdom (19th dynasty, ca. 1280 BCE). However, Yoyotte (1962) and Sauneron (1964) argue that the list is actually a copy from a much older template of the late Old Kingdom (6th dynasty, ca. 2260 BCE; Yoyotte, 1962, p. 105; Sauneron, 1964, p. 56.4; also Geßler-Löhr, 1983, p. 402). In addition, a block from the temple of Min at Koptos depicts Sesostris I (12th dynasty, 1919–1875 BCE) in front of the lioness goddess Bastet with the caption "Bastet, lady of the *Isheru*". Here, the use of the settlement determinative ⊗ in the writing shows again that this name was used as a toponym, yet its exact location remains unknown (Petrie, 1896, Pl. X.2; Geßler-Löhr, 1983, p. 404; Gomàa, 1987, p. 209). In the light of this unique evidence, it remains impossible to decide where the *Isheru* from the inscription on the statue from Meidum was located (cf. Yoyotte, 1962, pp. 99–101; Geßler-Löhr, 1983, p. 403; was it Memphis or Meidum?).

Specific information about sacred waters of the temple of Wadjet at Buto comes from an inscription at the temple of Mut at Karnak from the Ptolemaic Period (second–first century BCE). The text tells the story of an assemblage of the deities of Egypt at Buto where the gods and goddesses of the Ennead are ordered to dig out a canal for Wadjet: "the gods of the Ennead, as follows: 'you shall travel to the hill-country of Buto … were you shall dig out a canal for the mighty one. You shall draw its water with both of your hands [so?] her [temple?] is encircled by its canal because she is content in the great primeval ocean"' (Geßler-Löhr, 1983, p. 403; Sauneron, 1983, p. 20, Taf. X.11–13).

The Greek historian Herodotus (ca. 450 BCE) describes a lake at this temple: "In this way the shrine is for me the most marvellous of all things to see in this temple; the second place has an island called Chemmis. This lies in a deep and wide lake close to the temple at Buto, and the Egyptians say that it floats" (Hd. II. 156.1; Wilson, 2015, p. 221; Nesselrath, 2017, p. 194).

Thus the essential information provided by the texts is as follows:

1. There was a canal at the temple(?) of Wadjet at Buto in order to pacify her dangerous temper.
2. There was also a lake close to the temple with a floating vegetated island called Chemmis.

Chemmis is the Greek term for the Egyptian toponym *Akhbit* – "papyrus thicket of the bee", with "bee" as the heraldic animal designating the geographical area of the delta. *Akhbit* is well known from written sources, mostly of a mythological and religious background from the time of the Pyramid Texts (ca. 2350 BCE) onwards. There, it means the hiding place of the goddess Isis where she raised her infant son and crown prince Horus, in order to keep the god Seth, Horus' murderous uncle, from harming him. Gardiner (1944), who investigated all available textual references, discussed the possibility that the toponym *Akhbit* was used to designate not one but two different locations: the first site was an *Akhbit* in the temple district of Buto, as mentioned by Herodotus. This was probably an artificial replica of the mythological hideout of the young god Horus in the papyrus marshes, designed as a vegetated island set in a sacred lake. On the other hand, according to textual evidence that treats *Akhbit* as a real locality and not as a specific element within the temple precinct, the second was a natural landscape area with papyrus marshes, which inspired the mythos. However, this *Akhbit* would have to be localized in the vicinity of Buto as well (Gardiner, 1944, pp. 53–58).

2.2 Geoarchaeology

At Buto, the temple of Wadjet was located at the northeastern Kom B (Hartung et al., 2009, p. 184). In fact, not much

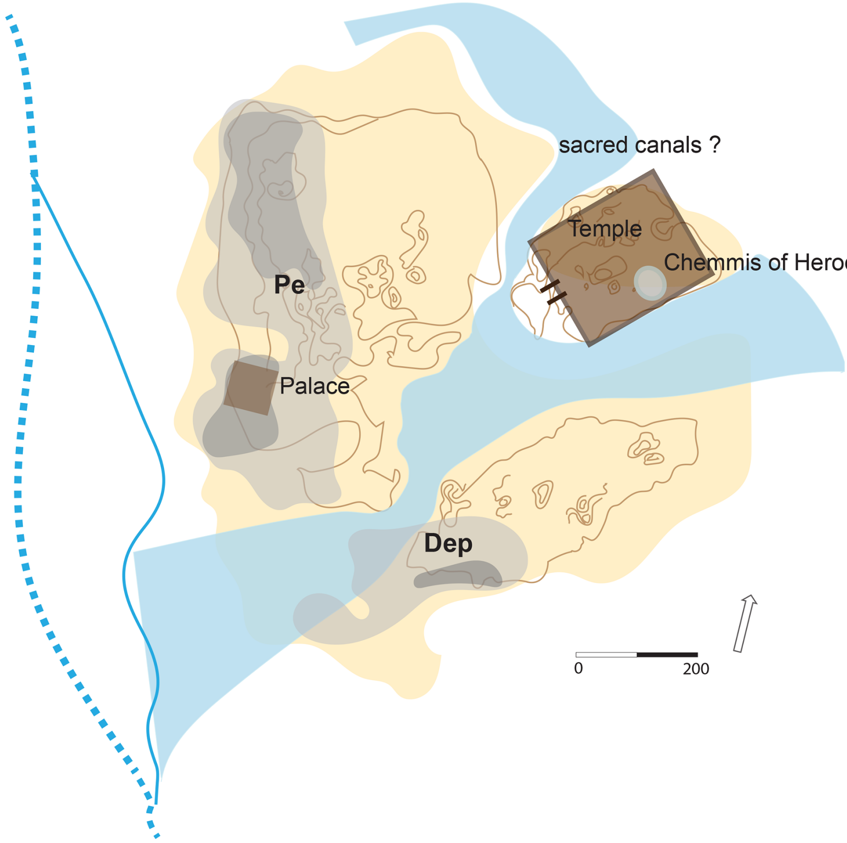

Figure 1. Topographic model of Buto with hypothetic course of the local canals at the temple. Topographic model after Hartung (2018, p. 102, Fig. 1).

survived of this building. Apparently, an enclosure wall of mud bricks of ca. 300 m by 200 m encircled the temple in the Late Dynastic Period. Its main entrance was on its western side (von der Way, 1999, p. 184; Leclère, 2008, pp. 205–208). Test trenches and drillings indicate the construction of a foundation made of sand in the Saite Period (seventh–sixth century BCE; Faltings et al., 2000, pp. 162–165). However, when looking at the elevation model of Buto (Hartung et al., 2009, p. 174, Abb. 27), a prominent depression between the northeastern, northwestern and southern parts of the tell, i.e. Kom A, B and C, is noticeable. One could speculate if this almost horseshoe-shaped depression could have formed a natural *Isheru*, presumably during the time of the inundation, when depressions were probably water-bearing.

At any case, a definitive answer could only be expected from the analysis of sediments of cores taken in that area. Although Hartung et al. (2009, p. 174, Abb. 27) conducted extensive drilling campaigns at the site, they focused mainly on the western stretch of the tell, leaving the area in question still unexplored. Interestingly, a single core drilling conducted by Faltings et al. (2000, pp. 167–168) in the eastern part of the temple precinct revealed green-greyish clayey mud with organic remains of plants, shells and fish bones, providing evidence of the former existence of a stagnant water body in this area.

Still ongoing is a long-term research programme on the natural landscape of the wider area around Buto. Based on core drillings and the digital and visual analysis of satellite imagery, Wunderlich (1989) detected massive peat layers to the north of Buto as far as Lake Burullus, indicating the former existence of a vast swampy area. These swamps originated from a belt of semi-marine lagoons, resulting from the marine transgression after the end of the last glacial period.

Figure 2 shows the extension of the consolidated *gezira* sands on which the settlement of Buto was founded and to its north the size and limits of the peat horizon to the north as attested by core drillings conducted by Wunderlich (1989). The peat horizon is the remnant of the above-mentioned semi-marine lagoon. C-14 datings on a number of test samples from the peat horizon (location indicated in Fig. 2) show that the lagoon belt moved inland to up to around 2 km north of Buto from 5050 to 4050 BCE. With the lowering of the sea level, the swamp dried up again from the fourth millennium BCE onwards (Wunderlich, 1989, pp. 106–110; Wunderlich and Ginau, 2014/2015, pp. 488–494).

Therefore, at the time of the beginning of the settlement at Buto in the second half of the fourth millennium BCE (Falt-

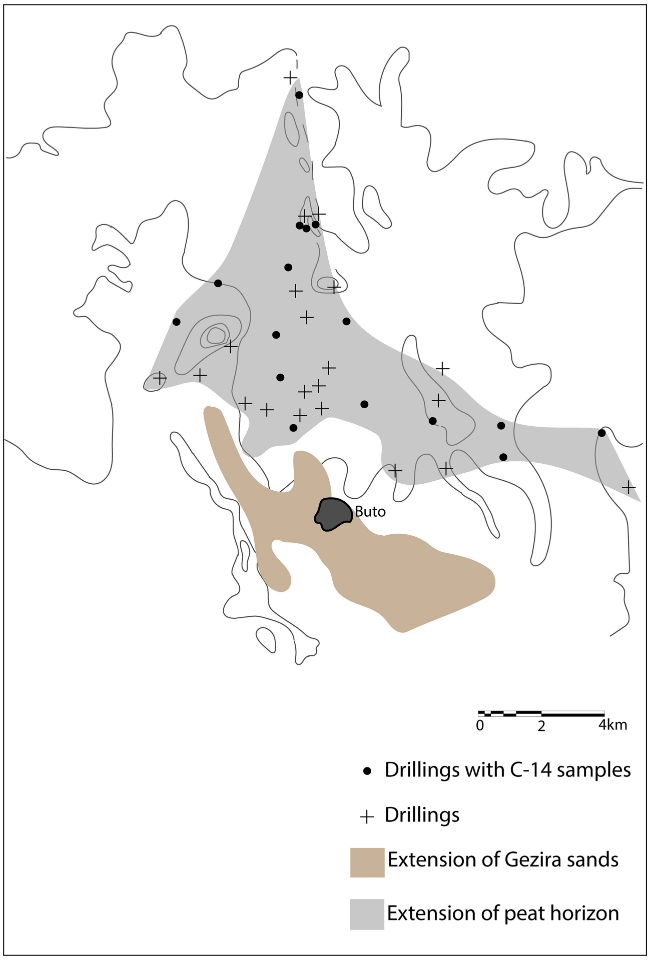

Figure 2. Geomorphology of Buto according to geophysical investigations, by courtesy of Jürgen Wunderlich (altered after Wunderlich, 1989, p. 108, Abb. 33).

ings, 1998, p. 373), the occupants of Buto could still explore large areas with open water surfaces and a dense vegetation of papyrus and other helophytes. Such a natural landscape would certainly match with the idea of the mythological papyrus marshes.

3 Sais

Sais was the main cult place of the goddess Neith, a goddess of deltaic origins (Wilson, 2006, pp. 2–3; Wilson, 2011, pp. 186–187), who since the earliest times belonged to the most important female deities of Egypt. As stated above, besides her anthropomorphic image often wearing the red crown of Lower Egypt, Neith could appear in the shape of a fearsome lioness goddess, sometimes associated with Sekhmet and Bastet (El-Sayed, 1982, p. 136).

3.1 Textual sources

Some important information concerning a lake at the temple of Neith at Sais under the reign of Amasis (570–526 BCE) comes from a biographical inscription on the dorsal pillar of the statue of an official named Horkhebi who states: "I dug a lake on the eastern side of the canal *ww*. [Its] length: 68 cubits, width: 65[?] cubits, lined with stone, with 8 staircases and walls around it [. . .] in it for Neith and the gods of the nome of Sais by order of the Dual king Amasis, son of Neith" (Geßler-Löhr, 1983, pp. 233–235).

The inscription on the statue of a woman from the early Ptolemaic Period usually cited in the literature amongst the textual evidence (Leclant and De Meulenaere, 1957, p. 36; Geßler-Löhr, 1983, p. 237; Zecchi, 1996, pp. 32–33; Wilson, 2019, p. 17) should be omitted as the reading of the group of signs in question is unsure and might refer to the offerings rather than to the lake.[1]

Herodotus describes the lake of the temple at Sais as follows: "Great stone obelisks stand in this sacred precinct, and a lake adjoins, beautifully lined with a crepidoma of stone all around; it is, as it seemed to me, as big as the lake at Delos, the so-called Circular Pond" (Hd. II. 170; Wilson, 2015, p. 228; Nesselrath, 2017, p. 200; also Wilson 2006, pp. 36–37).

These texts bear witness to the existence of a sacred lake in the precinct of the temple of Neith at Sais. The biographical inscription of Horkhebi provides some details on the dimensions and the location of the lake, which will be discussed below (Sects. 3.2 and 4).

3.2 Geoarchaeology

Similar to Buto, Sais was originally a twin tell, with the settlement started on two neighbouring *geziras*, to the west and east of a natural canal that evolved out of a lake between the two elevations (Wilson, 2006, pp. 203–204).

According to the drillings conducted by the team of Wilson (2006), an ancient water canal once flowed close to the eastern side of the so-called northern enclosure, an area to the north of the site. In this area to the north of the site was once located the temple of Sais, now completely destroyed. There might have been another palaeo-canal to the east, yet the traces found there indicate a more recent dating for this waterway (Wilson, 2006, pp. 177–204, 252–256).

On the eastern side of the northern enclosure, a possibly natural spring still flows. It may have already existed in ancient times. Wilson (2006) also reports the discovery of several limestone blocks at the site of this spring, which might have belonged to the lining of the sacred lake. According to her the spring could have been the source of the sacred lake of the temple (Wilson, 2006, p. 256). This fits well with the biographical text of Horkhebi cited above, who describes the

[1] My thanks go to Karl Jansen-Winkeln for his helpful comments on this text.

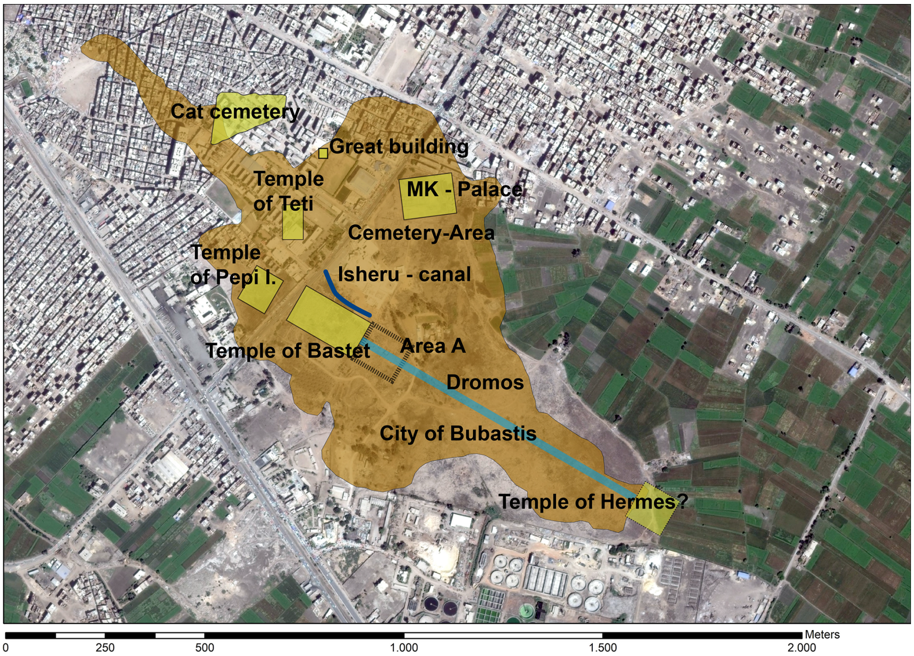

Figure 3. The course of the northern sacred canal at Bubastis according to the latest geophysical investigations. © Google Maps, modified by Eva Lange-Athinodorou.

construction of a sacred lake at the temple, more precisely an artificial water basin, lined with stone blocks and accessible via staircases leading down to the water.

4 Bubastis

Attestations for the cult of Bastet date back to the second dynasty (ca. 2850 BCE). If Bubastis was already the main cult place of this goddess in these early times is difficult to establish, as the earliest evidence of the cult of Bastet there dates back to the sixth dynasty only (Lange, 2016, pp. 310–313). We have, however, ample textual and archaeological evidence that she was the main goddess of Bubastis from then on until the time of the Roman emperors (Naville, 1891; de Wit, 1956, pp. 292–297).

4.1 Textual sources

The sacred waters of Bubastis appear prominently in the written record. Papyrus Brooklyn 47.218.84, a mythological compendium on the cities of the delta from the second part of the seventh century BCE, contains two references to it. The first says about the goddess, "She is on the pedestal of 'throwing down the enemies'. A falcon tames her, two hippo deities surround her, an *Henet* water is all around her, the length of which is . . . 7(?) (cubits and the width) 42 (cubits)" (pBrooklyn 47.218.84, IX.4; Meeks, 2006, p. 20). The term *Henet* that refers to the waters surrounding the temple of Bastet can generally designate various types of natural bodies of water, such as Nile branches, canals and lakes (Yoyotte, 1962, p. 88.4; Geßler-Löhr, 1983, p. 407, footnote 1348; Meeks, 2006, pp. 100–101).

Another paragraph in the same papyrus calling those waters *Isheru* informs us about the triumphal appearance of Bastet as the defeater of Seth in her sacred barque during her annual festival: "And they row her in the Oryx antelope on the *Isheru* at the moment as she saved the Udjat-Eye from him". (pBrooklyn 47.218.84, IX.7–8; Meeks, 2006, p. 20; Bohms, 2013, pp. 36–42). A very vivid depiction of this scene appears on the fragment of a stela from the Late Period. It was discovered at Bubastis at the cemetery of the cats, the sacred animals of the goddess (El-Sawi, 1977). Here we find all the elements described in the papyrus: the statue of the goddess in her shrine sitting in a barque, the stern of which is shaped like the head of an oryx antelope, the animal of Seth, representing the enemy she had subdued. Under the barque, zigzag lines indicate the water of the sacred canal as well (cf. also Geßler-Löhr, 1983, p. 407 and Fig. 74; Schorsch, 2015).

Herodotus describes the environments of the temple of Bastet at Bubastis in detail: "Except the entrance, the rest is an island. The canals, which come from the Nile, are not joining one another, but each one extends to the entrance of the temple; the one surrounds the one side, the other the other side and each one is 100 feet wide and shadowed by trees" (Hd. II. 138.1; Wilson, 2015, pp. 208–209; Nesselrath, 2017, p. 184).

The above-mentioned texts all come from the second part of the first millennium BCE. Still, how far the *Isheru* at Bubastis really dates back is unclear. The above-mentioned relief block (cf. Sect. 1.1) from the early 12th dynasty from Koptos names Bastet as the Lady of Isheru. Yet, the location of the *Isheru* mentioned on this block does not necessarily have to be at Bubastis, contrary to some attempts to locate it there (Sauneron, 1964, pp. 52, footnote 33; Yoyotte, 1962, pp. 103–104).

4.2 Geoarchaeology

Core drillings at Bubastis conducted by Ullmann et al. (2019, pp. 190, 195–197) revealed that the temple of Bastet sits on the elevated part of a NW–SE-oriented *gezira* of Pleistocene origin. Furthermore, it is possible that Bubastis, like Buto and Sais, was actually built not only on one elevation but also on a twin tell. In that case, the temple area was located on the southern mound, while the cemeteries were established at the northern one.

Recently, DCR soundings and ERT by Amr Abd el-Raouf pointed to the existence of a canal, close to the temple of Bastet. Core drillings and sediment analyses by Julia Meister corroborated those finds, placing a canal around 50–60 m to the north of the outer wall of the temple (Lange-Athinodorou et al., 2019). The results of the combined geophysical analysis led to the detection of around a 300 m length of a canal, its width measuring between 20 and 30 m (cf. Fig. 3; Lange-Athinodorou et al., 2019). This canal was most probably the northern part of the canal system that surrounded the temple, namely the *Isheru* or *Henet* of the Egyptian texts.

The dominant infill of the canal with fine-grained sediments as well as their high content of organic matter indicates that very slowly flowing water accumulated them. Parallel sediment laminations point to a periodic influx of fresh water, coming from a larger river, possibly a nearby Nile tributary. Eventually, the canal at the temple was cut off and became stagnant water, gradually silting up (Lange-Athinodorou et al., 2019, pp. 6–8, 11). A dating of the canal and its active periods is still difficult and must await further chronological analysis. However, the textual sources show that the canal system was existent at least in the time from the seventh to the fifth century BCE.

5 Discussion

The survey of the textual and geoarchaeological evidence represented in Sects. 1.1–3.2 allows some tentative reconstructions and comparisons of the lakes and canals in, around and nearby the temples of Buto, Sais and Bubastis with respect to their different hydrogeographic and geomorphological contexts. In addition, I will discuss the question as to whether the canals and lakes at those sites are of a natural or artificial origin.

For Buto, a text from the Ptolemaic Period at Karnak points to the existence of a sacred canal *around* the temple. By contrast, Herodotus refers to a "deep and wide" lake with an island somewhere close to the temple (cf. Sect. 1.1). As one can see in the case of Bubastis, Herodotus did differentiate between lakes and canals thoroughly. Therefore, the two texts might actually describe two distinct sacred waters at Buto: a probably horseshoe-shaped canal surrounding the temple mound and a lake within the temple enclosure wall. A drilling core in the eastern part of the temenos, south of the main axis of the temple, indicates that the sacred lake could have been somewhere in this area (cf. above Sect. 1.2). However, without further core drillings there is no way of determining its dimensions. Furthermore, no core drillings, sediment analyses and geoelectric soundings are available yet from the depression around the temple mound, where the canal of Wadjet could have flowed as described in the Ptolemaic text. Its existence in that vicinity is definitely a hypothesis worth testing by the means of geoarchaeological methods in the future. Another interesting, yet admittedly still unproven, possibility is that the palaeo-landscape with large marshlands to the north of Buto, as revealed by the geophysical survey there (cf. Sect. 2.1), might have inspired the mythos of the hiding of the child god Horus by his mother Isis in the papyrus thickets. In this process, the natural landscape, i.e. the marshlands called *Akhbit*, would have undergone a mythological interpretation and could later on be used as an ideal model providing the scenery for this specific mythos in Egyptian religious texts.

At Sais, we encounter a different situation. The texts unanimously describe a sacred lake, which Herodotus reports was established within the temenos area. The earlier text of Horkhebi adds its dimensions: the basin he built would have measured 35.63 m by 34.06 m, thus forming an almost square structure. Measuring 100 m by 70 m, the lake at Delos, which Herodotus uses for comparison, was, however, much larger (Nesselrath, 2017, p. 788, no. 264).

More complicated is the localization of the lake with regards to the canal of the name *ww* in Horkhebi's inscription. At first glance, one is inclined to identify this waterway with the palaeo-canal to the east of the temple area (cf. Sect. 2.2). Yet, as Wilson (2006, p. 257) points out, this poses problems, because Horkhebi clearly states, "I dug a lake on the *eastern* side of the canal *ww*" (emphasis added). The eastern side of the palaeo-canal is far outside of the temenos area. In this case, the artificial lake would have been nowhere within the enclosure wall of the temple, which seems to be very improbable. Moreover, the position of the spring, as the possible source of the lake, can be localized to the *west* of the palaeo-canal and hence doubtless well within the temple district (Wilson, 2006, p. 262, Fig. 8). Therefore, the *ww* canal should not be identified with the palaeo-canal to the east detected by core drillings. Rather, the *ww* canal was probably flowing somewhere to the west of the northern enclosure. The canal detected in this area is however a more recent structure.

More evidence is available for Bubastis: the main sacred body of water of the temple was doubtlessly a structure of two canals coming from a Nile branch. The temple mound therefore must truly have given the impression of an island, quite as Herodotus described it. As was shown above (Sect. 3.2), one of the paragraphs of Papyrus Brooklyn provides information on its dimensions: “an *Henet* water is all around her, the length of which is ... 7(?) (cubits and the width) 42 (cubits).” Unfortunately, the first specification in the papyrus is illegible. The width of the canal given by the ancient texts on the other hand is very close to the facts discovered by the geophysical analysis: the 42 cubits of Papyrus Brooklyn are a little more than 22 m. The description of Herodotus states 30 m for the width instead. These different statements of the dimensions in Papyrus Brooklyn and Herodotus might be explained by the fact that the canal was part of a dynamic hydrographic system. Its water level and dimensions therefore changed not only from season to season with the changing water volume of the Nile and its distributaries but also on a long-term scale. In Bubastis, another artificial basin might have also existed within the temple enclosure such as in Buto and Sais, but to date, there is no indication of it.

Finally, the question arises as to whether the sacred canals and lakes at Buto, Sais and Bubastis were of natural or artificial origin. In the case of the canals at Bubastis, the results of the geoarchaeological investigation do not yet allow a definitive answer. It is, however, conceivable that the natural hydrogeographic situation with two canals surrounding the elevated part of the *gezira* led to the founding of the temple of Bastet there. The main reasons for choosing this position were very probably the specific requirements of the cult of the lioness goddess (cf. Sect. 5; also Yoyotte, 1962, pp. 108–109). In later times, people might have artificially maintained the function of the canal as a navigable waterway by digging out accumulating sediments on a more or less regular basis. Regarding the canal around the temple mound at Buto, a similar situation is imaginable but awaits future investigations as well. The temple lake at Sais might have been based on a comparable process of enhancing a natural situation by artificial means: assumedly, a natural spring in the western part of the temenos area was the source of water that filled an artificial basin built of limestone blocks. Finally, whether the sacred lake within the temple of Wadjet was in any way similar to the one at Sais cannot be answered without further data.

The question remains around which reasons might have caused the specific connection of the horseshoe-shaped lakes and canals and the temples of goddesses. One answer lies in the geomorphological situation of the temple sites in the delta. Here, temples were built on elevations, while the depressions close to them would be at least seasonally water-bearing. In that case, a half-circular shape of the pool or canal would emerge as in the cases of Buto and Bubastis. As horseshoe-shaped lakes were preferred near temples of goddesses in the Nile Valley as well, several scholars argue that their natural prototypes might have been temporary fan-shaped lakes evolving on the estuaries of the wadis after seasonal rainfall. Such temporary lakes provided water for a variety of wildlife and therefore also attracted hunting lion prides (Tillier, 2010, p. 173, footnote 46). People would observe lionesses at those natural lakes not only hunting but also lovingly caring for their cubs. By analogy, people might have imagined that this kind of landscape was favourable for lioness goddesses as well. The water surrounding their temples would cool and calm their temper and bring out their positive, caring and protective nature. Therefore, locations surrounded by lakes or canals would have been thought to have been the ideal setting for their cult.

According to the narration of Herodotus, countless people celebrated festivals at Bubastis in honour of Bastet, which seem to have been ecstatic and orgiastic. The celebrations involved drunkenness and displays of many kinds of ecstatic activities like wild dancing and singing (Hd. II. 59.1–60.1; Wilson, 2015, pp. 161–162; Nesselrath, 2017, pp. 144–145). The already cited texts of Papyrus Brooklyn include a tale about Bastet, who saved the eye of Horus from Seth at Bubastis and was rowed on the sacred canals displaying her triumph over the enemy (cf. Sect. 3.1). This is actually the description of a river procession with a cult statue of Bastet in her barque shrine as the culmination of the festival. Surely, the appearance of the triumphant goddess would be the summit of a celebration passionately attended by the thousands of pilgrims who journeyed to her city every year to attend her festival.

6 Summary and conclusions

Elemental components of sacred landscapes at Buto, Sais and Bubastis were the canals and lakes in close proximity to the temples of the goddesses who were venerated in those cities. Geoarchaeological investigations not only bear witness to their existence but also indicate their dimensions and locations and help to reconstruct the hydrogeography and palaeolandscape they were connected to. So far, the analysis of the data gained by geoarchaeological methods leads to interesting results on the specifics of the lakes and canals at the three sites used as case studies: a sacred canal of the *Isheru* type and a sacred lake within the temple enclosure most probably defined the sacred landscape of Buto. At Sais, an existing sacred lake of possibly natural origin was enhanced for continuous use with an enclosure of stone blocks. The large *Isheru*-type canals of Bubastis enclosed the temple almost completely.

On the other hand, textual records are useful with regard to the understanding and reconstruction of the importance of sacred waters in the cult and the local mythology of Wadjet, Neith and Bastet. All of them were goddesses considered to be of an ambivalent nature: mighty, protecting and dangerous, the latter preferably to the enemies of the king; yet the rage of the goddesses could turn against even their admirers at any moment or, alternatively, into a peaceful calm temper (Lange-Athinodorou et al., 2019, pp. 554–561, 580–581). A canal system enclosing their temple or at least a lake close to the sanctuary was believed to be necessary to cool and please their unpredictable fiery temper.

Furthermore, the sacred canals were not only a tool to please and cool the mood of the goddesses; they were also a key element in the performance of their cults. The rich textual and pictorial evidence at Bubastis could be used as a role model of the events taking place on and around the sacred waters of Buto and Sais. Although there is no comparable textual evidence, it is well imaginable that Wadjet and Neith had festivals of their own with their barques appearing on their sacred canals and lakes during religious festivals. We know of such ceremonies at the temples of Sekhmet at Memphis, Mut at Karnak and Hathor at Dendera to name but a few (Geßler-Löhr, 1983, pp. 401–424; Tillier, 2010, pp. 170–171).

The results of the geophysical survey of the environs of Buto now widen the horizon much further. The evidence of a large palaeo-swamp north of Buto leads to the question as to whether human experience of this impressive landscape resulted in the concept of the papyrus marshes of *Akhbit* as the hiding place of Horus, a centrepiece of Egyptian mythology. If correct, this could highlight the cognitive process of connecting natural landscapes with mythological narratives: certain features of natural landscapes of the delta, even far from temple buildings, were incorporated into the imaginary sacred landscapes of the delta in ancient Egyptian minds.

Data availability. All relevant data and references are cited in this article.

Competing interests. The author declares that there is no conflict of interest.

Special issue statement. This article is part of the special issue "Geoarchaeology of the Nile Delta". It is a result of the workshop "Geoarchaeology of the Nile Delta: Current Research and Future Prospects", Würzburg, Germany, 29–30 November 2019.

Acknowledgements. I would like to thank the participants of the workshop for an interesting discussion, as well as the anonymous reviewers for their input.

Financial support. This open-access publication was funded by Julius-Maximilians-Universität Würzburg.

Review statement. This paper was edited by Becky Briant and reviewed by two anonymous referees.

References

Bohms, I.: Säugetiere in der altägyptischen Literatur, Ägyptologie 2, Lit-Verlag, Berlin, Münster, 2013.

Boreik, M., Gabolde, L., and Graham A.: Karnak's quaysides: evolution of the embankments from the Eighteenth Dynasty to the Graeco-Roman Period, in: The Nile: natural and cultural landscape in Egypt, edited by: Willems, H. and Dahms, J.-M., transcript, Bielefeld, 97–144, 2017.

Cordoba, C.: Geoarchaeology, The Human-Environmental Approach, I. B. Tauris, London, New York, Oxford, New Delhi, Sydney, 2020.

Darnell, J. C.: Opet festival, in: UCLA Encyclopedia of Egyptology online (1.1), edited by: Dieleman, J. and Wendrich, W., available at: https://escholarship.org/uc/item/4739r3fr (last access: 27 June 2020), 2010.

David, B. and Thomas, J.: Landscape archaeology: introduction, in: Handbook of landscape archaeology, edited by: David, B. and Thomas, J., Routledge, New York, 27–43, 2016.

De Wit, C.: Le rôle et le sens du lion dans l'Égypte ancienne, E.J. Brill, Leiden, 1951.

El-Sawi, A.: Preliminary report on Tell Basta excavations, Seasons 1969, 1970, 1971, Zeitschrift für Ägyptische Sprache und Altertumskunde, 104, 127–131, 1977.

El-Sayed, R.: La déesse Neith de Saïs, BdE 86, Institut français d'Archéologie orientale, Le Caire,1982 (in French).

Faltings, D., Ballet, P., Förster, F., French, P., Ihde, C., Sahlmann, H., Thomalsky, J., Thumshirn, C., and Wodzinska, A.: Zweiter Vorbericht über die Arbeiten in Buto von 1996 bis 1999, Mitteilungen des Deutschen Archäologischen Instituts, Abteilung Kairo, 56, 131–179, 2000 (in German).

Faltings, D.: Recent excavations in Tell El-Fara'in Buto: new finds and their chronological implications, in: Proceedings of the Seventh International Congress of Egyptologists, Cambridge, 3–9 September 1995, edited by: Eyre, C. J., Peeters, Leuven, 365–375, 1998 (in German).

Gardiner, A. H.: Horus the Behdetite, Journal of Egyptian Archaeology, 30, 23–60, 1944.

Geßler-Löhr, B.: Die heiligen Seen ägyptischer Tempel: ein Beitrag zur Deutung sakraler Baukunst im alten Ägypten, Hildesheimer Ägyptologische Beiträge, 21, Gerstenberg, Hildesheim, 1983.

Gomaà, F.: Die Besiedlung Ägyptens während des Mittleren Reiches II: Unterägypten und die angrenzenden Gebiete. Beihefte zum Tübinger Atlas des Vorderen Orients, Reihe B (Geisteswissenschaften) 66, Reichert, Wiesbaden, 1987.

Hartung, U., Ballet, P., Effland, A., French, P. G., Hartmann, R., Herbich, T., Hoffmann, H., Hower-Tilmann, E., Kitagawa, C., Kopp, P., Kreibig, W., Lecuyot, G., Lösch, S., Marouard, G., Zink, A., Nerlich, A., and Pithon M.: Tell el-Fara'in – Buto: 10, Vorbericht, Mitteilungen des Deutschen Archäologischen Instituts Kairo, 65, 83–190, 2009 (in German).

Hartung, U.: Recent investigations of Early Dynastic building structures at Tell el-Fara'in/Buto, in: Ancient Egyptian and ancient Near Eastern palaces, volume I: Proceedings of the conference on palaces in ancient Egypt, edited by: Bietak, M. and Prell, Silvia, London, UK, 12–14 June 2013, 101–112, 2018.

Lange, E.: The lioness goddess in the Old Kingdom Nile Delta: a study in local cult topography, in: Sapientia Felicitas: Festschrift für Günter Vittmann zum 29. Februar 2016, edited by: Lippert,

S. L., Schentuleit, M., and Stadler, M. A., CENiM, 14, 301–324, 2016.

Lange-Athinodorou, E.: Der "Tempel des Hermes" und die Pfeile der Bastet: zur Rekonstruktion der Kultlandschaft von Bubastis, in: En détail – Philologie und Archäologie im Diskurs, edited by: Brose, M., Dils, P., Naether, F., Popko, L., and Raue, D., De Gruyter, Berlin/Boston, Festschrift für Hans-Werner Fischer-Elfert 1, 549–585, https://doi.org/10.1515/9783110629705-025, 2019.

Lange-Athinodorou, E., Abd El-Raouf, A., Ullmann, T., Trappe, J., Meister, J., and Baumhauer, R.: The sacred canals of the temple of Bastet at Bubastis (Egypt): new findings from geomorphological investigations and Electrical Resistivity Tomography (ERT), J. Archaeol. Sci.-Rep., 26, 1–13, https://doi.org/10.1016/j.jasrep.2019.101910, 2019.

Leclant, J. and De Meulenaere, H.: Une statuette égyptienne à Délos, Kêmi 14, 34–42, 1957 (in French).

Leclère, F.: Les villes de Basse Égypte au Ier millénaire av. J.-C.: analyse archéologique et historique de la topographie urbaine, 2 vols. Bibliothèque d'étude 144, Institut français d'archéologie orientale, Le Caire, 2008 (French)

Mariette, A.: Abydos: description des fouilles exécutées sur l'emplacement de cette ville, Librairie A. Franck; Imprimerie nationale, Paris, 1869 (in French).

Meeks, D. : Mythes et légendes du Delta d'après le papyrus Brooklyn 47.218.84, Mémoires publiés par les membres de l'Institut français d'archéologie orientale 125, Institut Français d'Archéologie Orientale, Le Caire, 2006 (in French).

Montet, P.: Le lac sacré de Tanis, Académie des Inscriptions et Belles-Lettres (Extrait des Mémoires de l'Académie, Tome XLIV), Paris, 1966 (in French).

Naville, E: Bubastis (1887–1889), EEF 8, London, 1891.

Nesselrath, H.-G.: Herodot: Historien, Alfred Kröner Verlag, Stuttgart, 2017 (in German).

Petrie, W. M. F.: Koptos, Bernard Quaritch, London, 1896.

Said, R.: The geological evolution of the River Nile, Springer Verlag, New York, Heidelberg, Berlin, 1981.

Said, R.: The river Nile: geology, hydrology and utilization, Pergamon Press, Oxford, New York, Seoul, Tokyo, 1993.

Sauneron, S.: La porte ptolémaïque de l'enceinte de Mout à Karnak, Mémoires publiés par les membres de l'Institut français d'archéologie orientale, 107, Institut français d'archéologie orientale, Cairo, 1983 (French).

Sauneron, S.: Villes et légendes d'Égypte, Bulletin de l'Institut Français d'Archéologie Orientale (BIFAO), Cairo, 62, 33–57, 1964 (in French).

Schorsch, D.: Bastet goes boating, Bulletin of the Egyptological Seminar (BES), 19, 571–584, 2015.

Tillier, A.: Notes sur l'icherou, Égypte Nilotique et Méditerranéenne, 3, 167–176, 2010.

Ullmann, T., Lange-Athinodorou E., Göbel, A., Büdel, C., and Baumhauer, R.: Preliminary results on the paleo-landscape of Tell Basta/Bubastis (eastern Nile delta): an integrated approach combining GIS-based spatial analysis, geophysical and archaeological investigations, Quatern. Int., 511, 185–199, 2019.

van den Brink, E. C. M.: A geo-archaeological survey in the north-eastern Nile Delta, Mitteilungen des Deutschen Archäologischen Instituts, Abteilung Kairo, 43, 7–31, 1986.

von der Way, T.: Buto, in: Encyclopedia of the archaeology of ancient Egypt, edited by: Bard, K. and Shubert, S. B., London, 180–184, 1999.

Wilson, N. G.: Herodoti Historiae, Oxford University Press, Oxford, 2015.

Wilson, P.: Gateway to the underworld: the cult areas at Sais, Studies in Ancient Egypt and Sudan, 24, 341–364, 2019.

Wilson, P.: The survey of Saïs (Sa el-Hagar) 1997–2002, Egypt Exploration Society, Excavation Memoir 77, Egypt Exploration Society, London, 2006.

Wilson, P.: Sais I: The Ramesside-Third Intermediate Period at Kom Rebwa, Egypt Exploration Society, Excavation Memoir 98, Egypt Exploration Society, London, 2011.

Wunderlich, J.: Untersuchungen zur Entwicklung des westlichen Nildeltas im Holozän, Marburger geographische Schriften, Marburg/Lahn, Germany, 1989.

Wunderlich, J. and Ginau, A.: Paläoumweltwandel im Raum Tell el Fara'in/Buto: Ergebnisse und Perspektiven geoarchäologischer Forschung, Mitteilungen des Deutschen Archäologischen Instituts Kairo, 70–71, 485–497, 2014/2015 (in German).

Yoyotte, J.: Études géographiques, II: les localités méridionales de la région memphite et le "Pehou d'Héracléopolis", Revue d'égyptologie, 14, 75–111, 1962 (in French).

Zecchi, M.: A study of the Egyptian god Osiris Hemag. Archeologia e storia della civiltà egiziana e del vicino Oriente antico – Materiali e studi 1, La Mandragora, Imola, 1996.

E&G Quaternary Sci. J., 70, 83–92, 2021
https://doi.org/10.5194/egqsj-70-83-2021

Open Access E&G Quaternary Science Journal

Research article

Significant depositional changes offshore the Nile Delta in late third millennium BCE: relevance for Egyptology

Jean-Daniel Stanley and Sarah E. Wedl

Mediterranean Basin (MEDIBA) Program, 6814 Shenandoah Court, Adamstown, Maryland 21710, USA

Correspondence: Jean-Daniel Stanley (stanleyjd0@gmail.com)

Relevant dates: Received: 28 July 2020 – Accepted: 17 December 2020 – Published: 22 February 2021

How to cite: Stanley, J.-D. and Wedl, S. E.: Significant depositional changes offshore the Nile Delta in late third millennium BCE: relevance for Egyptology, E&G Quaternary Sci. J., 70, 83–92, https://doi.org/10.5194/egqsj-70-83-2021, 2021.

Abstract: No environmental factor has been as critically important for Egypt's ancient society through time as sufficiently high annual flood levels of the Nile River, the country's major source of fresh water. However, interpretation of core analysis shows reduced depositional accumulation rates and altered compositional attributes of the sediment facies deposited seaward of the Nile Delta during a relatively brief period in the late third millennium BCE. These changes record the effects of displaced climatic belts, decreased rainfall, lower Nile flows, and modified oceanographic conditions offshore in the Levantine Basin, primarily from 2300 to 2000 BCE, taking place at the same time as important geological changes identified by study of cores collected in the Nile Delta. It turns out that integrated multidisciplinary Earth science and archaeological approaches at dated sites serve to further determine when and how such significant changing environmental events had negative effects in both offshore and landward areas.

This study indicates these major climatically induced effects prevailed concurrently offshore and in Nile Delta sites and at about the time Egypt abandoned the Old Kingdom's former political system and also experienced fragmentation of its centralized state. In response, the country's population would have experienced diminished agricultural production leading to altered societal, political, and economic pressures during the late Old Kingdom to First Intermediate Period at ca. 2200 to 2050 BCE.

Kurzfassung: Für die Gesellschaft des Alten Ägypten war im Laufe der Zeit kein anderer Umweltfaktor so entscheidend wie die ausreichend hohen jährlichen Hochwasserstände des Nils, der wichtigsten Süßwasserquelle des Landes. Allerdings deuten Bohrkernanalysen darauf hin, dass während eines relativ kurzen Zeitraums gegen Ende des 3.Jahrtausends v. u. Z. geringere Ablagerungsraten sowie Veränderungen in der Zusammensetzung der Sedimentfazies auftraten, die sich meerwärts des Nildeltas akkumulierten. Diese Veränderungen resultierten aus einer Verschiebung der Klimagürtel, geringeren Niederschlägen und Nilabflüssen sowie veränderten ozeanographischen Bedingungen im Levantinischen Becken um etwa 2300 bis 2000 v. u. Z., einer Zeit weiterer geologischer Veränderungen, deren Effekte sich ebenfalls in den Bohrkernen nachweisen lassen. Wie sich nun zeigt, helfen integrierte multidisziplinäre geowissenschaftliche und archäologische Untersuchungen im Umfeld archäologischer Stätten dabei, näher zu bestimmen, wann und wie sich solche bedeutenden Umweltereignisse negativ auswirkten, sowohl vor der Küste, als auch im Delta selbst.

Die Ergebnisse dieser Studie legen nahe, dass sich diese großen klimabedingten Effekte gleichzeitig vor der Küste und im Umland archäologischer Stätten im Nildelta nachweisen lassen, ungefähr im gleichen Zeitraum, als in Ägypten das politische System des Alten Reiches zerfiel und die Fragmentierung des zuvor zentralistischen Staates einsetzte. Eine mögliche Konsequenz daraus wäre der Rückgang der landwirtschaftlichen Produktion, was wiederum zu veränderten gesellschaftlichen, politischen und wirtschaftlichen Bedingungen für die Bevölkerung des Landes vom späten Alten Reich bis zur Ersten Zwischenzeit um ca. 2200 bis 2050 v. u. Z. geführt haben könnte.

1 Introduction

Climatic conditions evolved considerably during the Middle to Late Holocene as interpreted by study of the sedimentary record examined in Egypt, northeastern Africa, and the Levant (Said, 1993; Gasse, 2000; Bar-Matthews and Ayalon, 2011; Marriner et al., 2013; Kaniewski et al., 2018). The present survey focuses primarily on significantly decreased sediment accumulation rates and marked lithofacies changes seaward of the Nile Delta that became more pronounced after the African Humid Period (AHP), from about 5000 to 4000 years ago (Maldonado and Stanley, 1976; Krom et al., 2002; Stanley et al., 2003; Ducassou et al., 2009; Kholeif and Mudie, 2009; Blanchet et al., 2013; Revel et al., 2015). Stratigraphic, lithological, and compositional attributes of deposits accumulating in lower Egypt and the delta during that period record increased effects of aridity and desertification (Calvert and Fontugne, 2001; Stanley et al., 2003; Ducassou et al., 2009; Kholeif and Mudie, 2009; Kholeif and Ibrahim, 2010; Bernhardt et al., 2012; Blanchet et al., 2013; Marriner et al., 2013; Pennington et al., 2019). Altered monsoonal rainfall patterns and intensities induced erosional changes in Nile highland source terrains south of Egypt, including Ethiopia and the East African lakes region, which modified the hydrography of both the Blue Nile and the White Nile during the Holocene (Gasse, 2000; Blanchet et al., 2015; Woodward et al., 2015). These changes induced substantially lower Nile flows northward to and across the Sudan and Egypt and significantly reduced rates of fresh water and sediment discharged into the delta (Stanley, 2019). Interpreting possible climatic effects seaward of the delta in the Mediterranean during this period is of major consideration in the present study.

The millennium from ca. 5000 to 4000 years BP (before present) comprises Egypt's early dynasties (numbered I to XI). This time span includes the Early Dynastic Period and Old Kingdom to the First Intermediate Period as established archaeologically (Shaw, 2000; Bard, 2008). It was during pharaonic rule of the Old Kingdom that Egypt's civilization was already reaching stunning levels, including major phases of social and municipal expansion, monumental construction projects along the Nile, and impressive artistic development (Shaw, 2000). Toward the latter part of that millennium, however, some notable degradation occurred, such as of pyramids (see Fig. 5 herein for example) during Egypt's late Old Kingdom and First Intermediate Period. These took place at, or about, the time when environmental conditions were evolving extensively, not only in the Nile Delta but also offshore as highlighted in the present review. Whether the country's population could have been affected by such altered climatic conditions at that time will be considered herein.

2 General background

Depositional changes observed offshore are recorded between the outer continental shelf and more distal, deeper slope sectors north of the delta in the eastern Mediterranean (Ducassou et al., 2009; Kholeif and Ibrahim, 2010). Studies at sea here (Fig. 1a) in recent years have recorded altered attributes through time in radiocarbon-dated sediment core sections, including markers such as texture, mineralogy and isotopes, and biogenic components. Together, these reveal that after ca. 5000 years BP proportions of eolian sediment, derived from both proximal and more distal arid terrains and deserts, were increasing in both deltaic and offshore deposits. By ca. 4000 years BP observations indicate that desert conditions had fully reached Egypt's Sahara (Calvert and Fontugne, 2001; Krom et al., 2002; Marriner et al., 2013; Blanchet et al., 2013; Pennington et al., 2019). For the purposes here we define three periods: from $\sim 11\,000$ to ~ 8000 years BP is Early Holocene, from ~ 8000 to ~ 4500 years BP is Middle Holocene, and from ~ 4500 years BP to present is Late Holocene. The Middle to Late Holocene is a time of prime interest here that has experienced significant shifts in amounts of water and sediment derived from Blue Nile, and to a lesser extent White Nile, upland source areas that were dispersed downslope to lower Egypt, its delta plain, and offshore. For example, Revel et al. (2015) proposed that decreased proportions of clastic sediments from Ethiopia's Blue Nile were at times derived from ca. 6 to 3.1 ka. Such changes resulted from altered rainfall patterns in East African highland source areas and increased aridification (Marriner et al., 2013; Revel et al., 2015) that markedly reduced sediment discharged by Nile flows at the coastal margin. This resulted in lower proportions of fluvial terrigenous and volcanically derived material released over more limited deltaic and offshore areas (Stanley and Warne, 1993).

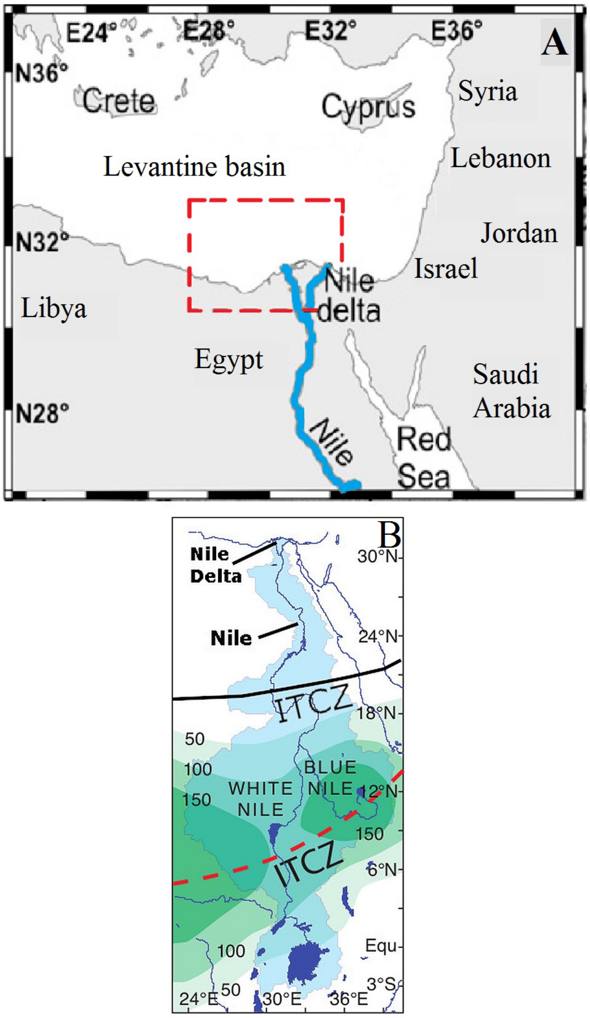

Figure 1. **(a)** Levantine Basin in the eastern Mediterranean showing the study area NW of Egypt's lower Nile River and delta. **(b)** Nile catchment basin (in blue) shows two approximate latitudinal positions of the June–July–August Intertropical Convergence Zone (ITCZ): solid black line denotes monsoonal shift to the north during Early to Middle Holocene; dashed red line denotes its Late Holocene move toward present position farther to the south. Numbers 50 to 150 are rainfall values (in mm), for the monsoon season (after Marriner et al., 2012, their Fig. 1b, modified here by authors of this article).

Egypt's then modest population along the Nile valley and lower river stretches had initially used a portion of deltaic plain terrains for pasturing and later for cultivation. The latter depended increasingly on channelization and diversion of water for irrigation from the Nile, that country's major source of fresh water (Butzer, 1976, 1984). Critical in this respect is the amount of freshwater discharge reaching the delta that responded largely to regional climate change induced by north–south latitudinal migration of the Intertropical Convergence Zone (ITCZ; Fig. 1b). Nile discharge fluctuations were also induced by more frequent and periodically intense El Niño–Southern Oscillation (ENSO) cycles that, at a centennial scale, affected water flow and sediment delivery to lower Egyptian sectors and its coast (Said, 1993; Krom et al., 2002; Marriner et al., 2012).

The focus here is on altered sediment databases recorded offshore Egypt that can be compared with those of similar age previously examined in the Nile Delta and farther inland. Data from dated sediment cores in the delta's northern sector and coastal area identify a period of markedly decreased depositional rates. This phase prevailed primarily during a 200- to 300-year period, between ca. 4300 and 4000 years BP (Stanley, 2019), and spans that of a climatically altered period generally termed the "ca. 4200 year BP event". This phase has been discussed by climatologists, geographers, sedimentologists, palynologists, and others, who have examined the Holocene record in different sectors of the eastern Mediterranean, Levant, and beyond (Weiss et al., 1993; Bar-Matthews and Ayalon, 2011; Kaniewski et al., 2018).

Other natural phenomena considered include neotectonic activity, as recorded by stratal deformation and offsets observed in seismic subbottom surveys that could have triggered some downslope displacement of sediment by gravitative flows such as turbidites and slumps during the Holocene. Near-surface displacement may have been set in motion by deep-seated underlying salt tectonics, isostatic readjustment of consolidated strata at depth, or shifts triggered by episodic shallow earthquake motion in the late Quaternary and continuing to the present (Ross and Uchupi, 1977; Kebeasy, 1990; Bellaiche et al., 1999; El-Sayed et al., 2004). Eustatic sea-level rise could also account for some changes in offshore sedimentation, especially during the period when the >100 m rise in sea level occurred from the Late Pleistocene (ca. 18 000 years BP) to the Middle Holocene (ca. 7500 years BP). This rapid rate of rise then decreased markedly by about 7500 to 6000 years BP to an elevation of -8 to -6 m below present sea level and then further declined by ca. 4000 years BP, attaining a level of about -3 to -2 m beneath the present level (Fleming et al., 1998; Sivan et al., 2001). The shelf's once subaerially exposed surface was submerged as the shoreline retreated landward toward the south. The delta's coastal margin from ca. 6000 to 4000 years BP (Fig. 2) appears to have reached its northward position on what once had been near the mid-shelf (Stanley and Warne, 1993). It then continued its southward retreat as a function of coastal erosion and concurrent subsidence of the inner shelf to mid-shelf and low-lying northern delta substrate (Stanley and Clemente, 2017; Stanley, 2019).

2.1 Early to Middle Holocene Nile offshore sedimentation

Seafloor deposits of Holocene age seaward of the delta, examined in about 150 gravity and piston sediment cores by specialists in diverse fields, were recovered across extensive offshore areas. These are curated in marine research centers

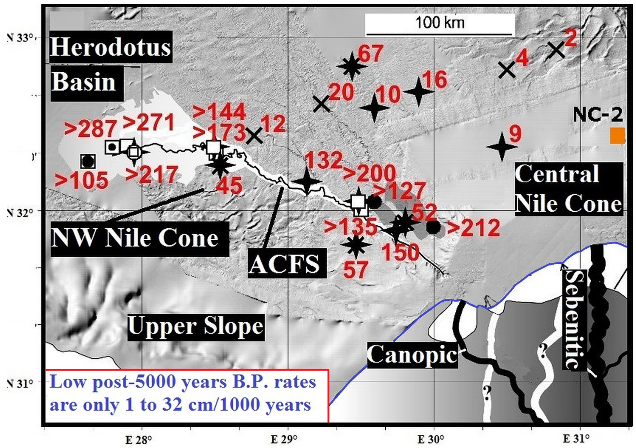

Figure 2. Study area off the NW Nile Delta (in lower right of figure) shows the Herodotus Basin (> 3000 m), NW and central sectors of the Nile Cone, Alexandria canyon–fan system (ACFS), corner of delta in northern Egypt, and positions of 23 cores offshore. Numbers in red: sedimentation rates in centimeters per 1000 years for lower core sections dated from ca. 10 000 to ca. 5000 years BP (data after Ducassou et al., 2009, their Figs. 13 and 14, modified here by the authors of this article). These record high rates of Nile sediment discharge during wetter climate. Different symbols at each core site identify major sediment types. In marked contrast, upper sections of the same cores, dated from ca. 5000 years BP to Late Holocene, record much lower rates of Nile discharge (only 1 to 32 cm per 1000 years; also after Ducassou et al., 2009) during the period of increased aridity.

and museum collections, including those in Egypt (Kholeif and Mudie, 2009), Europe (Ducassou et al., 2009), the United States (Maldonado and Stanley, 1976), and elsewhere. Core samples serve to compare dated Early (from ∼ 11 000 years BP) to dated Late Holocene lithofacies changes between Egypt's Nile continental shelf and deeper sectors. Focus here is on offshore slope deposits that accumulated on the upper surface of a large elongated bulge off Egypt, termed the Nile Cone, which extends seaward of the delta's shelf and upper slope. The study area is primarily on the pronounced cone sector that trends northwest of the delta's shelf edge (> 200 m depth) to the deep (> 3000 m) Herodotus Basin plain (Fig. 2). Seafloor isobaths in this area are shown in Ducassou et al. (2009) and are well defined on larger-scale charts such as the one compiled by the US Defense Mapping Agency Hydrographic Center (1972, N.O. 310) at a scale of 1 : 2 849 300.

The cone in this sector is ∼ 225 km long, increases in width downslope to ∼ 250 km at its base, and covers ca. 50 000 km^2. An elongate submarine canyon, traced on the surface of the NW cone, meanders downslope (Fig. 2); it extends from off-Nile mouths of the modern Rosetta and former Canopic branches to the lower cone. This Alexandria canyon–fan system (ACFS) actively distributed sediment seaward, primarily prior to ca. 5000 years BP during the Middle Holocene. Sedimentation patterns distributed on the Nile shelf, between the delta and its upper fan, have been defined by Summerhayes et al. (1978), Sestini (1992), and also Egyptian agencies including the Coastal Research Institute and the National Institute of Oceanography and Fisheries.

Shelf and upper-slope sediments record influences of the Late Holocene to recent wind- and wave-driven bottom current transport, the latter presently most active along the inner shelf and mid-shelf. These processes shift shallow seafloor sediment mainly eastward and, locally, seaward off the shelf (UNESCO/UNDP and Arab Republic of Egypt, 1978; Frihy and Dewidar, 2003; Kholeif and Mudie, 2009). Materials normally originating on the shelf and recovered in upper-slope and deeper Nile Cone cores indicate seaward displacement at times of intensified coastal margin circulation that swept the seafloor. Sedimentary structures and the composition of strata show that, once off the shelf, some sediments were shifted farther downslope by gravitative processes such as turbidity currents and mass flows. These mechanisms displaced clay and silt and, to a lesser extent, sand of fluvial Nile and eolian origin, along with shelf material of terrigenous, carbonate, and biogenic origin. Core analyses reveal transport of these components in varying proportions via the ACFS and NW cone's surface to more distal sectors primarily during the Early to Middle Holocene (Stanley and Maldonado, 1977; Ducassou et al., 2009; Kholeif and Ibrahim, 2010). It is also likely that some of the finer sediment components and low accumulation rates may indicate displacement from the NW-oriented cone eastward toward the central Nile Cone as well.

Sediments displaced from land to considerable distances offshore during that period were derived primarily from Nile flood discharge, which is strong in summer, across the delta's coastal margin and then seaward. These largely land-derived materials could be further shifted downslope and dispersed as they settled across climatically controlled, well-stratified intermediate and bottom water masses. One of these sediments distributed well offshore is sapropel, a depositional sequence typically comprising a dark gray to black, mostly silt and clay, organic-rich sediment unit of variable thickness (log in Fig. 3).

This dark unit accumulated beneath oxygen-deficient bottom water and reached euxinic seafloor conditions. High amorphic organic carbon content (58 %–72 %) indicates good preservation of autochthonous planktonic organic matter (Kholeif and Ibrahim, 2010). Stagnation in deep water, increases in primary productivity, and other associated oceanographic conditions are discussed by Rohling and Hilgen (1991) and Krom et al. (2002). Gray deposits, below and above the dark unit, were deposited on the seafloor in less well stratified water and only partially reduced oxygenated conditions.

The youngest sapropel sequence, termed S1, is dated to the AHP, from the Early to Middle Holocene (ca. 9500 to 6000 years BP). The climate during its deposition, one of ex-

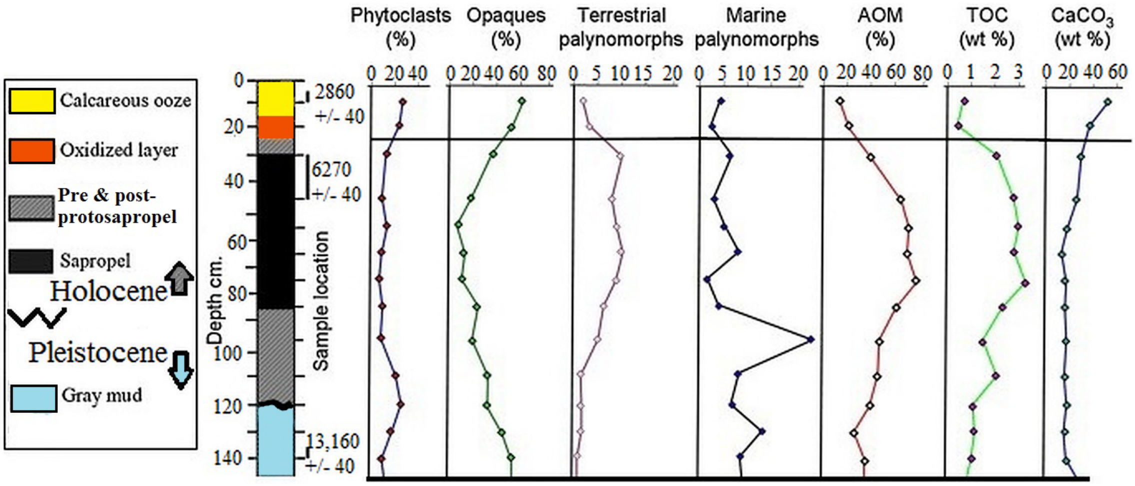

Figure 3. Stratigraphic log of core NC-2 (location shown in Fig. 2) records an Early to Middle Holocene sapropel S1 sequence formed during a period of ca. 3500 years and a much thinner Middle to Late Holocene upper core section of oxidized layer and calcareous ooze. Note proportions of compositional components that change markedly at about 25 cm from core top, at ca. late 4000 years BP (after Kholeif and Ibrahim, 2010). AOM is amorphous organic matter, and TOC is total organic carbon.

tensive to moderate rainfall, was in large part a response to northward displacement of the ITCZ (Fig. 1b; Said, 1993; Krom et al., 2002; Marriner et al., 2013). The S1 sequence is recovered at water depths usually greater than 500 to 600 m on the cone (Maldonado and Stanley, 1976; Ducassou et al., 2009). Complete S1 sequences can range from ~ 50 to > 200 cm in thickness. The gray deposits underlying and covering the dark gray to black unit usually include finely laminated silty clay and clayey silt mixes; their sedimentary structures indicate some were emplaced by bottom currents and others by fine-grained turbidity currents. The age and composition of these deposits indicate they were released beyond the delta's shelf during the AHP when East African source lake levels, Nile floods, and amounts of sediment discharge were at or near the optimum (Fig. 4a, b) and maximum aridity did not yet prevail (Gasse, 2000; Kholeif and Mudie, 2009; Revel et al., 2015; Pennington et al., 2017). Compositional analyses of both deltaic and offshore core facies indicate that the upper Blue Nile volcanic province in Ethiopia (Fig. 4c) was the major source of sediment released to and beyond the delta during that period.

2.2 Reduced depositional rates after 5000 years BP

Uppermost sedimentary sequences recovered in cores seaward of the delta and discussed here have received much less attention than the underlying sapropel sequences discussed in the previous section. Their lithofacies and compositional attributes differ significantly from the older S1 sequence. Notably, most sections are much thinner, generally only ~ 20 to 30 cm or less (Stanley and Maldonado, 1977). From the base upward, these present partially laminated silty clay and clayey silt layers that, in some cores, change upward and display a mottled tan, brown, or orange coloration, which is indicative of increasingly oxygenated water conditions above the S1 sequence (Fig. 3). These younger sections commonly evolve upward to a bioturbated silt and clay ooze, rich in calcareous carbonate content (up to 50 %), and grain size that can become coarser toward the core top. Although recovered at considerable water depth, some upper deposits include shallow seafloor components derived from the shelf; these became incorporated with deeper-water materials during downslope transport. Such strata may present sedimentary structures indicative of displacement by bottom currents or by relatively low density sand and silt to fine-grained turbidite flows. Uppermost sediments were released above older S1 sequences not only within the ACFS but also on adjacent cone surfaces (Fig. 2). Their lithologic attributes, much different from those of underlying S1 sequences, resulted from southern displacement of the ITCZ (Fig. 1b) and also from some effects of ENSO cycles during and after the Middle Holocene (Marriner et al., 2013; Pennington et al., 2017).

Average sediment accumulation rates in 23 cores recovered along the SE to NW trending Nile Cone were calculated for two age groups in each core based on sediment thickness and radiocarbon dates using planktonic foraminifera (Ducassou et al., 2009; Kholeif and Mudie, 2009; Kholeif and Ibrahim, 2010; Blanchet et al., 2013). An older group comprises lower core sections dated from ca. 10 000 to ca. 5000 years BP and usually includes the S1 sequence. Depositional rates for this Early to Middle Holocene period range from > 287 to 2 cm per 1000 years (Fig. 2). The average overall rate for all Early to Middle Holocene values in the 23 cores is ~ 106 cm per 1000 years. When examining the same offshore cores but using samples from the upper units dated from ca. 5000 years BP to the Late Holocene, measure-

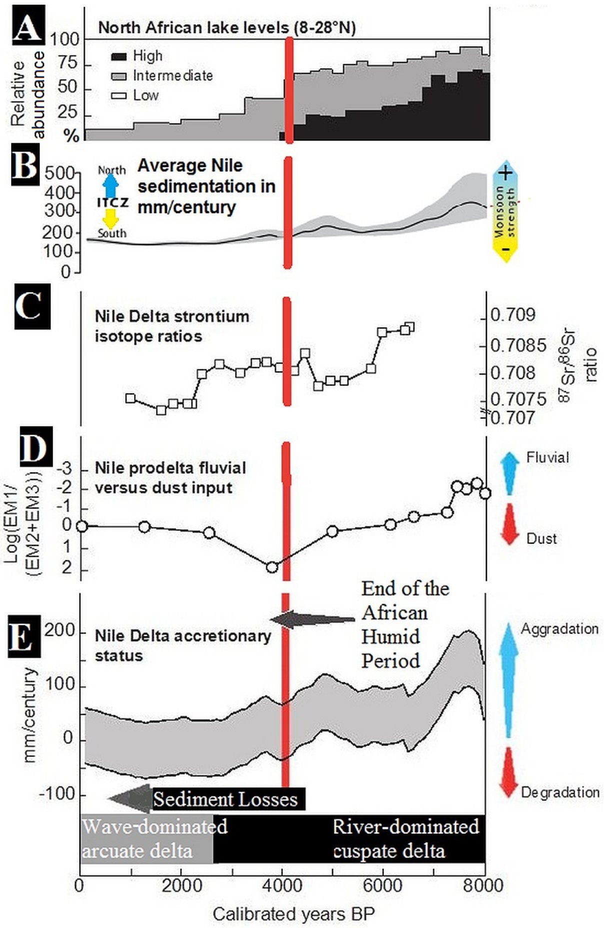

Figure 4. Sedimentation and compositional data respond to climatic change affecting **(a)** highland Nile source area, and **(b–e)** Nile Delta and offshore settings from ca. 8000 years BP to present (modified after Marriner et al., 2012, 2013). Changes in the Nilotic hydrological system and associated depositional responses during the Holocene include those before, at, and after ca. late 4000 years BP (vertical red time marker). These were induced largely by displacement of the monsoon system and associated climatic controls, including migrating ITCZ and ENSO events.

ments of their depositional rates are very much decreased (Fig. 2) and range from only 32 to 1 cm per 1000 years (data in Ducassou et al., 2009). The overall averaged value for all 23 upper core sections provides a much reduced average depositional rate of only ~ 8.4 cm per 1000 years, or under $\sim 10\,\%$ of the average accumulation rate of underlying Early to Middle Holocene S1 sequences. This records that the former turbidite-rich downslope depositional system had decreased substantially largely as a function of the Nile's much-altered hydrology and reduced sediment dispersal seaward of the delta, responses largely due to markedly changing climatic conditions that were seriously affecting this region in the Late Holocene. It is also possible that a center of sedimentation was shifting toward the east.

2.3 Effects of increased aridity and lower Nile flows

Of note are a number of altered compositional and textural attributes recorded offshore in upper core sections (Fig. 3) that correlate with some of similar age identified in the Nile Delta (Fig. 4 and Stanley, 2019). Together these serve as proxies to help interpret regional environmental changes occurring after 5000 years BP and especially in late 4000 years BP. The much thinner accumulation of Late Holocene and younger oxidized mud and carbonate ooze (log in Fig. 3) was deposited under conditions of relatively low Nile input responding to the considerably modified climate (Kholeif and Mudie, 2009). Conditions had become increasingly arid, and sediment discharge by the Nile was much reduced during formation of the upper marl section (Calvert and Fontugne, 2001). The major increase in hyper-aridity occurred ca. 4200–4000 years BP, contemporaneously with the time when the whole of the Egyptian Sahara had become a desert as cited earlier (Pennington et al., 2019).

In contrast with underlying sapropel sequences, the uppermost sediment sections comprise markedly decreased amorphous organic matter (AOM), total organic carbon (TOC), terrestrial pollen, and spores (Fig. 3). Uppermost core units, on the other hand, are defined by their high $CaCO_3$ content (up to 50 %) closely associated with increasingly warm climate and decreasing moisture (Kholeif and Mudie, 2009). Moreover, increased quartz grain roundness and size and especially a peak in the Ca/Ti ratio at that time indicate an eolian influx linked to hyper-aridity (Zhao et al., 2017; Pennington et al., 2019). Upper core sections also record increased proportions of Mg calcite and illite (Calvert and Fontugne, 2001) and higher amounts of opaque fractions (Kholeif and Ibrahim, 2010). Such arid periods are typically characterized by a larger input of coarser particles due to reworking of older deposits (Ducassou et al., 2009) and also of kaolinite derived largely from desert source areas in North Africa (Calvert and Fontugne, 2001).

Also noted were periodic decreases in Ethiopian-derived Blue Nile clastic sediment dispersed between 6000 and 3100 years BP (Krom et al., 2002; Revel et al., 2015). This is recorded by a marked minimum in strontium isotopic ratios (Fig. 4c), an indication of decreased Blue Nile sedimentation offshore (Krom et al., 2002). Relative increases in White Nile runoff were measured at times when Blue Nile fluvial input decreased relative to that of higher eolian transport (Fig. 4d). Minimal Nile discharge occurred in the upper layer offshore during its deposition under oxic bottom water conditions and good ventilation within the water column (Fig. 4e; cf. Kholeif and Mudie, 2009; Kholeif and Ibrahim, 2010). A decrease in fluvial discharge from about 6500 to 2800 $m^3\,s^{-1}$ and also in both flood frequency and intensity are estimated during the past 5000 years (Ducassou et al., 2009). These resulted in decreased sedimentation rates to less than 1 $mm\,yr^{-1}$ during some low-flood periods (Blanchet et al., 2013). Rather than primary responses to tectonic motion, eustatic sea-level rise, or human intervention, most lithofacies and compactional changes recorded by upper marine core sections were induced by the broad, powerful influences of regional climate shift.

3 Archaeological implications

Of prime consideration is whether the evolving natural events discussed in the previous sections would have had sufficient input to trigger societal changes in Egypt in late 4000 years BP, during the latter part of the Old Kingdom (ca. 2278–2181 BCE) and the First Intermediate Period (ca. 2181–2055 BCE) (dates after Shaw, 2000). Archaeologists tend to focus on the primary roles of evolving social, political, and/or economic factors during that timeframe and, to a lesser extent, on the potential effects of climate change. Their studies of this period tend to evaluate the role of environmental impacts on Egypt in one of three different ways: (1) little or no environmental changes occurred, were not influential, or had little societal effect at about this time (Moreno Garcia, 2015); (2) some environmental changes may have occurred but were not primarily responsible for triggering or activating major societal changes recorded during that period (Seidlmayer, 2000; Moeller, 2005); or (3) environmental conditions seriously impacted Egypt and were largely responsible for some extensive, and possibly traumatic, scenarios leading to social, political, and economic upheaval (the so-called "Dark Age" scenarios) then affecting the country such as those summarized by Vandier (1936), Bell (1971), and Hassan (2007).

For a recent example of archaeological support for the concepts of group (1) above, one can read the following: "Contrary to traditional interpretations of the end of the Old Kingdom, recent archaeological research shows no trace of climatic or subsistence crisis" (Moreno Garcia, 2015, p. 79). In contrast, it is noted that some historical documents previously cited by Egyptologists of group (3) to support arguments favoring major climate change and its dire effects on society at the end of the Old Kingdom are now recognized as having been documented long after the actual period that they describe. Moreover, others referring to documents used by group (3) to describe a major breakdown of the social order at that time have also indicated that considerable discretion should be used. For example, some suggest that Egyptian writings during those early years had a tendency to exaggerate the extent of damage and disorder and thus should be cautiously interpreted before using these as firm and accurate evidence of such past events (Freeman, 1996).

Archaeologists generally agree, however, that a centralized government long and firmly controlled by a sequential reign of pharaohs had all but ceased by the end of the Old Kingdom, and Egypt proceeded for a century, or perhaps somewhat longer, without such an authoritative leader as head of state. This occurred shortly after the lengthy reign of Pepy II, estimated at some time between $\sim$ 2284 BCE and $\sim$ 2184 BCE. Following closely, the pharaoh was replaced by a series of concurrent nomarchs, or governors, charged with organizing and directing many of the primary activities in Egypt's many nomes, or geographic districts. In addition to these major political alterations during the First Intermediate Period, it is proposed here that the country's stability would have been weakened by the powerful environmental factors triggered by major climate change at about the same time as recorded in this study. The quality of construction at this time, in some cases, may have decreased markedly (Fig. 5). In particular, a period of marked increased aridity and decline in moisture and rainfall leading to intermittent low Nile floods lasting a century or longer likely led to episodic conditions of diminished cultivation and reduced harvests. Additionally, such periods of decreased food supplies and their less-than-well-organized storage and equitable distribution to the population had the potential to last for several years at a time, some triggering serious societal consequences (Weiss and Bradley, 2001). These conditions, in turn, would probably have also given rise to some documented migration from the delta to areas in middle and upper Egypt, some of which were then perhaps less acutely impacted by the altered environmental factors in lower Egypt.

To help resolve whether the timing of environmental impacts on Egypt can be correlated with historic events at the end of the Old Kingdom and during the First Intermediate Period, it would be useful to encourage collections and detailed mineralogical and geochemical study of sediment drill cores recovered within, and also adjacent to, established archaeological sites of that time period. Collecting closely spaced core samples and dating where possible with plant fossils in delta and marine microfossils offshore using carbon-14 dating, along with other refined dating methodologies, coupled with detailed compositional analyses at the same stratigraphic levels are now necessary tasks of primary geoarchaeological importance. For example, it should be recognized that proportions of some sediment components in both offshore and deltaic samples would likely have been altered during transport, sometimes for long distances and over a considerable period of time, prior to their final deposition at a core's recovery site on land or at sea. At least some particles and isotopic components that comprise a sample would likely not have been displaced during one single short-period transport event from source to final depositional site but rather by what is termed a longer "stop-and-go" sedimentation process (Stanley, 2019). This displacement would have involved several downslope reworking phases by repeated deposition and storage–erosion and displacement–redeposition episodes over time. As a consequence, a date obtained by calibrated C-14 or other means may well record an age for sample particles that is likely to be older than the actual younger date of a sample's final deposition. Thus, some dates obtained in both Nile Delta and offshore cores can record a time that can be on the order of 50 to 100 or more years older than what is likely to be their actual younger dates of final deposition (see

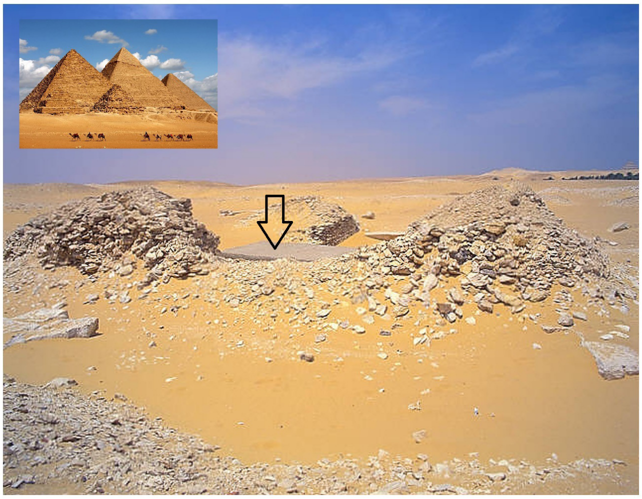

Figure 5. Pyramid of Ibi (Qakare) at South Saqqara, Egypt, built after the end of the Old Kingdom during the Eighth Dynasty of the First Intermediate Period. Ibi is little known and is believed to have ruled for about 2 years, from ca. 4109 to 4107 years BP. The structure includes a descending passage (see arrow) that leads to the burial chamber, and of its original height of ca. 21 m, only ~ 3 m now rests above the desert floor. Built largely of flat brick-size stones, it has been subject to destruction by weathering, structural failure, and theft of its rock material. In contrast, the upper inset shows the older, much larger, and better-constructed Old Kingdom Fourth Dynasty pyramids at Giza. From right to left are those of Khufu (ca. 4550 years BP), Khafre (ca. 4520 years BP), and Menkaure (ca. 4490 years BP). Khufu's pyramid, the highest (146 m), is formed of ~ 2 million large blocks of rock weighing 2.5 to 15 t. (Images publicly available as stock photographs.)

Dee, 2017). Caution is warranted particularly when interpreting sediment accumulation dates, especially in cases where a frequent reversal of sample ages (older dated samples above younger ones) occur as one proceeds upward from the base of a core study section.

4 Conclusions

The stratigraphic and sedimentological changes recorded both seaward of and in the Nile Delta proper during the Middle to Late Holocene examined herein resulted primarily from altered and reduced Nile flow conditions rather than from other natural factors and human intervention. It is proposed that marked climatic change led to intensified aridification, a decline in rainfall, diminished Nile flood levels, and a consequent periodic decline in agricultural production in late 4000 years BP. Such events would have negatively impacted Egypt's population toward the end of the Old Kingdom and in the early to middle First Intermediate Period. Of note in this respect is Herodotus (1987), who in his *The History* written in about 440 BCE, raised a pertinent question (Book II, Sect. 14): "If no rain falls in their land at all, and if the river cannot rise high enough to flood their fields . . . then . . . what will be left for Egyptians that live there, but starvation?" This commentary could pertain to an actual event that occurred prior to or during Herodotus' travel in Egypt or is perhaps meant as a predictor of future major climate changes such as increased droughts (Tabari and Willems, 2018; Nashwan et al., 2020) and of a substantial human-induced decreased-Nile-flow misfortune, such as by closure of the now near-completed Grand Ethiopian Renaissance Dam (GERD) placed across the Blue Nile in Ethiopia, the largest such structure in Africa (Stanley and Clemente, 2017). At the very least, these latter two factors alone warrant prompt and serious consideration that should lead to vital protection measures for Egypt. With its present population about 100 times greater than at the end of the Old Kingdom, the country cannot now readily withstand a 20 % to 30 % or more reduction in its present Blue Nile freshwater supply. Studies of this region's past history, such as those that integrate environmental and archaeological conditions in the late 4000 years BP, may provide some useful points serving as a basis to help interpret the present and also to better prepare for possible negative conditions in the years ahead.

Data availability. Information provided throughout the text is available in prior published studies by the first author (Jean-Daniel Stanley) and other authors cited throughout the text and listed in the references. These studies are readily available, and their data sets are publicly accessible therein. Data were gathered from prior original studies and are not stored in a separate database or website elsewhere.

Author contributions. This manuscript was prepared by JDS and SEW; conceptualization and project administration were completed by JDS, and visualization was completed by both SEW and JDS.

Competing interests. The authors declare that they have no conflict of interest.

Special issue statement. This article is part of the special issue "Geoarchaeology of the Nile Delta". It is a result of the workshop "Geoarchaeology of the Nile Delta: Current Research and Future Prospects", Würzburg, Germany, 29–30 November 2019.

Acknowledgements. The Smithsonian Institution's National Museum of Natural History, Washington, DC, is acknowledged for funding years of fieldwork seaward of and in Egypt's Nile Delta and for laboratory analyses that led to this study. Appreciation is expressed to Emmanuelle Ducassou, Université de Bordeaux, France; Suzan Kholeif, National Institute of Oceanography and Fisheries, Alexandria, Egypt; and Nick Marriner, Université de Franche-Comté, Besançon, France, for permission to use several of their published figures presented herein. Also thanked are Christopher E. Bernhardt, US Geological Survey; Paige Eager, Hood College; Adrienne N. Ellis, Adamstown, Maryland; and the two anonymous scholars for their useful reviews. The editors of this volume very kindly invited our contribution and assisted us in taking final steps for its publication.

Financial support. The article processing charge was funded by the Quaternary scientific community, as represented by the host institution of EGQSJ, the German Quaternary Association (DEUQUA).

Review statement. This paper was edited by Julia Meister and reviewed by two anonymous referees.

References

Bar-Matthews, M. and Ayelon, A.: Mid-Holocene climate variations revealed by high-resolution speleothem records from Soreq Cave, Israel and their correlation with cultural changes, The Holocene, 21, 163–171, https://doi.org/10.1177/0959683610384165, 2011.

Bard, K. A.: An Introduction to the Archaeology of Ancient Egypt, Blackwell Publishing, Maulden, Massachusetts, 400 pp., ISBN-13: 978-1405111485, 2008.

Bell, B.: The dark ages in ancient history, Am. J. Archaeol., 75, 1–26, https://doi.org/10.2307/503678, 1971.

Bellaiche, G., Zitter, T., Droz, L., Gaullier, V., Mart, Y., and Mascle, J.: Le cône sous-marin profound du Nil: principaux résultats de la campagne Prismed II du N.O. L'Atlante, Océanographie, 329, 727–733, https://doi.org/10.1016/S1251/8050(00)88492-X, 1999.

Bernhardt, C. E., Norton, S. P., and Stanley, J.-D.: Nile delta vegetation response to Holocene climate variability, Geology, 40, 615–618, https://doi.org/10.1130/G33012.1, 2012.

Blanchet, C. L., Tjallingii, R., Frank, M., Lorenzen, J., Reitz, A., Brown, K., Feseker, T., and Brückman, W.: High- and low-latitude forcing of the Nile River regime during the Holocene inferred from laminated sediments of the Nile deep-sea fan, Earth Planet. Sc. Lett., 364, 98–110, https://doi.org/10.1016/j.epsl.2013.01.009, 2013.

Blanchet, C. L., Contoux, C., and Leduc, G.: Runoff and precipitation dynamics in the Blue and White Nile catchments during the mid-Holocene: A data-model comparison, Quaternary Sci. Rev., 130, 222–230, https://doi.org/10.1016/j.quascirev.2015.07.014, 2015.

Butzer, K. W.: Early Hydraulic Civilization in Egypt, University of Chicago Press, Chicago, Illinois, 134 pp., ISBN: 0-226-08634-8, 1976.

Butzer, K. W.: Long-term Nile flood variation and political discontinuities in Pharaonic Egypt, in: From Hunters to Farmers: The Causes and Consequences of Food Production in Africa, edited by: Clark, J. D. and Brandt, S. A., University of California Press, Berkeley, California, 102–112, ISBN: 0520045742, 1984.

Calvert, S. E. and Fontugne, M. R.: On the late Pleistocene-Holocene sapropel record of climatic and oceanographic variability in the eastern Mediterranean, Paleoceanography, 16, 78–94, https://doi.org/10.1029/1999PA000488, 2001.

Dee, M. W.: Absolute dating climatic evidence and the decline of Old Kingdom Egypt, in: The Late Third Millenium in the Ancient Near East. Chronology, C-14, and Climate Change, edited by: Hoflmayer, F., University of Chicago, Oriental Institute Seminars no. 11, Chicago, Illinois, 323–331, 2017.

Ducassou, E., Migeon, S., Mulder, T., Murat, A., Capotondi, L., Bernasconi, S., and Mascle, J.: Evolution of the Nile deep-sea turbidite system during the Late Quaternary: influence of climate change on fan sedimentation, Sedimentology, 56, 2061–2090, https://doi.org/10.1111/j.1365-3091.2009.01070.x, 2009.

El-Sayed, A., Kerrat, I., and Hussein, H. M.: Seismicity and seismic hazard in Alexandria and its surroundings, Pure Appl. Geophys., 161, 1003–1019, https://doi.org/10.1007/s00024-003-2488-8, 2004.

Fleming, K., Johnston, P., Zwartz, D., Yokoyama, Y., Lambeck, K., and Chappell, J.: Refining the eustatic sea-level curve since the last Glacial Maximum using far- and intermediate-field sites, Earth Planet. Sc. Lett., 163, 327–342, https://doi.org/10.1016/S0012-821X(98)00198-8, 1998.

Freeman, C.: Egypt, Greece and Rome: Civilizations of the Ancient Mediterranean, Oxford University Press, Oxford, England, 784 pp., ISBN: 9780199651924, 1996.

Frihy, O. E. and Dewidar, K. M.: Patterns of erosion/sedimentation, heavy mineral concentration and grain size to interpret boundaries of littoral sub-cells of the Nile Delta, Egypt, Mar. Geol., 199, 27–43, https://doi.org/10.1016/S0025-3227(03)00145-2, 2003.

Gasse, F.: Hydrological changes in the African tropics since the last glacial maximum, Quaternary Sci. Rev., 19, 189–211, https://doi.org/10.1016/S0277-3791(99)00061-X, 2000.

Hassan, F. A.: Droughts, famine, and the collapse of the Old Kingdom: Re-reading Ipuwer, in: The Archaeology and Art of Ancient Egypt, edited by: Hawass, Z. A. and Richards, J., Publications du Conseil Suprême des Antiquités de l'Egypte, Cairo, Egypt, 1, 357–379, ISBN: I0977-437-241-7, 2007.

Herodotus: The History, translated by: Grene, D., The University of Chicago Press, Chicago, Illinois, 710 pp., ISBN: 9780226327723, 1987.

Kaniewski, D., Marriner, N., Cheddadi, R., Guiot, J., and Van Campo, E.: The 4.2 ka BP event in the Levant, Clim. Past, 14, 1529–1542, https://doi.org/10.5194/cp-14-1529-2018, 2018.

Kebeasy, R.M.: Seismicity, in: The Geology of Egypt, edited by: Said, R., A.A. Rotterdam, the Netherlands, Balkama, 51–59, ISBN: 978-9061918561, 1990.

Kholeif, S. and Ibrahim, M. I.: Palynofacies analysis of inner continental shelf and middle slope sediments offshore Egypt, southeastern Mediterranean, Geobios, 43, 333–347, https://doi.org/10.1016/j.geobios.2009.10.006, 2010.

Kholeif, S. and Mudie, P.: Palynological records of climate and oceanic conditions in the late Pleistocene and Holocene of the Nile Cone, southeastern Mediterranean, Egypt, Palynology, 33, 1–24, https://doi.org/10.2113/gspalynol.33.1.1, 2009.

Krom, M. D., Stanley, J.-D., Cliff, R. A., and Woodward J. C.: Nile River sediment fluctuations over the past 7000 years and their key role in sapropel development, Geology, 30, 71–74, https://doi.org/10.1130/0091-7613(2002)030<0071:NRSFOT>2.0.CO;2, 2002.

Maldonado, A. and Stanley, J.-D.: The Nile Cone: submarine fan development by cyclic sedimentation, Mar. Geol., 20, 27–40, https://doi.org/10.1016/0025-3227(76)90073-6, 1976.

Marriner, N., Flaux, C., Kaniewski, D., Morhange, C., Leduc, G., Moron, V., Chen, Z., Gasse, F., Empereur, J.-Y., and Stanley, J.-D.: ITCZ and ENSO-like pacing of Nile delta hydrogeomorphology during the Holocene, Quaterernary Sci. Rev., 45, 73–84, https://doi.org/10.1016/j.quascirev.2012.04.022, 2012.

Marriner, N., Flaux, C., Morhange, C., and Stanley, J.-D.: Tracking Nile Delta vulnerability to Holocene change, PLoS One, 8, 1–9, https://doi.org/10.1371/journal.pone.0069195, 2013.

Moeller, N.: The First Intermediate Period: A time of famine and climate change?, Egypt and the Levant, 15, 153–167, 2005.

Moreno Garcia, J.: Climatic change or sociopolitical transformation? Reassessing late 3rd millennium BC in Egypt, in: 2200 BC – A Climatic Breakdown as a Cause for the Collapse of the Old World, edited by: Meller, H., Arz, H. W., Jung, R., and Risch, R., Landesamt für Denkmalpflege und Archäologie Sachsen-Anhalt – Landesmuseums für Vorgeschichte, Halle, 79–94, 2015.

Nashwan, N. S., Shahid, S., and Chung, E.-S.: High-resolution climate projections for a densely populated Mediterranean region, Sustainability, 12, 23 pp., https://doi.org/10.3390/su12093684, 2020.

Pennington, B. T., Sturt, F., Wilson, P., Rowland, J., and Brown, A.: The fluvial evolution of the Holocene Nile Delta, Quaternary Sci. Rev., 170, 212–231, https://doi.org/10.1016/j.quascirev.2017.06.017, 2017.

Pennington, B. T., Hamdan, M. A., Pears, B. R., and Sameh, H. I.: Aridification of the Egyptian Sahara 5000–4000 cal BP revealed from x-ray fluorescence analysis of Nile Delta sediments at Kom al-Ahmer/Kom Wasit, Quatern. Int., 514, 108–118, https://doi.org/10.1016/j.quaint.2019.01.015, 2019.

Revel, M., Ducassou, E., Skonieczny, C., Colin, C., Bastian, L., Bosch, D., Migeon, S., and Mascle, J.: 20,000 years of Nile River dynamics and environmental changes in the Nile catchment area as inferred from Nile upper continental slope sediments, Quaternary Sci. Rev., 130, 200–221, https://doi.org/10.1016/j.quascirev.2015.10.030, 2015.

Rohling, E. J. and Hilgen, F. J.: The eastern Mediterranean climate at times of sapropel formation: a review, Geol. Mijnbouw, 70, 253–264, ISBN: 0016-7746, 1991.

Ross, D. A. and Uchupi, E.: Structure and sedimentary history of southeastern Mediterranean sea – Nile Cone area, AAPG Bull., 61, 872–902, https://doi.org/10.1306/C1EA4397-16C9-11D7-8645000102C1865D, 1977.

Said, R.: The River Nile: Geology, Hydrology, and Utilization, Pergamon Press, Tarrytown, New York, 320 pp., ISBN: 0-08-041886-4, 1993.

Seidlmayer, S.: The First Intermediate Period, in: The Oxford History of Ancient Egypt, edited by: Shaw, I., Oxford University Press, Oxford, England, 118–147, ISBN: 978-0-19-280458-7, 2000.

Sestini, G.: Implications of climatic changes for the Nile Delta, in: Climatic Change and the Mediterranean, edited by: Jeftic, L., Milliman, J. D., and Sestini, G., Edward Arnold, London, England, 535–601, ISBN: 0-340-55329-4, 1992.

Shaw, I. (Ed.): The Oxford History of Ancient Egypt, Oxford University Press, Oxford, England, 552 pp., ISBN: 978-0-19-280458-7, 2000.

Sivan, D., Wdowinski, S., Lambeck, K., Galili, E., and Raban, A.: Holocene sea-level changes along the Mediterranean coast of Israel, based on archaeological observations and numerical model, Palaeogeogr Palaeocl., 167, 101–117, https://doi.org/10.1016/S0031-0182(00)00234-0, 2001.

Stanley, J.-D.: Egypt's Nile Delta in late 4000 Years BP: Altered flood levels and sedimentation, with archaeological implications, J. Coastal. Res., 35, 1036–1050, https://doi.org/10.2112/JCOASTRES-D-19-00027.1, 2019.

Stanley, J.-D. and Clemente, P. L.: Increased land subsidence and sea-level rise are submerging Egypt's Nile Delta coastal margin, GSA Today, 27, 4–11, https://doi.org/10.1130/GSATG312A.1, 2017.

Stanley, J.-D. and Maldonado, A.: Nile Cone: Late Quaternary stratigraphy and sediment dispersal, Nature, 266, 129–135, https://doi.org/10.1038/266129a0, 1977.

Stanley, J.-D. and Warne, A. G.: Nile Delta: recent geological evolution and human impact, Science, 260, 628–634, https://doi.org/10.1126/science.260.5108.628, 1993.

Stanley, J.-D., Krom, M. D., Cliff, R. A., and Woodward, J. C.: Nile flow failure at the end of the Old Kingdom, Egypt: Strontium isotopic and petrologic evidence, Geoarchaeology, 18, 395–402, https://doi.org/10.1002/gea.10065, 2003.

Summerhayes, C., Sestini, G., Misdorp, R., and Marks, N.: Nile Delta: nature and evolution of continental shelf sediment systems, Mar. Geol., 27, 43–65, https://doi.org/10.1016/0025-3227(78)90073-7, 1978.

Tabari, H. and Willems, P.: More prolonged droughts by the end of the century in the Middle East, Environ. Res. Lett., 13, 104005, https://doi.org/10.1088/1748-9326/aae09c, 2018.

UNESCO/UNDP and Arab Republic of Egypt: Coastal Protection Studies, Project Findings and Recommendations, UNDP/EGY/73/063, Final Report, UNESCO, Paris, FNR/SC/OSP/78/230, 483 pp., 1978.

U.S. Defense Mapping Agency Hydrographic Center: Mediterranean Sea, Washington, D.C., Chart N.O. 310, 1972.

Vandier, J.: La Famine dans l'Egypte Ancienne, Recherches d'Archéologie, de Philologie et d'Histoire, Institut Français d'Archéologie Orientale, Cairo, Egypt, tome 7, 176 pp., 1936.

Weiss, H. and Bradley, R. S.: What drives societal collapse?, Science, 291, 609–610, https://doi.org/10.1126/science.1058775, 2001.

Weiss, H., Courty, M. A., Wetterstrom, W., Guichard, F., Senior, L., Meadow, R., and Curnow, A.: The genesis and collapse of 3rd millennium north Mesopotamian civilization, Science, 261, 995–1004, https://doi.org/10.1126/science.261.5124.995, 1993.

Woodward, J., Macklin, M., Fielding, L., Millar, I., Spencer, N., Welsby, D., and Williams, M.: Shifting sediment sources in the world's longest river: A strontium isotope record for the Holocene Nile, Quaternary Sci. Rev., 130, 124–140, https://doi.org/10.1016/j.quascirev.2015.10.040, 2015.

Zhao, X., Liu, Y., Salem, A., Marks, L., Welc, F., Sun, Q., Jiang, J., Chen, J., and Chen, Z.: Migration of the intertropical convergence zone in North Africa during the Holocene: evidence from variations in quartz grain roundness in the lower Nile Valley, Egypt, Quatern. Int., 449, 22–28, https://doi.org/10.1016/j.quaint.2017.06.036, 2017.

E&G Quaternary Sci. J., 70, 93–104, 2021
https://doi.org/10.5194/egqsj-70-93-2021

Open Access E&G Quaternary Science Journal

Research article

The late Holocene record of Lake Mareotis, Nile Delta, Egypt

Clément Flaux[1], Matthieu Giaime[2,a], Valérie Pichot[3], Nick Marriner[4], Mena el-Assal[5], Abel Guihou[6], Pierre Deschamps[6], Christelle Claude[6], and Christophe Morhange[6]

[1]Mosaïques Archéologie, Cournonterral, 34660, France
[2]Department of Geography, Durham University, Durham DH1 3LE, UK
[3]CEAlex, CNRS, USR3134, Alexandria, Egypt
[4]Chrono-Environnement, CNRS-UFC, UMR 6249, Besançon, 25000, France
[5]Department of Geography, Faculty of Humanities, King Khalid University, Abha, 62529, Saudi Arabia
[6]Aix Marseille Univ, CNRS, IRD, INRAE, Coll France, CEREGE, Aix-en-Provence, 13090, France
[a]present address: Institute of Environmental Science and Technology (ICTA-UAB), Universitat Autònoma de Barcelona, Bellaterra, 08193 Catalonia, Spain

Correspondence: Clément Flaux (c.flaux@mosaiquesarcheologie.com)

Relevant dates: Received: 28 August 2020 – Revised: 8 February 2021 – Accepted: 17 February 2021 – Published: 8 April 2021

How to cite: Flaux, C., Giaime, M., Pichot, V., Marriner, N., el-Assal, M., Guihou, A., Deschamps, P., Claude, C., and Morhange, C.: The late Holocene record of Lake Mareotis, Nile Delta, Egypt, E&G Quaternary Sci. J., 70, 93–104, https://doi.org/10.5194/egqsj-70-93-2021, 2021.

Abstract: Lake Maryut (northwestern Nile Delta, Egypt) was a key feature of Alexandria's hinterland and economy during Greco-Roman times. Its shores accommodated major economic centers, and the lake acted as a gateway between the Nile valley and the Mediterranean. It is suggested that lake-level changes, connections with the Nile and the sea, and possible high-energy events considerably shaped the human occupation history of the Maryut. To reconstruct Lake Maryut hydrology in historical times, we used faunal remains, geochemistry (Sr isotopic signature of ostracods) and geoarcheological indicators of relative lake-level changes. The data show both a rise in Nile inputs to the basin during the first millennia BCE and CE and a lake-level rise of ca. 1.5 m during the Roman period. A high-energy deposit, inferred from reworked radiocarbon dates, may explain an enigmatic sedimentary hiatus previously attested to in Maryut's chronostratigraphy.

Kurzfassung: In griechisch-römischer Zeit spielte der Maryut-See (nordwestliches Nil-Delta, Ägypten) eine wirtschaftliche Schlüsselrolle im Hinterland von Alexandria. An seinen Ufern befanden sich wichtige Wirtschaftszentren und der See fungierte als Bindeglied zwischen dem Niltal und dem Mittelmeer. Es ist zu vermuten, dass Schwankungen des Seespiegels, Verbindungen zum Nil und zum Mittelmeer und mögliche Hochenergieereignisse die menschliche Besiedlungsgeschichte des Maryut-Sees beachtlich geprägt haben. Um die Hydrologie des Maryut-Sees in historischer Zeit zu rekonstruieren, untersucht diese Studie Faunenreste, geochemische (Sr-Isotopensignaturen von Ostrakoden) und geoarchäologische Indikatoren, die relative Schwankungen des Seespiegels anzeigen. Die Ergebnisse zeigen sowohl einen Anstieg der Nileinträge in den See während des ersten Jahrtausends v. Chr. und n. Chr. als auch einen Anstieg des Seespiegels um ca. 1,5 m während der Römerzeit. Ein Hochenergieereignis, ausgewiesen durch umgelagerte ^{14}C Alter, könnte die Ursache eines rätselhaften Hiatus in den Profilen sein, der zuvor in der Chronostratigraphie des Maryut-Sees nachgewiesen wurde. (*Abstract was translated by Martin Seeliger.*)

1 Introduction

Lake Mareotis, precursor of the modern Maryut lagoon located just south of Alexandria (Egypt), constituted a dense traffic waterway during antiquity (Empereur, 1998), straddling the northwestern Nile Delta. Extensive archeological surveys have shed new light on the intense occupation of its shores between the 4th century BCE and the 7th century CE (Blue and Khalil, 2010). An archeological synthesis at the scale of the western delta has demonstrated that paleowaterways and the overall hydraulic configuration shaped the geography of ancient settlements (Wilson, 2012). Our knowledge and representation of the ancient water network is primarily based upon historical statements, in particular Strabo (Strabo, XVII, 1, 7; translation Yoyotte et al., 1997), according to whom Lake Mareotis was connected to the Nile through several canals on its southern and eastern sides. Lake-level oscillations were then mediated by Nile floods. Nonetheless, this vision furnishes a static view of the lake, whose shores were occupied for a period of 1000 years or more, as recently underscored at Kom el-Nogous close to Taposiris Magna (Fig. 1), occupied during the New Kingdom (Redon et al., 2017). Following Stanley (2019) quoting Butzer (1976, p. 56), "it has become difficult to ignore the possibility that major segments of ancient Egyptian history may be unintelligible without recourse to an ecological perspective." We suggest that this statement resonates strongly with the human occupation history of Lake Mareotis, as originally perceived by De Cosson (1935).

Lake Mareotis is part of the coastal belt of the Nile Delta, spread over a structural boundary which separates Pleistocene coastal sandstone ridges to the west and northwest from the Holocene Nile Delta to the east and southeast (Fig. 1). This situation at the deltaic margin made it very sensitive to hydrological changes, modulated by Holocene relative sea-level changes (e.g., Goiran et al., 2018) and Nile flow modifications (e.g., Sun et al., 2019). We have previously exploited Lake Mareotis sedimentary archives in order to reconstruct its Holocene history (Flaux et al., 2011, 2012, 2013, 2017), aiming to elucidate the ancient geography and hydrology of the lake. The marine transgression of the area is dated to 7.5 ka cal BP. Nile inputs then became progressively predominant in Maryut's hydrology (7–5.5 ka cal BP) in the context of the African Humid Period (AHP). Between 5.5 and 2.8 ka cal BP, the end of the AHP is translated by a progressive hydrological shift from a Nile-dominated to a marine-dominated lagoon. A hiatus in Maryut's sedimentary record precludes investigating the lagoon system between 2.8 and 1.7 ka cal BP. The final phase from 1.7 to 0.2 ka cal BP was characterized by dominant freshwater inputs except between 1.1 to 0.7 ka cal BP, when a Maryut relative lowstand and seawater intrusion are attested. New biosedimentological, geochemical, radiocarbon and geoarcheological data have helped to shed new light on the evolution of Lake Mareotis' water budget during historical times. In particular, this paper aims to better constrain hydrological conditions of the lake during the Greco-Roman period and probe the sedimentary hiatus previously described within the lake sequence (Goodfriend and Stanley, 1996; Flaux et al., 2012).

2 Materials and methods

This study is based on sedimentary sequences retrieved from archeological structures and Lake Maryut. All localities have been benchmarked relative to mean sea level (tide-gauge data from Alexandria taken in 1906) using a differential GPS.

Akadémia and Kôm de la Carrière are two Roman archeological sites lying on the southwestern waterfront of Lake Maryut (Fig. 1). At Akadémia, one sedimentary core was taken from a flooded kiln chamber (core AKA19; 30°59′16.74″ N 29°40′23.56″ E). Another core (AKA12; 30°59′12.31″ N 29°40′07.68″ E; WGS84 coordinate system) was retrieved from the sedimentary filling of a water-wheel well (Egyptian sakieh). Cores were taken in 2015 using a percussion corer Cobra TT and relevant sediment samples were extracted for wet sieving and binocular observation of the sand fraction. The base of the kiln chamber is used as an upper limit of the water table and the base of the well as a lower one. The chronology of both structures, based on their archeological dating (Pichot and Flaux, 2015; Pichot, 2017), shows the evolution of the water-table elevation, related to the adjacent Lake Maryut base level.

At Kôm de la Carrière eight sedimentary cores were collected in 2015 from a ancient silted quarry (Fig. 2). Core AMR-3 (31°01′07.15″ N, 29°44′07.27″ E; WGS84 coordinate system), drilled in the center of the basin, underwent sediment grain size and ostracod analyses at Durham University. We used wet sieving to quantify the sediment texture, including the coarse fraction (>2 mm), sand fraction (50 µm–2 mm) and silty-clay fraction (<50 µm). Ostracods were picked from the >125 µm fraction using a binocular microscope and identified to species level (Athersuch et al., 1989). The core chronology is based on three radiocarbon dates (Table 1), as well as ceramics studied at the Centre d'Etudes Alexandrines (CEAlex; CNRS, Alexandria).

The stratigraphy of Maryut lagoon's southeastern basin was investigated using the new sedimentary section M83, collected in 2014 from the section of a drain crossing the for-

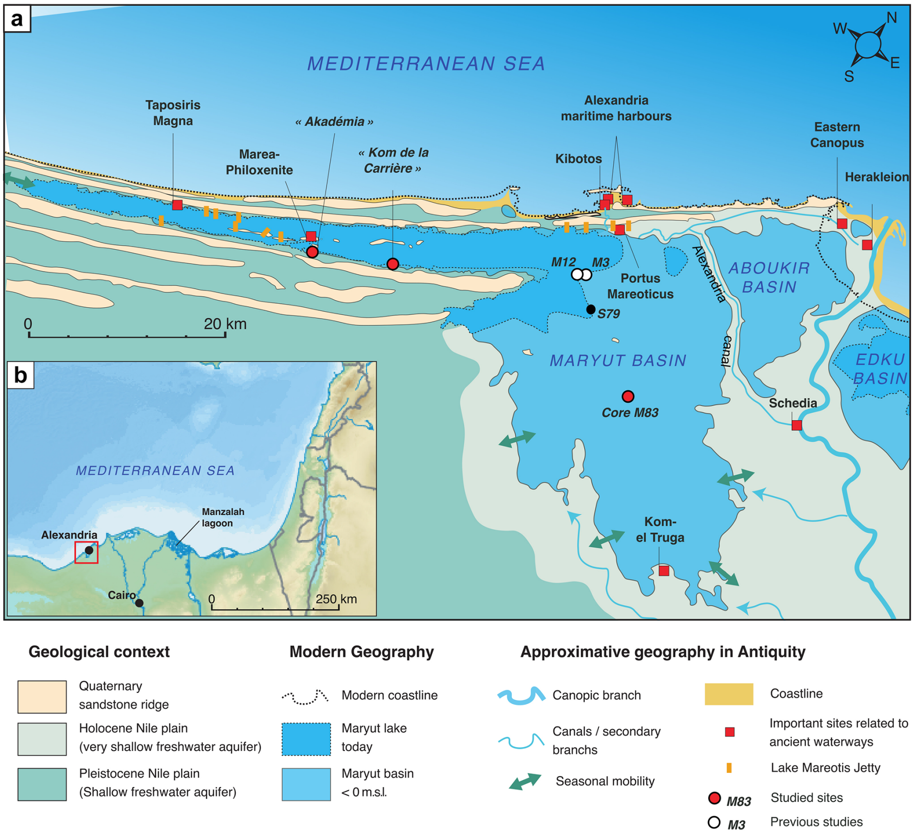

Figure 1. **(a)** Geomorphological map of Lake Mareotis at the northwestern edge of the Nile Delta. **(b)** Location of the study area along the southeastern Mediterranean Sea.

mer lagoon bottoms, now cultivated (Fig. 1; 31°2′39.24″ N, 30°2′21.52″ E; WGS84 coordinate system). A continuous set of 66 samples, each 2 cm thick, was taken from a 1.4 m thick sequence. Bio-sedimentary analyses were undertaken at CEREGE (CNRS, France). We used wet sieving to quantify the sediment texture (including the coarse fraction (>2 mm), sand fraction (50 µm–2 mm) and silty-clay fraction (<50 µm). Ostracods were picked from the >125 µm fraction using a binocular and identified to species level (Athersuch et al., 1989). Sorted mollusk shells were assigned to ecological assemblages according to modern faunal groups observed on the Nile coast (Bernasconi and Stanley, 1994). Magnetic susceptibility measurements were undertaken using a Bartington MS2 magnetic susceptibility meter and are reported as mass-specific magnetic susceptibility in SI units (10^{-8} m^3 kg^{-1}). Strontium isotopes were measured on ostracod valves for 29 samples (ca. 30 when available; Table 2). Reinhardt et al. (1998) analyzed Sr isotopic ratios on surface and subsurface shell samples taken from Manzala lagoon in the eastern Nile Delta and showed that this proxy could be used to reconstruct the recent desalinization of the lagoon, attributed to increasing Nile inflow from the modern irrigation system. Similar results were obtained from the modern northwestern Nile coast (Flaux, 2012, vol. III, p. 13–20) and applied to Maryut's Holocene sedimentary archives (Flaux et al., 2013). For the ^{87}Sr / ^{86}Sr analyses of section M83, we selected the euryhaline ostracod *Cyprideis torosa* due to the species' wide tolerance to hydrological changes (Frenzel and Boomer, 2005). Clean shells were selected and washed with Milli-Q water and then dissolved in a 3 N HNO_3 solution. Sr separation and purification techniques used Sr Spec resin following the procedure modified by Pin et al. (1994). Sr isotopic measurements were performed with a NEPTUNE+ Multicollector ICP-MS at CEREGE. A total of 13 replicate analyses of the NBS 987 standard yielded a ^{87}Sr / ^{86}Sr ratio of 0.710264 ± 0.000023 (2σ), providing a standard error of ±32 ppm (parts per million). The chronology of core M83 is based on seven radiocarbon dates (Table 1).

3 Georcheological indicators

3.1 Sediment record from a silted quarry at Kôm de la Carrière

The Kôm de la Carrière site is located on the southwestern shore of Lake Maryut (Fig. 1) at the foothill of a Pleistocene ridge mostly made of poorly consolidated aeolian oolitic carbonate sands (Gebel Maryut ridge; El Asmar and Wood,

Table 1. Radiocarbon data from the Kôm de la Carrière site (core AMR-3) and section M83. The ^{14}C activity was calibrated using the software Calib 8.2 (http://calib.org, last access: February 2021) and the IntCal20 curve (Reimer et al., 2020). No reservoir age correction was applied to radiocarbon ages (see discussion in Flaux et al., 2012, p. 3497). Extracted collagen was used for the bone sample Poz-88215.

Laboratory code	Conventional ^{14}C age	Error	Material	Calibrated BCE/CE (*IntCal20; 2σ*)
Poz-114734	111.84 pMC	0.54 pMC	Plant remains	Recent
Poz-114735	1050	80	Plant remains	774–1198 CE
Poz-114736	2205	30	Organic sediment	371–175 BCE
Beta - 406936	130	30	Charcoal	1673–1942 CE
Poz-89003	2310	50	*Bittium reticulatum* shell	537–203 BCE
Poz-89004	2465	30	*Bittium reticulatum* shell	760–418 BCE
Poz-88215	>46.000	–	Burnt bone fragment	>45 700 BCE
SacA 16171	2655	30	*Cerastoderma* valve	898–788 BCE
Poz-88214	1195	30	Organic residue	706–950 CE
Poz-89005	1845	30	*Bittium reticulatum* shell	122–308 CE

Table 2. Sr isotope data from the ostracod *Cyprideis torosa* extracted in section M83.

Sample depth below the surface (cm)		Sr isotopic ratio		
		Cyprideis torosa number of valves	^{87}Sr / ^{86}Sr	StdErr (abs)
2	4	31	0.7088923	6.8995×10^{-06}
6	8	32	0.7086547	7.1254×10^{-06}
10	12	32	0.7086056	7.3353×10^{-06}
16	18	30	0.7089906	6.8555×10^{-06}
22	24	25	0.7088767	8.4143×10^{-06}
32	34	32	0.7090380	7.2522×10^{-06}
36	38	37	0.7090952	5.6228×10^{-06}
40	42.5	29	0.7090651	7.8184×10^{-06}
45	46	28	0.7084412	7.0303×10^{-06}
50	52	32	0.7085629	6.9299×10^{-06}
54	56	33	0.7083908	6.9392×10^{-06}
58	60	46	0.7083415	6.1782×10^{-06}
66	68	38	0.7084961	7.3548×10^{-06}
68	70	29	0.7086069	7.2733×10^{-06}
74	76	23	0.7085054	7.3531×10^{-06}
78	80	26	0.7086150	6.7636×10^{-06}
82	84	23	0.7087141	7.1005×10^{-06}
86	88	16	0.7084723	6.7583×10^{-06}
92	94	20	0.7086781	6.4997×10^{-06}
98	100	23	0.7083944	8.8246×10^{-06}
102	104	26	0.7086270	7.0049×10^{-06}
108	110	26	0.7081114	7.7709×10^{-06}
110	112	25	0.7087512	0.00002
114	116	25	0.7087348	4.73×10^{-06}
116	118	30	0.7089914	6.9982×10^{-06}
118	120	38	0.7089995	4.94×10^{-06}
122	123	34	0.7090287	1.83×10^{-05}
126	128	17	0.7090530	4.57×10^{-06}
130	135	57	0.7086334	4.68×10^{-06}

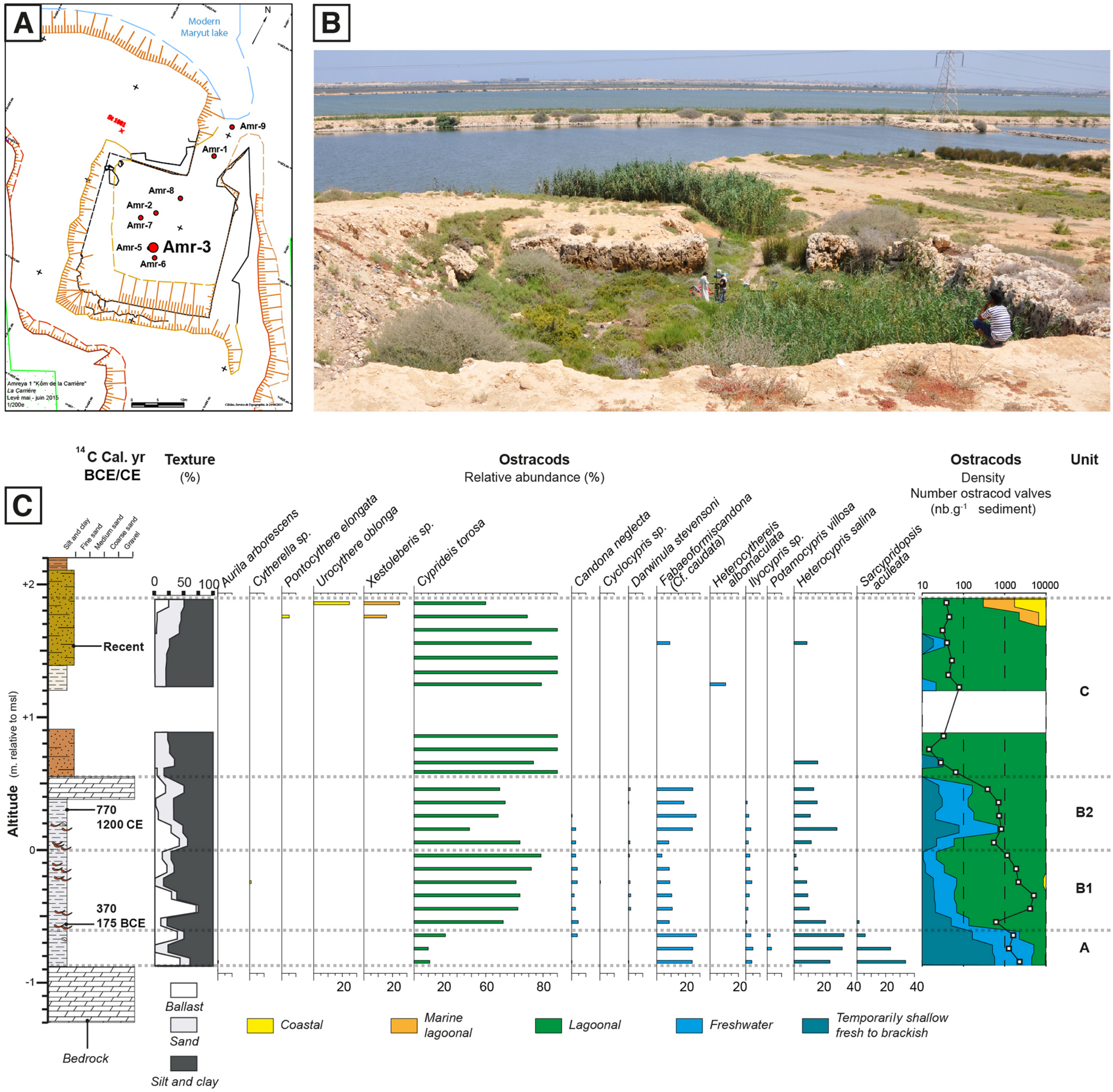

Figure 2. Kôm de la Carrière archeological site. Map **(a)** and photograph **(b)** of the silted quarry open toward Lake Maryut (© CEAlex archive). The quarry was hypothetically used as a lake harbor. Eight cores were taken from the silted quarry to test this hypothesis. Stratigraphy and ostracod species and assemblages of core AMR-3 are given in **(c)**.

2000). This bedrock has been carved in the form of a box-shaped quarry opening onto Lake Maryut (Fig. 2), which led El-Fakharani (1991) to suggest that this structure was later used as a protected harbor in ancient times. Core AMR-3 was taken from the silted quarry in order to test this hypothesis. Three main units were elucidated along the sedimentary sequence.

Unit A is composed of light gray silts and clays (56 %). The sand and gravel fractions respectively represent 17 % and 27 % of the sediment texture. The ostracods comprise an association of freshwater to brackish (86 %) and lagoonal (14 %) species. *Heterocypris salina* and *Sarcypridopsis aculeata*, indicative of temporary fresh to brackish water environments, constitute 52 % of the ostracod assemblage. The density is <1000 valves per 10 g of sediment.

Unit B comprises 63 % silts and clays, 17 % sands, and 20 % gravels. The gravels fraction is dominated by ceramic fragments. There is no color change in relation to unit A. The unit is dated between 370–175 cal BCE and 775–1200 cal CE (1050 ± 80 BP) (Table 1; Fig. 2).

The study of the ostracods allowed us to divide unit B into two subunits. Subunit B1 shows a high density of ostracods (between 530 and 4800 valves for 10 g of sediment). The ecology shows that lagoonal (*C. torosa*) ostracods dominate this assemblage (75 % of the valves). The remaining 25 % comprise freshwater (*Fabaeformiscandona* cf. *caudata*, *Candona neglecta*, *Iliocypris* sp.) and fresh to brackish water species (*Heterocypris salina*). In subunit B2 the faunal density is lower and never exceeds 800 valves per 10 g of sediment (mean density = 511 valves for 10 g of sediment). Fresh to brackish water species represent 45 % of the faunal assemblage, and *C. torosa* is still dominant with 55 % of the identified valves.

Unit C is sandier (27 %), but silts and clays still dominate the total texture (70 %). The gravels represent (3 %) of the sediment aggregate. The faunal density is very low with a maximum density of around 75 valves for 10 g of sediment in the middle of the unit. *C. torosa* is also dominant in this unit, comprising 93 % of the valves. Freshwater species are sporadically present in some samples and represent up to 5 % of the total assemblage.

3.2 Sediment record from a kiln firing chamber and a sakieh well at Akadémia

Akadémia is located on the southwestern shore of Lake Maryut, close to the ancient site of Marea-Philoxenite, ca. 8 km southwest of Kôm de la Carrière (Fig. 1) on the piedmont of the same Gebel Maryut Pleistocene ridge. Archeological remains at Akadémia are composed of an amphora workshop (kilns, activity level and a big waste dump) and a wine press from the 2nd century CE and hydraulic structures from the 5th to early 7th century CE. The plan view of one of the amphora kilns shows a semi-buried circular structure 12.65 m in outside diameter and 7.7 m in inside diameter. The firing chamber of the amphora kiln was cored in order to probe its volume and infilling (core AKA19; Fig. 3). The base of the firing chamber was found 4 m below the oven floor at 0.6 m below msl (mean sea level). The first deposit is a composite, comprising eight layers, 0.1 to 10 cm thick, of ashen and char sediments intercalated with silty sands and fragments of fired clay bricks. This first deposit translates the kiln activity. It is mainly overlain by fragments of fired clay bricks within a sandy silt matrix, related to the abandonment and the infilling stage of the structure. Four well-defined layers of clayey silts, 5–10 cm thick and including a few specimens of the freshwater ostracod *Ilyocypris* sp., were intercalated in the coarse sedimentary infilling.

Core AKA12 retrieved the infilling of a sakieh well found on the western part of Akadémia and is dated to the 5th to early 7th centuries CE (Fig. 3). The sequence is 3.8 m thick. At the base, unit A is made of alternating fine to coarse oolitic sand layers, including a few shell fragments and aeolianite gravels corresponding to the upper altered bedrock. The first depositional layer in the well comprises hydromorphic clayey sandy silts (unit B) with a few specimens of the freshwater ostracod *Candona sp.* and potsherd fragments. Unit C is broadly made up of a conglomerate of gravels and pebbles within a brown silty-sand matrix. This unit C, 1.5 m thick, likely derived from the abandonment and partial destruction of the sakieh's structure. The latter was stabilized during the last deposition of unit D, characterized by homogeneous yellowish brown silty sands. The well's base was found at 0.6 m below msl, while an estimate for the sakieh's hydraulic wheel diameter and position (Pichot and Empereur, 2013, Annexe IV, p. 88) shows that the water level in the sakieh's well when in use was around 1 m above msl (Fig. 3).

4 Sediments from section M83 (Fig. 4)

4.1 Unit A: the Maryut marine lagoon

The upper unit A comprises an alternation of shell-rich and dark mud layers deposited at the centimetric scale. Shell-rich layers comprise very abundant shell fragments and well-preserved and abundant gastropods, mollusks and ostracod valves, the latter sometimes still in connection. Species density is high and diversity low, dominated by *Hydrobia ventrosa* (50 %–95 %), followed by *Cerastoderma glaucum*, *Loripes lacteus*, *Bittium reticulatum* and *Abra* sp. The ostracod assemblage appears monospecific, represented by the ubiquist, euryhaline and opportunist species *Cyprideis torosa* (Frenzel and Boomer, 2005). The $^{87}Sr/^{86}Sr$ values of *Cyprideis torosa* valves taken from this unit are around 0.7090 except one sample close to 0.7086. The upper unit A ends with the deposition of a 4 cm thick layer almost exclusively composed of shell fragments from the same species as the unit A assemblage.

4.2 Units B and C: reworked Lake Mareotis muds?

Unit B is 0.8 m thick and comprises homogeneous silty clays (90 %–95 % of the bulk sediment), dark gray to brown, with a lumpy structure. Gypsum dominates the composition of the sand fraction mainly in discoidal lenticular forms. In sectional view, fine white gypsum was observed in the form of nodules and a mycelium-like morphology. Macrofauna and microfauna are scarce in this unit, but nonetheless the gastropods *Planorbis planorbis* and the ostracod *Ilyocypris* sp. are present, indicators of lightly brackish conditions, together with lagoonal and marine lagoonal species. These low-brackish conditions are confirmed by the $^{87}Sr/^{86}Sr$ signature that decreases significantly to 0.70805 at the base of the unit, although the whole facies is characterized by important fluctuations ranging between 0.70805 and 0.7087

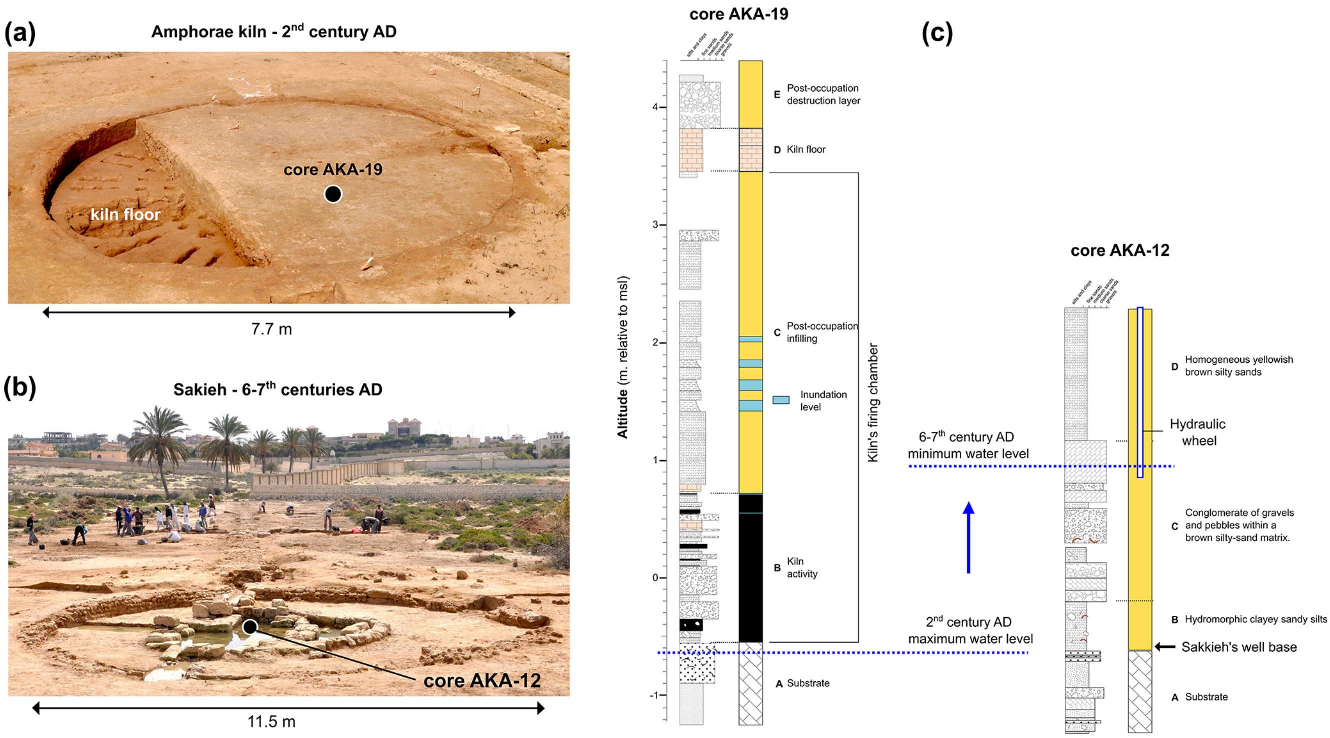

Figure 3. Akadémia archeological site. **(a)** A 2nd century CE amphora kiln. **(b)** A 5th to early 7th century CE sakieh (Egyptian water wheel) 500 m westward from the kiln. Both structures are located at ca. 150 m from the modern lakeshores in a similar configuration at the foothill of a Pleistocene coastal ridge covered by late Quaternary aeolian sands. **(c)** Comparison between cores AKA-19 and AKA-12 stratigraphies. The water table must have been below the kiln chamber during its use, then above the lower water wheel, showing a rise between the 2nd to the 5th century CE.

(Fig. 4). The transition between units A and B is characterized by a decrease in the faunal density and Sr isotope ratio and a sudden increase in magnetic susceptibility from 0 to $70 \times 10^{-8}\,m^3\,kg^{-1}$.

The next unit C comprises compact dark gray clayey silts with a lumpy structure. There is a rich gypsum layer with a pseudo-mycelium structure. Macrofauna density remains are just a few individuals per 100 g of dry sediment, although it peaks to >10 individuals towards the lower half of the unit, dominated by lightly brackish species (*Planorbis planorbis* and *Bellamya* sp.); *Cyprideis torosa* density increases rapidly from tens to hundreds of individuals from the base of unit C then decreases to tens of individuals per gram of sediments. The $^{87}Sr/^{86}Sr$ ratio in unit C ranges between 0.7083 and 0.70855.

Radiocarbon data from units B and C show great inconsistency (Fig. 4). Three samples, taken from the base of unit B, display ages ranging from 900 BCE to 950 CE. A shell from the middle of unit B was dated to 760–420 BCE, while a burnt bone taken from the same level dates to late Pleistocene times (>45 700 BCE; Fig. 4). Lastly, the upper unit C was dated from 540 to 200 BCE. Such a discrepancy, coupled with age inversions, suggests that units B and C consist of reworked muds. Given the macrofauna and $^{87}Sr/^{86}Sr$ and ^{14}C data, these muds were mostly reworked from lightly brackish lake bottoms deposited between the first millennium BCE and the first millennium CE.

4.3 Unit D: Lagoon regression

The lower and upper interfaces of unit D were sharply defined. The facies shows an increase in fine-sand inputs that reach ca. 50 % of the sediment bulk. Sands are dominated by quartz minerals. A laminated structure is partially preserved with alternations of sand-rich and mud-rich infra-millimetric layers. The faunal assemblage is characterized by the return of lagoonal species sensu stricto and an increase in *Cyprideis torosa* densities up to several thousand individuals per gram of dry sediment. Three $^{87}Sr/^{86}Sr$ values display a narrow range between 0.709 and 0.7091 and signal the return of marine-dominated conditions.

4.4 Unit E: final lagoon stage

Unit E provides the last record of section M83. The sand fraction, dominated by quartz minerals, decreases to 25 %–50 % in the lower half and 10 %–25 % in the upper part. The unit contains a few individuals of lagoonal shells (*Hydrobia* sp. and *Cerastoderma glaucum*). The $^{87}Sr/^{86}Sr$ ratio comprises

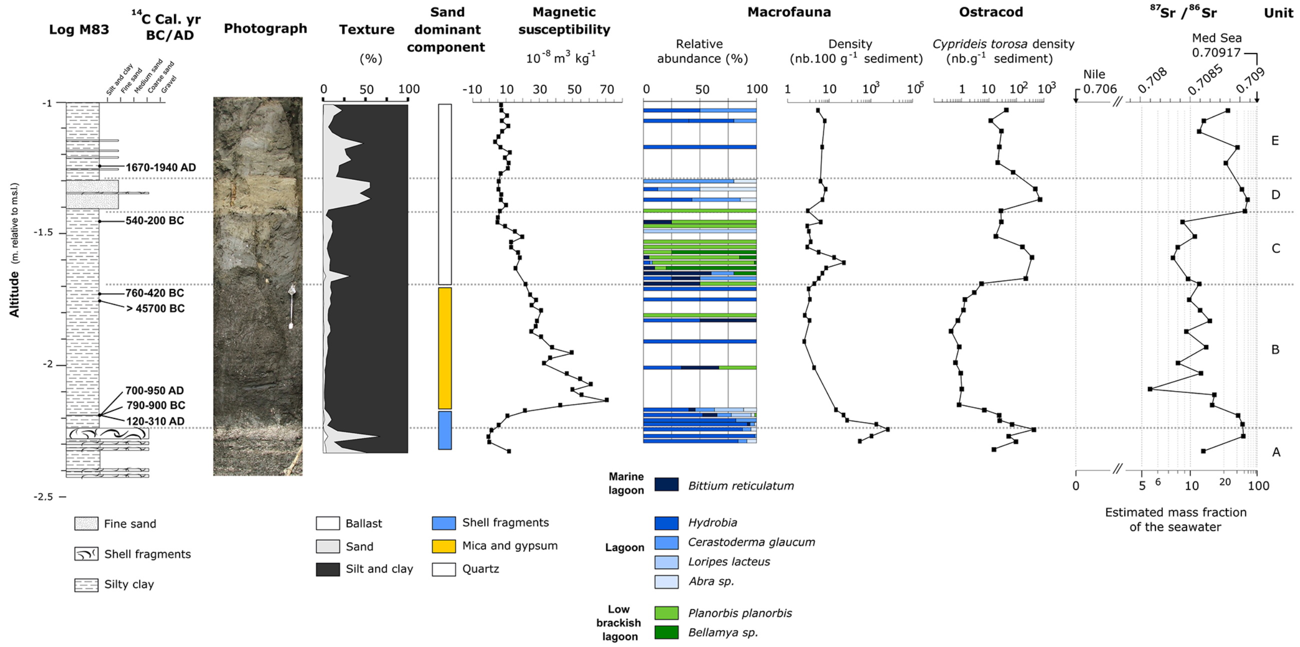

Figure 4. Multi-proxy analysis of section M83 taken from southeastern Lake Maryut (Fig. 1). The mass fraction of seawater was estimated via a two-component mixing equation using modern seawater and Nile river water $^{87}Sr/^{86}Sr$ signatures (details in Reinhard et al., 1998 and Flaux et al., 2013)

a wider range between 0.7086 and 0.709, indicating a fluctuating water budget from fluvial to marine dominated. A charcoal sample was radiocarbon dated to the modern period, in agreement with historical accounts from the 16th to the 18th centuries CE, which describe, from year to year, alternating lacustrine, lagoonal and salt marsh landscapes in the Maryut basin (Flaux et al., 2012).

5 Lake Mareotis' contrasting sedimentary record

5.1 Lake Mareotis desalinization during the first millennium BCE and Roman water-level rise

Mixed sediments deposited in section M83 have nevertheless recorded, according to fauna and $^{87}Sr/^{86}Sr$, dominant Nile inputs to Maryut's water budget for a broad period spanning the first millennium BCE to the first millennium CE. This assessment is confirmed by lagoonal to freshwater ostracods found in core AMR-3 taken in a sheltered context in relation to Maryut's southeastern central basin, i.e., the semi-closed inundated quarry located along the western Maryut margin (Fig. 2). These data show that Lake Mareotis was connected to the Nile. Geoarcheological data at Akadémia and Kôm de la Carrière confirm and refine hydrological conditions in Greco-Roman times.

At Akadémia, the kiln and the sakieh lie 500 m from each other in a similar geomorphological context at the foothill of a Pleistocene coastal ridge covered by late Quaternary aeolian sands (El-Asmar and Wood, 2000) ca. 150 m from the modern Lake Maryut shoreline. The base of the kiln's firing chamber lies at a similar depth to the base of the sakieh well, suggesting a rise in the water table between the 2nd (kiln activity) and the 5th to early 7th (sakieh activity) centuries CE, which is in accordance with clayey silt layers including a few specimens of the freshwater ostracod *Ilyocypris* sp., translating stagnant water after the inundation of the firing chamber posterior to its use (Fig. 3). In light of estimates for the sakieh's hydraulic wheel diameter and position (Pichot and Empereur, 2013, Annexe IV, p. 88), a minimum rise in the water table of 1.5 m is inferred (Fig. 3). Because the water table, given the shoreline context of the site and the porosity of loose sediments that compose the substrate of both structures, is probably controlled by the base level of Lake Maryut, it is suggested that Akadémia's remains have recorded a rise in Lake Mareotis' level during Roman times.

The study at Kôm de la Carrière has revealed that the quarry was excavated before or at the beginning of the Hellenistic period at a time when the level of the lake was below mean sea level (msl), given that it is not possible to extract the stones below shallow water (Fig. 2). Following a subsequent rise in water level, the quarry was transformed into a lightly brackish to freshwater basin connected to Lake Mareotis (unit A) and maybe used as a protected harbor. Alternatively, the quarry could have been excavated while disconnected from the lake before the excavation of a canal towards the lake. However, the great porosity of the bedrock, made of poorly consolidated fine to coarse sand layers, and the proximity of the lake go against this hypothesis. Our chronological framework shows that the onset of sedimentation is not much earlier than 370–195 cal years BCE (terminus post quem), which is consistent with excavations and archeological surveys undertaken upon the adjacent Kôm, showing an occupation spanning the Greco-Roman period (Pichot, 2017). Moreover, the basin silted during or after the late Roman period and later, as suggested by late Roman sherds discovered in most of the cores drilled into the silted quarry. Ostracod assemblages from this silting stage (units B1 and B2) comprise 25 % freshwater (*Fabaeformiscandona* cf. *caudata*, *Candona neglecta*, *Iliocypris* sp.) and fresh to brackish water species (*Heterocypris salina*), demonstrating important freshwater inputs, although *Cyprideis torosa* dominates the assemblages and attests to important variations in salinity, possibly related to seasonal Nile floods, in particular in subunit B1. Units B2 and C were deposited between 0 and 1.9 m above msl (Fig. 2), suggesting that Lake Maryut was disconnected from the sea at the time of deposition and mainly supplied by Nile inflow.

Geoarcheological indicators therefore suggest that (1) Lake Mareotis was a lightly brackish lagoon and (2) its level increased by at least ca. 1.5 m between the 2nd and the 5th centuries CE and lay above msl. Late Pleistocene stiff muds lying below Holocene sediments (Chen and Stanley, 1993) represent a relatively impermeable substratum that could have favored the water-level rise and stabilization above msl. It is not clear, however, whether the lake level stabilized above msl or was a seasonal high level linked to the Nile flood. More data are required to better document the dating and nature of this hydrological change, which is crucial for the interpretation of lakeshore archeological sites. For example, the lake-level rise could partially explain the apparent abandonment of Lake Mareotis' southwestern waterfront during the 3rd–4th centuries CE (Pichot, 2017).

5.2 Origin of reworked sediments in section M83: a tsunamite?

M83 chronological framework records a mixed sediment layer (units B and C) deposited between two non-reworked laminated facies (units A and D). The lower unit A is composed of shell-rich layers with a marine $^{87}Sr/^{86}Sr$ signature (Fig. 4) intercalated with mud layers. This biofacies is widely attested across Maryut sedimentary archives (Warne and Stanley, 1993; Goodfriend and Stanley, 1996; Flaux et al., 2011, 2012, 2013) and formed within a marine lagoon whose deposition ended at the beginning of the first millennium BCE. The upper unit D comprises aeolian sands alternating with muds (unit D), which is consistent with the lake's drying up stage recorded through evaporitic crust dated from the end of the 1st millennium CE (Flaux et al., 2012). Consistently, units B and C show ^{14}C datings from the 1st millennia BCE and CE, but the ages are completely reworked within these units, and a sample of late Pleistocene age was incorporated into the sediment matrix. This facies presents (i) dating inversions, (ii) incoherent juxtaposition of marine lagoonal, lagoonal and lightly brackish faunistic assemblages (unit B), (iii) heterogeneous Sr isotopic ratios (0.70805 and 0.7087), (iv) abrupt changes in the magnetic susceptibility signature of the sediments at the base of the unit B, and (v) a broken shell layer observed at the interface between units A and B (Fig. 4). These elements may suggest that units B and C resulted from the reworking of Lake Mareotis mud bottoms reworked by a high-energy event. At the lake scale, previous chronologies have highlighted an enigmatic sedimentary hiatus. For instance, in core M12, located in the deeper central part of the lake (Fig. 1), the shell-rich facies (identical to M83's unit A) is directly overlain by a gypsum-rich facies (consistent with M83's unit D), meaning that sediments from the first millennium BCE to the first millennium CE are missing (Flaux et al., 2012 and 2013). In section M3, the upper shelly facies dated from the beginning of the first millennium BCE is overlain by lightly brackish muds from the 2nd–3rd centuries CE (Flaux et al., 2012). Radiocarbon dates from section M83 suggest that sediments may have been reworked from the northern deeper part of the basin and were redeposited southeastwards. Goodfriend and Stanley (1996) previously described reworked sediments in core S79 (location in Fig. 1). Faunal assemblages and ^{14}C and $\delta^{13}C$ analyses of shells from the upper 2 m of the sequence show a mixed layer composed of younger freshwater (*Corbicula* sp., 855 uncal BP) and older reworked lagoonal (*Cerastoderma* sp., 3900 uncal BP) species. The scenario means that the tsunami wave would have overflowed above the coastal ridge (5 m high above msl in its lower parts) and across the urban topography of Alexandria, then eroded lake-bottom sediments finally redeposited towards the southeast. In section M83, the shell fragment layer capping unit A and mixed marine to low-brackish species from unit B could have resulted from tsunami wave trains, while dominant lightly brackish fauna in unit C would translate as backwash flow from lake margins. M83's hypothetical tsunamite would have been formed some 20 km from the sea (Fig. 1). Mega-tsunami sediment imprints can be found several kilometers from the coast (Scheffers and Kelletat, 2003), and reworked silt and clays found at site M83 may represent the distal sediment plume.

According to historical sources, eight tsunamis or high-energy marine events struck the coast of Alexandria during antiquity (Goiran, 2012). Previous research has focused on their sedimentological signatures in cores from Alexandria's ancient maritime harbors. Goiran et al. (2005) identified a coarse deposit with older reworked dates, mixed fauna and coarse sediment inputs, including shock impacts on quartz grains (Goiran, 2012). Radiocarbon dates framing the coarse deposit suggest that it has recorded the tsunami wave that hit Alexandria in 811 or 881 CE (Goiran, 2012). Stanley and Bernasconi (2006) observed a possible tsunamite facies with mixed fauna and slump-like sediment strata. Overall, both studies identified, in several coastal sequences of Alexandria's eastern harbor, a centennial- to millennial-scale sedimentary hiatus, as in some of the Lake Mareotis' sequences. It remains, however, difficult to link ancient processes to missing sediments. In Lake Mareotis, section M83 may have recorded mixed sediment reworked from the lake bottoms. The younger reworked age is chronologically consistent with the high-energy event, providing a terminus post quem to 700–950 cal CE. In core M12, given that the gypsum-rich layer following the sedimentary hiatus was dated between the 9th and the 12th centuries CE (Flaux et al., 2012), the 811 or 881 CE tsunami wave may have impacted not only Alexandria's coastal waterfront (Goiran, 2012) but also its southern lakeside. In section M3, however, the sedimentary hiatus spans a shorter period, up to the 2nd–3rd centuries CE, meaning that an older tsunami would have eroded these lake bottoms. Three tsunamic layers deposited during the last 2000 years were found within coastal lagoons protected by 2–20 m high dunes on the northwestern coast of Egypt (Salama et al., 2018).

Alternatively, recurrent gypsum in pseudo-mycelium form observed in units B and C, as well as their lumpy sediment structure and dark color likely related to higher organic input, suggests the development of pedogenic features at site M83. Soil development would necessarily imply that Lake Mareotis retreated from this area and would likely derive from the lake-level lowstand previously recorded after evaporitic deposits in sequences M3 and M12 between the 9th to the 12th centuries CE (Flaux et al., 2012). Soil biological activity or agricultural plowing could also explain reworking dating along units B and C. Although this alternative hypothesis does not explain the enigmatic sedimentary hiatus recorded from the deeper part of the lake, it shows that the tsunami hypothesis requires deeper investigation. Synolakis and Fryer (2001) and Marriner et al. (2017) caution that every coastal enigma does not necessarily have a tsunami explanation.

6 Conclusion

Lake Mareotis was densely occupied during Greco-Roman times. The present contribution aims to better constrain hydrological conditions of the lake during this period. Faunal remains, the Sr isotopic signature of ostracods and geoarcheological indicators of lake levels show both a rise in Nile inputs to the basin during the first millennia BCE and CE and a lake-level rise of ca. 1.5 m during the Roman period. Such changes highlight a complex co-evolution of Alexandria's lakeside occupation history and Nile flow changes, the latter being divided into fluctuating distributaries at the delta scale that were furthermore diverted by irrigation and drainage networks (e.g., Blouin, 2006). From a forward-looking viewpoint, the Alexandria canal (see location in Fig. 1) may have played a crucial role in the evolution of Lake Mareotis' water budget: (1) it has partially diverted the Canopic Nile flow towards the delta's western margin, and (2) it has disconnected the lake from the Aboukir lagoon and thus from the sea, favoring Lake Mareotis' desalinization and allowing its level to rise above msl, as observed at Akadémia and Kôm de la Carrière archeological sites. In any case, desalinization of the northwestern Nile Delta margin could have been key in the development of human occupation in this area during the first millennium BCE. At this time, Lake Mareotis became the natural conveyor for drainage and irrigation water. Since the Hellenistic period at least, there was increasing management of the water system around Lake Mareotis, a process which was accelerated during the Roman period (Pichot, 2017) and may have played a significant role in driving lake-level changes.

Lake Mareotis' configuration was transformed by the 9th century CE from a high-level, hypohaline coastal lake to a sebkha. While we previously related this environmental change to the progressive silting up of the Canopic branch and northwestern delta irrigation system, our new results instead highlight an environmental change related to the impact of possible high-energy event(s). A reconstruction of Lake Mareotis history requires new approaches and perspectives (Crépy and Boussac, 2021).

Data availability. All data generated during this study are included in this article or are available from the corresponding author upon request.

Author contributions. CF, MG, VP, NM, MeA, AG, PD, CC and CM conceived the study and wrote the paper. CF, VP, NM, CM and MeA performed fieldwork and provided chronostratigraphies. MG performed ostracod analyses. CF, AB, PP and CC performed Sr isotopes analyses.

Competing interests. The authors declare that they have no conflict of interest.

Special issue statement. This article is part of the special issue "Geoarchaeology of the Nile Delta". It is not associated with a conference.

Acknowledgements. We thank Hélène Mariot for taking care of CEREGE's clean lab. Matthieu Giaime acknowledges the support of the Institute of Advanced Studies and the Department of Geography at Durham University. We thank two anonymous referees for constructive comments on an earlier version of the manuscript. We thank Martin Seeliger for kindly translating the abstract into German.

Financial support. This research has been supported by the ANR (France) (grant no. ANR-12-SENV-0008-03), the Investissement d'Avenir (France) (grant no. EQUIPEX ASTER-CEREGE), and the Durham Junior Research Fellowship (grant no. 609412).

Review statement. This paper was edited by Julia Meister and reviewed by two anonymous referees.

References

Athersuch, J., Horne, D. J., and Whittaker, J. E.: Marine and Brackish Water Ostracods (Superfamilies Cypridacea et Cytheracea): Keys et Notes for the Identification of the Species, Brill Archive, New Work, USA, 1989.

Bernasconi, M. P. and Stanley, D. J.: Molluscan biofacies and their environmental implications, Nile delta lagoons, Egypt, J. Coast. Res., 10, 440–465, 1994.

Blouin, K.: Homme et milieu dans le nome mendésien à l'époque romaine (1er au 6e s.), PhD thesis, University of Nice Sophia Antipolis, France and University of Laval, Québec, Canada, 558 pp., 2006 (in French).

Blue, L. and Khalil, E. (Eds.): Lake Mareotis: Reconstructing the Past, Proceedings of the International Conference on the Archaeology of the Mareotic Region, Bar International Series 2113, Oxford, England, 2010.

Butzer, K. W.: Early Hydraulic Civilization in Egypt, University of Chicago Press, Chicago, USA, 1976.

Chen, Z. and Stanley, D. J.: Alluvial stiff muds (late Pleistocene) underlying the lower Nile delta plain, Egypt: petrology, stratigraphy and origin, J. Coast. Res., 9, 539–576, 1993.

Crépy, M. and Boussac, M.-F.: Western Mareotis lake(s) during the Late Holocene (4th century BCE–8th century CE): diachronic evolution in the western margin of the Nile Delta and evidence for the digging of a canal complex during the early Roman period, E&G Quaternary Sci. J., 70, 39–52, https://doi.org/10.5194/egqsj-70-39-2021, 2021.

De Cosson, A.: Mareotis, Being a Short Account of the History of Ancient Monuments of the North-western Desert of Egypt and of Lake Mareotis, Country Life Ltd., London, USA, 1935.

El-Asmar, H. M. and Wood, P.: Quaternary shoreline development: the northwestern coast of Egypt, Quaternary Sci. Rev., 19, 1137–1149, https://doi.org/10.1016/S0277-3791(99)00097-9, 2000.

El-Fakharani, F. A.: The Kibotos of Alexandria, Studi Miscellanei, 28, 21–28, 1991.

Empereur, J.-Y.: Alexandrie redécouverte. Fayard, Paris, 254 pp., 1998.

Flaux, C.: Holocene Coastal Palaeo-environment of Maryut Lake in the Northwestern Nile delta, Egypt, PhD thesis, Aix-Marseille University, Marseille, France, 413 pp., 2012.

Flaux, C., Morhange, C., Marriner, N., and Rouchy, J.-M.: Bilan hydrologique et biosédimentaire de la lagune du Maryût (delta du Nil, Egypte) entre 8000 et 3200 ans cal. B.P., Géomorphologie, 3, 261–278, https://doi.org/10.4000/geomorphologie.9474, 2011.

Flaux, C., El-Assal, M., Marriner, N., Morhange, C., Rouchy, J.-M., Soulié-Märsche, I., and Torab, M.: Environmental changes in the Maryut lagoon (northwestern Nile delta) during the last 2000 years, J. Archaeol. Sci., 39, 3493–3504, https://doi.org/10.1016/j.jas.2012.06.010, 2012.

Flaux, C., Claude, C., Marriner, N., and Morhange, C.: A 7500 years strontium isotope record from the northwestern Nile delta (Maryut lagoon, Egypt), Quaternary Sci. Rev., 78, 22–33, https://doi.org/10.1016/j.quascirev.2013.06.018, 2013.

Flaux, C., El-Assal, M., Shaalan, C., Marriner, N., Morhange, C., Torab, M., Goiran, J.-P., and Empereur, J.-Y.: Geoarchaeology of Portus Mareoticus: Ancient Alexandria's lake harbour (Nile Delta, Egypt), J. Archaeolog. Sci. 13, 669–681, https://doi.org/10.1016/j.jasrep.2017.05.012, 2017.

Frenzel, P. and Boomer, I.: The use of ostracods from marginal marine, brackish waters as bioindicators of modern and Quaternary environmental changes, Palaeogeogr. Palaeocl., 225, 68–92, 2005.

Goiran, J.-P.: Caractérisation d'un dépôt de tsunami dans le port antique d'Alexandrie par l'étude exoscopique des quartz: apports et limites de la méthode, in: Archéosismicité & Tsunamis en Méditerranée, Approches croisées, edited by: Rébé-Marichal, I., Laurenti, A., Boehm, I., and Goiran, J.-P., Editions APS, Perpignan, France, 157–190, 2012 (in French).

Goiran, J.-P., Marriner, N., Morhange, C., Abd El-Maguid, M., Espic, K., Bourcier, M., and Carbonel, P.: Évolution géomorphologique de la façade maritime d'Alexandrie (Egypte) au cours des six derniers millénaires, Méditerranée, 104, 61–65, https://doi.org/10.4000/mediterranee.2132, 2005 (in French).

Goiran, J.-P., Vittori, C., Noirot, B., and Torab, M.: Relative Sea Level Variations at Alexandria (Nile Delta, Egypt) over the Last Millennia: Archaeological Implications for the Ancient Harbour, Verlag der Österreichischen Akademie der Wissenschaften, Wien, 2018.

Goodfriend, G. A. and Stanley, J.-D.: Reworking and discontinuities in Holocene sedimentation in the Nile delta: documentation from amino acid racemization and stables isotopes in mollusks shells, Mar. Geol., 129, 271–283, https://doi.org/10.1016/0025-3227(96)83348-2, 1996.

Marriner, N., Kaniewski, D., Morhange, C., Flaux, C., Giaime, M., Vacchi, M., and Goff, J.: Tsunamis in the geological record: Making waves with a cautionary tale from the Mediterranean, Sci. Adv., 3, 10, https://doi.org/10.1126/sciadv.1700485, 2017.

Pichot, V.: Aux portes d'Alexandrie. Le développement de la Maréotide hellénistique et romaine, PhD thesis, Lyon 2 Lumière University, Lyon, France, 1391 pp., 2017 (in French).

Pichot, V. and Empereur, J.-Y.: Rapport de la campagne de fouille juin–août 2013 sur le site d'Akadémia (Égypte), Rapport pour le Ministère de l'Europe et des affaires étrangères, CEAlex, Alexandria, Egypt, 102 pp., 2013 (in French).

Pichot, V. and Flaux, C.: Les fours à amphores du Haut-Empire du site d'Akadémia (Maréotide): campagne de fouille et carottages 2014, Bulletin de liaison de la Céramique Égyptienne (BCE), 25, 259–276, 2015 (in French).

Pin, C., Briot, D., Bassin, C., and Poitrasson, F.: Concomitant separation of strontium and samarium-neodymium for isotopic analysis in silicate samples, based on specific extraction chromatography, Anal. Chim. Acta, 298, 209–217, 1994.

Redon, B., Vanpeene, M., and Pesenti, M.: La vigne a été inventée dans la ville égyptienne de Plinthine, A propos de la découverte d'un fouloir saïte à Kôm el-Nogous (Maréotide), Bulletin de l'Institut français d'archéologie orientale (BIFAO), 116, 303–323, https://doi.org/10.4000/bifao.440, 2017 (in French).

Reimer, P., Austin, W., Bard, E., Bayliss, A., Blackwell, P., Bronk Ramsey, C., Butzin, M., Cheng, H., Edwards, R. L., Friedrich, M., Grootes, P. M., Guilderson, T. P., Hajdas, I., Heaton, T. J., Hogg, A. G., Hughen, K. A., Kromer, B., Manning, S. W., Muscheler, R., Palmer, J. G., Pearson, C., van der Plicht, J., Reimer, R. W., Richards, D. A., Scott, E. M., Southon, J. R., Turney, C. S. M., Wacker, L., Adolphi, F., Büntgen, U., Capano, M., Fahrni, S. M., Fogtmann-Schulz, A., Friedrich, R., Köhler, P., Kudsk, S., Miyake, F., Olsen, J., Reinig, F., Sakamoto, M., Sookdeo, A., and Talamo, S.: The IntCal20 Northern Hemisphere Radiocarbon Age Calibration Curve (0–55 cal kBP), Radiocarbon, 62, 725–757, https://doi.org/10.1017/RDC.2020.41, 2020.

Reinhardt, E. G., Stanley, J.-D., and Patterson, R. T.: Strontium isotopic paleontological method as a high-resolution paleosalinity tool for lagoonal environments, Geology, 26, 1003–1006, 1998.

Salama, A., Meghraoui, M., El Gabry, M., Maouche, S., Hussein, M. H., and Korrat, I.: Paleotsunami deposits along the coast of Egypt correlate with historical earthquake records of eastern Mediterranean, Nat. Hazards Earth Syst. Sci., 18, 2203–2219, https://doi.org/10.5194/nhess-18-2203-2018, 2018.

Scheffers, A. and Kelletat, D.: Sedimentologic and geomorphologic tsunami imprints worldwide – a review, Earth-Sci. Rev., 63, 83–92, 2003.

Stanley, J.-D.: Egypt's Nile Delta in Late 4000 Years BP: Altered Flood Levels and Sedimentation, with Archaeological Implications, J. Coast. Res., 35, 1036–1050, https://doi.org/10.2112/JCOASTRES-D-19-00027.1, 2019.

Stanley, J.-D. and Bernasconi, M. P.: Holocene Depositional Patterns and Evolution in Alexandria's Eastern Harbor, Egypt, J. Coast. Res., 22, 283–297, https://doi.org/10.2112/04-0348.1, 2006.

Sun, Q., Liu, Y., Salem, A., Marks, L., Welc, F., Ma, F., Zhang, W., Chen, J., Jiang, J., and Chen, Z.: Climate-induced discharge variations of the Nile during the Holocene: Evidence from the sediment provenance of Faiyum Basin, north Egypt, Global Planet. Change, 172, 200–210, 2019.

Synolakis, C. and Fryer, G. J. : Review of: Tsunami: The underrated hazard, EOS, 82, 588, https://doi.org/10.1029/01EO00342, 2001.

Warne, A. G. and Stanley, D. J.: Late Quaternary evolution of the northwest Nile delta and adjacent coast in the Alexandria region, Egypt, J. Coast. Res., 9, 26–64, 1993.

Wilson, P.: Waterways, settlements and shifting power in the northwestern Nile Delta, Water Hist., 4, 95–117, https://doi.org/10.1007/s12685-012-0053-z, 2012.

Yoyotte, J., Charvet, P., and Gompertz, S.: Strabon, le voyage en Egypte, un regard romain, Nil Edition, Paris, France, 1997.

E&G Quaternary Sci. J., 70, 105–128, 2021
https://doi.org/10.5194/egqsj-70-105-2021

Open Access E&G Quaternary Science Journal

A composite ^{10}Be, IR-50 and ^{14}C chronology of the pre-Last Glacial Maximum (LGM) full ice extent of the western Patagonian Ice Sheet on the Isla de Chiloé, south Chile (42° S)

Juan-Luis García[1], Christopher Lüthgens[2], Rodrigo M. Vega[3], Ángel Rodés[4], Andrew S. Hein[5], and Steven A. Binnie[6]

[1]Instituto de Geografía, Facultad de Historia, Geografía y Ciencia Política, Pontificia Universidad Católica de Chile, Avenida Vicuña Mackenna 4860, Macul, Santiago, 782-0436, Chile
[2]Institute for Applied Geology, University of Natural Resources and Life Sciences (BOKU), Vienna, 1190, Austria
[3]Instituto de Ciencias de la Tierra, Facultad de Ciencias, Universidad Austral de Chile, Valdivia, 5091000, Chile
[4]Scottish Universities Environmental Research Centre, Rankine Avenue, Scottish Enterprise Technology Park, East Kilbride, G75 0QF, UK
[5]School of GeoSciences, University of Edinburgh, Edinburgh, Scotland, EH8 9XP, UK
[6]Institut für Geologie und Mineralogie, Universität zu Köln, Zülpicher Str. 49b, Gebäude 310, 50674, Köln, Germany

Correspondence: Juan-Luis García (jgarciab@uc.cl)

Relevant dates: Received: 11 August 2020 – Revised: 5 February 2021 – Accepted: 23 March 2021 – Published: 20 May 2021

How to cite: García, J.-L., Lüthgens, C., Vega, R. M., Rodés, Á., Hein, A. S., and Binnie, S. A.: A composite ^{10}Be, IR-50 and ^{14}C chronology of the pre-Last Glacial Maximum (LGM) full ice extent of the western Patagonian Ice Sheet on the Isla de Chiloé, south Chile (42° S), E&G Quaternary Sci. J., 70, 105–128, https://doi.org/10.5194/egqsj-70-105-2021, 2021.

Abstract: Unanswered questions about the glacier and climate history preceding the global Last Glacial Maximum (LGM) in the southern temperate latitudes remain. The Marine Isotope Stage (MIS) 3 is normally understood as a global interstadial period; nonetheless its climate was punctuated by conspicuous variability, and its signature has not been resolved beyond the polar realms. In this paper, we compile a ^{10}Be depth profile, single grain infrared (IR) stimulated luminescence dating and ^{14}C samples to derive a new glacier record for the principal outwash plain complex, deposited by the western Patagonian Ice Sheet (PIS) during the last glacial period (Llanquihue Glaciation) on the Isla de Chiloé, southern Chile (42° S). In this region, the Golfo de Corcovado Ice Lobe left a distinct geomorphic and stratigraphic imprint, suitable for reconstructing former ice dynamics and timing of past climate change. Our data indicate that maximum glaciation occurred by 57.8 ± 4.7 ka without reaching the Pacific Ocean coast. Ice readvanced and buttressed against the eastern side of the Cordillera de la Costa again by 26.0 ± 2.9 ka. Our data further support the notion of a large ice extent during parts of the MIS 3 in Patagonia and New Zealand but appear to contradict near contemporaneous interstadial evidence in the southern midlatitudes, including Chiloé. We propose that the PIS expanded to its full-glacial Llanquihue moraines, recording a rapid response of southern mountain glaciers to the millennial-scale climate stadials that punctuated the MIS 3 at the poles and elsewhere.

Kurzfassung: Hinsichtlich der Glazial- und Klimageschichte vor dem letztglazialen Maximum (LGM) in den temperierten Breiten der Südhemisphäre sind derzeit vielen Fragen noch unbeantwortet. Das Marine Isotopenstadium (MIS) 3 wird gemeinhin als globale interstadiale Phase verstanden, die jedoch durch phasenweise starke Variabilität gekennzeichnet war, deren Verlauf jenseits der Polargebiete jedoch noch nicht aufgelöst werden konnte. In dieser Studie werden ein 10Be Tiefenprofil, Datierungsergebnisse von Einzelkorn-Lumineszenz-Messungen mittels infraroter (IR) Stimulation und Alter von 14C Datierungen kompiliert, um für den Haupt-Sander-Komplex, der vom westlichen Patagonischen Eisschild (PIS) während des letzten Glazials (Llanquihue Vereisung) auf der Isla de Chiloé (südliches Chile, 42° S) aufgebaut wurde, eine neue Vereisungschronologie aufzubauen. In dieser Region ermöglichen die deutliche geomorphologische und stratigraphische Prägung durch den Golfo de Corcovado Lobus die Rekonstruktion von vergangener Eisdynamik und der Zeitstellung klimatischer Veränderungen. Unsere Ergebnisse besagen, dass sich die maximale Eisausdehnung um 57.8 ± 4.7 ka einstellte. Der Pazifik wurde hierbei nicht erreicht. Ein erneuter Eisvorstoß entlang der östlichen Flanke der Cordillera de la Costa kann um 26.0 ± 2.9 ka nachgewiesen werden. Unsere Daten unterstützen damit die Auffassung von der Existenz großer Eisausdehnungen im MIS 3 in Patagonien und Neuseeland, aber scheinen jedoch zeitgleiche Erkenntnisse aus benachbarten Regionen zum Interstadial der südlichen Mittelbreiten, einschließlich Chiloé, zu konterkarieren. Wir erklären die Ausdehnung des PIS zu den Llanquihue Endmoränen als schnelle, kurzfristige Reaktion südlicher Gebirgsgletscher auf kurze (tausendjährige Zeitskale) stadiale Phasen innerhalb des MIS 3 Interstadials, die bereits an den Polen und andernorts nachgewiesen werden konnten.

1 Introduction

We lack thorough knowledge on the timing of the local Last Glacial Maximum (lLGM) for the Southern Hemisphere mountain glaciers because the dating of their terminal moraines and associated outwash plains has remained spatially variable. Understanding the glacial fluctuations throughout this recent glacial period (e.g., Marine Isotope Stage, MIS, 4 through MIS 2) is a prerequisite for uncovering the cause and climate mechanisms driving southern glaciation and the interhemispheric linkages of climate change (Denton et al., 1999a). Similarly, defining the ice extent is key for understanding the magnitude of the last glaciation in the southern Andes (e.g., the lLGM) and thereby the main paleoclimatological, geomorphological and paleoecological implications. In addition to MIS 2, new records indicate extensive glaciers during MIS 3, MIS 4 and late MIS 5 in southern Patagonia and New Zealand, but uncertainty remains as to whether this is a common feature of southern midlatitude glacial history (Schaefer et al., 2015; Williams et al., 2015; Darvill et al., 2015; Kelley et al., 2014; García et al., 2018; Davies et al., 2020; Mendelová et al., 2020; Shulmeister et al., 2010). Moreover, the MIS 3 is normally referred to as a global interstadial period when southern conifer forest expanded to ice-free low-land areas, but glaciers are also known to have advanced in southern Chile and New Zealand by this time (Villagrán et al., 2004; Kelley et al., 2014; Darvill et al., 2015; García et al., 2018). Despite the fact that paleoclimate records are well-resolved in the polar regions, main knowledge gaps remain for the terrestrial southern midlatitudes before the global LGM time frame.

Here, we present new geochronological data from a ^{10}Be depth profile, infrared (IR) stimulated luminescence dating using single grains of potassium-rich feldspar (Fs) and ^{14}C samples of the two Cucao main outwash terraces (Cucao_T1 and Cucao_T2) on the Isla de Chiloé, south Chile (42° S) (Figs. 1 and 2). These extensive outwash plains were deposited by the Golfo de Corcovado Ice Lobe of the northwest Patagonian Ice Sheet (PIS) during the Llanquihue Glaciation (i.e., the last glacial period). Together with Cucao_T1 and Cucao_T2, multiple pairs of outwash terraces occupying similar morphostratigraphic positions occur on the lee side of the Cordillera de la Costa and represent the full glacial extent in Chiloé (Fig. 1). These outwash terraces can be traced to ice-contact slopes on the east side of the Cordillera de la Costa as they have been previously mapped (García, 2012). Thus, the dating of the Cucao_T1 and Cucao_T2 terraces can help reconstruct the lLGM of the PIS and the overall glacier and climate history that preceded the well-known LGM (MIS 2) in the region (Mercer, 1976; Laugénie, 1982; Porter, 1981; Bentley, 1997; Denton et al., 1999b). Our record builds on previous work in the Chilean Lake District (CLD) by dating glacially derived sediments that can be directly related to a landform, thereby determining the extent of glacier advances during the last glacial period. Dating landforms beyond the ^{14}C range in Chiloé is challenging. Exposed bedrock and boulders resting on glacial landforms are very rare, rendering commonly used cosmogenic nuclide exposure-dating techniques impractical. Here, we constrain the timing of maximum ice extent, as recorded by glacial landform and deposit associations, by applying a composite geochronologic approach.

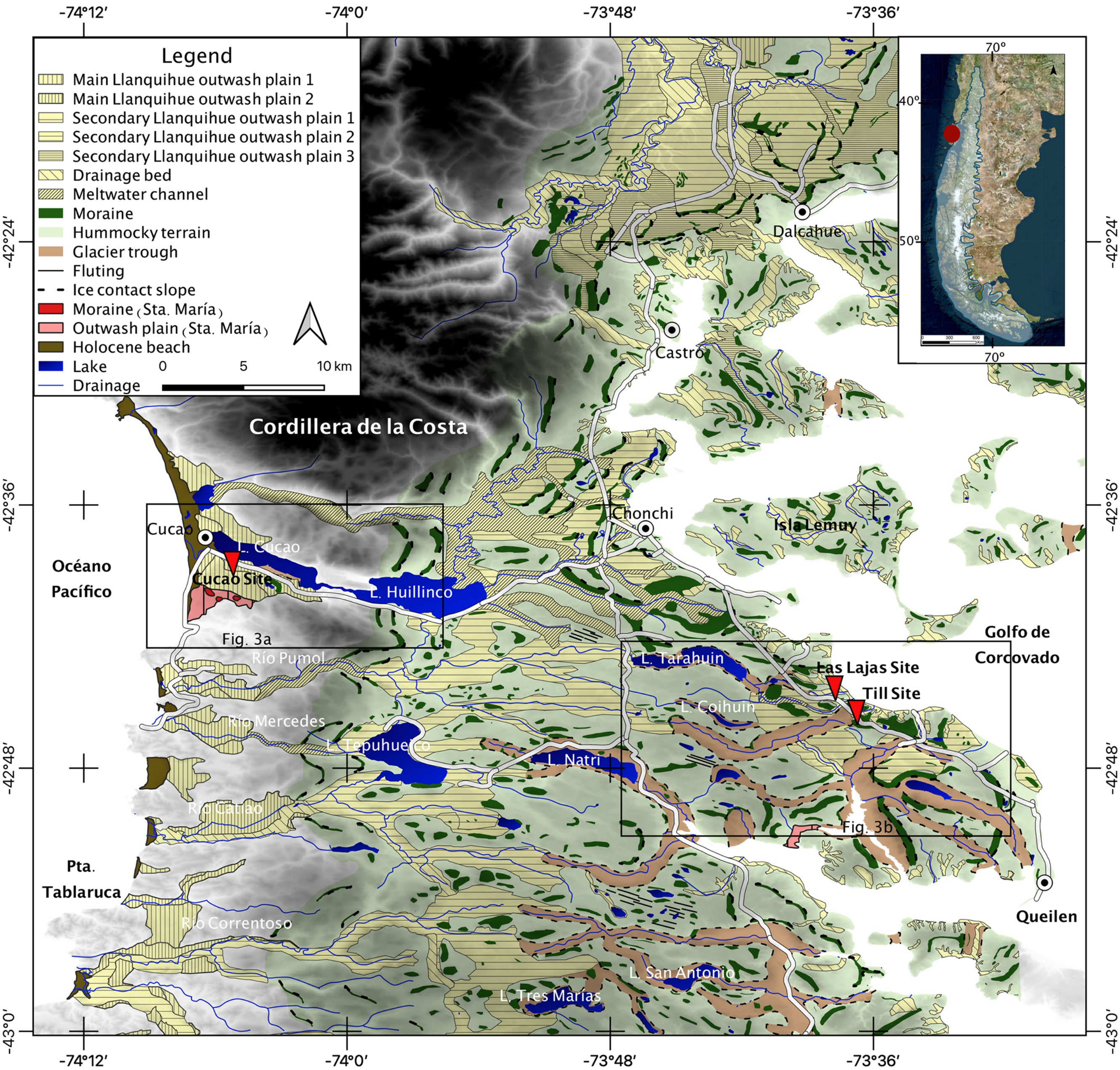

Figure 1. The Cucao site in the context of the former Patagonian Ice Sheet (PIS) and the glacial geomorphologic setting of the Archipiélago de Chiloé. The red circle in the inset indicates the location of the study area in the northwest sector of the former PIS (outlined). Note the location of stratigraphic sites presented in this study and mentioned in the text. For the sake of space, the Cucao site in the map indicates the geographic location of all seven sites studied within this sector. For more details, see Figs. 2 and 3a. Geomorphic map modified from García (2012). Base map is the 30 × 30 Shuttle Radar Topography Mission (SRTM) extracted from NASA JPL (2013).

1.1 The Llanquihue Glaciation

The Llanquihue Glaciation is the local name for the last glacial period in southern Chile, particularly the CLD and the Archipiélago de Chiloé (39–42° S) (Heusser and Flint, 1977; Porter, 1981; Laugénie, 1982; Denton et al., 1999b; García, 2012). Glacial landforms and sediments from the last ice period display excellent preservation and limited weathering, respectively. García (2012) suggested that a mountain style of glaciation characterized the CLD. Different subglacial landforms, including drumlinoid and fluting landforms, within extensive, mostly uninterrupted ice-marginal positions denote rather an ice-sheet style of glaciation to the south on the Isla Grande de Chiloé. For instance, a west–east transect across the moraine field in the CLD and northern Isla de Chiloé reveals a stepwise topography punctuated by dis-

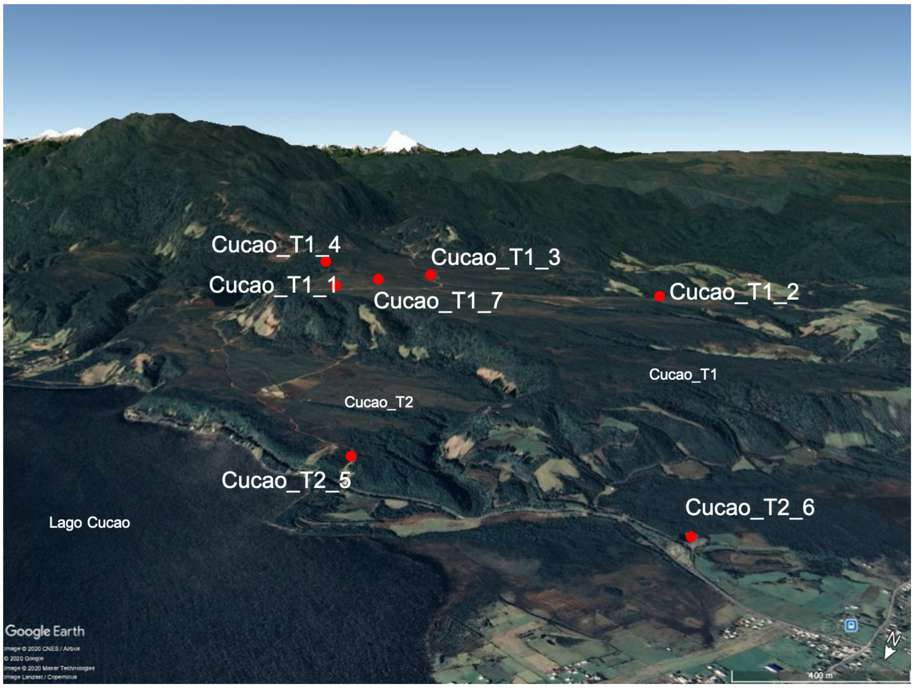

Figure 2. Oblique view of the Cucao_T1 and Cucao_T2 outwash terraces and the studied Cucao sites. All Cucao sites occur in these terraces on the western side of the Cordillera de la Costa. View is to the south-southeast. Ice flow from the upper left. Base image from © Google Earth.

tinct ice-contact slopes, composite moraines, and associated main and subsidiary outwash plains (Andersen et al., 1999; Denton et al., 1999b). To the south of Dalcahue, a double moraine and ice-contact slope preserved on the eastern slope of the Cordillera de la Costa represents the outermost extents of the ice during the Llanquihue Glaciation in Chiloé (García, 2012). Beyond this ice-marginal position, meltwater channels carved the bedrock and fed outwash terraces on the Pacific mountain side. Accordingly, the Huillinco and Cucao lakes (Fig. 1), which interrupt the continuity of the Cordillera de la Costa, likely allowed the ice to trespass towards the west. Otherwise, the ice buttressed on the eastern mountain side. It has been suggested that the outer Llanquihue landforms (i.e., the early Llanquihue time) were deposited during the Marine Isotope Stage (MIS) 4 (e.g., Denton et al., 1999b; García, 2012). This conclusion is based on the landform and sediment preservation, together with the infinite uncalibrated age $> 50\,000$ ^{14}C yr BP, of the Taiquemó record (Heusser et al., 1999), which is located inboard from the early Llanquihue moraine in northern Chiloé. In addition, sea surface temperatures (SSTs) offshore northern Chiloé uncover the coldest glacial conditions in the ocean during MIS 4 (Kaiser et al., 2005). Nonetheless, the early Llanquihue landforms have remained mostly undated, which in turn is the main research focus of this paper.

The MIS 3 in Chiloé and the CLD have been regarded as an interstadial period based on pollen and sub-fossil-tree records constrained by finite and mostly infinite ^{14}C ages (e.g., Heusser et al., 1999; Roig et al., 2001; Villagrán et al., 2004). At this time conifer forests dominated, indicating a relatively mild and humid climate (Villagrán et al., 2004). However, high variability between arboreal and herbaceous vegetation also occurred, which suggests climate instability through the MIS 3 (Heusser et al., 1999). The same conclusion can be extracted from the SST record offshore Chiloé (Kaiser et al., 2005).

For MIS 2, Denton et al. (1999b) determined the timing of at least four glacial advances in the CLD and northern Isla Grande de Chiloé, which significantly added to the previous work in the region (Mercer, 1976; Porter, 1981; Bentley, 1997). From their radiocarbon chronology, Denton et al. (1999b) defined the timing of the LGM to between 34.3 and 18.0 cal kyr BP. In central Chiloé, a glacial advance occurred before 28 cal kyr BP and at 26.0 cal kyr BP (García, 2012). The regional equilibrium line altitude (ELA) was depressed ~ 1000 m relative to the present (Porter, 1981; Hubbard et al., 2005). This corresponds to an estimated drop of 6 to 8 °C in mean summer temperature and mean annual precipitation ~ 2000 mm yr^{-1} greater than present (Heusser et al., 1996, 1999; Villagrán, 1988, 1990). The end of the LGM was marked by abrupt glacial retreat after 18 cal kyr BP, both in the CLD and Chiloé (Lowell et al., 1995; Denton et al., 1999b).

1.2 Regional setting

The Archipiélago de Chiloé is separated from the mainland by the Golfo de Ancud and Golfo de Corcovado, where intervening seawaters can reach > 400 m but mostly less than 200 m depth. The western Patagonian Andes facing Chiloé reach higher elevations and contain a significantly larger number of glaciers than the CLD to the north, with ice caps on peaks > 2000 m a.s.l. (Barcaza et al., 2017).

South of 40° S, the southwesterly circulation is present throughout the year (Garreaud et al., 2009). This zonal wind extends through the whole troposphere and occurs as a mostly symmetric belt in the southern midlatitudes. The westerly wind belt in the Pacific occurs in a zone constrained mainly by the effect of the subtropical anticyclone and the polar front, and today it produces a precipitation peak at 45–47° S (Miller, 1976). Seasonal expansion (winter) and contraction (summer) of the westerly wind belt and associated storm circulation govern the climate along extratropical Chile. Chiloé intersects the northern margin of the westerly wind belt, which results in humid winters (> 1000 mm of precipitation between May–August in Castro; Luebert and Pliscoff, 2006) and rather dry summers due to the blocking effect of the Pacific high-pressure cell (Miller, 1976; Garreaud et al., 2009). In South America, precipitation to the west of the southern Andes chain is positively correlated to the westerly wind strength, while the opposite occurs to the east of the Andes, where a rain shadow dominates (Garreaud, 2007). Mean air temperatures in Chiloé fluctuate from about 8 °C in winter to 14 °C in summer, reflecting a west-coast, southern-midlatitude maritime climate regime. Nonetheless, freezing temperatures can occur late in the autumn. Climate variability at decadal to interdecadal timescales is affected by pressure anomalies in the Antarctic and the southern midlatitudes (the Southern Annular Mode, SAM) thus controlling the strength and position of the westerly wind, precipitation yields and surface air temperatures south of 40° S (Garreaud et al., 2009, 2013).

Offshore Chiloé, the north branch of the Antarctic Circumpolar Current (ACC) shows the steepest thermal latitudinal gradient (Kaiser et al., 2005). This abrupt change in SST temperatures is linked with the southwesterly wind's northern boundary (Strub et al., 1998). Just south of Chiloé, the ACC separates into the northward Humboldt Current and the southward Cape Horn Current (Lamy et al., 2015). The Humboldt Current transports subantarctic surface waters of the ACC along the Chilean coast with mean annual SST offshore Chiloé reaching ∼ 13 °C (Kaiser et al., 2005). The ocean and atmosphere circulation are intimately linked and experienced large changes during the LGM affecting the PIS fluctuations (Lamy et al., 2015).

2 Methods

For studying the Cucao terraces, we selected a total of seven sites, including sediment pits and road sediment sections in both Cucao_T1 and Cucao_T2 (Figs. 2 and 3a). The number and distribution of sites help us to constrain the age of these glaciofluvial landforms. Most of sites occur on top of the glaciofluvial plains (sites Cucao_T1_1–3 and _7) except for Site Cucao_T1_4, Site Cucao_T2_5 and Site Cucao_T2_6, which occur by the edge of the terraces. We also study a stratigraphic section in eastern Chiloé (the Till site) which, together with the Las Lajas site (García, 2012), adds context for interpreting Cucao data.

2.1 Mapping and sedimentology

The mapping produced here builds on previous work in the area (Heusser and Flint, 1977; Andersen et al., 1999; García, 2012). We took advantage of new sediment exposures in the study area to produce more detailed observations of sediments and landforms during multiple field campaigns developed between 2016–2019. For better description and interpretation of the geomorphology, we analyzed SRTM_GL1 (Nasa JPL, 2013) and reexamined aerial photographs of the study area. Sediment analysis includes modified facies codes based on Miall (1985, 2006), Eyles et al. (1983), and Maizels (1993). We applied traditional sedimentology and geomorphology techniques in order to describe the glacial and proglacial environments as a basis for our dating approach.

2.2 Geochronology

2.2.1 Radiocarbon

We radiocarbon dated both bulk organic sediment and wood samples. We targeted in situ organic stratigraphic units or reworked organic mud clasts embedded in outwash sediments. The interpretation of our ^{14}C data varied depending on the setting, as described in the results section. All ^{14}C ages in this paper are presented as the mean ± uncertainty of the reported 2σ range except where indicated. The ages were calculated using CALIB REV7.1 online web calculator (Stuiver et al., 2020) and the Southern Hemisphere ^{14}C calibration curve (Hogg et al., 2013). The ^{14}C calibrated ages include > 0.9 probability within the 2σ range. This is true for all data presented except sample CUCAOT1-1803_III (> 0.7).

2.2.2 The ^{10}Be depth profile

We selected a stratigraphic column at the Site Cucao_T1_3 section with an accessible sediment depth reaching ∼ 300 cm (Fig. 4). This site is suitable for building a ^{10}Be depth profile as the sediments appear to have been deposited on top of each other in a continuous and rapid fashion (Hein et al., 2009; Darvill et al., 2015). Nonetheless, the sediment section where

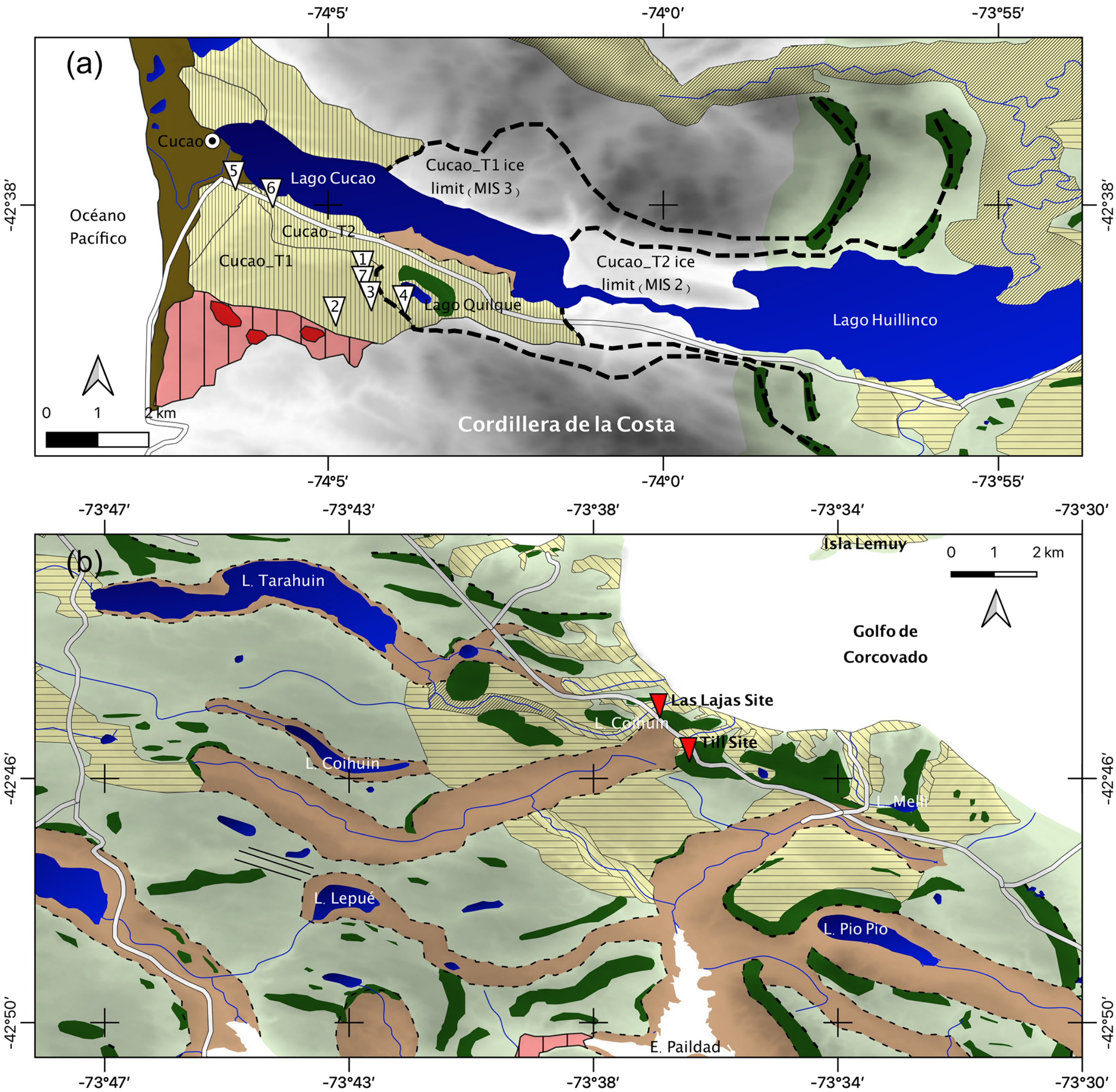

Figure 3. Geomorphic maps showing the morphostratigraphic relationships between the Cucao sites **(a)** and Las Lajas and Till sites **(b)**. Also shown in **(a)** are the inferred ice limits (dashed lines) associated with the deposition of Cucao_T1 and Cucao_T2 terraces. Both of these terraces are separated by a distinct fluvial scarp that in part could have been formed as an ice contact slope (see text for discussion). Legend codes in Fig. 1.

the ^{10}Be profile was sampled includes a top organic soil (upper 35–20 cm) that overlies outwash sediment, and therefore no surface cobbles were found for dating. An iron-rich layer occurs at 70 cm below the original surface within the outwash sediments. Above this iron layer, the sediment can appear oxidized, which is not the case towards the bottom of the sediment section.

The most critical parameter to model how the ^{10}Be accumulates underground is the evolution of the surface erosion/accretion affecting the depth of the quartz grains (samples) through time. This is because the cosmogenic ^{10}Be production rate decreases exponentially with cumulative mass depth (expressed in g cm^{-2}). To relate cumulative mass depth to the sampling depth within a sediment layer requires an estimate of the overlying bulk soil density. For our model, we considered the outwash sediment bulk density to be between 1.9 and 2.2 g cm^{-3}, based on the visual estimation of porosity between 20 % and 30 %, with variable moisture between 30 % and 60 %, and for a grain density of 2.6 g cm^{-3}. This density range coincides with the densities of gravel-bearing unconsolidated materials listed in Manger (1963). We include the top organic soil (see Sect. 3) in this range. For

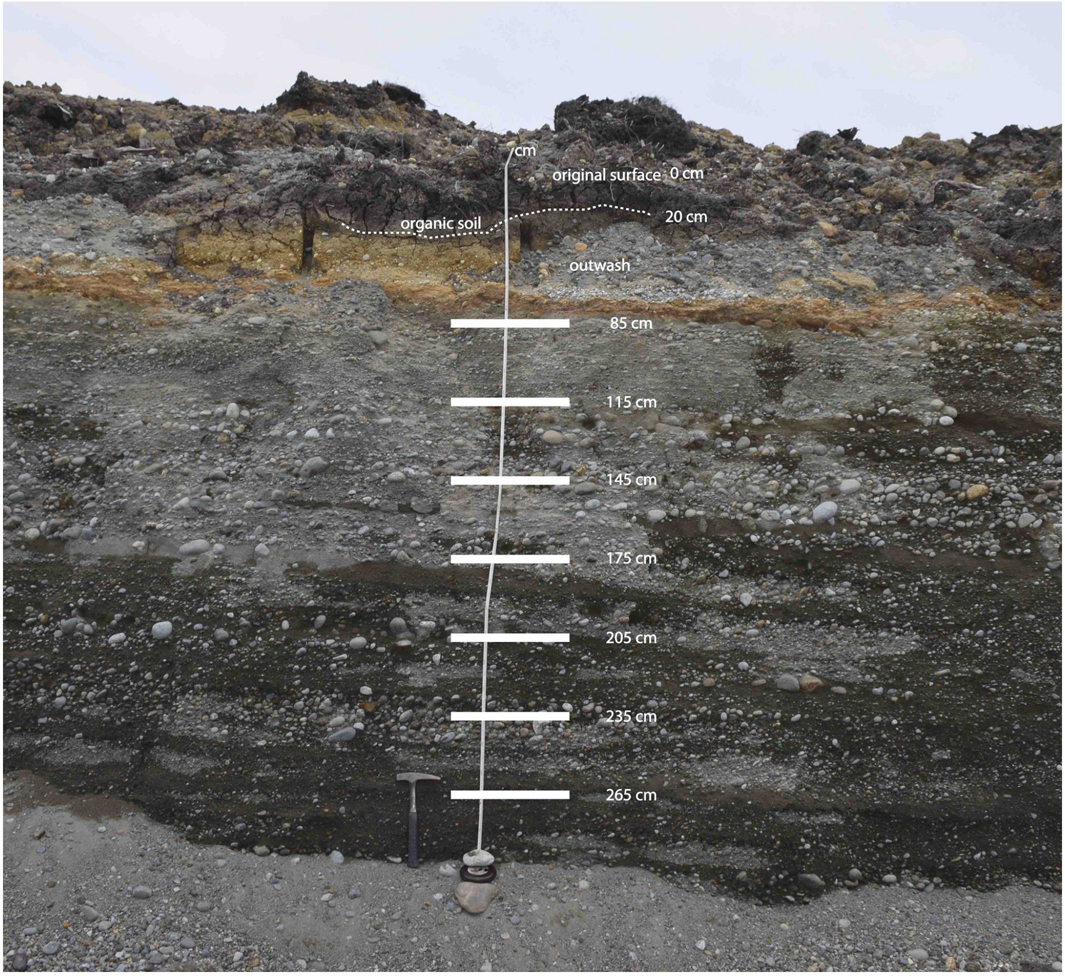

Figure 4. Cucao_T1 ^{10}Be depth profile produced in Cucao_T1_3 site. Note the original surface (underlying not in situ mixed soil remains) and the in situ organic soil and outwash sediment surface contact (dashed white line). Solid white rectangles indicate ^{10}Be sample locations with associated depths.

testing our ^{10}Be profile models for Cucao_T1_terrace, ^{10}Be concentrations produced in situ were measured in quartz obtained from seven amalgamated sand and pebble sample layers. We collected about 3 cm thick layers each 30 cm between 85–265 cm depth (Fig. 4). Model concentrations were calculated at the center of the sampling layers. We did not sample the top 50 cm of the outwash to avoid vertical sediment mixing due to potential root development near the surface.

Sediment ^{10}Be sample preparation as an accelerator mass spectrometry (AMS) target was done at University of Edinburgh's cosmogenic nuclide laboratory. The ^{10}Be was selectively extracted from 20 to 26 g of pure quartz following standard methods (Bierman et al., 2002; Kohl and Nishiizumi, 1992). The samples and the process blanks ($n = 1$) were spiked with ~ 0.25 mg ^{9}Be carrier (Scharlau Be carrier, 1000 mg L^{-1}, density 1.02 g mL^{-1}). The samples were prepared as BeO targets for AMS analysis following procedures detailed by Hein (2009). Measurements of ^{10}Be/^{9}Be ratios were undertaken at CologneAMS (Dewald et al., 2013), normalized to the revised standard values reported by Nishiizumi et al. (2007). Blank ^{10}Be/^{9}Be ratios ranged between 1 % and 5 % of sample ^{10}Be/^{9}Be ratios. Table 1 shows other ^{10}Be data from this study.

The ^{10}Be accumulation was modeled following the formulae of Lal (1991). The time was discretized to accommodate the change in the samples' depths due to the accumulation of the overlaying organic sediment. Monte-Carlo simulations (as in Hidy et al., 2010) were used to find the fitting values of the following free parameters: (1) the age of the outwash sedimentary package, (2) the age of the overlaying organic soil and (3) the initial ^{10}Be accumulated before the outwash deposition, which is considered to be constant along the outwash profile. Random values of bulk density between 1.9 and 2.2 g cm^{-3} were considered for the entire profile. Probabilities corresponding to the chi-square values of the individual models were used to calculate the probabil-

Table 1. The ^{10}Be data for depth profiles in the Cucao_T1 terrace.

Sample ID	Latitude (dd)	Longitude (dd)	Altitude (m a.s.l.)	Depth (cm)	Thickness (cm)[a]	Quartz mass (g)	^{10}Be measured (10^4 atom g^{-1}) ($\pm 1\sigma$)[b]
Cucao_115	42.6659	74.0777	112	85	3.0	23.5264	12.144 ± 1.393
Cucao_145				115	3.0	22.2588	8.376 ± 1.086
Cucao_175				145	3.0	24.3108	6.747 ± 0.404
Cucao_205				175	3.0	22.3157	6.301 ± 0.753
Cucao_235				205	3.0	22.466	4.302 ± 0.734
Cucao_265				235	3.0	26.6511	2.384 ± 0.209
Cucao_295				265	3.0	24.8943	4.125 ± 0.869

[a] This is the approximate thickness of the layer of amalgamated sediment collected at each specified depth. [b] Nuclide concentrations are normalized to revised ^{10}Be standards and half-life (1.36 ± 0.07 Myr) of Nishiizumi et al. (2007) and include propagated AMS sample and lab-blank uncertainty and 2 % carrier mass uncertainty. Quartz density is 2.7 g cm^{-3}. Topographic shielding at the profile site is negligible (0.9999).

ity density distributions of the parameters. The method described in Rodés et al. (2011) was used to select the models fitting the data within a 1σ confidence level. We initially modeled the effect of gradual (linear with time) accretion of the organic sediment. The Be-10 profiles under the organic sediment generated by these models were identical to those generated for instantaneous deposition of the organic sediment layer at an intermediate time (between the outwash formation and today). Therefore, the formation age of the organic sediment was considered an unknown variable in the models presented here in order to simulate all extreme scenarios. As the timing of the process that produced the organic soil is unknown, two scenarios were considered. Scenario "a" does not consider the shielding produced by the organic layer, as would be appropriate if the latter was formed recently or for a limited time span. The models fitting this scenario provide a minimum estimate for the outwash deposition age as they consider the conditions that maximize the ^{10}Be production rate at the sample depths. Scenario "b" considers that the organic layer could be deposited anytime between the outwash deposition and today. The models fitting this scenario should cover all the possible and the less restrictive age ranges for the deposition of the Cucao_T1 outwash. The models assume no surface erosion occurred after outwash deposition as negligible erosion rates are expected in abandoned outwash plains in relatively short time spans (i.e., the last glacial period) (Hein et al., 2009). We used ^{10}Be production rates of 4.0678, 0.0383 and 0.0404 atoms g^{-1} and attenuation lengths of 160, 2481 and 1349 g cm^{-2}, for spallation and fast and stopping muons, respectively. This is in agreement with the average production rate corresponding to the Lago Argentino calibration data in Patagonia (Kaplan et al., 2011) scaled according to the online calculators formerly known as the CRONUS-Earth online calculators v.3 (Balco et al., 2008) for the last ~ 100 kyr and using the scaling scheme of LSDn (Lifton et al., 2014). The LSDn is based on models derived from theory and includes estimates for a time-dependent magnetic field (Lifton et al., 2014). Although the selection of this scaling scheme does not affect our conclusions, we chose to use the Lago Argentino calibration and LSDn scaling scheme in order to facilitate the direct comparison of our ages with other published cosmogenic ages in Patagonia (e.g., Davies et al., 2020).

2.2.3 Luminescence dating approach

We collected luminescence samples by driving opaque tubes into soft sand sediments within the outwash deposits of Cucao_T1 (sites _1, _2 and _3; four samples) and Cucao_T2 (sites _5 and _6; two samples). Luminescence dating techniques in general allow for the determination of depositional ages of sediments by calculating the point in time when the sediments were last exposed to daylight (during transport) and subsequently shielded from daylight (deposition). The build-up of a latent luminescence signal in quartz- and potassium-rich feldspar minerals is time dependent and induced by naturally occurring radiation (cosmic radiation and ionizing radiation from naturally occurring radionuclides). Once the stored luminescence signal (termed equivalent dose) and the rate of ionizing radiation impacting the sample over time (termed the dose rate) are known, a luminescence age can be determined using the following general age equation: age (a) = equivalent dose (Gy) / dose rate (Gy a^{-1}). For further details on luminescence dating in general, please see the following overview papers: Preusser et al. (2008), Rhodes (2011), Wintle (2008), and Smedley et al. (2016).

All sample preparation and subsequent measurements were conducted at the Vienna Laboratory for Luminescence dating (VLL) on RISØ DA20 luminescence reader systems, one of which is equipped with an 830 nm infrared laser for the stimulation of the luminescence signal of potassium-rich feldspar single grains (Bøtter-Jensen et al., 2000, 2003). All measurements were conducted using potassium-rich feldspar because quartz from Patagonia has frequently been shown to be unsuitable for dating purposes (García et al., 2019; Duller, 2006; Glasser et al., 2006; Harrison et al., 2008; Blomdin et al., 2012; Smedley et al., 2016). All sample preparation was conducted at the VLL under subdued red light conditions to extract pure separates of potassium-rich feldspar (procedures described in detail in Lüthgens et al., 2017). Because waterlain samples in general are prone to incomplete bleaching of the luminescence signal prior to burial (insufficient exposure to daylight to reset the luminescence signal to zero), and that effect is intensified by the slow bleaching properties of potassium-rich feldspar, a single grain dating approach was adopted to detect and correct for the effects of incomplete bleaching. This methodological approach has been described in detail in García et al. (2019). All measurements were conducted using an IR-50 (infrared stimulated luminescence at a temperature of 50 °C) SAR (single aliquot regenerative) dose protocol, using the most easily bleachable K-feldspar (potassium-rich feldspar) signal (Blomdin et al., 2012). Rejection criteria ($<30\,\%$ recycling ratio, $<30\,\%$ recuperation, $<20\,\%$ test dose error) are based on results from dose recovery experiments resulting in recovery ratios in agreement with unity within error. Equivalent dose values were calculated using the bootstrapped three-parameter minimum age model (BS-MAM; Galbraith et al., 1999; Cunningham and Wallinga, 2012) with a threshold value of $40 \pm 10\,\%$ for the expected overdispersion. The threshold value is based on the results from dose recovery experiments and the characteristics of the best-bleached natural sample (Figs. 5 and 6). All statistical evaluation was done using the R luminescence package of Kreutzer et al. (2012). The contents of naturally occurring radionuclides (^{238}U and ^{232}Th decay chains, as well as ^{40}K) contributing to the external dose rate were determined using high-resolution, low-level gamma spectrometry (Baltic Scientific Instruments 40 % p-type HPGe detector). The dose-rate and age calculation was conducted using the software ADELE (Kulig, 2005), and all ages were corrected for fading (athermal signal loss over time; Wintle, 1973) using the approach of Huntley and Lamothe (2001) based on an average fading rate (g value of 4.4 ± 0.27) from multiple samples determined following the approach of Auclair et al. (2003) on multi-grain aliquots, as suggested by Blomdin et al. (2012). All details concerning the experimental setup are described in García et al. (2019) and the supplement on luminescence dating in that paper. A typical dose response curve and a typical equivalent dose distribution are provided in Figs. 5 and 6 for sample VLL-0291-L. In the text, we provide the calculated IR-50 age $\pm 1\sigma$.

3 Results

Whereas the higher Cucao_T1 outwash plain occurs at ~ 140 m a.s.l., the lower Cucao_T2 occurs at ~ 70 m a.s.l. Nonetheless, both landforms show relatively high topographic gradients between $\sim 2\,\%$ (Cucao_T1) and $\sim 1.3\,\%$ (Cucao_T2). Multiple outwash levels exist in between these two large outwash plains, but they are only local in extent. A main geomorphic feature is a ~ 30 m tall scarp that separates Cucao_T1 and Cucao_T2 terraces (Fig. 3a). To the west, the Cucao_T2 terrace is punctuated by a hummocky terrain adjacent to the T1 terrace scarp where the Quilque lake develops (Fig. 3a). The most prominent mounds are covered by dense forests, but a recently cleared inner ridge exhibits a diamictic surface with several rounded cobbles and small boulders on top partly covered by soil development. Overall, these landforms resemble a type of moraine relief surrounded by Cucao_T2 outwash plain. The links between this moraine landform and the outwash terraces are discussed below in Sect. 4.

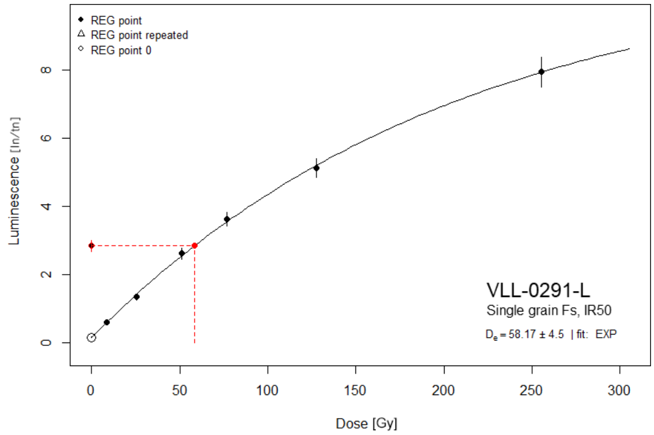

Figure 5. Representative dose response curve for a single K-feldspar grain of sample VLL-0291-L. Plot generated using the R luminescence package of Kreutzer et al. (2012).

3.1 Sedimentology

We selected a total of six sites for stratigraphic sediment interpretation: Cucao_T1 is characterized by the description of sites _1–_4. Cucao_T2 is characterized based on sites _5 and _6 (see Figs. 2 and 3a for location and Table 2 for site details). Sedimentological description and interpretation provided here for Cucao_T1 and Cucao_T2 terraces allow us to discuss the type of glacial and proglacial setting during maximum glaciation in Chiloé. Site Cucao_T1_7 outcrops on the side of a road as a nearly 50 cm peat deposit, and therefore no sediment description was made here.

3.1.1 Site Cucao_T1_1

The exposure consists of a series of crudely bedded, well-rounded, clast- to matrix-supported gravels (Gmg, Gcg), arranged in 0.3–0.5 m subhorizontal beds (Fig. 7a). Predominant grain size is within the pebble range, although cobble-rich bodies are common. Both upward-coarsening and upward-finning beds occur, matrix content generally

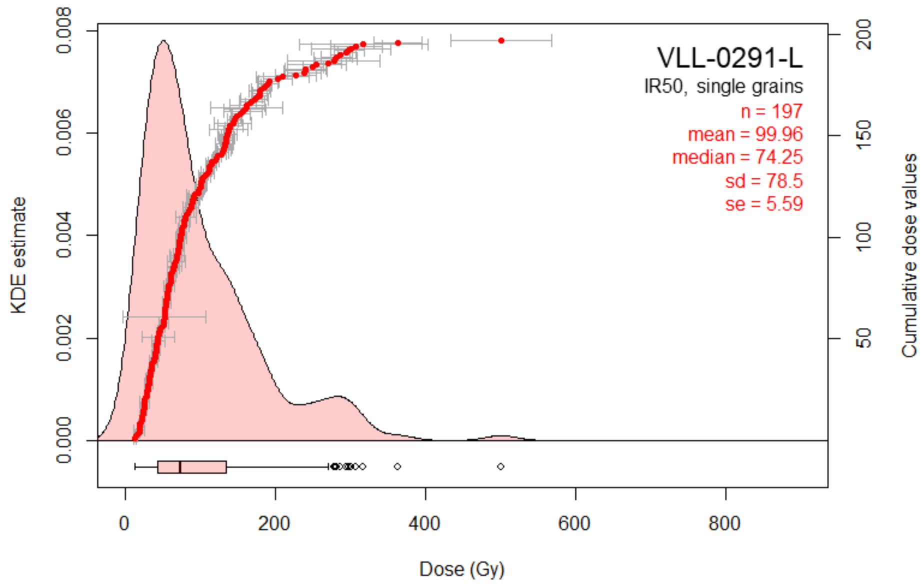

Figure 6. Equivalent dose distribution for sample VLL-0291-L. KDE plot (kernel density estimate) generated using the R luminescence package of Kreutzer et al. (2012). The graph shows an asymmetric, right-skewed distribution, which is typical for incompletely bleached samples.

decreasing from base to top and usually culminating in a clast-supported veneer. Beds are laterally extensive (> 10 m) and mostly bounded by flat subhorizontal surfaces occasionally disrupted by shallow, narrow channel bodies filled with matrix-supported, massive, cobble-rich, imbricated gravels (Gmm, Gmi). Polymict material is predominantly of Andean origin (volcanic and intrusive rocks).

Interpretation. Gcg and Gmg are interpreted as being the product of turbulent and cohesive debris flows, respectively. Laterally extensive beds, making up most of the exposed sequence, are interpreted as being the result of unconfined sheet floods. Most beds are capped by a clast-supported veneer inferred to represent winnowed sediments. Shallow channel bodies filled by Gmm and Gmi facies are taken to indicate, respectively, cohesive and turbulent, channelized, possibly erosive debris flow deposits. The whole section would thus be composed of gravitationally resedimented glacial sediments chiefly through the action of both channelized and unchannelized debris flows.

3.1.2 Site Cucao_T1_2

This is a road cut exhibiting a series of rounded, poorly to moderately sorted, matrix- to clast-supported gravel and sand layers disposed in ∼ 0.1–0.3 m thick subhorizontal beds (Fig. 7e–f). Gravel is mostly within the range of pebbles. Crudely bedded, matrix-supported, chaotic and usually coarsening upwards beds (Gmm, Gmg) form laterally extensive lenses. Clast- to matrix-supported, crudely bedded and imbricated gravel layers (Gmi, Gh) alternate with parallel-stratified, pebbly sand layers (Sh) forming a series of fining upwards sequences. Lateral extension is often truncated by concave-upwards basal surfaces of channel-shaped bodies up to 0.9–1.2 m deep filled with similar sediments. Within these fills, festoon patterns are common (St, Gt). A few outsized muddy intraclasts occur throughout the exposure.

Interpretation. Gmm and Gmg facies are interpreted as cohesive through turbulent debris flow deposits. Gmi, Gh and Sh are related to traction deposits under waning flow conditions associated with periodical shifts in hydraulic regime. Channel bodies' frequently truncating strata are taken as the product of a highly unstable, rapidly shifting distributary system made up of narrow, shallow channels.

3.1.3 Site Cucao_T1_3

This is a gravel pit, 8 m deep at most and topped by an organic soil unit (Fig. 7b–d). Exposure here consists of a series of poorly to moderately sorted, well-rounded, clast- to matrix-supported gravel and sand layers. Beds are between 0.1 and 0.4 m thick and several meters wide, with sharp subhorizontal or concave-upwards bounding surfaces often cutting underlying stratification at low angles. Both upward coarsening and upward fining layers occur, though the latter is more common. Beds usually show crude horizontal stratification (Gh, Sh) and trough or tabular cross-bedding (Gt–Gp, St–Sp). Small scours ∼ 0.9 m wide and ∼ 0.5 m deep filled with clast-supported, open-framework large pebbles to small cobbles (Go) are present as isolated features or within larger, 2–3 m wide and ∼ 1.5 m deep multistory channels. Matrix-supported, chaotic gravels (Gmm) occur almost exclusively

Table 2. Sediment sections analyzed in this study.

Site name	Dec. lat S/long W	Elevation (m a.s.l.)	Samples	Sediment interpretation
Cucao_T1_1	42.6585/74.0740	124	IR-50: Cucao_T1_1601	Turbulent and cohesive debris flows; unconfined sheet floods
Cucao_T1_2	42.6693/74.0905	79	IR-50: Cucao_T1_1602	Cohesive through turbulent debris flow deposits intercalated with traction deposits
Cucao_T1_3	42.6659/74.0777	112	IR-50: Cucao_T1_1603i_ii ^{14}C: Cucao_T1_1603A_A2; Cucao_T1_1803_I_II_III ^{10}Be: Cucao_T1_1601_85_115_145_175_205_235_265	Traction sediments within streamflows; deposition within a shallow braided distributary system
Cucao_T1_4	42.6681/74.0624	145	–	Main channel fill facies topped by glacial diamicton
Cucao_T1_7	42.6600/74.0752	120	^{14}C: Cucao_T1_1804_I_II_III	Peat deposit with wood over T1 outwash
Cucao_T2_5	42.6418/74.1034	10	IR-50: Cucao_T2 1604	Braided river system within a distal ice margin environment
Cucao_T2_6	42.6418/74.0892	26	IR-50: Cucao_T2 1606; ^{14}C: Cucao_T2-1801	Braided river system within a distal ice margin environment
Till site	42.7682/73.6195	151	–	Subglacial traction till
Las Lajas site*	42.7601/73.6316	151	–	Two glacial diamictons that sandwich an 80 cm peat layer

* García (2012).

within these fills. A few outsized, rounded, mud intraclasts lie within Sh and Gh facies.

Interpretation. Facies Gh, Gt–Gp, Sh and St–Sp are consistent with deposition from traction load within streamflows. Gmm facies are interpreted as debris flow deposits. Low-angle cutting is inferred to represent reactivation surfaces, reflecting a change in hydrological conditions between series of stacked traction carpets (i.e., third order surfaces in Miall, 2006). Wider multistory channel elements would represent entrenched channels active during low water stages. Altogether, deposits suggest an environment with a highly variable discharge that is prone to periodical flooding and channel instability. The whole sequence is here inferred to represent deposition within a shallow braided distributary system, with a minor contribution – or low preservation – of debris flows. The presence of mud intraclast can suggest incipient soil development within interfluves.

3.1.4 Site Cucao_T1_4

This consists of clast-supported, poorly to moderately sorted, trough cross-bedded gravel and sand (Gt, St) (Fig. 8). They are arranged in 0.5–1 m deep and > 3 m wide channel-shaped bodies. Towards the terrace edge, an inclined erosion surface cuts through all strata and is mantled by a chaotic to crudely bedded diamicton (Dmm).

Interpretation. Gt–St facies in Sect. 4 are related to a channel fill. Being deeper and wider than most channels described so far, these facies could relate to the main route feeding the distributary system alluded to before. The erosion surface towards the terrace edge is interpreted as an ice-contact surface capped by melt-out till (Dmm).

3.1.5 Sites Cucao_T2_5 and _6

Both sites occur within the edge of Cucao_T2 terrace, near the southern coast of Lake Cucao (Fig. 3a). Exposed sedi-

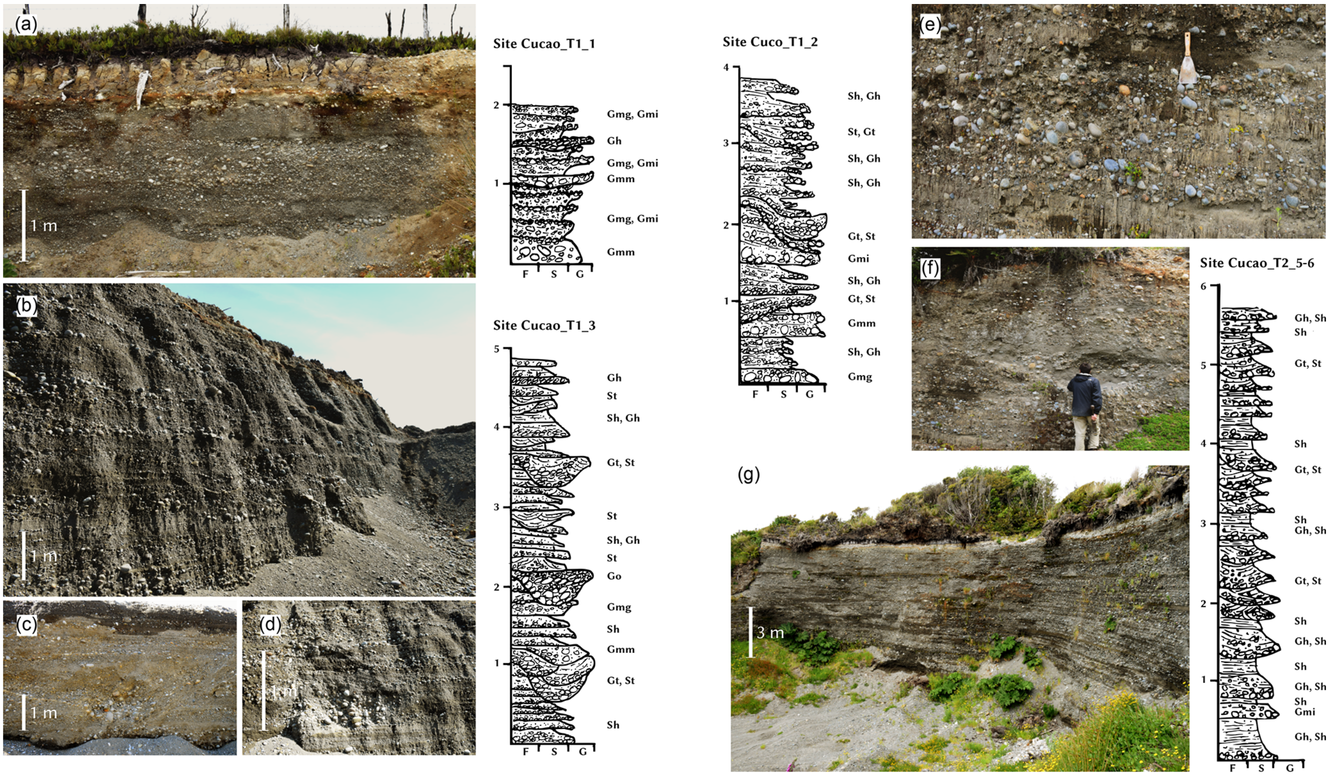

Figure 7. Generalized stratigraphic columns and sedimentary attributes for studied sites within Cucao terraces. **(a)** Cucao_T1_1, laterally extensive gravel beds, mostly bounded by flat subhorizontal surfaces but occasionally filling shallow channel-shaped depressions. **(b)** Cucao_T1_3 wide view. Note pebble to small cobble layer at the base of most lower bounding surfaces. **(c, d)** Detail of small channel bodies within Cucao_T1_3. Images come from two opposing walls about 3 m apart and capture the same channel element: a small open-framework gravel-filled (Go) channel in **(d)** grading downflow to a wider multistory filled channel in **(c)**. This is interpreted as an entrenched gully. **(e, f)** Cucao_T1_2: **(f)** shows a general view capturing one of the channel-shaped bodies referred to in the description, while **(e)** shows a detail of stacked gravel and sand layers that characterize this exposure. **(g)** Cucao_T2_5–6, general view of sediments in Site 6. Because of similarities between both sites (5 and 6) we only show a single column that represents Cucao_T2 sediments.

Figure 8. Site Cucao_T1_4 stratigraphic section. The image shows the two main sediment units described here. An outwash of gravel and sand (Gt, St) underlie melt-out till (Dmm); both units are separated by an ice-contact surface (white arrows), suggesting overriding ice.

ments are very similar, consisting of a series of laterally extensive, 0.1–0.5 m thick sand and pebble beds (Fig. 7g). Beds are mostly composed of a fining-upwards sequence grading from gravel (pebbles and small cobbles) to sand. Sediment is moderately to well sorted, rounded and mostly clast-supported. Channel-shaped bodies 3–5 m wide filled with lateral accretion deposits (St-Sp; Gt-Gp) are fairly common. Beds stack on each other with flat, sharp contacts or low-angle surfaces. There are occasional channel-shaped bodies, 1–2 m thick, filled with well-rounded, well-sorted cobbles.

Interpretation. Dilute stream flow processes within a braided river system. This is the classical sandur deposit within a distal ice-margin environment.

3.1.6 The Till site

This site is located on the southern side of the Chonchi-Queilén route to the east of central Isla de Chiloé (Figs. 1 and 3b). It is a sediment pit 1.5 km to the south after the detour to Las Lajas. The pit was excavated in the south-western side of a glacially molded hill. A hummocky terrain betters characterized the surroundings including kilometer-scale hills standing several tens of meters above surrounding elongated depressions (Fig. 3b). The excavation walls expose several meters of indurated gravel-rich glacial diamictons making up most of the morainic relief. Sediment structures including a fissility appearance, rudimentary bedding, and well-faceted and striated clasts can be best interpreted as subglacial traction till (Fig. 9) (Menzies, 2012; Menzies et al., 2006; Evans et al., 2006). Intercalated laminated fine sediment occurs within the section, but this is not widespread.

3.1.7 Las Lajas site

García (2012) first described this site, located by the Las Lajas detour on the Chonchi-Queilén route (Figs. 3b and 10). It includes two glacial diamictons that sandwich an 80 cm thick peat layer. Whereas the lower diamicton–peat surface contact shows a disconformity, higher up the peat grades conformably into glaciolacustrine sediments and sands overlain by the upper diamicton. The ^{14}C dates from the base and top of the peat yielded 28.2 ± 0.4 and 25.7 ± 0.4 cal kyr BP, respectively.

3.2 Chronology

3.2.1 Radiocarbon dating

We obtained a total of nine ^{14}C samples from Cucao_T1 and Cucao_T2 sites (Table 3). In Site Cucao_T1_3 two bulk ^{14}C samples from a single organic clast embedded in outwash sediment yielded 27.7 ± 0.2 and 31.5 ± 0.3 cal kyr BP, respectively. This clast was embedded in the sediment section nearby where we obtained the luminescence and ^{10}Be samples (see below). Also in Site Cucao_T1_3, we obtained three ^{14}C samples from wood pieces protruding out from the upper organic soil unit which ranged from 0.2 ± 0.07 to 7.5 ± 0.07 cal kyr BP. Site Cucao_T1_7 is a rather small (few tens of centimeters thick) sediment exposure on a road side where peat with wood outcrops on top of the Cucao_T1 terrace surface. The ^{14}C ages of three wood samples ranged from 44.7 ± 0.8 cal kyr BP to > 45.0 ^{14}C kyr BP.

In Cucao_T2, we obtained an age of 4.9 ± 0.07 cal kyr BP from the organic soil unit overlying the outwash sediment in Site Cucao_T2_6.

3.2.2 Luminescence dating

We obtained a total of six luminescence samples in both Cucao_T1 (sites Cucao_T1_1–_3) and Cucao_T2 (sites Cucao_T2_5 and _6). The results from high-resolution, low-level gamma spectrometry are summarized in Table 4. All samples were found to be in secular equilibrium. With regard to the equivalent dose determination, all samples showed indicators for incomplete bleaching prior to burial (right skewed dose distributions and high overdispersion values $> 50\,\%$). Because of that, all equivalent doses were calculated using the bootstrapped MAM (Galbraith et al., 1999; Cunningham and Wallinga, 2012). The age and dose-rate calculation was done using the software ADELE (Kulig, 2005). All ages were corrected for fading using the approach of Huntley and Lamothe (2001). All details are provided in Table 5.

At Site Cucao_T1_1 we obtained a sample (VLL-0287-L – Cucao-T1-1601) from a sand unit 100 cm below the surface and derived an age of 33.6 ± 3.5 ka. At Site Cucao_T1_2, a single sample (VLL-0288-L – Cucao-T1-1602) was obtained from a sand lens 255 cm below the surface and yielded an age of 51.9 ± 6.0 ka. At Site Cucao_T1_3, we obtained two samples (VLL-0289-L – Cucao-T1-1603 i and ii of which only i was dated) from the same sand unit at 350 cm below surface which yielded an age of 56.7 ± 5.3 ka. From the lower Cucao_T2 terrace, an age of 28.1 ± 2.6 ka was obtained at Site Cucao_T2_5 (VLL-0290-L – Cucao-T2-1604) and of 23.9 ± 2.0 ka at Site Cucao_T2_6 (VLL-0291-L – Cucao-T2-1606) at 1000 and 600 cm below surface, respectively.

3.2.3 The ^{10}Be depth profile dating

Figure 11a shows that the ^{10}Be concentration declines exponentially with depth, consistent with post-deposition isotope production in a stable outwash plain and no mixing of sediment. One exception occurred towards the base of the profile where some sediment mixing could have occurred as higher concentration of ^{10}Be were measured here. Our experiments show that the modeled ^{10}Be age seems somewhat sensitive to the position of the original outwash surface below the top organic soil unit (20 or 35 cm) and to a lesser degree to the sediment density (1σ range between 1.9 and 2.2 g cm^{-3}) (Fig. 11b iv). The modeling yielded low values for ^{10}Be inheritance (1σ range between 0 and 11 000 ^{10}Be atoms g^{-1}, as expected in glacial sediments; Fig. 11b iii). Based on these boundary conditions, the Cucao-T1 outwash age ranges between 45 and 100 ka (Fig. 11i, c), conditioned by the age of the organic soil formation. Accordingly, if the soil formed or was present as it is today for a short time (i.e., centennial to millennial timescales), the Cucao-T1 age would be closer to the younger limit (45 ka); alternatively, if the soil formed together with the outwash abandonment, the Cucao-T1 age would be closer to the older limit (100 ka). All other possible scenarios for organic soil formation would yield intermediate ages for Cucao-T1 outwash deposition (between 45 and 100 ka).

4 Discussion

4.1 The Cucao_T1 and Cucao_T2 ages

Based on the ^{14}C ages obtained for the peat unit capping the outwash sediment at Site Cucao_T1_7, we can determine that fluvioglacial activity linked to Cucao_T1 ended by 44.7 ± 0.8 to > 48.3 cal kyr BP. In other words, the outwash minimum age is the ^{14}C saturation age. This minimum age based on radiocarbon agrees with the depositional lumines-

Figure 9. The Till site stratigraphic section. **(a)** Geomorphic context of the section (red box) on the distal side of a drumlinoid landform (view to the south from the Las Lajas site). Ice flowed from the left (east). **(b)** Detail of the subglacial till making up most of the sediment section.

cence ages of 51.9 ± 6 and 56.7 ± 5.3 ka (Cucao-T1-1602 and Cucao-T1-1603 i) which occur near the younger ^{10}Be model age limit. The two luminescence ages are in good agreement within error, which strengthens the reliability of the ages and the chosen luminescence dating approach. The IR-50 age obtained for Cucao-T1-1601 yielding 33.6 ± 3.5 ka is not in agreement with the previous reasoning. Because all methodological steps involved to obtain that age are in agreement with the quality criteria applied for all luminescence samples in this study, the age must be regarded as a reliable luminescence age from a methodological point of view. However, there are a number of environmental uncertainties which may explain the age underestimation of that sample: this sample was taken close to the sediment surface at approximately 1 m depth. Bioturbation (plant roots, digging activities of animals) may be relevant when a sample is taken close to the surface. Although no indication of such processes was detectable in the field, it cannot be ruled out that grains from the soil surface may have been relocated to deeper layers by bioturbation processes. This would result in a shift of the equivalent dose distribution to a lower dose which corresponds to a younger age. A second scenario might be that the sediment of the Cucao-T1-1601 site was locally redeposited in an event not related to the primary terrace formation. As there is no age control from radiocarbon at that site, this may have to be considered as a valid option and is further discussed in the context of the formation of the Cucao_T2 terrace level. Considering the ^{14}C ages from Site Cucao_T1_7, it is clear that the Cucao-T1-1601 IR-50 sample must be regarded as a minimum age for the Cucao_T1 terrace formation.

In order to determine the age of the Cucao_T1 terrace, we have considered two different scenarios ("a" and "b") that best reconcile the ^{14}C, IR-50 and ^{10}Be chronologies obtained for this outwash. For both scenarios we have calculated the

Table 3. The ^{14}C dates from this study.

Site name	Sample ID	Lab code	Material	^{14}C age (year BP)	Error 1σ (year BP)	2σ range calendar age (year BP)	Median probability (cal year BP)	Interpretation
Cucao_T1_3	CUCAOT1-1603A2	Beta 456717	Bulk sediment	27 820	120	31 226–31792	31 482	Organic clast embedded in outwash sediment; likely contaminated with young carbon
Cucao_T1_3	CUCAOT1-1603A	D-AMS 020993	Bulk sediment	23 687	127	27 526–27 968	27 747	Organic clast embedded in outwash sediment; likely contaminated with young carbon
Cucao_T1_3	CUCAOT1-1803_I	D-AMS 031033	Wood	772	25	649–722	672	Minimum age of soil on top of Cucao_T1 outwash
Cucao_T1_3	CUCAOT1-1803_II	D-AMS 031034	Wood	6591	40	7415–7565	7461	Minimum age of soil on top of Cucao_T1 outwash
Cucao_T1_3	CUCAOT1-1803_III	D-AMS 031035	Wood	188	25	135–283	182	Minimum age of soil on top of Cucao_T1 outwash
Cucao_T1_7	CUCAOT1-1804_I	D-AMS 031036	Wood	> 45 000		> 47 030–49 603	> 48 312	Minimum age for Cucao_T1 outwash deposition/abandonment
Cucao_T1_7	CUCAOT1-1804_II	D-AMS 031037	Wood	41 781	496	44 245–46 012	45127	Minimum age for Cucao_T1 outwash deposition/abandonment
Cucao_T1_7	CUCAOT1-1804_III	D-AMS 031038	Wood	41 273	411	43 905–45 481	44 713	Minimum age for Cucao_T1 outwash deposition/abandonment
Cucao_T2_6	CUCAOT2-1801	D-AMS 031053	Bulk sediment	4391	31	4843–4979	4919	Minimum age of soil on top of Cucao_T2 outwash

Table 4. Results from radionuclide analysis and dose-rate calculation.

Sample lab code	Sample field code	^{238}U ($Bq\,kg^{-1}$)	^{232}Th ($Bq\,kg^{-1}$)	^{40}K ($Bq\,kg^{-1}$)	Overall dose-rate Fs ($Gy\,kyr^{-1}$)[a]
VLL-0287-G	Cucao_T1 1601	14.7 ± 1.1	21.5 ± 1.8	314.0 ± 18.9	2.41 ± 0.17
VLL-0288-G	Cucao_T1 1602	14.8 ± 1.2	21.8 ± 1.2	342.0 ± 20.5	2.45 ± 0.17
VLL-0289-G	Cucao_T1 1603i/ii[b]	15.7 ± 1.1	21.5 ± 1.2	351.0 ± 21.1	2.47 ± 0.18
VLL-0290-G	Cucao_T2 1604	15.1 ± 1.2	20.3 ± 1.1	341.0 ± 20.5	2.49 ± 0.17
VLL-0291-G	Cucao_T2 1606	13.9 ± 1.0	20.0 ± 1.3	333.0 ± 20.0	2.33 ± 0.16

[a] Cosmic dose rate determined according to Prescott and Stephan (1982) and Prescott and Hutton (1994), taking the geographical position of the sampling spot (longitude, latitude, and altitude), the depth below surface and the average density of the sediment overburden into account. An uncertainty of 10 % was assigned to the calculated cosmic dose rate. External and internal dose rate calculated using the conversion factors of Adamiec and Aitken (1998) and the β-attenuation factors of Mejdahl (1979), including an α-attenuation factor of 0.08 ± 0.01, an internal K content of 12.5 ± 0.5 % (Huntley and Baril, 1997) and an estimated average water content of 15 ± 5 % throughout burial time. Values covering almost dry to almost saturated conditions. Error was propagated to the overall dose-rate calculation. [b] Only sample Cucao_T1 1603i was measured because both samples were taken in direct vicinity from the same sediment layer.

probability distributions in Bayesian terms. In both scenarios, all ages obtained for the Cucao_T1 outwash deposition are older than the ^{14}C ages from Site Cucao_T1_7. The scenario "a" considers the ^{10}Be age as a minimum (i.e., corresponding to a short-lived organic soil development) and the luminescence ages as the depositional age of the outwash sediment. The scenario "b" considers the wide ^{10}Be age range (i.e., corresponding to an organic soil development at any time since the Cucao_T1 outwash abandonment), together with the luminescence ages, as the deposi-

Table 5. Summary of IR-50 data.

Sample lab code	Sample field code	Fs SG (n)[1]	σb^2 (%)[2]	Fs IR-50 D_e (Gy)[3]	Dose rate Fs (Gy kyr^{-1})[4]	Fs IR-50 age (ka) faded[5]	Fs IR-50 age (ka) fading corr.[6]
VLL-0287-L	Cucao_T1 1601	83	67 ± 6	50.5 ± 3.5	2.41 ± 0.17	20.9 ± 2.1	33.6 ± 3.5
VLL-0288-L	Cucao_T1 1602	78	51 ± 5	78.3 ± 4.9	2.45 ± 0.17	31.9 ± 3.0	51.9 ± 6.0
VLL-0289-L	Cucao_T1 1603i/ii	83	50 ± 4	85.9 ± 3.8	2.47 ± 0.18	34.8 ± 2.9	56.7 ± 5.3
VLL-0290-L	Cucao_T2 1604	82	73 ± 6	43.9 ± 2.5	2.49 ± 0.17	17.6 ± 1.5	28.1 ± 2.6
VLL-0291-L	Cucao_T2 1606	197	71 ± 4	34.9 ± 1.7	2.33 ± 0.16	15.0 ± 1.3	23.9 ± 2.0

[1] Number of single grains (SGs) passing all rejection criteria. [2] Overdispersion calculated using the CAM (Galbraith et al., 1999). [3] Equivalent dose (D_e) calculated using the bootstrapped MAM-3 (Galbraith et al., 1999; Cunningham and Wallinga, 2012) for all samples. [4] Overall dose rate. [5] Ages calculated using the software ADELE (Kulig, 2005). [6] Fs-based ages corrected for fading according to the method of Huntley and Lamothe (2001) using the R luminescence package (Kreutzer et al., 2012)

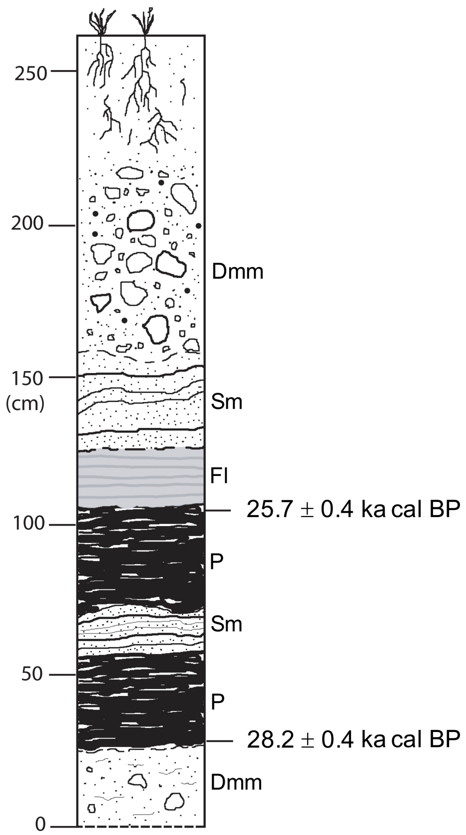

Figure 10. Stratigraphic column of the Las Lajas site. Two diamictons (Dmm) sandwich a peat soil (P) and inorganic glacial finer sediments (Sm, Fl). The upper peat layer dates a glacial advance on the site as evidenced by the upward coarsening of the sediments. Modified from García (2012).

tional ages of the outwash. For scenario "a", the resulting age is 57.8 ± 4.7 ka, and for scenario "b" the resulting age is $55.5^{+29}_{-6.5}$ ka.

The data show that both scenarios yield statistically the same most likely age but differ in precision (Figs. 12a, b). The overlap between luminescence ages and ^{10}Be fitting models (youngest outwash ages in Fig. 11c) suggest that most of the organic soil unit has been in its present form and thickness for a limited time span. The older ^{14}C ages (Site 7) also suggest that scenario "a" is most probable, which implies that the shielding of cosmogenic radiation by the organic unit has not been significant since the Cucao_T1 outwash deposition (MIS 3). A question may arise regarding the range of ^{14}C ages we obtained from the organic sediment capping the Cucaco_T1 outwash in two different sites, including MIS 3 (Cucao_T1_Site 7) and Holocene (Site 3) dates. Taking the data at face value, and in the light of ^{10}Be and IR-50 data, it is unlikely that an organic soil as thick (and dense) as in Site Cucao_T1_7 has been present since $\geq 48.3 \pm 1.3$ cal kyr BP. The implication is that the top organic soil was not preserved throughout the MIS 3 and MIS 2 until the present. In fact, we do not find MIS 3 but only Holocene ^{14}C ages in Site 3, supporting a young organic cover (Table 3). This points to an unsteady organic layer cover (e.g., mostly absent or of limited thickness) after the Cucao_T1 deposition. Therefore, our preferred modeled age, when IR-50, ^{10}Be and ^{14}C data match, is 57.8 ± 4.7 ka for the Cucao_T1 outwash deposition. This age identifies the early Llanquihue Glaciation in Chiloé (i.e., the lLGM).

The two luminescence IR-50 ages obtained from samples related to the Cucao_T2 terrace yielded ages in good agreement within error. The calculated mean age of 26.0 ± 2.9 ka obtained for the Cucao_T2 terrace corroborates that this terrace represents a younger, inboard glacial extent. The increased geomorphic activity in the area during the formation of the Cucao_T2 terrace level likely included enhanced incision into the Cucao_T1 terrace level and increased remobilization of sediments on the Cucao_T1 terrace. This initial phase of climate deterioration potentially resulted in the remobilization of material on the Cucao_T1 terrace level, followed by incision and subsequent build-up of the Cucao_T2 terrace on a lower level. The initial phase of remobilization and incision may be represented by the IR-50 age of sample Cucao-T1-1601, which was taken close to the present Cucao_T1 terrace surface (and present-day Cucao_T1–Cucao_T2 scarp) and yielded an age of $33.6 \pm$

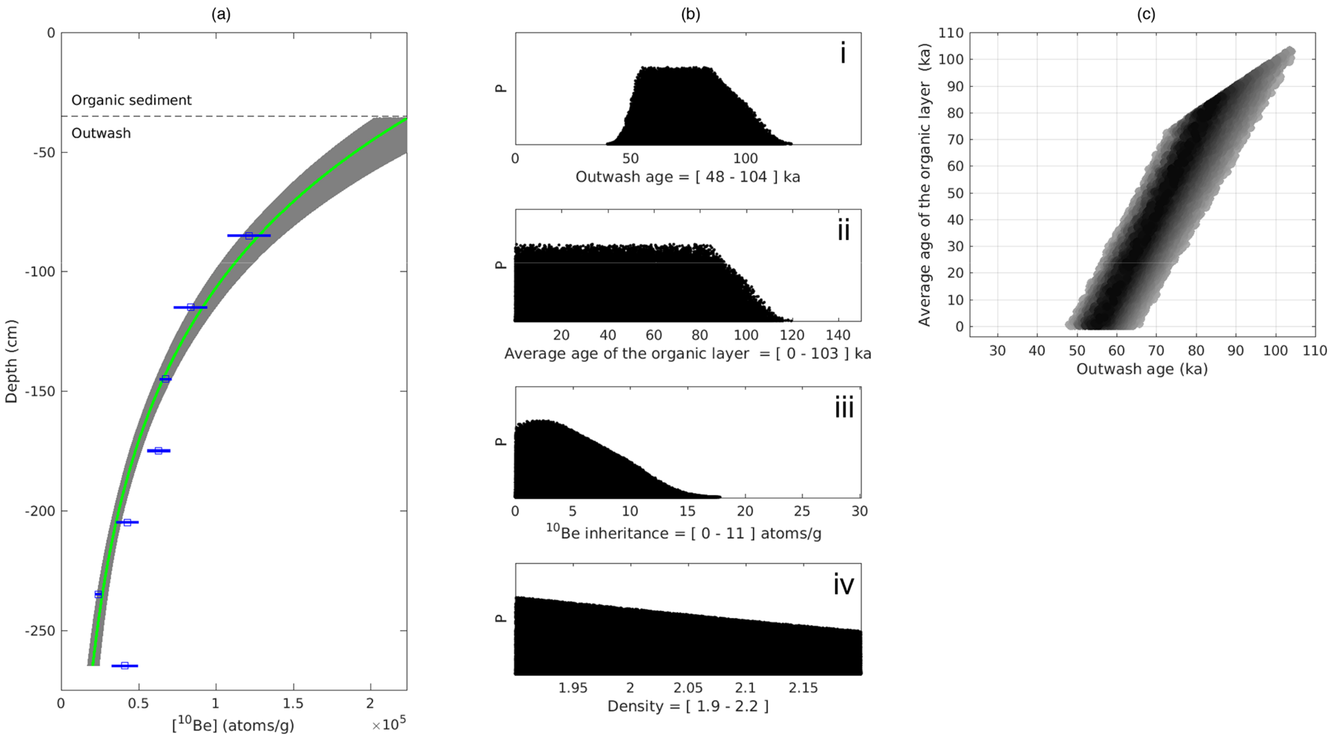

Figure 11. Site Cucao_T1_3 ^{10}Be depth profile results. **(a)** Depth profile with cosmogenic samples and vertical distribution of the outwash and the overlaying organic sediments: Be-10 data in blue, best fit of the Be-10 accumulation models in green and 1σ fitting models in grey. **(b)** Probability density distributions of the parameters considered in the models shown in **(a)**. **(c)** The 1σ results of the fitting ages for the deposition of the outwash and the organic layer in different shades of grey based on their probabilities.

3.5 ka, which is only slightly older than the luminescence ages obtained from the Cucao_T2 terrace sediments.

4.2 The local LGM ice limit

Based on the mapping, sediment preservation and age of the landforms, each Cucao outwash plain Cucao_T1 and Cucao_T2 could be linked to expanded ice marginal positions within the last glacial period (Fig. 3a). García (2012) mapped a double Llanquihue age ice-contact slope widespread on the eastern slope of the Cordillera de la Costa that was linked to a double system of outwash terraces on the western mountainside, such as Cucao_T1 and Cucao_T2. In this scenario, the PIS buttressed against the Cordillera de la Costa (here up to ∼ 500 m a.s.l.), which acted as a barrier for the Golfo de Corcovado Ice Lobe's expansion towards the open Pacific Ocean. The mountain range is punctuated by meltwater channels that grade to the outwash plains to the west. Opposite, the Huillinco–Cucao basin (Fig. 1) allowed a narrow tongue of ice to flow through the coastal mountains. Here, the exact ice marginal positions attained during the Cucao_T1 and Cucao_T2 outwash depositions are not obvious. It is possible that part of the scarp separating Cucao_T1 from Cucao_T2 can be regarded as a reworked ice contact slope (Fig. 3a). Several sources of evidence could support this scenario indicating ice proximity: (1) a glacial diamicton outcropping at the proximal edge of T1 in Site Cucao_T1_4, (2) the Cucao_T1 terrace high dipping angle of ∼ 2 % and (3) the ice proximal facies (e.g., debris flows) intercalated with better sorted outwash outcroppings in the studied sediment sections within Cucao_T1 terrace (Figs. 7 and 8). On the other hand, the lower Cucao_T2 deposition can be linked to an inboard ice margin at the proximal edge of this outwash plain (Fig. 3a). The morainic relief confining the Quilque lake can be interpreted as a hummocky moraine formed as part of a dead-ice topography related to the deglacial phase after the terminal position against the ice contact slope of Cucao_T1 terrace or, alternatively, as a push complex during active ice recession (Evans and Twigg, 2002). Sediment slumps from the T1 ice-contact slope during a paraglacial phase are also a possibility during deglaciation.

The inferred ice limits imply that ice reached more or less similar positions, first at 57.8±4.7 ka (Cucao_T1 terrace) and then 26.0±2.9 ka (Cucao_T2 terrace), with ice covering most of the island to the Cordillera de la Costa or slightly beyond this point along the Huillinco–Cucao basin.

An extended ice position to the Cordillera de la Costa at 26.0 ± 2.9 ka may be in conflict with a previous interpretation of the Las Lajas site (García, 2012). Here, the upper diamicton was interpreted as being deposited at the ice margin by 25.7 ± 0.4 cal kyr BP. This ice advance was pre-

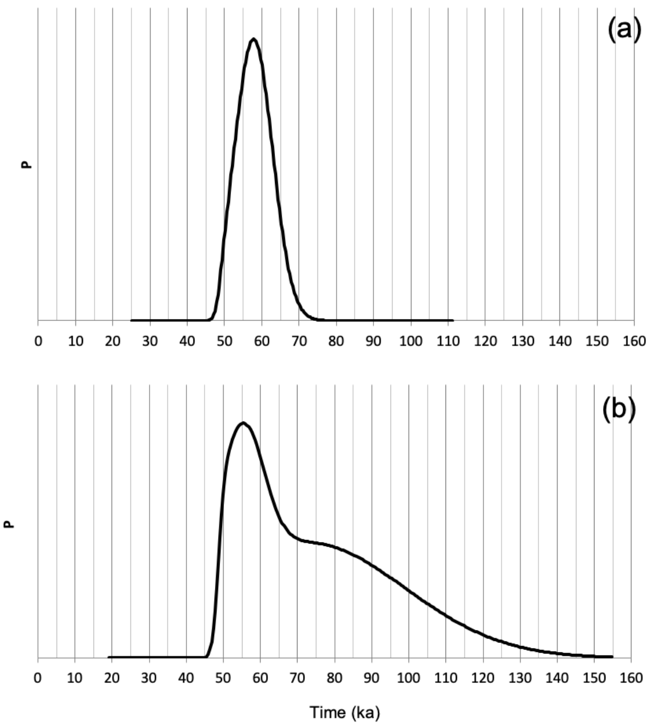

Figure 12. Scenarios "a" and "b" probability distributions of ^{10}Be, ^{14}C and IR-50 data. Both scenarios coincide in the best Bayesian age but differ in terms of precision. In **(a)**, scenario "a" considers that the organic soil as it is today has been present in the site for only a short time (centuries to millennia). The kernel density estimation of the age of the outwash has been calculated as $p(\mathrm{TOSL}|t) \cdot p(T^{14}\mathrm{C} < t) \cdot p(T^{10}\mathrm{Be} < t)$, where $p(\mathrm{TOSL}|t)$ is the sum of the probabilities corresponding to the IR-50 ages, and $p(t > T^{14}\mathrm{C})$ and $p(t > T^{10}\mathrm{Be})$ are the cumulative sum of the probabilities corresponding to the minimum ^{14}C and ^{10}Be ages, respectively. In this case, we only considered the probabilities of the minimum ^{10}Be age corresponding to an age of 0 for the organic soil ($y = 0$ in Fig. 11c; 56.5 ± 8.5 ^{10}Be ka). In **(b)**, scenario "b" considers that the organic soil was formed anytime between outwash deposition and today. The kernel density estimation of the age of the outwash has been calculated as $p(\mathrm{TOSL}|t) \cdot p(T^{14}\mathrm{C} < t) \cdot p(T^{10}\mathrm{Be}|t)$, where $p(T^{10}\mathrm{Be}|t)$ corresponds to the ^{10}Be age obtained in Fig. 11 (72.5 ± 26.5 ^{10}Be ka). Note that here only the ^{14}C ages are considered as minimum ages.

ceded by ice-free conditions interpreted from the peat layer between 28.2 ± 0.4 and 25.7 ± 0.4 cal kyr BP when ice should have resided up-glacier from the Las Lajas site (i.e., reduced ice standing to the east of Isla de Chiloé). Then, the Cucao_T2 outwash deposition can only have occurred between 26 cal kyr BP and 23.1 ka, if the age control from both sites (the IR-50 and ^{14}C ages) is considered using 1σ range. Several lines of evidence suggest that the ice expanded westward to the Cordillera de la Costa by 25.7 ± 0.4 cal kyr BP to deposit the Cucao_T2 terrace. First, it seems difficult to reconcile an ice margin at eastern Chiloé building the western Cucao_T2 outwash plain ≥ 20 km away. No topographic match seems plausible. Second, ice must have overridden Las Lajas when it expanded westward to the Cordillera de la Costa. Third, nearby sediment and the geomorphic record denote that subglacial morphogenesis originated by overriding ice. The Till site, near Las Lajas, exposes well-preserved subglacial traction till (Figs. 3b and 9). Nearby exposures along the Chonchi-Queilén route in eastern Chiloé (Fig. 1) commonly denote outwash sediments being capped with erosional surfaces by glacial diamictons, showing overriding ice during ice expansion (García, 2012). Fluting and drumlinoid landforms cored by till then can suggest that rapid-flowing ice expanded all the way to the Cordillera de la Costa in central Chiloé during the Llanquihue Glaciation. In the light of the new morphostratigraphic observations and geochronologic data, we thus suggest the Golfo de Corcovado Ice Lobe expanded towards the Cordillera de la Costa to deposit the Cucao_T2 outwash by 25.7 ± 0.4 cal kyr BP, thus overriding central Chiloé during the global LGM. Just north in the CLD, glaciers reached their most extensive positions by about 26 ka also, as suggested by Denton et al. (1999b). Antarctic ice cores show stadial conditions between ~ 28 and 24 ka peaking at ~ 26 ka that seem to be mirrored by SST offshore Chiloé (WAIS Divide Project Members, 2015; Lamy et al., 2004).

4.3 The pre-LGM Llanquihue Glaciation

Precise geochronologic records of glacial activity during the early to middle MIS 3 are rare in the CLD. Moreover, no records of MIS 4 glaciation exist on land. On the other hand, available radiocarbon data have precisely constrained glacial fluctuations during the LGM (Mercer, 1972, 1976; Porter, 1981; Denton et al., 1999b). Therefore, only a limited understanding of glacial fluctuations during pre-LGM time exists today. Available dating for the early Llanquihue drift is mostly equivocal because either the stratigraphic context is not well understood or dates reported are not sufficiently precise ages for dating putative pre-LGM glacial advance(s) (Porter, 1981; Denton et al., 1999b). For instance, the "crossroad stratigraphic site" west of Lago Llanquihue (Denton et al., 1999b; Porter, 1981; Mercer, 1976) includes deformed weathered pyroclastic organic sediments including wood and charcoal sandwiched by pre-Llanquihue (below) and Llanquihue (above) till. Minimum ages ranging from $> 39.6 \pm 0.7$ to 57.8 ^{14}C kyr BP obtained from the nonglacial sediments do not closely constrain the age of glacial advances represented by the till units. Nearby the "crossroad site", a reworked organic clast into Llanquihue outwash yielded > 44.4 ^{14}C kyr BP (Denton et al., 1999b; Mercer, 1976). Similarly, the bottom sediments of the Puerto Octay and the Bahía Frutillar Bajo sections show Llanquihue drifts deposited before 41.3 ± 0.7 and 45.4 ± 2.0 cal kyr BP, respectively (Denton et al., 1999b). To the north, an early Llanquihue glacial advance > 56.0 ^{14}C kyr BP occurred in Lago Ranco, as suggested by ^{14}C dating of a log in peat that occurs stratigraphically linked to interpreted till sediments (Mercer, 1976). Porter (1981) reported a wood age of 45.7 ± 1.0 cal kyr BP from an interdrift in situ stump in Punta Penas. In Punta Pelluco, wood in a similar stratigraphic context yielded > 40.0 ^{14}C kyr BP (Porter, 1981). All these records suggest Llanquihue glacial expansions during pre-LGM times, but it remains unclear the precise dates of the events. In contrast, the Taiquemó record in Chiloé provides unique details regarding the Llanquihue Glaciation (Heusser et al., 1999). The Taiquemó mire is located inboard from the outermost early Llanquihue moraine. The basal minimum limiting age of Taiquemó of > 49.9 ^{14}C kyr BP suggests this early Llanquihue landform was deposited by this time. Dating of the Taiquemó basal sediments beyond the ^{14}C technique suggest that an early glacial maximum occurred before > 50.0 ^{14}C kyr BP when a pollen peak in Gramineae overlaps with a jump in magnetic susceptibility and a minimum in loss on ignition (Heusser et al., 1999).

Although dating control is limited (i.e., available dates occur at the limit and beyond the ^{14}C possibilities, > 50 ^{14}C kyr BP), evidence suggests that interstadial periods dominated by tree species adapted to cool and humid conditions occurred during the MIS 3 (Heusser et al., 1999; Villagrán et al., 2004, 2019). A reasonable scenario is that these ecosystems spread during the Antarctic millennial-scale interstadial periods that punctuated the MIS 3, for instance, at ~ 60 ka (Antarctic Isotope Maximum, AIM, 17) and/or at ~ 54 ka (AIM 14) (WAIS Divide Project Members, 2015). Near the base of the Taiquemó record a peak in warm temperatures was interpreted from a broad peak in loss of ignition and a Gramineae minimum within subantarctic evergreen forest conditions (Heusser et al., 1999) which could have been accompanied by the expansion of conifer forest to the low lands of Chiloé (Villagrán et al., 2004). Therefore, we suggest that the Cucao_T1 glacial advance was triggered by a millennial-scale climate deterioration that followed an interstadial peak (e.g., the AIM 17). This PIS glacial expansion by 57.8 ± 4.7 ka into the outermost ice-contact slope in Chiloé coincided with a decreasing SST trend that lasted several millennia and culminated offshore Chiloé ~ 4–5 °C below the early Holocene value (Kaiser et al., 2005). The Antarctic temperature stack (Parrenin et al., 2013), which mimics the WAIS divide ice core δ^{18}O record (WAIS Divide Project Members, 2015), records a stadial period culminating at ~ 57 ka when atmospheric temperatures reached 6–7°C below those of the present day. Presumably, during this Antarctic stadial the westerly wind belt shifted north, associated with extended sea ice and the expansion of Antarctic and subantarctic atmospheric and oceanic conditions into lower latitudes (Lamy et al., 2015). The expanded westerly wind belt linked to an enhanced northern ACC boundary brought depressed SST and air temperatures and high precipitation to the latitude of Chiloé, thus forcing a PIS advance here by the early MIS 3.

4.4 MIS 3 paleoclimate

This section discusses the MIS 3 paleoclimate in the context of glacial fluctuations of the PIS and other Southern Hemisphere mountain glaciers. Globally, the MIS 3 is a long-term interstadial phase when ice sheets were reduced, sea level reached intermediate stands, and temperatures were mild (Shackleton et al., 2000; Ivy-Ochs et al., 2008; Parducci et al., 2012; Dalton et al., 2019). The peak of the MIS 3 warmth occurred at ~ 60 ka, the first in a sequence of prominent millennial-scale climate changes (e.g., Dansgaard–Oeschger and AIM events) recorded at both polar hemispheres during this period (Jouzel et al., 2007). Nonetheless, the climate variability in the MIS 3 is conspicuous not only in the polar records but elsewhere (Mayr et al., 2019).

After MIS 4, climate in New Zealand and southern Chile was rather mild. In New Zealand, the Aurora Interstadial lasted until about 43 ka, but it was interrupted by stadial conditions, first at 49–47 ka and then at 42–38 ka, when Southern Alps glaciers readvanced (Williams et al., 2015; Kelley et al., 2014; Doughty et al., 2015). Between 37–31 ka, a new phase of mild interstadial temperatures was recorded in New Zealand, after which temperatures declined into the MIS 2 global LGM phase (Putnam et al., 2013; William et al., 2015; Darvill et al., 2016). In southern Chile, Heusser et al. (1999) recorded interstadial temperatures and humid conditions until about > 50 ka when temperatures started a cooling trend that extended until the global LGM. Ice-free areas later overridden by glacier or ice proximal outwash deposits occurred between about 43–33 ka, thus indicating mid-to-late MIS 3 ice fluctuations (Denton et al., 1999b). Similarly, high and low frequencies of Gramineae punctuated the MIS 3, thus being indicative of millennial-scale temperature changes throughout the MIS 3 (Heusser et al., 1999). Distal to the PIS front, interstadial conifer forests are known to have grown in areas later overridden by ice, as recorded by peat layers containing tree trunks on sea-cliff exposures and also by tree stumps standing in life position at present-day intertidal sea shores (Roig et al., 2001; Villagrán et al., 2004, 2019). Along the eastern coastal cliffs of Chiloé multiple peat layers are intercalated with finely laminated glacial sediments assumed to be early MIS 3 in age, suggesting short-term environmental variability (Villagrán et al., 2004, 2019). Moreover, these glacial-sourced sediments suggest that the PIS front, although located up ice from Isla de Chiloé, was not much further to the east during the MIS 3. A similar conclusion can be derived from the alternating peat and lake facies that punctuate the Taiquemó record between about > 50–40 ka (Heusser et al., 1999). Altogether, the available records show that not only did mild atmospheric conditions punctuate the MIS 3, but rather this was a variable climatic period both in the middle and high latitudes. In fact, Lovejoy and Lambert (2019) noted that the highest climate variability occurs during the middle of a glacial cycle (e.g., MIS 3), the opposite being true at the ends (i.e., the LGM) when a rather stable climate predominates. These authors studied the European Project for Ice Coring in Antarctica (EPICA) dust flux frequency record, which is known to be linked to Patagonian climate and glacial fluctuations, among others factors (Lambert et al., 2008), and which therefore provides a direct link between southern middle and high latitudes (Sugden et al., 2009; Kaiser and Lamy, 2010). During mid-glacial climates, transition times and amplitudes of Antarctic dust flux variability occurred at centennial to millennial timescales implying that large PIS ice lobe extent variability occurred also at these time frequencies in response to climate change forcing (see Lovejoy and Lambert, 2019). Therefore, an extensive northern PIS glacial expansion at 57.8 ± 4.7 ka in Chiloé, together with that recorded by the PIS in Torres del Paine, Última Esperanza and Bahía Inútil by ~ 48 ka (Sagredo et al., 2011; Darvill et al., 2015; García et al., 2018) and in New Zealand at ~ 49–47 and 42–38 ka (Kelley et al., 2014; William et al., 2015), suggests a distinct return to glacial conditions in the southern midlatitudes within the MIS 3.

5 Conclusions

Full glacial advances by the Golfo de Corcovado Ice Lobe of the northwest Patagonian Ice Sheet (PIS) occurred by 57.8 ± 4.7 and 26.0 ± 2.9 ka on the Isla de Chiloé and respectively deposited the outer Cucao_T1 and Cucao_T2 outwash plains enclosing the Lago Cucao basin. The latter ice advance could be tied to a previously dated advance to 25.7 ± 0.3 cal kyr BP that better constrains its age (García, 2012). The extent of the now inexistent Golfo de Corcovado Ice Lobe was > 100 km during both glacial expansions, which did not reach the Pacific Ocean during the Llanquihue Glaciation. The early Llanquihue ice expansion during the MIS 3 occurred intercalated with interstadial periods, which denotes the sensitive response of the Patagonian glaciers to centennial- to millennial-scale climate fluctuations. Southern midlatitude glacial advances interrupting the apparent mild climate that characterized the early MIS 3 imply that this time period was rather characterized by large and rapid climate oscillations not only at the poles but elsewhere.

Code availability. All details with regard to the codes used in this study are available from the references provided in the text. The primary sources also contain information about the availability of the code.

Data availability. All relevant data have been included in the published version of this paper. Otherwise, please submit any requests to jgarciab@uc.cl.

Author contributions. JLG conceived the project. JLG and RMV collected the ^{10}Be, IR-50 and ^{14}C samples and performed the sediment description in the field. ASH and SAB performed the ^{10}Be laboratory and AMS work. JLG performed the ^{14}C laboratory work. CL performed the IR-50 laboratory work and luminescence age calculation. AR and ASH performed the ^{10}Be and Bayesian modeling. All authors contributed to interpret the data and write the paper.

Competing interests. The authors declare that they have no conflict of interest.

Acknowledgements. The authors acknowledge the support from the Chile FONDECYT. We thank the valuable comments of two reviewers that improved the quality of this paper.

Financial support. This research has been supported by the Chile FONDECYT (grant no. 1161110).

The article processing charge was funded by the Quaternary scientific community, as represented by the host institution of EGQSJ, the German Quaternary Association (DEUQUA).

Review statement. This paper was edited by Becky Briant and reviewed by Gordon Bromley and one anonymous referee.

References

Adamiec, G. and Aitken, M.: Dose-rate conversion factors: update, Ancient TL, 16, 37–50, 1998.

Andersen, B. G., Denton, G. H., and Lowell, T. V.: Glacial geomorphologic maps of Llanquihue drift in the area of the southern Lake District, Chile, Geogr. Ann. A, 81, 155–166, https://doi.org/10.1111/1468-0459.00056, 1999.

Auclair, M., Lamothe, M., and Huot, S.: Measurement of anomalous fading for feldspar IRSL using SAR, Radiat. Meas., 37, 487–492, https://doi.org/10.1016/S1350-4487(03)00018-0, 2003.

Balco, G., Stone, J. O., Lifton, N. A., and Dunai, T. J.: A complete and easily accessible means of calculating surface exposure ages or erosion rates from ^{10}Be and ^{26}Al measurements, Quat. Geochronol., 3, 174–195, https://doi.org/10.1016/j.quageo.2007.12.001, 2008.

Barcaza, G., Nussbaumer, S. U., Tapia, G., Valdés, J., García, J. L., Videla, Y., Albornoz, A., and Arias, V.: Glacier inventory and recent glacier variations in the Andes of Chile, South America, Ann. Glaciol., 58, 166–180, https://doi.org/10.1017/aog.2017.28, 2017.

Bentley, M. J.: Relative and radiocarbon chronology of two former glaciers in the Chilean Lake District, J. Quaternary Sci., 12, 25–33, https://doi.org/10.1002/(SICI)1099-1417(199701/02)12:1<25::AID-JQS289>3.0.CO;2-A, 1997.

Bierman, P. R., Caffee, M. W., Davies, P. D., Marsella, K., Pavich, M., Colgan, P., Mickelson, D., and Larsen, J.: Rates and Timing of Earth Surface Processes From In Situ-Produced Cosmogenic Be-10, Rev. Mineral. Geochem., 50, 147–205, https://doi.org/10.2138/rmg.2002.50.4, 2002.

Blomdin, R., Murray, A., Thomsen, K., Buylaert, J.-P., Sohbati, R., Jansson, K., and Alexanderson, H.: Timing of the deglaciation in southern Patagonia: Testing the applicability of K-Feldspar IRSL, Quat. Geochronol., 10, 264–272, https://doi.org/10.1016/j.quageo.2012.02.019, 2012.

Bøtter-Jensen, L., Bulur, E., Duller, G., and Murray, A.: Advances in luminescence instrument systems, Radiat. Meas., 32, 523–528, https://doi.org/10.1016/S1350-4487(00)00039-1, 2000.

Bøtter-Jensen, L., Andersen, C., Duller, G., and Murray, A.: Developments in radiation, stimulation and observation facilities in luminescence measurements, Radiat. Meas., 37, 535–541, https://doi.org/10.1016/S1350-4487(03)00020-9, 2003.

Cunningham, A. and Wallinga, J.: Realizing the potential of fluvial archives using robust OSL chronologies, Quat. Geochronol., 12, 98–106, https://doi.org/10.1016/j.quageo.2012.05.007, 2012.

Dalton, A. S., Finkelstein, S. A., Forman, S. L., Barnett, P. J., Pico, T., and Mitrovica, J. X.: Was the Laurentide Ice Sheet significantly reduced during Marine Isotope Stage 3? Geology, 47, 111–114, https://doi.org/10.1130/G45335.1, 2019.

Darvill, C. M., Bentley, M. J., Stokes, C. R., Hein, A. S., and Rodés, A.: Extensive MIS 3 glaciation in southernmost Patagonia revealed by cosmogenic nuclide dating of outwash sediments, Earth Planet. Sc. Lett., 429, 157–169, https://doi.org/10.1016/j.epsl.2015.07.030, 2015.

Darvill, C. M., Bentley, M. J., Stokes, C. R., and Shulmeister, J.: The timing and cause of glacial advances in the southern mid-latitudes during the last glacial cycle based on a synthesis of exposure ages from Patagonia and New Zealand, Quaternary Sci. Rev., 149, 200–214, https://doi.org/10.1016/j.quascirev.2016.07.024, 2016.

Davies, B. J., Darvill, C. M., Lovell, H., Bendle, J. M., Dowdeswell, J. A., Fabel, D., García, J.-L., Geiger, A., Glasser, N. F., Gheorghiu, D. M., Harrison, S., Hein, A. S., Kaplan, M. R., Martin, J. R. V., Mendelova. M., Palmer, A., Pelto, M., Rodés, A., Sagredo, E. A., Smedley, R., Smellie, J. L., and Thorndycraft, V. R.: The evolution of the Patagonian Ice Sheet from 35 ka to the present day (PATICE), Earth-Sci. Rev., 204, 103152, https://doi.org/10.1016/j.earscirev.2020.103152, 2020.

Denton, G. H., Heusser, C. J., Lowell, T. V., Moreno, P. I., Andersen, B. G., Heusser, L. E., Schlühter, C., and Marchant, D. R.: Interhemispheric linkage of paleoclimate during the last glaciation, Geogr. Ann. A, 81, 107–153, https://doi.org/10.1111/1468-0459.00055, 1999a.

Denton, G. H., Lowell, T. V., Moreno, P. I., Andersen, B. G., and Schlühter, C.: Geomorphology, stratigraphy, and radiocarbon chronology of Llanquihue Drift in the area of the Southern Lake District, Seno de Reloncaví and Isla Grande de Chiloé, Geogr. Ann. A, 81, 167–229, https://doi.org/10.1111/1468-0459.00057, 1999b.

Dewald, A., Heinze, S., Jolie, J., Zilges, A., Dunai, T., Rethemeyer, J., Melles, M., Staubwasser, M., Kuczewski, B., Richter, J., Radtke, U., von Blanckenburg, F., and Klein, M.: CologneAMS, a dedicated center for accelerator mass spectrometry in Germany, Nucl. Instrum. Meth. B, 294, 18–23, https://doi.org/10.1016/j.nimb.2012.04.030, 2013.

Doughty, A. M., Schaefer, J. M., Putnam, A. E., Denton, G. H., Kaplan, M. R., Barrell, D. J. A., Andersen, B. G., Kelley, S. E., Finkel, R. C., and Schwartz, R.: Mismatch of glacier extent and summer insolation in Southern Hemisphere mid-latitudes, Geology, 43, 407–410, https://doi.org/10.1130/G36477.1, 2015.

Duller, G. A. T.: Single grain optical dating of glacigenic deposits, Quat. Geochronol., 1, 296–304, https://doi.org/10.1016/j.quageo.2006.05.018, 2006.

Evans, D. J. A. and Twigg, D. R.: The active temperate glacial landsystem: a model based on Breiðamerkurjökull and Fjallsjökull, Iceland, Quaternary Sci. Rev., 21, 2143–2177, https://doi.org/10.1016/S0277-3791(02)00019-7, 2002.

Evans, D. J. A., Phillips, E. R., Hiemstra, J. F., and Auton, C. A.: Subglacial till: formation, sedimentary characteristics and classification, Earth-Sci. Rev., 78, 115–176, https://doi.org/10.1016/j.earscirev.2006.04.001, 2006.

Eyles, N., Eyles, C. H., and Miall, A. D.: Lithofacies types and vertical profile models, an alternative approach to the description and environmental interpretation of glacial diamict and diamictite sequences, Sedimentology, 30, 393–410, https://doi.org/10.1111/j.1365-3091.1983.tb00679.x, 1983.

Galbraith, R., Roberts, R., Laslett, G., Yoshida, H., and Olley, J.: Optical dating of single and multiple grains of Quartz from Jinmium rock shelter, northern Australia: Part I, experimental design and statistical models, Archaeometry, 41, 339–364, https://doi.org/10.1111/j.1475-4754.1999.tb00987.x, 1999.

García, J.-L.: Late Pleistocene ice fluctuations and glacial geomorphology of the Archipiélago de Chiloé, southern Chile, Geogr. Ann. A, 94, 459–479, https://doi.org/10.1111/j.1468-0459.2012.00471.x, 2012.

García, J.-L., Hein, A. S., Binnie, S. A., Gómez, G. A., González, M. A., and Dunai, T. J.: The MIS 3 maximum of the Torres del Paine and Última Esperanza ice lobes in Patagonia and the pacing of southern mountain glaciation, Quaternary Sci. Rev., 185, 9–26, https://doi.org/10.1016/j.quascirev.2018.01.013, 2018.

García, J.-L., Maldonado, A., de Porras, M. E., Nuevo Delaunay, A., Reyes, O., Ebensperger, C. A., Binnie, S. A., Lüthgens, C., and Méndez, C.: Early deglaciation and paleolake history of Río Cisnes Glacier, Patagonian Ice Sheet (44° S), Quaternary Res., 91, 194–217, https://doi.org/10.1017/qua.2018.93, 2019.

Garreaud, R. D.: Precipitation and circulation covariability in the extratropics, J. Climate, 20, 4789–4797, https://doi.org/10.1175/JCLI4257.1, 2007.

Garreaud, R. D., Vuille, M., Compagnucci, R., and Marengo, J.: Present-day South America climate, Palaeogeogr. Palaeocl., 281, 180–195, https://doi.org/10.1016/j.palaeo.2007.10.032, 2009.

Garreaud, R. D., Lopez, P., Minvielle, M., and Rojas, M.: Large-scale control on the patagonian Climate, J. Climate, 26, 215–230, https://doi.org/10.1175/JCLI-D-12-00001.1, 2013.

Glasser, N., Harrison, S., Ivy-Ochs, S., Duller, G., and Kubik, P.: Evidence from the Rio Bayo valley on the extent of the north Patagonian ice field during the late Pleistocene-Holocene transition, Quaternary Res., 65, 70–77, https://doi.org/10.1016/j.yqres.2005.09.002, 2006.

Harrison, S., Glasser, N., Winchester, V., Haresign, E., Warren, C., Duller, G., Bailey, R., Ivy-Ochs, S., Jansson, P., and Kubik, P.: Glaciar León, Chilean Patagonia: late-Holocene chronology and geomorphology, Holocene, 18, 643–652, https://doi.org/10.1177/0959683607086771, 2008.

Hein, A. S.: Quaternary Glaciations in the Lago Pueyrredon Valley, Argentina, PhD thesis, The University of Edinburgh, Edinburgh, Scotland, 2009.

Hein, A. S., Hulton, N. R. J., Dunai, T. J., Schnabel, C., Kaplan, M. R., Naylor, M., and Xu, S.: Middle Pleistocene glaciation in Patagonia dated by cosmogenic-nuclide measurements on outwash gravels, Earth Planet. Sc. Lett., 286, 184–197, https://doi.org/10.1016/j.epsl.2009.06.026, 2009.

Heusser, C. J. and Flint, R. F.: Quaternary glaciations and environments of northern Isla Grande de Chiloé, Chile, Geology, 5, 305–308, https://doi.org/10.1130/0091-7613(1977)5<305:QGAEON>2.0.CO;2, 1977.

Heusser, C. J., Lowell, T. V., Heusser, L. E., Hauser, A., Andersen, B. G., and Denton, G. H.: Full-glacial–late-glacial palaeoclimate of the Southern Andes: evidence from pollen, beetle, and glacial records, J. Quaternary Sci., 11, 173–184, https://doi.org/10.1002/(SICI)1099-1417(199605/06)11:3<173::AID-JQS237>3.0.CO;2-5, 1996.

Heusser, C. J., Heusser, L. E., and Lowell, T. V.: Paleoecology of the southern Chilean Lake District – Isla Grande de Chiloé during middle-Late Llanquihue glaciation and deglaciation, Geogr. Ann. A, 81, 231–284, https://doi.org/10.1111/1468-0459.00058, 1999.

Hidy, A. J., Gosse, J. C., Pederson, J. L., Mattern, J. P., and Finkel, R. C.: A geologically constrained Monte Carlo approach to modeling exposure ages from profiles of cosmogenic nuclides: An example from Lees Ferry, Arizona, Geochem. Geophy. Geosy., 11, Q0AA10, https://doi.org/10.1029/2010GC003084, 2010.

Hogg, A. G., Hua, Q., Blackwell, P. G., Niu, M., Buck, C. E., Guilderson, T. P., Heaton, T. J., Palmer, J. G., Reimer, P. J., Reimer, R. W., Turney, C. S. M., and Zimmerman, S. R. H.: SHCal13 Southern Hemisphere Calibration, 0–50 000 Years cal BP, Radiocarbon, 55, 1889–1903, https://doi.org/10.2458/azu_js_rc.55.16783, 2013.

Hubbard, A., Hein, A. S., Kaplan, M. R., Hulton, N. R. J., and Glasser, N.: A reconstruction of the late glacial maximum ice sheet and its deglaciation in the vicinity of the Northern Patagonian Icefield, South America, Geogr. Ann. A, 87, 375–391, https://doi.org/10.1111/j.0435-3676.2005.00264.x, 2005.

Huntley, D. and Baril, M.: The K content of the K-feldspars being measured in optical and thermoluminescence dating, Ancient TL, 15, 11–13, 1997.

Huntley, D. and Lamothe, M.: Ubiquity of anomalous fading in K-feldspars and the measurement and correction for it in optical dating, Can. J. Earth Sci., 38, 1093–1106, https://doi.org/10.1139/e01-013, 2001.

Ivy-Ochs, S., Kerschner, H., Reuther, A., Preusser, F., Heine, K., Maisch, M., Kubik, P. W., and Schlüchter, C.: Chronology of the last glacial cycle in the European Alps, J. Quaternary Sci., 23, 559–573, https://doi.org/10.1002/jqs.1202, 2008.

Jouzel, J., Masson-Delmotte, V., Cattani, O., Dreyfus, G. Falourd,S., Hoffmann, G. Minster, B., Nouet, J., Barnola, J. M., Chappellaz, J., Fischer, H., Gallet, J. C., Johnsen, S., Leuenberger, M., Loulergue, L., Luethi, D., Oerter, H., Parrenin, F., Raisbeck, G., Raynaud, D., Schilt, A., Schwander, J., Selmo, E., Souchez, R., Spahni, R., Stauffer, B., Steffensen, J. P., Stenni, B., Stocker, T. F., Tison, J. L., Werner, M., and Wolff, E. W.: Orbital and millennial Antarctic climate variability over the past 800 000 years, Science, 317, 793–796, https://doi.org/10.1126/science.1141038, 2007.

Kaiser, J. and Lamy, F.: Links between Patagonian Ice Sheet fluctuations and Antarctic dust variability during the last glacial period (MIS 4-2), Quaternary Sci. Rev., 29, 1464–1471, https://doi.org/10.1016/j.quascirev.2010.03.005, 2010.

Kaiser, J., Lamy, F., and Hebblen, D.: A 70 kyr sea surface temperature record off southern Chile (Ocean Drilling Program Site 1233), Paleoceanography, 20, PA4009, https://doi.org/10.1029/2005PA001146, 2005.

Kaplan, M. R., Strelin, J. A., Schaefer, J. M., Denton, G. H., Finkel, R. C., Schwartz, R., Putnam, A. E., Vandergoes, M. J., Goehring, B. M., and Travis, S. G.: In-situ cosmogenic 10Be production rate at Lago Argentino, Patagonia: implications for late-glacial climate chronology, Earth Planet. Sc. Lett., 309, 21–32, https://doi.org/10.1016/j.epsl.2011.06.018, 2011.

Kelley, S. E., Kaplan, M. R., Schaefer, J. M., Andersen, B. G., Barrell, D. J. A., Putnam, A. E., Denton, G. H., Schwartz, R., Finkel, R. C., and Doughty, A. M.: High-precision ^{10}Be chronology of moraines in the Southern Alps indicates synchronous cooling in Antarctica and New Zealand 42 000 years ago, Earth Planet. Sc. Lett., 405, 194–206, https://doi.org/10.1016/j.epsl.2014.07.031, 2014.

Kohl, C. P. and Nishiizumi, K.: Chemical isolation of quartz for measurement of *in-situ*-produced cosmogenic nuclides, Geochim. Cosmochim. Ac., 56, 3583–3587, https://doi.org/10.1016/0016-7037(92)90401-4, 1992.

Kreutzer, S., Schmidt, C., Fuchs, M., Dietze, M., and Fuchs, M.: Introducing an R package for luminescence dating analysis, Ancient TL, 30, 1–8, 2012.

Kulig G.: Erstellung einer Auswertesoftware zur Altersbestimmung mittels Lumineszenzverfahren unter spezieller Berücksichtigung des Einflusses radioaktiver Ungleichgewichte in der ^{238}U-Zerfallsreihe, B.Sc. thesis, Technische Universität Bergakademie, Freiberg, Germany, 35 pp., 2005.

Lal, D.: Cosmic ray labeling of erosion surfaces: in-situ nuclide production rates and erosion models, Earth Planet. Sc. Lett., 104, 424–439, https://doi.org/10.1016/0012-821X(91)90220-C, 1991.

Lambert, F., Delmonte, B., Petit, J., Bigler, M., Kaufmann, P., Hutterli, M., Stocker, T., Ruth, U., Steffensen, J., and Maggi, V.: Dust-climate couplings over the past 800 000 years from the EPICA Dome C ice core, Nature, 452, 616–619, https://doi.org/10.1038/nature06763, 2008.

Lamy, F., Kaiser, J., Ninnemann, U., Hebbeln, D., Arz, H. W., and Stoner, J.: Antarctic timing of surface water changes off Chile and Patagonian Ice Sheet response, Science, 304, 1959–1962, https://doi.org/10.1126/science.1097863, 2004.

Lamy, F., Arz, H. W., Kilian, R., Lange, C. B., Lembke-Jene, L., Wengler, M., Kaiser, J., Baeza-Urrea, O., Hall, I. R., Harada, N., and Tiedemann, R.: Glacial reduction and millennial scale variations in Drake Passage throughflow, P. Natl. Acad. Sci. USA, 112, 13496–13501, https://doi.org/10.1073/pnas.1509203112, 2015.

Laugénie, C.: La Région des Lacs, Chili Meridional, PhD diss., Universit de Bordeaux, France, 1982.

Lifton, N., Sato, T., and Dunai, T.: Scaling in situ cosmogenic nuclide production rates using analytical approximations to atmospheric cosmic-ray fluxes, Earth Planet. Sc. Lett., 386, 149–160, https://doi.org/10.1016/j.epsl.2013.10.052, 2014.

Lovejoy, S. and Lambert, F.: Spiky fluctuations and scaling in high-resolution EPICA ice core dust fluxes, Clim. Past, 15, 1999–2017, https://doi.org/10.5194/cp-15-1999-2019, 2019.

Lowell, T. V., Heusser, C. J., Andersen, B. G., Moreno, P. I., Hauser, A., Heusser, L. E., Schlüchter, C., Marchant, D. R., and Denton, G. H.: Interhemispheric correlation of late Pleistocene glacial events, Science, 269, 1541–1549, https://doi.org/10.1126/science.269.5230.1541, 1995.

Luebert, F. and Pliscoff, P.: Sinopsis bioclimática y vegetacional de Chile, Editorial Universitaria, Santiago, Chile, ISBN 956-11-1832-7, 2006.

Lüthgens, C., Neuhuber, S., Grupe, S., Payer, T., Peresson, M., and Fiebig, M.: Geochronological investigations using a combination of luminescence and cosmogenic nuclide burial dating of drill cores from the Vienna Basin, Z. Dtsch. Ges. Geowiss., 168, 115–140, https://doi.org/10.1127/zdgg/2017/0081, 2017.

Maizels, J.: Lithofacies variations within sandur deposits: the role of runoff regime, flow dynamics and sediment supply characteristics, Sediment. Geol., 85, 299–325, https://doi.org/10.1016/0037-0738(93)90090-R, 1993.

Manger, G. E.: Porosity and bulk density of sedimentary rocks, USGS Publications Warehouse, Washington D.C., Bulletin 1144-E, 55 pp., https://doi.org/10.3133/b1144E, 1963.

Mayr, C., Stojakowits, P., Lempe, B., Blaauw, M., Diersche, V., Grohganz, M., López Correa, M., Ohlendorf, C., Reimer, P., and Zolitschka, B.: High-resolution geochemical record of environmental changes during MIS 3 from the northern Alps (Nesseltalgraben, Germany), Quaternary Sci. Rev., 218, 122–136, https://doi.org/10.1016/j.quascirev.2019.06.013, 2019.

Mejdahl, V.: Thermoluminescence dating: beta attenuation in quartz grains, Achaeometry, 21, 61–73, 1979.

Mendelová, M., Hein, A. S., Rodés, A., and Xu, S.: Extensive mountain glaciation in central Patagonia during marine isotope stage 5, Quaternary Sci. Rev., 227, 105996, https://doi.org/10.1016/j.quascirev.2019.105996, 2020.

Menzies, J.: Strain pathways, till internal architecture and microstructures – perspectives on a general kinematic model – a "blueprint" for till development, Quaternary Sci. Rev., 50, 105–124, https://doi.org/10.1016/j.quascirev.2012.07.012, 2012.

Menzies, J., van der Meer, J. J. M., and Rose, J.: Till – as a glacial "tectomict", its internal architecture, and the development of a "typing" method for till differentiation, Geomorphology, 75, 172–200, https://doi.org/10.1016/j.geomorph.2004.02.017, 2006.

Mercer, J. H.: Chilean glacial chronology 20 000 to 11 000 carbon – 14 years ago: some global comparisons, Science 172, 1118–1120, https://doi.org/10.1126/science.176.4039.1118, 1972.

Mercer, J. H.: Glacial history of southernmost South America, Quaternary Res., 6, 125–166, https://doi.org/10.1016/0033-5894(76)90047-8, 1976.

Miall, A. D.: Architectural-Element Analysis: A New Method of Facies Analysis Applied to Fluvial Deposits, Earth-Sci. Rev., 22, 261–308, https://doi.org/10.1016/0012-8252(85)90001-7, 1985.

Miall, A. D.: The Geology of Fluvial Deposits: Sedimentary facies, basin analysis and petroleum geology, Springer, Berlin, Germany, 582 pp., https://doi.org/10.1007/978-3-662-03237-4, 2006.

Miller, J. H.: The climate of Chile, in: Climates of Central and South America, edited by: Schwerdtfeger, W., World Survey of Climatology, Elsevier, Amsterdam, The Netherlands, 113–145, 1976.

NASA JPL: NASA Shuttle Radar Topography Mission Global 1 arc second, NASA EOSDIS Land Processes DAAC, USA, https://doi.org/10.5067/MEaSUREs/SRTM/SRTMGL1.003, 2013.

Nishiizumi, K., Imamura, M., Caffee, M. W., Southon, J. R., Finkel, R. C., and McAninch, J.: Absolute calibration of Be-10 AMS standards, Nucl. Instrum. Meth. B, 258, 403–413, https://doi.org/10.1016/j.nimb.2007.01.297, 2007.

Parducci, L., Jorgensen, T., Tollefsrud, M. M., Elverland, E., Alm, T., Fontana, S. L., Bennett, K. D., Haile, J., Matetovici, I., Suyama, Y., Edwards, M. E., Andersen, K., Rasmussen, M., Boessenkool, S., Coissac, E., Brochmann, C., Taberlet, P., Houmark-Nielsen, M., Larsen, N. K., Orlando, L., Gilbert, M. T. P, Kjær, K. H., Greve, Alsos, I. G., and Willerslev, E.: Glacial survival of boreal trees in northern Scandinavia, Science, 335, 1083–1086, https://doi.org/10.1126/science.1216043., 2012.

Parrenin, F., Masson-Delmotte, V., Koehller, P., Raynud, D., Paillard, D., Schwander, J., Barbante, C., Landais, A., Wegner, A., and Jouzel, J.: Synchronous change of atmospheric CO_2 and Antarctic temperature during the last deglacial warming, Science, 339, 1060–1063, https://doi.org/10.1126/science.1226368, 2013.

Porter, S.: Pleistocene Glaciations in the Southern Lake District of Chile, Quaternary Res., 8, 2–31, https://doi.org/10.1016/0033-5894(81)90013-2, 1981.

Prescott, J. and Hutton J.: Cosmic ray distributions to dose rates for luminescence and ESR dating: large depths and long-term variations, Radiat. Meas., 23, 497–500, https://doi.org/10.1016/1350-4487(94)90086-8, 1994.

Prescott, J. and Stephan, L.: The contribution of cosmic radiation to the environmental dose for thermoluminescent dating – Latitude, altitude and depth dependencies, PACT. Revue du Groupe Européen d'Etudes pour les Techniques Physiques, Chimiques et Mathématiques Appliquées à l'Archéologie, 6, 17–25, 1982.

Preusser, F., Degering, D., Fuchs, M., Hilgers, A., Kadereit, A., Klasen, N., Krbetschek, M., Richter, D., and Spencer, J. Q. G.: Luminescence dating: basics, methods and applications, E&G Quaternary Sci. J., 57, 95–149, https://doi.org/10.3285/eg.57.1-2.5, 2008.

Putnam, A. E., Schaefer, J. M., Denton, G. H., Barrell, D. J. A., Birkel, S. D., Andersen, B. G., Kaplan, M. R., Finkel, R. C., Schwartz, R., and Doughty, A. M.: The Last Glacial Maximum at 44° S documented by a ^{10}BE moraine chronology at Lake Ohau, Southern Alps of New Zealand, Quaternary Sci. Rev., 62, 114–141, https://doi.org/10.1016/j.quascirev.2012.10.034, 2013.

Rhodes, E.: Optically Stimulated Luminescence Dating of Sediments over the Past 200 000, Annu. Rev. Earth. Pl. Sc., 39, 461–488, https://doi.org/10.1146/annurev-earth-040610-133425, 2011.

Rodés, Á., Pallàs, R., Braucher, R., Moreno, X., Masana, E., and Bourlés, D. L.: Effect of density uncertainties in cosmogenic ^{10}BE depth-profiles: dating a cemented Pleistocene alluvial fan (Carboneras Fault, SE Iberia), Quat. Geochronol., 6, 186–194, https://doi.org/10.1016/j.quageo.2010.10.004, 2011.

Roig, F. A., Le-Quesne, C., Boninsegna, J. A., Briffa, K. R., Lara, A., Grudd, H., Jones, P. D., and Villagrán, C.: Climate variability 50 000 years ago in mid-latitide Chile as reconstructed from tree rings, Nature, 410, 567–570, https://doi.org/10.1038/35069040, 2001.

Sagredo, E. A., Moreno, P. I., Villa-Martinez, R., Kaplan, M. R., Kubik, P. W., and Stern, C. R.: Fluctuations of the Última Esperanza ice lobe (52° S), Chilean Patagonia, during the last glacial maximum and termination 1, Geomorphology, 125, 92–108, https://doi.org/10.1016/j.geomorph.2010.09.007, 2011.

Schaefer, J. M., Putnam, A. E., Denton, G. H., Kaplan, M. R., Birkel, S., Ninneman, U. S., Barker, S., Schwartz, R., Andersen, B. J., and Schluechter, C.: The southern glacial maximum 65 000 years ago and its unfinished termination, Quaternary Sci. Rev., 114, 52–60,https://doi.org/10.1016/j.quascirev.2015.02.009, 2015.

Shackleton, N. J., Hall, M. A., and Vincent, E.: Phase relationships between millennial-scale events 64 000–24 000 years ago, Paleoceanography, 15, 565–569, https://doi.org/10.1029/2000PA000513, 2000.

Shulmeister, J., Thackray, G. D., Rieser, U., Hyatt, O. M., Rother, H., Smart, C. C., and Evans, D. J.: The stratigraphy, timing and climatic implications of glaciolacustrine deposits in the middle Rakaia Valley, South Island, New Zealand, Quaternary Sci. Rev., 29, 2362–2381, https://doi.org/10.1016/j.quascirev.2010.06.004, 2010.

Smedley, R. K., Glasser, N. F., and Duller, G. A. T.: Luminescence dating of glacial advances at Lago Buenos Aires (∼ 46° S), Patagonia, Quaternary Sci. Rev., 134, 59–73, https://doi.org/10.1016/j.quascirev.2015.12.010, 2016.

Strub, P. T., Mesias, J. M., Montecino, V., Ruttlant, J., and Salinas, S.: Coastal ocean circulation off western South America, in: The Global Coastal Ocean: Regional Studies and Synthesis, edited by: Robinson, A. R. and Brink K. H., John Wiley, New York, USA, 273–315, 1998.

Stuiver, M., Reimer, P. J., and Reimer, R. W.: CALIB 7.1 [WWW program], available at: http://calib.org, last access: 16 April 2020.

Sugden, D. E., McCulloch, R. D., Bory, A. J.-M., and Hein, A. S.: Influence of Patagonian glaciers on Antarctic dust deposition during the last glacial period, Nat. Geosci., 2, 281–285, https://doi.org/10.1038/ngeo474, 2009.

Villagrán, C.: Expansion of Magellanic moorland during the Late Pleistocene: palynological evidence from northern Isla Grande de Chiloé, Quaternary Res., 30, 304–314, https://doi.org/10.1016/0033-5894(88)90006-3, 1988.

Villagrán, C.: Glacial, Late-Glacial, and Post-Glacial climate and vegetation of the Isla Grande de Chiloé, Southern Chile (41–44° S), Quat. S. Am. A., 8, 1–15, 1990.

Villagrán, C., León, A., and Roig, F. A.: Paleodistribución del alerce y ciprés de las Guaitecas durante períodos interestadiales de la Glaciación Llanquihue: provincias de Llanquihue y Chiloé, Región de Los Lagos, Chile, Rev. Geol. Chile, 31, 133–151, https://doi.org/10.4067/S0716-02082004000100008, 2004.

Villagrán, C., Abarzúa, A. M., and Armesto, J.: Nuevas evidencias paleobotánicas y filogeográficas en torno a la historia Cuaternaria de los bosques subtropical-templados de la Cordillera de la Costa de Chile, in: Biodiversidad y Ecología de los bosques costeros de Chile, edited by: Smith-Ramirez, C. and Squeo, F., Editorial Universidad de Los Lagos, Chile, 3–21, 2019.

WAIS Divide Project Members: Precise interpolar phasing of abrupt climate change during the last ice age, Nature, 520, 661–665, https://doi.org/10.1038/nature14401, 2015.

Williams, P. W., McGlone, M., Neil, H., and Zhao, J.-X.: A review of New Zealand palaeoclimate from the last interglacial to the global last glacial maximum, Quaternary Sci. Rev., 110, 92–106, https://doi.org/10.1016/j.quascirev.2014.12.017, 2015.

Wintle, A.: Anomalous Fading of Thermo-luminescence in Mineral Samples, Nature, 245, 143–144, https://doi.org/10.1038/245143a0, 1973.

Wintle, A.: Luminescence dating: where it has been and where it is going, Boreas, 37, 471–482, https://doi.org/10.1111/j.1502-3885.2008.00059.x, 2008.

E&G Quaternary Sci. J., 70, 129–143, 2021
https://doi.org/10.5194/egqsj-70-129-2021

Open Access E&G Quaternary Science Journal

Research article

Sandhills, sandbanks, waterways, canals and sacred lakes at Sais in the Nile Delta

Penelope Wilson[1] **and Hosni Ghazala**[2]

[1]Department of Archaeology, Durham University, Durham DH1 3LE, United Kingdom
[2]Geology Department, Mansoura University, Mansoura, Dakhalia Governorate, Egypt

Correspondence: Penelope Wilson (penelope.wilson@durham.ac.uk)

Relevant dates: Received: 30 July 2020 – Revised: 7 April 2021 – Accepted: 16 April 2021 – Published: 25 May 2021

How to cite: Wilson, P. and Ghazala, H.: Sandhills, sandbanks, waterways, canals and sacred lakes at Sais in the Nile Delta, E&G Quaternary Sci. J., 70, 129–143, https://doi.org/10.5194/egqsj-70-129-2021, 2021.

Abstract: The paper explores the relationship between the archaeological zones of the ancient city of Sais at Sa el-Hagar, Egypt, and the natural landscape of the western central Nile Delta and, in particular, the extent to which the dynamic form of the landscape was an element in the choice of settlement location. Furthermore, settlement at Sais has been determined to have existed at several locations in the immediate environs of the current archaeological zones from the Neolithic period, around 4000 BCE (Before Common Era), to the modern day, suggesting that the local environment was conducive to sustainable settlement, culminating in the establishment of a capital city in the 7th century BCE. The nature of the settlement, its immediate environs and waterway systems will, thus, be described, based on correlation of geological, geophysical, remote sensing and archaeological data, in order to establish if and when human interactions in the landscape can be determined to be reactive or proactive.

Kurzfassung: Der Beitrag untersucht die Beziehung zwischen den archäologischen Arealen der antiken Stadt Sais (heute: Sa el-Hagar, Ägypten) und der natürlichen Landschaft des westlichen Zentrums des Nildeltas und insbesondere, welche Rolle die dynamische Landschaftsentwicklung bei der Wahl des Siedlungsstandortes spielte. Dies geschieht vor dem Hintergrund, dass von der neolithischen Periode um 4000 v. Chr. bis in die Neuzeit verschiedene Siedlungsareale an mehreren Stellen in der unmittelbaren Umgebung der heutigen archäologischen Bereiche von Sais existierten, was darauf hindeutet, dass die lokale Umwelt dieses Ortes günstige Bedingungen für eine nachhaltige Besiedlung bot, ein Umstand, der in der Etablierung von Sais als Hauptstadt Ägyptens im siebten Jahrhundert v. Chr. gipfelte. Basierend auf der Korrelation von geologischen, geophysikalischen, Fernerkundungs- und archäologischen Daten wird dementsprechend im Folgenden der Charakter der Siedlung, ihrer unmittelbaren Umgebung und des zugehörigen Flussnetzes im Hinblick darauf beschrieben, ob eine auch zeitlich genauer zu fassende Bestimmung menschlicher Interaktionen mit der Landschaft als reaktiv oder proaktiv möglich ist. *(Abstract was translated by Eva Lange-Athinodorou.)*

1 Introduction

The archaeological site of Sais at Sa el-Hagar, Gharbiyah Governorate, Egypt (Fig. 1), has been studied since 1997, within its palaeo- and modern landscape, through a programme of archaeological survey and excavation combined with geoelectrical resistivity and magnetic survey as well as a manual drill coring programme (Wilson, 2006). The overall aim of the work was to understand the relationship and interactions between the archaeological settlement areas and the natural landscape features, in particular the waterways and buried sandbanks, from the period of the first human settlement at the site in Neolithic times, ca. 4000 BCE (Before Common Era), until the present day (Wilson et al., 2014). Furthermore, the dynamics of the landscape and human activity can be analysed for information about the extent to which the choice of area for settlement was dictated by naturally occurring favourable conditions, such as buried sand features and/or levees or levees, or by human political and economic choices connected with land and river management (Hritz, 2014, pp. 230–243). This paper will analyse the extent to which different types of data from geophysical, archaeological, remote sensing and ancient textual information can be combined to correlate and extend the interpretation of single data sets, in order to track waterways, buried sandhills, human settlement and other landscape interventions over the longue durée of 6000 years at Sa el-Hagar in a floodplain dominated by an ancient river system.

2 Methods

The study area is the floodplain the west of the Rashid (Rosetta) branch of the Nile where there are a number of towns and villages within a drain and canal network, mostly consolidated in the 19–20th century by the engineers of Muhammad Ali and the Ministry of Public Works (Barois, 1904, pp. 119–124). First, to reconstruct the palaeolandscape of the area, the University of Mansoura team made 19 deep-drill cores, up to 23 m deep, and six transects of 41 vertical electrical soundings (VESs; using a Schlumberger array) to trace the development of the landscape from the Pleistocene to the Holocene eras (Fig. 2; Ghazala, 2005; El-Shahat et al., 2005).

In addition, information from historical satellite imagery, such as CORONA and Google Earth, and from individual Landsat 5 images was also compared with the geophysical survey data to detect subsurface relict waterways (Abrams and Comer, 2013; see Pope and Dahlin, 1989; for Egypt, see Wunderlich, 1989). Then, from 1999 onwards, the geoarchaeological programme of the Durham–Ministry of Antiquities mission made over 300 shallow cores with a manual Eijkelkamp drill auger in the area (Wilson, 2006). The analysis of the core material showed that the human material culture layers usually do not extend beyond 6 to 7 m below the ground surface, except in some higher ground in the Kom Rebwa archaeological area. Deposits recorded in augers in the surface and buried archaeological zones included reworked primary settlement material, buried primary archaeological strata and, in some places, up to 8 m of continuous anthropogenic strata and layers of archaeological material apparently separated by alluvial sediments. Elsewhere, the augers contained purely geological sediments consisting of silts, hard compact clay and sandy-silt mixtures, as well as medium and fine sands (Wilson, 2006). Further data were collected from archaeological excavations (Ex's) in the Great Pit area (Ex 8) and in Kom Rebwa (Ex's 1–12), where fine-grained archaeological strata can be compared with drill auger data from the same place (Wilson, 2011; Wilson et al., 2014) to correlate the two sets of material more closely, to provide an understanding of anthropogenic material within drill cores and to integrate the geological and archaeological material. Finally, an ancient textual source was compared with the excavated and survey data to determine the limits of the source in answering specific questions without further topographical information. The correlation of the data can be used to refine chronological developments of human activity as it was played out in the dynamic floodplain environment.

3 The geological framework

Analysis of the underlying geology of the delta has identified the following four main phases and strata (Pennington, 2017; Pennington et al., 2017): at the base, the Mit Ghamr formation comprises Pleistocene medium coarse sands with an uneven surface, created by downcutting river systems (in some areas, the Mit Ghamr surface is covered by a layer of aeolian and reworked fluvial sand); next, and key to the period of human activity in the delta, is the deposition of the Bilqas 2 mud around 8000–7000 BP (Before Present) upon the surface of the Pleistocene fluvial sand, creating an undulating topography in the delta, with some sandhills, dynamic anastomosing channel networks, swampy floodplain and peat formation in some areas. Starting in the central and southern delta, there was a transition from the large-scale crevassing action of the river to the meandering river channels (Pennington et al., 2016) and from the Bilqas 2 muds to the Bilqas 1 layer around 6000–5500 BP, so that, by ca. 4500 BP, all of the delta was covered in Bilqas 1 sediments. This layer of brown silt clay ranged from 2 to 9.9 m thick and contains limestone nodules and gypsum rosettes according to periods of warm, arid conditions. The upper alluvial mud is essentially the layer in which human activity is detected.

In the Sa el-Hagar area, the detailed geological reconstruction of the area (Fig. 3) is based on the VES and deep-drill cores (Ghazala, 2005; Ghazala et al., 2005) and modelled scenarios of the main geologic strata from deep cores and the shallow-core drilling programme (Pennington, 2017, pp. 176–183). The analyses suggests that buried sandhills are located under the village of Kawady northeast of Sais, run-

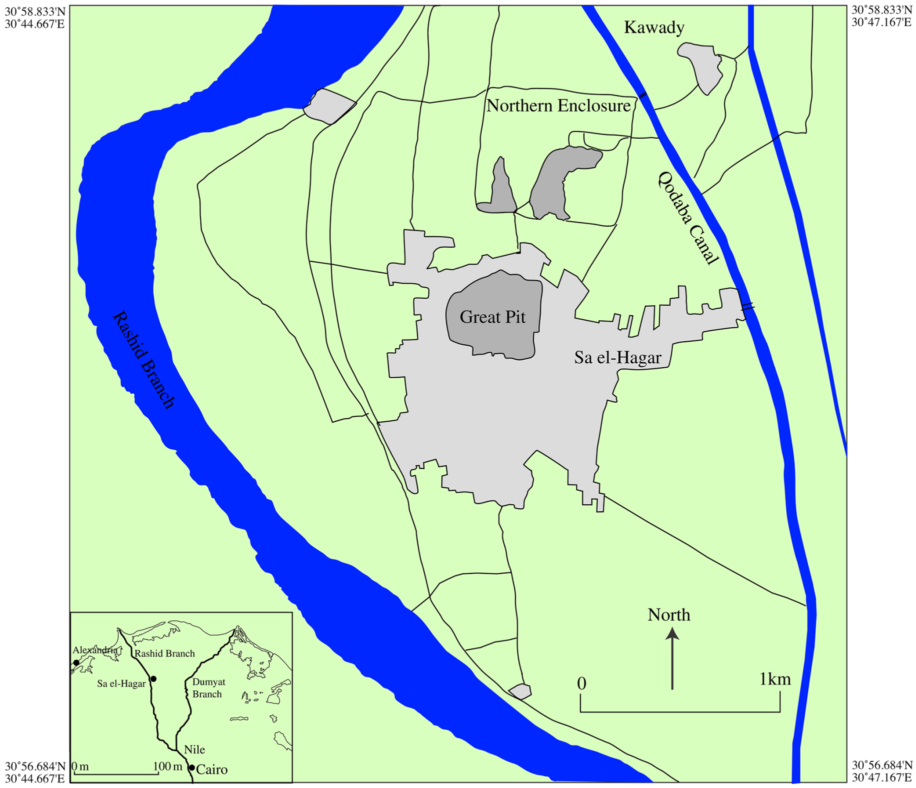

Figure 1. Map showing the location of the area of Sais, the archaeological zones and the modern town of Sa el-Hagar in the Nile Delta.

ning southward, and another sandbank runs along the eastern river bank on the western side of the area. In the region, other buried, elevated sands lie to the west of Basioun and in a large body running north to south to the east of the Sais area. The latter may have been a significant sand body separating the western river channels (the Canopic and Saitic branches) from the Sebennytic branch running through the centre of the delta.

The uneven Mit Ghamr surface also suggests that there were deep swampy basins north of Sais and, potentially, the course of a deep, older river channel to the east of Basioun flowing northward to Shubra Tana but with a distributary branching west, under what is now called the Great Pit, then turning in a meander back to the northeast and under what is now called the Northern Enclosure. A younger channel, mirroring the channel of the distributary but just a little south of it, has also been detected on the western side of the village of Sa el-Hagar and west of the Northern Enclosure. It seems likely that, over time, the river has continued this westward meander to its present location, leaving behind reworked sandbars on the inside of the bend of the modern Rashid or Rosetta branch at Sa el-Hagar. The environment in the period 4000–3500 BCE could be characterised as one of swamps and anastomosing river course, with higher land in isolated locations (Pennington, 2017, pp. 180–183), therefore making it ideal for settlement and river exploitation during the Neolithic period.

4 Data correlations

This section discusses the correlation of different types of data and their analysis.

4.1 Correlating geological survey and drill augers to the south of Sa el-Hagar

Shallow drill augers to the southeast of the village of Sa el-Hagar (Fig. 4), contained thick bands of bivalve mollusc shells, confirming the reconstruction of a series of channels or waterbodies here at one time, i.e. the cores labelled C107, C103, C102, C101 and C182 and C183 (Fig. 5). The thick shell bands were also associated with silts and sands that were blueish or turquoise in colour and were, thus, at the interface between the Bilqas 1 and Mit Ghamr formation. C119 and C120 to the east, and between the two transects above, are shown for comparison without the thick bands of shell material and only have a few fragments representing the floodplain of the channels. It can also be noted that C107 and C102 had pottery fragments underneath the shell layers, suggesting that prehistoric human activity had been interrupted by a new channel in the same location (see below).

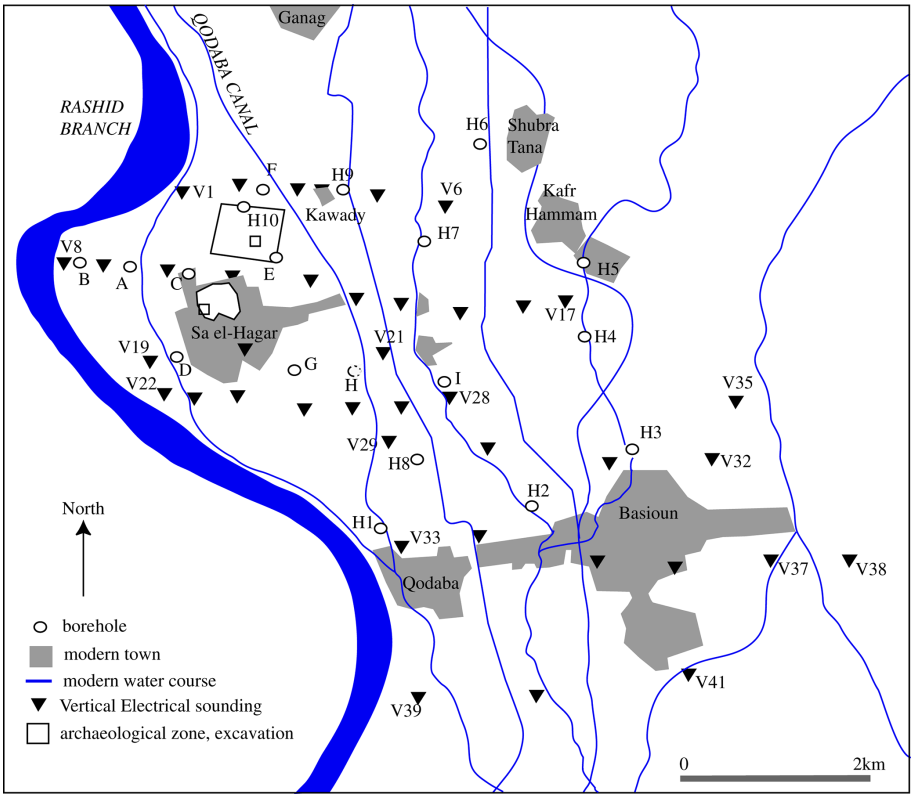

Figure 2. Area of Sa el-Hagar with the location of VES transects and deep-drill augers (after Ghazala, 2005).

4.2 Correlating the geophysical model, remote sensing data and drill auger data

The proposed younger channel has left a strong signal in satellite imagery and drill augers on the western side of the Northern Enclosure archaeological area. A Landsat 5 TM (thematic mapper) image of wavelength 5 (shortwave infrared; USGS, 2020) shows a dark band along the western side of the enclosure, almost parallel to it, due to relative water retention of sediments, and is most likely to be related to grain-size effects of buried river branches (see Ullmann et al., 2020; this Special Issue; Fig. 6). The band is an average of 200 m in width, similar to the narrow part of the modern Rashid branch bend at Sa el-Hagar.

A transect of the drill augers (C5, C191, C189, C63; Fig. 5) in the location of the band (Fig. 7) shows an upper 2.8 m of sediments with anthropogenic material in it, including broken limestone, orthoquartzites and pottery; then there are bands of finer silts and sands with broken bivalve mollusc shells (*Cyrenidae* family) in a 30 cm thick band, from 4 to 4.30 m below the ground surface in C189 and 3.5–4 m below the surface in C191. In the latter cores, the shell and sediment deposits continue for as much as 6.68 m belowground. But in C189, the core has a band of further anthropogenic material; apparently the channel cut into a previous area of human activity or deposition of material. In C189, there was especially dense anthropogenic material, and in fact, the core was stopped when the drill head hit a stone and could not proceed further at 7.25 m below the ground.

The pottery and other burnt material recovered from the lower part of the cores was potentially Predynastic in date, and this depth of material might well link with the prehistoric layers to the south in Ex 8 (see below). The satellite image, thus, seems to show the buried presence of a filled-in channel, with the sediments on top of the shell layer retaining more water than the sediments on either side. Such a strong signal cannot be detected in the satellite imagery elsewhere in the Sa el-Hagar area, and it may be that elsewhere the surface layers are too disturbed or built over by modern structures, as in the area to the south of Sa el-Hagar.

4.3 Correlating geological soundings and archaeological excavation

The river channel shift from the Great Pit area to the west can perhaps be detected in archaeological excavations in the Great Pit. A date can also be suggested for the movement of the channel. In Ex 8, the earliest level found was a fish midden of the Neolithic period, ca. 4300–4000 BCE, after radiocarbon dating and comparison of the pottery and lithics with other Neolithic sites in Egypt (Wilson el al., 2014). By correlating the archaeological section and drill augers (Fig. 8), it

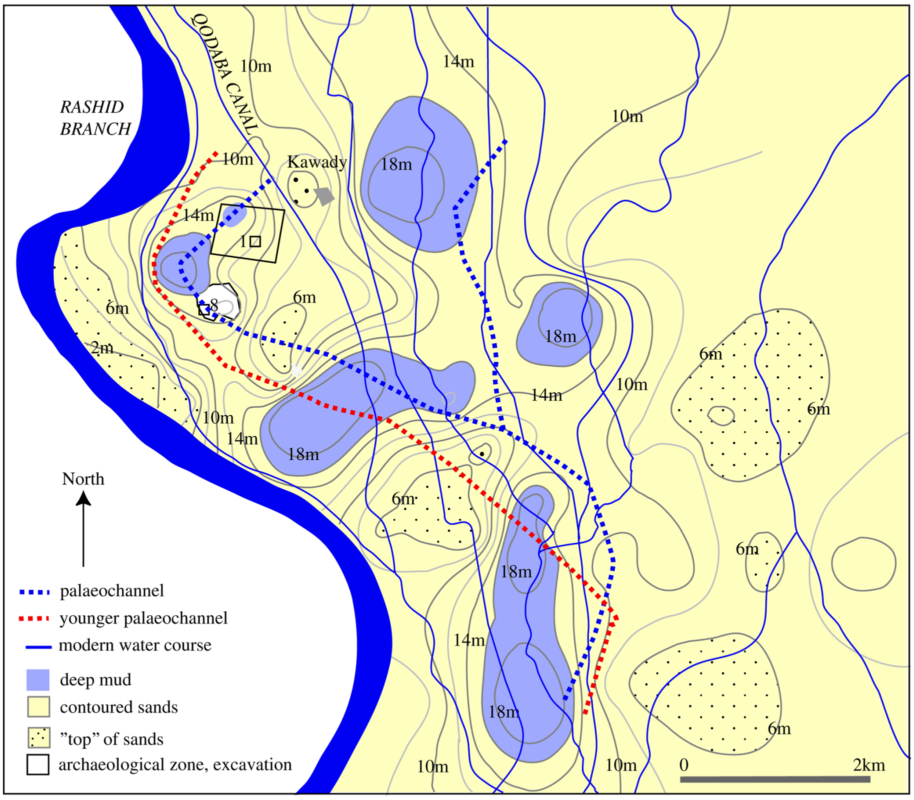

Figure 3. Map of the Sa el-Hagar area, with reconstructed subsurface sand contours up to 18 m below the ground, and the palaeochannel locations.

seems that the fish midden was situated on the western side of a riverbank (Mit Ghamr formation), which was then subject to flooding (Bilqas 1), and a settlement was established in the same location, which had evidence for semi-domesticated cattle, pigs and sheep goats. The area may have been subject to an arid period before the inundation increased to such an extent that the settlement area was abandoned and left to alluvial deposition (Bilqas 2) for some time until a reoccupation in the Buto–Maadi period, ca. 3500 BCE. The change in the alluvial regime could represent the shift of the river from the older channel to the younger channel, at which point human activity, if not settlement, resumed on the alluvium in the same place, at around 3500 BCE, until the Early Dynastic period around 3000 BCE, but was then situated on the eastern bank of a river channel.

The date of the change between 4000 and 3500 BCE seems to agree well with recent radiocarbon dates and pollen data from Sa el-Hagar (Zhao et al., 2020) that show the beginning of cultivated (domesticated) *Poaceae* cereal in the area during a period of warmer climate and expansion of the wetlands between 4750–3850 BCE (zone III), followed by a drier period with shrinkage of the wetland 3850–3550 BCE (zone IV) and then the recovery of the wetland from 3550–2250 BCE before the onset of a global, drier arid event 2250–2050 BCE. The key period of zones III to IV, when the older deep channel was abandoned through reduced water burden or a crevasse splay, was detected from coring at depths of 6.32 to 5.48 m below the ground (e.g. C41 in the north (Fig. 4) and C107 and C102 in the southeast; Fig. 5), consistent with reaching the Neolithic levels in Ex 8. In C107, there were blue-green coloured silts at the end of the core, and from this location, the bank of a possible water body would be on the same trajectory as the bank in Ex 8. Furthermore, C107 has a thick layer of settlement and anthropogenic material under the shell layer, but it is on top of coarse sands, at about 6.4 m below the ground surface, which may be redolent of the Pleistocene sand surface. The change in the river channel may have meant the replacement of human activities focussed on the exploitation of the river and water bodies in the Neolithic period, with humans settling on alluvial land with high areas and swampy backwaters that were attractive for settlement and exploitation of the agricultural, wetland and riverine resources in the Late Predynastic and Early Dynastic periods (ca. 3500–3000 BCE; Wilson, 2014).

The stratigraphic record, however, cannot be followed further in the Ex 8 area because, directly upon the Buto–Maadi period layers, is material from the destroyed structures dating to the Saite period at the end of the 6th century BCE. It seems likely that, in the Saite period, the area was cleared down to the sandy sediments for the purpose of founding new

Figure 4. Map of drill core transects discussed in the article in the area of Sa el-Hagar. This figure has been generated from QGIS (Quantum GIS) and satellite images. © Google Earth.

monumental structures in the area. Whatever happened there in the intervening 2800 years was removed by human action, demonstrating that, although riverine activity can have short-term and long-term impacts, human intervention on geological layers can also be substantial.

5 Analysing the archaeological data from drill cores

According to the scenarios above, the current configuration of the river to the west, and perhaps other channels to east, of Sa el-Hagar suggests that there has been little change since the beginning of the Dynastic period and that anthropogenic material occurs in the 6 m or so of alluvium after the Bilqas 1–Bilqas 2 transition. The identification of settlement layers and alluvial layers from drill cores alone, without contextual data, can be difficult. At Sa el-Hagar there are areas of positive archaeological settlement data, which can help in the analysis of core material where there are no other contextual data.

5.1 Northern Enclosure – monumentalised settlement

The Northern Enclosure area, although much flattened and denuded now, once contained massive mud brick and stone structures, including an enclosure wall some 700 m by 680 m in dimension, which is now reduced to a track (Wilson, 2006, pp. 99–115). The archaeological material in the enclosure has been extensively removed so that it is not even certain that this was the location of the famous temple of Neith. The drill augers have proved useful in the enclosure, not only identifying the depth of settlement and archaeological material but also, in some places, the nature of that material (Figs. 4, orange dots, and 9).

A transect across the Northern Enclosure (Fig. 9) shows the landscape in which the settlement is situated and the deep bands of human material culture (Wilson, 2006, pp. 180–202). C53 is the channel, and its in-fill is to the west of the Northern Enclosure described above. The area seems to be virgin land and has no anthropogenic material in it, i.e. archaeological material defined as pottery, stone, burnt mate-

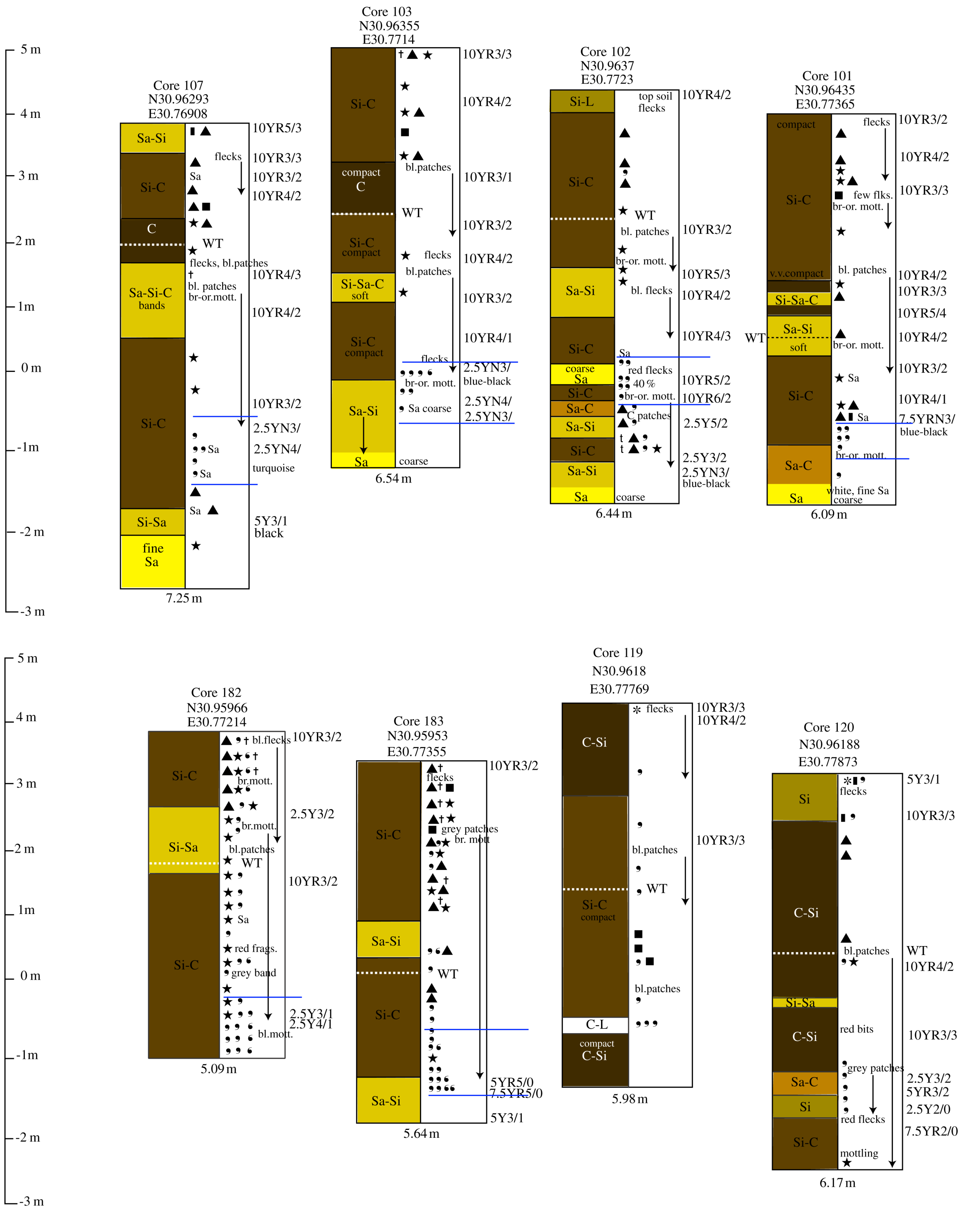

Figure 5. Transects southeast of Sa el-Hagar showing the following thick shell bands (blue lines): C107, C103, C102, C101 and C182 and C183, with C119 and C120 for comparison (see Fig. 13 for the key to cores).

Figure 6. Extract from Landsat 5 data, showing the subsurface water features west of the Northern Enclosure at Sa el-Hagar (water absorbs infrared energy and gives no return; thus, this detail appears to be greyish black). Base map source: USGS Landsat 5; 14 February 1998 (original image courtesy of the U.S. Geological Survey).

rial and bone concentrations. By contrast, C54, just inside the enclosure, shows dense stone fragment layers, which are the remains of destroyed stone structures in the top 5 m of the core. The stone fragments are of limestone, granite and orthoquartzite, especially in a band 4–5 m below the ground, and these were the standard materials used for monumental structures. The stone layer is directly situated upon compact clay, which could be a natural levee acting as a foundation or a mud brick construction, in turn, upon other settlement material. The sequence may suggest that there was a building or gateway in the western side of the enclosure built upon pre-existing settlement layers. Earlier human activity was evidenced within alluvial layers, to a depth of at least 8 m below the modern ground level in C54. C52, to the east of C54 inside the Northern Enclosure, has silt clay and clay upper material, and there is a stone debris layer between 4 and 5 m from ground level, perhaps the foundations of a stone structure, apparently upon clay mud, with a thin band of pottery at 6.25 m signalling an initial settlement layer upon compact clay river levee material. C50 in the northern wall of the enclosure also has thick layers of stone debris (limestone, granite and orthoquartzite) with pottery for a depth of almost 7 m, including a black gloss sherd, with brown and orange-red bands (3.5 × 2.7 × 0.4 cm; C50 and C43) that may be east Greek in origin, and this, thus, points to a date in the 7th–6th century BCE. The latter would directly suggest a Saite period date for some aspect of the stone structure, and its depth at 5.22 m below ground level shows the difficulties of dating archaeological layers in terms of the depth alone. There are also thick layers of stone material, for example in C57 between 4.5 and 6 m below the ground. But above the stone debris is a band of anthropogenic material, from 3.14 to 4.5 m, suggesting that the stone debris is from an earlier phase of monumental building in the eastern part of the enclosure. It may be that the stone structures were reorganised in a new phase of the site's history. In the eastern enclosure wall it is possible that the upper metre is the last part of the mud brick wall, which seems to have been founded on earlier settlement material, including an alluvial or mud band between and 2 and 3 m below ground. Other stone debris was recorded at the entrance to the Northern Enclosure in C47 and C48 (not illustrated), where the drill head could not penetrate the debris easily; this may suggest a gateway entrance to the enclosure or part of a monumental area.

As the enclosure is an identifiable archaeological zone with two low mound areas known that are protected Antiquities land, it is not unexpected to find considerable evidence of human activity, as detailed above. But the material from the cores can be directly compared with material from archaeological excavations, especially in Ex 1. Starting from datable layers and working downward through known archaeological features, the information from the drill cores can be contextualised, to some extent. C58 was drilled through a mud brick wall dating to the late Ramesside period (ca. 1189–1077 BCE) and was compared with subsequent excavation in this area (Wilson, 2011, p. 25; Fig. 25). The wall was known to have a height of over 1 m but was not completely excavated; in the core, the upper 1.64 m was a homogeneous mixture of silt clay with some pottery fragments, which is expected as walls were constructed by reusing settlement muds with pottery added for strength. The base of the wall seemed to be indicated by a layer of sand, possibly within a foundation trench or on top of earlier settlement debris to a depth of 2.76 m and aligned in the excavation section with the base of a series of ovens constructed in the area enclosed by the wall. The excavation ended after about 3 m of depth from the ground level due to reaching the water table and a layer of mud with blueish-black clay lumps in it, which was perhaps an alluvial layer. Pottery dating to the Old Kingdom had been found in this lower level. The drill core was able to proceed further, reaching the base of the alluvial layer at 3.64 m from its start, and another strong settlement layer was encountered, possibly topped by a burial ground due to the bones found between 3.64 and 4.9 m. The drill auger then continued through alluvial layers, including an apparent in-filled channel at 6.7–8 m, and through a compact clay levee down to 9.5 m. In archaeological terms, the presence of Old Kingdom layers within alluvial mud underlying the New Kingdom material is interesting. Little Middle Kingdom material has been found at Sais, and the period is regarded as having had high inundations (Vercoutter, 1966; Bell, 1975), which may have affected settlements adversely. The alluvial band between the two dateable settlement layers may thus

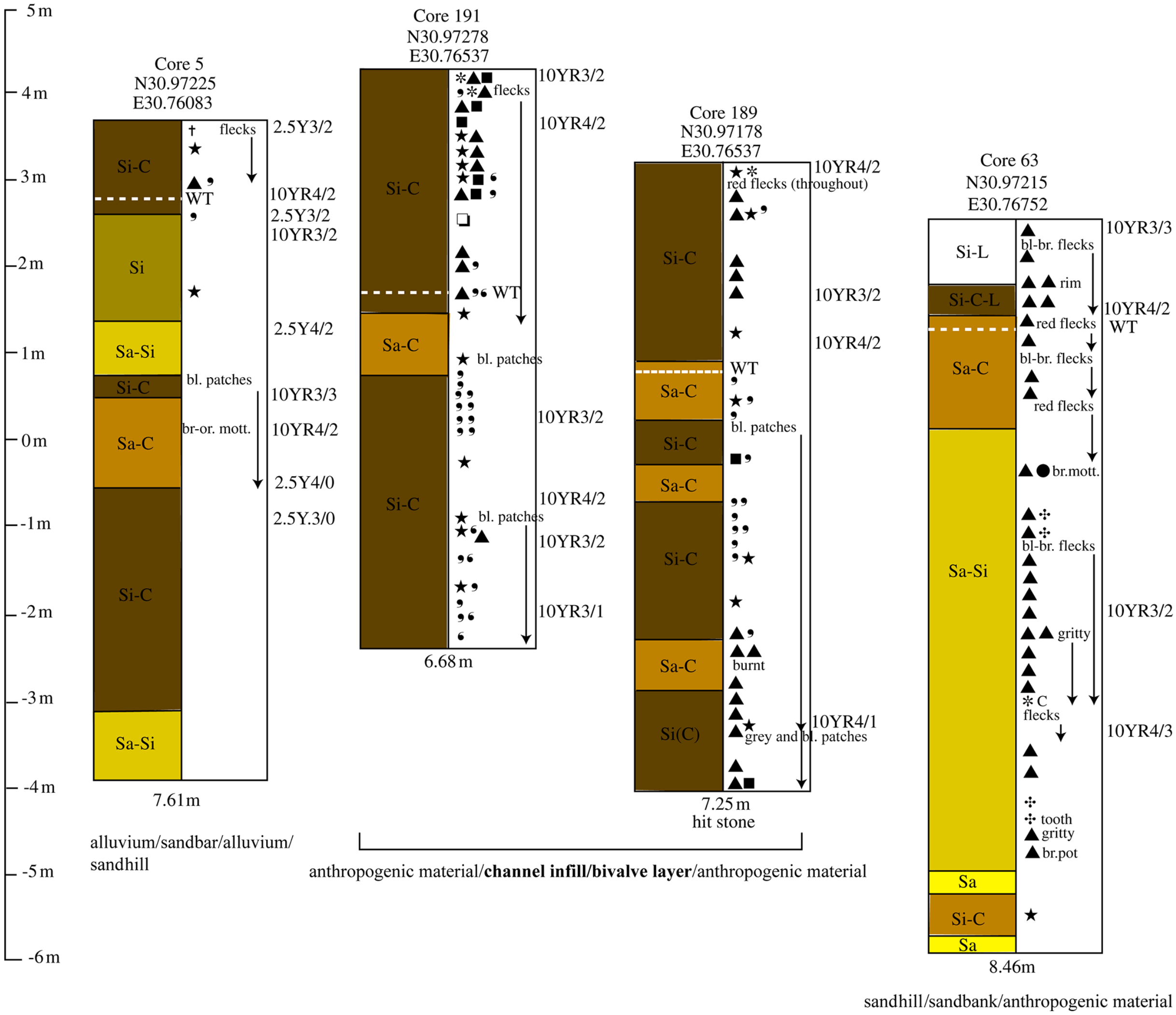

Figure 7. Transect (cores 5, 191, 189, 63) to the west of the Northern Enclosure, showing the channel and difference between alluvial and archaeological zones. Ground heights are taken from TanDEM-X data. (See Fig. 13 for the key to cores.)

be significant, implying that the old settlement area had been flooded. In the eastern side of the enclosure, C160 was made through Ex 5, and C161 was made through Ex 6. In Ex 5, upper levels dating to the Third Intermediate Period (TIP), ca. 1000–800 BCE, were found to be upon a cemetery, perhaps of the New Kingdom, and contained disturbed material from the late Second Intermediate Period, ca. 1500 BCE; Ex 6 had a similar stratigraphy but was closely dated by TIP structures lying over early New Kingdom burials (ca. 1400 BCE). In the drill cores, there were several phases of settlement material from the ground surface, with changes in the matrices perhaps indicating phases of activity. The drill core information is useful in pinpointing the depths of archaeological material that are otherwise not possible to access. With better typologies of the pottery, it may be possible to have more confidence in dating the small, but numerous, fragments that have been collected from the drill cores, as has been done at Buto (Hartung et al., 2009, pp. 172–188) and at Thebes (Toonen et al., 2017). In C161, there was almost constant settlement debris to a depth of 8.88 m below the ground, suggesting long-lived and continuous human activity over a long period, especially allowing for the fact that the upper level begins at about 800 BCE, because any later settlement material has been removed. The deepest hand-drilled core in the enclosure area is C8, to a depth of 10.51 m at the edge of the eastern side of the Antiquities land (not illustrated). This core has deep strata of possible reworked anthropogenic material – which means that the layers are not so well defined, but there is good deal of pottery and other material – to 4.75 m and then alluvial layers or solid mud material in bands upon a thin layer of degraded pottery fragments at 7.8 to 8 m and compact alluvial levee clay to 10.5 m. It seems, therefore, that below the 8 m limit there is no anthropogenic material at the site, and we may regard this as the Neolithic boundary. Similarly, Man-

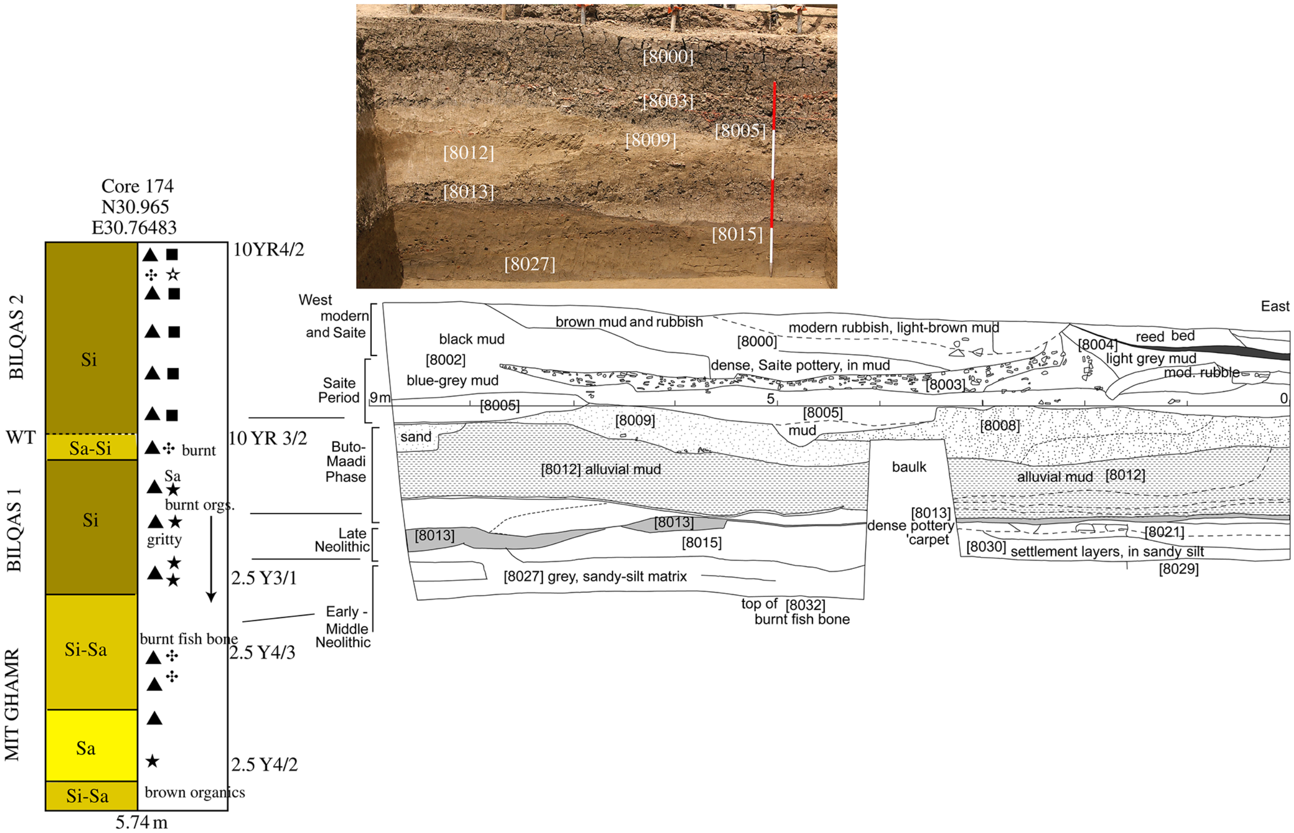

Figure 8. Correlation of archaeological strata in excavation 8 with drill core 174. Original data were taken from Angus Graham. (See Fig. 13 for the key to cores.)

soura cores E, to a depth of 11 m, and H10 (for location, see Fig. 2), to a depth of 16 m, detected anthropogenic material only in the upper 6 m of the cores.

5.2 Kawady sandhill and archaeology

A second archaeological zone is at Kawady (Ezbet Mohamed Ismail) to the northeast of the Saite area, where there is a buried sandhill (Figs. 2 and 3). According to theories of settlement patterns in Ancient Egypt, such a high-sand area should have provided an attractive place for settlement on the sides of the sandbank, with cemeteries being placed on the top to avoid the annual flooding. Excavations by the Egyptian Antiquities Service in 1961–1962 and 1965 discovered an elite cemetery area to the west of Kawady village, most likely consisting of a mausoleum structure that had contained limestone and basalt sarcophagi and a shrine to a local saint called Wahibre in the Saite period (Bakry, 1968). Drill cores in this area have located the sand lying relatively close to the surface, overlain by sandy silts that are often blue–black in colour (Fig. 11).

On top of these sands are strong anthropogenic signals from the ground level as far as the sand, suggesting that, indeed, this sandhill was an attractive area for human activity. In C20, C21 and C23, the stone debris in bands down to 1.5 m below the ground may correlate with the Saite elite cemetery area. Further work is needed on the identification of the pottery fragments to show whether this area was used from much earlier periods. The drill cores and vertical electrical soundings from villages further to the east at Shubra Tana, Kafr and Bahr el-Hamam also suggest that there is archaeological material at depth here. Although coring in all places has indicated human material culture in the upper layers, including observed Roman amphorae, deeper deposits have only been identified in Kafr el-Hamam C2 (G6) between 2 and 4 m, which may well be ancient, but it is unclear how ancient. The pattern of waterways, the positioning of settlements and the Roman–Late Roman material from some of the villages may suggest that this area was part of the irrigation system established during the Roman period in the area. As the system is visible in the current landscape, it cannot be very ancient, i.e. Late Roman or medieval at most, and is more likely from the 19th century during the irrigation projects from the Muhammad Ali era onwards.

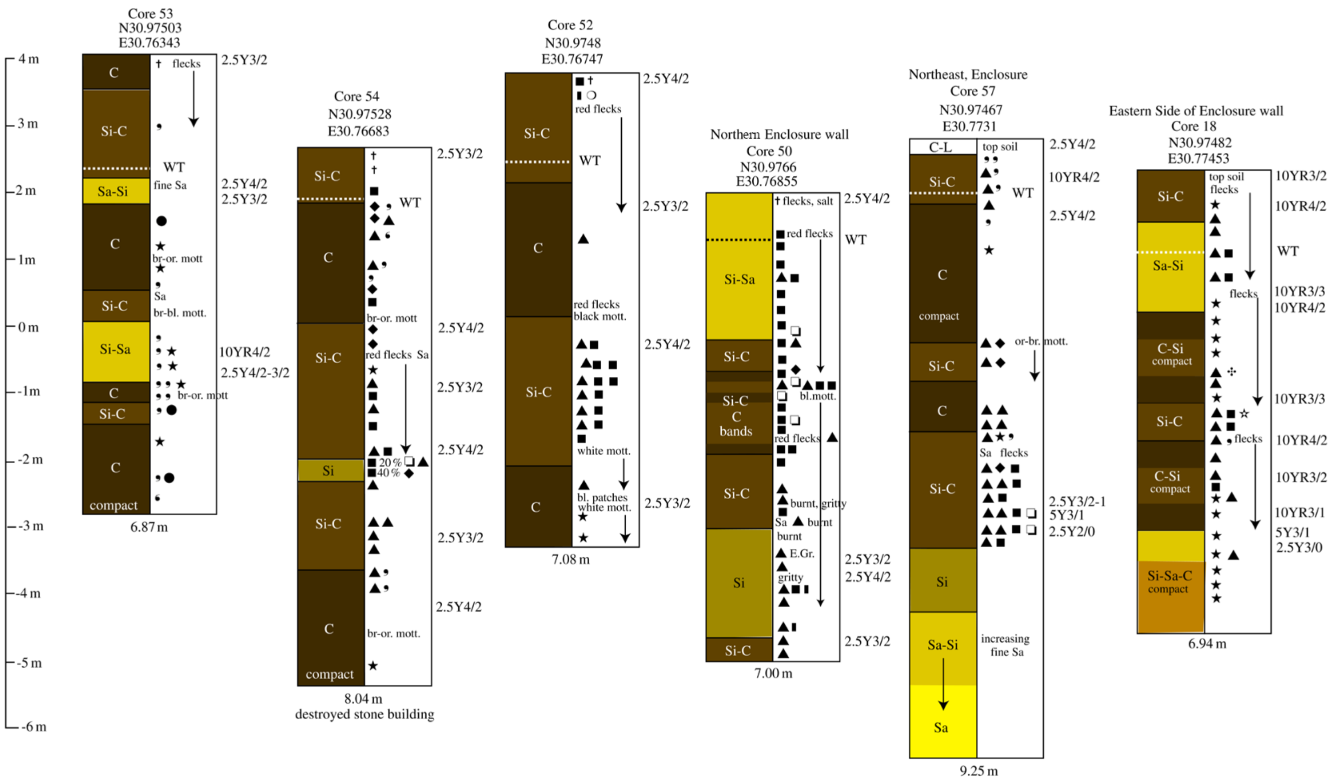

Figure 9. Transect of drill cores across the Northern Enclosure at Sa el-Hagar (C53, C54, C52, C50, C57 and C18) (see Fig. 13 for the key to cores).

5.3 A new southern settlement?

The geological reconstruction of the area to the southeast (Fig. 3) shows buried high ground that may also have been a focus for human activity that is no longer visible as an archaeological zone but can be detected in drill augers. Analysis of the core data has determined the following four types of core data at Sais: (1) human (anthropogenic) material culture (HMC) for the whole length of the drill core, with a high level of confidence that pottery, for example, had not dropped down into the borehole from the upper layers of the cores (Fig. 9, C50; Fig. 10, C161; Fig. 12, C155); (2) a layer of HMC at the top band, then a gap of alluvial material before a further buried band of HMC (Fig. 12, C143); (3) HMC in a strong or weak band in the top 1.2 m of the core (Fig. 12, C148); (4) strongly indicated HMC in the lower bands of the core. In the case of type (3), such cores can perhaps be taken cautiously as being the kind of archaeology they indicate. If the HMC content is weak and consists of top-soil-containing material from manuring or is in the modern town where settlement layers can be thick, then it may indicate relatively modern activity.

In the agricultural area south of Sa el-Hagar, type (2) drill auger cores, comprising two bands of HMC separated by alluvium, are evidenced by 25 drill cores in the area southeast of the village alone, mostly in the area that was flooded by the palaeochannel that moved to the west. In a transect across the area (Fig. 4 red dots; Fig. 12), the upper layers of human material culture, for example in C148, contain fired brick and sherds that may be from the Roman period and modern material. The settlement material in the lower core bands, for example C143 and C151, is overlain and on top of alluvium and channel deposits and is not easy to date due to the small size of the pottery fragments. The fact that the material is in dense bands, along with some charcoal and brown-orange mottling suggests that the anthropogenic material is a primary deposit, and it is also spread over a wide area. The presence of another archaeological zone at Sa el-Hagar raises questions about what would have been the settlement or even the urban constitution of ancient Sais. With areas in the north, in the Great Pit and under the modern village, and to the southeast and perhaps areas around Sais, the conurbation seems to be a loose federation of settlements, perhaps operating at slightly different chronological time frames, but suggesting a dynamic and changing urban catchment area that was responsive to changes in the alluvial character of the river and its branches.

6 Ancient topographies

There is a description of part of the topography of Sais from an inscription on a granite statue in the Greco-Roman

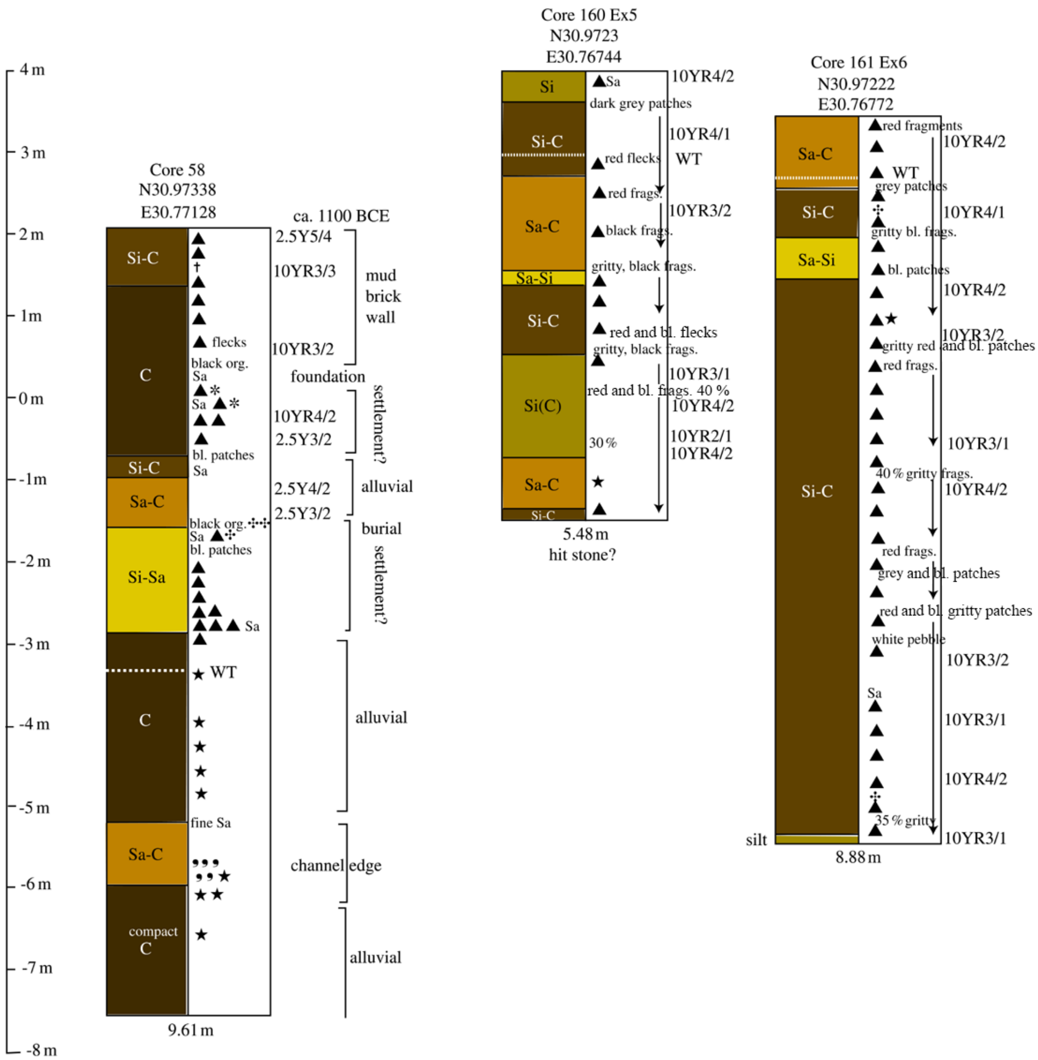

Figure 10. Drill cores in excavation trenches for Ex 1 (C58), Ex 5 (C160) and Ex 6 (C161) (see Fig. 13 for the key to cores).

museum in Alexandria (inventory no. 26532). The headless statue of man kneeling to present an offering table records the excavation of a lake at Sais by the "Administrator of the temples of Neith, Lector Priest, great Physician of Pharaoh, Royal Chancellor and Sole Companion Horkhebi" (Bakry, 1970; Geßler-Löhr, 1983, pp. 233–237). The decree from Ahmose II for the lake's construction was to enable water to be provided for purification purposes in the temple of Neith.

> I excavated the lake on the east side of the *Wuwu* Canal; its width was 68 cubits, its length of 65 cubits and built of [lime]stone, 8 stairways in it and walls around it.

The lake would have been a stone-lined structure with dimensions of around 34 by 32.5 m, perhaps like the sacred lake at the Dendera temple in upper Egypt, for example (it is about 25 by 35 m in size and lined with sandstone blocks). The location "east of the Double Canal" may suggest that a local canal system could feed water into the lake to keep the lake supplied. The writing with two quail chick signs between two canal signs has suggested the translation "Double Canal", but can the inscription be used to locate either the sacred lake or the "Double Canal"? And how does this fit within the geoarchaeological topography of Sais as a whole? The sacred lake should have been in the sacred enclosure area near the temple of Neith, which was most likely in the Northern Enclosure. In this case, the canal would be to the west of the enclosure and may have been in the channel noted there and described above. The lake would be somewhere in the area of the western part of the enclosure. Unfortunately, the inscription does not give enough information to be certain about where to look for the sacred lake, although the buried stone debris features noted above may, at some point in the future, prove to be indicators of some such feature. The ancient texts then provide details which cannot yet be verified

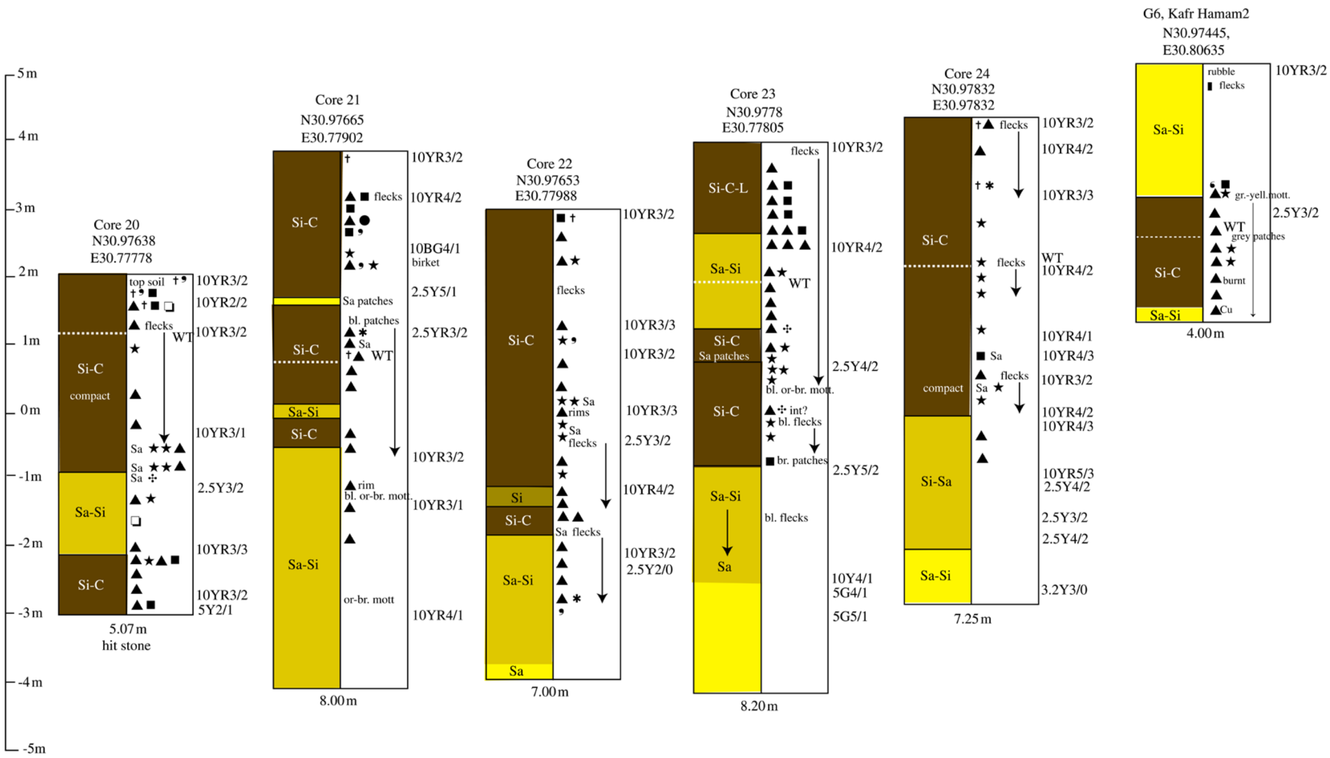

Figure 11. Transect in the Kawady elite cemetery area (C20, C21, C22, C23, C24 and KH2) (see Fig. 13 for the key to cores).

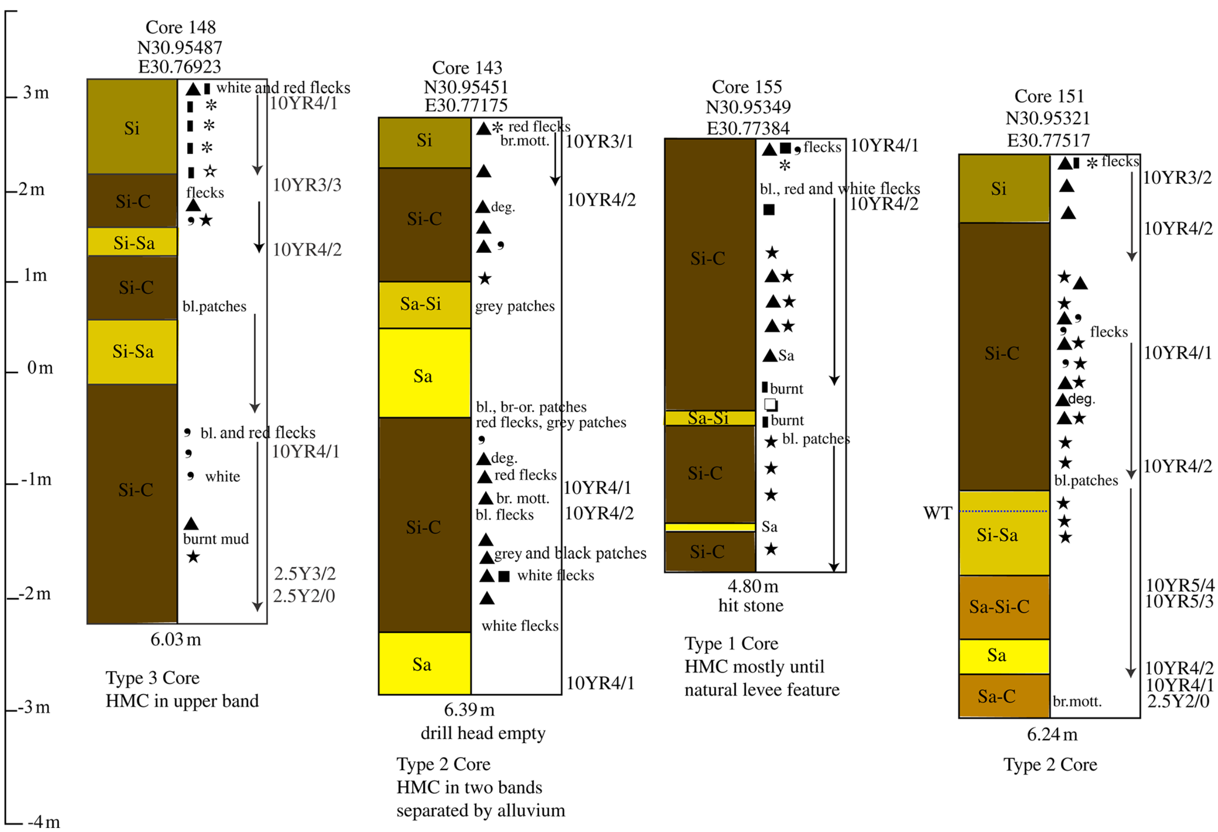

Figure 12. Transect south of Sa el-Hagar (C148, C143, C155 and C151) (see Fig. 13 for the key to cores).

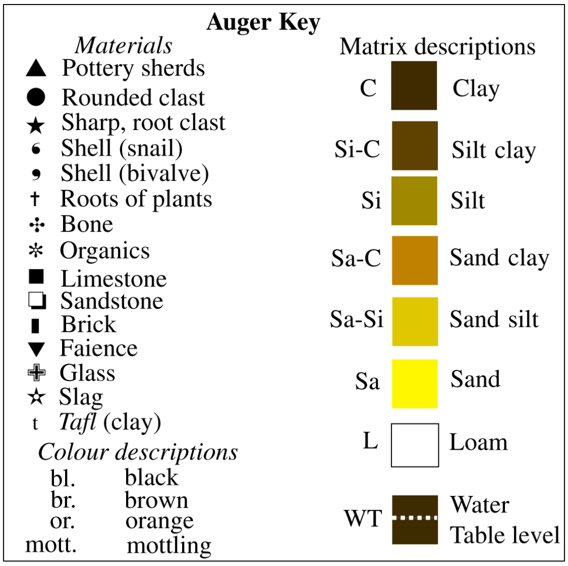

Figure 13. Key for the auger logs.

on the ground and, so, are limited in specific identifications of water features at Sais.

7 Summary

The analysis of the subsurface material contributes to understanding why the area at Sais area was suitable for sustained settlement. First, the underlying sand and channels of the meandering river system meant that there was always some high, non-flooded land available, either because it was naturally high or humanly managed so that it was high (settlement tell) and dry (mud brick enclosure), with high ground for a cemetery. Second, the period of the initiation of the deposition of the Bilqas mud was a decisive change in settlement and riverine exploitation at Sais. The old palaeochannel system with Neolithic settlement on the west bank of the channel was replaced by a more stable river system, with settlements on the east bank. Third, the Sais archaeological zone is extensive, with settlements changing their original locations in the area, being abandoned and then returning to previously inhabited places. The complex record therefore contains evidence of human reactions to larger environmental changes and proactive interventions in the construction of agricultural and settlement facilities.

By linking some of the archaeological material with geological data, it is possible to go some way towards understanding the components of a settled area, especially if it is buried under modern towns and agricultural land. A city like Sais may have consisted of, perhaps, numerous settlements at any one time that were distributed around the general area. In ancient times, such settlements may have been part of the estates controlled by Sais itself from the main temple zones, and together the settlements may have constituted an administrative unit. Further analysis of drill auger material, more targeted work in conjunction with floodplain geologists and dating and pollen analysis will yield significant information when collated and analysed. Most exciting is the potential for sites that have been mostly destroyed and removed to yield their information and further expand our knowledge of settlement patterns and the relationship with waterway dynamics in the Nile Delta floodplain.

Data availability. Data for the drill cores are available from the Archaeology Data Service at https://doi.org/10.5284/1081997 (Wilson, 2020).

The Landsat 5 imagery in Fig. 6 is part of the USGS Landsat 5 product (01198021202520009) from 14 February 1998, with 5 band wavelengths equal to 1.55 and 1.75. The radiometric gains and/or bias are equal to.0.1080784,−0.3700000.

Author contributions. PW compiled the article, maps and auger interpretations. HG carried out the deep-drill coring and VES work and interpretation.

Competing interests. The authors declare that they have no conflict of interest.

Special issue statement. This article is part of the special issue "Geoarchaeology of the Nile Delta". It is a result of the workshop "Geoarchaeology of the Nile Delta: Current Research and Future Prospects", Würzburg, Germany, 29–30 November 2019.

Acknowledgements. Thanks are due to the following people: the drill teams (Ahmed el Bishe, Esmaiein el Bishe and Ibrahim Darawy) and their supervisors (Daniel Lines, Joshua Trampier, Karen Exell, Shakira Christodoulou, Gregory Gilbert and Mohamed Gaber). The professors Adam El-Shahat, Hosni Ghazala, Mahmoud El-Gamili and Zeinab el-Sayed Belal and their teams from Mansoura University are thanked. For the discussions, we thank Benjamin Pennington, Angus Graham, Judith Bunbury, Willem Toonen and Israel Hinojosa-Baliño. For logistical support and local information, we extend our gratitude to the Ministry of Antiquities Tanta and Cairo, Inspectors Said el Assal, Emad el Shenawy and Fatma Ragab, the Egypt Exploration Society and Durham University.

Review statement. This paper was edited by Christopher Lüthgens and reviewed by Julia Meister and one anonymous referee.

References

Abrams, M. and Comer, D.: Multispectral and hyperspectral technology and archaeological applications, in: Mapping archaeological landscapes from space, edited by: Comer, D. C. and Harrower, M. J., Springer, New York, NY, 57–72, 2013.

Bakry, H. S.: A Family from Sais, Mitteilungen des Deutschen Archäologischen Instituts, Abteilung Kairo, 23, 69–74, 1968.

Bakry, H. S.: Two Saite Monuments of Two Master Physicians, Oriens Antiquus 9, 333–341, pl. XXXVIII–XL, 1970.

Barois, J.: Les irrigations en Égypte, first edn., librarie Polytechnique Ch. Béranger, Paris, 1904.

Bell, B.: Climate and the History of Egypt: the Middle Kingdom, Am. J. Archaeol., 79, 223–269, 1975.

El-Shahat, A., Ghazala, H., Wilson, P., and Belal, Z.: Lithofacies of the upper quaternary sequence of Sa el-Hagar area, Gharbiya Governorate, Nile Delta, Egypt, Journal of Geology and Geophysics, Mansoura University, 32, 79–110, 2005.

Geßler-Löhr, B.: Die heiligen Seen ägyptischer Tempel: ein Beitrag zur Deutung sakraler Baukunst im alten Ägypten, Hildesheimer Ägyptologische Beiträge, 21, Gerstenberg Verlag, Hildesheim, 1983.

Ghazala, H.: Landscape evolution during the Holocene at Sais Area based on the drilled boreholes and geoelectrical survey, unpublished report for the Sais Mission, 2005.

Ghazala, H., El-Shahat, A., Abdel Raouf, O., Wilson, P., and Belal, Z.: Geoelectrical investigations around Sa el-Hagar archaeological site, Gharbiya Governorate, Nile Delta, Egypt, Journal of Geology and Geophysics, Mansoura University, 32, 121–137, 2005.

Hartung, U., Ballet, P., Effland, A., French, P. G., Hartmann, R., Herbich, T., Hoffman, H., Hower-Tilmann, E., Kitagawa, C., Kopp, P., Kreibig, W., Lecuyot, G., Lösch, S., Marouard, G., Zink, A., Nerlich, A., Pithon, M.: Tell el-Fara'in – Buto. 10. Vorbericht, Mitteilungen des Deutschen Archäologischen Instituts, Abteilung Kairo 65, 172–188, 2009.

Hritz, C.: Contributions of GIS and Satellite-based Remote Sensing to Landscape Archaeology in the Middle East, J. Archaeol. Res., 22.3, 229–276, 2014.

Pennington, B. T.: Environmental Change in Deltaic Settings and the Emergence of Civilization. A study in palaeolandscape construction focussing on the mid-Holocene Nile Delta, available at: https://eprints.soton.ac.uk/424723/1/Ben_Pennington_PhD_Thesis_final_copy.pdf (last access: 13 May 2021), unpublished PhD Dissertation, Southampton University, Southampton, UK, 2017.

Pennington, B. T., Bunbury, J., and Hovius, N.: Emergence of Civilization, Changes in Fluvio-Deltaic Style and Nutrient Redistribution Forced by Holocene Sea-Level Rise, Geoarchaeology, 31, 194–210, 2016.

Pennington, B. T., Sturt, F., Wilson, P., Rowland, J., and Brown, A. G.: The fluvial evolution of the Holocene Nile delta, Quaternary Sci. Rev., 170, 212–231, https://doi.org/10.1016/j.quascirev.2017.06.017, 2017.

Pope, K. O. and Dahlin, B. H.: Ancient Maya Wetland Agriculture: New Insights from Ecological and Remote Sensing Research, J. Field Archaeol., 16.1, 87–106, 1989.

Toonen, W. H., Graham, A., Pennington, B. T., Hunter, M. A., Strutt, K. D., Barker, D. S., Masson-Berghoff, A., and Emery, V. L.: Holocene fluvial history of the Nile's west bank at ancient Thebes, Luxor, Egypt and its relation with cultural dynamics and basin-wide hydroclimatic variability, Geoarchaeology, 33, 273–290, 2017.

Ullmann, T., Nill, L., Schiestl, R., Trappe, J., Lange-Athinodorou, E., Baumhauer, R., and Meister, J.: Mapping buried paleogeographical features of the Nile Delta (Egypt) using the Landsat archive, E&G Quaternary Sci. J., 69, 225–245, https://doi.org/10.5194/egqsj-69-225-2020, 2020.

USGS: Fact Sheet 2015-3081, ver. 1.2, available at: https://pubs.usgs.gov/fs/2015/3081/fs20153081.pdf (last access: 18 May 2021), Landsat Earth Observation Satellites, 2020.

Vercoutter, J.: Semna South fort and the records of the Nile levels at Kumma, Kush: Journal of the Sudan Antiquities Service, 14, 125–164, 1966.

Wilson, P.: The Survey of Saïs (Sa el-Hagar), 1997–2002, Egypt Exploration Society, Excavation Memoir 77, Egypt Exploration Society, London, 2006.

Wilson, P.: Sais I: The Ramesside-Third Intermediate Period at Kom Rebwa, Egypt Exploration Society, Excavation Memoir 98, Egypt Exploration Society, London, 2011.

Wilson, P.: The Prehistoric Sequence at Sais: Temporal and Regional Connections, in: The Nile Delta as a centre of cultural interactions between Upper Egypt and the Southern Levant in the 4th millennium BC, edited by: Maczynska, A., Poznan Archaeological Museum, Poznan, Poland, 299–318, 2014.

Wilson, P., Gilbert, G., and Tassie, G.: Sais II: The Prehistoric Period, Egypt Exploration Society, Excavation Memoir 107, Egypt Exploration Society, London, 2014.

Wilson, P.: Royal City of Sais, York: Archaeology Data Service [distributor], https://doi.org/10.5284/1081997, 2020.

Wunderlich, J.: Untersuchungen zur Entwicklung des westlichen Nildeltas im Holozän, PhD thesis, Philipps-Universität, Marburg, West Germany, 1989.

Zhao, X., Thomas, I., Salem, A., Alassal, S., Liu, Y., Sun, Q., Chen, J., Fuwei, M., Finlayson, B., and Chen, Z.: Holocene climate change and its influence on early agriculture in the Nile Delta, Egypt, Paleogeography, Palaeoclimatology, Palaeoecology, 547, 109702, https://doi.org/10.1016/j.palaeo.2020.109702, 2020.

E&G Quaternary Sci. J., 70, 145–150, 2021
https://doi.org/10.5194/egqsj-70-145-2021

Open Access E&G Quaternary Science Journal

Express report

A first outline of the Quaternary landscape evolution of the Kashaf Rud River basin in the drylands of northeastern Iran

Azra Khosravichenar[1,2], Morteza Fattahi[3], Alireza Karimi[4], Hassan Fazeli Nashli[5], and Hans von Suchodoletz[2]

[1]Department of Human Evolution, Max Planck Institute for Evolutionary Anthropology, 04103 Leipzig, Germany
[2]Department of Geography, Leipzig University, 04103 Leipzig, Germany
[3]Institute of Geophysics, University of Tehran, Tehran 14155-6466, Iran
[4]Department of Soil Science, Faculty of Agriculture, Ferdowsi University of Mashhad, Mashhad 917794-8974, Iran
[5]Department of Archaeology, University of Tehran, Tehran 14155-6466, Iran

Correspondence: Azra Khosravichenar (azra_khosravichenar@eva.mpg.de)

Relevant dates: Received: 28 March 2021 – Revised: 29 April 2021 – Accepted: 7 May 2021 – Published: 2 June 2021

How to cite: Khosravichenar, A., Fattahi, M., Karimi, A., Fazeli Nashli, H., and von Suchodoletz, H.: A first outline of the Quaternary landscape evolution of the Kashaf Rud River basin in the drylands of northeastern Iran, E&G Quaternary Sci. J., 70, 145–150, https://doi.org/10.5194/egqsj-70-145-2021, 2021.

1 Introduction

Naturally fragile drylands are among the most sensitive regions to climate change and human activities. More than 80 % of Iran is drylands today, of which large parts represent human settlement centers (Amiri and Eslamian, 2010). Furthermore, the region forms a natural bridge between southwestern, southern, and central Asia for human groups that mainly used three main migration corridors throughout the Pleistocene and Early Holocene (Vahdati Nasab et al., 2013). To better deal with current and future geomorphological and ecological changes in this partly densely settled region and to better understand the geomorphic and paleoenvironmental background of former human dispersal, regional knowledge about such changes on longer centennial to millennial timescales is necessary. Whereas loess–paleosol sequences offer quite well-based information about Late Quaternary paleoenvironmental changes in northern Iran (Kehl, 2009; Lauer et al., 2017), such knowledge is still rather fragmentary for the drylands of eastern and northeastern Iran and is mostly limited to incomplete sediment records of playa lakes or alluvial fans (Walker and Fattahi, 2011; Fattahi and Walker, 2016).

Fluvial archives are very sensitive to climatic and base-level changes, tectonics, or human activity, making them valuable archives of former geomorphic and paleoenvironmental changes (Macklin and Lewin, 2008; Walker and Fattahi, 2011; Faust and Wolf, 2017; von Suchodoletz et al., 2015, 2018). Therefore, we recently studied the high mountain Kalshour catchment in northeastern Iran, with a size of some square kilometers, and linked fluvial activity with regional geomorphological and hydrological changes and global solar and temperature fluctuations (Khosravichenar et al., 2020). However, to obtain robust geomorphic and paleoenvironmental information for the larger region, studies of river systems with catchments of several hundreds to thousands of square kilometers are necessary (Faust and Wolf, 2017) but are still lacking for this region. To fill this gap and to offer future research perspectives for this region, we studied the Kashaf Rud River basin in northeastern Iran with a catchment of several thousand square kilometers during a field expedition in 2019 (Fig. 1). This drylands river basin formed part of a Pleistocene to Holocene human migration corridor, linking western and central Asia (Vahdati Nasab et al., 2013; Fig. 1). Our goal was to build up a first field-based outline of the Quaternary landscape evolution of the

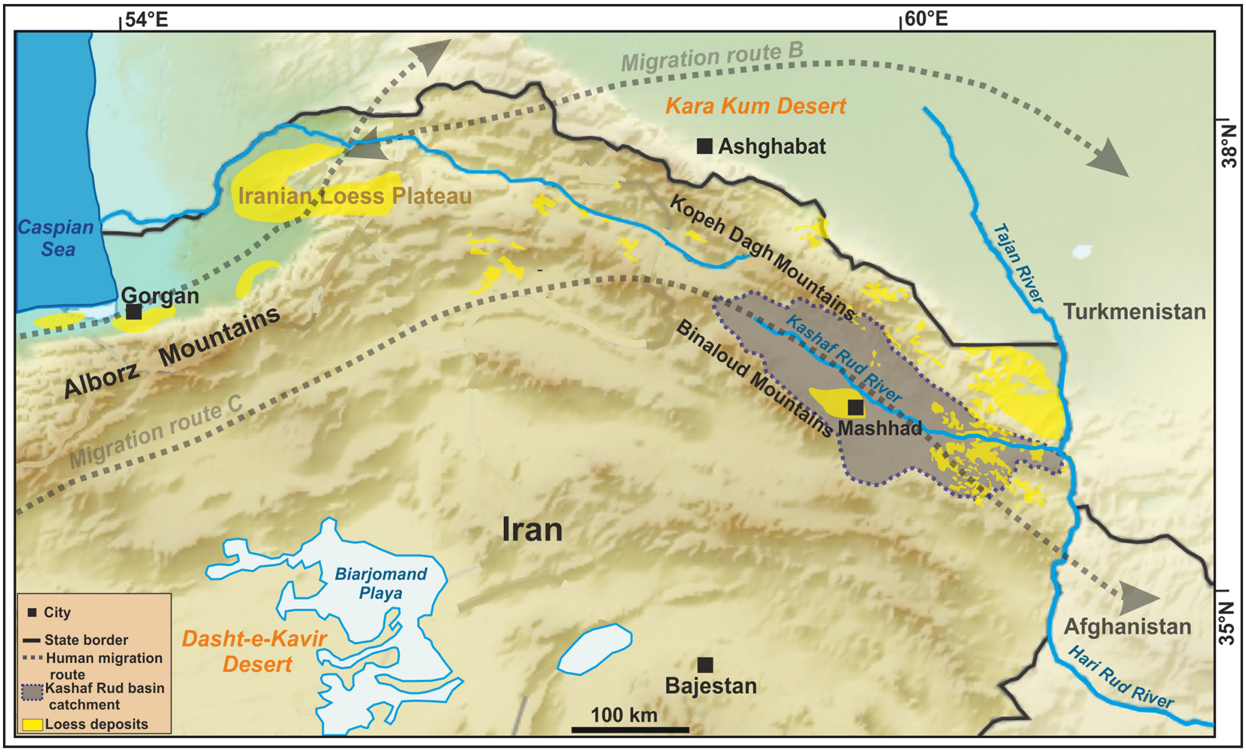

Figure 1. Location of the Kashaf Rud River basin (gray shaded area) in northeastern Iran (digital elevation model sources: GTOPO30, https://earthexplorer.usgs.gov, last access: 1 March 2020; ALOS PALSAR, https://vertex.daac.asf.alaska.edu, last access: 1 March 2020), with loess distribution (geological maps of Khorasan 1 : 1000 and 1 : 250 000; Lauer et al, 2017) and Pleistocene to Holocene human migration corridors B and C (Vahdati Nasab et al., 2013).

river basin to (i) demonstrate its good suitability as a fluvial archive for Late Quaternary geomorphic and paleoenvironmental changes in the drylands of eastern and northeastern Iran and (ii) offer a first diachronic geomorphic frame for human migrations in a largely unexplored former main human migration corridor (Fig. 1).

2 Study area and methods

The ca. 290 km long northwest–southeast flowing Kashaf Rud River has a catchment of ca. 16 800 km^2 and a mean annual discharge of ca. 0.64 $m^3\,s^{-1}$ (station Olang-e-Azadi 1992–2007; Regional Water Company of Khorasan Razavi; Fig. 2a). The regional climate is arid to semi-arid today (precipitation ca. 150–550 mm a^{-1}; https://globalweather.tamu.edu, last access: 1 March 2020). Large parts of the basin are currently covered with patchy loess and loess derivatives (Karimi et al., 2011; Fig. 1), and the basin formed part of Pleistocene to Holocene human migration corridor C of Vahdati Nasab et al. (2013; Fig. 1). Accordingly, Middle and especially Lower Paleolithic stone artifacts were found at several sites (Fig. 2a). In the course of the archeological investigations during the 1970s, the regional landscape context was also partly studied (Ariai and Thibault, 1975; Jamialahmadi et al., 2008).

We investigated a ca. 45 km long part of the river valley east of the city of Mashhad during a field expedition in 2019 and mapped the main geomorphological and sedimentological features. Here, the riverbed shows altitudes between 900 and 630 m a.s.l., and precipitation is around 250 mm a^{-1} (https://en.climate-data.org, last access: 1 March 2020).

3 Results

The studied part of the Kashaf Rud River valley is currently only sparsely vegetated, so its geomorphology and stratigraphical features are well recognizable. The current river flows in a deeply incised gorge-like valley (maximal width ca. 0.8–1.5 km; Fig. 2b). In agreement with the findings of Ariai and Thibault (1975), throughout most of the study area three main morphological terrace levels were observed that are largely naturally outcropped today, offering excellent conditions for geomorphological and sedimentological investigations (Fig. 3).

– *T-1.* In the lowest and youngest aggradational terrace level (surface ca. 2–4 m above current river bed; Figs. 2b, 3a, c, g, h), meters-thick, mostly yellowish to ochreous loamy to silty sediments overlie basal gravels and sand. We observed no paleosols within these sedi-

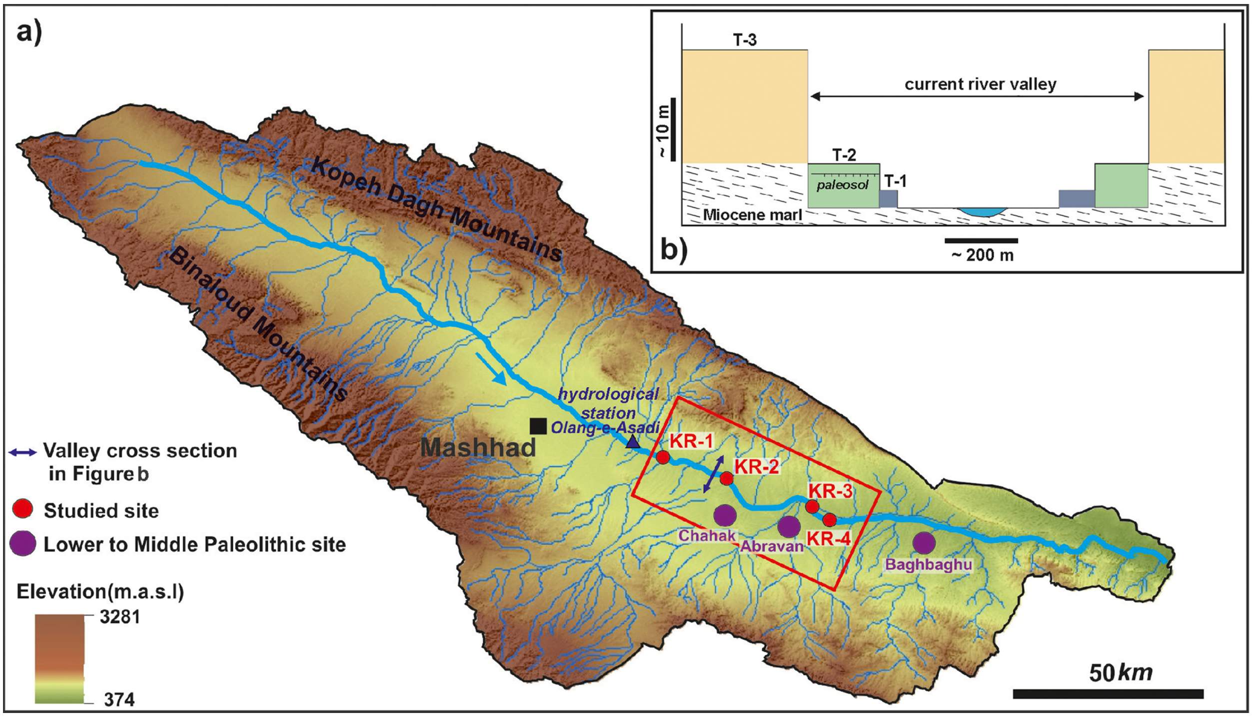

Figure 2. **(a)** The Kashaf Rud River basin with the study area (red rectangle) and Lower to Middle Paleolithic sites (Ariai and Thibault, 1975; Jamialahmadi et al., 2008). **(b)** Schematic cross section through the river valley between sites KR-1 and KR-2, with the different terrace levels (for the location, please see panel **a**).

ments, and the fluvial layers are often easily recognizable (Fig. 3h).

- *T-2*. In the middle aggradational terrace level (surface ca. 5–7 m above current river bed; Figs. 2b, 3a–g), meters-thick, mostly yellowish to ochreous loamy to silty sediments overlie basal gravels and sand. At most sites, the fluvial layers are easily recognizable (Fig. 3d). At site KR-1, one weak, slightly reddish and clayey paleosol was found (Fig. 3b). Furthermore, at site KR-3 a brownish clayey paleosol was found (Fig. 3e, f). At the latter site, the river flows in an artificial canal some 100 m north of the natural river bed (Fig. 3e). Here, the fluvial sediments are covered by up to > 1 m silty to gravelly sediments originating from the northern slope (Fig. 3e, f).

- *T-3*. In this highest and oldest aggradational terrace level (surface 40–50 m above current river bed; Figs. 2b, 3c, e, g), decameters-thick sediments, mostly consisting of partly solidified intercalated gravel, sand, and silt layers overlie Miocene marl (Fig. 3g inset). In the upper part, Lower Paleolithic finds were made by Ariai and Thibault (1975). This level was strongly incised when the deeply incised current valley was formed (Fig. 2b), and it marks the surface of a former flat valley with an extension of some kilometers.

4 Discussion and conclusions

By combining our field observations with former findings of Ariai and Thibault (1975), we reconstructed the main steps of the Quaternary landscape evolution of the Kashaf Rud River basin as follows:

i. *Multi-phased fluvial and lacustrine aggradation of gravelly, sandy and silty material in level T-3, indicating varying hydrological conditions in the Kashaf Rud River basin (Fig. 4a; Ariai and Thibault, 1975)*. This level must have shown a large extension and a relatively flat topography (Fig. 2b). The higher proportion of gravelly and especially sandy material compared with the following periods indicates a lower importance of silty loess in the landscape during that time. Although the archeological finds of Ariai and Thibault (1975) from the upper part of these sediments were not numerically dated, they are comparable to east African Oldowan tool collections. Therefore, the sediments of terrace level T-3 must have been aggraded during the Early Quaternary.

ii. *Fluvial incision of T-3 (Fig. 4b)*. Given that following level T-2 was aggraded at least from the current river bed, the incision reached down at least to this level. The deep incision shaped the current gorge-like river valley.

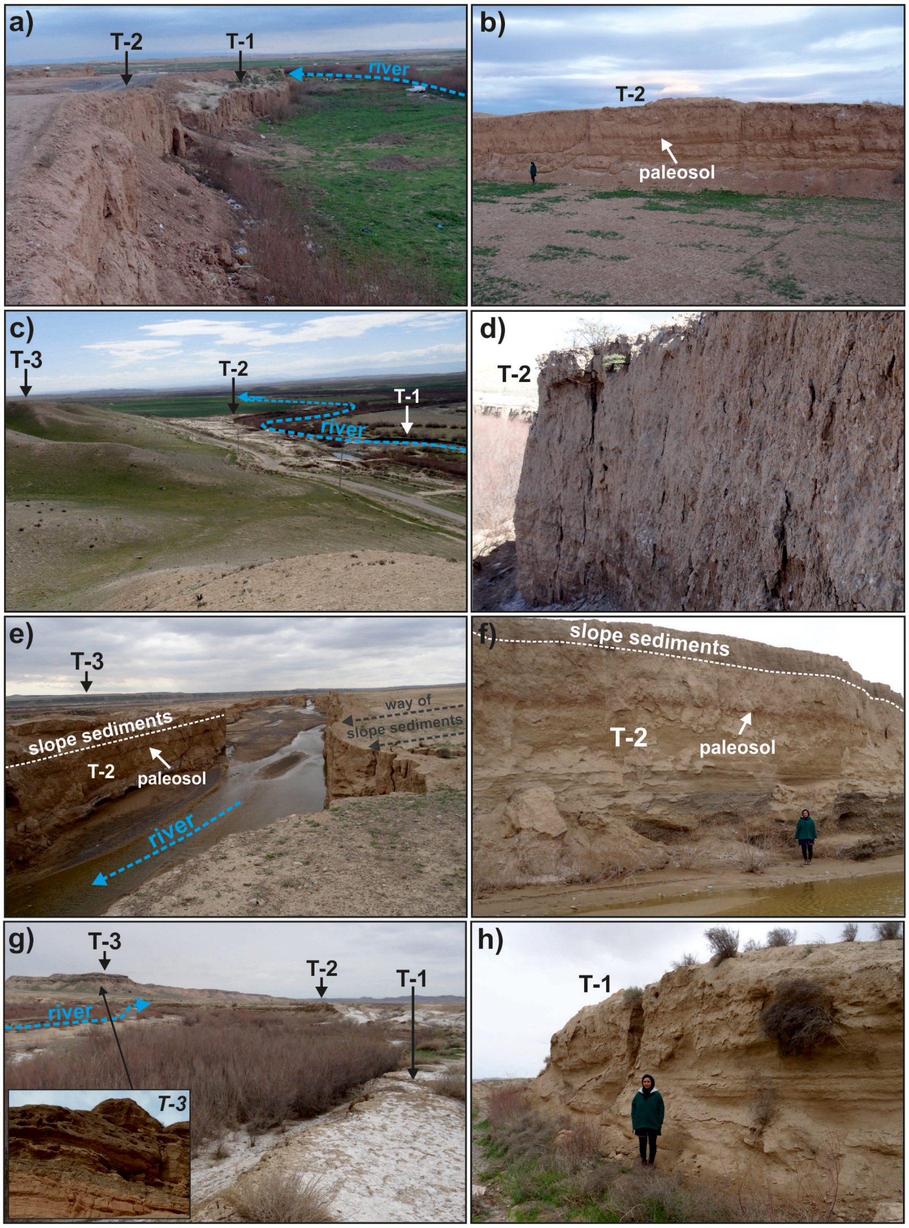

Figure 3. **(a, b)** Site KR-1 (36°14′1.32″ N, 59°55′32.04″ E) shows the two mainly silty terrace levels T-1 and T-2, with at least one weak paleosol in the sediments of T-2 **(b)**. **(c, d)** Site KR-2 (36°10′34.60″ N, 60°4′3.45″ E) shows the two mainly silty terrace levels T-1 and T-2 and terrace level T-3. In level T-2, the fluvial layers are still easily visible **(d)**. **(e, f)** Site KR-3 (36°10′34.60″ N, 60°4′3.45″ E) shows the mainly silty terrace level T-2. Anthropogenic activity diverted the river bed some 100 m towards the north, where it forms a steep 7–9 m deep canyon today. Here, the fluvial sediments of T-2 show a well-developed paleosol and are overlain by up to > 1 m thick gravelly to silty slope sediments. **(g, h)** Site KR-4 (36°4′33.35″ N, 60°18′39.63″ E) shows the two mainly silty terrace levels T-1 and T-2 and the gravelly to silty level T-3. The fluvial layers are still easily visible in T-1 **(h)**. The inset in panel **(g)** shows the detail of the sediments in level T-3.

iii. *Multi-phased fluvial aggradation of level T-2 (Fig. 4c).* The dominance of yellowish to ochreous loamy to silty sediments suggests that they mainly originate from eolian loess that is found in the catchment today (Fig. 1) and shows similar grain sizes and colors (Karimi et al., 2011; Lauer et al., 2017). Loess deposition in northern Iran is known since the Middle Pleistocene (Kehl, 2009). Consequently, we suggest that level T-2 has been deposited since that time. During certain periods, the loess deposits in the river basin must have been strongly reworked by fluvial processes so that they were accumulated as fluvial sediments in the main river valley. Accordingly, Karimi et al. (2011) observed Late Pleistocene periods of strong fluvial reworking of loess de-

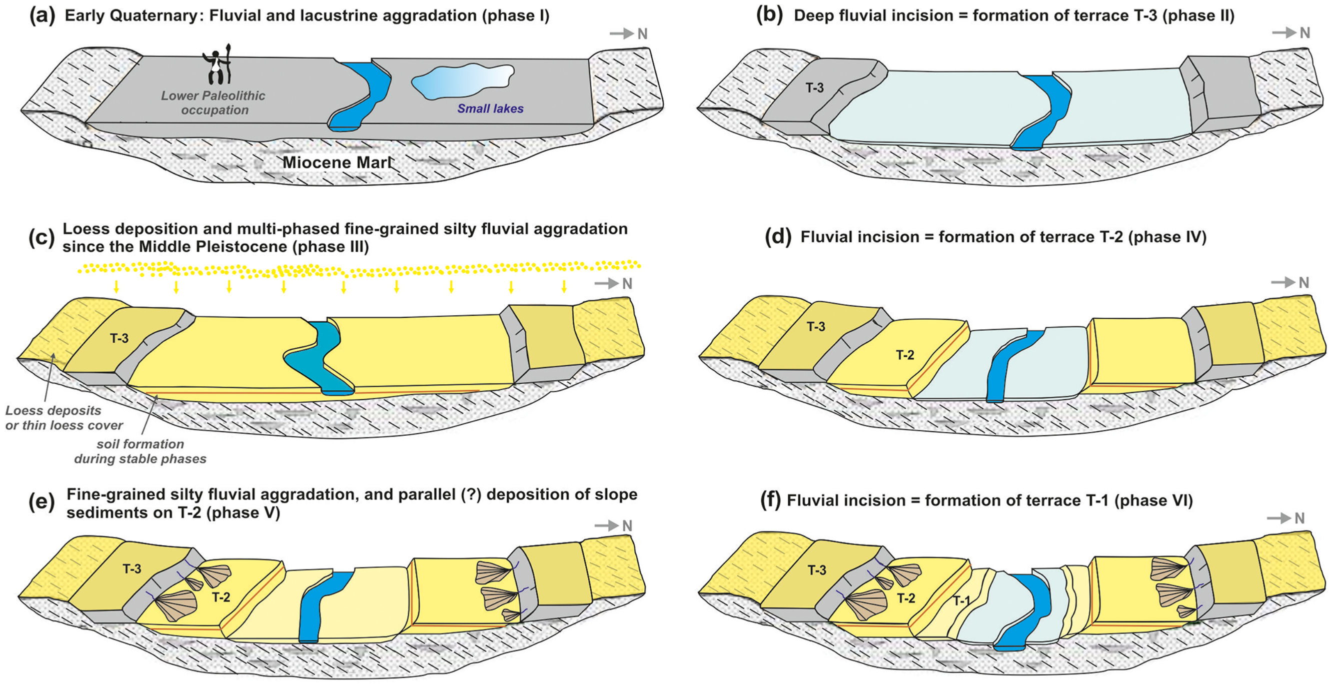

Figure 4. Compiled Quaternary landscape evolution of the Kashaf Rud River basin.

posits in the southwestern part of the Kashaf Rud River basin. At sites KR-1 and KR-3, at least one paleosol was observed in the sediments of level T-2. Therefore, aggradation must have encompassed different phases that were interrupted by at least one period of floodplain stability with soil formation (von Suchodoletz et al., 2018).

iv. *Fluvial incision of T-2 (Fig. 4d).* Given that following level T-1 was aggraded at least from the current river bed, the incision reached down at least to this level.

v. *Fluvial aggradation of level T-1, and coverage of level T-2 by slope deposits (Fig. 4e).* Similar to level T-2, in level T-1 mostly yellowish to ochreous loamy to silty loess-borne sediments were aggraded. Furthermore, a strong erosional landscape dynamic is indicated by slope deposits that cover the fluvial sediments of level T-2 at site KR-3 (Fig. 3e, f). Based on our current knowledge, it is not clear whether these two processes were concomitant.

vi. *Fluvial incision of level T-1 (Fig. 4f).* This incision formed the current river bed.

Terrace levels T-1–T-3 are just morphological forms, so similar levels in different parts of the valley could potentially have been aggraded during different phases (von Suchodoletz et al., 2015; Kolb et al., 2016). Therefore, the Quaternary evolution of the Kashaf Rud River basin must have been much more complex than outlined here. However, already our first field-based findings demonstrate significant geomorphic changes in the basin during the Quaternary. Besides long-term environmental changes, these were possibly also linked with reactions of the river system towards relatively rapid Late Pleistocene and Holocene global climate changes (Macklin and Lewin, 2008). In this context, it remains an open question how far such processes influenced human migrations and activities in human migration corridor C (Fig. 1).

Generally, our field-based results demonstrate the high potential of the well-outcropped sediments in the Kashaf Rud River basin as archives for Late Quaternary geomorphic and linked paleoenvironmental changes in the drylands of eastern and northeastern Iran that must also have influenced human migrations and activities in this region. Specifically, given the high silt content of terrace levels T-1 and T-2, these potentially form complementary sediment archives to formerly studied regional loess–paleosol sequences (Karimi et al., 2011; Lauer et al., 2017); that is, in case of erosion of the loess, corresponding fluvial sediments should have been deposited in the Kashaf Rud River valley. Therefore, more detailed studies of the sediments in the Kashaf Rud river basin, using analytical methods, such as numerical dating and paleoecological analyses, are necessary to contribute to geomorphological, paleoenvironmental, and geoarcheological research, filling a significant knowledge gap in this largely unexplored region.

Data availability. No data sets were used in this article.

Author contributions. AzK, MF and HvS planned and carried out the fieldwork. AlK contributed to the information on regional loess and HFN on regional archaeology.

Competing interests. The authors declare that they have no conflict of interest.

Acknowledgements. We thank Mohamed Fatemi (Mashhad), Ulrich Göres (Dresden) and Klaus von Suchodoletz (Ballwitz) for their help during fieldwork.

Financial support. The article processing charges for this open-access publication were covered by the Max Planck Society.

Review statement. This paper was edited by Julia Meister and reviewed by one anonymous referee.

References

Amiri, M. J. and Eslamian, S. S.: Investigation of climate change in Iran, Journal of Environmental Science and Technology, 3, 208–216, 2010.

Ariai, A. and Thibault, C.: Nouvelles precisions a propos de l'outillage paléolithique ancient sur galets du Khorassan (Iran), Paléorient, 3, 101–108, 1975.

Fattahi, M. and Walker, R.: Optical dating of Holocene lake bed sediments of the Nimbluk Plain, Khorasan, Northeast Iran: Implications for the climate change and palaeoenvironment, Journal of the Earth and Space Physics, 41, 1–12, 2016.

Faust, D. and Wolf, D.: Interpreting drivers of change in fluvial archives of the Western Mediterranean – A critical view, Earth-Sci. Rev., 174, 53–83, https://doi.org/10.1016/j.earscirev.2017.09.011, 2017.

Jamialahmadi, M., Vahdati Nasab, H., Fazeli Nashli, H., and Beshkani, A.: Kashafrud revisited: discovery of new Palaeolithic sites in north-eastern Iran. Antiquity 82, project gallery, available at: http://www.antiquity.ac.uk/projgall/nasab317 (last access: 10 February 2021), 2008.

Karimi, A., Frechen, M., Khademi, H., Kehl, M., and Jalalian, A.: Chronostratigraphy of loess deposits in northeast Iran, Quat. Int., 234, 124–132, https://doi.org/10.1016/j.quaint.2009.08.002, 2011.

Kehl, M.: Quaternary climate change in Iran – the state of knowledge, Erdkunde, 63, 1–17, https://doi.org/10.3112/erdkunde.2009.01.01, 2009.

Khosravichenar, A., Fattahi, M., Amini, H., and von Suchodoletz, H.: The potential of small mountain river systems for paleoenvironmental reconstructions in drylands – an example from the Binaloud Mountains in northeastern Iran, Geosciences, 10, 448, https://doi.org/10.3390/geosciences10110448, 2020.

Kolb, T., Fuchs, M., and Zöller, L.: Deciphering fluvial landscape evolution by luminescence dating of river terrace formation: A case study from Northern Bavaria, Germany, Suppl., Z. Geomorphol., 60, 29–48, 2016.

Lauer, T., Vlaminck, S., Frechen, M., Rolf, C., Kehl, M., Sharifi, J., Lehndorff, E., and Khormali, F.: The Agh Band loess-paleosol sequence – A terrestrial archive for climatic shifts during the last and penultimate glacial-interglacial cycles in a semiarid region in northern Iran, Quat. Int., 429, 13–30, https://doi.org/10.1016/j.quaint.2016.01.062, 2017.

Macklin, M. G. and Lewin, J.: Alluvial responses to the changing Earth system, Earth Surf. Proc. Land., 33, 1374–1395, https://doi.org/10.1002/esp.1714, 2008.

Vahdati Nasab, H., Clark, G. A., and Torkamandi, S.: Late Pleistocene dispersal corridors across the Iranian Plateau: A case study from Mirak, a Middle Paleolithic site on the northern edge of the Iranian Central desert (Dasht-e Kavir), Quat. Int., 300, 267–281, https://doi.org/10.1016/j.quaint.2012.11.028, 2013.

von Suchodoletz, H., Menz, M., Kühn, P., Sukhishvili, L., and Faust, D.: Fluvial sediments of the Algeti River in southeastern Georgia - An archive of Late Quaternary landscape activity and stability in the Transcaucasian region, Catena, 130, 95–107, https://doi.org/10.1016/j.catena.2014.06.019, 2015.

von Suchodoletz, H., Zielhofer, C., Hoth, S., Umlauft, J., Schneider, B., Zeeden, C., Sukhishvili, L., and Faust, D.: North Atlantic influence on Holocene flooding in the southern Greater Caucasus, Holocene, 28, 254–269, https://doi.org/10.1177/0959683617735584, 2018.

Walker, R. T. and Fattahi, M.: A framework of Holocene and Late Pleistocene environmental change in eastern Iran inferred from the dating of periods of alluvial fan abandonment, river terracing, and lake deposition, Quat. Sci. Rev., 30, 1256–1271, https://doi.org/10.1016/j.quascirev.2011.03.004, 2011.

E&G Quaternary Sci. J., 70, 151–164, 2021
https://doi.org/10.5194/egqsj-70-151-2021

Open Access E&G Quaternary Science Journal

Research article

Reconstruction of former channel systems in the northwestern Nile Delta (Egypt) based on corings and electrical resistivity tomography (ERT)

Marina Altmeyer[1], Martin Seeliger[1], Andreas Ginau[1], Robert Schiestl[2], and Jürgen Wunderlich[1]

[1]Department of Physical Geography, Goethe University Frankfurt, Frankfurt a. M., 60438, Germany
[2]Department of Ancient History, Ludwig Maximilian University of Munich, Munich, 80539, Germany

Correspondence: Marina Altmeyer (marina.altmeyer@gmx.de)

Relevant dates: Received: 30 September 2020 – Revised: 30 March 2021 – Accepted: 16 April 2021 – Published: 18 June 2021

How to cite: Altmeyer, M., Seeliger, M., Ginau, A., Schiestl, R., and Wunderlich, J.: Reconstruction of former channel systems in the northwestern Nile Delta (Egypt) based on corings and electrical resistivity tomography (ERT), E&G Quaternary Sci. J., 70, 151–164, https://doi.org/10.5194/egqsj-70-151-2021, 2021.

Abstract: The current state of research about ancient settlements within the Nile Delta allows the hypothesizing of fluvial connections to ancient settlements all over the Nile Delta. Previous studies suggest a larger Nile branch close to Kom el-Gir, an ancient settlement hill in the northwestern Nile Delta. To contribute new knowledge to this little-known site and prove this hypothesis, this study aims at using small-scale paleogeographic investigations to reconstruct an ancient channel system in the surroundings of Kom el-Gir. The study pursues the following: (1) the identification of sedimentary environments via stratigraphic and portable X-ray fluorescence (pXRF) analyses of the sediments, (2) the detection of fluvial elements via electrical resistivity tomography (ERT), and (3) the synthesis of all results to provide a comprehensive reconstruction of a former fluvial network in the surroundings of Kom el-Gir. Therefore, auger core drillings, pXRF analyses, and ERT were conducted to examine the sediments within the study area. Based on the evaluation of the results, the study presents clear evidence of a former channel system in the surroundings of Kom el-Gir. Thereby, it is the combination of both methods, 1-D corings and 2-D ERT profiles, that derives a more detailed illustration of previous environmental conditions which other studies can adopt. Especially within the Nile Delta which comprises a large number of smaller and larger ancient settlement hills, this study's approach can contribute to paleogeographic investigations to improve the general understanding of the former fluvial landscape.

Kurzfassung: Der derzeitige Stand der Forschung über antike Siedlungen im Nildelta erlaubt es, Hypothesen fluvialer Verbindungen zu antiken Siedlungen im gesamten Nildelta aufzustellen. Frühere Studien deuten auf einen größeren Nilarm in der Nähe des Kom el-Girs, einem antiken Siedlungshügel im nordwestlichen Nildelta, hin. Um neue Erkenntnisse zu dieser wenig bekannten Stätte zu gewinnen und diese Hypothese zu beweisen, zielt diese Studie auf kleinräumige paläogeographische Untersuchungen zur Rekonstruktion eines antiken Kanal-/Rinnensystems in der Umgebung des Kom el-Girs ab. Die Studie verfolgt: (1) die Identifizierung von Sedimentationsmilieus mittels stratigraphischer und pXRF-

Analysen, (2) den Nachweis fluvialer Strukturen mittels elektrischer Widerstandsmessung (ERT) und (3) die Synthese aller Ergebnisse, um eine umfassende Rekonstruktion eines ehemaligen fluvialen Netzwerkes in der Umgebung des Kom el-Girs zu erstellen. Dazu wurden Rammkernsondierungen, pXRF-Analysen und elektrische Widerstandsmessungen (ERT) durchgeführt, um die Sedimente innerhalb des Untersuchungsgebietes zu beschreiben. Die Auswertung der Ergebnisse zeigt deutliche Hinweise auf ein ehemaliges Kanal-/Rinnensystem in der Umgebung des Kom el-Girs. Dabei ist es die Kombination beider Methoden, der 1D-Bohrungen und 2D-ERT-Profile, die eine detailliertere Darstellung früherer Umweltbedingungen ermöglicht und die von anderen Studien übernommen werden kann. Besonders im Nildelta mit seiner großen Anzahl kleinerer und größerer antiker Siedlungshügel, kann der Ansatz dieser Studie in weiteren paläogeographischen Untersuchungen Anwendung finden, um das allgemeine Verständnis ehemaliger Flusslandschaften zu verbessern.

1 Introduction

The Nile Delta (Fig. 1) has been settled and cultivated since the Neolithic period as the earliest known archeological remains within the delta from ca. 4530 BCE reveal (Butzer, 2002). The connection of ancient settlements to former Nile branches is considered an essential factor for the vitality of a settlement to supply people and animals with fresh water, to irrigate fields, or as a connection to the transport system (Bietak, 1975; Lange et al., 2016; Schiestl, 2018; Ginau et al., 2019). Therefore, elevated levees or relict dunes near watercourses offered favorable conditions to settle due to the combination of assured protection from the annual Nile flood while providing access to water supply (Wunderlich, 1989; El Gamili et al., 2001; Schiestl, 2018). Based on a high-resolution TanDEM-X image, Ginau et al. (2019) presented the first detailed illustration of a former fluvial landscape (Fig. 2) in the regional context of the northwestern Nile Delta. Kom el-Gir (KeG), an ancient settlement site in the area of interest (Figs. 2, 3), presumably represents a favored place with a hypothesized connection to a larger former Nile branch (Schiestl, 2019). To prove this assumption, this study aims to explore the subsurface sediments in the surroundings of KeG to obtain a comprehensive view of the paleoenvironmental conditions in this area. In this context, core drillings are widely adopted for scientific investigations into paleoenvironmental reconstructions (Marriner et al., 2012; Pint et al., 2015; Morhange et al., 2016; Seeliger et al., 2018). In addition to core drillings, electrical resistivity tomography (ERT) offers great opportunities for near-subsurface investigations in general (Toonen et al., 2018; Wunderlich et al., 2018) and was previously applied within the Nile Delta (El Gamili et al., 1994, 2001).

Therefore, the study applies a combination of methods to

1. identify and classify sedimentary environments (e.g., riverbed/channel, floodplain) via coring followed by portable X-ray fluorescence (pXRF) analyses of sampled sediments
2. detect fluvial elements (e.g., channel, levee, floodplain) along transects via electrical resistivity tomography (ERT)
3. interpret and correlate all results to combine the point-like coring data with the two-dimensional data of the ERT in order to derive a reconstruction of a former channel system.

2 Study area

2.1 Geographical setting

KeG is located in the northwestern Nile Delta, approx. 20 km south of Lake Burullus and 16 km east of the Rosetta branch (Figs. 1, 2). It represents a former settlement hill with a present-day extent of approx. 20 ha and a maximum elevation of ca. 5 m above the Nile Delta floodplain.

The lithology of the Nile Delta floodplain is characterized by alluvial accumulations dominated by late Neo-Nile deposits (Bilqas Formation), which are overlying the Pre-Nile sediments (Mit Ghamr Formation) at greater depths (Rizzini et al., 1978; Pennington et al., 2017; Gebremichael et al., 2018). Today's uppermost deposits, the so-called Nile mud, represent aggrading clastic sediments that mainly originated as Nile alluvium from the Ethiopian Highlands during the Holocene. Within the delta, the predominantly clayey and silty sediments reach a thickness of 10–15 m (Andres and Wunderlich, 1986; Wunderlich, 1988, 1989; Woodward et al., 2015; Ginau et al., 2019). These sediments overlie deposits, which mainly consist of fine to medium sands. They are distinguished from the overlying sediments by lighter colors and the appearance of a post-sedimentary lime formation within the upper section. This lime formation was dated by Wunderlich (1989) and verified the sedimentation during the Pleistocene (Wunderlich, 1989; El Gamili et al., 1994).

2.2 Historical background of KeG

Recent investigations of the *kom*'s area and pottery from the surface and from corings on the site date the settlement from

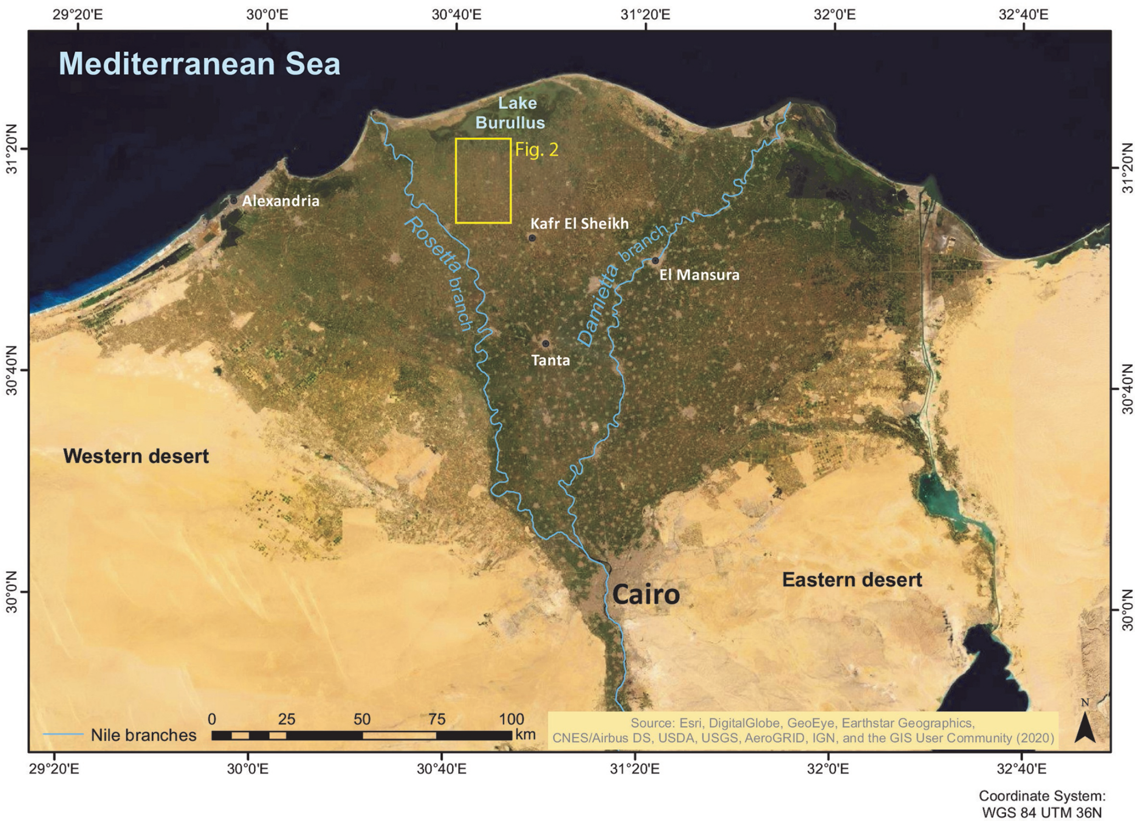

Figure 1. Regional area of interest (yellow frame) located in the northwestern Nile Delta.

the Ptolemaic (late 4th–1st century BCE) to the Late Roman period (4th–7th century CE) (Schiestl, 2012; Schiestl and Herbich, 2013; Schiestl, 2019). Investigations via magnetic prospection further revealed a densely occupied settlement covered with buildings 8 to 10 m wide as well as additional bigger enclosures. Those are interpreted as a temple enclosure and a Late Roman fort (Schiestl and Rosenow, 2016). Within the Nile Delta, it is the first archeological evidence for the existence of a Roman fort (Schiestl and Herbich, 2013; Schiestl, 2015, 2019). As transport by ship was common during those days, the presumed function and given knowledge about the founding of former settlements support the hypothesis that KeG was connected to a substantial watercourse (Ginau et al., 2019; Schiestl, 2019).

3 Material and methods

To combine and correlate the results of all applied methods, lateral and vertical changes in the subsurface sediment stratigraphy were investigated performing auger core drillings, followed by pXRF analyses of the core sediments as well as electrical resistivity tomography (ERT) measurements.

3.1 Geoarcheological fieldwork

Auger core drillings were performed using a vibracorer (Wacker EH 23/230) with open steel auger heads of 8, 6, and 5 cm diameter and 1 m length. The drillings reached a maximum depth of 11 m. These recorded the Holocene sedimentary sequence, which normally has a thickness of less than 10 m (Wunderlich and Andres, 1991). The positions of each drilling location to the north and east of KeG (Fig. 3) were based on prior investigations of Ginau et al. (2019) and measured using a global navigation satellite system (Topcon GR-5, accuracy of ≤ 2 cm in all three dimensions). The altitude given in m a.s.l. (meters above recent sea level) is based on the local reference system, established by the German Archaeological Institute (in German, Deutsches Archäologisches Institut – DAI) and its excavation team of Buto (Ginau et al., 2019). Retrieved sediments were lithologically described via grain size and lime content (10 % HCl) estimations according to German soil classification (Ad-Hoc-AG Boden, 2005). In addition to this, color (Munsell soil color charts) and special findings (ceramic fragments, mollusks, shell fragments, charcoal, plant remains, etc.) were documented. Based on the specific sedimentological characteristics of the core material, bulk samples for laboratory analyses were taken from the open sediment cores.

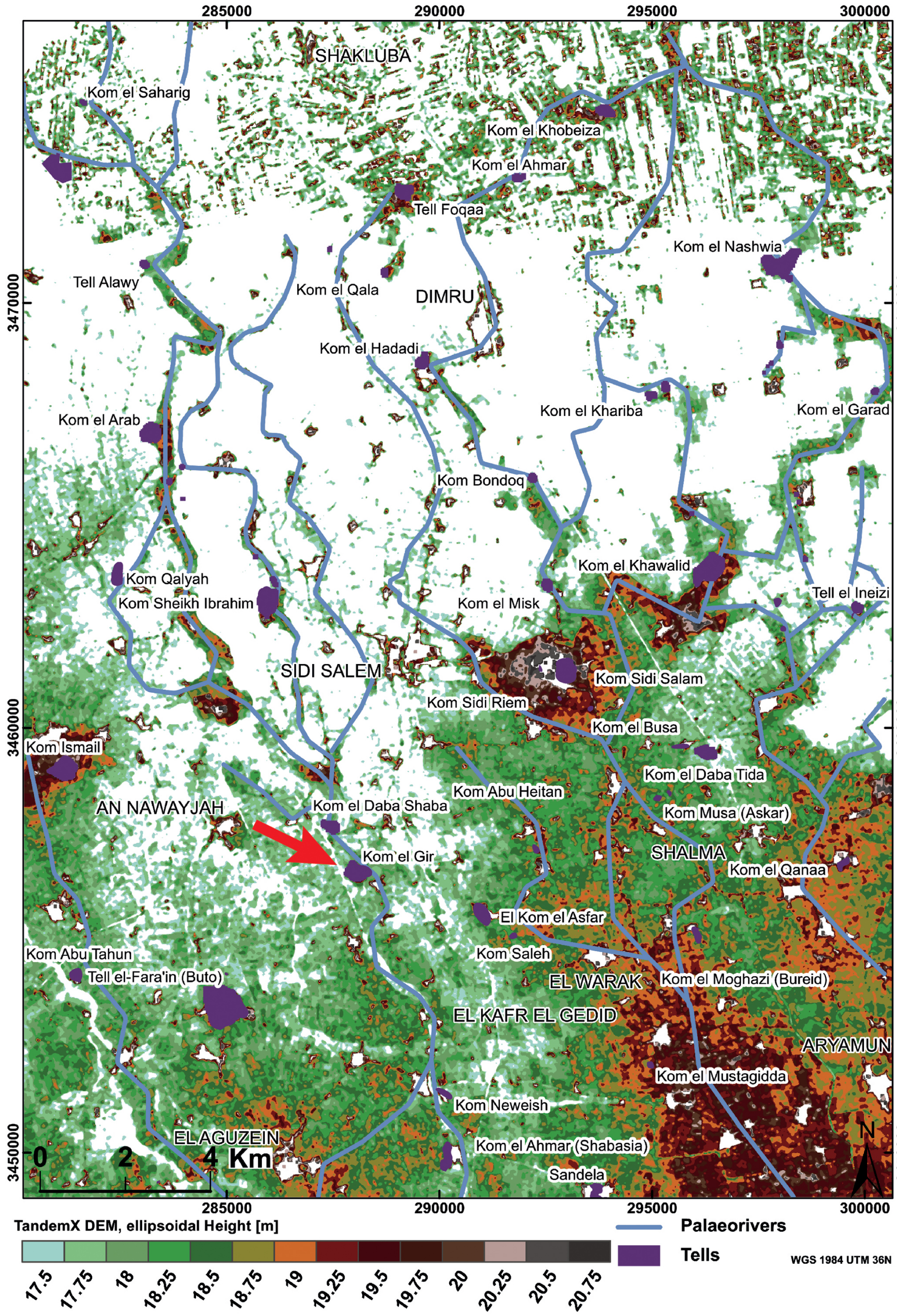

Figure 2. TanDEM-X image of the regional area of interest in the northwestern Nile Delta. The red arrow highlights Kom el-Gir (Ginau et al., 2019; German Aerospace Center).

3.2 Geochemical analysis via pXRF

All sample preparation procedures for the subsequent pXRF analyses adhered to a standardized process flow to reduce the influences on the samples, especially due to missing laboratory facilities and equipment on-site. For each core sample, a reduced sediment mass representing a mix of the overall sample was dried in an oven at 100 °C for at least 12 h. To produce a homogenous, fine-grained powder, the dried samples were ground in an agate mortar. Through this approach, the results of the conducted pXRF analysis are representative and a true achievement of the respective geochemical signals of the sample is ensured. The ground sample powder was packed into a special XRF plastic cylinder and coated with a 4 µm thick XRF foil that allows the best penetration of the fluorescence radiation (Ginau et al., 2019). The sediment samples were analyzed using a Niton XL3t 980-He portable XRF (pXRF) device equipped with an Ag anode.

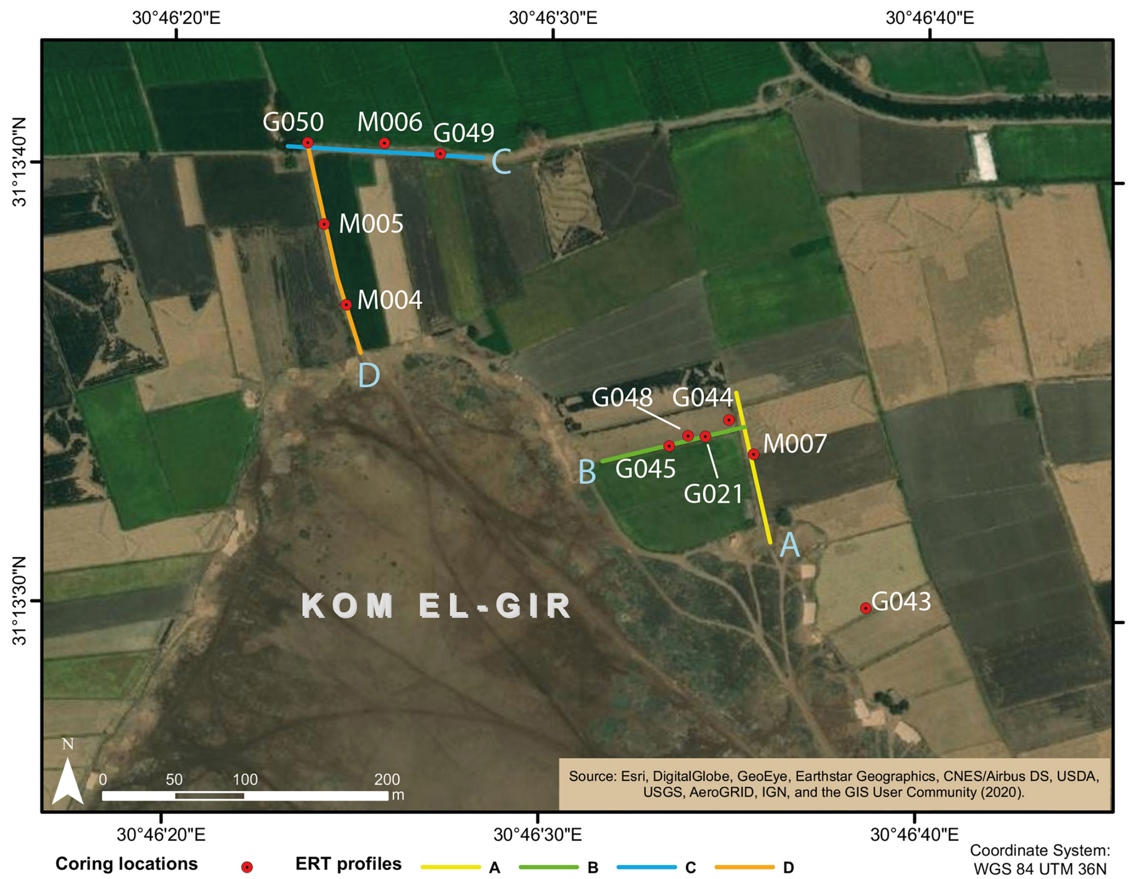

Figure 3. Locations of performed corings and ERT profiles within the study area located north and northeast of KeG.

The measurements were performed under standardized conditions using a measurement chamber. According to testing and calibration within prior research work, the measurement parameters were set to 180 s using the AllGeo mode that combines the soil and mining mode of the device. During measurements, helium was induced into the detector unit of the device. The application of helium allows the reduction of the measurement times and preserves the necessary precision for the detection of light elements such as phosphor (Ginau et al., 2020).

3.3 Data analysis

In addition to the applied methods performed on-site, possible sources of error were considered in order to prepare and analyze the sampled data. Therefore, zero values or values below the limit of detection (LOD), which occur due to the inaccurate precision of the measurement method, were excluded according to the calculated detection limits of Ginau et al. (2020). Based on relevant literature and given geochemical signals used in paleoenvironmental studies (Kern et al., 2019), specific elements or element ratios were selected as potential proxies (Table 1).

3.4 Electrical resistivity tomography (ERT)

In total, four profiles (100–150 m length) of electrical resistivity measurements reaching from the edges of KeG into the adjacent fields were made employing a multi-electrode setup with 24 electrodes using Lippmann 4point light HP equipment. This was considered the appropriate method to detect lateral facies changes down to sounding depths of ca. 10 m. The resistivity distribution was determined by inversions according to the Levenberg–Marquardt algorithm. The profiles were placed alongside the positions of recently performed corings (Fig. 3) to correlate the results of both applied methods. Profiles A–C are presented in Fig. 5, whereas profile D was excluded due to problems during the measurements.

4 Results

To investigate the study area, seven corings were performed in the northern and northeastern surroundings of KeG (Fig. 3). Due to the small extent of the study area and resulting resemblance of the retrieved core sediments, coring M006 is presented exemplarily in detail (Fig. 4).

Table 1. Selected elements used as geochemical proxies.

Element	Proxy for	Corresponding references
Zr	terrigene influence	Eckert (2014)
Fe, Al	fluvial influence (strongly enriched in Blue Nile draining), terrigenous origin	Vött et al. (2002), Revel et al. (2010), Eckert (2014), Pint et al. (2015), Pennington et al. (2019)
Fe, S	reducing/anoxic conditions	Revel et al. (2010), Eckert (2014), Martinez-Ruiz et al. (2015), Pennington et al. (2019), Emmanouilidis et al. (2020)
Ca	eolian deposit	Woronko (2012)
Cu	anthropogenic influence	Pint et al. (2015), Delile et al. (2018)
Element ratio		
Ca/Fe	dominating terrestrial (or fluvial) influences (in favor of iron)	Pint et al. (2015)
Ca/Ti	relative contributions of eolian (in favor of Ca) vs. fluvial (in favor of Ti) input	Vött et al. (2002), Blanchet et al. (2015), Pint et al. (2015), Castañeda et al. (2016), Pennington et al. (2019)
Cu/Zn	nature of river sediments (natural watercourses vs. human-constructed canals)	Ginau et al. (2019)

4.1 Coring M006

M006 (31.22794° N, 30.773801° E; 2.178 m a.s.l., depth: 11 m) is situated approx. 135 m north of the northern edge of the present-day *kom* area (Figs. 3, 4). The lowermost sediments between 11.00 and 6.00 m b.s. (meters below modern surface) are made of well-sorted silty medium sand, associated with ceramic fragments and mica. The pXRF values of this section reveal strongly fluctuating Ca/Fe and Ca/Ti ratios and Fe and Al concentrations. The S concentration of the lowermost section is around 250 ppm with an increasing trend towards upper sections. The Cu/Zn ratio shows strong fluctuations between 0.0 and 2.0 while the Zr concentration fluctuates around 320 ppm up to ca. 3.00 m b.s.

Between 6.00 and 2.70 m b.s., the sediment sequence shows alternating layers (mm–cm) of silty fine sand and medium sand. The intercalation of fS and mS shows more fluctuations in the element ratios with a high peak (2.7 for Ca/Fe and 9.0 for Ca/Ti) in favor of Ca at approx. 4.50 m b.s. Fe and Al concentrations remain fluctuating before values reveal a gradual increasing trend from 4.00–2.70 m b.s. After an S peak of 500 ppm, the values gradually decrease with a few anomalies. Only within the upper fS unit is no S concentration detected. The Cu/Zn ratio as well as Zr further fluctuates until 3.00 m b.s. where the Zr concentration begins to increase gradually.

Within the overlying material (2.70–1.70 m b.s.), silty fine sand dominates the sediment sequence. The Ca/Fe and Ca/Ti ratios consistently range around 0.5 (Ca/Fe) and 3.0 (Ca/Ti), while the Fe and Al concentrations are generally high with a gradual increase towards the upper sediment section. In contrast to lower core sections, the Cu/Zn ratio shows slightly fewer variations and weaker amplitudes. At 1.90 m b.s., the Zr concentration reaches its maximum of approx. 680 ppm within the uppermost Ufs unit.

Between 1.70 and 1.00 m b.s., silty fine sand within the lower section gradually transitions into fine sandy silt towards the upper parts. In contrast to underlying sections, these sediments reveal a medium lime content of c1–c3. Between 2.00 and 0.30 m b.s., the S concentration ranges around 0 and 350 ppm.

The uppermost material (1.00–0.30 m b.s.) consists of clay intercalated by silty clay, showing decreasing Ca/Fe and Ca/Ti ratios in favor of Ca, while Fe and Al concentrations gradually increase. The Zr concentration reveals gradually decreasing values around 240 ppm.

4.2 ERT profiles

The ERT profiles measured the electrical resistivity of the subsurface sediments over a length of 100–150 and 8–10 m depth with a total resistivity range from less than 2.5 Ωm to approx. 40.0 Ωm (Figs. 3, 5).

The lowest resistivity (<2.5–10.0 Ωm) was predominantly measured within the topmost subsurface sediments, partially reaching into deeper surface areas and occurring as lenses (Fig. 5a, b). Medium values of electrical resistivity (10.0–20.0 Ωm) are observed within various profile areas. They are present within middle profile sections as well as within near-tell areas. Sediments of higher electrical resistivity (20.0–40.0 Ωm) are predominantly located below the top layer of low resistivity and within deeper profile sections. They

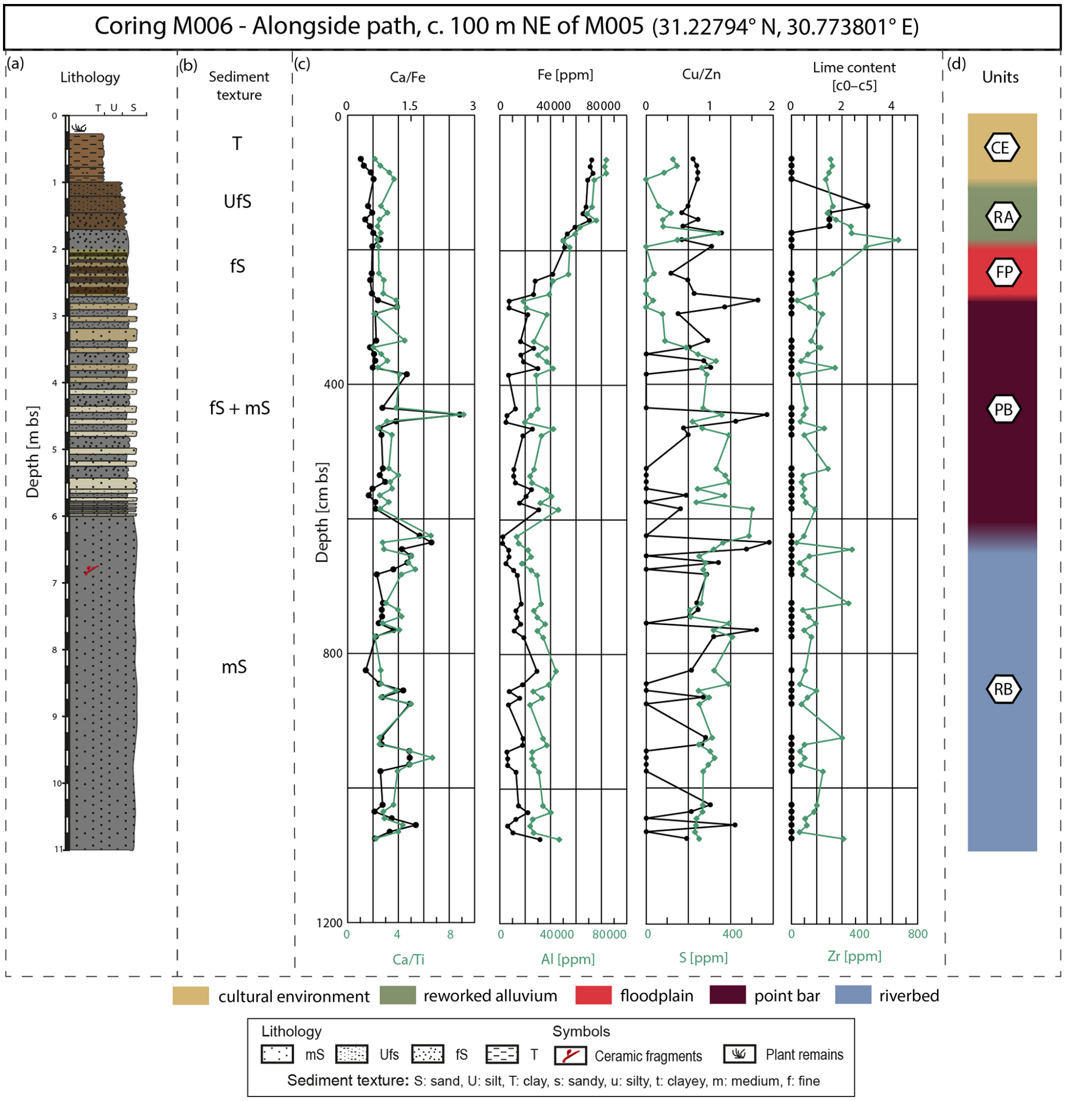

Figure 4. Lithostratigraphy **(a)** and sediment texture **(b)** as well as pXRF results of selected proxies **(c)** for coring M006. For unit interpretation **(d)** see Sect. 5.

mainly occur as depressions representing channel-like features.

4.3 ERT profile C

In addition to coring M006 (Fig. 4), ERT profile C (Fig. 5c), which includes the coring site of M006, is exemplarily described in detail. The modeled ERT image is subdivided into three sections, showing distinct differences in electrical resistivity of the sediments. The material of the uppermost 1.50 m b.s. reveals low to medium resistivity values (5.0–11.0 Ωm), reaching further down to 4.00 m b.s. within the western profile part. Sediments below this layer reveal high electrical resistivity (20.0–40.0 Ωm), almost visible over the entire profile length and depth. Only between profile meters 20 and 50 does the material within the lowermost 2 m possess lower resistivity values around 10.0 Ωm. Besides, the material of high resistivity is sharply defined by sediments with medium (15.0–16.0 Ωm) resistivity. The boundary of medium values is visible in the top transition area and lower-lying parts.

5 Discussion

5.1 Interpretation and discussion of core data

5.1.1 Classification of sedimentary units

Based on the coring results, eight distinct units (Fig. 6) are identified that represent the sedimentary environments in which the sediments once accumulated or that predominantly influenced them.

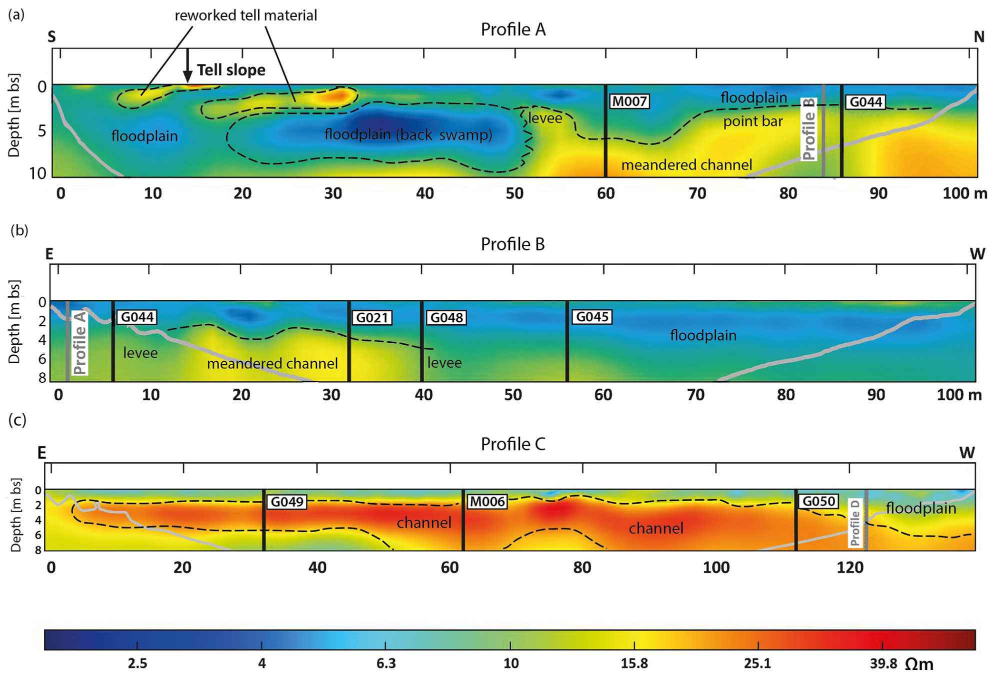

Figure 5. Modeled ERT images of **(a)** profile A, **(b)** profile B, and **(c)** profile C with identified subsurface channel elements. The color scale visualizes the resistivity of the subsurface sediments, ranging from blue, representing low resistivity to red, representing high resistivity. Further features such as locations of several corings conducted in this area are also indicated. The grey lines mark the boundaries of uncertain result reliability towards the start and end of the profile. For profile location see Fig. 3.

- *Unit BA (basement).* The dark grey to whitish colored fine to medium sands (Fig. 6a, b) with partially horizontal color shifts to greenish and yellowish hues indicate former fluvial origin. Studies of regional sediments show that those deposits are usually overlain by peat or organic-rich layers and reveal elevated lime concentrations within upper parts (Wunderlich, 1989; Ginau et al., 2019).

- *Unit LE (levee).* The yellowish-brown coarser sandy sediments are intercalated with thin, fine-grained dark brown loam layers (Fig. 6d). Those sediment alternations are interpreted as a result of flood events with gradually decreasing flow velocities within areas adjacent to channels. The periodical flood sediments accumulated as darker and fine-grained layers in between the sandy deposits, shaping elevated overbank structures (Wunderlich, 1989; Toonen et al., 2012; El Bastawesy et al., 2020). A trend of increasing sediment accumulation is also reflected by gradually increasing Zr concentrations, which mainly originate from erosional processes, reflecting the terrigenous character of the sediments (Eckert, 2014). Furthermore, alternating flood and drought phases are reflected by intense fluctuations in the Cu/Zn ratio (Ginau et al., 2019).

- *Unit RB (riverbed).* The grey-colored material (Fig. 6e) with partially greenish to dark olive hues varies between fine-grained sediments and coarse sand, associated with findings of ceramic fragments, pebbles, or mollusks which serve as proxies for a former channel environment (Giaime et al., 2018; Ginau et al., 2019). The Ca/Ti and Ca/Fe ratios in favor of Ti and Fe, additionally indicate former fluvial conditions (Pint et al., 2015; Castañeda et al., 2016; Croudace et al., 2019; Pennington et al., 2019). Fe with its terrigenous origin is strongly enriched in the sediments transported by the Blue Nile, possibly fed by erodible Fe-rich silicate rocks present within the Ethiopian drainage basin (Revel et al., 2010; Ménot et al., 2020). Continuous fluctuations in the measured pXRF data underline the fluvial nature of this unit. The geochemical variability reveals changing streamflow conditions associated with alternating floods and droughts (Stanley et al., 2003; Ginau et al., 2019).

- *Unit PB (point bar).* The dark greenish-grey as well as light whitish coarser sediments are strongly laminated with dark grey to greyish-brown silts (Fig. 6c). The elements and associated ratios show a similar geochemical variability to those of unit RB. Fluctuations within the Fe and Al concentrations as well as the Cu/Zn ratio indicate the accumulation within a fluvial system (Stanley et al., 2003; Ginau et al., 2019). The visible lamination of the sand section with silty strata highlights changing hydrodynamics (Vött et al., 2002; Goiran et al., 2014).

Figure 6. Exemplary core sediments corresponding to the different sedimentary units. Selected sediments of the coring material representing the identified units. **(a, b)** unit basement, **(c)** unit point bar, **(d)** unit levee, **(e)** unit riverbed, **(f, g)** unit reworked alluvium, **(h, i)** unit floodplain, **(j)** unit cultural debris, and **(k)** unit cultural environment.

The Ca/Fe and Ca/Ti ratios show peaks towards Ca, indicating predominantly eolian input at certain intervals (Woronko, 2012; Blanchet et al., 2015; Pint et al., 2015; Pennington et al., 2019). Partially present high S concentrations reflect the existence of reducing conditions, detectable within silty sediments corresponding to phases of low-energy flow or stagnant water (Goiran et al., 2014; Martinez-Ruiz et al., 2015).

- *Unit FP (floodplain).* The light brown to greenish-grey and dark grey varying sediments range from clay to coarser sand (Fig. 6h, i). The small-scale layering of multiple accumulated sections of silty clay and medium sand indicates a change in the energetic environmental conditions caused either by variations in sediment load and flood height or by alternating channel courses and associated marginalizing energetic conditions. The fluctuating Cu/Zn ratio reflects phases of floods and droughts (Stanley et al., 2003; Ginau et al., 2019). A partially elevated lime content, the Ca/Ti ratio in favor of Ca, and plant remains support the assumption that sediments were accumulated within an area of dominating eolian input during dryer periods (Woronko, 2012; Pint et al., 2015). During warm and dry periods without flood events, ascendant water mobilization possibly led to Ca precipitation (Vött et al., 2002; Pennington et al., 2019). The fine-grained material is partially rich in organics characterized by a distinct sulfidic smell and a blackish color, which developed due to the existence of a long-lasting brackish water body (Wunderlich, 1989; Ginau et al., 2019). Coarser sediments either were accumulated within close distance of an active channel or can be interpreted as crevasse splays, transported over longer distances from the stream course due to the higher streamflow velocity of flood events (Wunderlich, 1989; Toonen et al., 2012; Ginau et al., 2019).

- *Unit CD (cultural debris).* The red-brick-colored composition of brick and ceramic fragments (Fig. 6j) shows distinct boundaries of under- and overlying sediments. Although, the unit can be clearly distinguished visually, differences in its geochemistry compared to the overlying reworked alluvium (see unit RA) are not detectable.

- *Unit RA (reworked alluvium).* The dark yellowish-brown clayey to fine sandy material (Fig. 6f, g) represents the Nile alluvium characteristic for this region (Wunderlich, 1989; Ginau et al., 2019). High element loadings of Fe and Al, indicating that the deposited sediments are fluvially transported material with a terrigenous origin, underline the presumed source (Revel et al., 2010; Eckert, 2014; Pint et al., 2015; Pennington et al., 2019). The unit contains cultural components such as charcoal, ceramic, and brick fragments that presumably influenced the sediment's geochemistry and altered the geochemical signal, leading to differing geochemical distributions and elemental loadings compared to those of a floodplain area without human influences. Thus, the sediments of this unit rather show steady to gradual element distributions. The visible gradual increase in element loadings, such as Fe and Al, without severe geochemical distinctions, further indicate anthropogenic influences (Ginau et al., 2017, 2019; Pennington et al., 2019).

- *Unit CE (cultural environment).* The dark greyish-brown sediments composed of varying amounts of clay, silt, and fine sand (Fig. 6k) are predominantly formed by human activity. A high quantity of anthropogenic remains such as ceramic or brick fragments, charcoals, mortar, and plastic bags among other findings such as plant remains, lime concretions, and pebbles are present.

5.1.2 Interpretation of coring M006

The results of core M006 (Fig. 4) lead to a differentiation of five units (Fig. 7). The lowermost unit (11.00–6.00 m b.s.) is represented by unit RB. The presence of a ceramic fragment embedded within coarse sand underlines a sediment transport by a turbulent flow (Goiran et al., 2014). The overlying sediments (6.00–2.80 m b.s.) are attributed to unit PB. A visible lamination within the sediment texture and the coarse material underlines this interpretation. The material above (2.80–2.00 m b.s.) is identified as unit FP. The existence of fine sand and the number of color differences within the sediments suggest a fluvial origin, presumably with minor distance to the actual channel stream (Toonen et al., 2020). The sediments above (2.00–1.25 m b.s.) are transitioning into unit RA. Although no anthropogenic remains are visible, increasing Fe and Al concentrations and the depth of the unit within the drilling core indicate anthropogenic influences. The uppermost material (1.25–0.00 m b.s.) predominantly shows strongly enriched Fe and Al concentrations without the presence of ceramic fragments or other remains as well. Nevertheless, it is to be identified as unit CE, considering the core location and implied influences of human activity.

5.2 Interpretation of ERT profile C

The images of all three ERT profiles (Fig. 5) reveal clear indicators for buried channel features. Specifically, the resistivity distribution of profile C (Fig. 5c) shows two deep structures with high values (at 55–70 and 80–120 m), presumably representing relict riverbeds as channel sediments contain fine to coarser sand (Ginau et al., 2019). A zone of medium resistivity values (at 70–80 m) in lower-profile sections leads to the interpretation of a sand/point bar between the two channels.

Lower hydrodynamics within such stream-protected areas entail dominating accumulation processes. An alternating streamflow leads to the deposition of sediments with varying grain sizes. The lithological character of the deposits most likely reveals laminations of coarse and fine-grained sediments (Wunderlich, 1989; Goiran et al., 2014; Toonen et al., 2018). Thus, due to the portions of coarse-grained material, the electrical resistivity potentially reveals higher values as well. High ERT values above this presumed sand/point bar indicate overlying channel deposits. Therefore, a first channel construction with two branches and a corresponding sand bar in between is assumed. A potential increasing discharge may have initiated the extending of these streams into one wider channel (channel Ia) that also incorporates the area between 10–50 m (Fig. 5c). However, the eastern half of the profile may also represent a floodplain close to the detected channel. The slightly decreasing electrical resistivity towards the eastern profile end may correspond to the decrease in the mean deposit grain size with distance to an active stream (Toonen et al., 2020). Following this idea, a corresponding floodplain on the western edge at approx. 120–140 m is to be expected.

5.3 Channel-network reconstruction

The obtained data distinctively reveal evidence of buried channel elements embedded in the subsurface sediments of the study area. The core sediments of M006 and the ERT profile C reveal the presence of coarse sand sequences that reach from near-surface areas (approx. 3.00 m b.s.) to deeper sections. These deep-reaching coarse deposits could only have been accumulated within a stream course with high hydrodynamics and flow velocity (Wunderlich, 1989; Goiran et al., 2014). Further corings (M004, M005) in this area also comprise coarse-grained sediments within deeper sections that are classified as unit RB according to their lithology and pXRF data (Fig. 7). In addition to this, M004 incorporates a preserved FP unit below the riverbed section, indicating lower hydrodynamics, which only partially eroded these floodplain deposits. Therefore, it is to be assumed that the location of coring M004 represents marginal areas of the former channel environment. The identified sedimentary units (unit PB and unit FP) within upper sections of M004 and M005 indicate the channel relocation towards the north. Thereby, the interpretations of the ERT profile C lead to the assumption that this profile cuts the former channel nearly orthogonally, indicating the presence of an additional stream.

This presumption is revised with the aid of the topographic map of the *Survey of Egypt* (Fig. 8) that presents contour lines in this area. At the considered location, the contour lines are narrower, which indicates a slightly steeper slope (Fig. 8). A potentially increasing flow energy of the channel may have initiated a further discharge course. Within deeper sections of the ERT profile, two identified depressions suggest the first initiation of two smaller streams before extending into one larger stream. Based on the ERT and coring results, revealing near-surface locations of these channel elements, it is assumed that the channel (channel Ia) silted up later than the channel incorporating M004 and M005 (channel Ib).

The northeast-located corings and ERT measurements also reveal evidence of a former channel (channel II).

Based on the interpretation of the ERT profiles A and B (Fig. 5a, b), the stream is interpreted as a smaller side channel. Although the dimensions of the defunct paleochannel cannot be drawn with certainty, the interpretations of the results lead to this schematic reconstruction (Fig. 8). In consideration of the corings G044 and G048, the pXRF data of the sediments furthermore indicate a low-energy stream. They also align with additional results by Ginau et al. (2019), concluding there was a former channel (coring G21 Fig. 5b) in the eastern surroundings of KeG. Based on its infill comprising loamy fine sand, the authors attributed the stream to a low-energy domain that also revealed characteristics of a natural channel (Ginau et al., 2019). In addition to this, the existent RB units within the performed corings transitioning into FP units and the thickness of these sections suggest an earlier siltation than in the northern channel.

The applied multi-proxy approach allowed the small-scale reconstruction of a former channel system within the study area. However, the sole use of a pXRF approach may be problematic as the Nile Delta sediments possess strong conformities regarding their chemical composition. This can be explained by the consistent sources of the Nile sediments, which did not vary due to climate fluctuations or human in-

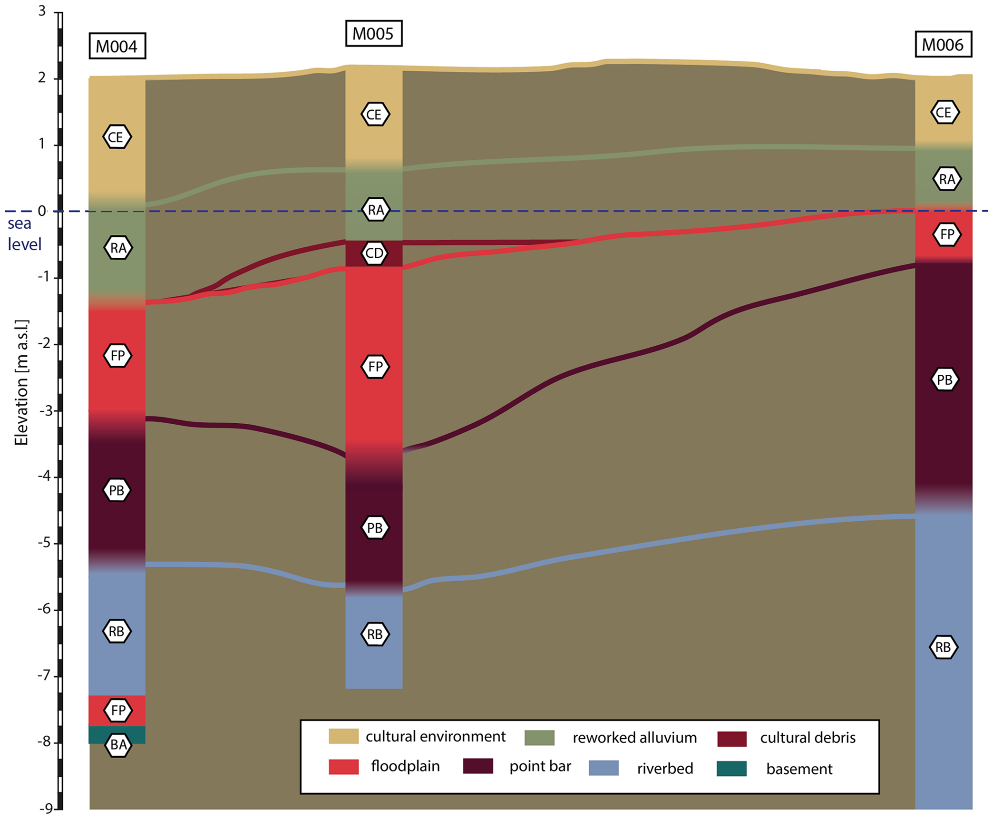

Figure 7. Identified units of coring M004, M005, and M006 representing the environmental evolution in this part of the study area. Corings are presented schematically; for core locations see Fig. 3.

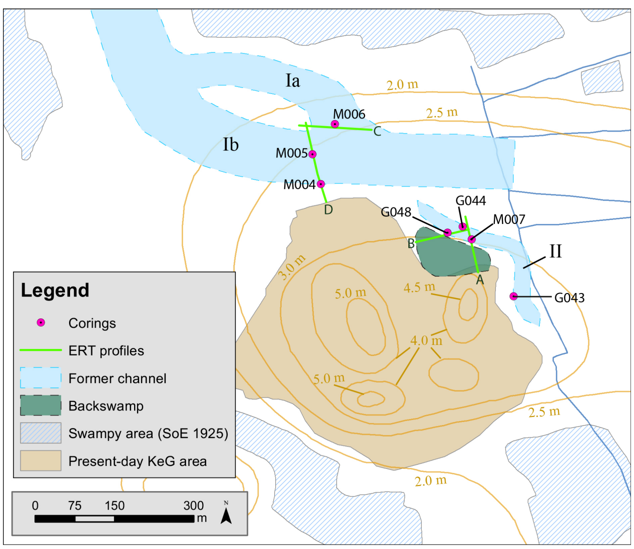

Figure 8. Reconstructed channel systems in the northern and north-eastern surroundings of KeG. Based on topographic map of the *Survey of Egypt* from 1925 (scale 1 : 25 000).

fluences. Thus, the pXRF values within this study are only to be considered in combination with the lithological sediment description. However, additional studies may further develop this multi-proxy approach and add more sedimentary and geochemical analyses to the state of research.

6 Conclusion

Through the pXRF analyses of the coring material, eight sedimentary environments are classified that provide subsequent insights into the evolution of the coring sites and former environmental conditions of the study area.

These analyses and the ERT images reveal clear evidence for deposits of defunct channels in the area close to KeG. While deep-reaching sandy deposits in the northern research area represent a former stream (channel Ia, Ib) with high hydrodynamics, the northeast-located sediments show only features of a smaller channel (channel II) with lower flow velocity. In summary, by combining pXRF analyses, lithology, and ERT measurements, a comprehensive small-scale reconstruction of a former fluvial network was elaborated in the area northeast of KeG. Therefore, combining these methods yields a massive benefit in answering the assumptions of Schiestl (2019) about the Nile Delta's fluvial landscape. The used approach may be a choice for investigations of several other settlement hills in the nearby area (Fig. 2).

Although the pXRF analyses and ERT measurements provide no indications of the width of the former streams, topographic maps and current satellite images suggest a framework for the potential dimensions of at least one of the identified channels by the arrangement of fields southeast of KeG. Furthermore, due to a lack of dating facilities, it is not possible to relate the channels to each other or the period of their activity. In this context, future research may provide improved reconstructions and extended insights regarding this topic and the illustrated channel network as well as its dimensions. Datings, microfossil analyses, and further multi-proxy approaches may contribute additional knowledge about the channel system and their activity periods.

Data availability. The TanDEM-X digital elevation model is used with the permission of the German Aerospace Center (DLR), based on the data requested via the proposal (DEM_HYDR1426) by Andreas Ginau, Robert Schiestl, Jürgen Wunderlich, Eva Lange-Athinodorou, and Tobias Ullmann.

All further data generated during this study are included in this article or are available from the corresponding author upon request.

Author contributions. MA, MS, and JW designed this study. All authors performed the fieldwork, mainly comprising drilling, sediment sampling, and leveling the coring locations via GNSS. AG, MA, and MS carried out the pXRF analyses. MA wrote the first draft of the manuscript that was later improved by all co-authors. MA created all figures. JW acquired the funding for this research. RS provided the archeological and historical background for this paper.

Competing interests. The authors declare that they have no conflict of interest.

Special issue statement. This article is part of the special issue "Geoarchaeology of the Nile Delta". It is a result of the workshop "Geoarchaeology of the Nile Delta: Current Research and Future Prospects", Würzburg, Germany, 29–30 November 2019.

Acknowledgements. The fieldwork was conducted as part of the regional survey around Buto (Tell el-Fara'in), with a particular focus on Kom el-Gir. This project is undertaken under the auspices of the Cairo Department of the German Archaeological Institute (DAI). We thank Viktor Nawa and Mona Maier-Rotter for performing the ERT measurements. Thanks to the entire DAI team, especially the first director of the DAI Cairo Department Stephan Seidlmayer for his hospitality and support during the field campaigns. We thank the Egyptian Ministry of State for Antiquities for their assistance and support of our work in the field and for granting the research permits. Furthermore, we thank the two anonymous reviewers for their valuable comments.

Financial support. This study was funded by the Deutsche Forschungsgemeinschaft (DFG, German Research Foundation) (grant no. 392434407).

This open-access publication was funded by the Goethe University Frankfurt.

Review statement. This paper was edited by Tobias Ullmann and reviewed by two anonymous referees.

References

Ad-Hoc-AG Boden: Bodenkundliche Kartieranleitung, Bundesanstalt für Geowissenschaften und Rohstoffe in Zusammenarbeit mit den Staatlichen Geologischen Diensten, 5, Hannover, Germany, 2005.

Andres, W. and Wunderlich, J.: Untersuchungen zur Paläogeographie des westlichen Nildeltas im Holozän, Marburger Geographische Schriften, 100, 117–131, 1986.

Bietak, M.: Tell el-Dab'a II: Der Fundort im Rahmen einer archäologisch-geographischen Untersuchung über das ägyptische Ostdelta, Verlag d. Österr. Akademie d. Wissenschaft, Vienna, Austria, 1975.

Blanchet, C. L., Contoux, C., and Leduc, G.: Runoff and precipitation dynamics in the Blue and White Nile catchments during the mid-Holocene: A data-model comparison, Quaternary Sci. Rev., 130, 222–230, https://doi.org/10.1016/j.quascirev.2015.07.014, 2015.

Butzer, K. W.: Geoarchaeological Implications of Recent Research in the Nile Delta, in: Egypt and the Levant. Interrelations from the 4th throught the early 3rd Millennium B.C.E., New Approaches to Anthropological Archaeology, edited by: van den Brink, E. C. M. and Levy, T. E., Leicester University Press, London/New York, 83–97, 2002.

Castañeda, I. S., Schouten, S., Pätzold, J., Lucassen, F., Kasemann, S., Kuhlmann, H., and Schefuß, E.: Hydroclimate variability in the Nile River Basin during the past 28,000 years, Earth Planet. Sc. Lett., 438, 47–56, https://doi.org/10.1016/j.epsl.2015.12.014, 2016.

Croudace, I. W., Löwemark, L., Tjallingii, R., and Zolitschka, B.: Current perspectives on the capabilities of high resolution XRF core scanners, Quatern. Int., 514, 5–15, https://doi.org/10.1016/j.quaint.2019.04.002, 2019.

Delile, H., Goiran, J. P., and Blichert-Toft, J.: The contribution of geochemistry to ancient harbor geoarcheology: The example of Ostia Antica, Quaternary Sci. Rev., 193, 170–187, https://doi.org/10.1016/j.quascirev.2018.06.019, 2018.

Eckert, S.: The past and present trace metal budget of the Black Sea: a comparison of the Holocene and Eemian marine ingression, PhD thesis, Carl von Ossietzky Universität, University Oldenburg, Germany, 120 pp., 2014.

El Bastawesy, M., Gebremichael, E., Sultan, M., Attwa, M., and Sahour, H.: Tracing Holocene channels and landforms of the Nile Delta through integration of early elevation, geophysical, and sediment core data, The Holocene, https://doi.org/10.1177/0959683620913928, 2020.

El Gamili, M. M., Shaaban, F. F., and El-Morsi, O. A.: Electrical resistivity mapping of the buried stream channel of the Canopic Branch in the Western Nile Delta, Egypt, J. Afr. Earth Sci., 19, 135–148, https://doi.org/10.1016/0899-5362(94)90046-9, 1994.

El Gamili, M. M., Ibrahim, E. H., Hassaneen, A. R. G., Abdalla, M. A., and Ismael, A. M.: Defunct Nile Branches Inferred from a Geoelectric Resistivity Survey on Samannud area, Nile Delta, Egypt, J. Archaeol. Sci., 28, 1339–1348, https://doi.org/10.1006/jasc.2001.0761, 2001.

Emmanouilidis, A., Messaris, G., Ntzanis, E., Zampakis, P., Prevedouros, I., Bassukus, D. A., and Avramidis, P.: CT scanning, X-ray fluorescence: Non-destructive techniques for the identification of sedimentary facies and structures, Revue de micropaléontologie, 67, 100410, https://doi.org/10.1016/j.revmic.2020.100410, 2020.

Gebremichael, E., Sultan, M., Becker, R., El Bastawesy, M., Cherif, O., and Emil, M.: Assessing land deformation and sea encroachment in the Nile Delta: a radar interferometric and inundation modeling approach, J. Geophys. Res.-Sol. Ea., 123, 3208–3224, https://doi.org/10.1002/2017JB015084, 2018.

Giaime, M., Morhange, C., Marriner, N., López-Cadavid, G. I., and Artzy, M.: Geoarchaeological investigations at Akko, Israel: New insights into landscape changes and related anchorage locations since the Bronze Age, Geoarchaeology, 33, 641–660, https://doi.org/10.1002/gea.21683, 2018.

Ginau, A., Schiestl, R., Kern, F., and Wunderlich J.: Identification of historic landscape features and settlement mounds in the Western Nile Delta by means of remote sensing time series analysis and the evaluation of vegetation characteristics, J. Archaeol. Sci.: Reports, 16, 170–184, https://doi.org/10.1016/j.jasrep.2017.09.034, 2017.

Ginau, A., Schiestl, R., and Wunderlich J.: Integrative geoarchaeological research on settlement patterns in the dynamic landscape of the northwestern Nile delta, Quatern. Int., 511, 51–67, https://doi.org/10.1016/j.quaint.2018.04.047, 2019.

Ginau, A., Steiniger, D., Hartmann, R., Hartung, U., Schiestl, R., Altmeyer, M., Seeliger, M., and Wunderlich, J.: What settlements leave behind – pXRF compositional data analysis of archaeological layers from Tell el-Fara'in (Buto, Egypt) using machine learning, Palaeogeogr. Palaeocl., 546, 109666, https://doi.org/10.1016/j.palaeo.2020.109666, 2020.

Goiran, J. P., Salomon, F., Mazzini, I., Bravard, J. P., Pleuger, E., Vittori, C., Boetto, G., Christiansen, J., Arnaud, P., Pellegrino, A., Pepe, C., and Sadori, L.: Geoarchaeology confirms location of the ancient harbour basin of Ostia (Italy), J. Archaeol. Sci., 41, 389–398, https://doi.org/10.1016/j.jas.2013.08.019, 2014.

Kern, O. A., Koutsodendris, A., Mächtle, B., Christanis, K., Schukraft, G., Scholz, C., Kotthoff, U., and Pross, J.: XRF core scanning yields reliable semiquantitative data on the elemental composition of highly organic-rich sediments: Evidence from the Füramoos peat bog (Southern Germany), Sci. Total Environ., 697, 134110, https://doi.org/10.1016/j.scitotenv.2019.134110, 2019.

Lange, E., Ullmann, T., and Baumhauer, R.: Remote sensing in the Nile Delta: spatio-temporal analysis of Bubastis/Tell Basta, Egypt and the Levant, 26, 377–392, available at: https://www.jstor.org/stable/44243959 (last access: 10 August 2020), 2016.

Marriner, N., Flaux, C., Kaniewski, D., Morhange, C., Leduc, G., Moron, V., Chen, Z., Gasse, F., Empereur, J. Y., and Stanley, J.-D.: ITCZ and ENSO-like pacing of Nile delta hydro geomorphology during the Holocene. Quaternary Sci. Rev., 45, 73–84, https://doi.org/10.1016/j.quascirev.2012.04.022, 2012.

Martinez-Ruiz, F., Kastner, M., Gallego-Torres, D., Rodrigo-Gámiz, M., Nieto-Moreno, V., and Ortega-Huertas, M.: Paleoclimate and paleoceanography over the past 20,000 yr in the Mediterranean Sea Basins as indicated by sediment elemental proxies, Quaternary Sci. Rev., 107, 25–46, https://doi.org/10.1016/j.quascirev.2014.09.018, 2015.

Ménot, G., Pivot, S., Bouloubassi, I., Davtian, N., Hennekam, R., Bosch, D., Ducassou, E., Bard, E., Migeon, S., and Revel, M.: Timing and stepwise transitions of the African Humid Period from geochemical proxies in the Nile deep-sea fan sediments, Quaternary Sci. Rev., 228, 106071, https://doi.org/10.1016/j.quascirev.2019.106071, 2020.

Morhange, C., Giaime, M., Marriner, N., abu Hamid, A., Bruneton, H., Honnorat, A., Kaniewski, D., Magni, F., Porotov, A. V., Wante, J., Zviely, D., and Artzy, M.: Geoarchaeological evolution of Tel Akko's ancient harbor (Israel). J. Archaeol. Sci., 7, 71–81, https://doi.org/10.1016/j.jasrep.2016.03.046, 2016.

Pennington, B. T., Sturt, F., Wilson, P., Rowland, J., and Brown, A. G.: The fluvial evolution of the Holocene Nile Delta, Quaternary Sci. Rev., 170, 212–231, https://doi.org/10.1016/j.quascirev.2017.06.017, 2017.

Pennington, B. T., Hamdan, M. A., Pears, B. R., and Sameh, H. I.: Aridification of the Egyptian Sahara 5000–4000 cal BP revealed from x-ray fluorescence analysis of the Nile Delta sediments at Kom al-Ahmer/Kom Wasit, Quatern. Int., 514, 108–118, https://doi.org/10.1016/j.quaint.2019.01.015, 2019.

Pint, A., Seeliger, M., Frenzel, P., Feuser, S., Erkul, E., Berndt, C., Klein, C., Pirson, F., and Brückner, H.: The environs of Elaia's ancient open harbour-a reconstruction based on macrofaunal evidence, J. Archaeol. Sci., 54, 340–355, https://doi.org/10.1016/j.jas.2014.06.011, 2015.

Revel, M., Ducassou, E., Grousset, F. E., Bernasconi, S. M., Migeon, S., Révillon, S., Mascle, J., Murat, A., Zaragosi, S., and Bosch, D.: 100,000 years of African monsoon variability recorded in sediments of the Nile margin, Quaternary Sci. Rev., 29, 1342–1362, https://doi.org/10.1016/j.quascirev.2010.02.006, 2010.

Rizzini, A., Vezzani, F., Cococcetta, V., and Milad, G.: Stratigraphy and sedimentation of a Neogene – Quaternary section in the Nile Delta area (ARE), Mar. Geol., 27, 327–348, https://doi.org/10.1016/0025-3227(78)90038-5, 1978.

Schiestl, R.: Investigating ancient settlements around Buto, Egyptian Archaeology, 40, 18–20, 2012.

Schiestl, R.: Landschaftsarchäologie und regionale Siedlungsnetzwerke um den Fundplatz Tell el-Fara'in, Gouvernorat Kafr esch-Scheich. Die Arbeiten des Jahres 2012, e-Forschungsberichte, 1, 11–13, available at: https://www.dainst.org/documents/10180/727267/eFB2015-1_Schiestl_Buto.pdf/cff14d7c-eb23-4be5-bde9-911156900701 (last access: 31 May 2021), 2015.

Schiestl, R.: Gouvernorat Kafr esch-Scheich, Ägypten. Landschaftsarchäologie und regionale Siedlungsnetzwerke um den Fundplatz Tell el-Fara'in (Buto) im Nildelta. Die Arbeiten des Jahres 2018, e-Forschungsberichte 2018, 2, 44–46, available at: https://publications.dainst.org/journals/index.php/efb/article/view/2149 (last access: 24 May 2021), 2018.

Schiestl, R.: Gouvernorat Kafr esch-Scheich, Ägypten. Landschaftsarchäologie und regionale Siedlungsnetzwerke um den Fundplatz Tell el-Fara'in im Nildelta und Untersuchungen am antiken Fundplatz Kom el-Gir. Die Arbeiten des Jahres 2018 und Frühjahres 2019, e-Forschungsberichte, 2, 51–55, https://doi.org/10.5282/ubm/epub.69238, 2019.

Schiestl, R. and Herbich, T.: Kom el-Gir in the western Delta, Egyptian Archaeology, 42, 28–29, 2013.

Schiestl, R. and Rosenow, D.: Prospektion am Kom el-Gir: eine Einführung in eine neue Siedlung des Deltas, Mitteilungen des Deutschen Archäologischen Instituts, Abteilung Kairo, 72, 169–196, 2016.

Seeliger, M., Pint, A., Frenzel, P., Weisenseel, P. K., Erkul, E., Wilken, D., Wunderlich, T., Başaran, S., Bücherl, H., Herbrecht, M., Rabbel, W., Schmidts, T., Szemkus, N., and Brückner, H.: Using a multi-proxy approach to detect and date a buried part of the Hellenistic City Wall of Ainos (NW Turkey), Geosciences, 8, 357, https://doi.org/10.3390/geosciences8100357, 2018.

Stanley, J. D., Krom, M. D., Cliff, R. A., and Woodward, J. C.: Short contribution: Nile flow failure at the end of the Old Kingdom, Egypt: strontium isotopic and petrologic evidence, Geoarchaeology, 18, 395–402, https://doi.org/10.1002/gea.10065, 2003.

Toonen, W. H. J., Kleinhans, M. G., and Cohen, K. M.: Sedimentary architecture of abandoned channel fills, Earth Surf. Proc. Land., 37, 459–472, https://doi.org/10.1002/esp.3189, 2012.

Toonen, W. H. J., Graham, A., Pennington, B. T., Hunter, M. A., Strutt, K. D., Barker, D. S., Masson-Berghoff, A., and Emery, V. L.: Holocene fluvial history of the Nile's west bank at ancient Thebes, Luxor, Egypt, and its relation with cultural dynamics and basin-wide hydroclimatic variability, Geoarchaeology, 33, 273–290, https://doi.org/10.1002/gea.21631, 2018.

Toonen, W. H. J., Munoz, S. E., Cohen, K. M., and Macklin, M. G.: High-Resolution Sedimentary Paleoflood Records in Alluvial River Environments: A Review of Recent Methodological Advances and Application to Flood Hazard Assessment, in: Palaeohydrology, Geography of the Physical Environment, edited by: Herget, J. and Fontana, A., Springer, Cham, Switzerland, https://doi.org/10.1007/978-3-030-23315-0_11, 213–228, 2020.

Vött, A., Handl, M., and Brückner, H.: Rekonstruktion holozäner Umweltbedingungen in Arkanien (Nordwestgriechenland) mittels Diskriminanzanalyse von geochemischen Daten, Geologica et Palaeontologica, 36, 123–147, 2002.

Woodward, J., Macklin, M., Fielding, L., Millar, I., Spencer, N., Welsby, D., and Williams, M.: Shifting sediment sources in the world's longest river: A strontium isotope record for the Holocene Nile, Quaternary Sci. Rev., 130, 124–140, https://doi.org/10.1016/j.quascirev.2015.10.040, 2015.

Woronko, B.: Late-Holocene dust accumulation within the ancient town of Marea (coastal zone of the South Mediterranean Sea, N Egypt), Quatern. Int., 266, 4–13, https://doi.org/10.1016/j.quaint.2011.09.010, 2012.

Wunderlich, J.: Investigations on the development of the western Nile Delta in Holocene times, in: The Archaeology of the Nile Delta: Problems and Priorities, edited by: van den Brink, E. C. M., Neth. Found. Archaeol. Res. Egypt, Amsterdam, the Netherlands, 251–257, 1988.

Wunderlich, J.: Untersuchungen zur Entwicklung des westlichen Nildeltas im Holozän, Marburger Geographische Schriften, 114, Marburg/Lahn, Germany, 1989.

Wunderlich, J. and Andres, W.: Late Pleistocene and Holocene evolution of the western Nile delta and implications for its future development, in: Von der Nordsee bis zum Indischen Ozean, Erdkundliches Wissen, edited by: Brückner, H. and Radtke, U., Franz Steiner Verlag, Stuttgart, Germany, 105–120, 1991.

Wunderlich, T., Fischer, P., Wilken, D., Erkul, E., Mecking, R., Günther, T., Heinzelmann, M., Vött, A., and Rabbel, W.: Constraining electric resistivity tomography by direct push electric conductivity logs and vibracores: An exemplary study oft he Fiume Morto silted riverbed (Ostia Antica, western Italy), Geophysics, 83, B87–B103, https://doi.org/10.1190/geo2016-0660.1, 2018.

E&G Quaternary Sci. J., 70, 165–169, 2021
https://doi.org/10.5194/egqsj-70-165-2021

Open Access E&G Quaternary Science Journal

Express report

Spatial survey of tephra deposits in the middle Lahn valley (Hesse, Germany)

Collin J. Weber, Volker M. H. Dickhardt, and Stefan Harnischmacher

Department of Geography, Philipps-University Marburg, Marburg, 35032, Germany

Correspondence: Collin J. Weber (collin.weber@geo.uni-marburg.de)

Relevant dates: Received: 26 March 2021 – Revised: 11 May 2021 – Accepted: 1 June 2021 – Published: 1 July 2021

How to cite: Weber, C. J., Dickhardt, V. M. H., and Harnischmacher, S.: Spatial survey of tephra deposits in the middle Lahn valley (Hesse, Germany), E&G Quaternary Sci. J., 70, 165–169, https://doi.org/10.5194/egqsj-70-165-2021, 2021.

1 Introduction

Tephra deposits and especially Laacher See tephra (LST) deposits resulting from the Laacher See eruption (12.9 ka) are an important stratigraphic marker for the Allerød period in central Europe (van den Bogaard and Schmincke, 1995). Within the central German low mountain range (Rhenish Massif and eastern areas) the LST was found within soils (initial deposits, sheltered slope positions) and valleys (relocated deposits) (Bos and Urz, 2003; Hahn and Opp, 2005). The Niederweimar gravel quarry, located on the lower terrace in the middle reach of the Lahn River valley south of Marburg (Hesse, Germany), is known for its high-resolution stratigraphy of Quaternary gravel deposits and late glacial, as well as Holocene, floodplain fines (Lomax et al., 2018). This particular stratigraphy is mainly achieved by the up to 2 m thick LST deposits, which consist of pure LST beds and a multitude of fine LST bands (partly interbedded with black sands or interrupted by clay bands). The origin of the LST in the floodplain is attributed to an extensive deposition (aeolian, directly in the floodplain), as well as later fragmentation of the tephra deposits by surface erosion and renewed deposition of LST from the catchment area through changing river systems (Bos and Urz, 2003; Lomax et al., 2018). The surroundings of the gravel quarry are also rich in archaeological finds reaching more or less continuously from the Mesolithic (11.7 to 7.5 ka) to the Middle Ages (Bos and Urz, 2003; Lomax et al., 2018). Further well-summarized information about the situation within the Niederweimar gravel quarry can be found in Lomax et al. (2018) or on the website of the archaeological survey of Hesse (https://lfd.hessen.de/, last access: 21 March 2021).

The evidence of LST in the Lahn valley, as in other valley sediments, is often limited to gravel pits (other larger excavations). These pits and their profiles offer very good insights (e.g. detailed lithostratigraphic description of profiles), but they are always limited to a comparatively small spatial section of the entire floodplain (gravel pit area). Therefore, the objective of the presented study is to provide a spatial survey of LST deposits in the middle Lahn valley, covering the entire floodplain cross section. The following two questions form the focus of the spatial survey. (1) How is the lateral and vertical extension of the LST deposits within the Lahn valley floodplain? (2) Does the spatial distribution provide overarching information about the deposition dynamics of the LST? For this purpose, a transect-based survey with qualitative analysis of LST grains based on density separation and visual identification (stereomicroscope) was applied.

2 Methods

Survey and sampling of tephra samples was conducted at three floodplain transects (including active floodplain zone and lower terrace) in the south of Niederweimar gravel quarry where the floodplain shows one of its greatest transverse expansions (Fig. 1). Transects cover a maximum width of 973.9 m and are at 170.9 m a.s.l. (above sea level) with a height difference of ±1.4 m. Sampling was carried out with the help of a hand auger (Pürckhauer, Ø 2 cm, 2 m depth) and pile core probing (Ø 6–8 cm, 3 m depth). Soil properties and stratigraphy were documented in the field according to the national standard soil classification scheme (KA5, Ad-hoc AG Boden, 2005). Tephra-containing layers were identified visually (visible tephra grains) or by smeary consistence (owing to higher contents of allophane) (Jahn et al., 2006), proportion documented (percentage of tephra grains estimated by area according to KA5), and extracted for further analysis.

Samples for method validation and as comparison material (reference samples) were taken from a recently excavated profile (32U 480710 5621590) in the Niederweimar gravel quarry, which was excavated during archaeological work. The profile consists of Holocene floodplain loams (silt to sandy loam) above four LST layers (sandy loam, partwise alternating with black sands and ripple) and flood loam (late Pleistocene) at the base (Fig. 2). Three samples were taken from the upper (LST bands mixed with sandy loam), middle (thick LST bands, between black sands) and lower (LST bands interrupted by black sands with ripple shapes) parts of the LST layer (Fig. 2).

Reference samples and samples from the transects were dried at 100 °C (drying chamber) under weight loss control, subsequently carefully ground, and sieved to < 2 mm (stainless steel sieve, Retsch, Haan, Germany). Subsample material (20g per sample) was then mixed with 150 mL saturated NaCl solution (density adjusted, $\rho = 1.2\,\mathrm{g\,cm^{-3}}$) within glass beakers, stirred (1 min, magnetic stirrer) and allowed to sediment for 20 min. This allows the tephra grains to be separated from other mineral components (sand to clay grains), despite the heavy minerals contained (Lomax et al., 2018), because the grains float in the dry state due to their many cavities (volcanic origin). The floating tephra grains were then sieved to > 50 µm (Atechnik, Leinburg, Germany) to separate clay and/or silt particles and filtered by vacuum filtration (cellulose filter, LLG-Labware, Meckenheim, Germany) to rinse out remaining salts. Dried filters were visually examined using a stereomicroscope (Motic SMZ-161 TL, Motic, Hong Kong). From the reference samples, 30 randomly selected tephra grains were extracted and measured (Moticam, Motic, Hong Kong). Samples from the transects were inspected according to the presented method, and the presence of tephra grains or their fragments was considered a positive finding. In addition, 19 samples containing proven LST were selected, and the particle size distribution was determined according to DIN ISO 11277 (2002) and the integral suspension pressure method (Durner et al., 2017).

3 Results and discussion

In total 56 tephra containing stratigraphically distinguishable layers were identified and sampled. Qualitative tephra analyses within the laboratory show a positive rate of 69.6 % in which case tephra could be detected under the microscope for the 56 samples. In 30.4 % of the layers, no tephra grains or larger fragments could be found even if the Greasing effect occurred in the field. The applied method is therefore suitable for qualitative detection, is fast and inexpensive, and can be extended by other methods such as mineral analysis and dating. Tephra grains occur usually entire with grey-brown to greenish colours, clear holes and glassy surface structure (Fig. 2). The length to width ratio of the grains from a random sample of 30 grains comprises an average length of 782.7 (±288.4) µm and width of 557.12 (±179.5) µm. Grain surface and average and maximum length (1565.9 µm) correspond clearly to the reference samples (same colour, holes and glassy structure) with an average length of 724.3 (±245.6) µm.

Tephra layers come up at average depths of 68.6 cm below surface and end at average depths of 166.5 cm (±46.3 cm). Tephra layers have thicknesses from 6.0 up to 132.0 cm with an average thickness of 52.0 cm (Figs. 1b and 2). Grain size analyses of tephra-containing layers has a mean distribution of 30.2 % clay, 46.8 % silt and 23.1 % sand. However, the share of sand is ranging between 2.7 % and 57.9 %, resulting in the samples comprising the grain size classes clay, silty clay, silty clay loam to silt loam (outliers within loam and sandy loam), and they are thus very heterogeneous.

Stratigraphic classification of tephra layers corresponds to the findings of our reference profile and other profiles within the Niederweimar quarry (e.g. Lomax et al., 2018): The tephra layers are covered by Holocene floodplain sediments (floodplain loams, silty loams) and rarely with single clay layers or isolated gravel deposits. The lowermost tephra layers, partly with the same pattern of banding (LST bands and black sands) (Fig. 2), however, are only poorly visible within the drill sample in contrast to quarry profiles. Below the tephra, a thin band (approx. 5 cm) of sand with gravel occurs, followed by a thick layer of clay (dark and rich in organic matter), before the gravel deposits of the lower terrace begin.

Regarding the vertical and lateral spatial distribution of tephra layers it can be stated that it is present nearly all over the floodplain area of the middle Lahn valley. The interpolation of the upper and lower tephra boundaries (Fig. 1b) shows that it is independent of the terrain surface today. This indicates that the tephra follows the morphology of Pleistocene gravel and flood loam deposits, as observed within the quarry (reference profile). The tephra is missing at the edge of the floodplain (drill point 101a: transition to the lower slope, colluvial formation), in the area of the active floodplain (drill points 108a and 2010a: river erosion) and in parts with inactive channel situations (drill point 304b) where Pleistocene

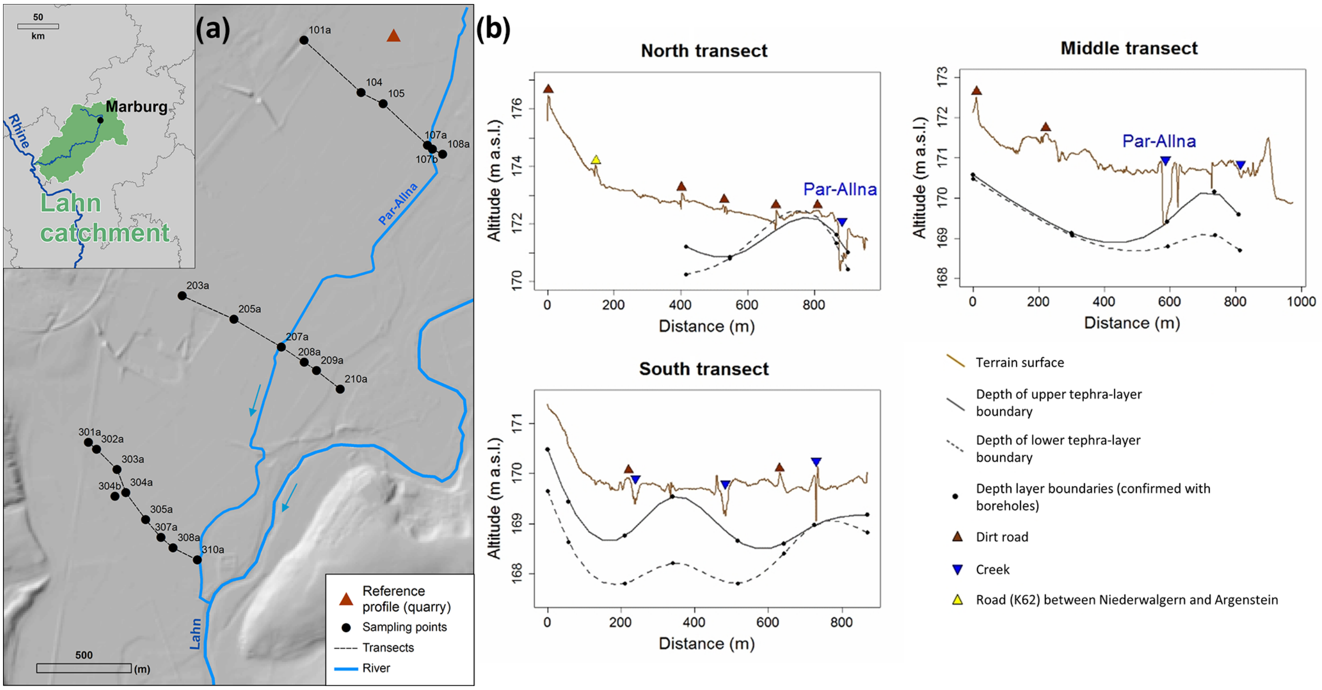

Figure 1. Study area located within the Lahn River catchment in the south of Marburg and transects with interpolated upper and lower tephra boundaries. **(a)** Transects with sampling points (drill cores) and location of reference profile within the quarry. **(b)** Interpolated upper and lower tephra boundaries under terrain surface. Deviation in the interpolation (lower limit) results from large distances between the boreholes (no borehole due to missing permission). Data basis: Hessian State Agency for Soil Management and Geoinformation (HVBG, 2019).

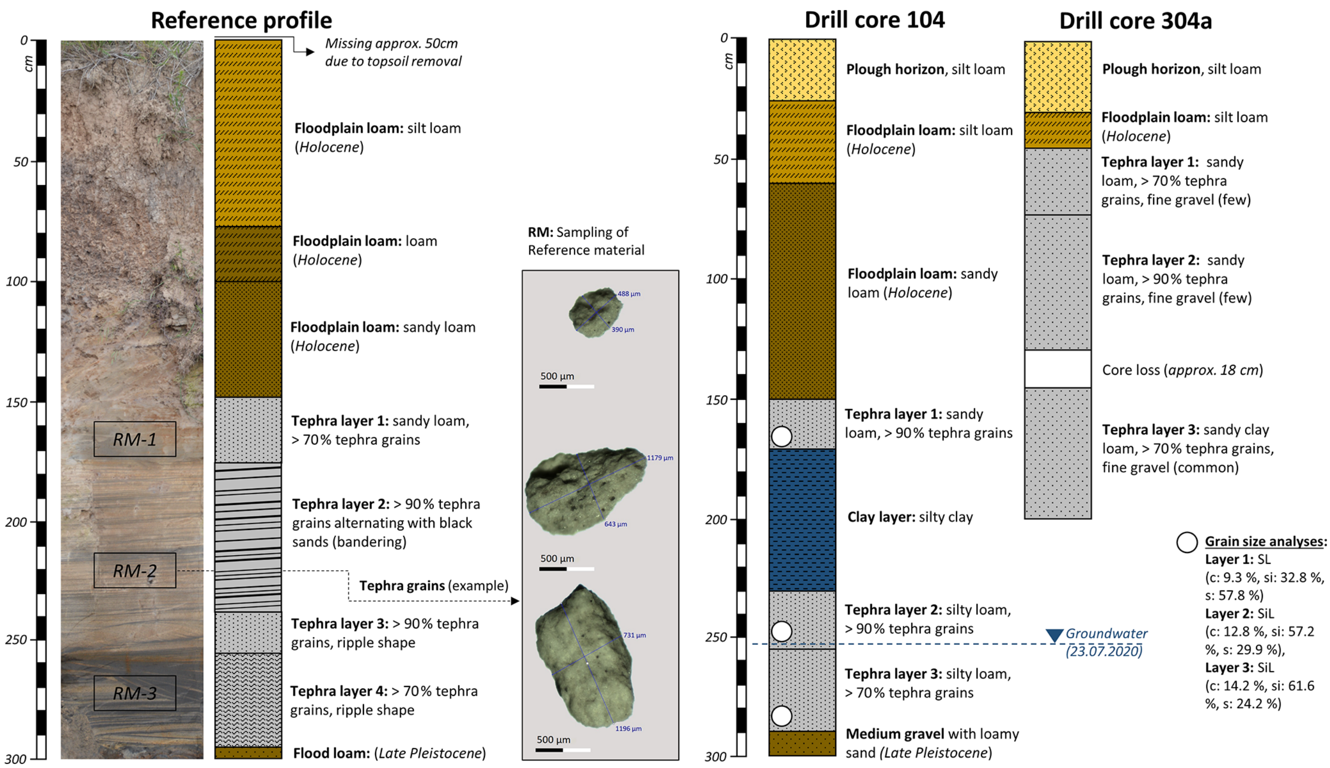

Figure 2. Lithological description of reference profile (with exemplary separated tephra grains) and exemplary drill cores (104: north transect; 304a: south transect).

gravel structures are found directly below the terrain surface. The interpolation also indicates, despite spatial inaccuracies, that the position of the lower tephra border allows for a partwise reconstruction of the terrain surface that existed at the time of deposition, with structures of various flow channels preformed in the Pleistocene.

Regarding the depositional conditions for LST within the Lahn River valley the heterogeneous grain size distribution indicates slow to medium flow velocities (clay–silt deposition) during LST deposition. From the findings presented in this report an area-wide deposition of LST in the middle Lahn valley can be assumed, which encompasses the entire width of the floodplain. LST deposits seem to follow the structure of preformed Pleistocene flow channels throughout the floodplain, as already stated for the quarry profiles (Bos and Urz, 2003; Lomax et al., 2018). The heterogeneous grain size distribution, banding of the LST with sandy loam intermediate layers and the absence of LST in the floodplain margin and active floodplain area (erosion) indicate fluvial deposition. Therefore, it can be concluded that the LST deposits originate from the entire upper catchment area and have been reworked within the entire floodplain.

4 Conclusion

The present survey shows an area-wide occurrence of LST deposits within the floodplain area of the middle Lahn valley. Vertical extension of LST deposits seems to follow preformed Pleistocene channel structures. The spatial distribution of LST deposits allows for an overreaching consolidation of former findings regarding the LST deposition and origin: LST deposition took place during the Allerød period, when river systems change due to climatic shifts. The findings presented here support the assumption that large quantities of LST have been deposited and relocated in the floodplain, which must originate mainly from fluvial transport originating from the entire catchment area instead of direct aeolian deposition. The widespread distribution of the sediments alone suggests large quantities of LST. Even though the analyses of quarry profiles have provided major insights about LST deposition in previous research, the presented results offer a spatial view that goes beyond this and contribute to the reconstruction of preformed Pleistocene channel structures. As the pure LST deposits occurring in the Lahn valley represent a special stratigraphic unit, further research should aim to clarify the details of LST deposition, exact sequence of events and former river system characteristics by a holistic spatial methodological approach in the future and also in other regions. In relation to the more than 11 000 years of documented settlement history within the study area, the immense occurrence and widespread distribution of tephra deposits may have influenced land use and cultivation opportunities across different cultures. Despite the fact that the aeolian deposition, fluvial transport and redeposition of a massive amount of tephra at the beginning of the Holocene had an immense impact on the landscape and humans at that time, the deposits that are still present today provide an enhancement of the soil properties. In contrast to other valleys without these amounts of tephra, the alluvial floodplain soils of the middle Lahn valley can probably have a higher water holding capacity in dry periods, as well as a positive influence on groundwater reserves due to the tephra grains even if their soil cultivation might be affected by compaction (stagnic properties, stagnosols) in some places. Further interdisciplinary research from the fields of soil science and archaeology should examine the considerations and effects of the tephra deposits beyond their use as stratigraphic markers.

Data availability. The digital elevation model is used with the permission of the Hessian State Agency for Soil Management and Geoinformation. All further data generated during this study are included in this article or are available from the corresponding author upon request.

Author contributions. CJW conceived the project. CJW and VMHD collected reference samples and performed the profile description in the field. VMHD performed the spatial survey and further sample collection. CJW and VMHD have developed, tested and applied the density separation method for tephra grain extraction. VMHD performed the laboratory work. All authors contributed to the interpretation of the data and have contributed to the manuscript's initial and review processes.

Competing interests. The authors declare that they have no conflict of interest.

Disclaimer. Publisher's note: Copernicus Publications remains neutral with regard to jurisdictional claims in published maps and institutional affiliations.

Acknowledgements. The authors would like to thank the operators of the Niederweimar gravel quarry, as well as the Wissenschaftliche Baugrund-Archäologie e.V. (WiBA), namely Benedikt König for access to new excavations. Likewise, the authors would like to acknowledge the landowners for access to their land, as well as the handling editor and one anonymous referee for the improvement of our contribution.

Review statement. This paper was edited by Elisabeth Dietze and reviewed by one anonymous referee.

References

Ad-hoc AG Boden: Bodenkundliche Kartieranleitung (Manual of soil mapping) (KA5), Bundesanstalt für Geowissenschaften und Rohstoffe, Hannover, Vol. 5, 438 pp., ISBN 9783510959204, 2005.

Bos, J. A. A. and Urz, R.: Late Glacial and early Holocene environment in the middle Lahn river valley (Hessen, central-west Germany) and the local impact of early Mesolithic people – pollen and macrofossil evidence, Veg. Hist. Archaeobot., 12, 19–36, https://doi.org/10.1007/s00334-003-0006-7, 2003.

Durner, W., Iden, S. C., and von Unold, G.: The integral suspension pressure method (ISP) for precise particle-size analysis by gravitational sedimentation, Water Resour. Res., 53, 33–48, https://doi.org/10.1002/2016WR019830, 2017.

Freund, H. and Urz, R.: Ein frühweichselzeitliches Profil aus der Niederterrasse der mittleren Lahn (Weimar-Niederweimar, Hessen) – geologische, pollenanalytische und makrorestanalytische Untersuchungen. E&G – Quaternary Sci. J., 50, A. 08, https://doi.org/10.23689/fidgeo-1332, 2000 (in German).

Hahn, J. and Opp, C.: Geochemische Eigenschaften von Laacher See-Tephra enthaltenden Bodensubstraten in eruptionsnaher underuptionsferner Position, Geol. Jb. Hessen 137, 65–77, 2011.

Jahn, R., Blume, H. P., Asio, V. B., Spaargaren, O., and Schad, P.: Guidelines for soil description, Food and Agriculture Organization of the United Nations (FAO), Rome, Vol. 4, 97 pp., ISBN 9789251055212, 2006.

Lomax, J., Steup, R., Shumilovskikh, L., Hoselmann, C., Sauer, D., van Diedenhoven, V., and Fuchs, M.: Field Trip B (27 September 2018): Quaternary environments of Giessen and its surrounding areas, DEUQUA Spec. Pub., 1, 15–28, https://doi.org/10.5194/deuquasp-1-15-2018, 2018.

Mäckel, R.: Untersuchungen zur jungquartären Flußgeschichte der Lahn in der Gießener Talweitung, E&G Quaternary Sci. J., 20, 138–174, https://doi.org/10.3285/eg.20.1.14, 1969.

Van den Bogaard, P.: $^{40}Ar/^{39}Ar$ ages of sanidine phenocrysts from Laacher See Tephra (12,900 yr BP): Chronostratigraphic and petrological significance, Earth Planet. Sc. Lett, 133, 163–174, 1995.

Van den Bogaard, P. and Schminke, H. U.: Laacher See Tephra: A widespread isochronous Late Quaternary tephra layer in central and Northern Europe, Geol. Soc. Am. Bull., 96, 1554–1571, https://doi.org/10.1130/0016-7606(1985)96<1554:LSTAWI>2.0.CO;2, 1995.

E&G Quaternary Sci. J., 70, 171–186, 2021
https://doi.org/10.5194/egqsj-70-171-2021

Open Access E&G Quaternary Science Journal

Research article

Revisiting the subalpine Mesolithic site Ullafelsen in the Fotsch Valley, Stubai Alps, Austria – new insights into pedogenesis and landscape evolution from leaf-wax-derived *n*-alkanes, black carbon and radiocarbon dating

Michael Zech[1,2,★], Marcel Lerch[1,2,★], Marcel Bliedtner[3], Tobias Bromm[2], Fabian Seemann[1], Sönke Szidat[4], Gary Salazar[4], Roland Zech[3], Bruno Glaser[2], Jean Nicolas Haas[5], Dieter Schäfer[6], and Clemens Geitner[7]

[1]Heisenberg Chair of Physical Geography with Focus on Paleoenvironmental Research, Department of Geosciences, Technische Universität Dresden, Helmholtzstr. 10, 01096 Dresden, Germany
[2]Soil Biogeochemistry Group, Institute of Agronomy and Nutritional Sciences, Martin-Luther University Halle-Wittenberg, Von-Seckendorff-Platz 3, 06120, Halle (Saale), Germany
[3]Chair of Physical Geography, Institute of Geography, Friedrich Schiller University of Jena, Löbdergraben 32, 07743 Jena, Germany
[4]Department of Chemistry, Biochemistry and Pharmaceutical Sciences & Oeschger Centre for Climate Change Research, University of Bern, Freiestrasse 3, 3012 Bern, Switzerland
[5]Institute of Botany, University of Innsbruck, Sternwartestr. 15, 6020 Innsbruck, Austria
[6]Institute of Archaeology, University of Innsbruck, Langer Weg 11/3, 6020 Innsbruck, Austria
[7]Institute of Geography, University of Innsbruck, Innrain 52, 6020 Innsbruck, Austria
★These authors contributed equally to this work.

Correspondence: Michael Zech (michael.zech@tu-dresden.de)

Relevant dates: Received: 11 January 2021 – Revised: 29 May 2021 – Accepted: 16 June 2021 – Published: 13 July 2021

How to cite: Zech, M., Lerch, M., Bliedtner, M., Bromm, T., Seemann, F., Szidat, S., Salazar, G., Zech, R., Glaser, B., Haas, J. N., Schäfer, D., and Geitner, C.: Revisiting the subalpine Mesolithic site Ullafelsen in the Fotsch Valley, Stubai Alps, Austria – new insights into pedogenesis and landscape evolution from leaf-wax-derived *n*-alkanes, black carbon and radiocarbon dating, E&G Quaternary Sci. J., 70, 171–186, https://doi.org/10.5194/egqsj-70-171-2021, 2021.

Abstract: Archaeological research in high mountain regions has gotten a lot more attention since the discovery of the copper age mummy called "Ötzi" in the Ötztaler Alps in 1991. In the Tyrolean Stubai Alps, the Mesolithic site Ullafelsen at 1869 m a.s.l. (above sea level) close to the recent upper timberline in the Fotsch Valley represents, on the one hand, a very important archaeological reference site and offers, on the other hand, intriguing research questions related to, amongst others, pedogenesis. Given that no biomarkers and stable isotopes have been hitherto investigated, we aimed at contributing with respective analyses and additional radiocarbon dating to a better understanding of the landscape evolution and pedogenesis on and around the Ullafelsen.

Our results for modern vegetation suggest that leaf-wax-derived *n*-alkanes allow us to chemotaxonomically distinguish between subalpine deciduous trees (nC_{27} predominance) versus (sub)alpine grasses, herbs and dwarf shrubs (nC_{29}, nC_{31} and/or nC_{33} predominance). Except for *Juniperus*, conifers produce no or extremely low n-alkane contents. Although no clear vegetation changes could be inferred from the n-alkane patterns of the investigated soil profiles, the total n-alkane content (TAC) was developed for the first time as an unambiguous proxy for distinguishing between buried (= fossil) topsoils (2Ahb horizons) and humus-enriched subsoils such as Bh horizons of podzols. Based on this leaf wax proxy, we can rule out that the 2Ahb?/Bh? horizons under question on the Ullafelsen are buried topsoils as suggested previously. Dating of the H_2O_2-pretreated soil samples yielded ^{14}C ages for the podzol Bh horizons ranging from 6.7 to 5.4 cal kyr BP. This is clearly younger than the overlying Mesolithic living floor (LL) (10.9 to 9.5 cal kyr BP) but pre-dates the assumed intensification of alpine pasturing from the Bronze Age onwards. Both the LL and the directly overlying OAh3 horizon yielded black carbon maxima and benzene polycarboxylic acid patterns reflecting fire-induced human impact during the Mesolithic. The discrepancy between the Mesolithic charcoal ^{14}C ages (ages of $\geq$ 9.5 cal kyr BP) versus the ^{14}C ages obtained for bulk n-alkanes ranging from 8.2 to 4.9 cal kyr BP suggests that non-alkane-producing conifers predominated the vegetation on and around the Ullafelsen after the Mesolithic occupation. Only with the anthropo-zoological lowering of the timberline associated with alpine pasturing since the Neolithic and especially the Bronze Age has an n-alkane-producing vegetation cover (grasses, herbs or dwarf shrubs) started to predominate.

Kurzfassung: Mit dem Fund der kupferzeitlichen Mumie „Ötzi“ in den Ötztaler Alpen im Jahr 1991 hat die Hochgebirgsarchäologie viel Aufmerksamkeit erfahren. So wurde unter anderem der fürs Mesolithikum sehr bedeutende Fundplatz Ullafelsen in 1869 m ü.NN. nahe der oberen Waldgrenze im Fotschertal in den Stubaier Alpen entdeckt, der auch aus bodengenetischer Sicht spannende Fragen aufwirft. Ziel der vorliegenden Arbeit ist es, basierend auf Biomarker- und Stabilisotopenanalysen sowie zusätzlichen Radiokohlenstoffdatierungen (^{14}C) einen Beitrag zum besseren Verständnis der Landschaftsentwicklung und Bodengenese des Untersuchungsgebietes zu leisten.

Unsere Ergebnisse zeigen, dass blattwachsbürtige n-Alkane als Lipidbiomarker eine chemotaxonomische Unterscheidung von subalpinen Laubbäumen (Dominanz von nC_{27}) und (sub)alpinen Gräsern, Kräutern und Sträuchern (Dominanz von nC_{29}, nC_{31} und/oder nC_{33}) erlauben. Dagegen produzieren Nadelbäume mit Ausnahme von *Juniperus* keine oder kaum n-Alkane. Zwar lassen sich basierend auf den n-Alkanmustern keine eindeutigen Vegetationsänderungen für die untersuchten Bodenprofile vom Ullafelsen belegen; dafür konnten die n-Alkangehalte (TAC) erstmalig als aussagekräftiger Proxy für die Unterscheidung von begrabenen ehemaligen (= fossilen) Oberböden (2Ahb Horizonte) und humusangereicherten Unterböden (wie Bh Horizonten von Podsolen) entwickelt werden. Basierend auf diesem Blattwachsproxy kann für die fraglichen 2Ahb?/Bh? Horizonte am Ullafelsen zweifelsfrei ausgeschlossen werden, dass es sich so wie bisher vermutet um begrabene spätglaziale Oberböden handelt. Die Datierung H_2O_2-behandelter Bodenproben dieser podsolbürtigen Bh Horizonte lieferte ^{14}C-Alter zwischen 6.7 bis 5.4 cal kyr BP. Das ist stratigraphisch inkonsistent und deutlich jünger als der überlagernde und anhand von Holzkohlen auf 10.9 bis 9.5 cal kyr BP datierte mesolithische Begehungshorizont (LL) aber älter als die ab der Bronzezeit einsetzende Almwirtschaft. Sowohl Black Carbon (BC) Maxima als auch die Muster von Benzolpolycarbonsäuren (BPCAs) als BC Biomarker in der LL und dem unmittelbar überlagernden OAh3 Horizont belegen den menschlichen Einfluss durch Feuer während des Mesolithikums. Während die mesolithischen Holzkohlen ^{14}C Alter $\geq$ 9.5 cal kyr BP liefern, deuten die ^{14}C Alter von 8.2 bis 4.9 cal kyr BP für n-Alkane darauf hin, dass unmittelbar nach der mesolithischen Besiedelung am Ullafelsen eine Vegetation vorgeherrscht haben muss, die kaum n-Alkane produziert hat (= Nadelbäume). Erst mit der anthropozoologisch bedingten Absenkung der Waldgrenze durch Almwirtschaft seit dem Neolithikum und insbesondere während der Bronzezeit begann n-alkanproduzierende Vegetation (Gräser, Kräuter und Zwergsträucher) vorzuherrschen.

1 Introduction

Archaeological research in high mountain regions has gotten a lot of attention since the discovery of the copper age mummy called "Ötzi" in the Ötztaler Alps in 1991. Results of former archaeological research projects show that Mesolithic hunter-gatherers lived in the Alpine regions from the beginning of the Holocene (Fontana et al., 2016, and publications in the special issue MesoLife). For instance, Cornelissen and Reitmaier (2016) presented detailed respective evidence from the central and southeastern Swiss Alps. In the Tyrolean Stubai Alps, the Mesolithic site Ullafelsen at 1869 m a.s.l. (above sea level) and its surroundings in the Fotsch Valley represent a very important archaeological reference site (Schäfer, 2011a) (Fig. 1). Thousands of archaeological artefacts and several fire places were found, which provide evidence of the presence and the human–environment interaction of our ancestors (Schäfer, 2011b). Accordingly, the Ullafelsen was used as a summer camp during the Preboreal and the Boreal from around 10.9 to 9.5 kyr BP. Apart from high mountain archaeology, the "Mesolithic project Ullafelsen" included many more scientific disciplines, ranging from geology, petrography, geomorphology, sedimentology and soil science to (paleo)botany (Schäfer, 2011a).

From a pedological and sedimentological perspective, a striking and frequently occurring light layer (LL) attracted much attention on the Ullafelsen (Geitner et al., 2011, 2014). In the subalpine zone, light horizons typically developed as eluvial albic horizons (*E* horizons) due to biotic and climatic factors favouring podzolisation (Zech and Wilke, 1977; Egli et al., 2008). On the Ullafelsen, the LL reveals, however, several characteristics that are untypical for *E* horizons, and the LL is considered as the Mesolithic living floor. Indeed, most of the artefacts and fire places were found in and on the LL (Fig. 2). Based on stratigraphical features and related soil analyses, Geitner et al. (2011, 2014) suggested that the LL developed by aeolian dust deposition during the Younger Dryas (YD) and that it overlies a late glacial buried topsoil (2Ahb) that developed during the favourable climatic conditions of the Bølling–Allerød period. Unequivocal evidence for the existence of this late glacial 2Ahb horizon is, however, hitherto missing, and neither micromorphological nor preliminary ^{13}C nuclear magnetic spectroscopy results were able to resolve this issue.

Over the past decades, analytical progress has allowed us to develop new methods in the field of biogeosciences based on the investigation of organic marker molecules (biomarkers) and stable isotopes (e.g. Glaser, 2005; Zech et al., 2011b), which complements more traditional analytical approaches. For instance, black carbon (BC) based on the analyses of benzene polycarboxylic acids (BPCAs) as organic marker molecules can serve as a proxy for fire-derived carbon and aromatic-structured molecules in general even if char particles are not preserved (Glaser et al., 1998, 2001; Glaser and Birk, 2012; Lehndorff et al., 2015). Similarly, plant leaf-wax-derived *n*-alkane biomarkers are preserved in soils and sediments over at least glacial–interglacial timescales, have potential in chemotaxonomic studies and thus allow us to reconstruct vegetation changes from palaeoenvironmental archives even if the preservation of pollen is poor (Zech et al., 2012; Lemma et al., 2019; Trigui et al., 2019). Moreover, compound-class radiocarbon dating of bulk *n*-alkanes was developed during the last years and allows us to address both potential pre-ageing and potential post-depositional rejuvenation of *n*-alkanes in sedimentary archives (Zech et al., 2017; Lerch et al., 2018; Bliedtner et al., 2020). Last but not least, other molecular lipid biomarkers allow us to infer, for instance, dietary information in geoarchaeological studies (Grillo et al., 2020), and the stable nitrogen isotopic composition ($\delta^{15}N$) of soils allows us to infer the human-induced opening of the N cycle (Zech et al., 2011a). Such biomarker and stable isotope studies had been hitherto not tested and applied within the "Mesolithic project Ullafelsen".

The overall aim of this geoarchaeological follow-up study was, therefore, to contribute particularly with biomarker and stable isotope analyses, as well as with radiocarbon dating, for a better understanding of the pedogenesis, the human impact and the landscape evolution on and around the Mesolithic site Ullafelsen. More specifically, we addressed the following questions. (i) Is the humus-enriched subsoil horizon on the Ullafelsen a buried topsoil (2Ahb horizon) or humus-enriched by podzolisation (Bh horizon)? (ii) Do biomarker and stable isotope results validate the LL as the Mesolithic living floor and/or eluvial albic horizon? (iii) Do *n*-alkane biomarkers allow us to chemotaxonomically distinguish the dominant vegetation types around the Ullafelsen and is there any evidence for late glacial and Holocene vegetation changes from *n*-alkanes on the Ullafelsen? (iv) Is there evidence for human impact from black carbon on the Ullafelsen? (v) Can we gain new insights from merging existing knowledge with new biomarker-based findings?

2 Material and methods

2.1 Study area: the Ullafelsen in the Fotsch Valley, Stubai Alps, Austria

The study area was described in detail previously (Schäfer, 2011a). In brief, the approximately 13 km long Fotsch Valley is situated in the northern part of the Stubai Alps southwest of Innsbruck (Fig. 1). In the south, the highest mountain is the Hohe Villerspitze at 3087 m a.s.l.; in the north, the Fotsch Creek discharges into the Melach River (tributary of the Inn River) in the Sellrain Valley and the village of Sellrain at about 900 m a.s.l.

Geologically, the Fotsch Valley is part of the "Ötztal-Stubai crystalline complex", which belongs to the Austroalpine nappes. Its metamorphic rocks, which are mainly Para- and Orthogneisses, primarily built up the valley. In

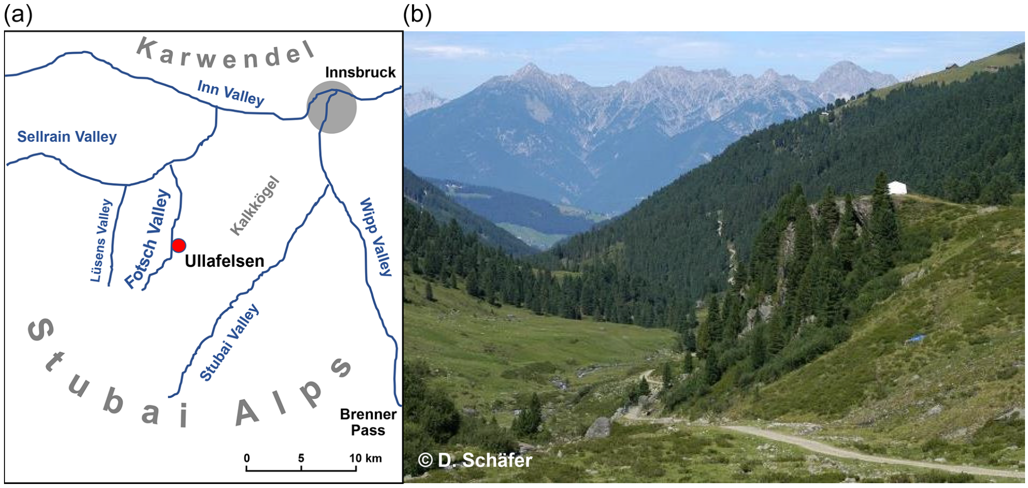

Figure 1. **(a)** Map showing the location of the Mesolithic site Ullafelsen in the Fotsch Valley southwest of Innsbruck, Austria. **(b)** Northward view from the inner Fotsch Valley over the Ullafelsen (1869 m a.s.l.) near the recent upper timberline located at 1800–2000 m a.s.l. (the white tent indicates the archaeological excavation) and toward the Karwendel mountain range in the Northern Limestone Alps (from Schäfer, 2011b).

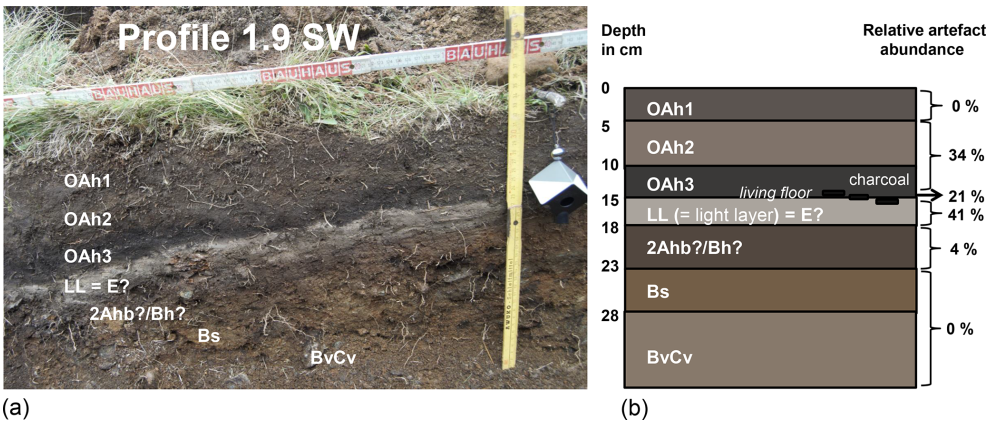

Figure 2. **(a)** Soil profile 1.9 SW on the Ullafelsen with the strikingly humus-enriched OAh3 and 2Ahb?/Bh? horizons. The latter was suggested by Geitner et al. (2011) to be a buried topsoil (→ 2Ahb) that was buried by aeolian deposition during and after the Younger Dryas. **(b)** Schematic horizontation of the soil profiles on the Ullafelsen; actually, the profiles reveal a high heterogeneity. The LL (light layer) reveals the highest relative artefact abundance, is overlain by several fire places on the Ullafelsen and is considered as the living floor of the Mesolithic hunter-gatherers. Please note that in previous publications (Geitner et al., 2011, 2014) the topsoil horizons were classified as Ah horizons. Due to TOC concentrations partly $\geq 15\,\%$ we add the classification as O layers.

the southern part, mountain peaks (e.g. Villerspitzen) are of amphibolite (Nittel, 2011). During glacial times, the Fotsch Valley became U-shaped by glacial erosive processes; the Ullafelsen at 1869 m a.s.l. (47.14702° N, 11.21475° E) represents a rock hummock (Fig. 1). Several moraine walls at around 2000 m a.s.l. in the valley were assigned to the Egesen Stadial (Younger Dryas). The deposition of the innermost moraines during the early Preboreal around 11.0 kyr ago is explicitly not excluded by Kerschner (2011) and might be explained with a glacier advance caused by pronounced humid conditions and a solar activity minimum during the “Preboreal Humid Phase” around 11.2 kyr BP (Hepp et al., 2019). Nowadays, only a small glacier, the Fotscher Ferner, remains on the southernmost slopes of the valley.

Climatically, the Fotsch Valley is situated within the European west wind belt characterised by moderate climate and in a transition zone between the Northern and the Central Alps (Schlosser, 2011). The microclimate strongly depends on local conditions and orography with thermally and orographically induced wind systems being very regular.

The vertical vegetation gradients in the Fotsch Valley are similar to other parts of the Central Alps (Kemmer, 2011). Montane spruce forests with *Picea abies* dominance grow up to an elevation of 1600 m a.s.l. Above, it is replaced by the subalpine Arolla pine forest (*Pinus cembra*). While the potential timberline reaches up to 2200 m a.s.l., the actual timberline at 1800–2000 m a.s.l. is considered to have been lowered by anthropo-zoological disturbances associated with alpine pasturing. The study site Ullafelsen lies at the timberline and is characterised by the transition to (sub)alpine dwarf shrubs and pastures. Above 2300 m a.s.l., alpine grasslands (*Nardus stricta*, *Caricion curvulae*) and vegetation adapted to snow (*Salicion herbaceae*) dominate (Kemmer, 2011). Additionally, *Alnus* and *Betula* shrubs occur along creeks and *Sphagnum* and *Carex* peat bogs with associated respective vegetation developed especially in the (sub)alpine zone.

Leptosols and Cambisols are the dominant reference soil groups occurring in the alpine and the montane zone, respectively. In the subalpine zone, Podzols are frequently found especially under (sub)alpine dwarf shrub vegetation, and Histosols have developed in flatter valley floors and in slope positions. As emphasised in the introduction, the light layer LL on the Ullafelsen (see Fig. 2) reveals several characteristics that are untypical for Podzol *E* horizons (Geitner et al., 2011, 2014). For instance, it is covered by an up to 15 cm thick OAh topsoil horizon, and the boundary between these units is often quite sharp. The LL is moreover considered as the Mesolithic living floor because in and on the LL most of the artefacts and fire places were found (Fig. 2). Geitner et al. (2011, 2014) suggested that the LL developed by aeolian dust deposition during and after the Younger Dryas (YD) and that it overlies a late glacial buried topsoil (2Ahb) that developed during the favourable climatic conditions of the Bølling–Allerød period. While unequivocal evidence for the existence of a late glacial 2Ahb horizon is hitherto missing, podzolisation processes alone can undoubtedly not explain the pedogenesis of the soil profiles on the Ullafelsen. Sedimentation processes are needed, too. The radiocarbon-dated fire places overlying the LL related to the presumed Mesolithic living floor serve as valuable chronological markers and date to the Preboreal and the Boreal periods from around 10.9 to 9.5 cal kyr BP (re-calibrated from Schäfer, 2011b) (Table S1 in the Supplement). Last but not least, recent optically stimulated luminescence (OSL) dating of the LL yielding an age of 10.9 ± 1.8 ka corroborates – despite the large age uncertainties – this chronology and the idea of aeolian dust input during the late-glacial–Holocene transition (Michael Meyer, personal communication, University of Innsbruck, Austria, 2021).

2.2 Sampling of modern vegetation and soil profiles

In total, 20 leaf samples of typical and dominant vegetation types were collected from the Ullafelsen and surroundings in July 2015 and from the nearby Potsdamer Hütte peat bog (1970 m a.s.l.) and surroundings in August 2019. The sample set comprises coniferous trees ($n=2$; *Picea abies*, *Pinus cembra*), *Juniperus communis* ($n=1$; considered separate from coniferous trees), deciduous trees ($n=2$; *Betula pendula*; *Alnus viridis*), alpine dwarf shrubs ($n=4$, *Vaccinium vitis-idaea*, *Vac. myrtillus*, *Calluna vulgaris*, *Rhododendron ferrugineum*), herbs ($n=5$; *Potentilla erecta*, *Cardamine amara*, *Epilobium palustre*, *Saxifraga spec.*, *Viola palustris*), mosses ($n=4$; *Moss spec.*, *Sphagnum rubellum*, *Sphag. cuspidatum*, *Amblystegiaceae*) and grasses ($n=2$; not specified).

Four profile walls from the archaeological excavation (1.1 B5W, 1.1 B5S, 1.1 C4W and 1.1 G5N) and three profile walls from a nearby trench (1.9 NE, 1.9 NW and 1.9 SW) on the Ullafelsen (Fig. 3) were sampled by horizon in August 2017, resulting in 37 soil samples in total. Note that the schematic horizons as described in Fig. 2 are not fully developed in all profiles. The samples were classified by horizon, and only those samples that could be unambiguously assigned were used for the further data evaluation ($n=33$): OAh1 ($n=3$), OAh2 ($n=3$), OAh3 ($n=3$), LL ($n=8$), 2Ahb?/Bh? ($n=6$), Bs ($n=5$) and BvCv ($n=5$). Moreover, a buried fire place was discovered several metres northeast of the excavation (RP20) (Fig. 3). There, three charcoal samples from 10, 15 and 20 cm depth were taken for radiocarbon dating.

In addition, 40 soil samples were taken from 13 profile walls elsewhere in the (sub-)alpine zone of the Fotsch Valley. Classification included *E* ($n=7$) and 2Ahb?/Bh? ($n=15$) horizons; those samples serve as reference for the geoarchaeological samples from the Ullafelsen. Both 2Ahb and Bh horizons are to be expected in the study area due to podzolisation and slope dynamics. A detailed overview of all investigated profiles and samples including all results is provided in the Supplement (Table S2 and Fig. S1).

2.3 Biogeochemical analyses and radiocarbon dating

The soil samples were air dried, sieved (< 2 mm) and finely ground. Total carbon (TC) and total nitrogen (N), as well as the stable carbon and nitrogen isotopic composition ($\delta^{13}C$ and $\delta^{15}N$, respectively), were determined using an elemental analyser coupled to an isotope ratio mass spectrometer (EA-IRMS). Given the non-carbonate parent rock material and the low pH values (< 4 in $CaCl_2$) of the soils (Geitner et al., 2011), we consider in the following TC values to reflect total organic carbon (TOC). The natural abundances of ^{13}C and ^{15}N are expressed in the usual δ scale; precision as determined by replication measurements of standards was 0.26 ‰ and 0.32 ‰, respectively.

Total lipid extracts from leaf and soil samples were obtained using Soxhlet and ultrasonic extraction following standard procedures (e.g. Lerch et al., 2018), and dichloromethane and methanol (9 : 1) were used as the solvent mixture. The aliphatic fraction including the *n*-alkanes was separated over aminopropyl pipette columns by eluting with hexane. The *n*-alkane identification and quantification were performed using a gas chromatograph–flame ionisa-

Figure 3. North-northwest view over the Ullafelsen at the upper timberline showing the geoachaeological excavation area 1.1 with the reopened and resampled profiles 1.1 B5, 1.1 C4 and 1.1 G5 and the newly opened and sampled profile, 1.9, several metres towards the southeast.

tion detector (GC-FID; GC-2010, Shimadzu) and external n-alkane standards. The total n-alkane contents (TACs) were calculated as the sum of nC_{21} to nC_{35} and are expressed in micrograms per gram ($\mu g\, g^{-1}$) for the leaf samples and additionally in micrograms per gram TOC for the soil samples. The cursive n refers to unbranched and saturated hydrocarbon homologues; subscript numbers refer to the number of carbon atoms of the respective n-alkane homologues. For further data evaluation and interpretation, we additionally calculated the odd-over-even predominance (OEP) according to Eq. (1),

$$\mathrm{OEP} = \frac{nC_{27} + nC_{29} + nC_{31} + nC_{33}}{nC_{26} + nC_{28} + nC_{30} + nC_{32}}, \quad (1)$$

the average chain length (ACL) according to Eq. (2),

$$\mathrm{ACL} = \frac{27 \times nC_{27} + 29 \times nC_{29} + 31 \times nC_{31} + 33 \times nC_{33}}{nC_{27} + nC_{29} + nC_{31} + nC_{33}}, \quad (2)$$

and an n-alkane ratio based on Schäfer et al. (2016) (Eq. 3):

$$n\text{-Alkane ratio} = \frac{nC_{31} + nC_{33}}{nC_{27} + nC_{31} + nC_{33}}. \quad (3)$$

Black carbon (BC) was analysed using benzene polycarboxylic acids (BPCAs) as molecular fire markers following Glaser et al. (1998). In brief, hydrolysis was realised using 10 mL of 4M trifluoroacetic acid (TFA) for 4 h at 105 °C (Brodowski et al., 2005). The residues were digested with 65 % nitric acid for 7 h at 170 °C, 100 µg of phthalic acid were added as internal standard, and the filtrates were cleaned over Dowex 50W resin columns. After the addition of Biphenylen-2,2-dicarboxylic acid as recovery standard and after derivatisation, the BPCAs were detected and quantified using a GC-FID (GC-2010, Shimadzu) equipped with a 30 m SPB-5 column (Supelco) and an external standard mixture.

The results of the above-described analyses are depicted in the form of box plot diagrams in Figs. 4, 5 and 6. The box plots indicate the median (solid line between the boxes), the interquartile range (IQR) with the lower (25 %) and upper (75 %) quartiles, lowest values still within $1.5 \times$ IQR of the lower quartile, highest values still within the $1.5 \times$ IQR of the upper quartile, and outliers (dots).

Radiocarbon (^{14}C) dating at the Ullafelsen site was performed on four untreated soil samples and five soil samples that were pretreated with HCl and H_2O_2 from the 2Ahb?/Bh? horizon, on seven bulk n-alkane samples from the LL, and on three charcoal samples from RP20 that were also pretreated with HCl (see Table 1). The HCl and H_2O_2 pretreatment aimed at removing young carbon pools in order to yield ages for old and resilient soil organic carbon pools reflecting the start of humus enrichment. The H_2O_2 pretreatment followed the method described by Favilli et al. (2009). Similarly, the ^{14}C dating of the bulk n-alkanes (following the method described by Zech et al., 2017 and Lerch et al., 2018) aimed at yielding maximum ages based on the insight that n-alkanes are not water-soluble and thus not rejuvenated by podzolisation processes. This is corroborated by extremely low concentrations of unsaturated hydrocarbons in dissolved organic

Table 1. Results of radiocarbon analyses for untreated and pretreated soil samples, charcoal, and bulk n-alkanes from the Ullafelsen.

Sample name	Lab code	Material and description	µg C	$\delta^{13}C$ (‰)	Measured $F^{14}C$	Error	^{14}C age (years BP)	Error (years)	Calibrated age (2σ) Intcal20 (cal yr BP)	Mean age Intcal20 (cal yr BP)	±
1.1 C4w 2Ahb?Bh?	BE 12069.1.1	Bulk soil, no pretreatment	156	−27.7	0.7686	0.0096	2114	101	1839–2338	2096	135
1.1 B5s 2Ahb?Bh?	BE 12070.1.1	Bulk soil, no pretreatment	118	−27.2	0.7507	0.0092	2304	98	2057–2705	2337	162
1.1 G5n 2Ahb?Bh?	BE 12071.1.1	Bulk soil, no pretreatment	121	−29.4	0.7193	0.0092	2647	103	2374–2997	2738	146
1.9 NW 2Ahb?Bh?	BE 12072.1.1	Bulk soil, no pretreatment	99	−28.1	0.7211	0.0090	2627	100	2371–2956	2704	144
1.1. C4w 2Ahb?Bh?	BE 13619.1.1	Bulk soil, HCl pretreatment	80	−33.0	0.6903	0.0095	2977	111	2860–3396	3142	143
1.1. B5s 2Ahb?Bh?	BE 13620.1.1	Bulk soil, HCl pretreatment	126	−33.3	0.6562	0.0100	3385	122	3371–3967	3646	151
1.9. NW 2Ahb?Bh?	BE 13621.1.1	Bulk soil, HCl pretreatment	211	−32.7	0.6827	0.0134	3066	157	2853–3633	3242	194
1.1. B5w 2Ahb?Bh?	BE 13622.1.1	Bulk soil, HCl pretreatment	204	−32.5	0.7408	0.0106	2410	115	2157–2749	2490	153
1.1. G5n 2Ahb?Bh?	BE 13623.1.1	Bulk soil, HCl pretreatment	164	−32.9	0.6681	0.0096	3240	115	3174–3822	3471	144
1.1. C4w 2Ahb?Bh?	BE 13614.1.1	Bulk soil, H_2O_2 pretreatment	120	−28.2	0.5063	0.0092	5467	145	5925–6598	6245	167
1.1. B5s 2Ahb?Bh?	BE 13615.1.1	Bulk soil, H_2O_2 pretreatment	120	−27.9	0.4844	0.0089	5823	148	6306–6982	6647	175
1.9. NW 2Ahb?Bh?	BE 13616.1.1	Bulk soil, H_2O_2 pretreatment	140	−30.6	0.4928	0.0104	5684	170	6027–6936	6505	190
1.1. B5w 2Ahb?Bh?	BE 13617.1.1	Bulk soil, H_2O_2 pretreatment	148	−27.7	0.5553	0.0094	4725	136	4985–5745	5423	177
1.1. G5n 2Ahb?Bh?	BE 13618.1.1	Bulk soil, H_2O_2 pretreatment	132	−27.5	0.5141	0.0085	5344	132	5760–6401	6118	143
RP20 HK 10 cm	BE 9779.1.1	Charcoal, HCl pretreatment	160	−23.6	0.3253	0.0095	9020	235	9535–10760	10 144	329
RP20 HK 15 cm	BE 9780.1.1	Charcoal, HCl pretreatment	175	−24.7	0.3447	0.0097	8556	227	9026–10190	9608	306
RP20 HK 20 cm	BE 9781.1.1	Charcoal, HCl pretreatment	147	−24.8	0.3213	0.0094	9120	235	9555–11069	10 292	347
1.1 B5s LL	BE 8926.1.1	Bulk n-alkanes	74	−29.8	0.4480	0.0066	6451	118	7076–7579	7351	117
1.1 B5w LL	BE 8927.1.1	Bulk n-alkanes	80	−30.9	0.5852	0.0077	4303	106	4575–5284	4902	181
1.1 C4w LL	BE 8928.1.1	Bulk n-alkanes	42	−30.0	0.4100	0.0064	7163	126	7695–8288	7987	133
1.1 G5n LL	BE 8929.1.1	Bulk n-alkanes	116	−30.5	0.4458	0.0071	6490	128	7159–7618	7385	121
1.9 SW LL	BE 8930.1.1	Bulk n-alkanes	43	−31.9	0.3959	0.0067	7444	136	7976–8518	8241	132
1.9 NO LL	BE 8931.1.1	Bulk n-alkanes	41	−33.2	0.5140	0.0077	5346	120	5900–6395	6121	129
1.9 NW LL	BE 8932.1.1	Bulk n-alkanes	69	−36.6	0.4503	0.0079	6410	142	6995–7574	7302	147

matter of Podzols as recently reported by Maria et al. (2019) based on high-resolution mass spectrometry.

Radiocarbon analyses were carried out at the Laboratory for the Analysis of Radiocarbon with accelerator mass spectrometry (LARA AMS) of the University of Bern, Switzerland (Szidat et al., 2014). Samples were packed and weighted into tin boats (Elementar, $6 \times 6 \times 12$ mm). The ^{14}C dating was performed on the Mini Carbon Dating System (MICADAS) AMS coupled online to an Elementar analyser (Wacker et al., 2010; Ruff et al., 2010). Results are reported as fraction modern ($F^{14}C$), i.e. the activity ratio of a sample related to the modern level. All $F^{14}C$ results were corrected for cross-contamination and constant contamination according to the contamination drift model of Salazar et al. (2015). The ^{14}C ages were calibrated to calendar ages (cal yr BP) with the IntCal20 calibration curve (Reimer et al., 2020) using OxCal (Bronk Ramsey, 2009).

3 Results and discussion

3.1 Total *n*-alkane contents and patterns of modern vegetation

The total *n*-alkane contents (TACs) of the leaf samples range from 0 to 1819 $\mu g\, g^{-1}$ (*Picea abies* and *Betula pendula*, respectively) (Fig. 4). This is within the range reported in the literature (Zech et al., 2012; Tarasov et al., 2013; Schäfer et al., 2016; Bliedtner et al., 2018; Trigui et al., 2019; Struck et al., 2020) and provides evidence that *Betula*, *Alnus* and many other deciduous trees produce high amounts of *n*-alkanes. By contrast, except for *Juniperus*, coniferous trees and mosses are characterised by very low TACs. This "blindness" of *n*-alkane biomarkers for coniferous trees needs to be considered when aiming at reconstructing vegetation history such as shifts of the upper timberline based on *n*-alkane patterns from soils and sediments.

Figure 4 moreover depicts the *n*-alkane patterns of deciduous trees being significantly different compared to other vegetation types. The ACL yielded a mean value of 27.4 for the two deciduous tree samples. For comparison, the mean ACL values for herbs, grasses and alpine dwarf shrubs are much higher, ranging from 29.9 to 30.4. Similarly, the $(nC_{31} + nC_{33}) / (nC_{27} + nC_{31} + nC_{33})$ ratio of the deciduous tree samples is very low (0.06), whereas the mean *n*-alkane ratios of the other vegetation types are much higher (ranging from 0.63 to 0.95). This finding provides evidence that the chemotaxonomic differentiation between trees and shrubs versus grasses and herbs as suggested by, for example, Zech et al. (2009) needs regional calibration and/or validation (e.g. Schäfer et al., 2016; Bliedtner et al., 2018; Lemma et al., 2019; Trigui et al., 2019; Struck et al., 2020). In our Ullafelsen case study, the chemotaxonomic potential for reconstructing vegetation changes can be specified in terms of subalpine deciduous trees (*Betula* and *Alnus*) versus alpine grass, juniper and dwarf shrubland (including herbs), whereas the *n*-alkane biomarkers are "blind" for coniferous trees dominating the montane zone.

3.2 TOC, TOC / N, $\delta^{13}C$, $\delta^{15}N$ and BC contents of soil profiles on the Ullafelsen

The TOC contents of the soil profiles on the Ullafelsen cover a wide range from 0.3 % to 28.8 % (Fig. 5). High TOC contents and stocks are indeed to be expected especially in subalpine soils near the timberline (Egli et al., 2006). Apart from high TOC values in the OAh1 horizon (ranging from 14.2 % to 19.3 %), TOC maxima occur in the OAh3 and the 2Ahb?/Bh? horizons (Fig. 5). In fact, the two highest TOC values (25.0 % and 28.8 %) of this dataset were measured for the OAh3 horizon of profiles 1.1 G5N and 1.9 NW. This is in agreement with the OAh3 horizon on the Ullafelsen being often characterised by dark colours (indicating humus enrichment) and often containing charcoal particles (cf. Fig. 2). TOC maxima in the 2Ahb?/Bh? horizon range from 4.8 % to 8.3 % and are expected both in the case of the burial of a former topsoil and in the case of podzolisation. Hence, the TOC results do not allow us to distinguish between these two options.

The TOC / N ratio on the Ullafelsen ranges from 12.4 to 37.2 (Fig. 5). Such high ratios also in the subsoils are typical for podzols (Zech et al., 2014) or charcoal-rich Anthrosols (Glaser et al., 2001; Glaser and Birk, 2012). Apart from the one outlier in the LL of profile 1.1 G5W (37.2), the highest TOC / N ratios are observed in the OAh3 horizon (ranging from 27.7 to 33.8). This again reflects geochemically that the OAh3 horizon overlies the LL as the Mesolithic living floor and often contains charcoal particles characterised by high TOC / N ratios (Fig. 2).

The $\delta^{13}C$ values range from −26.3 ‰ to −24.4 ‰ and are thus well within the range to be expected for soils under C_3 vegetation (Glaser, 2005). Due to low pH values of our samples and the risk of $\delta^{13}C$ biases (Brodie et al., 2011), we refrained from an HCl pretreatment prior to sample analyses. At the same time, carbonates are known to be ^{13}C-enriched. Traces of dolomite were reported to occur sporadically especially in the LL and are considered residues of late glacial aeolian dust input (Geitner et al., 2011, 2014). Aeolian dust input is well known for the Northern Limestone Alps, too (Küfmann, 2003, 2008; Gild et al., 2018), and needs also to be considered as a process for the Middle and Late Holocene coverage of the Mesolithic living floor LL on the Ullafelsen. However, neither the LL nor the overlying horizons indicate a dolomite-induced ^{13}C enrichment. By contrast, the LL yielded the most negative $\delta^{13}C$ values (Fig. 5). We suggest that this reflects the preferential removal of ^{13}C-enriched and water-soluble soil organic carbon pools such as pectin, sugars and amino acids compared to ^{13}C-depleted and water-insoluble pools such as lignins and lipids (cf. Glaser, 2005) by podzolisation.

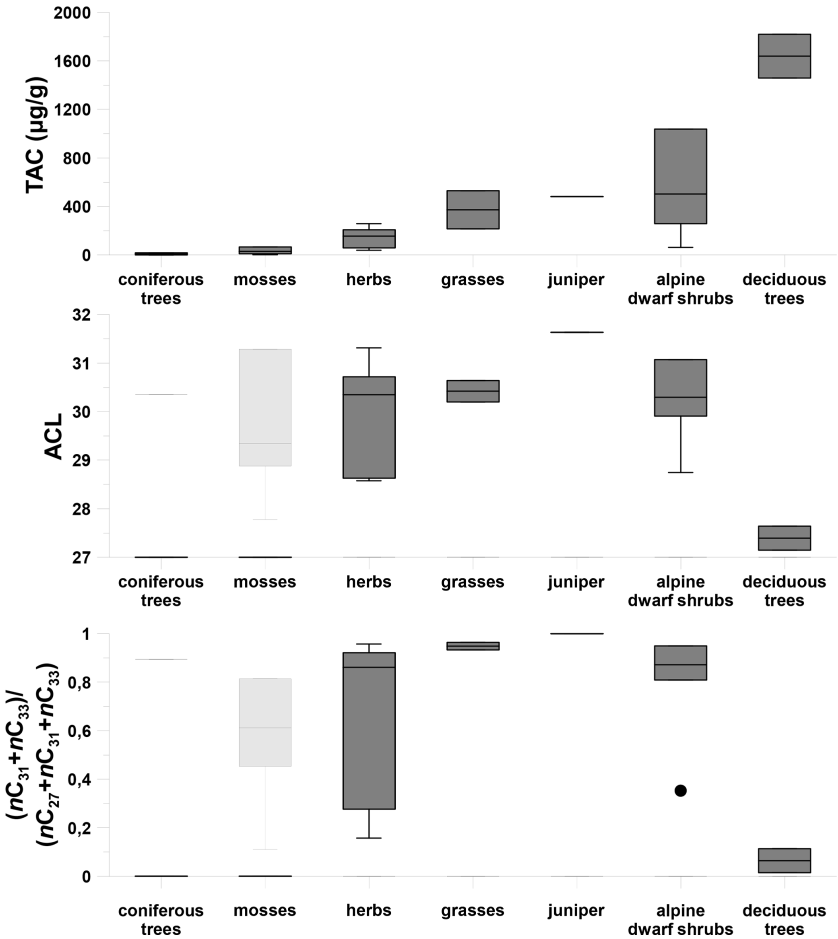

Figure 4. Total n-alkane content (TAC), average chain length (ACL) and n-alkane ratio – $(nC_{31}+nC_{33})/(nC_{27}+nC_{31}+nC_{33})$ – of typical and dominant vegetation types on and around the Ullafelsen. Note that the very low TACs of coniferous trees (excluding juniper) and mosses (grey bar) hinder reconstructing respective vegetation changes using ACL and n-alkane ratios from soils.

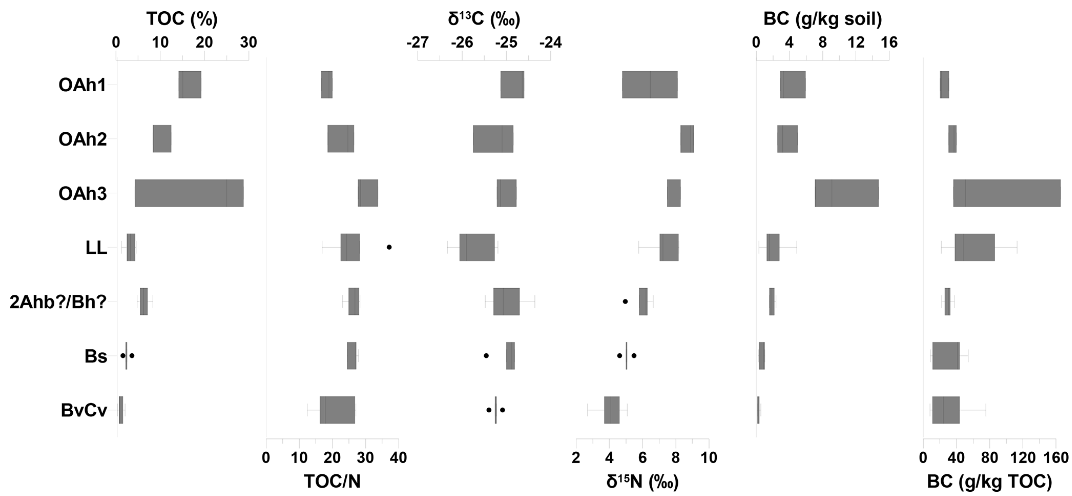

Figure 5. Box plots illustrating the total organic carbon content (TOC), the carbon to nitrogen ratio (TOC / N), the stable carbon isotopic composition δ^{13}C, the stable nitrogen isotopic composition δ^{15}N and the black carbon content (BC) in both grams per kilogram ($\mathrm{g\,kg^{-1}}$) soil and grams per kilogram TOC for the investigated soil profiles.

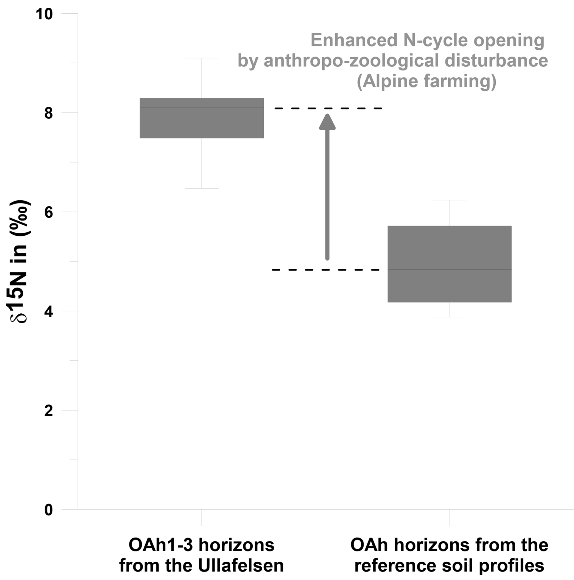

Figure 6. Box plots illustrating the comparison of the δ^{15}N results of the OAh1-3 horizons from the Ullafelsen versus the δ^{15}N results of the OAh horizons from the reference soil profiles.

Figure 5 moreover depicts the δ^{15}N values which range from 2.7 ‰ to 9.1 ‰, with the upper part of the profiles being characterised by more positive values. Although shifts towards more positive δ values by degradation need to be considered both for δ^{13}C and δ^{15}N values of soils and sediments (Zech et al., 2007), δ^{15}N is best described as an integrating indicator of the N cycle. Accordingly, ecosystem disturbances associated with the opening of the N cycle result in more positive δ^{15}N values. For instance, Zech et al. (2011a) reported that intensively grazed pastures in the high-mountain areas of the eastern Pamirs are significantly ^{15}N-enriched by 3.5 ‰ compared to less exploited pastures. The high δ^{15}N values in the upper part of the Ullafelsen soil profiles therefore probably reflect the anthropo-zoological disturbance by Alpine farming (trampling and dung/urine by cows and sheep) since the Bronze Age (Haas et al., 2007; Pindur et al., 2007). On average, the OAh horizons from the Ullafelsen yield a δ^{15}N value of 7.7 ‰ compared to a δ^{15}N value of 4.6 ‰ for the OAh horizons of all reference soil profiles (Table S2 and Fig. 6). The δ^{15}N values of the LL are not statistically significantly more positive compared to the *E* horizons of the reference soil profiles and thus do not provide any evidence for the human-induced disturbance during the Mesolithic.

The BC contents on the Ullafelsen reach up to 14.7 g kg^{-1} soil and 165.4 g kg^{-1} TOC (Fig. 5). For comparison, the famous and anthropogenically developed "Terra Preta" in the Amazonian Basin yielded similarly high BC contents of around 11 ± 5 g kg^{-1} soil and around 200 ± 30 g kg^{-1} TOC (Glaser et al., 2001). For the Nordic Dark Earth of Slavic settlements, Wiedner et al. (2015) reported BC contents of up to 7.5 g kg^{-1} soil compared to a maximum 1.1 g kg^{-1} soil in reference soils. On the Ullafelsen, the OAh3 horizon reveals a distinct BC maximum (Fig. 5). When referring to grams per kilogram TOC, the LL also yielded higher BC contents than other horizons. This finding nicely reflects the field observations as documented during the (geo-)archaeological excavations that the fire places and the highest char particle abundance typically occur in or directly above the Mesolithic living floor LL. One might be surprised that the BC contents are not zero in the subsoil horizons Bv and BvCv where no char particles occur. However, BPCAs are not exclusive biomarkers for char. Humic and fulvic acids, as well as lignin-like structures, are compound classes typically dominating in dissolved organic matter of Podzols, and they are built up of (partly condensed) aromatic macromolecules, too. The latter, therefore, also produce BPCAs during the analytical BC analyses and are actually to be expected in subsoils of Podzols. Last but not least, we calculated the ratio of the individual BPCAs with five and six carboxylic groups (B5CA / B6CA) (Table 2). For the OAh3 horizon and the LL, where we argue that increased BC contents are fire-induced, we detected ratios of 0.65 and 0.60, respectively. According to Wolf et al. (2013), ratios < 0.8 are indicative of domestic fires, whereas ratios > 0.8 are typical for forest ground or grass fires. The low B5CA / B6CA ratios hence provide evidence that the charcoal in and on the LL of the Ullafelsen is of human rather than natural origin.

3.3 The *n*-alkane contents and patterns of soil profiles on the Ullafelsen

The total *n*-alkane contents (TACs) in the OAh horizons range from 3 to 148 µg g^{-1} soil and from 61 to 648 µg g^{-1} TOC, respectively (Fig. 7). For comparison, the TACs of the OAh horizons of the reference soils range from 13 to 106 µg g^{-1} soil and from 238 to 635 µg g^{-1} TOC, respectively (cf. Table S2, data not illustrated). The OEP values range from 4.1 to 24.3 and are highest in the topmost OAh1 horizon (Fig. 7). This indicates fresh leaf wax input by plant litter on top and a certain degree of *n*-alkane degradation (cf. Zech et al., 2011c) in the deeper horizons. Both the TAC and the OEP values of the Ullafelsen are well within the range to be expected for very organic-rich mineral topsoils (Schäfer et al., 2016; Bliedtner et al., 2018; Lemma et al., 2019; Trigui et al., 2019; Struck et al., 2020).

Strikingly, the LL contains very low TACs, and no *n*-alkanes at all were detectable in most 2Ahb?/Bh?, Bs and BvCv horizons (Fig. 7) despite partly strong modern root penetration occurring in these latter subsoil horizons (Geitner et al., 2011). This finding is in agreement with previous studies reporting that roots do not or at least only negligibly contribute to the *n*-alkane pools of subsoils and sediments (Zech et al., 2012; Häggi et al., 2014). Moreover, this finding undoubtedly rules out the assumption that the 2Ahb?/Bh? horizon on the Ullafelsen could be a buried late glacial top-

Table 2. Mean BPCA pattern (in %) and B5CA / B6CA ratio of soil horizons on the Ullafelsen.

Horizon	B3CA	±	B4CA	±	B5CA	±	B6CA	±	B5CA / B6CA
OAh1 ($n = 3$)	8	3	31	5	27	4	34	4	0.80
OAh2 ($n = 3$)	8	2	28	4	28	1	36	5	0.79
OAh3 ($n = 3$)[1]	6	1	23	1	28	4	43	4	0.65
LL ($n = 8$)[1]	5	3	24	3	27	3	44	6	0.60
2Ahb?/Bh? ($n = 6$)[2]	4	2	21	6	23	2	51	7	0.45
Bs ($n = 5$)[2]	4	4	30	11	24	2	42	13	0.57
BvCv ($n = 5$)[2]	2	5	47	35	27	20	23	32	1.17

[1] BC content maxima and the finding of char particles in the OAh3 horizon and the LL indicate that the respective BPCAs are primarily fire-derived. [2] The absence of char particles and the identification of these horizons as Podzol subsoils suggest that the respective BPCAs are not fire-derived but primarily originate from translocated and adsorbed dissolved organic matter.

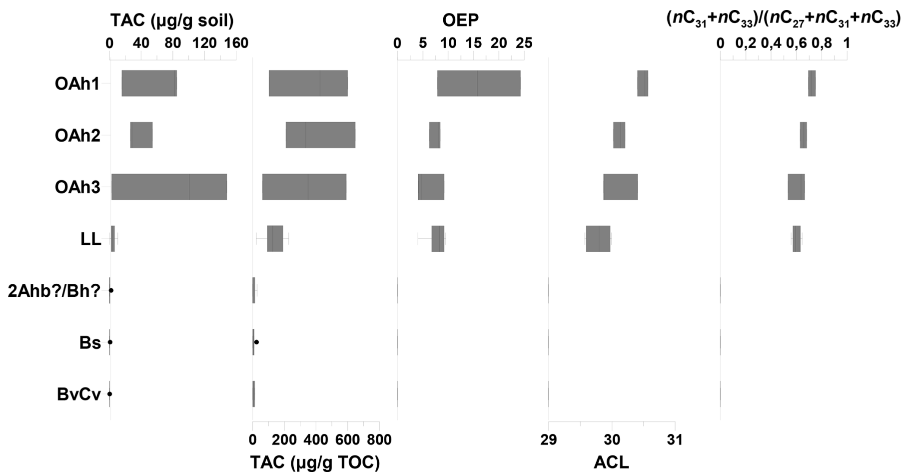

Figure 7. Box plots illustrating the total n-alkane content (TAC) in both micrograms per gram soil and micrograms per gram TOC, the odd-over-even predominance (OEP), the average change length (ACL), and the n-alkane ratio $(nC_{31} + nC_{33}) / (nC_{27} + nC_{31} + nC_{33})$ for the investigated soil profiles.

soil (2Ahb). In the latter case, leaf wax n-alkanes would have been deposited on and incorporated in this horizon. The humus accumulation of this horizon under discussion must therefore be attributed to other processes than leaf litter deposition, namely to organic matter translocation by podzolisation (→ Bh horizon) and to a certain degree also to root input and rhizodeposition[1].

For comparison, 15 horizons from the reference soil profiles were classified during fieldwork as 2Ahb, Bh or 2Ahb?/Bh? horizons. Figure 8 illustrates that the TACs for these samples yielded a bimodal histogram distribution. Either the samples yielded TACs of $> 500\,\mu g\,g^{-1}$ TOC, revealing that these are indeed 2Ahb horizons, or they yielded TACs of mostly $< 100\,\mu g\,g^{-1}$ TOC, revealing that these are Bh horizons.

[1]Please note once again that n-alkanes are important constituents of leaf waxes and are hardly biosynthesised by roots. Moreover, n-alkanes are not water-soluble and thus not prone to translocation processes in soils (except for in particle-bound form by lessivation).

The ACL values from the Ullafelsen soil profiles range from 29.6 to 30.6 with a trend towards higher values from the LL to the OAh1 horizon (Fig. 7). Similarly, the $(nC_{31} + nC_{33}) / (nC_{27} + nC_{31} + nC_{33})$ ratio ranges from 0.53 to 0.75 and shows a slight increase from the LL to the OAh1 horizon, too. The ACL range thus corresponds well with the ACL values of the modern reference herbs, grasses and alpine dwarf shrubs with no indication of a significant contribution of deciduous trees (cf. Fig. 4). By contrast, the $(nC_{31} + nC_{33}) / (nC_{27} + nC_{31} + nC_{33})$ ratio of the soils is lower than the ratio yielded for the modern reference grasses and alpine dwarf shrubs; they fall within the range yielded for the modern reference herbs. On the one hand, we can certainly rule out a deciduous tree predominance on the Ullafelsen from these results. On the other hand, one may be tempted to reconstruct vegetation changes in terms of a herb predominance during the formation of the LL followed by an increasing grass and alpine shrub contribution towards the OAh1 horizon. However, we suggest caution against such a more in-depth vegetation reconstruction because n-alkane ra-

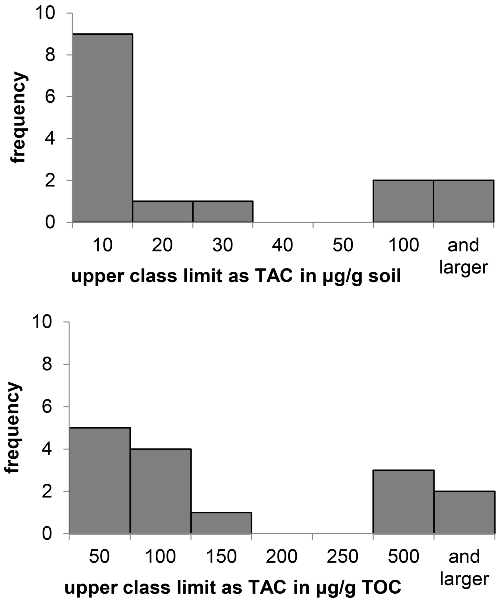

Figure 8. Histograms depicting the bimodal distribution of total *n*-alkane contents of 2Ahb?/Bh? horizons from reference soil profiles in the Fotsch Valley.

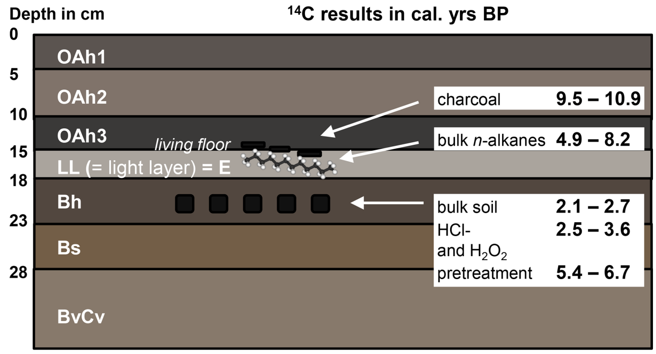

Figure 9. Results of radiocarbon analyses for untreated and pretreated soil samples, charcoal, and bulk *n*-alkanes from the Ullafelsen shown in stratigraphical position.

tios are known to be affected by degradation (Zech et al., 2011c, 2012; Schäfer et al., 2016), and the above-presented OEP results clearly suggest that the *n*-alkanes in the OAh1 horizon are less degraded than the *n*-alkanes of the underlying horizons.

3.4 Bulk, charcoal and *n*-alkane ^{14}C ages of soil profiles on the Ullafelsen

Four bulk soil samples from the 2Ahb?/Bh? horizon on the Ullafelsen were ^{14}C dated without any pretreatment. These analyses yielded calibrated ages ranging from 2.7 ± 0.1 to 2.1 ± 0.1 cal kyr BP (Table 1 and Fig. 9), which is much younger compared to the charcoals found in and above the LL and thus overlying the 2Ahb?/Bh? horizon. According to Schäfer (2011b), the fire places date between 10.9 and 9.5 cal kyr BP, and the fire place RP20 discovered and dated within this follow-up study dates between 10.3 ± 0.3 and 9.6 ± 0.3 cal kyr BP (Table 1). This prominent ^{14}C age inversion has to be interpreted in terms of a strong rejuvenation of the bulk soil organic carbon in the 2Ahb?/Bh? horizon. Both modern root input and modern podzolisation need to be considered. Typically, podzolisation occurs in mineral soils covered by an acidic O layer rich in decomposing conifer needles or dwarf shrub litter. Although the Ullafelsen is nowadays grass-predominant, the up to 15 cm thick OAh horizon is characterised by very low pH values of 3.7 (Geitner et al., 2011) favouring podzolisation. In order to remove young carbon pools and thus to yield ages for old and resilient soil organic carbon pools reflecting the start of humus enrichment, we applied both HCl and H_2O_2 pretreatment to five 2Ahb?/Bh? samples. Accordingly, HCl pretreatment yielded calibrated ^{14}C ages ranging from 3.6 ± 0.2 to 2.5 ± 0.2 cal kyr BP, and H_2O_2 pretreatment (after Favilli et al., 2009) yielded calibrated ^{14}C ages ranging from 6.7 ± 0.2 to 5.4 ± 0.2 cal kyr BP (Table 1 and Fig. 9). Hence, radiocarbon dating does not provide evidence for a late glacial or an Early Holocene 2Ahb?/Bh? formation pre-dating the Mesolithic living floor LL.

Last but not least, seven bulk *n*-alkane samples from the LL of soil profiles on the Ullafelsen yielded ^{14}C ages dating between 8.2 ± 0.1 and 4.9 ± 0.2 cal kyr BP (Table 1 and Fig. 9). This is younger than one might expect at first glance because the Mesolithic living floor LL was utilised from 10.9 to 9.5 cal kyr BP according to the radiocarbon dating of the fire places. Given that a noteworthy post-depositional rejuvenation of *n*-alkane pools in subsoils by roots and aqueous translocation can be excluded (Zech et al., 2017; Lerch et al., 2018), this finding suggests that during and shortly after the Mesolithic occupation no vegetation prevailed on the Ullafelsen producing significant amounts of *n*-alkanes. As discussed in Sect. 3.1, most conifers produce no or negligible amounts of *n*-alkanes. A conifer-predominated vegetation cover on the Ullafelsen at 1869 m a.s.l. directly after the Mesolithic occupation is indeed to be expected according to timberline reconstructions in the region. For instance, Staffler et al. (2011) and Kutschera et al. (2014) reported that in the neighbouring Ötztal the timberline was at around 2450 m a.s.l. between ∼ 10 to 5 cal kyr BP. Subsequently, the timberline was depressed by several hundred metres due to an intensification of alpine pasturing. Similarly, the Neolithic presence of humans and their domestic livestock is documented for the Zillertal Alps from about 6.1 cal kyr BP onwards (Haas et al., 2007; Pindur et al., 2007). We infer that on the Ullafelsen a noteworthy *n*-alkane production by grasses, herbs and dwarf shrubs predominating in the alpine pastures started only during the Neolithic or the Bronze Age. A more in-depth chronological assessment for the Fotsch Valley requires other environmental archives than the Ullafelsen soil

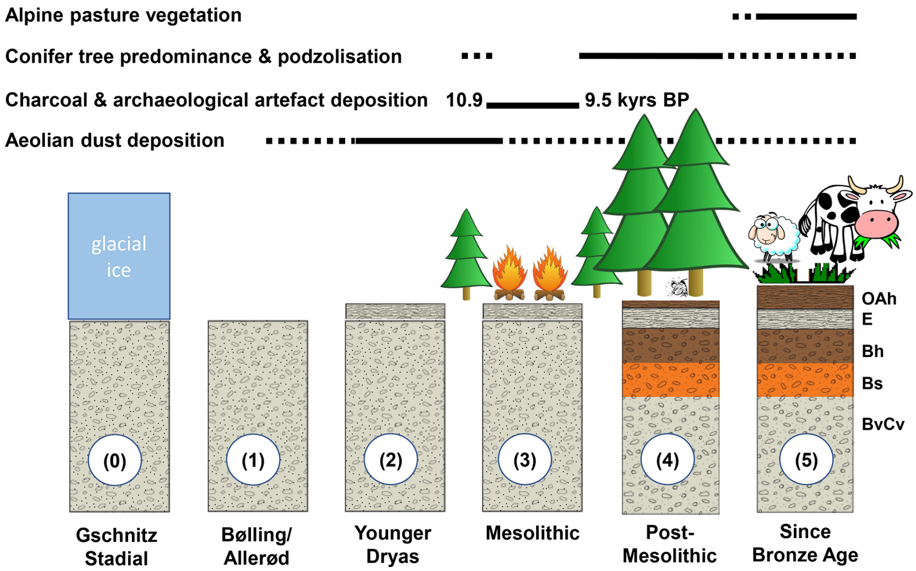

Figure 10. Didactically simplified revised scenario illustrating the hypothetical sequence of pedogenetic phases at the Ullafelsen (after Geitner et al., 2011, 2014).

profiles, such as peat bogs as high-resolution archives, and is a work in progress.

4 Conclusions, synthesis and outlook

Revisiting the Mesolithic site Ullafelsen in the Fotsch Valley with hitherto not applied biomarker, stable isotope and additional radiocarbon dating tools paid off. Based on our results and the discussion, the following conclusions can be drawn.

The total n-alkane content (TAC) was developed for the first time as an unambiguous proxy for distinguishing between buried (= fossil) 2Ahb topsoils and humus-enriched subsoils such as Bh horizons of podzols. Based on this proxy, we can rule out that the 2Ahb?/Bh? horizon on the Ullafelsen is a buried topsoil. It developed by podzolisation as a Bh horizon below the LL and above a Bs horizon.

The LL is corroborated as the Mesolithic living floor and at the same time as an eluvial albic *E* horizon. It is characterised by the most negative $\delta^{13}C$ values of the soil profiles on the Ullafelsen. This can be attributed to the selective removal of water-soluble soil organic carbon pools by eluviation. The LL and the overlying OAh3 horizon yielded distinct fire-induced BC maxima, with B5CA / B6CA ratios pointing to human-induced fires rather than natural fires.

High $\delta^{15}N$ values in the LL and the overlying OAh horizons indicate anthropo-zoological disturbance and N-cycle opening by alpine farming (trampling and dung/urine input). Given that a Mesolithic human disturbance cannot be inferred from these results, ongoing work focusses, amongst others, on human- versus herbivore-specific faecal sterol and bile acid biomarkers.

Leaf-wax-derived n-alkane biomarkers allow us to chemotaxonomically distinguish between subalpine deciduous trees (nC_{27} predominance) versus (sub)alpine grasses, herbs and dwarf shrubs (nC_{29}, nC_{31} and/or nC_{33} predominance). Except for *Juniperus*, conifers produce no or extremely low n-alkane contents.

We caution against an in-depth vegetation reconstruction based on the rather small variability in n-alkane patterns on the Ullafelsen due to degradation effects. Yet, ^{14}C ages of bulk n-alkanes ranging from 8.2 to 4.9 cal kyr BP compared to Mesolithic charcoal ^{14}C ages ranging from 10.9 to 9.5 cal kyr BP suggest that an n-alkane-producing vegetation cover (grasses, herbs or dwarf shrubs) did not start to predominate immediately after the Mesolithic abandonment. Instead, non-n-alkane-producing conifers should have dominated the vegetation cover, which is in agreement with timberline reconstructions for the Central Alps.

Our new data and insights into pedogenesis, human impact and landscape evolution from the Ullafelsen complement and partly revise previous studies and scenarios (Fig. 10). (1) While Geitner et al. (2011, 2014) suggested that the humus-rich horizon under the LL represents a late glacial buried topsoil, we did not find respective evidence either based on our leaf-wax-derived n-alkane analyses or based on our applied radiocarbon dating approaches. Similarly, no ^{14}C ages pre-dating the Holocene were obtained for basal samples of three peat bogs cored in the Fotsch Valley. (2) According to Geitner et al. (2011, 2014), aeolian dust deposition contributed to the build-up of the LL during the Younger Dryas and continued during the Holocene. This allowed the OAh horizons to build-up. (3) During the Mesolithic occupation, artefacts and charcoal were deposited on the LL.

(4) However, we suggest in our revised scenario that the light-coloured feature of the LL developed primarily only after the Mesolithic abandonment, namely when conifer vegetation dominated the Ullafelsen from 9.5 cal kyr BP onwards and abundant conifer needle litter favoured podzolisation. Only during that period did the pronounced bleaching of the LL and thus the transformation of the LL into an *E* horizon occur. Synchronously, the underlying Bh and Bs horizons started to develop. (5) A major human-induced vegetation change should have occurred with the onset and the intensification of alpine pasturing during the Neolithic and the Bronze Age. The low pH values (< 4) suggest that podzolisation still continues under the modern-day pasture vegetation predominated by grasses, herbs and dwarf shrubs.

Further follow-up studies in the Fotsch Valley focus on (i) the spatial distribution patterns of geochemical (TOC, TOC / N, P, Fe) and isotope (δ^{15}N, δ^{13}C) patterns on the Ullafelsen, (ii) the identification of human- versus herbivore-specific faecal sterol and bile acid biomarkers, and (iii) investigating high-resolution peat archives.

Data availability. Data are available in the Supplement.

Supplement. The supplement related to this article is available online at: https://doi.org/10.5194/egqsj-70-171-2021-supplement.

Author contributions. MZ developed the project idea in collaboration with BG, DS and CG. Fieldwork was done by MZ, ML, JNH, DS and CG. ML carried out most of the laboratory work with contributions made by MZ, MB, TB, FS and GS. MZ prepared the manuscript, and all co-authors, including SöS and RZ, contributed to the discussion of the results and read and approved the manuscript.

Competing interests. The authors declare that they have no conflict of interest.

Disclaimer. Publisher's note: Copernicus Publications remains neutral with regard to jurisdictional claims in published maps and institutional affiliations.

Acknowledgements. We are very grateful to quite a number of students who supported our field and laboratory work within student projects and bachelor and master theses, namely Sabrina Andruch, Lilly Biedermann, Mikesch Blümlein, Larisa Boysen, Lukas Epp, Nina Feistmantl, Corinna Heinrich, David Horn, Tina Jahn, Martin Kaufhold, Marco Pacher, Tugba Ayla Schlegel, Katharina Schneider, Melissa Sehrt and Marika Stutzriemer. We also greatly acknowledge Sixten Bussemer and Jaroslaw Waroszewski for support of fieldwork and valuable discussions on pedogenesis, Ingrid Kögel-Knabner, Markus Steffens and Heike Knicker for valuable discussions on ^{13}C-NMR, Jörg Löffler for valuable discussions on ^{14}C dating, Michael Meyer for communicating the OSL age obtained for the LL, Oliver Kiewert and his team from the Bergheim Fotsch for excellent food and accommodation, and last but not least Marianne Zech (formerly Benesch) and Heike Maennicke for support of lab work and their cheerful cohesion of our working group. We kindly thank Hans von Suchodoletz for his committed editorial handling and two anonymous reviewers for their constructive comments and suggestions.

Financial support. This research has been supported by the Deutsche Forschungsgemeinschaft (grant nos. ZE 844/12-1 and GL 327/23-1).

This open-access publication was funded
by the Technische Universität Dresden (TUD).

Review statement. This paper was edited by Hans von Suchodoletz and reviewed by two anonymous referees.

References

Bliedtner, M., Schäfer, I. K., Zech, R., and von Suchodoletz, H.: Leaf wax *n*-alkanes in modern plants and topsoils from eastern Georgia (Caucasus) – implications for reconstructing regional paleovegetation, Biogeosciences, 15, 3927–3936, https://doi.org/10.5194/bg-15-3927-2018, 2018.

Bliedtner, M., von Suchodoletz, H., Schäfer, I., Welte, C., Salazar, G., Szidat, S., Haas, M., Dubois, N., and Zech, R.: Age and origin of leaf wax *n*-alkanes in fluvial sediment–paleosol sequences and implications for paleoenvironmental reconstructions, Hydrol. Earth Syst. Sci., 24, 2105–2120, https://doi.org/10.5194/hess-24-2105-2020, 2020.

Brodie, C. R., Leng, M. J., Casford, J. S. L., Kendrick, C. P., Lloyd, J. M., Yongqiang, Z., and Bird, M. I.: Evidence for bias in C and N concentrations and δ^{13}C composition of terrestrial and aquatic organic materials due to pre-analysis acid preparation methods, Chem. Geol., 282, 67–83, https://doi.org/10.1016/j.chemgeo.2011.01.007, 2011.

Brodowski, S., Rodionov, A., Haumaier, L., Glaser, B., and Amelung, W.: Revised black carbon assessment using benzene polycarboxylic acids, Org. Geochem., 36, 1299–1310, https://doi.org/10.1016/j.orggeochem.2005.03.011, 2005.

Bronk Ramsey, C.: Bayesian Analysis of Radiocarbon Dates, Radiocarbon, 51, 337–360, https://doi.org/10.1017/S0033822200033865, 2009.

Cornelissen, M. and Reitmaier, T.: Filling the gap: Recent Mesolithic discoveries in the central and south-eastern Swiss Alps, Quatern. Int., 423, 9-22, 2016.

Egli, M., Mirabella, A., Sartori, G., Zanelli, R., and Bischof, S.: Effect of north and south exposure on weathering rates and clay mineral formation in Alpine soils, Catena, 67, 155–174, 2006.

Egli, M., Mirabella, A., and Sartori, G.: The role of climate and vegetation in weathering and clay mineral formation in late Quaternary soils of the Swiss and Italian Alps, Geomorphology, 102, 307–324, 2008.

Favilli, F., Egli, M., Brandova, D., Ivy-Ochs, S., Kubik, P., Maisch, M., Cherubini, P., and Haeberli, W.: Combination of numerical dating techniques using ^{10}Be in rock boulders and ^{14}C of resilient soil organic matter for reconstructing the chronology of glacial and periglacial processes in a high alpine catchment during the Late Pleistocene and Early Holocene, Radiocarbon, 51, 537–552, 2009.

Fontana, F., Visentin, D., and Wierer, U.: MesoLife. A Mesolithic perspective on Alpine and neighbouring territories, Quatern. Int., 423, 1–4, 2016.

Geitner, C., Bussemer, S., Ehrmann, O., Ikinger, A., Schäfer, D., Traidl, R., and Tscherko, D.: Bodenkundlich-stratigraphische Befunde am Ullafelsen im hinteren Fotschertal sowie ihre landschaftsgeschichtliche Interpretation, in: Das Mesolithikum-Projekt Ullafelsen (Teil 1). Mensch und Umwelt im Holozän Tirols 1, edited by: Schäfer, D., Philipp von Zabern, Innsbruck, Austria, 2011.

Geitner, C., Schäfer, D., Bertola, S., Bussemer, S., Heinrich, K., and Waroszewski, J.: Landscape archaeological results and discussion of Mesolithic research in the Fotsch valley (Tyrol), in: From the foreland to the Central Alps – Field trips to selected sites of Quaternary research in the Tyrolean and Bavarian Alps (DEUQUA EXCURSIONS), edited by: Kerschner, H., Krainer, K., and Spötl, C., Geozon, Berlin, Germany, 106–115, 2014.

Gild, C., Geitner, C., and Sanders, D.: Discovery of a landscape-wide drape of late-glacial aeolian silt in the western Northern Calcareous Alps (Austria): First results and implications, Geomorphology, 301, 39–52, 2018.

Glaser, B.: Compound-specific stable-isotope (δ^{13}C) analysis in soil science, J. Plant Nutr. Soil Sc., 168, 633–648, 2005.

Glaser, B. and Birk, J.: State of the scientific knowledge on properties and genesis of Anthropogenic Dark Earths in Central Amazonia (*terra preta de Índio*), Geochim. Cosmochim. Ac., 82, 39–51, 2012.

Glaser, B., Haumeier, L., Guggengerger, G., and Zech, W.: Black carbon in soils: the use of benzenecarboxylic acids as specific markers, Org. Geochem., 29, 811–819, 1998.

Glaser, B., Haumaier, L., Guggenberger, G., and Zech, W.: The “*terra preta*” phenomenon: a model for sustainable agriculture in the humid tropics, Naturwissenschaften, 88, 37–41, 2001.

Grillo, K., Dunne, J., Marshall, F., Prendergast, M., Casanova, E., Gidna, A., Janzen, A., Karega-Munene, Keute, J., Mabulla, A., Robertshaw, P., Gillard, T., Walton-Doyle, C., Whelton, H., Ryan, K., and Evershed, R.: Molecular and isotopic evidence for milk, meat, and plants in prehistoric eastern African herder food systems, P. Natl. Acad. Sci. USA, 117, 9793–9799, https://doi.org/10.1073/pnas.1920309117, 2020.

Haas, J. N., Walde, C., and Wild, V: Prähistorische Lawinen und ihr Einfluss auf die subalpinen Vegetation der Schwarzensteinalm im Zemmgrund (Zillertal, Tirol, Österreich), in: Nachweis und Analyse holozäner Lawinenereignisse in den Zillertaler Alpen, Österreich, Band 16, edited by: Luzian, R. and Pindur, P., Mitteilungen der Kommission für Quartärforschung, Vienna, Austria, 185–220, 2007.

Häggi, C., Zech, R., McIntyre, C., Zech, M., and Eglinton, T. I.: On the stratigraphic integrity of leaf-wax biomarkers in loess paleosols, Biogeosciences, 11, 2455–2463, https://doi.org/10.5194/bg-11-2455-2014, 2014.

Hepp, J., Wüthrich, L., Bromm, T., Bliedtner, M., Schäfer, I. K., Glaser, B., Rozanski, K., Sirocko, F., Zech, R., and Zech, M.: How dry was the Younger Dryas? Evidence from a coupled δ^2H–δ^{18}O biomarker paleohygrometer applied to the Gemündener Maar sediments, Western Eifel, Germany, Clim. Past, 15, 713–733, https://doi.org/10.5194/cp-15-713-2019, 2019.

Kemmer, I.: Die rezente Vegetation im inneren Fotschertal / Nördliche Stubaier Alpen, in: Das Mesolithikum-Projekt Ullafelsen (Teil 1). Mensch und Umwelt im Holozän Tirols 1, edited by: Schäfer, D., Philipp von Zabern, Innsbruck, Austria, 2011.

Kerschner, H.: Spätglaziale Gletschervorstöße im Fotschertal, in: Das Mesolithikum-Projekt Ullafelsen (Teil 1). Mensch und Umwelt im Holozän Tirols 1, edited by: Schäfer, D., Philipp von Zabern, Innsbruck, Austria, 97–105, 2011.

Küfmann, C.: Soil types and eolian dust in high-mountainous karst of Northern Calcareous Alps (Zugspitzplatt, Wetterstein Mountains, Germany), Catena, 53, 211–227, 2003.

Küfmann, C.: Are Cambisols in alpine karst autochthonous or eolian in origin?, Arct. Antarct. Alp. Res., 40, 506–518, 2008.

Kutschera, W., Patzelt, G., Wild, E. M., Haas-Jettmar, B., Kofler, W., Lippert, A., Oeggl, K., Pak, E., Priller, A., Steier, P., Wahlmüller-Oeggl, N., and Zanesco, A.: Evidence for early human presence at high altitudes in the Ötztal Alps (Austria/Italy), Radiocarbon, 56, 923–947, 2014.

Lehndorff, E., Linstädter, J., Kehl, M., and Weniger, G.-C.: Fire history reconstruction from Black Carbon analysis in Holocene cave sediments at Ifri Oudadane, Northeastern Morocco, Holocene, 25, 398–402, 2015.

Lemma, B., Mekonnen, B., Glaser, B., Zech, W., Nemomissa, S., Bekele, T., Bittner, L., and Zech, M.: Chemotaxonomic patterns of vegetation and soils along altitudinal transects of the Bale Mountains, Ethiopia, and implications for paleovegetation reconstructions – Part II: lignin-derived phenols and leaf-wax-derived *n*-alkanes, E&G Quaternary Sci. J., 68, 189–200, https://doi.org/10.5194/egqsj-68-189-2019, 2019.

Lerch, M., Bliedtner, M., Roettig, C.-B., Schmidt, J.-U., Szidat, S., Salazar, G., Zech, R., Glaser, B., Kleber, A., and Zech, M.: Lipid biomarkers in aeolian sediments under desert pavements – potential and first results from the Black Rock Desert, Utah, USA, and Fuerteventura, Canary Islands, Spain, E&G Quaternary Sci. J., 66, 103–108, https://doi.org/10.5194/egqsj-66-103-2018, 2018.

Maria, E., Crancon, P., Lespes, G., and Bridoux, M.: Spatial variation in the molecular composition of dissolved organic matter from the Podzol soils of a temperate Pine Forest, ACS Earth and Space Chemistry, 3, 1685–1696, 2019.

Nittel, P.: Geologie, Hydrogeologie und Geomorphologie des Fotschertals – Kartierungsergebnisse Projekt “Sellrain” 2006, in: Das Mesolithikum-Projekt Ullafelsen (Teil 1). Mensch und Umwelt im Holozän Tirols 1, edited by: Schäfer, D., Philipp von Zabern, Innsbruck, Austria, 2011.

Pindur, P., Schäfer, D., and Luzian, R.: Nachweis einer bronzezeitlichen Feuerstelle bei der Schwarzensteinalm im Oberen Zemmgrund, Zillertaler Alpen, Mitt. Österr. Geogr. G., 149, 181–198, 2007.

Reimer, P. J., Austin, W. E. N., Bard, E., Bayliss, A., Blackwell, P. G., Bronk Ramsey, C., Butzin, M., Cheng, H., Edwards, R. L., Friedrich, M., Grootes, P. M., Guilderson, T. P., Hajdas, I., Heaton, T. J., Hogg, A. G., Hughen, K. A., Kromer, B., Manning,

S. W., Muscheler, R., Palmer, J. G., Pearson, C., van der Plicht, J., Reimer, R. W., Richards, D. A., Scott, E. M., Southon, J. R., Turney, C. S. M., Wacker, L., Adolphi, F., Büntgen, U., Capano, M., Fahrni, S. M., Fogtmann-Schulz, A., Friedrich, R., Köhler, P., Kudsk, S., Miyake, F., Olsen, J., Reinig, F., Sakamoto, M., Sookdeo, A., and Talamo, S.: The IntCal20 Northern Hemisphere radiocarbon age calibration curve (0–55 cal kBP), Radiocarbon, 62, 725–757, https://doi.org/10.1017/RDC.2020.41, 2020.

Ruff, M., Fahrni, S., Gäggeler, H. W., Hajdas, I., Suter, M., Synal, H.-A., Szidat, S., and Wacker, L.: On-line Radiocarbon Measurements of Small Samples Using Elemental Analyzer and MICADAS Gas Ion Source, Radiocarbon, 52, 1645–1656, https://doi.org/10.1017/S003382220005637X, 2010.

Salazar, G., Zhang, Y. L., Agrios, K., and Szidat, S.: Development of a method for fast and automatic radiocarbon measurement of aerosol samples by online coupling of an elemental analyzer with a MICADAS AMS, Nucl. Instrum. Meth. B, 361, 163–167, https://doi.org/10.1016/j.nimb.2015.03.051, 2015.

Schäfer, D.: Das Mesolithikum-Projekt Ullafelsen (Teil 1). Mensch und Umwelt im Holozän Tirols (Band 1), Philipp von Zabern, Innsbruck, Austria, 560 pp., 2011a.

Schäfer, D. (Ed.): Das Mesolithikum-Projekt Ullafelsen – Landschaftlicher Rahmen und archäologische Befunde. Arbeitsstand 2009/2010, in: Das Mesolithikum-Projekt Ullafelsen (Teil 1). Mensch und Umwelt im Holozän Tirols 1, Philipp von Zabern, Innsbruck, Austria, 2011b.

Schäfer, I. K., Lanny, V., Franke, J., Eglinton, T. I., Zech, M., Vysloužilová, B., and Zech, R.: Leaf waxes in litter and topsoils along a European transect, SOIL, 2, 551–564, https://doi.org/10.5194/soil-2-551-2016, 2016.

Schlosser, E.: Das Fotschertal – regionale Klimatologie und gebirgsmeterologische Aspekte, in: Das Mesolithikum-Projekt Ullafelsen (Teil 1). Mensch und Umwelt im Holozän Tirols Band 1, edited by: Schäfer, D., Philipp von Zabern, Innsbruck, Austria, 2011.

Staffler, H., Nicolussi, K., and Patzelt, G.: Postglaziale Waldgrenzentwicklung in den Westtiroler Zentralalpen, Gredleriana, 11, 93–114, 2011.

Struck, J., Bliedtner, M., Strobel, P., Schumacher, J., Bazarradnaa, E., and Zech, R.: Leaf wax n-alkane patterns and compound-specific $\delta^{13}C$ of plants and topsoils from semi-arid and arid Mongolia, Biogeosciences, 17, 567–580, https://doi.org/10.5194/bg-17-567-2020, 2020.

Szidat, S., Salazar, G. A. Vogel, E., Battaglia, M., Wacker, L., Synal, H.-A., Türler, A.: ^{14}C Analysis and Sample Preparation at the New Bern Laboratory for the Analysis of Radiocarbon with AMS (LARA), Radiocarbon, 56, 561–566, https://doi.org/10.2458/56.17457, 2014.

Tarasov, P., Müller, S., Zech, M., Andreeva, D., Diekmann, B., and Leipe, C.: Last glacial vegetation reconstructions in the extreme-continental eastern Asia: Potentials of pollen and n-alkane biomarker analyses, Quatern. Int., 290–291, 253–263, https://doi.org/10.1016/j.quaint.2012.04.007, 2013.

Trigui, Y., Wolf, Y., Sahakyan, L., Hovakimyan, H., Sahakyan, K., Zech, R., Fuchs, M., Wolpert, T., Zech, M., and Faust, D.: First calibration and application of leaf wax n-alkane biomarkers in loess-paleosol sequences and modern plants and soils in Armenia, Geosciences, 9, 263, https://doi.org/10.3390/geosciences9060263, 2019.

Wacker, L., Bonani, G., Friedrich, M., Hajdas, I., Kromer, B., Němec, M., Ruff, M., Suter, M., Synal, H.-A., and Vockenhuber, C.: MICADAS: Routine and High-Precision Radiocarbon Dating, Radiocarbon, 52, 252–262, https://doi.org/10.1017/S0033822200045288, 2010.

Wiedner, K., Schneeweiß, J., Dippold, M., and Glaser, B.: Anthropogenic Dark Earth in Northern Germany – The Nordic Analogue to terra preta de Índio in Amazonia, Catena, 132, 114–125, 2015.

Wolf, M., Lehndorff, E., Wiesenberg, G., Stockhausen, M., Schwark, L., and Amelung, W.: Towards reconstruction of past fire regimes from geochemical analysis of charcoal, Org. Geochem., 55, 11–21, 2013.

Zech, M., Zech, R., and Glaser, B.: A 240,000-year stable carbon and nitrogen isotope record from a loess-like palaeosol sequence in the Tumara Valley, Northeast Siberia, Chem. Geol., 242, 307–318, 2007.

Zech, M., Buggle B., Leiber, K., Marković, S., Glaser, B., Hambach, U., Huwe, B., Stevens, T., Sümegi, P., Wiesenberg, G., and Zöller, L.: Reconstructing Quaternary vegetation history in the Carpathian Basin, SE Europe, using n-alkane biomarkers as molecular fossils: problems and possible solutions, potential and limitations, Eiszeitalter und Gegenwart – Quaternary Sci. J., 58, 148–155, 2009.

Zech, M., Bimüller, C., Hemp, A., Samimi, C., Broesike, C., Hörold, C., and Zech, W.: Human and climate impact on ^{15}N natural abundance of plants and soils in high mountain ecosystems – a short review and two examples from the Eastern Pamirs and Mt. Kilimanjaro, Isot. Environ. Healt. S., 47, 286–296, 2011a.

Zech, M., Zech, R., Buggle, B., and Zöller, L.: Novel methodological approaches in loess research – interrogating biomarkers and compound-specific stable isotopes, E&G Quaternary Sci. J., 60, 13, https://doi.org/10.3285/eg.60.1.12, 2011b.

Zech, M., Pedentchouk, N., Buggle, B., Leiber, K., Kalbitz, K., Markovic, S., and Glaser, B.: Effect of leaf litter degradation and seasonality on D/H isotope ratios of n-alkane biomarkers, Geochim. Cosmochim. Ac., 75, 4917–4928, 2011c.

Zech, M., Rass, S., Buggle, B., Löscher, M., and Zöller, L.: Reconstruction of the late Quaternary paleoenvironment of the Nussloch loess paleosol sequence, Germany, using n-alkane biomarkers, Quaternary Res., 78, 326–335, 2012.

Zech, M., Kreutzer, S., Zech, R., Goslar, T., Meszner, S., McIntyre, C., Häggi, C., Eglinton, T., Faust D., and Fuchs, M.: Comparative ^{14}C and OSL dating of loess-paleosol sequences to evaluate post-depositional contamination of n-alkane biomarkers, Quaternary Res., 87, 180–189, 2017.

Zech, W. and Wilke, B.: Vorläufige Ergebnisse einer Bodenchronosequenzstudie im Zillertal, Mitteilungen der Deutschen Bodenkundlichen Gesellschaft, 25, 571–586, 1977.

Zech, W., Schad, P., and Hintermaier-Erhard, G.: Böden der Welt, Springer Spektrum Verlag, https://doi.org/10.1007/978-3-642-36575-1, 2014.

E&G Quaternary Sci. J., 70, 187–190, 2021
https://doi.org/10.5194/egqsj-70-187-2021

Open Access E&G Quaternary Science Journal

Preface

Preface: Special issue “Geoarchaeology of the Nile Delta”

Julia Meister[1], Eva Lange-Athinodorou[2], and Tobias Ullmann[1]

[1]Chair of Physical Geography, Institute of Geography and Geology, University of Würzburg, 97074 Würzburg, Germany
[2]Chair of Egyptology, Institute for Ancient Studies, University of Würzburg, 97070 Würzburg, Germany

Correspondence: Julia Meister (julia.meister@uni-wuerzburg.de)

Relevant dates: Received: 9 June 2021 – Revised: 30 June 2021 – Accepted: 2 July 2021 – Published: 23 July 2021

How to cite: Meister, J., Lange-Athinodorou, E., and Ullmann, T.: Preface: Special issue “Geoarchaeology of the Nile Delta”, E&G Quaternary Sci. J., 70, 187–190, https://doi.org/10.5194/egqsj-70-187-2021, 2021.

1 Geoarchaeology of the Nile Delta: research context and emerging fields

The Egyptian Nile Delta is the largest delta system in the Mediterranean region, covering about 24 000 km^2. As the most fertile region in North Africa, it is nowadays heavily used for agriculture and is home to about 60 million inhabitants. Today, there are only two estuarine branches in the Nile Delta (the Rosetta and Damietta branches), while for antiquity there are textual descriptions of up to seven major Nile branches that flowed through the delta. Major ancient Egyptian cities are found only in their immediate vicinity as these waterways were of great importance for intra-Egyptian traffic and trade, as well as for the availability of water. In addition, settlements were often built on their embankments for protection against the seasonal Nile floods. The Holocene dynamics of the ancient river network, therefore, influenced the ancient settlement activity in the Nile Delta (Butzer, 2002). However, these branches have been silted up or canalized and are usually no longer recognizable in the modern landscape, while the historical data allow for only a rough estimate of the former river courses and their chronology. Hence, the reconstruction of Holocene delta environments plays a central role in the study of human–environment interactions in ancient Egypt, and researchers working on this topic recognized the importance of the large river branches early on.

A pioneer in this field was Manfred Bietak who reconstructed the river courses of the eastern delta on the basis of the contour maps of the Survey of Egypt (Bietak, 1975). In the following years, the geoarchaeological survey of the Amsterdam University Expedition continued this line of research in the northeastern delta with more detailed investigations on the early historical periods of ancient Egypt (van den Brink et al., 1986; van Wesemael, 1988; de Wit, 1993). At the same time, the geological exploration, especially of the northern delta, progressed through the extensive drilling campaigns of the Mediterranean Basin Program of the Smithsonian Institute from 1985 to 1994, analysing a total of 87 boreholes on- and offshore. This project generated large amounts of new data on the Late Pleistocene and Holocene delta evolution (e.g. Coutellier and Stanley, 1987; Stanley and Warne, 1993; Stanley et al., 1996, 2004). Further on, the team of Jürgen Wunderlich (Goethe University Frankfurt) established a project on the Holocene development of the western Nile Delta, building a bridge between geography, geoarchaeology, and Egyptology (Wunderlich, 1988, 1989; Andres and Wunderlich, 1991). This project is still ongoing in cooperation with Robert Schiestl (University of Munich) and the German Archaeological Institute (DAI) in Cairo (Ginau et al., 2017, 2019, 2020; Altmeyer et al., 2021). In recent years further geoarchaeological ventures evolved in the Nile Delta. To name two, the “Delta Survey” of the Egypt Exploration Society has created a database available online of all visited tells throughout the delta, which is continually updated (Wilson and Grigoropoulos, 2009; Spencer, 2016), and it is also worth mentioning that there is the ongoing geoarchaeological exploration of the sacred landscape of Bubastis being carried

Published by Copernicus Publications on behalf of the Deutsche Quartärvereinigung (DEUQUA) e.V.

out by the University of Würzburg (Lange-Athinodorou et al., 2019; Ullmann et al., 2019, 2020).

2 The contributions to this volume

This special issue includes primarily studies presented at the DFG-funded (German Research Foundation) international workshop "Geoarchaeology of the Nile Delta: Current Research and Future Prospects", which took place in Würzburg in November 2019, pooling geoarchaeological case studies from different regions of the Nile Delta. Encompassing the broad interdisciplinary audience of the meeting, the nine articles in this special issue report on current geoarchaeological research projects in the Nile Delta and the application of innovative methods and approaches in this context, reflecting the wide range of current developments and challenges in geoarchaeological research in this region.

The study of Altmeyer et al. (2021) presents results on geophysical, stratigraphic, and pXRF surveys in the surroundings of the site Kom el-Gir in the northwestern Nile Delta. The synthesis of these investigations allows for a comprehensive reconstruction of a former fluvial network in the immediate surroundings of this site and confirms previous studies that suggested a larger Nile branch in this region.

The study of Crépy and Boussac (2021) investigates the palaeohydrology of ancient Lake Mareotis in the northwestern Nile Delta near the Mediterranean coast of Egypt, precursor of the modern Mariut lagoon, which acted as a gateway between the Nile valley and the Mediterranean Sea in ancient times. To reconstruct the extension of the western lake(s) at different periods, this study is based on the reassessment of geoarchaeological data and the analysis of early scholars' accounts, maps, and satellite images. The data show that Lake Mareotis experienced a drawdown in its western part during the 1st millennium BCE, followed by the formation of several distinct lakes and building activities in emerging areas during the Hellenistic period. During the 2nd century CE several canals were dug to connect the sites of the western wadi Mariut to the eastern part of the Mariut basin, leading to a reconfiguration of the lake(s).

Based on the assumption that lake-level changes, connections with the Nile and the sea, and possible high-energy events considerably controlled the human occupation history of ancient Lake Mareotis, the study of Flaux et al. (2021) reconstructs the lake's hydrology in historical times using faunal remains, geochemistry, and geoarchaeological indicators of relative lake-level changes. The data show both an increase in Nile sediment inputs to the basin during the 1st millennia BCE and CE and a lake-level rise of ca. 1.5 m during the Roman period. A high-energy deposit may explain an enigmatic sedimentary hiatus previously documented in the chronostratigraphy of the lake sediments.

The article of Khaled (2021) points out that the vast and fertile agricultural lands of the Nile Delta formed the backbone of the economy of the Old Kingdom. Foodstuffs and a wide variety of goods that were produced in this area were mandatory for the conduction of royal building projects like, for example, the erection of pyramids at the royal cemeteries in Sakkara, Giza, and other sites. To establish unhindered access to these resources, an effective administrative system came into place, based on the territorial distribution of the delta into districts, the so-called nomes. In these nomes, agricultural units ("domains") produced, collected, and delivered agricultural products for the needs of the royal household. New pictorial and written evidence from the causeway of the pyramid of King Sahure at Abusir provides us with fresh information on the territorial administration of the Nile Delta in the 5th dynasty.

For a long time, ancient Egyptian texts and descriptions of Greek and Roman historiographers were the only available sources of information about water bodies as parts of the sacred landscape of temples in the Nile Delta. The recent introduction and application of geoarchaeological methods in archaeological projects, however, led to an unprecedented accumulation of new geophysical, sedimentological, and archaeological data which can be utilized to identify and locate lakes, canals, and river branches in close vicinity to the temple areas. The study of Lange-Athinodorou (2021) reviews the available geoarchaeological information on the temples of the cities of Buto, Sais, and Bubastis, which were home to important goddesses acknowledged all over Egypt, and compares these with the information coming from textual sources. The combined results allow for reconstructions of the most elemental parts of the sacred landscapes of those shrines, their role in religious and daily life activities, and their surrounding hydro-geography and natural landscapes.

In the absence of geoarchaeological indications, Schiestl (2021) applied a combined analysis of historical sources, satellite imagery, and the TanDEM-X digital elevation model to investigate the Butic Canal, a waterway that crossed the northern Nile Delta in a transversal way during Roman times. The detection of debris from the excavation of the canal, which became visible as a linear elevated feature in the digital elevation model, allowed for the identification of the eastern section of the canal. The discovery is of relevance as this artificial watercourse resulted from the need for a more economic and less time-consuming transportation route through the delta, and it was a manifestation of imperial investments in the infrastructure of the eastern part of the Roman Empire.

The study of Stanley and Wedl (2021) addresses the question of how climate and environmental changes affected the societies of Ancient Egypt. By examining marine sediments in the Levantine Basin, they were able to demonstrate reduced depositional accumulation rates and altered compositional attributes of the sediment facies mainly from 2300 to 2000 BCE. These effects were presumably triggered by displaced climatic belts leading to decreased rainfall and lower Nile flows, as well as modified oceanographic conditions. As a result agricultural production probably decreased significantly, possibly leading to a changed social, political, and economic situation that could have promoted the disintegration of the political system at the end of the Old Kingdom.

The study of Ullmann et al. (2020) analyses Landsat remote sensing data, acquired between 1985 and 2019 for the entire Nile Delta, to detect surface anomalies that are potentially related to buried near-surface palaeogeographical features. Using the normalized difference wetness index calculated for months with low and high evapotranspiration, anomalies in the immediate surroundings of several Pleistocene sand hills ("geziras") and tells of the eastern delta were identified. This approach allowed them to map the potential near-surface continuation of these geziras and the indication of buried river branches in the northern and eastern Nile Delta.

The paper of Wilson and Ghazala (2021) investigates the embedding of the ancient city of Sais (Sa el-Hagar) within the surrounding natural landscape of the western-central Nile Delta and explores the possibility that certain features of the landscape influenced the choice of the settlement location. By combining geological, geophysical, remote sensing, and archaeological data, this study aims to describe and reconstruct the deltaic environs and hydro-geography of Sais. A special focus lies on the question of if research can determine the specific nature of human interactions with the landscape, i.e. if human occupants reacted in a proactive or reactive manner. The study shows that over a period of several millennia (i.e. from around 4000 BCE to the modern day) the settlement at Sais occupied several locations in the immediate environs of a moving Nile branch. Ultimately, the positive effects of the local hydrography led to the establishment of a capital city in the 7th century BCE.

3 Current challenges and future research

The aforementioned emerging fields of geoarchaeological research are accompanied by several challenges. These include the rapid expansion of modern settlements due to the rapidly growing population, leading to overbuilding and thus the endangerment of archaeological sites. In addition, the continuing sea-level rise is gradually submerging the coastal regions of the Nile Delta. In order to quickly advance research and to generate as much data as possible in the relatively short time remaining, as well as to further develop the field of geoarchaeology in the Nile Delta, the cooperation of existing projects and the establishment of new projects in close collaboration with the Ministry of State for Antiquities of Egypt is therefore all the more important in the coming years. Moreover, the application and further development of interdisciplinary methods and models have a key position in this process.

Code and data availability. Information provided throughout the text is available in previously published studies by authors cited throughout the text and listed in the references.

Author contributions. The manuscript was prepared by JM, ELA, and TU.

Disclaimer. Publisher's note: Copernicus Publications remains neutral with regard to jurisdictional claims in published maps and institutional affiliations.

Special issue statement. This article is part of the special issue "Geoarchaeology of the Nile Delta". It is a result of the workshop "Geoarchaeology of the Nile Delta: Current Research and Future Prospects", Würzburg, Germany, 29–30 November 2019.

Acknowledgements. We gratefully thank all authors for their contributions to this special issue. We also kindly thank Hans von Suchodoletz and one anonymous reviewer for constructive comments and suggestions.

Financial support. This open-access publication was funded by Julius-Maximilians-Universität Würzburg.

Review statement. This paper was edited by Hans von Suchodoletz and reviewed by one anonymous referee.

References

Altmeyer, M., Seeliger, M., Ginau, A., Schiestl, R., and Wunderlich, J.: Reconstruction of former channel systems in the northwestern Nile Delta (Egypt) based on corings and electrical resistivity tomography (ERT), E&G Quaternary Sci. J., 70, 151–164, https://doi.org/10.5194/egqsj-70-151-2021, 2021.

Andres, W. and Wunderlich, J.: Late Pleistocene and Holocene Evolution of the Eastern Nile Delta and Comparisons with the Western Delta, in: Von der Nordsee bis zum Indischen Ozean. Ergebnisse der 8. Jahrestagung des AK Geographie der Meere und Küsten, 13.–15. Juni 1990, Düsseldorf, edited by: Brückner, H. and Ratdke, U., Stuttgart, 121–130, 1991.

Bietak, M.: Tell el-Dab'a II, Der Fundort im Rahmen einer archäologisch-geographischen Untersuchung über das ägyptische Ostdelta, Austrian Academy of Sciences Press, Wien, 1975.

Butzer, K. W.: Geoarchaeological implications of recent research in the Nile Delta, in: Egypt and the Levant: Interrelations from the 4th through the Early 3rd Millennium BCE, edited by: van den Brink, E. C. M. and Levy, T. E., Leicester University Press, London, New York, 83–97, 2002.

Coutellier, V. and Stanley, D. J.: Late Quaternary stratigraphy and paleogeography of the eastern Nile Delta, Egypt, Mar. Geol., 77, 257–275, https://doi.org/10.1016/0025-3227(87)90116-2, 1987.

Crépy, M. and Boussac, M.-F.: Western Mareotis lake(s) during the Late Holocene (4th century BCE–8th century CE): diachronic evolution in the western margin of the Nile Delta and evidence for the digging of a canal complex during the early Roman period, E&G Quaternary Sci. J., 70, 39–52, https://doi.org/10.5194/egqsj-70-39-2021, 2021.

de Wit, H. E.: The evolution of the eastern Nile Delta as a factor in the development of human culture, in: Environmental change and human culture in the Nile Basin and Northern Africa until the second millennium B.C, edited by: Krzyżaniak, L., Kobusiewicz, M., and Alexander, J., Poznan Archaeological Museum, Poznań, 305–320, ISBN 978-83-900434-1-8, 1993.

Flaux, C., Giaime, M., Pichot, V., Marriner, N., el-Assal, M., Guihou, A., Deschamps, P., Claude, C., and Morhange, C.: The late Holocene record of Lake Mareotis, Nile Delta, Egypt, E&G Quaternary Sci. J., 70, 93–104, https://doi.org/10.5194/egqsj-70-93-2021, 2021.

Ginau, A., Schiestl, R., Kern, F., and Wunderlich, J.: Identification of historic landscape features and settlement mounds in the Western Nile Delta by means of remote sensing time series analysis and the evaluation of vegetation characteristics, J. Archaeol. Sci. Rep., 16, 170–184, https://doi.org/10.1016/j.jasrep.2017.09.034, 2017.

Ginau, A., Schiestl, R., and Wunderlich, J.: Integrative geoarchaeological research on settlement patterns in the dynamic landscape of the northwestern Nile delta, Quat. Int., 511, 51–67, https://doi.org/10.1016/j.quaint.2018.04.047, 2019.

Ginau, A., Steiniger, D., Hartmann, R., Hartung, U., Schiestl, R., Altmeyer, M., Seeliger, M., and Wunderlich, J.: What settlements leave behind – pXRF compositional data analysis of archaeological layers from Tell el-Fara'in (Buto, Egypt) using machine learning, Palaeogeogr. Palaeocl., 546, 109666, https://doi.org/10.1016/j.palaeo.2020.109666, 2020.

Khaled, M. I.: Nomes of Lower Egypt in the early Fifth Dynasty, E&G Quaternary Sci. J., 70, 19–27, https://doi.org/10.5194/egqsj-70-19-2021, 2021.

Lange-Athinodorou, E.: Implications of geoarchaeological investigations for the contextualization of sacred landscapes in the Nile Delta, E&G Quaternary Sci. J., 70, 73–82, https://doi.org/10.5194/egqsj-70-73-2021, 2021.

Lange-Athinodorou, E., El-Raouf, A. A., Ullmann, T., Trappe, J., Meister, J., and Baumhauer, R.: The sacred canals of the Temple of Bastet at Bubastis (Egypt): New findings from geomorphological investigations and Electrical Resistivity Tomography (ERT), J. Archaeol. Sci. Rep., 26, 101910, https://doi.org/10.1016/j.jasrep.2019.101910, 2019.

Schiestl, R.: A new look at the Butic Canal, Egypt, E&G Quaternary Sci. J., 70, 29–38, https://doi.org/10.5194/egqsj-70-29-2021, 2021.

Spencer, J.: The Delta Survey, 2009–2015, Egypt Exploration Society, Excavation Memoir 112, London, 31 pp., ISBN 978 0 85698 225 5, 2016.

Stanley, D. J. and Warne, A. G.: Nile Delta: Recent Geological Evolution and Human Impact, Science, 260, 628–634, https://doi.org/10.1126/science.260.5108.628, 1993.

Stanley, D. J., McRea, J. E., and Waldron, J. C.: Nile Delta drill core and sample database for 1985–1994: Mediterranean Basin (MEDIBA) Program, Smithson. Contrib. Mar. Sci., 1–428, https://doi.org/10.5479/si.01960768.37.1, 1996.

Stanley, J., Warne, A., and Schnepp, G.: Geoarchaeological Interpretation of the Canopic, Largest of the Relict Nile Delta Distributaries, Egypt, J. Coast. Res., 203, 920–930, https://doi.org/10.2112/1551-5036(2004)20[920:GIOTCL]2.0.CO;2, 2004.

Stanley, J.-D. and Wedl, S. E.: Significant depositional changes offshore the Nile Delta in late third millennium BCE: relevance for Egyptology, E&G Quaternary Sci. J., 70, 83–92, https://doi.org/10.5194/egqsj-70-83-2021, 2021.

Ullmann, T., Lange-Athinodorou, E., Göbel, A., Büdel, C., and Baumhauer, R.: Preliminary results on the paleo-landscape of Tell Basta /Bubastis (eastern Nile delta): An integrated approach combining GIS-Based spatial analysis, geophysical and archaeological investigations, Quat. Int., 511, 185–199, https://doi.org/10.1016/j.quaint.2017.12.053, 2019.

Ullmann, T., Nill, L., Schiestl, R., Trappe, J., Lange-Athinodorou, E., Baumhauer, R., and Meister, J.: Mapping buried paleogeographical features of the Nile Delta (Egypt) using the Landsat archive, E&G Quaternary Sci. J., 69, 225–245, https://doi.org/10.5194/egqsj-69-225-2020, 2020.

van den Brink, E. C. M., van Wesemael, B., and Dirksz, P.: A geoarchaeological survey in the north-eastern Nile Delta, Mitteilungen Dtsch. Archäol. Inst. Abt. Kairo, 43, 7–31, 1986.

van Wesemael, B.: The relation between natural landscape and distribution of archaeological remains in the Northeastern Nile Delta, in: The archaeology of the Nile Delta, Egypt: problems and priorities, in: Proceedings of the seminar held in Cairo, 19–22 October 1986, on the occasion of the fifteenth anniversary of the Netherlands Institute of Archaeology and Arabic Studies in Cairo, edited by: van den Brink, E. C. M., Amsterdam, 125–139, 1988.

Wilson, P. and Ghazala, H.: Sandhills, sandbanks, waterways, canals and sacred lakes at Sais in the Nile Delta, E&G Quaternary Sci. J., 70, 129–143, https://doi.org/10.5194/egqsj-70-129-2021, 2021.

Wilson, P. and Grigoropoulos, D.: The West Nile Delta Regional Survey, Beheira and Kafr El-Sheikh Provinces, Egypt Exploration Society, Excavation Memoir 86, London, 490 pp., ISBN 978 0 85698 194 4, 2009.

Wunderlich, J.: Investigations on the development of the Western Nile Delta in Holocene times, in: The archaeology of the Nile Delta, Egypt: problems and priorities, Proceedings of the seminar held in Cairo, 19–22 October 1986, edited by: van den Brink, E. C. M., Amsterdam, 251–257, 1988.

Wunderlich, J.: Untersuchungen zur Entwicklung des westlichen Nildeltas im Holozän, Marburger Geographische Gesellschaft, Marburg/Lahn, ISBN 978-3-8835-3038-3, 1989.

E&G Quaternary Sci. J., 70, 191–195, 2021
https://doi.org/10.5194/egqsj-70-191-2021

Open Access E&G Quaternary Science Journal

Express report

Local mineral dust transported by varying wind intensities forms the main substrate for loess in Kashmir

Christian Zeeden[1], Jehangeer Ahmad Mir[2], Mathias Vinnepand[1], Christian Laag[1,3], Christian Rolf[1], and Reyaz Ahmad Dar[2]

[1]Rock Physics & Borehole Geophysics, Leibniz Institute for Applied Geophysics (LIAG), 30655 Hanover, Germany
[2]Department of Earth Sciences, University of Kashmir, Srinagar, 190006, India
[3]Institut de Physique du Globe de Paris, Université de Paris, CNRS, Paris, 75005, France

Correspondence: Christian Zeeden (christian.zeeden@leibniz-liag.de)

Relevant dates: Received: 4 May 2021 – Revised: 21 June 2021 – Accepted: 23 July 2021 – Published: 24 August 2021

How to cite: Zeeden, C., Mir, J. A., Vinnepand, M., Laag, C., Rolf, C., and Dar, R. A.: Local mineral dust transported by varying wind intensities forms the main substrate for loess in Kashmir, E&G Quaternary Sci. J., 70, 191–195, https://doi.org/10.5194/egqsj-70-191-2021, 2021.

1 Introduction and site descriptions

Airborne mineral dust particles of dominantly silt size are the main substrate for loess deposits, which provide valuable and widespread palaeo-environmental archives. Especially during the Quaternary period, loess–palaeosol sequences (LPSs) formed through consolidation and largely climate-dependent post-depositional modifications of mineral dust, e.g. along the mid-latitudes in Eurasia. The enormous spatial spread of these archives exceeds the extent of any other Quaternary terrestrial sediment record. Consequently, LPSs are a key for studying the impact of oscillating and competing supra-regional climate systems to sub-systems on diverse temporal and spatial scales. While Eurasian LPSs have been decently studied (e.g. Fischer et al., 2021; Jia et al., 2018; Zeeden et al., 2016; Vlaminck et al., 2016), information on age and physical properties of equivalents across the Indian subcontinent remains sparse (Dar and Zeeden, 2020). This limits our understanding of the origin of loess deposits and associated major wind directions and wind intensities for the Indian subcontinent throughout the Quaternary and how these factors differ from locations across Eurasia. Studies on Kashmir loess led to valuable stratigraphic descriptions (Bronger et al., 1987) and a first temporal framework (Singhvi et al., 1987), but few physical proxy data are available (Dar and Zeeden, 2020, and references therein). In this study, we present a first high-resolution investigation of room-temperature magnetic susceptibility and grain size data of loess deposits in the Kashmir region and compare our results with these from other LPSs in Eurasia. We aim to pave the way for further studies addressing differences in palaeo-environmental conditions between the Indian subcontinent and Eurasia, which are likely to reflect the impact of competing supra-regional climate systems (Indian monsoon, westerlies) varying over time.

In this study, we focus on the Wanihama section (34°10′05.7″ N, 74°51′03.5″ E) ∼ 4 km NE of Srinagar and the Khan Sahib section (33°56′08.9″ N, 74°39′29.5″ E), ∼ 30 km SW of Srinagar (both in Kashmir, Fig. 1). The sections were sampled continuously in 0.02 m resolution. Stratigraphic descriptions of the profiles are from bottom to top, in order of deposition. Only limited material could be removed from the hardened deposits at the outcrop behind the Wanihama Middle School (see Fig. 1a, c), where sampling was conducted in 2019. The base of the outcrop is characterised by chestnut-coloured lacustrine loamy and sandy deposits with no visible bedding. From 0.2 up to 0.5 m, sediments are enriched with silty material whilst the sand content

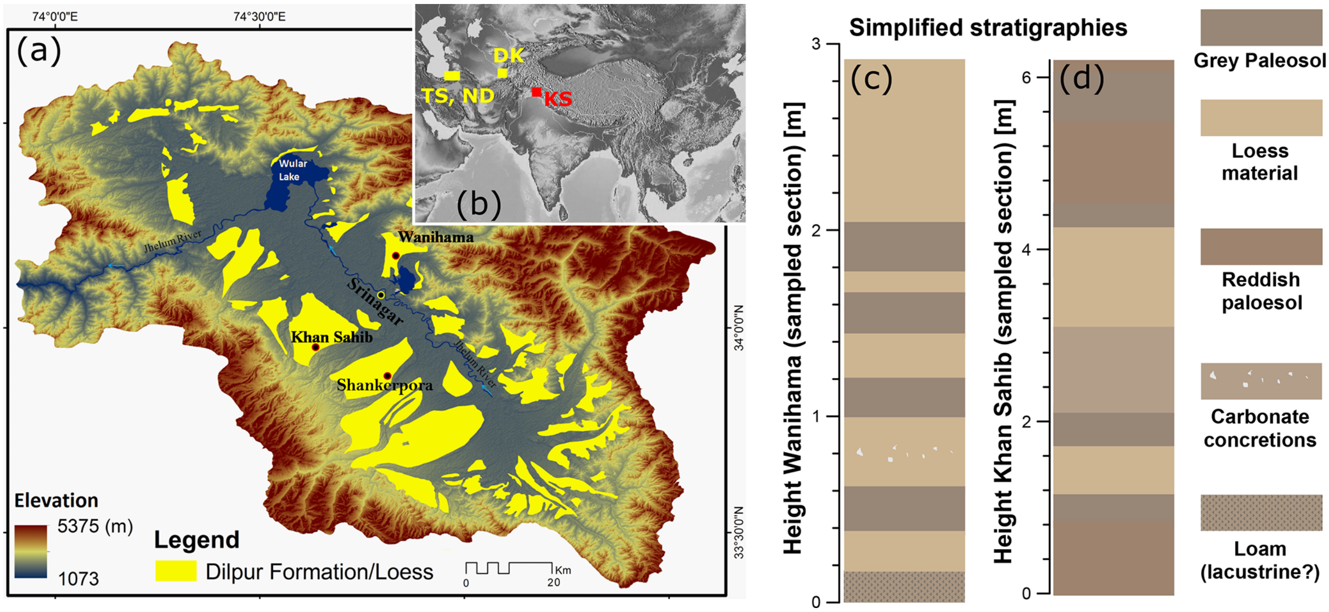

Figure 1. **(a)** Distribution of loess in Kashmir and **(b)** location of the studied Wanihama and Khan Sahib sections in supra-regional and regional context (after Dar and Zeeden, 2020). KS denotes Kashmir loess, DK Darai Kalon, and TS and ND Toshan and Now Deh, respectively. Profile sketches of the profiles Wanihama **(c)** and Khan Sahib (**d**, on the right) show alternating loess and palaeosol units indicating climate sensitivity of the archives. Sampling resolution was 0.02 m.

decreases distinctly. Note that this interval contains varying amounts of ~ 1 mm sized carbonate nodules. Until 0.8 m, the sediment gets lighter until a medium silt component dominates the grain size range (prevailing up to the top of the sampled section). From 0.8 up to a height of 1.70 m the hues of the record turn brown again with a distinct gradient towards darker brown hues at the top of this interval. Ochre-coloured sediments occur from ~ 1.7–1.8 m. These are followed by brown silt until 2.2 m. The part from 2.2 m up to the top of the LPS is characterised by light ochre silt including preserved palaeo-root channels.

In 2020, we sampled 6.20 m of the Khan Sahib section (Fig. 1a, d). Sampling started at the base within a brown silt. Palaeosols with clearly enhanced clay contents and (sub)polyhedric structures are identified at ~ 1, 2, 4.5 and 5.8 m height of the LPS. These at 2, 4.5 and 5.8 m exhibit a grey to brown colour. In contrast, the palaeosol at ~ 1 m height is brown to black and mostly clay- and organic-rich. All palaeosols are separated by lighter packages of loess or weaker pedogenesis. Due to similarities of the stratigraphies of the records under study with parts of a 17 m thick LPSs at Shankerpora, Kashmir (Fig. 1a), temporally placed into the last glacial cycle (Meenakshi et al., 2018), we start from the premise that both studied sections formed during the late last glacial cycle in the interval between oxygen isotope stages (OISs) 4 to 2.

2 Geophysical sediment properties: methods and results

For magnetic susceptibility measurements we dried, disintegrated, and homogenised the samples and transferred the material into 6.4 cm^3 non-magnetic plastic boxes. Subsequently, the mass-normalised magnetic susceptibility (χ) was measured using a MAGNON VFSM susceptibility bridge. Frequencies of 505 Hz (low frequency; χ_{lf}) and 5050 Hz (high frequency; χ_{hf}) and a field intensity of 400 A m^{-1} were used. $\Delta\chi$ denotes the difference between χ_{lf} and χ_{hf} and is indicative of fine magnetic grain sizes. Grain sizes were determined using a Beckman Coulter LS 13320 PIDS using methods as described in Vlaminck et al. (2016).

The χ_{lf} ranges from 25×10^{-8} to 144×10^{-8} $m^3\,kg^{-1}$ with a mean of 82×10^{-8} $m^3\,kg^{-1}$ at Wanihama (Fig. 2a). At the Khan Sahib section, the χ_{lf} ranges from 28×10^{-8} to 170×10^{-8} $m^3\,kg^{-1}$ with a mean of 75×10^{-8} $m^3\,kg^{-1}$ (Fig. 2b). The $\Delta\chi$ lies in the range from 2.5 % to 10.7 % for the Wanihama and from 3.1 % to 10.9 % for the Khan Sahib section. The grain size distributions plotted in Fig. 3 have a dominant peak at the boundary from middle to coarse silt around 10–30 µm throughout, with rather small differences between soils and loess. All but one sample from 0.98 m of the Wanihama section exhibit at least one additional component with a local maximum in grain size ranging around 50–500 µm (Fig. 3). Overall, the palaeosol samples exhibit finer modes than the loess samples. The two loess samples (from Wanihama 1.48 m, Khan Sahib 6.18 m) contain dif-

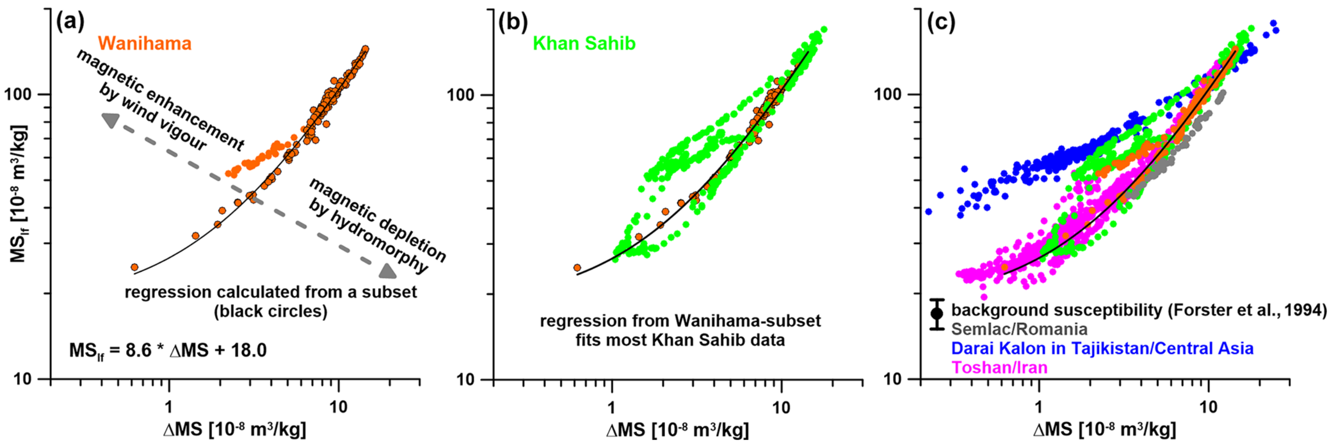

Figure 2. Magnetic enhancement at **(a)** Wanihama including an enhancement line for the lower 2.4 m. **(b)** Enhancement plot for Khan Sahib including the data from Wanihama. **(c)** Data from both Kashmir localities with comparison to reference data from Semlac, Romania (Zeeden et al., 2016); Darai Kalon, Tajikistan (Jia et al., 2018); and Toshan, Iran (Vlaminck et al., 2016). Note that only data from the last glacial–interglacial cycle are plotted and that plots are double logarithmic.

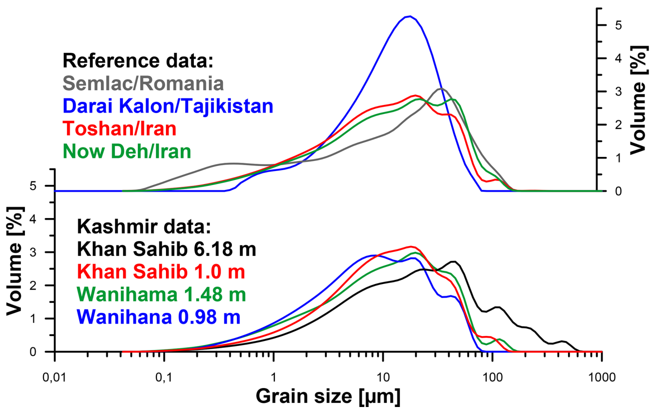

Figure 3. Grain size properties of Kashmir loess, also in comparison with data from Semlac, Romania; Toshan, Iran; and Now Deh, Iran. Reference data from ~30 ka are plotted for Semlac and Darai Kalon (Zeeden et al., 2016; Lu et al., 2020), and mean grain size distributions for Toshan and Now Deh (Vlaminck et al., 2016; Kehl et al., 2021). Note that also Shah et al. (2021) reported grain size data from Kashmir which are dominated by silt.

ferent amounts of sand and are varying in their multimodal properties. Note that some multimodal properties may be measuring artefacts (cf. Schulte et al., 2018).

3 Kashmir loess deposits within a Eurasian context

Overall, χ properties of the studied sections in Kashmir are similar to loess in Eurasia, although the reference data were partly measured using different field frequencies and intensities. Figure 2c shows a comparison to magnetic enhancement from Semlac in Romania (Zeeden et al., 2016), Darai Kalon in Tajikistan (Jia et al., 2018), Toshan in Iran (Vlaminck et al., 2016) and the background susceptibility determined by Forster et al. (1994). The Kashmir loess shows higher χ than loess from Romania and lower values compared to loess from Tajikistan. Magnetic enhancement of Kashmir loess was quite strong during stadial phases of the last glacial cycle. Enhancement was partly even stronger than for full interglacial soils in Europe,but not as strong as in full interglacial soils in central Asia (Fig. 2c). Besides classical magnetic enhancement, an additional effect influences the relationship between χ_{lf} and $\Delta\chi$ leading to prominently elevated values of the $\chi_{lf}/\Delta\chi$ ratio. We relate this to wind vigour effects (Begét and Hawkins, 1989) associated with strong winds delivering coarser material (with elevated $\chi_{lf}/\Delta\chi$) from source areas in proximity to the studied LPS in Kashmir (Fig. 2). When comparing the Kashmir dataset to last glacial data from localities in Eurasia (using their respective age models; Fig. 2c), it becomes apparent that magnetic enhancement is similar to datasets from Romania and Iran. In contrast, magnetic enhancement of Tajik loess shows relatively elevated χ and/or reduced $\Delta\chi$. The dataset from Kashmir bridges these two data populations/trends and shows features of both. Kashmir grain size properties exhibit a ~10 µm median, and the grain size distribution is similar to loess from OIS 3 at Darai Kalon, Tajikistan (Lu et al., 2020; see Fig. 3), loess grain size at Toshan, Iran (Vlaminck et al., 2016), and loess at Now Deh, Iran (Kehl et al., 2021). At Toshan and Now Deh, finer grain sizes were interpreted to indicate the input of mineral dust from distal source areas (Kehl et al., 2021; Vlaminck et al., 2016). At Darai Kalon, the grain sizes > 25 µm are considered to be driven by local near-surface wind intensity (Lu et al., 2020), which may be the case here, too. For the Kashmir loess, our grain size data indicate no sediment transport over the mostly > 2000 m high surrounding mountain ranges suggesting that the dust source is located in the Kashmir Valley or its direct surroundings. This implies that low SiO_2 / AL_2O_3 ratios reported by Ahmad and Chandra (2013) are a product of sediment origin besides transport, and possibly reworking of sedimentary rocks in Kashmir, and may not require transport over high mountain ranges. We interpret components around $\sim 100/150\,\mu m$ to indicate transport modes during strong wind events.

4 Conclusions

Magnetic enhancement of Kashmir loess was quite strong during stadial phases of the last glacial cycle. It reached interglacial intensity when compared to selected places in central Asia (Fig. 2c). Beside classical magnetic enhancement, an additional effect influences the relationship between χ_{lf} and $\chi_{fd}/\Delta\chi$. We assign this to wind vigour with strong winds transporting coarser material with elevated $\chi_{lf}/\Delta\chi$ ratios during the most loessic and coarse-grained intervals, pointing to local transport of a considerable amount of the material. The loess in Kashmir shows features of both "classical" magnetic enhancement (Forster et al., 1994) and wind-vigour effects. Grain sizes of Kashmir loess exhibit modes mostly around 5–20 µm, similar to some data from central Asia (Lu et al., 2020; Vlaminck et al., 2016; Kehl et al., 2021). Grain size distributions do not suggest transport over high mountain ranges that would be required for non-local sources in Kashmir. Therefore, and because of wind vigour effects, we suggest that the Kashmir loess is at least predominantly of local origin. The thick deposits of loess from the last glacial cycle in Kashmir (e.g. > 8, ~ 10, ~ 18 m for the last glacial–interglacial cycle; Dar and Zeeden, 2020; Meenakshi et al., 2018; Singhvi et al., 1987; Shah et al., 2021; and references in these) support this interpretation, as it appears unlikely that such substantial sediment masses were transported over the > 2000 m high mountain ranges surrounding Kashmir.

Data availability. The magnetic susceptibility and grain size data will be made available in the PANGAEA database.

Author contributions. CZ designed the study. Sampling was done by JAM, RAD and CZ. Samples were analysed by CL, MV, CZ and CR. Interpretation and manuscript writing was led by CZ but was a joint effort of all authors (CZ, JAM, MV, CL, CR, RAD).

Competing interests. Christian Zeeden is an associate editor of *E&G Quaternary Science Journal*. The authors declare no other competing interests.

Disclaimer. Publisher's note: Copernicus Publications remains neutral with regard to jurisdictional claims in published maps and institutional affiliations.

Acknowledgements. We thank the staff of the Wanihama Middle School for providing the access to the Wanihama section and general support. Sumiko Tsukamoto is thanked for the fantastic teamwork in the framework of the project "Loess in India: recorder of the Indian Monsoon system". Samples were processed in the LIAG laboratories. We thank especially Kathrin Worm and Sonja Riemenschneider for their help with sample processing and measurements. We thank Hao Lu and Martin Kehl for sharing grain size data from Darai Kalon and Toshan, Now Deh, respectively. We also thank Tobias Sprafke and another reviewer for their constructive feedback through the review process, which helped to improve this article. This is IPGP contribution number 4235.

Financial support. This research was funded by the Deutsche Forschungsgemeinschaft (DFG, German Research Foundation; grant no. 432194908).

Review statement. This paper was edited by Tobias Sprafke and reviewed by one anonymous referee.

References

Ahmad, I. and Chandra, R.: Geochemistry of loess-paleosol sediments of Kashmir Valley, India: Provenance and weathering, J. Asian Earth Sci., 66, 73–89, https://doi.org/10.1016/j.jseaes.2012.12.029, 2013.

Begét, J. E. and Hawkins, D. B.: Influence of orbital parameters on Pleistocene loess deposition in central Alaska, Nature, 337, 151–153, https://doi.org/10.1038/337151a0, 1989.

Bronger, A., Pant, R. K., and Singhvi, A. K.: Pleistocene climatic changes and landscape evolution in the Kashmir Basin, India: Paleopedologic and chronostratigraphic studies, Quat. Res., 27, 167–181, https://doi.org/10.1016/0033-5894(87)90075-5, 1987.

Dar, R. A. and Zeeden, C.: Loess-Palaeosol Sequences in the Kashmir Valley, NW Himalayas: A Review, Front. Earth Sci., 8, 113, https://doi.org/10.3389/feart.2020.00113, 2020.

Fischer, P., Jöris, O., Fitzsimmons, K. E., Vinnepand, M., Prud'homme, C., Schulte, P., Hatté, C., Hambach, U., Lindauer, S., Zeeden, C., Peric, Z., Lehmkuhl, F., Wunderlich, T., Wilken, D., Schirmer, W., and Vött, A.: Millennial-scale terrestrial ecosystem responses to Upper Pleistocene climatic changes: 4D-reconstruction of the Schwalbenberg Loess-Palaeosol-Sequence (Middle Rhine Valley, Germany), CATENA, 196, 104913, https://doi.org/10.1016/j.catena.2020.104913, 2021.

Forster, T., Evans, M. E., and Heller, F.: The frequency dependence of low field susceptibility in loess sediments, Geophys. J. Int., 118, 636–642, https://doi.org/10.1111/j.1365-246X.1994.tb03990.x, 1994.

Jia, J., Lu, H., Wang, Y., and Xia, D.: Variations in the Iron Mineralogy of a Loess Section in Tajikistan During the Mid-Pleistocene and Late Pleistocene: Implications for the Climatic Evolution in Central Asia, Geochem. Geophy. Geosy., 19, 1244–1258, https://doi.org/10.1002/2017GC007371, 2018.

Kehl, M., Vlaminck, S., Köhler, T., Laag, C., Rolf, C., Tsukamoto, S., Frechen, M., Sumita, M., Schmincke, H.-U., and Khormali, F.: Pleistocene dynamics of dust accumulation and soil formation in the southern Caspian Lowlands – New insights from the loess-paleosol sequence at Neka-Abelou, northern Iran, Quat. Sci. Rev., 253, 106774, https://doi.org/10.1016/j.quascirev.2020.106774, 2021.

Lu, H., Jia, J., Yin, Q., Xia, D., Gao, F., Liu, H., Fan, Y., Li, Z., Wang, X., Berger, A., Oimahmadov, I., and Gadoev, M.: Atmospheric dynamics patterns in southern central Asia since 800 ka revealed by loess-paleosol sequences in Tajikistan, Geophys. Res. Lett., 47, e2020GL088320, https://doi.org/10.1029/2020GL088320, 2020.

Meenakshi, Kumar, P., Shrivastava, J. P., Chandra, R., Chopra, S., Roonwal, G. S., and Sharma, R.: High resolution 14C AMS ages (∼ 50 ka) of organic matter associated with the loess-palaeosol Holocene-Late Pleistocene (8–130 ka) sediments of Dilpur Formation, Karewa Group, Kashmir, India, Quat. Geochronol., 47, 170–179, https://doi.org/10.1016/j.quageo.2018.06.004, 2018.

Schulte, P., Sprafke, T., Rodrigues, L., and Fitzsimmons, K. E.: Are fixed grain size ratios useful proxies for loess sedimentation dynamics? Experiences from Remizovka, Kazakhstan, Aeolian Res., 31, 131–140, https://doi.org/10.1016/j.aeolia.2017.09.002, 2018.

Shah, R. A., Achyuthan, H., Lone, A. M., Jaiswal, M. K., and Paul, D.: Constraining the timing and deposition pattern of loess-palaeosol sequences in Kashmir Valley, Western Himalaya: Implications to paleoenvironment studies, Aeolian Res., 49, 100660, https://doi.org/10.1016/j.aeolia.2020.100660, 2021.

Singhvi, A. K., Bronger, A., Pant, R. K., and Sauer, W.: Thermoluminescence dating and its implications for the chronostratigraphy of loess-paleosol sequences in the Kashmir Valley (India), Chem. Geol. Isot. Geosci. Sect., 65, 45–56, https://doi.org/10.1016/0168-9622(87)90061-3, 1987.

Vlaminck, S., Kehl, M., Lauer, T., Shahriari, A., Sharifi, J., Eckmeier, E., Lehndorff, E., Khormali, F., and Frechen, M.: Loess-soil sequence at Toshan (Northern Iran): Insights into late Pleistocene climate change, Quat. Int., 399, 122–135, https://doi.org/10.1016/j.quaint.2015.04.028, 2016.

Zeeden, C., Kels, H., Hambach, U., Schulte, P., Protze, J., Eckmeier, E., Marković, S. B., Klasen, N., and Lehmkuhl, F.: Three climatic cycles recorded in a loess-palaeosol sequence at Semlac (Romania) – Implications for dust accumulation in south-eastern Europe, Quat. Sci. Rev., 154, 130–142, https://doi.org/10.1016/j.quascirev.2016.11.002, 2016.

E&G Quaternary Sci. J., 70, 197–199, 2021
https://doi.org/10.5194/egqsj-70-197-2021

Open Access E&G Quaternary Science Journal

Thesis abstract

The Quaternary palaeobotany of Madeira and Azores volcanic archipelagos (Portugal): insights into the past diversity, ecology, biogeography and evolution

Carlos A. Góis-Marques[1,2,3]

[1]Departamento de Geologia, Faculdade de Ciências da Universidade de Lisboa, Campo Grande, 1749-016, Lisbon, Portugal
[2]Instituto Dom Luiz (IDL), Laboratório Associado, Universidade de Lisboa, Campo Grande, 1749-016, Lisbon, Portugal
[3]Madeira Botanical Group (GBM), Faculdade de Ciências da Vida, Universidade da Madeira, Campus da Penteada, 9000-390, Funchal, Portugal

Correspondence: Carlos A. Góis-Marques (c.goismarques@gmail.com)

Relevant dates: Received: 14 May 2021 – Accepted: 9 August 2021 – Published: 6 September 2021

How to cite: Góis-Marques, C. A.: The Quaternary palaeobotany of Madeira and Azores volcanic archipelagos (Portugal): insights into the past diversity, ecology, biogeography and evolution, E&G Quaternary Sci. J., 70, 197–199, https://doi.org/10.5194/egqsj-70-197-2021, 2021.

Supervisor: José Madeira (University of Lisbon)
Co-supervisors: José María Fernández-Palacios (University of La Laguna), Miguel Menezes de Sequeira (University of Madeira)
Dissertation online: https://doi.org/10.13140/RG.2.2.25325.10729

Palaeobotanical research on oceanic islands has been largely ignored despite its importance for providing empirical proof to disentangle insular plant diversity, evolution, ecology and biogeography. Here we use the oceanic archipelagos of Madeira and the Azores as a "testing ground" (Fig. 1a), via fieldwork and laboratorial and collection-based research, to demonstrate the existence of well-preserved and palaeobiologically informative plant fossils (Góis-Marques, 2020). In Madeira, mid-19th century collections from the São Jorge leaf bed (Fig. 2b) were stratigraphically and taxonomically reappraised, revealing the presence of the stink-laurel forest at 7–1.8 Ma, similar to the extant community (Góis-Marques et al., 2018). Porto da Cruz sediment exploration and new ^{40}Ar–^{39}Ar dating revealed the existence at 1.3 Ma of the extinct *Eurya stigmosa* (Theaceae) (Fig. 1d; Góis-Marques et al., 2019d), the neoendemic *Melanoselinum decipiens* (Apiaceae) (Fig. 1c; Góis-Marques et al., 2019a) and the probable ancestor of the Madeiran besom heath, *Erica* sect. *Chlorocodon* (Ericaceae). Preliminary prospection and dating of limnic sediments revealed the presence of suitable Pleisto-Holocene palynological content for palaeoecological reconstruction. In the Azores archipelago, the historical fossil collection (Góis-Marques and Menezes de Sequeira, 2015) and palaeobotanical review revealed the existence of plant fossils on all the islands (Fig. 1g; Góis-Marques et al., 2019b). On Faial, charcoalified wood found within the 1200-year BP ignimbrite (Fig. 1e) revealed the presence of abundant *Prunus lusitanica* subsp. *azorica* (Fig. 1f), today a rare endemic tree due to anthropic impacts (Góis-Marques et al., 2020). Fanal Bay leaf beds (Terceira) were prospected during 2016, revealing an in situ leaf litter forest, but these were destroyed in 2018 despite being within the Azores UNESCO global Geopark (Góis-Marques et al., 2019c). Here we demonstrate, for both archipelagos, the presence of an abundant and well-preserved plant fossil record, ranging probably from the Miocene but mostly Pleistocene to Holocene (Fig. 1g). These plant fossils are valuable, as they provide minimum ages for future phylogeny calibration and clues on the evolution of insular syndromes and allow the inference of

Published by Copernicus Publications on behalf of the Deutsche Quartärvereinigung (DEUQUA) e.V.

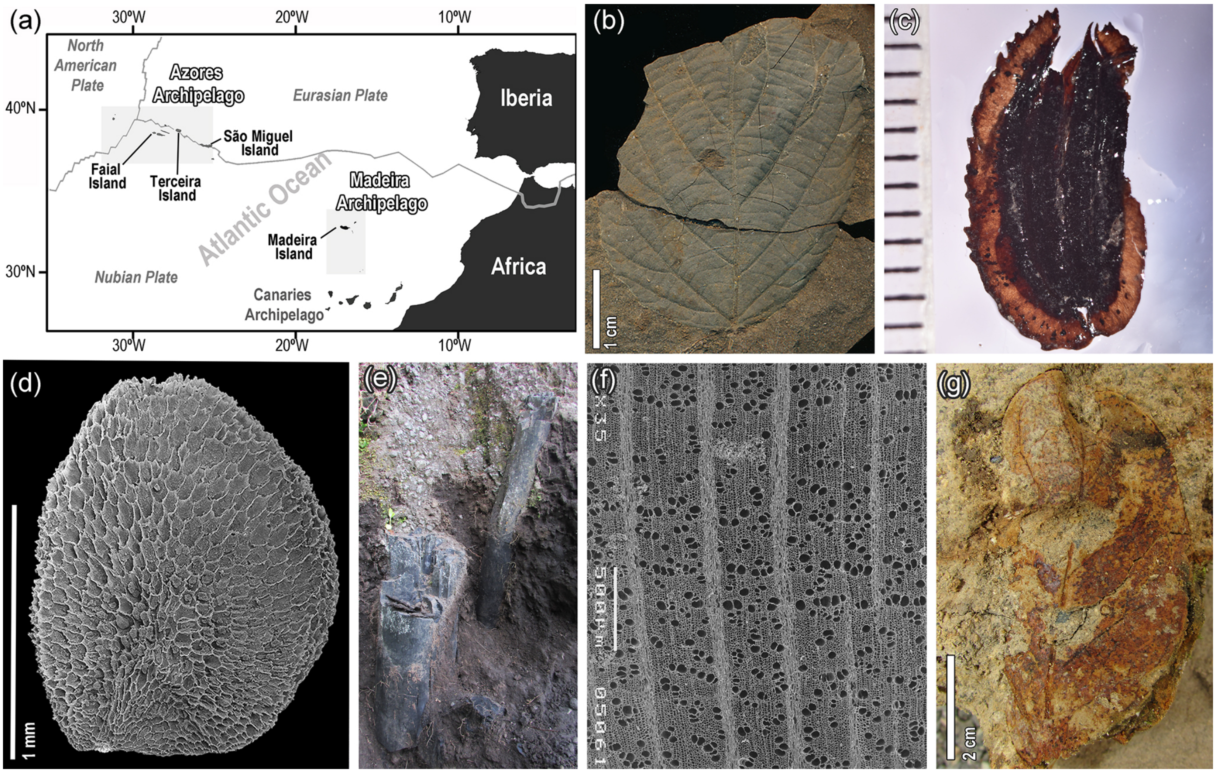

Figure 1. **(a)** Geographical locations and tectonic settings of the Madeira and Azores archipelagos and the respective islands studied in this thesis; **(b)** specimen ETH-Z-ERDW 5739 currently deposited at the Departement Erdwissenschaften-Eidgenössische Technische Hochschule (Zurich, Switzerland), collected in the mid-19th century in São Jorge, Madeira. This specimen was identified as *Corylus australis*, an extinct taxon described in Heer (1857) but revised in Góis-Marques et al. (2018) as a *Rubus* sp. leaflet, a native genus in Madeira; **(c, d)** fruit and seed fossils from the 1.3 Ma Porto da Cruz sediments, Madeira: **(c)** *Melanoselinum* (≡ *Daucus*) *decipiens* (Apiaceae) fossilized mericarps, representing the oldest fossil of a carrot and the first fossil evidence of insular woodiness (Góis-Marques et al., 2019a; scale bar in millimetres); **(d)** scanning electronic microscopy (SEM) image of a seed fossil of *Eurya stigmosa* (Theaceae), a new and extinct plant for Madeira. Reprinted from Góis-Marques et al. (2019d), © 2021 with permission from Elsevier; **(e)** charcoalified trunks buried in situ within a 1200-year BP ignimbrite on Faial, Azores; **(f)** SEM image of a transverse section of a charcoalified trunk of *Prunus lusitanica* subsp. *azorica* (found in the same locality shown in panel **e**); **(g)** example of an unidentified lauroid leaf fossil found in ash tuff 1200 years BP on Faial.

the anthropic impact on pristine insular vegetation. However, this information can only be retrieved if the palaeobotanical geoheritage in these archipelagos is protected and properly studied.

Data availability. The papers that constitute this thesis are published or submitted (see reference list).

Competing interests. The contact author has declared that there are no competing interests.

Disclaimer. Publisher's note: Copernicus Publications remains neutral with regard to jurisdictional claims in published maps and institutional affiliations.

Acknowledgements. This thesis was supported by the SYNTHESYS project (GB-TAF-3203; http://www.synthesys.info/, last acess: 10 May 2021), which is financed by the European Community Research Infrastructure Action under the FP7 Integrating Activities Programme.

Financial support. This research has been supported by the ARDITI – Regional Agency for the Development of Research, Technology and Innovation project (PhD grant: M1420-09-5369-FSE-000001).

The article processing charge was funded by the Quaternary scientific community, as represented by the host institution of *EGQSJ*, the German Quaternary Association (DEUQUA).

Review statement. This paper was edited by Daniela Sauer and reviewed by one anonymous referee.

References

Góis-Marques, C. A.: The Quaternary palaeobotany of Madeira and Azores volcanic archipelagos (Portugal): insights into the past diversity, ecology, biogeography and evolution, unpublished PhD thesis, Departamento de Geologia, Faculdade de Ciências da Universidade de Lisboa, Portugal, XLVIII+426 pp., 2020.

Góis-Marques, C. A. and Menezes de Sequeira, M.: Darwin, Hooker and Arruda Furtado and the palaeobotany of Azores: Rediscovering the first collections, Rev. Palaeobot. Palynol., 221, 47–51, https://doi.org/10.1016/j.revpalbo.2015.05.010, 2015.

Góis-Marques, C. A., Madeira, J., and Menezes de Sequeira, M.: Inventory and review of the Mio-Pleistocene São Jorge flora (Madeira Island, Portugal): palaeoecological and biogeographical implications, J. Syst. Palaeontol., 16, 159–177, https://doi.org/10.1080/14772019.2017.1282991, 2018.

Góis-Marques, C. A., de Nascimento, L., Fernández-Palacios, J. M., Madeira, J., and Menezes de Sequeira, M.: Tracing insular woodiness in giant *Daucus* (s.l.) fruit fossils from the Early Pleistocene of Madeira Island (Portugal), Taxon, 68, 1314–1320, https://doi.org/10.1002/tax.12175, 2019a.

Góis-Marques, C. A., de Nascimento, L., Menezes de Sequeira, M., Fernández-Palacios, J. M., and Madeira, J.: The Quaternary plant fossil record from the volcanic Azores Archipelago (Portugal, North Atlantic Ocean): a review, Hist. Biol., 31, 1267–1283, https://doi.org/10.1080/08912963.2018.1444761, 2019b.

Góis-Marques, C. A., Elias, R. B., Steinbauer, M. J., de Nascimento, L., Fernández-Palacios, J. M., Menezes de Sequeira, M., and Madeira, J.: The loss of a unique palaeobotanical site in Terceira Island within the Azores UNESCO global geopark (Portugal), Geoheritage, 11, 1817–1825, https://doi.org/10.1007/s12371-019-00401-1, 2019c.

Góis-Marques, C. A., Mitchell, R. L., de Nascimento, L., Fernández-Palacios, J. M., Madeira, J., and Menezes de Sequeira, M.: *Eurya stigmosa* (Theaceae), a new and extinct record for the Calabrian stage of Madeira Island (Portugal): $^{40}Ar/^{39}Ar$ dating, palaeoecological and oceanic island palaeobiogeographical implications, Quat. Sci. Rev., 206, 129–140, https://doi.org/10.1016/j.quascirev.2019.01.008, 2019d.

Góis-Marques, C. A., Rubiales, J., de Nascimento, L., Menezes de Sequeira, M., Fernández-Palacios, J. M., and Madeira, J.: Oceanic Island forests buried by Holocene (Meghalayan) explosive eruptions: palaeobiodiversity in pre-anthropic volcanic charcoal from Faial Island (Azores, Portugal) and its palaeoecological implications, Rev. Palaeobot. Palynol., 273, 104116, https://doi.org/10.1016/j.revpalbo.2019.104116, 2020.

Heer, O.: Ueber die fossilen Pflanzen von St. Jorge in Madeira, Neue Denkschr. Allg. schweiz. Ges. ges. Naturw., Band XV, 1–40, 1857.

E&G Quaternary Sci. J., 70, 201–203, 2021
https://doi.org/10.5194/egqsj-70-201-2021

Open Access E&G Quaternary Science Journal

Preface: Celebrating 70 years of "Eiszeitalter und Gegenwart" (*E&G*)

Frank Preusser[1], **Markus Fuchs**[2], **and Christine Thiel**[3]

[1]Institute of Earth and Environmental Sciences, University of Freiburg, 79104 Freiburg, Germany
[2]Department of Geography, Justus Liebig University Giessen, 35390 Giessen, Germany
[3]Federal Seismological Survey and Nuclear Test Ban Treaty, Federal Institute for Geoscience and Natural Resources, 30655 Hanover, Germany

Correspondence: Frank Preusser (frank.preusser@geologie.uni-freiburg.de)

Relevant dates: Published: 17 December 2021

How to cite: Preusser, F., Fuchs, M., and Thiel, C.: Preface: Celebrating 70 years of "Eiszeitalter und Gegenwart" (*E&G*), E&G Quaternary Sci. J., 70, 201–203, https://doi.org/10.5194/egqsj-70-201-2021, 2021.

The German Quaternary Association (Deutsche Quartärvereinigung, DEUQUA) was founded on 24 March 1948 in Hanover. Its journal "Eiszeitalter und Gegenwart" (*E&G*, literally "Ice Age and Present") was established in 1951 as an annual of the society, publishing scientific articles as well as book reviews, conference reports, and other pieces of information relating to the broad field of Quaternary research. Over the years, the journal not only changed publisher several times, but also shifted towards a pure scientific journal exclusively containing articles covering the entire spectrum of Quaternary research. To open the journal to a broader international readership, it was restructured and renamed *E&G Quaternary Science Journal* (*EGQSJ*) in 2007 and transferred into a non-profit open-access format, financed by the members of DEUQUA. Together with the open-access policy, all articles published in *E&G* since 1951 were digitised and made available online. However, even though the articles are freely available, of which quite a few contain rather outstanding contributions to and historic views of Quaternary research, there is a major drawback: the articles are written in German and have therefore received limited international attention.

To celebrate the 70th anniversary of the founding of *E&G*, this special issue features a retrospective of the early years of the journal. Articles published until 1980 were worked through by the DEUQUA executive board, which resulted in a selection of 12 manuscripts. These were not only translated into English, but also got an update of the figures to present-day standards. Our selection of manuscripts by no means intends to present the "best" articles published in *E&G* over its long history. Rather, we aim to cover a wide range of topics and articles that are still relevant from the present-day perspective or that represent benchmarks in the history of Quaternary research. Each translated article comes with a critical appraisal written by selected experts in the field. These retrospectives, a new category of publication, have been reviewed by independent referees and are collected in a special volume of *EGQSJ*. The translated articles are compiled in one open-access volume of DEUQUA Special Publications (*DEUQUASP*) and cross-linked with the retrospectives as well as with the original article published in German.

Clare Bamford (Freiburg) undertook the initial translations of the original articles, which were then further processed by the individual handling editors. They cross-checked the translated manuscripts with regard to correct use of terminology and content. It has to be noted that a direct translation from German to English terminology was not always straightforward and was partly even impossible. In such cases, footnotes have been added to the translated text for explanation. While an attempt was made to keep the translations as close as possible to the original style in order to not add any kind of interpretation, it was occasionally necessary to use rather loose translations to allow for readability. In this context, we would like to acknowledge the help of Michael Bolus (Tübingen), Norm Catto (St. Johns), Sven Lukas (Lund), and James Rose (London) with four of the articles. Figures were redrawn by Lisett Diehl (Gießen) after consultation with the handling editors, again staying as close as possible to the original style. Henrik Rother, editor of *DEUQUASP*, carried out a final language check of the translated articles.

The special issue starts with a translation of the foreword in the first issue of *E&G* (Woldstedt, 1951), summarising the context of the formation of DEUQUA and Quaternary research in the middle of the 20th century. The statement that Quaternary research aims "to contribute to understanding the present and our place in it" is, without any doubt, still valid today.

The article by Büdel (1951) is a remarkable summary regarding the knowledge of climatic zones of the Ice Age at that time. In the tribute by Jef Vandenberghe it is pointed out that this article is a precursor of the famous book "Klimageomorphologie" (Büdel, 1977), which was later translated into English (Büdel, 1982), thereby receiving widespread attention.

Louis (1952) focusses on the theory of glacial erosion in valleys, a topic that is still the subject of lively discussion today. As mentioned by Pierre Valla in his tribute, while the majority of the concepts and proposed controlling factors discussed by Louis (1952) are still valid today, the understanding of physical subglacial processes has significantly increased since.

Articles on Palaeolithic archaeology always attracted attention in the early years of *E&G*. This was also the case with the contribution by Narr (1952) on the stratigraphy of the Upper Palaeolithic, which synthesised the state of research of these days. As the tribute by Nicholas J. Conard notes, the article is "instructive in terms of both the history of research and as a reflection of what the goals of Palaeolithic archaeology could and should be today".

Woldstedt (1952) critically discusses the different components and issues of the formation of river terraces. As the tribute by James Rose, David R. Bridgeland, and Rob Westaway stresses, river terraces are important landforms for both science and society. In this respect, the article by Woldstedt (1952) has not lost its importance, and because of the debate on climate change and its consequences for fluvial geomorphology, the article is more relevant than ever.

A very detailed overview of the occurrence and distribution of terraces, loess, and palaeosols in Austria is given by Fink (1956). He attempted to divide Austria into different (climatic) loess regions, an approach which is in principle still valid today, as highlighted in the tribute article by Tobias Sprafke. Beyond that, the work of Fink (1956) impressively shows the true art of field observations, which is the basis for Quaternary research.

Flohn (1963) added the meteorological view to Quaternary research. At that time, (palaeo)climate research was not the focus of meteorology or the other way around. However, as Ulrich Cubasch, the author of the tribute article, states, "Flohn's paper presents the vision that meteorological modelling and Quaternary sciences will have an inter-dependence in future".

Loess research has always been of great importance in Quaternary science, and Ložek (1965) contributed to that with his work on loess formation and loess molluscs. In his article, he not only elaborated on the term "loessification", but also pointed out the importance of the malacofauna to the sediment and its use for reconstructing the loess formation. Denis-Didier Rousseau discusses these observations – focussing on the molluscs – and concludes that this paper is not only a very good review, but is also still relevant today.

Schwarzbach (1968) was one of the leading German Quaternary scientists of his time and in particular aimed at placing local and regional observations into the overall picture. His summary refers to both ice age hypotheses still being valid today as well as some that have been almost forgotten. As highlighted by Jürgen Ehlers, while palaeoclimate research has seen significant advancements over the past decades, there are still several questions that remain to be solved with regard to the mechanisms of natural climate change and hence the causes of widespread glaciations.

The plains of northern central Europe have been, for a long time, one of the key areas for the reconstruction of Quaternary environmental change. The review by Menke (1970) compiles the early work on pollen analyses in Schleswig-Holstein that has been of eminent importance for the understanding of past vegetation dynamics. While the general scheme has been verified in the following years, as stated by Roberta Pini in her tribute, the increased number of sites investigated and the advent of new approaches have led to a partly more detailed picture of past developments.

The article by Rohdenburg (1970) deals with morphodynamic activity and stability, a topic which is still controversially discussed within the Quaternary and geomorphology community up to now. Thus, as Dominik Faust and Markus Fuchs point out in their tribute, the fundamental ideas of Rohdenburg (1970) had a great influence on these disciplines, and the topic is more relevant than ever, especially since the effects of fauna and flora on geomorphological processes are intensively discussed today.

Smolíková (1971) not only brought to attention the relevance of soils and soil science for Quaternary research, but also presented the possibilities and importance of micromorphology in that field. To better understand the scientific background at the time of publication, Lenka Lisá and Aleš Bajer explain the then new ideas and understanding of soil science, highlighting that even though some of Smolíková's (1971) observations and her terminology have been revised, micromorphology still ought to be of great importance in Quaternary research to better understand the processes of soil formation under specific site and climate conditions.

The Lower Rhine Embayment is one of the major depocentres of Europe, with a complex sedimentation history since the Tertiary. As accentuated by Philip Gibbard in his tribute, the article by Boenigk (1978) provides a comprehensive picture of the palaeogeographical development and fluvial drainage patterns over time. This contribution is considered a key example of a critical assessment of regional data prior to aiming at correlations with other records, in particular those representing global-scale changes.

We hope that the selection of classic articles presented here not only elucidates some historic aspects, but also effectuates some critical reflections about the development of Quaternary research – both in the past as well as at present. Last but not least, we would like to express our deepest gratitude to the authors of the tribute articles and the referees for their contributions as well as all who helped with the production process. Special thanks go to Copernicus Publications, who generously covered the article processing charges for the *DEUQUASP* issue.

References

Boenigk, W.: Die flußgeschichtliche Entwicklung der Niederrheinischen Bucht im Jungtertiär und Altquartär, E&G Quaternary Sci. J., 28, 1–9, https://doi.org/10.3285/eg.28.1.01, 1978.

Büdel, J.: Die Klimazonen des Eiszeitalters, E&G Quaternary Sci. J., 1, 16–26, https://doi.org/10.3285/eg.01.1.02, 1951.

Büdel, J.: Klima Geomorphologie, Gebrüder Borntraeger, Berlin-Stuttgart, Germany, 1977.

Büdel, J.: Climatic Geomorphology, Princeton Univ. Press, Princeton, USA, 1982.

Fink, J.: Zur Korrelation der Terrassen und Lösse in Österreich, E&G Quaternary Sci. J., 7, 49–77, https://doi.org/10.3285/eg.07.1.07, 1956.

Flohn, H.: Zur meteorologischen Interpretation der pleistozänen Klimaschwankungen, E&G Quaternary Sci. J., 14, 153–160, https://doi.org/10.3285/eg.14.1.17, 1963.

Louis, H.: Zur Theorie der Gletschererosion in Tälern, E&G Quaternary Sci. J., 2, 12–24, https://doi.org/10.3285/eg.02.1.02, 1952.

Lozek, V.: Das Problem der Lößbildung und die Lößmollusken, E&G Quaternary Sci. J., 16, 61–75, https://doi.org/10.3285/eg.16.1.05, 1965.

Menke, B.: Ergebnisse der Pollenanalyse zur Pleistozän-Stratigraphie und zur Pliozän-Pleistozän-Grenze in Schleswig-Holstein, E&G Quaternary Sci. J., 21, 5–21, https://doi.org/10.3285/eg.21.1.01, 1970.

Narr, K. J.: Zur Stratigraphie jungpaläolithischer Typen und Typengruppen, E&G Quaternary Sci. J., 2, 50–62, https://doi.org/10.3285/eg.02.1.06, 1952.

Rohdenburg, H.: Morphodynamische Aktivitäts- und Stabilitätszeiten statt Pluvial- und Interpluvialzeiten, E&G Quaternary Sci. J., 21, 81–96, https://doi.org/10.3285/eg.21.1.07, 1970.

Schwarzbach, M.: Neuere Eiszeithypothesen, E&G Quaternary Sci. J., 19, 250–261, https://doi.org/10.3285/eg.19.1.21, 1968.

Smolíkovaá, L.: Gesetzmäßigkeiten der Bodenentwicklung im Quartär, E&G Quaternary Sci. J., 22, 156–177, https://doi.org/10.3285/eg.22.1.12, 1971.

Woldstedt, P.: Quartärforschung: Einleitende Worte, E&G Quaternary Sci. J., 1, 9–15, https://doi.org/10.3285/eg.01.1.01, 1951.

Woldstedt, P.: Probleme der Terrassenbildung, E&G Quaternary Sci. J., 2, 36–44, https://doi.org/10.3285/eg.02.1.04, 1952.

E&G Quaternary Sci. J., 70, 205–207, 2021
https://doi.org/10.5194/egqsj-70-205-2021

Open Access E&G Quaternary Science Journal

Retrospective

A tribute to Büdel (1951): The climatic zones of the ice age

Jef Vandenberghe

Dept. of Earth Sciences, Vrije Universiteit Amsterdam, Amsterdam, the Netherlands

Correspondence: Jef Vandenberghe (jef.vandenberghe@vu.nl)

Relevant dates: Received: 24 May 2021 – Revised: 24 July 2021 – Accepted: 30 October 2021 – Published: 17 December 2021

How to cite: Vandenberghe, J.: A tribute to Büdel (1951): The climatic zones of the ice age, E&G Quaternary Sci. J., 70, 205–207, https://doi.org/10.5194/egqsj-70-205-2021, 2021.

Special issue statement. This article is part of a special issue published on the occasion of the 70th anniversary of *E&G Quaternary Science Journal (EGQSJ)*. The special issue celebrates the journal's notable contribution to Quaternary research by revisiting selected milestone articles published in the long history of *EGQSJ*. The German Quaternary Association (DEUQUA) presents translations of the originals and critical appraisals of their impact in tandem anniversary issues of *DEUQUASP* and *EGQSJ*, respectively.

Original article: https://doi.org/10.3285/eg.01.1.02

Translation: https://doi.org/10.5194/deuquasp-3-11-2021

1 General background of Julius Büdel's paper

It may look as a coincidence that Julius Büdel published this paper at the introduction of the journal *EGQSJ* exactly 70 years ago. Climatic geomorphology is a subject that characterizes especially the focus of his early scientific work, while later Büdel was also known for his work on fluvial geomorphology. Although this paper is marked as a benchmark paper by the present-day editors of DEUQUA, it is striking that Büdel himself did not refer to it in his internationally famous book on *Klimageomorphologie* (climate geomorphology; Büdel, 1977; translated into English in 1982), but he preferred to refer to his slightly earlier lecture ("The system of climatic geomorphology" in 1948) at the "Geographentag" (day of geography) in München that was apparently the foundation of the present paper in *EGQSJ*.

Looking at the publication list of Büdel, it is clear that the *EGQSJ* paper was not an expression of sudden insight but should be considered as a first effort of general synthesis of his earlier papers on climatic zonation. Many other papers followed in the following years tackling specific cases of morphogenesis with strong links to climatic conditions in different climatic environments. Much later (1977) a new general synthesis appeared in his book *Klimageomorphologie* summarizing all his previous experience on the same subject and not limited solely to the (mostly periglacial) environments in the ice age. That work is much better known than his *EGQSJ* paper, especially after its translation into English (Büdel, 1982). As such, the *EGQSJ* paper may be considered as a precursor of that later famous book.

As the link between climate and morphogenesis was the main thread in Büdel's work it may be considered as an exponent of "climatic geomorphology". Apparently, Büdel was not the founding scientist in Germany to stress the importance of climate for morphological processes. In fact, he acquired this legacy from his tutors at university, Eduard Brückner and Albrecht Penck. Originally, this focus was a counterweight to the American school of geomorphological evolution theory, manifested by W.M. Davis, that was especially characterized by erosion on a tectonically predestined landscape. Büdel shared the focus on climate for landscape evolution with other famous European colleagues, like for instance Tricart (1954), while this philosophy of "climatic geomorphology" was traditionally kept alive in Germany, for instance by a younger generation of famous geomorphologists, like for instance Horst Hagedorn, his successor at Würzburg.

Later on, this climatic geomorphological approach was succeeded by more process-oriented strategies following advances made in dating and other analytical techniques and rather stressing quantification and physical and mathematical basics. They were clearly manifested in fluvial and hillslope geomorphology (e.g. Hack, Kirkby, Schumm, and Chorley to name only a few). But, even in those more recent approaches climate has not lost its principal role as a steering factor in the evolution of landscapes. In this respect, it is illustrative that Schumm in his famous 1977 monograph on the fluvial system devoted a whole chapter to "climate change and paleohydrology", while similarly, Chorley et al. (1984) in their geomorphology monograph included a full part on "climatic geomorphology".

2 The paper of Büdel

The present paper is especially remarkable since it approaches the geomorphological evolution during ice ages in its full complexity by the spatial shift in climatic zones from poles to Equator, rather than stressing the temporal evolution at specific locations in much research nowadays. In this respect, Büdel links the July temperature to the snowline elevations, in particular the 10.5 °C July isotherm. This gives him the link with the vegetation cover, in this case the tree line. It is the more particular that, according to Büdel, this line shows a nice E–W orientation despite strongly differing degrees of continentality. Further, Büdel concluded that the different regional positions of the limit of the treeless tundra with respect to the ice-sheet border were climatically derived (summer temperatures) and not the result of the proximity of the ice sheet. However, later it was demonstrated that other temperature values (mean annual or winter temperatures) or rates rather than summer temperatures characterize the ice-age climate and its extent.

Another link to the glacial climate than the polar tree line proposed by Büdel is the distribution of loess and the processing of loessic material starting from other fine-grained sediment. Büdel distinguishes a northern (or higher) zone dominated by frost weathering and slope processes and a southern (or lower) zone where loess is accumulated. The belt of loess deposition coincided with regions of (forest) steppe-like to tundra vegetation. The sharp northern margin of the loess deposition belt was well observed by Büdel (but its origin is still at present an unresolved problem) and facilitated by a tundra carpet and thus of climatic origin. He also observed very well that the zone between the polar forest and the ice border was much larger during the ice age than it is today. In addition, he emphasized that this zone was strongly diverse and should be subdivided in a frost-weathered zone, a forest tundra, loess tundra, loess steppe, and loess forest. A main element in Büdel's climatic geomorphological concept is his, quite provocative, link between climate (or altitudinal) zones and geomorphological processes, for instance processes of solifluction and cryoturbation in the higher zones versus windblown loess blankets in the lower zones. Later on, this strong relation between climate and process was contested in many cases and thus appeared too simple.

Another hitherto highly disputed problem of periglacial climate tackled by Büdel is the aeolian dust supplying wind direction. Büdel derived that the aeolian sediments were supplied by westerly storm winds, although those winds were possibly less frequent than the easterly winds. Only the lighter (finer-grained) loess may have been supplied by northern and eastern winds. This wind direction was later confirmed by model experiments (Renssen et al., 2007).

A remarkable point is also Büdel's statement on the independency of the extent of the ice sheet from the glacial climate. More particularly, he stresses the delay of the ice-sheet melting with respect to the maximum cold conditions. Indeed, the atmospheric cooling was the paramount process. Because of this inertia of the glacial ice-sheet expansion, growth and decay of that sheet cannot be used for a climatic subdivision. His suggestion to use loess appearance in the glacial stratigraphy is not so clearly elaborated and, moreover, not always accepted in recent loess studies. Büdel appears to observe a certain sedimentary regularity in loess deposition in a specific ice age reflecting climatic conditions, namely starting with a soliflucted loess in a humid (oceanic) setting and ending with an aeolian loess in dry (continental) conditions. At present, this conclusion seems also to be an oversimplification (e.g. Schaetzl et al., 2018).

Finally, Büdel devotes a short paragraph to fluvial development in a glacial period. He distinguishes two terrace levels during the ice age, the oldest one dating from the maximum cold phase, the younger one from the declining cold phase (Late Glacial). Here it seems that a more precise treatment is severely hampered by the absence of absolute dating. His work on fluvial evolution is discussed in much more detail in other and later publications (Büdel, 1972, 1977).

3 Significance of Büdel's paper

Although the introduction of climatic geomorphology had taken place before the publication of Büdel's 1950 paper, it represents a clear landmark in the reconstruction of past environments. The idea of the shifting climatic zones – clearly illustrated in Fig. 1 of his paper – was a significant novelty that contributed to the understanding of climatic changes during the Quaternary in general. It illustrates the growing belief in the middle of the previous century that the present landforms were not generated in the present-day climatic conditions (Louis, 1961). In his paper, Büdel focused on the last ice age by specifying characteristics of the periglacial environment, but the principals of the climatic zonation theory could be applied to all other climatic zones. Büdel's contribution is still relevant in modern times as the present-day climatic change – although artificially induced in contrast to the natural palaeoclimatic changes described by Büdel – will probably also invoke a poleward shift of climatic zones, accompanied by associated shifts of geomorphological environments and ecosystems. Certainly, at the time of writing his paper, Büdel did not realize that his approach of the shifting past climatic zones could contribute to understanding the implications of present-day climatic changes.

Without doubt, Büdel was a man of his time by the way he conceptualized this paper. It followed the tradition of deductive scientific thinking of his predecessors. It means he forwarded a reasonably thought out scientific theory and looked for proofs that could sustain his theory. At first sight, the paper looks very unusually structured in comparison with present-day usance of paper publishing. In fact, there is no formal structure as it is written in one single continuous text without any subdivision. This study did not start from a series of collected data, followed by their analysis and conclusions. It does not mean there are no proposed research objectives, nor background or final conclusions. No, they are present but not clearly delineated in separate sections as in present-day papers. For instance, results were mixed up with partial conclusions underway. This approach explains also the absence of any sedimentary analyses or systematic morphological descriptions. As a conclusion, it looks more like an opinion paper rather than a paper based on research strategy. I presume it would have been difficult for Büdel to get this paper accepted in a present issue of *EGQSJ*.

When reading this paper again, one should realize that, at that time, absolute and relative dating of sediments and detailed stratigraphy were still in their infancy. For instance, Büdel was still adhering to the number of four glacial periods within the Quaternary. This explains the quite rough stratigraphic positioning of loess series and terrace settings. In addition, also the use of sedimentological and biotic (e.g. pollen) analyses in palaeo-environmental reconstructions became familiar only at a (much) later stage.

Despite these particularities that were inherent to the time of his paper, Büdel supplemented a few remarkable conclusions that confirm his profound visionary spirit. I mention, for instance, the principle of delayed climatic impact on morphology and environments which was only fully exploited later on in fluvial geomorphology (Schumm, 1977; Vandenberghe, 1993). Another example is Büdel's, presently still valid, conclusion that all palaeoclimatic subdivision should be carried out by multidisciplinary analyses (Vandenberghe et al., 1998).

Financial support. The article processing charge was funded by the Quaternary scientific community, as represented by the host institution of *EGQSJ*, the German Quaternary Association (DEUQUA).

Review statement. This paper was edited by Christopher Lüthgens and reviewed by Dominik Faust.

References

Büdel, J.: Die Klimazonen des Eiszeitalters, E&G Quaternary Sci. J., 1, 16–26, https://doi.org/10.3285/eg.01.1.02, 1951.

Büdel, J.: Typen der Talbilding in verschiedenen klimamorphologischen Zonen, Z. Geomorphol. Suppl. Bd., 14, 1–20 1972.

Büdel, J.: Klima-Geomorphologie, Gebrüder Bornträger, Berlin, Germany, 304 pp, 1977.

Büdel, J.: Climatic Geomorphology, English translation by Fischer, L. and Busche, D., Princeton University Press, Princeton, NJ, USA, 443 pp., 1982.

Chorley, R. J., Schumm, S. S., and Sugden, D. E.: Geomorphology, Methuen, London, UK, New York, USA, 1984.

Louis, H.: Allgemeine Geomorphologie, 2nd edn., W. De Gruyter & Co., Berlin, Germany, 1961.

Renssen, H., Kasse, C., Vandenberghe, J., and Lorenz, S. J.: Weichselian Late Pleniglacial surface winds over northwest and central Europe: a model-data comparison. Journal of Quaternary Science 22, 281-293, 2007.

Schaetzl, R. J., Bettis III, A. E., Crouvi, O., Fitzsimmons, K. E., Grimley, D. A., Hambach, U., Lehmkuhl, F., Markovićh, S. B., Mason, J. A., Owczarek, P., Roberts, H. M., Rousseau, D.-D., Stevens, T., Vandenberghe, J., Zárate, M., Veres, D., Yang, S., Zech, M., Conroy, J. L., Dave, A. K., Faust, D., Hao, Q., Obreht, I., Prud'homme, C, Smalley, I., Tripaldi, A., Zeeden, C., and Zech, R.: Approaches and challenges to the study of loess – Introduction to the LoessFest Special Issue, Quaternary Res., 89, 563–618, 2018.

Schumm, S.: The fluvial system, Wiley-Interscience, New York, USA, 338 pp., 1977.

Tricart, J.: Cours de Géomorphologie: le modélé des pays froids, le modélé glaciaire et nival, CDU, Paris, France, 1954 (in French).

Vandenberghe, J.: Changing fluvial processes under changing periglacial conditions, Z. Geomorphol., Suppl. Bd., 88, 17–28, 1993.

Vandenberghe, J., Coope, G. R., and Kasse, C.: Quantitative reconstructions of palaeoclimates during the last interglacial-glacial in western and central Europe: an introduction, J. Quaternary Sci., 13, 361–366, 1998.

E&G Quaternary Sci. J., 70, 209–212, 2021
https://doi.org/10.5194/egqsj-70-209-2021

Open Access E&G Quaternary Science Journal

Retrospective

A tribute to Louis (1952): On the theory of glacial erosion in valleys

Pierre G. Valla

Institute of Earth Sciences (ISTerre), Université Grenoble Alps, Université Savoie Mont Blanc, CNRS, IRD, IFSTAR, 38000 Grenoble, France

Correspondence: Pierre G. Valla (pierre.valla@univ-grenoble-alpes.fr)

Relevant dates: Received: 30 July 2021 – Revised: 27 September 2021 – Accepted: 30 October 2021 – Published: 17 December 2021

How to cite: Valla, P. G.: A tribute to Louis (1952): On the theory of glacial erosion in valleys, E&G Quaternary Sci. J., 70, 209–212, https://doi.org/10.5194/egqsj-70-209-2021, 2021.

Special issue statement. This article is part of a special issue published on the occasion of the 70th anniversary of *E&G Quaternary Science Journal (EGQSJ)*. The special issue celebrates the journal's notable contribution to Quaternary research by revisiting selected milestone articles published in the long history of *EGQSJ*. The German Quaternary Association (DEUQUA) presents translations of the originals and critical appraisals of their impact in tandem anniversary issues of *DEUQUASP* and *EGQSJ*, respectively.

Original article: https://doi.org/10.10.3285/eg.02.1.02

Translation: https://doi.org/10.5194/deuquasp-3-19-2021

The scientific contribution of Herbert Louis (1952) focuses on glacial erosion and the development of glacial landscapes, and in this it nicely follows the expansion of scientific research on glacial geomorphology at the beginning of the 20th century. Pioneering work by Penck (1905) and De Martonne (1910) had already emphasized the importance of glacial topographic shaping at the Earth's surface, especially in high-latitude or high-elevation mountainous areas. In addition, glaciologists and glacial geomorphologists had already recognized at that time the profound topographic differences between ice-sheet (referred to as "regional-scale glaciation") and valley/alpine glacier (referred to as "local-scale glaciation") landscapes. Interestingly, the influence of initial (i.e., pre-glacial) relief and substrate (i.e., lithology, bedrock fracturing) on magnitudes and patterns of erosion has already been emphasized for valley glaciers, whereas it was thought to have had only little influence on the erosion dynamics of ice sheets.

At the time of Louis' (1952) contribution, large geomorphic evidence had been reported for the impact of valley glaciers on mountainous landscapes, with various case studies of observed specific and conspicuous features. However, there was no scientific consensus on the physical basis/theory for glacial erosion, with remaining active discussion within the community. One striking example of such debate is the occurrence and origin of steps and basins along glacial valleys (Lewis, 1947; Louis, 1952) and the widespread observations of U-shaped valley cross-sections (referred to as "trough valleys"). Glacial valley steps and basins have been proposed to have several possible origins, with enhanced ice flux at tributary confluences (e.g., Penck, 1905), the role of lithological spatial variations or the proposed view by some scientists that glacial valleys are bedforms of ice streams (i.e., a general term at the time for describing any body of moving ice). It is interesting to note that these hypotheses have been recently quantitatively assessed using numerical glacial modeling, showing a major impact of ice-flux increase at tributary junctions for glacial steps and basin development along the valley longitudinal profile (MacGregor et al., 2000), as well as the topographic influence on ice-stream dynamics (i.e., topographically constrained corridors of fast ice flow within ice sheets, e.g., Kessler et al., 2008). However, as also noted by Louis (1952) and others previously, not all observed glacial valley steps or basins can be linked to these proposed controlling factors. Pre-glacial relief inheritance has been suggested as an alternative hypothesis for these glacial features (De Martonne, 1910), and this point of view was actually also taken by Louis (1952). The importance of pre-glacial relief inheritance for glacial dynamics and topographic valley evolution is another important factor, which has also been highlighted recently using numerical modeling (e.g., Pedersen and Egholm, 2013).

The overall aim of Louis (1952) at the time had been to propose a physical interpretation of these widely observed glacial landscape features, building his hypothesis on field observations since no consensus on any physical basis for glacial erosion was present at that time. One major issue exposed in his contribution was that previously proposed explanations considered the erosive action of valley glaciers in the view of a viscous fluid with almost laminar flow. However, such glacier behavior would go against the presence of inherited steps in glacial valleys, which in the case of laminar flow should be erased by the glacier's action following ice acceleration at the glacial topographic step. Although the logical reasoning appears interesting and correct, it relies on a static view of glacier dynamics with the inheritance hypothesis for glacial valley steps, whereas more recent research has shown that these glacial features can emerge from internal glacier dynamics when considering small-scale subglacial processes (e.g., Anderson, 2014), subglacial hydrology and sediment transport (e.g., Herman et al., 2011) over long-term repetitive glaciations. However, Louis (1952) based his reasoning not only on observed glacial features but also on laboratory experiments which suggested that ice viscosity cannot be considered constant but rather changes with stress ratios, temperature or crystal orientation (Glen, 1955). As a consequence, Louis (1952) joined previously proposed hypotheses that rather considered the flow of a valley glacier as more similar to a plastic behavior, with which a critical stress is associated. Such behavior was later shown to be applicable under specific conditions to describe a valley glacier's height, length and longitudinal profile (Cuffey and Paterson, 2010).

With these observations and considerations, Louis (1952) proposed a physical theory for valley glacier flow and its erosional impact on bedrock in the view of the "block floe movement" (Fig. 1 in Louis, 1952), which is a block movement of a rigid ice mass that can break in specific parts along floes (e.g., seracs). Such valley glacier behavior would be, in the view of Louis (1952), compatible with the observation that the cross-section of the valley glacier does not necessarily change at topographic steps (which would be expected in the case of viscous fluid behavior) and that high friction within the ice itself would allow more plastic behavior in the longitudinal than in the transverse direction. Louis (1952) proposed a schematic view of individual rigid ice bodies that are pushing over an inclined (pre-glacial topographic inheritance) bedrock surface in response to gravity. By illustrating the force balance and spatial variations between ice rigid bodies, he proposed a transfer of basal pressure on the inclined bedrock surface as a driver for bedrock glacial erosion. This simple physical basis was appealing at that time, although not entirely physically based on subglacial processes as developed afterwards (Hallet, 1979), since this allowed the explanation of first-order glacial landscape features such as valley glacier steps and flats. Upstream of any topographic step, the reduction in effective pressure above the steepening of the topographic surface (resulting from ice thinning) would lead to minor erosional efficiency of the glacier, in concordance with specific glacial features such as "cirque sills". In addition, the increased bedrock stresses at the foot of topographic steps may favor basin development, in line with cirque creation or overdeepenings frequently encountered in alpine landscapes. Louis (1952) noted that glacial cirques and overdeepenings can be of only limited extent, since the bedrock counterslope would induce increased friction and thus reduced erosion, in agreement with the most recent views on the evolution of overdeepenings although the proposed processes differ with subglacial water and sediments involved (Cook and Swift, 2012). Finally, Louis (1952) also considered the possibility that valley glaciers can flow over a sediment/soil layer (i.e., soft-bed glacier dynamics) that he described as a "plastic intermediate zone" and to which his theoretical basis also applied. It is worth noting, however, that the proposed physical theory by Louis (1952) had been mainly justified, as explicitly expressed by himself in his contribution, to explain "aggravation of pre-existing irregularities of slope", i.e., landscape features in the longitudinal profile such as valley steps, flats and basins. In this line of thought, the "rigid block floe movement" theory allowed Louis (1952) to satisfactorily explain the variety of observed morphologies in glacial landscapes, giving at least some credit to it. One final observation that favored the rigid block theory of Louis (1952) at the time was the low variability in ice velocity from surface to bottom measurements. However, the reported observations at that time may have been recorded for a specific warm-based glacier where the ice flow would be dominated by basal sliding with respect to internal ice deformation. It is interesting to note that Louis (1952) partly envisaged the role of subglacial water in basal sliding in his contribution, referring to a valley glacier that "sits on a kind of lubricant".

After stating his theoretical hypothesis, Louis (1952) adopted a more consensual and intermediate position where he considered that the physical behavior of a valley glacier would lie between a viscous fluid and a flow of rigid individual bodies. In his view, the block floe movement hypothesis is most certainly not physically correct to describe the ice flow of valley glaciers, which can adopt end-member behaviors depending on several factors including topographic conditions. For him, the merit of his proposed physical theory was to open new directions and to raise questions for a better understanding of the variability in valley glaciers. In his view, the rigid behavior of the ice would be of prime importance for erosion dynamics and the evolution of glacial landscapes. He then posed the question of the observed variability in valley glacier behaviors as well as the diversity of observed glacial landscapes, which for him evidences contrasting erosional efficiency of valley glaciers in sculpting their bedrock. He phrased this as an open question, and this is still a matter of debate and active scientific research today (e.g., Herman et al., 2021). The proposed intermediate and compromise view of Louis (1952) concerning the flow of a valley glacier may also reflect the general thinking of the time within the scientific community, with the major achievement of Glen's law of non-linear viscous flow for glaciers and ice sheets, which was physically demonstrated a few years afterwards (Glen, 1955).

Another merit and interesting aspect of Louis' (1952) contribution was his conceptual investigation of the transverse profile of valley glaciers. In the final part of his contribution, he explored how important the varying contact pressure of flowing ice to the underlying bedrock (in both the ablation and the accumulation areas) might be and how this effect may partly explain the development of U-shaped glacial valleys with respect to the relative contribution of inherited pre-glacial relief features. He also raised a first-order question for the development of U-shaped valley morphology (Harbor, 1992), questioning whether this results from enhanced vertical or horizontal glacial erosion. In the view of Louis (1952), both situations can occur along a glacial valley profile and would depend on specific topographic conditions (i.e., the occurrence of longitudinal steps in a glacial profile). Finally, he developed his reasoning based on some key morphological observations (Figs. 2 and 3 in Louis, 1952) for the upper part of a glacier valley cross-section, above the U-shaped deeper part (referred to as the "valley trough"). This work is, to my knowledge, very specific and insightful, since the landforms around the glacial altitudinal limit ("trimline" as already exposed by Penck, 1905) have received only minor attention since then. For Louis (1952), the glacial landforms above the U-shaped valley part can be differentiated between steep slopes below the trimline (*Schliffkehle*) and subsequent low-slope areas (*Schliffbord*). Following Louis' (1952) view on inherited pre-glacial relief, such landforms may indicate the magnitude of lateral glacial erosion at the upper boundary (i.e., lateral margin of the valley glacier), which is emphasized at depth within the trough valley (U-shaped section of the valley transverse profile). These observations also raised the question of the geomorphological significance of the trimline as the topographic boundary for either the glacier maximum vertical extent or efficient glacial erosion, a point also recently raised by numerical studies of alpine glacier modeling (e.g., Seguinot et al., 2018).

Finally, Louis (1952) discussed the significance of the relatively low slope shoulder areas which are located above the U-shaped valley part (*Trogschulter*) as being either the result of lateral erosion by the glacier at high elevations or the inherited features from "over-printed old valley floor remnants". In his view, this question is not simple and the origin of glacial valley shoulders depends on both the initial topographic configuration (pre-glacial relief) and the differences in topographic slopes between the ridgelines (periglacial area) and the valley flanks (glacial area). In addition, he pointed to the need for a pronounced vertical structure (high total relief) for observing developed valley shoulders along glacial valley profiles. The question of pre-glacial inheritance vs. glacial erosional imprint for the occurrence of low-slope, high-elevation glacial shoulders or plateaux has been an important research topic in fjord environments, and their existence in alpine areas is also the subject of discussion. However, investigating the transition from glacial to periglacial landforms around the trimline has remained challenging, since several geomorphic processes are acting at these sites and may vary in both space (i.e., along the valley glacier longitudinal profile) and time (i.e., over repetitive glacial periods or within the course of an individual glacial cycle).

In summary, the reported observations and proposed physical explanations for glacial erosion and landscape features by Louis (1952) have the important merit of synthesizing key morphological evidence of glacier dynamics and of proposing a conceptual model for landscape evolution under glacier erosional imprint. Most of the concepts and proposed controlling factors of glacial erosion are still valid at present, although the implied physical subglacial processes and associated theoretical basis for glacial erosion have evolved substantially since Louis' (1952) contribution. Some important aspects of glacial landscapes still have to be investigated: (1) the relative importance of vertical vs. lateral glacial erosion for the valley cross-profile evolution and (2) the possible controlling mechanism(s) for the observed contrast and diversity of glacial landforms at high elevations, i.e., the contact between the glacially modified trough below the trimline with the frost-shattered terrain above it.

Financial support. The article processing charge was funded by the Quaternary scientific community, as represented by the host institution of *EGQSJ*, the German Quaternary Association (DEUQUA).

Review statement. This paper was edited by Frank Preusser and reviewed by Sven Lukas.

References

Anderson, R. S.: Evolution of lumpy glacial landscapes, Geology, 42, 679–682, https://doi.org/10.1130/G35537.1, 2014.

Cook, S. J. and Swift, D. A.: Subglacial basins: Their origin and importance in glacial systems and landscapes, Earth-Sci. Rev., 115, 332–372, https://doi.org/10.1016/j.earscirev.2012.09.009, 2012.

Cuffey, K. M. and Paterson, W. S. B.: The Physics of Glaciers, 4th edn., Academic Press, Elsevier – Amsterdam, 704 pp., ISBN: 9780123694614, 2010.

De Martonne, E.: L'érosion glaciaire et la formation des vallées alpines, Ann. Géogr., 19, 289–317, 1910.

Glen, J. W.: The creep of polycrystalline ice, P. Roy. Soc. A-Math. Phy., 228, 519–538, https://doi.org/10.1098/rspa.1955.0066, 1955.

Hallet, B.: A theoretical model of glacial abrasion, J. Glaciol., 23, 39–50, https://doi.org/10.3189/S0022143000029725, 1979.

Harbor, J. M.: Numerical modeling of the development of U-shaped valleys by glacial erosion, Geol. Soc. Am. Bull., 104, 1364–1375, https://doi.org/10.1130/0016-7606(1992)104<1364:NMOTDO>2.3.CO;2,1992.

Herman, F., Beaud, F., Champagnac, J.-D., Lemieux, J.-M., and Sternai, P.: Glacial hydrology and erosion patterns: a mechanism for carving glacial valleys, Earth Planet. Sc. Lett., 310, 498–508, https://doi.org/10.1016/j.epsl.2011.08.022, 2011.

Herman, F., De Doncker, F., Delaney, I., Prasicek, G., and Koppes, M.: The impact of glaciers on mountain erosion, Nature Reviews Earth & Environment, 2, 422–435, https://doi.org/10.1038/s43017-021-00165-9, 2021.

Kessler, M. A., Anderson, R. S., and Briner, J. P.: Fjord insertion into continental margins driven by topographic steering of ice, Nat. Geosci., 1, 365–369, https://doi.org/10.1038/ngeo201, 2008.

Lewis, W. V.: Valley steps and glacial valley erosion, Transactions and Papers, 13, 19–44, 1947.

Louis, H.: Zur Theorie der Gletschererosion in Tälern, E&G Quaternary Sci. J., 2, 12–24, https://doi.org/10.3285/eg.02.1.02, 1952.

MacGregor, K., Anderson, R., Anderson, S., and Waddington, E.: Numerical simulations of glacial-valley longitudinal profile evolution, Geology, 28, 1031–1034, https://doi.org/10.1130/0091-7613(2000)28<1031:NSOGLP>2.0.CO;2, 2000.

Pedersen, V. K. and Egholm, D. L.: Glaciations in response to climate variations pre-conditioned by evolving topography, Nature, 493, 206–210, https://doi.org/10.1038/nature11786, 2013.

Penck, A.: Glacial features in the surface of the Alps, J. Geol., 13, 1–19, available at: https://www.jstor.org/stable/30066319 (last access: 31 July 2021), 1905.

Seguinot, J., Ivy-Ochs, S., Jouvet, G., Huss, M., Funk, M., and Preusser, F.: Modelling last glacial cycle ice dynamics in the Alps, The Cryosphere, 12, 3265–3285, https://doi.org/10.5194/tc-12-3265-2018, 2018.

E&G Quaternary Sci. J., 70, 213–216, 2021
https://doi.org/10.5194/egqsj-70-213-2021

Open Access E&G Quaternary Science Journal

Retrospective

A tribute to Narr (1952): On the stratigraphy of Upper Palaeolithic types and type groups

Nicholas J. Conard[1,2]

[1]Department of Early Prehistory and Quaternary Ecology, University of Tübingen, Schloss Hohentübingen, 72070 Tübingen, Germany
[2]Senckenberg Centre for Human Evolution and Paleoenvironment, University of Tübingen, 72070 Tübingen, Germany

Correspondence: Nicholas J. Conard (nicholas.conard@uni-tuebingen.de)

Relevant dates: Received: 13 October 2021 – Accepted: 30 October 2021 – Published: 17 December 2021

How to cite: Conard, N. J.: A tribute to Narr (1952): On the stratigraphy of Upper Palaeolithic types and type groups, E&G Quaternary Sci. J., 70, 213–216, https://doi.org/10.5194/egqsj-70-213-2021, 2021.

Special issue statement. This article is part of a special issue published on the occasion of the 70th anniversary of *E&G Quaternary Science Journal (EGQSJ)*. The special issue celebrates the journal's notable contribution to Quaternary research by revisiting selected milestone articles published in the long history of *EGQSJ*. The German Quaternary Association (DEUQUA) presents translations of the originals and critical appraisals of their impact in tandem anniversary issues of *DEUQUASP* and *EGQSJ*, respectively.

Original article: https://doi.org/10.3285/eg.02.1.06

Translation: https://doi.org/10.5194/deuquasp-3-27-2021

Main text

Karl J. Narr's (1921–2009) paper in the inaugural volume of EAG presents a critical review of the taxonomy and organization of the European Upper Palaeolithic. At the same time, the contribution addresses the European cultural stratigraphic record within a theoretical framework grounded within the cultural historical approach. The paper touches upon questions related to cultural change and the appearance and spread of innovative technologies. Interestingly, the paper almost never mentions Upper Palaeolithic hunter-gatherers. At times the author gives the impression that it is the artefacts themselves that shaped Palaeolithic prehistory rather than past peoples. Narr drew heavily on key sites, many of which are still important today, and addressed research questions that are discussed as much now as in Narr's day prior to the advent of radiocarbon dating, climatic records based on deep sea cores or ice cores, aDNA, and many other sources of data that are central to research today.

If we consider the terminology that Narr used, the main cultural groups including the Chatelperronian, the Aurignacian, the Gravettian, the Solutrean and the Magdalenian are all terms used today. Narr, however, discussed numerous other cultural groups that today have fallen out of use and that few current researchers would recognize. The paper also addresses the strengths and weaknesses of Denis Peyrony's (1933) concept of the Perigordian tradition extending over most of the Upper Palaeolithic, and it ultimately favours Dorothy Garrod's (1938) concept of the Gravettian cultural group as a revision to both Breuil's (1912) concept of a long Aurignacian cultural tradition and Peyrony's system. In many respects, Narr's assessment is consistent with the general terminology of today, and Palaeolithic archaeologists still debate the origins and spread of cultural markers of the Upper Palaeolithic.

Given the lack of absolute dates for the Upper Palaeolithic sequence, it comes as no surprise that Narr constructed a stratigraphic system without explicit dates for the four stages he defines. These stages are further subdivided into substages. In this system, Narr, for example, argued that

Chatelperronian points and other Chatelperronian forms date no earlier than to Stage 1 in Western Europe, while at the same time we have the earliest appearance of Aurignacian points and carinated scrapers in Central Europe. These sorts of claims are consistent with recent work which suggests a temporal overlap between the Central European Aurignacian and the Western European Chatelperronian (Higham et al., 2012). In contemporary terms, we would see this period as corresponding to the millennia preceding the Heinrich 4 event and dating in the vicinity of 42–43 ka cal BP using the radiocarbon chronology (Fig. 1). Narr's figure on page 60 suggests that the Chatelperronian spread from Western Europe into Central Europe, bringing with it early Gravettian elements, which today is not a plausible point of view. Also, if we ask what Stage 1 meant to Narr, it becomes clear that his Stage 1, reflecting a warm period, mainly loamy cave deposits and the Göttweiger soil development of the loess stratigraphy, is completely out of date and irrelevant for current research. Furthermore, considerable research in recent years has shown that the cultural variability at the beginning of the Upper Palaeolithic reflects a fluid continuity within adaptive technological systems rather than unvarying typological patterns that are easily attributed to specific cultural groups (Bataille et al., 2018).

Moving up the stratigraphic sequence, Narr viewed the horizon of the Gravettian with Noailles burins as dating to no earlier than his Stage 3b in Western and Central Europe, while he argues that in Western Europe this time corresponds to the first appearance of triangularly retouched pieces. Stage 3b corresponds to the cold continental conditions at the end of Würm II. In caves, this period corresponds to a phase of deposition of coarse angular limestone debris and in the open air to the end of a phase of pure loess deposition within his Loess III. In a broad sense, this assessment is consistent with the placement of the Gravettian within a general phase of cold continental conditions in Europe leading up to the Last Glacial Maximum, but the details of the stratigraphic assessment are of little relevance today, as many new methods allow for an improved cultural chronology and palaeoenvironmental assessment.

A final example is the initial presence of double-rowed Magdalenian harpoons in Stage 4a, which corresponds to conditions in caves and the open air that are similar to those at the time of the appearance of Noailles burins. While one commiserates with the challenges that researchers faced in the middle of the 20th century, it is clear that these sorts of general stratigraphic assessments are not helpful today in establishing a reliable chronostratigraphic framework.

What I find exceptional about Narr's paper is the near absence of statements on specific ecological conditions and his apparent lack of interest in attempting to use faunal assemblages, which at that time were comparatively well-understood, for establishing reliable palaeoenvironmental interpretations. The relatively general stratigraphic and lithological correlations that Narr made are, while more or less valid, very broad and do not provide a high level of resolution. What is, however, clear from Narr's paper is that in a period prior to the advent of radiometric dating, diagnostic artefacts could in some cases be used to establish a degree of chronostratigraphic control. This use of cultural stratigraphic markers persists in some contexts today, but in many settings, radiometric dates are now given priority over assumptions about the temporal control provided by the presence or absence of specific artefact forms. In many settings today, archaeologists are expected to demonstrate that similar typological forms are indeed of similar age, while in the middle of the 20th century archaeological finds were often considered the best way to establish a relative chronology. Dating using cultural stratigraphy is still done today, but such arguments are often viewed as rough approximations for establishing temporal units.

Perhaps because of the concise nature of Narr's paper, he did not address taphonomy and site formation processes. While in Narr's day researchers were, of course, aware of stratigraphic complications caused by geological, biological and cultural processes, taphonomic studies and geoarchaeological studies today accompany nearly all publications of Pleistocene cultural materials (McPhail and Goldberg, 2018).

Despite his focus on the appearance and disappearance of artefact forms, Narr does at times make schematic remarks about Palaeolithic peoples. He correctly contrasted the biological reproduction of organisms with the cultural reproduction of artefacts. Although he was rarely explicit about his ideas in this respect, it seems that Narr viewed specific artefact forms as clear markers for the movements of populations of peoples. He touched upon the importance of innovations in material culture and the conservative nature of Palaeolithic material culture, but he made no explicit mention of how technological knowledge was passed down and modified from one generation to the next. He also did not remark on how people make artefacts, how both the people who make tools and the tools themselves experience a degree of selective pressure that, all else being equal, would favour human populations who are well-adapted to their ecological niche, and how changing ecological conditions would likely lead to technological adjustments being made in a group's material culture. It seems as if Narr was more interested in the artefacts than the people who made them. This comes as a surprise since, along with Hansjürgen Müller-Beck in Tübingen, Narr enjoyed the reputation of having considered the ethnographic record as providing insights into the lives of Palaeolithic peoples. In his paper from 1952, ice age hunter-gatherers remain invisible, and human agency is only found in the dark shadows cast by Palaeolithic artefacts. Today we are lucky to have ever-increasing amounts of hominin skeletal material. These fossil finds have fostered studies of individual life histories and reconstructions of ice age diet and lifeways. While the amount of information in aDNA is still relatively scant in the Palaeolithic, archaeo- and palaeogenetic research allows for analyses of the genetic relationships

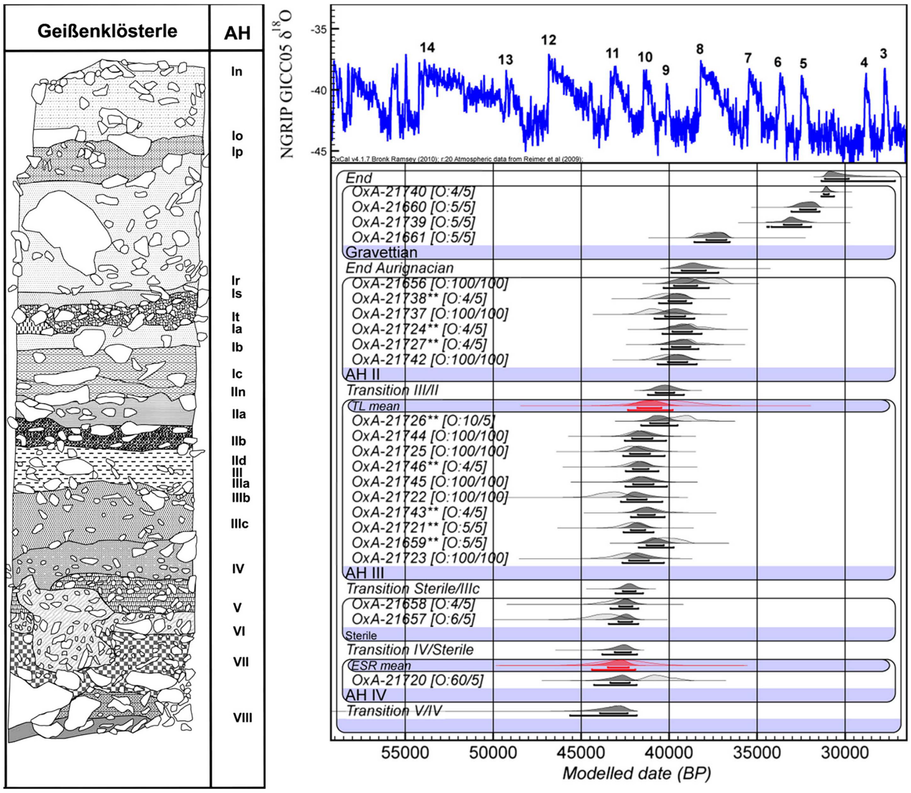

Figure 1. Geißenklösterle. Cultural and chronostratigraphic sequence with calibrated radiocarbon ages and proposed correlations with the NGRIP ice core record from Greenland (based on Higham et al., 2012).

of past individuals and populations in ways that would have been difficult to imagine in a time before the discovery of the structure of DNA and long before the development of routine studies of aDNA that have contributed greatly to our understanding of Palaeolithic population dynamics (Prüfer et al., 2021). Beyond work on aDNA, considerable progress has also been made on diachronic, demographic modelling of Upper Palaeolithic populations (Schmidt et al., 2021), a topic that received little attention at the time of Narr's research.

Turning to Palaeolithic material culture, Narr's paper makes it clear that he, like many of his contemporaries, was highly focused on the use of artefacts as type fossils or *fossiles directeurs*. He seems to have viewed the typological method uncritically, and he appears to have considered artefact types as explicit signatures of specific prehistoric cultures. Today there is a much stronger tendency to examine the specific technological means by which artefacts are made, as well as their life histories, with an awareness of how raw material availability and constraints dictated by mobility, curation and recycling can shape artefacts and artefact assemblages (Floss, 2012). Similarly, Narr, like his contemporaries, did not consider how functional studies and the study of residues could illuminate our understanding of the design and use of lithic, osseous and botanical artefacts (Plisson and Geneste, 1989). Current microscopic studies document the multifunctionality of tools and their life histories, thereby questioning the concept of tools reflecting singular functional needs of past people or rigid mental templates for tool design. While today's research will likely seem naïve to researchers 70 years from now, Palaeolithic archaeologists today have a more subtle understanding of artefact assemblages based on a wide range of experimental and analytical studies that were not available to Narr.

While Narr's paper was thoughtful and impressive for its day, 70 years later the paper is not read, and as far as I am able to determine it has never been cited in any internationally indexed publication. This underlines the fact that, although the paper contains many important ideas, the improvement of the empirical record of the stratigraphy, chronology and material culture of the Upper Palaeolithic has developed to the point that the paper today mainly has relevance solely in the context of the history of research. This is true of most syntheses of this age and highlights the importance of high-quality empirical data that are of lasting value. The lack of interest in the paper could also, in part, reflect the unwillingness of the scientific community in the late 20th and early 21st century to engage with the German research tradition in Palaeolithic archaeology. Only recently has this tendency begun to change with the international recognition of the importance of contemporary research in Germany, with the increasing number of international students seeking training in Germany and with ever more international researchers finding research positions in German-speaking Europe (Conard, 2010). Nonetheless, the history of research in Germany is a topic that is almost never addressed outside the Central European research tradition.

Financial support. This open-access publication was funded by the University of Tübingen.

Review statement. This paper was edited by Markus Fuchs and reviewed by Michael Bolus.

References

Bataille, G., Tafelmaier, Y., and Weniger, G.-C.: Living on the edge – a comparative approach for studying the beginning of the Aurignacian, Quatern. Int., 474, 3–29, https://doi.org/10.1016/j.quaint.2018.03.024, 2018.

Breuil, H.: Les subdivisions du paléolithique supérieur et leur signification, Congrès internat. d'anthrop. et archéol. Préhist., 14, 165–238, 1912.

Conard, N. J.: The Current State of "Paleohistory" in Germany, Mitteilungen der Gesellschaft für Urgeschichte, 19, 193–208, 2010.

Floss, H. (Ed.): Steinartefakte. Vom Altpaläolithikum bis in die Neuzeit, 1. Auflage, Tübingen Publications in Prehistory, Kerns Verlag, Tübingen, Germany, 2012.

Garrod, D. A. E.: The Upper Palaeolithic in the Light of Recent Discovery, P. Prehist. Soc., 4, 1–26, https://doi.org/10.1017/S0079497X00021113, 1938.

Higham, T., Basell, L., Jacobi, R., Wood, R., Ramsey, C. B., and Conard, N. J.: Testing models for the beginnings of the Aurignacian and the advent of figurative art and music: The radiocarbon chronology of Geißenklösterle, J. Hum. Evol., 62, 664–676, https://doi.org/10.1016/j.jhevol.2012.03.003, 2012.

Macphail, R. I. and Goldberg, P.: Applied soils and micromorphology in archaeology, in: Manuals in archaeology, Cambridge University Press, Cambridge, UK, https://doi.org/10.1017/9780511895562, 2018.

Narr, K. J.: Zur Stratigraphie jungpaläolithischer Typen und Typengruppen, E&G Quaternary Sci. J., 2, 50–62, https://doi.org/10.3285/eg.02.1.06, 1952.

Peyrony, D.: Les Industries " aurignaciennes " dans le bassin de la Vézère, Bull. Soc. Préhist. Fr., 30, 543–559, 1933.

Plisson, H. and Geneste, J. M.: Analyse technologique des pointes à cran solutréennes du Placard (Charente), du Fourneau du Diable, du Pech de la Boissiere et de Combe-Saunière (Dordogne), Paléo, 1, 65–106, https://doi.org/10.3406/pal.1989.954, 1989.

Prüfer, K., Posth, C., Yu, H., Stoessel, A., Spyrou, M. A., Deviese, T., Mattonai, M., Ribechini, E., Higham, T., Velemínský, P., Brůžek, J., and Krause, J.: A genome sequence from a modern human skull over 45,000 years old from Zlatý kůň in Czechia, Nat. Ecol. & Evol., 5, 820–825, https://doi.org/10.1038/s41559-021-01443-x, 2021.

Schmidt, I., Hilpert, J., Kretschmer, I., Peters, R., Broich, M., Schiesberg, S., Vogels, O., Wendt, K. P., Zimmermann, A., and Maier, A.: Approaching prehistoric demography: proxies, scales and scope of the Cologne Protocol in European contexts, Philos. T. Roy. Soc. B. 376, 20190714, https://doi.org/10.1098/rstb.2019.0714, 2021.

E&G Quaternary Sci. J., 70, 217–220, 2021
https://doi.org/10.5194/egqsj-70-217-2021

Open Access E&G Quaternary Science Journal

Retrospective

A tribute to Woldstedt (1952): Problems of terrace formation

James Rose[1,2], **David R. Bridgland**[3], **and Rob Westaway**[4,✝]

[1]Department of Geography, Royal Holloway, University of London, Egham, Surrey, TW20 0EX, UK
[2]British Geological Survey, Keyworth, Nottingham, NG12 5GG, UK
[3]Department of Geography, University of Durham, Durham, DH1 3LE, UK
[4]James Watt School of Engineering, University of Glasgow, James Watt (South) Building, Glasgow, G12 8QQ, UK
✝deceased

Correspondence: James Rose (jimrose@clara.co.uk, j.rose@rhul.ac.uk)

Relevant dates: Received: 7 June 2021 – Revised: 7 July 2021 – Accepted: 30 October 2021 – Published: 17 December 2021

How to cite: Rose, J., Bridgland, D. R., and Westaway, R.: A tribute to Woldstedt (1952): Problems of terrace formation, E&G Quaternary Sci. J., 70, 217–220, https://doi.org/10.5194/egqsj-70-217-2021, 2021.

Special issue statement. This article is part of a special issue published on the occasion of the 70th anniversary of *E&G Quaternary Science Journal (EGQSJ)*. The special issue celebrates the journal's notable contribution to Quaternary research by revisiting selected milestone articles published in the long history of *EGQSJ*. The German Quaternary Association (DEUQUA) presents translations of the originals and critical appraisals of their impact in tandem anniversary issues of *DEUQUASP* and *EGQSJ*, respectively.

Original article: https://doi.org/10.3285/eg.02.1.04

Translation: https://doi.org/10.5194/deuquasp-3-35-2021

1 Scientific background

River terraces are important landforms. For society, they provide safe spaces for human habitation in proximity to a water resource; a landscape suitable for agriculture, transport and an infinite range of human requirements including groundwater; minerals; and aggregates. For science, these landforms and sediments provide a proxy for understanding river development in response to a range of climatic, sea-level and tectonic forces, as well as an archive for the records of landscape evolution, climate change, geodiversity, biodiversity and human occupance.

River terraces have two components: (i) the first component is an erosional surface called a strath. This is a landform that has long challenged geomorphologists because of the difficulties of producing a relatively level erosional plain when the potential energy of a river means that it has a natural tendency to erode vertically. This landform did not attract Paul Woldstedt's attention. (ii) The second component is a depositional landform, with an upper surface, known as a tread, and a slope separating the tread from other treads or the river channel, known as a bluff (British English) or riser (American English). These features are composed predominantly of sand, sand and gravel, and coarser material up to boulder size. Treads are relatively level but complex surfaces reflecting deposition within a river channel, deposition on the surface beyond the river channel and intermittent erosional events.

Typically, river terraces form what is often known as a cross-valley staircase of treads and bluffs, which may be made of either erosional or depositional surfaces or an almost infinite combination of both (cut-and-fill terraces). The formation of these terrace staircases is a topic that has attracted much attention, and many substantive papers have presented models to explain the patterns of erosion and aggradation (see below and references therein). Explanations involve uplift or submergence of the land and steepening or flattening of the land, both of which determine accommodation space for river deposition. Explanations also involve increase or decrease in sediment supply to the river, increase or decrease in the size of sediment supplied to the river, increase or decrease in river discharge, and particularly variations in high-magnitude flood events. It is little wonder that the subject has attracted substantial research and numerous publications in geology and geomorphology (Pazzaglia, 2013). Likewise, the presence of plant, animal and human remains within the sediments, along with an understanding of the factors that cause changes in the patterns of erosion and aggradation, means that terraces have also attracted the attention of palaeobiologists, archaeologists, climate-change scientists and Quaternary scientists.

At about the same time as Woldstedt's *EGQSJ* article was published, Zeuner (1952) summarised the main factors considered to be responsible for the formation of river terraces as follows: tectonic processes: sea-level change (thalassostatic terraces), climate changes in the form of sediment supply from a glacier, and variations in river discharge and sediment supply due to changes in climate and vegetation cover. Zeuner also recognised that the climatic origin of river terraces meant that they had the potential to provide a chronology for the Quaternary with the recognition and ordering of cold and warm periods. Paul Woldstedt had much respect for Frederick Zeuner, and it was within this framework that he developed his concepts.

2 The formation of river terraces – characteristics and processes of formation according to Paul Woldstedt

Woldstedt addressed the issue of river terraces by describing critical evidence for each of the formational scenarios and ended by presenting a scheme for terrace formation that integrates much of that evidence (Fig. 1). This scheme is perceptive, widely applicable and relevant to present concepts. Nevertheless, he noted that "Die im Vorstehenden gemachten Ausführungen bieten mehr Problemstellungen als Lösungen" [The explanations given above offer more problems than solutions] (Woldstedt, 1952, p. 44) and looked forward to the results of future investigations.

The effects of climatic processes on terrace formation are examined with evidence from the Saale and Elbe regions of central Germany and the Thames and Somme regions of southern England and northern France. Within the framework of the climatic model, Woldstedt considered that the primary process for the formation of these terraces is deposition of glacial and periglacial deposits during periods of cold climate and erosion during periods of "passive" warm climates and that these activities are tuned to the glacial–interglacial cycles as identified by Penck and Brückner (1909). However, he was critically aware that this model is challenged because terrace deposits may be composed of both cold and warm climate sediments. He was aware that some of the warm climate proxies included in the terrace deposits may not be in situ, but he rejected derivation as a general explanation and stressed the fact that a single terrace may contain evidence of different climates and that this material may be located at either the bottom or the top of the sediment body. Furthermore he noted that the relative position of these warm and cold sediment units may vary within a catchment and between river systems.

In order to explain this apparent anomaly, he identified the importance of sea level as a factor able to control the process of deposition or erosion at the lower part of river systems. According to this proposition, a rise in sea level would cause a reduction in the gradient of the channel in the lower part of a river, resulting in aggradation during interglacials. At the same time, incision would characterise the development of the upper reaches. In contrast, during glacials when sea level was low, incision would take place in the lower parts of catchments due to a steepening of the channel and aggradation would take place in the upper reaches due to increased sediment supply from periglacial and glacial processes. The extent of incision or aggradation through a catchment would depend upon the duration of the period of low sea level, gradient of the seabed in the exposed offshore zone and the duration of the depositional processes in the upper reaches. He also took care to note that the tuning between the rise in sea level and sedimentation would not coincide directly with the climate at the river mouth, as there would be a lag in sea-level rise due to the time taken for global ice masses to melt. Likewise, he stressed that the rate of sea-level rise would determine the pattern of sedimentation. A rapid rise would submerge the river mouth, and sediment would be located offshore, so that aggradation in the lower part of the river valley would be limited. The effects of these processes are summarised in Fig. 1, which is based on Fig. 2 of Woldstedt (1952), and it is evident that the processes of terrace development are very complex.

Woldstedt examined the issue of a solely tectonic origin for river terraces by reference to work done on the river Rhine, in which it had been proposed that deposition took place during periods of tectonic stability and incision occurred during periods of uplift that tilted the river towards the sea. He rejected this model because it failed to take into account the consequences of sea-level change and variations in sediment supply caused by glaciation and periglaciation. Nevertheless, he fully acknowledged that tectonic activity would be a factor responsible for terrace formation but that it needed to be validated by available evidence.

In addition to the mechanisms described above, Woldstedt responded to the proposal that terraces would develop due to the blockage of a river by an ice sheet. He examined this issue by reference to the river Weser in northern Germany, in which it was recognised that an ice dam had created a proglacial lake in the river valley upstream of the Scandinavian ice margin. Paul Woldstedt reasoned that this process would have resulted in the formation of a delta in the

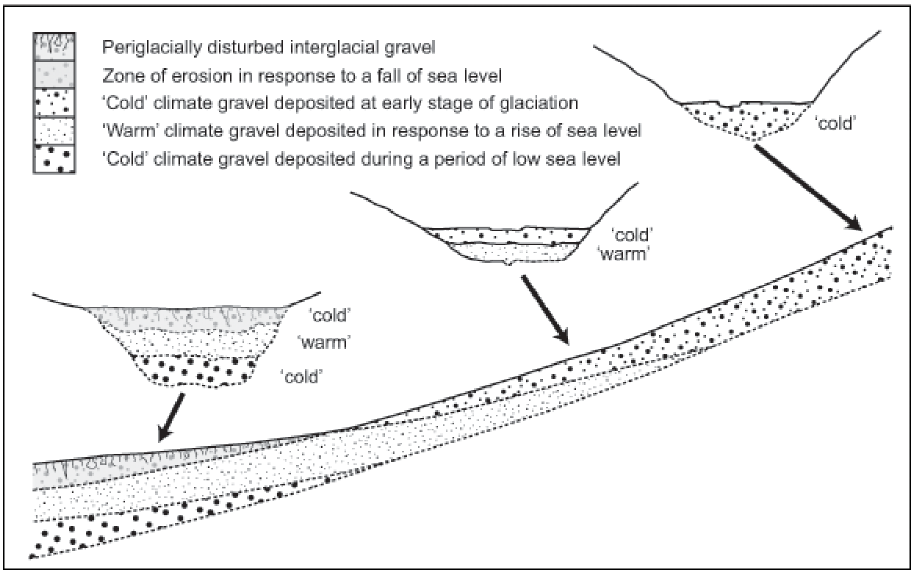

Figure 1. Redrawn version of Fig. 2 from Woldstedt (1952) with the addition of representative cross sections.

proglacial lake and that this would be of restricted extent, not significantly affecting existing river terraces. He also noted that it would be capable of being differentiated from terraces by the presence of deltaic topset and foreset sedimentary structures, supporting his case with a figure showing a stratigraphic succession indicating river gravels, overlain by lake sediments, and capped by glacial and glaciofluvial deposits. His proposition has been vindicated and expanded by recent work of Winsemann et al. (2015). Furthermore he noted that the subsequent deposition downstream of the ice dam would have a different lithological composition from material deposited in terraces in the upper part of the catchment.

3 The significance of Paul Woldstedt's contribution to the understanding of river terrace formation

The recognition that the pattern of terrace development varies along the length of a river catchment was a fundamental contribution to geomorphology and Quaternary science (Fig. 1). This premise requires that any study of river terraces must be aware of the potentially infinite variety of erosional/depositional permutations and approach the subject with this constraint in mind. The following section considers how science has responded to this requirement.

4 The formation of river terraces – a perspective from 2021

Since Woldstedt published his work in 1952, there has been an explosion of data collection and research on the topic of river terrace formation, illustrated best by the activities of the International Geoscience Programme: IGCP 449 "Global Correlation of Late Cenozoic Fluvial Deposits" and IGCP 518 "Fluvial Sequences as Evidence for Landscape and Climatic Evolution in the Late Cenozoic" (Bridgland and Westaway, 2014).

Nearly all of the new findings have been based on developments in technology and the application of knowledge from associated sciences. For instance methods of dating terrace deposits (Schaller et al., 2016) now include ^{14}C of organic material held within the terrace deposits; thermo-luminescence, optically stimulated luminescence and infrared-stimulated luminescence (TL, OSL and IRSL) of quartz and feldspar sand grains comprising terrace deposits; amino acid racemisation ratio (AAR) determinations of specific organic materials held in the sediments; and U-series ratio determinations of calcrete precipitates in caves and sediments or organic material from within the terrace. Additionally dating can be achieved by palaeomagnetism and cosmogenic nuclides produced in situ measured from depth profiles through the terraces and cosmogenic surface exposure dating of boulders at the terrace surface. Likewise stratigraphic links to datable materials such as basalt lavas can provide a fine age resolution using Ar / Ar or U–Pb ratio determinations. Geochronometrically constrained biostratigraphic assemblages, especially mammal assemblage zones (MAZ), have also been used to date the age of terrace deposits (Schreve et al., 2007).

The ability to assign an age to a terrace with some degree of confidence has meant that it is possible to further evaluate factors that have determined terrace formation. The most significant outcome has been the establishment of a relationship between river terrace formation and climate change expressed in the form of Milankovitch orbital forcing. In cool temperate latitudes, such as those considered by Woldstedt, three patterns of river development can be identified for the late Cenozoic (Rose, 2010; Bridgland and Westaway, 2014). Small-scale precession variations (22 kyr), prior to ca. 2.6 Ma, provided limited power for surface processes, and rivers transported fine-grained sediments over low-relief terrain, with limited terrace development. Between 2.6 and 0.9 Ma when obliquity forcing (44 kyr) was dominant, cold-climate processes introduced power into river systems that then began to shape the landscape and transport well-sorted, coarser-grained sediment with extensive but often poorly defined terraces. In contrast, over the past 0.9 Myr, eccentricity forcing on a 100 kyr timescale generated long periods of cold-climate processes and of river sedimentation and incision tuned to 100 kyr cycles. However, over this period, lowland glaciation could greatly complicate the products of river activity (as Woldstedt clearly recognised).

Tied into this approach, the application of stream power calculations explains the focus of incision, transport and deposition throughout a catchment-long profile (Pazzaglia, 2013).

$$\text{Stream power } \Omega = \rho g Q S, \tag{1}$$

where ρ is the density of the fluid, g is the acceleration due to gravity, Q is discharge and S is slope.

High power is generated by high (snowmelt) runoff, leading to the erosion, transport and deposition of readily available cold-climate-derived sediments. Low power is constrained by relatively low (vegetation-controlled) discharge and the concentration of sediment sources to within the river channel. Thus, in cold climates, incision is focussed on the upper parts of catchments and sedimentation takes place in lower reaches. Alternatively in climates permitting an effective vegetation cover, (limited) aggradation is focussed on the upper part of catchments, and channel incision is characteristic of lower reaches. In turn, the critically important finding that in areas of responsive mobile lower crust, incision in the upper parts of river systems and deposition in adjacent subsiding basins result, through positive feedback, in progressive, periodic land uplift and associated subsidence in the upper and lower parts of the catchments respectively (Bridgland and Westaway, 2014). It is under these conditions that the classic, incised terrace staircases developed.

With these building blocks of river terrace development in place, it is possible to provide some general explanations. In addition to the climatic controls outlined above, tectonic processes can increase or decrease stream power by altering gradients within a channel. The role of lags within the system, whereby one relationship (such as river aggradation or incision) can be maintained temporarily out of phase with a contemporary forcing factor, can explain variations within system models. Specifically, stream power distribution in cool temperate catchments can mean that aggradation can take place at a coastline during cold-climate periods of low sea level. Alternatively, if climatically forced processes operate for a relatively short duration, then sedimentation may not extend throughout a catchment and incision may occur in relation to an equivalent fall of sea level.

Financial support. The article processing charge was funded by the Quaternary scientific community, as represented by the host institution of *EGQSJ*, the German Quaternary Association (DEUQUA).

Review statement. This paper was edited by Markus Fuchs and reviewed by one anonymous referee.

References

Bridgland, D. R. and Westaway, R.: Quaternary fluvial archives and landscape evolution: a global synthesis, Proc. Geol. Assoc., 125, 600–629, 2014.

Pazzaglia, F. J.: 9.22 Fluvial Terraces, in: Treatise on Geomorphology, edited by: Shroder, J. F., Academic Press, London, UK, 379–412, 2013.

Penck, A. and Brückner, E.: Die Alpen im Eiszeitalter (3 vols), Tauchnitz, Leipzig, Germany, 1189 pp., 1909.

Rose, J.: The Quaternary of the British Isles: factors forcing environmental change, J. Quaternary Sci., 25, 399–418, 2010.

Schaller, M., Ehlers, T. A., Stor, T., Torrent, J., Lobato, L., Christl, M., and Vockenhuber, C.: Timing of European fluvial terrace formation and incision rates constrained by cosmogenic nuclide dating, Earth Planet. Sc. Lett., 451, 221–231, 2016.

Schreve, D. C., Keen, D. H., Limondin-Lozouet, N., Auguste, P., Santistebane, J. I., Ubilla, M., Matoshko, A., Bridgland, D. R., and Westaway, R.: Progress in faunal correlation of Late Cenozoic fluvial sequences 2000–4: the report of the IGCP 449 biostratigraphy subgroup, Quaternary Sci. Rev., 26, 2970–2995, 2007.

Winsemann, J., Lang, J., Roskosch, J., Polom, U., Böhner, U., Brandes, C., Glotzbach, C., and Frechen, M.: Terrace styles and timing of terrace formation in the Weser and Leine valleys, northern Germany: response of a fluvial system to climate change and glaciation, Quaternary Sci. Revi., 123, 31–57, 2015.

Woldstedt, P.: Probleme der Terrassenbildung, E&G Quaternary Sci. J., 2, 36–44, https://doi.org/10.3285/eg.02.1.04, 1952.

Zeuner, F. E.: Dating the Past, Methuen, London, UK, 1952.

E&G Quaternary Sci. J., 70, 221–224, 2021
https://doi.org/10.5194/egqsj-70-221-2021

Open Access E&G Quaternary Science Journal

Retrospective

A tribute to Fink (1956): On the correlation of terraces and loesses in Austria

Tobias Sprafke

Kompetenzzentrum Boden (Center of Competence for Soils), BFH-HAFL, Länggasse 85, 3052 Zollikofen, Switzerland

Correspondence: Tobias Sprafke (tobias.sprafke@bfh.ch)

Relevant dates: Received: 8 August 2021 – Accepted: 5 November 2021 – Published: 17 December 2021

How to cite: Sprafke, T.: A tribute to Fink (1956): On the correlation of terraces and loesses in Austria, E&G Quaternary Sci. J., 70, 221–224, https://doi.org/10.5194/egqsj-70-221-2021, 2021.

Special issue statement. This article is part of a special issue published on the occasion of the 70th anniversary of *E&G Quaternary Science Journal (EGQSJ)*. The special issue celebrates the journal's notable contribution to Quaternary research by revisiting selected milestone articles published in the long history of *EGQSJ*. The German Quaternary Association (DEUQUA) presents translations of the originals and critical appraisals of their impact in tandem anniversary issues of *DEUQUASP* and *EGQSJ*, respectively.

Original article: https://doi.org/10.3285/eg.07.1.07

Translation: https://doi.org/10.5194/deuquasp-3-41-2021

1 Historical context

Julius Fink did not discover a new continent, he did not develop a new research technique, he made no important archeological find, and he did not describe an unknown mineral or species. Fink created a holistic framework linking geology, physical geography, and soil science close to his hometown of Vienna. He collected detailed field evidence from numerous loam pits and other outcrops, thereby managing to solve a number of complications in a region that seemed well-studied but, looking in detail, was full of contradictory evidence. Fink had large shoes to fill when presenting his results on a five-day excursion following the DEUQUA meeting in Laufen near Salzburg (Austria) in 1955. His follow-up paper treated here established key concepts of loess and terrace stratigraphy and their geographical differences, largely valid today (Sprafke, 2016; Terhorst et al., 2015).

A major footprint before Fink was the seminal work of Penck and Brückner (1909) which established that at least four major glaciations occurred in the eastern Alps. These were (from oldest to latest): Günz, Mindel, Riss (i.e., penultimate glacial), and Würm (i.e., last glacial). Key pieces of evidence were glacial moraines linked to fluvioglacial terraces in the Alpine foreland, whereas the widespread loess cover played a minor role in this concept. As terraces were linked to moraines and thus to glacial periods, their loamy covers (absent on the lowermost, last glacial terrace) were attributed to interglacials. This misconception was soon invalidated: loess represents glacial periods, and intercalated paleosols represent interglacials or interstadials (Soergel, 1919).

Many footprints were left by generations of archeologists that made important discoveries in the Austrian loess landscapes, especially in the Krems–Wachau region. The Venus of Willendorf discovered in 1908 remains until now a symbol for the European Paleolithic. The nearby remarkable loess outcrops at Krems, Göttweig, and Paudorf, with their well-developed paleosols, played an important role in fierce discussions between Quaternary geologists and archeologists on how to subdivide the ice age and related Paleolithic cultures.

Probably the most immediate footprint for Fink was left by Götzinger (1936). On a field trip through the Alpine forelands in the context of the INQUA conference in Vienna, Götzinger internationally established the Krems, Göttweig, and Paudorf loess–paleosol sequences (LPSs) as type localities of Quaternary stratigraphy. The Krems, Göttweig, and Paudorf paleosols were thought to represent the "long" Mindel–Riss interglacial (∼ marine oxygen isotope stages (MISs) 11/9-7), the "last" Riss–Würm interglacial (∼ MIS 5e), and the single marked Würm interstadial (∼ MIS 3), respectively.

2 Loess and terrace stratigraphy

Today we know from continuous marine and ice core oxygen isotope records that over 50 glacial–interglacial cycles and numerous suborbital climatic oscillations occurred during the Quaternary. At the same time each landscape and archive has its distinct response to these paleoclimatic changes, hampering unified stratigraphies, especially when absolute dating techniques are not available. Until the 1950s, Quaternary research was essentially a field science, and the small national and international communities did field trips to personally observe and discuss stratigraphic evidence brought forward by colleagues.

Götzinger (1936) realized the potential of LPS in the Krems region to refine Quaternary stratigraphy and presented impressive outcrops at Paudorf, Göttweig, and Krems as type localities. Fink expressed his strong skepticism with this choice 20 years later as these localities had no clear connection to stratigraphically robust terraces. It was in the region between Salzburg and Linz (NW Austria), studied in detail by Penck and Brückner (1909), where Fink realized that the connection of fluvioglacial terraces (previously linked to glacial moraines) and loess was too obvious to be ignored: the lowermost terrace (in German: *Niederterrasse*) represents the last glacial period and is therefore free of loess, and the next higher terrace (in German: *Hochterrasse*) represents the penultimate glacial, contains the last interglacial paleosol, and is superimposed by a last glacial LPS. A thick LPS on higher terrace levels (different *Deckenschotter* units) can record several glacial–interglacial cycles.

In NW Austria, close to the former piedmont glaciers, Fink managed to convincingly complement the Penck and Brückner (1909) scheme with loess stratigraphy. The latter provided details of glacial paleoenvironments not visible from moraines and terraces (Terhorst et al., 2015). In NE Austria (N of Vienna), far from the piedmont paleoglaciers, Fink identified an overall similar stratigraphic pattern compared to the one of NW Austria, however with markedly different expressions of paleosols and sediments. He suggested a regional terrace stratigraphy for NE Austria based on the insights from geomorphology and loess stratigraphy, although he was less confident with this connection due to the influence of neotectonics in the Vienna Basin. The Krems region with its complex pattern of terraces and impressive LPS of highly variable ages was largely avoided in the stratigraphic schemes of Fink.

Despite regional differences of the LPSs, Fink created a robust stratigraphic framework for the Austrian loess landscapes in connection to terraces and based on this to glacial moraines. While he was skeptical about Götzinger's choice of type localities in the Krems region, he agreed to his notion that the last glacial period had only one clear interstadial. While Götzinger (1936) had used the Paudorf soil, Fink selected the Stillfried B paleosol of NE Austria and a marked tundra gley in NW Austria as stratigraphic markers for this single interstadial of the last glacial. This twofold last glacial period contrasted to the widely shared view of a tripartite subdivision of the last glacial period (Soergel, 1919; Woldstedt, 1956).

3 Paleoenvironments

From today's perspective, the pedostratigraphic advances by Fink seem of little relevance as we have modern techniques to date organic matter up to 50 ka and far older phases of sedimentation, using, e.g., optically stimulated luminescence dating (Thiel et al., 2011). With these tools we are able to detect local changes in sedimentation rates and pathways of pedogenesis, which we can link to regional paleoenvironments and even paleoclimatic evolution (Sprafke, 2016). Already Fink realized during his stratigraphic work that there are marked differences in LPS between NW Austria and NE Austria which correspond to different present-day climatic and ecological conditions. His German colleague, Brunnacker (1956), followed the same approach for Bavaria, differentiating loess facies regions according to (paleo-)climatic differences in N Bavaria (Franconia) and S Bavaria. In Austria the gradient between the "humid" and the "dry" loess landscape is stronger as the Bohemian Massif between these areas acts as a topographic barrier for moisture brought by the westerlies.

While Fink is internationally well-known for loess research, it should be highlighted that he contributed to numerous soil maps and considerably advanced soil geography in Austria and beyond. In his concept of loess landscapes, he virtuously linked geology, physical geography, and soil science. The humid loess landscape in NW Austria receives 600–800 mm mean annual precipitation, and present-day soils from loess are Luvisols that typically develop in deciduous forest ecosystems. To the east of the Bohemian Massif precipitation is only around 500 mm per year, and present-day soils largely correspond to Chernozems that form potentially in steppe ecosystems. Different morphologies of LPS E and W of the Bohemian Massif can be explained by overall similar paleoclimatic gradients (Sprafke, 2016).

Fink realized that similar to the present-day soil, interglacial paleosols of the humid loess landscape (developed in loess or terrace sediments) correspond to well-developed Luvisols, partly with strong redoximorphic features. The interglacial Luvisol remnants and polygenetic pedosediments on top are termed "Linzer Komplex". Superimposed are brown, decalcified loess sediments, at least one major tundra gley and calcareous loess. Unlike the present-day Chernozems, the last interglacial paleosol in the dry loess landscape corresponds to a Cambisol, thus indicating advanced weathering compared to the present-day soil but still more weakly developed in comparison to the last interglacial soil of the humid loess landscape. At the type locality Stillfried A, the "Stillfrieder Komplex", correlative to the "Linzer Komplex", consists of the last interglacial Cambisol and three Chernozems separated by loess layers. Stillfried B is a topographically higher profile with a weak paleosol, which is correlated to the major Würm interstadial (cf. Terhorst et al., 2015).

Although the localities of the Krems–Wachau region (e.g., Paudorf, Göttweig, Krems, Willendorf) were widely known to archeologists and Quaternary researchers, Fink avoids detailed discussions on loess profiles of what he calls a "transition region"; this area is defined as the Wachau Valley and the E margin of the Bohemian Massif. Fink gives an overview of the main stratigraphic features in this region and suggested that the local paleosols are comparable to those of the dry loess landscape, but early last glacial reworking is comparable to the humid loess landscape. Fink admits that the terrace stratigraphy is complicated in the transition region and that it is not possible to provide reliable links to the terrace scheme in NW Austria, close to the paleoglaciers, where we are in Fink's words "forced to accept" Penck's nomenclature. Fink regrets the lack of studies linking the NW Austrian terrace stratigraphies to those of the Krems region and the Vienna Basin – a problem that persists until today (Sprafke, 2016).

An important aspect of Fink's work is the correlations of his loess stratigraphies to those of other regions in the loess belt between Belgium and (former) Yugoslavia. Note that Fink expands his text to where he is able to report from his own field observations. It appears he trusts his own eyes more than what is said or even written in publications given his tendency to reinterpret findings from colleagues. This focus on one's own field observations appears unusual from a modern perspective, in which findings require independent support by quantitative data. Summarizing his discussion on profiles from other regions, Fink was able to connect his own findings to those of other loess landscapes as there are in general comparable patterns in loess–paleosol successions – a remarkable achievement without absolute chronology. Possibly the unified stratigraphy from (paleo-)climatically distinct regions allowed him to understand profiles in the oceanic and continental parts across the European loess belt.

4 Further development

In 1956, Fink realized that field evidence was insufficient to discuss the transition region in detail. Radiocarbon ages from so-called Paudorf soils and Göttweig soils of different archeological sites became available five years later, and Fink accepted an age of ca. 30 ka for the Paudorf interstadial, which he correlated to Stillfried B. Following Götzinger (1936), Fink (1961) proposed that the Göttweig soil correlates to the last interglacial and thus the lower parts of the "Stillfrieder Komplex" and "Linzer Komplex". At this time, the Quaternary research community agreed to abandon the tripartite subdivision of last glacial period, and Fink finally succeeded in integrating the transitional region with its famous loess sections into Austrian loess stratigraphy.

Also in 1961, at the loess symposium of the INQUA conference in Warsaw (Poland), Fink and colleagues established the INQUA subcommission of loess stratigraphy. The notion that the first well-developed brown loess paleosol (usually a truncated Luvisol) below the surface represented the last interglacial found wide acceptance as a "stratigraphic rule". On the first annual subcommission field trips in Central Europe, this rule worked well, but in the late 1960s after field trips to Hungary and Serbia, there were increasing doubts that the stratigraphic rule is universally applicable and that the type localities of the transition region in Austria were adequate. The loess subcommission reached full commission status during the INQUA congress in Paris 1969, but at the same time Fink had to announce unfortunate news. According to malacological and paleomagnetic results obtained by Czech colleagues from Krems, Göttweig, and Paudorf paleosols (e.g., Vojen Ložek, Jiří Kukla), the respective units were considerably older, i.e., Early Pleistocene, Middle Pleistocene, Last Interglacial, respectively (see Sprafke, 2016).

During the 1970s until his death, Fink worked with Jiri (George) Kukla on Pleistocene land–sea correlations, providing results from the Old Pleistocene loess records of Krems and Stranzendorf. With the emerging marine stratigraphy, loess lost its key role to subdivide the Quaternary – at least for European LPS because complete loess sections at the Chinese loess plateau attracted an increasing number of researchers. The classical tetraglacial scheme of Penck and Brückner (1909) remains useful in the forelands of the eastern Alps, but internationally it is only of historical relevance.

In the 1990s the establishment of luminescence dating led to some revival of loess research in Central Europe and some key sites like those in Lower Austria finally had absolute age information (Zöller et al., 1994). In the last decade, the growing interest in regional paleoclimate records and the paleoenvironmental contexts of Paleolithic humans have resulted in intensified research on loess (Lomax et al., 2014; Sprafke, 2016; Terhorst et al., 2015). It should not be forgotten that a key observation of Fink was the significance of LPS to understand past climate and landscape evolution, which appears largely blurred by the stratigraphic confusion during the following decades. The concept of loess landscapes highlights the imprint of (paleo-)climate on paleosol properties, which can be used to reconstruct regional effects of past climatic changes (Sprafke, 2016; Terhorst et al., 2015).

Nowadays, loam pits are rare, and field observations are often limited to sampling time. With the emergence of big data geoscience, the paper of Fink may to many just appear as historical science. However, key concepts developed in these times are still valid, and key challenges remain until today. Some details need revision; for example, the last glacial tundra gley of the humid loess landscape is most likely Upper Würm, as the Middle Würm is represented by brown soils, including the equivalent to the Lohne soil and Stillfried B (Terhorst et al., 2015). Despite modern geochronology techniques (e.g., advanced luminescence dating protocols, cosmogenic nuclide dating, and refined paleomagnetics) and advances in quantitative modeling, there remain many more open questions on loess and terrace stratigraphy in the Alpine foreland. Certainly, detailed and careful field observations complemented by appropriate modern analytical techniques and based on a holistic understanding of the complex interplay of natural processes are of great importance to resolve these questions and pedosedimentary and landscape evolution in general – a lesson we also learn from Fink.

Acknowledgements. Many thanks to Birgit Terhorst and Robert Peticzka for introducing me to Austrian loess, the fascinating world of Julius Fink. Also thanks to Bernhard Salcher for helpful review comments to improve this paper and many thanks to Christine Thiel for the editorial handling and important remarks during the preparation of this paper.

Financial support. The article processing charge was funded by the Quaternary scientific community, as represented by the host institution of *EGQSJ*, the German Quaternary Association (DEUQUA).

Review statement. This paper was edited by Christine Thiel and reviewed by Bernhard Salcher.

References

Brunnacker, K.: Regionale Bodendifferenzierungen während der Würmeiszeit, E&G Quaternary Sci. J., 7, 43–48, https://doi.org/10.3285/eg.07.1.06, 1956.

Fink, J.: Zur Korrelation der Terrassen und Lösse in Österreich, E&G Quaternary Sci. J., 7, 49–77, https://doi.org/10.3285/eg.07.1.07, 1956.

Fink, J.: Die Gliederung des Jungpleistozäns in Oesterreich, Mitteilungen der Geologischen Gesellschaft in Wien, 54, 1–25, 1961.

Götzinger, G.: Das Lößgebiet um Göttweig und Krems an der Donau, in: Führer für die Quartär-Exkursionen in Österreich, edited by: Götzinger, G., Geologische Bundesanstalt, Wien, pp. 1–11, 1936.

Lomax, J., Fuchs, M., Preusser, F., and Fiebig, M.: Luminescence based loess chronostratigraphy of the Upper Palaeolithic site Krems-Wachtberg, Austria, Quatern. Int., 351, 88–97, 2014.

Penck, A. and Brückner, E.: Die Eiszeiten in den nördlichen Ostalpen (= Die Alpen im Eiszeitalter Band 1), Tauchnitz, Leipzig, 393 pp., 1909.

Soergel, W.: Löße, Eiszeiten und paläolithische Kulturen. Eine Gliederung und Altersbestimmung der Lösse, Fischer, Jena, 177 pp., 1919.

Sprafke, T.: Löss in Niederösterreich – Archiv quartärer Klima- und Landschaftsveränderungen, Dissertation, Würzburg University Press, Würzburg, 272 pp., available at: https://opus.bibliothek.uni-wuerzburg.de/files/12778/978-3-95826-039-9_Sprafke_Tobias_OPUS_12778.pdf (last access: 26 November 2021), 2016.

Terhorst, B., Sedov, S., Sprafke, T., Peticzka, R., Meyer-Heintze, S., Kühn, P., and Solleiro Rebolledo, E.: Austrian MIS 3/2 loess–palaeosol records – Key sites along a west–east transect, Palaeogeogr. Palaeocl., 418, 43–56, 2015.

Thiel, C., Buylaert, J.-P., Murray, A. S., Terhorst, B., Tsukamoto, S., Frechen, M., and Sprafke, T.: Investigating the chronostratigraphy of prominent palaeosols in Lower Austria using post-IR IRSL dating, E&G Quaternary Sci. J., 60, 11, https://doi.org/10.3285/eg.60.1.10, 2011.

Woldstedt, P.: Über die Gliederung der Würm-Eiszeit und die Stellung der Lösse in ihr, E&G Quaternary Sci. J., 7, 78–86, https://doi.org/10.3285/eg.07.1.08, 1956.

Zöller, L., Oches, E. A., and McCoy, W. D.: Towards a revised chronostratigraphy of loess in Austria with respect to key sections in the Czech Republic and in Hungary, Quaternary Sci. Rev., 13, 465–472, 1994.

E&G Quaternary Sci. J., 70, 225–227, 2021
https://doi.org/10.5194/egqsj-70-225-2021

Open Access E&G Quaternary Science Journal

Retrospective

A tribute to Flohn (1963): On the meteorological interpretation of Pleistocene climate variations

Ulrich Cubasch

Department of Earth Science, Institute of Meteorology, Freie Universität Berlin,
Carl-Heinrich-Becker-Weg 6–10, 12165 Berlin, Germany

Correspondence: Ulrich Cubasch (cubasch@zedat.fu-berlin.de)

Relevant dates: Received: 25 May 2021 – Accepted: 30 October 2021 – Published: 17 December 2021

How to cite: Cubasch, U.: A tribute to Flohn (1963): On the meteorological interpretation of Pleistocene climate variations, E&G Quaternary Sci. J., 70, 225–227, https://doi.org/10.5194/egqsj-70-225-2021, 2021.

Special issue statement. This article is part of a special issue published on the occasion of the 70th anniversary of *E&G Quaternary Science Journal (EGQSJ)*. The special issue celebrates the journal's notable contribution to Quaternary research by revisiting selected milestone articles published in the long history of *EGQSJ*. The German Quaternary Association (DEUQUA) presents translations of the originals and critical appraisals of their impact in tandem anniversary issues of *DEUQUASP* and *EGQSJ*, respectively.

Original article: https://doi.org/10.3285/eg.14.1.17

Translation: https://doi.org/10.5194/deuquasp-3-61-2021

1 Context

Hermann Flohn's (1963) publication "On the meteorological interpretation of Pleistocene climate variations" discusses from the perspective of atmospheric sciences the state of knowledge of the Pleistocene climate, which in 1963 was mainly based on geological and geomorphological evidence. It interprets the Pleistocene cold and warm periods and the regionally detectable variations between wet and dry episodes via changes in the large-scale meteorological flow pattern. Flohn identifies gaps and inconsistencies in the prevailing explanations and expresses the hope that with improved methods, in particular enhanced age determination and derivation of paleotemperatures, the Pleistocene climate, which as he states "has been determined by the rampant phantasies of some popular authors" ("ungezügelten Phantasie populärer Autoren"), will be in the future "realistically and physically consistently described using numerical model calculations" ("mit rationalen, physikalisch-mathematisch fundierten Erwägungen und Modellrechnungen"). Flohn's paper was published in "Eiszeitalter und Gegenwart", and many of the references he cited are found in Quaternary science or geological journals. In 1963, research in paleoclimate changes and their meteorological interpretation was predominantly based on the proxy data of Quaternary sciences, and this topic had hardly entered the recognition of the meteorological community. In those days, meteorologists saw climate research as a necessary but unchallenging byproduct of their routine data collection. Flohn's paper presents the vision that meteorological modeling and Quaternary sciences will have an interdependence in the future. Triggered by the discussion about the influence of mankind on climate, from 1985 onwards the interdisciplinary research into the paleoclimate has been intensifying. The central question was and still is as follows: is the currently experienced global warming of anthropogenic origin (mainly by raising the concentration of greenhouse gases in the atmosphere) or does it stem from natural causes like changes in solar intensity, changes in the orbital parameters, or by the aerosols emitted during volcanic eruptions? In an ongoing international effort, ice and sediment cores have been collected, dated, and interpreted. Data representing the oceanic and atmospheric circulation have been sampled using in situ and satellite sources. Numerous numerical models have been developed which simulate the ocean, the atmosphere, the hydrosphere, and the biosphere and their interactions with each other. The effort is coordinated in various national, European, and international programs (WCRP, IGPB, PAGES, IODP). The results are summarized on a quasi-regular basis in the reports of the IPCC (https://www.ipcc.ch, last access: 6 December 2021). It has to be stressed that the current research on the atmospheric paleoclimate focuses on the Holocene due to the data availability and restrictions in the computing resources; the earlier periods of the Pleistocene climate are still being interpreted on the basis of geological evidence.

2 How has our current knowledge changed compared to that presented by Flohn in 1963?

At the beginning, Flohn's paper discusses the interaction of the meteorological flow regimes with the glaciation of the Northern Hemisphere, as well as the contribution of these flow regimes to the buildup of the glaciers and their the melting. The general assumption in 1963 was that during the glacials and interglacials the jet stream moves south- and northwards, respectively. The climate zones are shifted synchronously with the glaciation events, linked with a shift of pluvials. However, as Flohn pointed out, geological evidence indicates that this is not consistently the case. He raises the question of whether these inconsistencies are caused by uncertainties in the age determination or if a mechanism has been overlooked that causes regional pluvials to develop independently from the glaciation state. Nowadays changes in the large-scale precipitation pattern are attributed mainly to a shift in the Intertropical Convergence Zone (ITCZ), which follows the changes in the solar insolation induced by variations in the orbital parameters (Milankovic-cycles; Berger, 1978). These insolation changes are also seen as the main driver leading to glaciations (Kaspar and Cubasch, 2007; Wanner et al., 2008). The mechanisms Flohn had found missing are feedback processes, which according to current knowledge influence the formation of a regional wet climate. One feedback mechanism that has been known for a long time in agricultural meteorology consists of the feedback loop in which enhanced precipitation leads to more vegetation, which in turn reinforces the evaporation, which then leads to more precipitation. Its importance for the large-scale climate, however, was only discovered more than 30 years later by Claussen et al. (1999). He proved in model experiments that the vegetation cover of the Sahara is strongly dependent on this vegetation feedback. Flohn assumes that during some of the interglacials the Arctic was free of sea ice. He deduces that this reduces the meridional temperature gradient in the Northern Hemisphere and that this would lead to a stronger meridionalization of the airflow. This assumption is still followed today: with enhanced global warming, the Arctic ice cover is dwindling in the present. The IPCC projections for the high climate change scenarios indicate that the Arctic ice will almost completely disappear within the next 100 years (IPCC, 2013). It has been found by Francis und Vavrus (2015) that already now the decrease in the Arctic ice coverage leads to a diminished Equator–North pole temperature contrast, which induces a wavier jet stream. Flohn calculated that the changes in the radiative balance alone would not have been effective enough for the glacier melt and deduced that during the late- and post-glacials, the changes in the large-scale circulation must have enhanced the advection of warm air. He estimated that, in general, the available heat within the climate system is sufficient to explain the melting of the glaciers and the induced sea level rise. At a first glance, it is a bit surprising that Flohn focused on the atmospheric circulation and does not mention at all the contribution of the heat advection by oceanic currents. However, if one takes the standard German textbook on Oceanography (Dietrich et al., 1975) as an indicator of the state of knowledge of that time (12 years after Flohn's paper was published), only a very limited number of locally confined estimates of the heat transport by the Gulf Stream (some of them estimated during the 1930s) can be found but no comprehensive portrayal. It took more than a quarter of a century after Flohn's work until Broecker (1991) summarized the structure of three-dimensional oceanic circulation and its heat and freshwater transport in terms of a "great conveyor belt circulation". Flohn presents quantitative estimates of the amount of freshwater melting (freezing) during a deglaciation (glaciation). The order of magnitude of the glacier melting rates and the sea level change derived from the mass balance agree with the present-day estimate published by the IPCC (2013). Flohn points to the fact that large quantities of meltwater have to be transported in huge rivers. However, he does not go so far as to speculate what impact these freshwater masses would have on the oceanic circulation since, as mentioned before, little was known about the oceans in 1963. The idea that the amount of freshwater flowing into the North Atlantic ocean could lead to a change in the Gulf Stream circulation emerged about 20 years later after the analyses of sediment and ice cores (Broecker et al., 1985). It was later verified in model studies by Stocker und Wright (1991) and Rahmstorf (1995).

3 Summary

In summary, Flohn has compiled the indicators of the climate states during the Pleistocene and interpreted them with his extensive experience in atmospheric circulation. Even though he found contradictions and gaps in the available information, he was able to draw a consistent picture of the atmospheric circulation and its variability during that time period and offered a physically consistent explanation of the sea level change during a glaciation cycle. His main statements are still valid today. After decades of intensive research, one can nowadays fill some of the gaps and solve some of the contradictions. Substantial advances have been made in the understanding of the oceanic circulation, its role in the heat and freshwater transport, and its variability. Furthermore, the consideration of multiple feedback mechanisms of a biological, chemical, and physical nature led to an improved understanding of the reaction of the climate system to variations in the external forcings (solar radiation, orbital parameter, volcanic aerosols). Substantial deficits in our knowledge of the climate system still exist, particularly if one considers time periods prior to the Holocene (IPCC, 2013). The tendency to employ "rampant phantasies" to fill these gaps has not disappeared. Even almost 60 years after Flohn's paper and after a substantial increase in knowledge, the scientific community must continue to strive for an improved data coverage and understanding of processes so that the paleoclimate in its entirety can "realistically and physically consistently [be] described using numerical model calculations".

Financial support. The article processing charge was funded by the Quaternary scientific community, as represented by the host institution of *EGQSJ*, the German Quaternary Association (DEUQUA).

Review statement. This paper was edited by Christine Thiel and reviewed by one anonymous referee.

References

Berger, A.: Long-term variations of daily insolation and Quarternary climate changes, J. Atmos. Sci., 35, 2362–2367, https://doi.org/10.1175/1520-0469(1978)035<2362:LTVODI>2.0.CO;2,1978.

Broecker, W. S.: The Great Ocean Conveyor, Oceanography, 4, 79–89, https://doi.org/10.5670/OCEANOG.1991.07, 1991.

Broecker, W. S., Peteet, D. M., and Rind, D.: Does the ocean-atmosphere system have more than one stable mode of operation?, Nature, 315, 21–26, https://doi.org/10.1038/315021a0, 1985.

Claussen, M., Brovkin, V., Ganopolski, A., Hoelzmann, P., and Pachur, H.-J.: Simulation of an abrupt change in Saharan vegetation in the mid-Holocene, Geophys. Res. Lett., 26, 2037–2040, https://doi.org/10.1029/1999GL900494, 1999.

Dietrich G., Kalle, K., Krauss, W., and Siedler, G.: Allgemeine Meereskunde – Eine Einführung in die Ozeanographie. 3. Neubearbeitete Auflage, Gebrüder Borntraeger, Berlin, Germany, 593 pp., 1975.

Flohn, H.: Zur meteorologischen Interpretation der pleistozänen Klimaschwankungen, E&G Quaternary Sci. J., 14, 153–160, https://doi.org/10.3285/eg.14.1.17, 1963.

Francis, J. A. and Vavrus, S. J.: Evidence for a wavier jet stream in response to rapid Arctic warming, Environ. Res. Lett., 10, 014005, https://doi.org/10.1088/1748-9326/10/1/014005, 2015.

IPCC: Climate Change 2013 – The Physical Science Basis. Contribution of Working Group I to the Fifth Assessment Report of the Intergovernmental Panel on Climate Change, eidted by: Stocker, T. F., Qin, D., Plattner, G.-K, Tignor, M., Allen, S. K., Boschung, J., Nauels, A., Xia, Y., Bex, V., and Midgley, P.M., Cambridge University Press, Cambridge, UK and New York, NY, USA, https://doi.org/10.1017/CBO9781107415324.005, 2013.

Kaspar, F. and Cubasch, U.: Simulations of the Eemian interglacial and the subsequent glacial inception with a coupled ocean-atmosphere general circulation model, in: Development in Quaternary Science 7, The Climate of Past Interglacials, edited by: Sirocko, F., Claussen, M., Sanchez-Goni, M. F., and Litt. T., Elsevier, https://doi.org/10.1016/S1571-0866(07)80058-3, 2007.

Rahmstorf, S.: Bifurcations of the Atlantic thermohaline circulation in response to changes in the hydrological cycle, Nature, 378, 145–149, https://doi.org/10.1038/378145a0, 1995.

Stocker, T. F. and Wright, D. G.: Rapid transitions of the ocean's deep circulation induced by changes in surface water fluxes, Nature, 351, 729–732, https://doi.org/10.1038/351729a0, 1991.

Wanner, H., Beer, J., Crowley, T., Cubasch, U., Flückiger, J., Goosse, H., Grosjean, M., Kaplan, J., Küttel, M., Solomina, O., Stocker, T., Tarasov, P., Wagner, M., and Widmann, M.: Mid to late Holocene climate change – a comprehensive review, Quaternary Sci. Rev., 27, 1791–1828, https://doi.org/10.1016/j.quascirev.2008.06.013, 2008.

E&G Quaternary Sci. J., 70, 229–233, 2021
https://doi.org/10.5194/egqsj-70-229-2021

Open Access E&G Quaternary Science Journal

Retrospective

A tribute to Ložek (1965): The problem of loess formation and the loess molluscs

Denis-Didier Rousseau[1,2]

[1]Geosciences Montpellier, University of Montpellier, CNRS, Montpellier, France
[2]Lamont-Doherty Earth Observatory, Columbia University, New York, NY 10964, USA

Correspondence: Denis-Didier Rousseau (denis-didier.rousseau@umontpellier.fr)

Relevant dates: Received: 11 August 2021 – Revised: 6 September 2021 – Accepted: 5 November 2021 – Published: 17 December 2021

How to cite: Rousseau, D.-D.: A tribute to Ložek (1965): The problem of loess formation and the loess molluscs, E&G Quaternary Sci. J., 70, 229–233, https://doi.org/10.5194/egqsj-70-229-2021, 2021.

Special issue statement. This article is part of a special issue published on the occasion of the 70th anniversary of *E&G Quaternary Science Journal (EGQSJ)*. The special issue celebrates the journal's notable contribution to Quaternary research by revisiting selected milestone articles published in the long history of *EGQSJ*. The German Quaternary Association (DEUQUA) presents translations of the originals and critical appraisals of their impact in tandem anniversary issues of *DEUQUASP* and *EGQSJ*, respectively.

Original article: https://doi.org/10.3285/eg.16.1.05

Translation: https://doi.org/10.5194/deuquasp-3-67-2021

When addressing the nature and origin of loess deposits and the associated environment as deduced from terrestrial mollusc faunas, Vojen Ložek produced a synthetic review of the state of the art at that time (Ložek, 1965a). This synthesis was one among several papers that he published the same year in English about "The loess environment in Central Europe" (Ložek, 1965c) or "Problems of analysis of the Quaternary nonmarine molluscan fauna in Europe" (Ložek, 1965b). It was mainly based on his own experience of investigating terrestrial molluscs in Czechoslovakian Quaternary deposits.

In his seminal paper, Ložek addresses key issues, which remain valid and are still relevant nowadays – 56 years later! Ložek noticed the problem "that it is surprising how little attention has been paid to the mollusc fauna, which occurs so frequently in loess that it can rightly be considered one of the main characteristics of this sediment". Such a key statement still prevails today by comparison with other proxies which appear much more popular. This leads Ložek to conclude that "we still see that this goes far beyond the framework of the loess problem".

Ložek initially addresses the critical question of loess formation, indicating that at that time there were two schools: soil scientists and bio-geoscientists. Interestingly, such distinction remains until the present; however, the differentiation between the two today seems to rather correspond to a problem of the scale at which the relevant processes and mechanisms are analysed. Ložek gives preference to the aeolian hypothesis of loess formation, what he termed "Richthofenian hypothesis", by reference to Ferdinand von Richthofen, who first proposed that loess was aeolian in origin. He adds the critical assumption that "it is clear that the loess is to be regarded as the product of a peculiar environment which has no parallel in present-day Europe".

With Ložek's correct and concrete statement that "molluscs are best suited, as they are more abundant than the vertebrates in the loess and the related deposits", it is easier to understand the sampling protocol developed by Ložek and his followers. About 10 kg of sediment needs to be sampled and sieved in order to retrieve the remaining shells. During this procedure, bones or even skulls of micromammals and rodent teeth are frequently found among the numerous shells, making vertebrates a sub-product of mollusc studies!

Ložek states "molluscs are so widespread and common in loess that the presence of shells has to be seen as one of the main characteristics of loess". This statement may be biased by his own experience of central European mollusc assemblages, where this finding holds true. However, not noticing shells from an outcrop does not imply the absence of any shells in a loess sample, as they have a great variability in size. Ložek further states that the "largest number of finds is indisputably known from the loess areas of Germany and Czechoslovakia". This statement is clearly not precise enough. Is he considering the number of shells, i.e. abundance? Or is he considering the number of species, i.e. richness? There are other more precise ecological indices allowing for a description of mollusc communities, like diversity and equitability, which refers to the ecosystems they live in. Therefore, the conclusion reached can be totally different. Ložek's vague statement may, however, simply be reflecting the state of the art of terrestrial mollusc studies at that time. Expanding the geographical range of his statement, he acknowledges the lack of useful information from Asia and indicates a kind of parallelism of North American loess mollusc faunas with the ones from Europe, with "many developmental traits … specific to America". Although loess mollusc faunas have been identified in Chinese loess series, loess mollusc faunas in North America indeed show similar characteristics to those of Europe but with properties inherited from biological evolution: different species of the same genus but showing almost identical ecological requirements. Similarly, Ložek refers to the fading of the loess faunas towards the south, concluding that loess had been deposited with its associated mollusc faunas living in the sediment, although under different climate conditions. This leads Ložek to conclude that there must have been different climate zones in the Quaternary.

To explain the lack of efficient comparison with other regions, Ložek lists four reasons, which are still relevant and valid today. He emphasises the very need for careful observation of the shells and determination of the species. The identification at the species level is not always easy, and some variability exists in the shape and ornamentation of the shell of a single species. Careless and surficial investigations of the shells can significantly change the interpretation of a mollusc assemblage, which Ložek pointed out. This resulted in the identification of mollusc assemblages, named after key species, basically the *Pupilla* and the *Columella* faunas, with variations in their composition resulting from environmental conditions and geographical locations. Ložek summarised this interpretation, which is commented on in Table 1.

Making a turn to Asian loess, Ložek states that it "could perhaps be argued that loess in Asia formed under different conditions … and that the term mentioned should refer primarily to this environment". Over the last few decades it has been demonstrated that one ought to remove the "perhaps"; i.e. Asian loess did indeed form under different conditions with different sources than those of European loess.

Defining subzones among the loess landscapes, Ložek indicates that loess deposits mainly occurred in dry and low-elevation areas. Indeed, recent studies (e.g. Rousseau et al., 2014) have demonstrated that at least in Europe loess was deposited at lower elevations in relation to the dust transport dynamics and that the source of the transported material is mostly regional or local. Therefore, Ložek correctly speaks of fairly uniform faunas from a fairly uniform environment. However, he reconciles with the soil hypothesis by stating that the "fauna of the loess phases thus clearly testifies to peculiar soil conditions, and confirms that the loess is to be regarded not only as a product of wind sedimentation but also of a specific soil-forming process".

Ložek further tries to summarise the complexity of the loessification process, still referring to the presence of molluscs as a key indicator: "The mollusc analyses showed that the soil and environmental conditions were really quite peculiar and that the assumption of a special loessification process seems completely justified". Such a statement could be given nowadays without relying on the mollusc analyses, especially from sequences or deposits where there are no snails reported. However, the peculiarity of the mollusc assemblages was key to characterising the loess environments. From that, Ložek drew four general conclusions that are still valid even if the third one needs to be discussed a little more.

1. Ložek states, "thanks to the loessification process … The $CaCO_3$ precipitation and the specific iron compounds, which determines the colour of the loessification products, are characteristics features". The pale yellow colour of the unstratified loess units and the presence of carbonate concretions, the loess dolls, are indeed characteristic features allowing the clear identification of loess layers as described initially by von Leonard (Smalley et al., 2001).

2. Ložek states, "the formation of loess is not only due to the accumulation of dust". This is a correct statement! This assumption, however, was only expressed years later by Pecsi in his paper "Loess is not just the accumulation of dust" (Pecsi, 1990).

3. Ložek states, "the particular chemistry of loess deposits and weathering products allow the appearance and proliferation of some steppe molluscs and apparently also characteristic vegetation". I would rather reverse the arguments: the particular vegetation allows the appearance and proliferation of mollusc populations. Mollusc individuals and species grow and develop because environmental conditions allow them to do so: with vegetation not only to feed on but also to use to hide from temperature and precipitation variations. Moreover, the occurrence of carbonate in the dust or the soil would also favour the development of mollusc populations.

Table 1. Comments on Ložek's original statements about the loess mollusc faunas.

Original statement	Validity	Comment
(1) "The loess faunas represent closed autochthonous populations, which have no analogy in the present".	Partly yes	The *Pupilla* fauna fits with this statement, especially because of the particular association of the various *Pupilla* species, while the *Columella* fauna does not, as similar communities can partly be found presently in Europe.
(2) "They consist of a relatively small number of cold-hardy species, which indicate open, largely wood-free formations (and can live today in cold steppes, tundra as well as in the high mountains)".	Yes	This statement refers to a longitudinal and latitudinal knowledge and interpretation of the modern distribution of the species at that time that has evolved since then and that I used later in proposing reconstructing quantitative estimates of past temperatures and precipitation.
(3) "The mollusc fauna is characterised by a few special species that occur almost exclusively in loess; species common elsewhere are also represented by special races and forms and often have different ecological requirements compared to the present".	Yes	In fact, using biometry, I have demonstrated the occurrence of ecophenotypism not only in modern populations of *Pupilla muscorum* but also in fossil ones, especially in loess series with higher shells present in glacial deposits or more continental conditions, while shorter ones prevailed in interglacial units or in western environments (Rousseau, 1997). Similar variations have also been noticed with other eurytherm species like *Trochulus hispidus* (formerly *Trichia hispida*) or *Succinea oblonga*, present also in loess mollusc fauna through the *S. oblonga* elongate form in layers corresponding to the coldest conditions.
(4) "On the basis of detailed analyses of loess faunas, a whole series of mollusc communities have been distinguished, some of which are bound to certain areas, others to certain biotopes (e.g. through different relief conditions)".	Roughly speaking yes	This is correct, and one can follow the time evolution of the ecosystems in time from interglacial to glacial ones (Rousseau, 1987). Among the latter, "the loess fauna forms a closed monotonous unit that is clearly distinguishable from all other Quaternary mollusc communities". Rather than monotonous, I would rather qualify the loess fauna as particular as one could immediately refer to particular environmental conditions.
(5) "A loess fauna with the described characteristics is distributed in a huge area, in which currently very diverse mollusc communities live, which indicates a far-reaching leveling of the environmental conditions, which has no analogy in other sections of the Quaternary".	Yes	Loess deposits are capping worldwide areas, especially in the Northern Hemisphere corresponding to glacial open landscapes with very little vegetation. Such general environmental characteristics induce biomes that are relatively homogenous with slight local or regional adaptations, what Ložek calls "loess biotopes or loess environment". This is far different from environmental conditions mostly corresponding to interglacial conditions during which the local and regional specificities took over and which are expressed by more specialised and diverse biomes (here the association of vegetation and fauna).

However, it is possible to observe modern terrestrial snails living in a more acidic environment, but under such conditions, they often show very thin and fragile shells that will not be preserved after the death of the animal. Moreover, later Ložek states "the loess environment is especially favourable for snails but the species richness is quite limited due to harsh climate and aridity". A loess environment is favourable for snails if there is enough carbonate available to build their shells. In addition, the notion of harsh climate appears rather vague.

Apparently, Ložek refers to temperature, but as this is a limiting factor in general, some species can endure various temperature minimums, allowing them to be observed at very high latitudes or elevation. As a complement to these points, one should refer to the main limiting factors that constrain the growth of terrestrial molluscs found in the loess deposits: the impacts of both temperature and hibernation. Other factors like precipitation, moisture, and dust can also impact the growth of the terrestrial molluscs. Knowing these limitations allows us to understand the low number of species able to face the drastic environmental and climatic conditions under which the loess was deposited. In fact, loess faunas are composed theoretically of mollusc species, which are either eurytherm (large temperature range tolerance) or stenothermic (limited and specific temperature range tolerance). However, precipitation has been a second important limiting factor. This has been demonstrated by comparing loess faunas over Europe, showing a strong reduction in the richness westwards. Therefore, one ought to speak in terms of seasonality, especially of the interval from spring to autumn when the molluscs have some metabolic activity.

4. Ložek states, “the formation of loess and loess-like formations is thus closely linked to specific climatic and vegetation conditions”. This ought to be more precise. In fact, only during cold and glacial conditions are deflation areas created, which is a prerequisite for the production of aeolian material. In general, those areas are outwashes of glaciers or ice sheets, moraines, and riverbeds. The vegetation is important not only in the deposition area to trap the aeolian dust but also in the deflation area, in the emission process. Modelling studies (Sima et al., 2013) have demonstrated that if the vegetation is too high, later in spring, the aeolian material cannot be emitted and therefore transported. Conversely, if the vegetation has not grown enough but the ground is still frozen, the aeolian material cannot, irrespective of wind speed, be emitted.

In addition, Ložek discusses the hypothesis of interglacial loess, known today as typically a glacial sediment. He also states, “It is equally misleading to compare the present conditions in the alpine region of Central Europe mountains with the conditions of other areas during the loess phases”. This is only true with regard to the average annual temperature but does not apply to the humidity, which is very high in the mountains, while the loess climate must have been arid. Although such a statement may be appropriate concerning temperature, the degree of aridity must be questioned. Indeed, there must have been some seasonality allowing the vegetation to grow in spring and thus to trap the aeolian material (Sima et al., 2013).

Ložek discusses further what is called the loess interlayers, mostly found in pedocomplexes, which themselves are related to odd marine isotope stages (Kukla, 1977), and highlights the importance of the precise observation of the outcrop stratigraphy. This could be considered a misleading interpretation of the interglacial loess hypothesis. Indeed, some of these particular units have been named “markers” by Kukla (1977) and correspond to specific climate conditions. The best example is given from the Dolní Věstonice record of the last climate cycle, where several of these units have been described (Kukla and Ložek, 1961; Rousseau et al., 2013). In fact, when Ložek’s paper was published, interglacials were still interpreted as a single temperate episode, while later investigations demonstrated a much more complex history marked by the occurrence of stadials.

Ložek further points out the importance of aeolian activity “not being underestimated”. We know now that this activity is very basic as aeolian material is the source of the deposited material. This is indeed best evidenced when among the transported material elements, fossils or particular grains or granules, where characteristics of the source region can be found, supporting therefore the regional origin of the transported material.

Ložek also noted the bedding of some loess units. They are mostly related to slope deposits but may also be related to dust deposits on snow, resulting in such facies after the snow had melted. He states that, “at the time of loess accumulation at the foot of a slope, slope transport and the formation of coarser debris were limited to the lowest degree”. This appears logical because of not only the drier conditions of the dust deposition but also the substratum being frozen during most of the year, preventing major sediment movement. On the contrary, the soil complexes show units corresponding to slope deposits that were described by Kukla (1977) as pellet sands representing the erosion by heavy rains of sedimentary units deposited or developed on the slope itself. Other forms of laminations occur in western and eastern loess sequences, named “limon à doublets”, which are mostly post-sedimentary in origin.

Intense calcareous precipitation at the end of the cold periods is another misleading assumption by Ložek. In fact, the carbonate precipitation marks the lower limit of soil formation and development. The pedogenesis actually started at the top of the aeolian unit, after the dust accumulation had stopped, and produced large carbonate concretions at the base of the paleosols by leaching of the loess sediment. Therefore, precipitation of carbonates occurred during the interglacials and not at the end of cold periods.

With respect to loess deposition Ložek claims that “the entire environmental conditions at that time were very peculiar and … they have no equivalent in present day Europe”. He goes further by stating that loess characterises the late phases of highly glacial periods in the Pleistocene of Europe. We should amend this statement by saying that in general, loess is noticed and observed in deposits corresponding to glacial (odd marine isotope stages) or stadial conditions.

Some final reservations should be raised regarding one major point of Ložek's work: he claims that the mollusc fauna "differs sharply from all other cold and warm period communities, which is undoubtedly due to the condition of the substrate". According to present analyses and from the ecological requirement of the modern representatives of the identified species, this is not certain.

In conclusion, the present paper appeared 1 year after the release of Ložek's doctoral thesis "Quartärmollusken der Tschechoslowakei" (Ložek, 1964), in which he had developed many more points compared to what he addresses here. In his paper he chose to make his vision and the ones Czechoslovakian loess researchers had at that time visible to the international community. Ložek presented a detailed and complete state-of-the-art loess and mollusc study. This paper represents therefore an extraordinarily synthetic review, which still has a modern flavour as many of the aspects addressed remain relevant today. I am proud to have met Vojen Ložek in person several times and to have conducted fieldwork with him around Prague and in Moravia.

Acknowledgements. I would like to thank Frank Preusser, Markus Fuchs, and Christine Thiel for inviting me to participate in this very special tribute series and the anonymous reviewer for comments on the original draft. This is a LDEO contribution.

Financial support. The article processing charge was funded by the Quaternary scientific community, as represented by the host institution of *EGQSJ*, the German Quaternary Association (DEUQUA).

Review statement. This paper was edited by Christine Thiel and reviewed by one anonymous referee.

References

Kukla, G.: Pleistocene land-sea correlations. 1. Europe, Earth-Sci. Rev., 13, 307–374, 1977.

Kukla, G. and Ložek, V.: Loess and related deposits, in: Survey of Czechoslovak Quaternary, Czwartozed Europy Srodkowej i Wschodniej, INQUA 6th Int. Congr., Inst Geol Pr. Warszawa, 34, 11–28, 1961.

Ložek, V.: Quartärmollusken der Tschechoslowakei, Rozpr. Ustred. ustavu. Geol., Verlag der Tschechoslowakischen Akademie der Wissenschaften, Praha, 374 pp., 1964.

Ložek, V.: Das Problem der Lößbildung und die Lößmollusken, E&G Quaternary Sci. J., 16, 61–75, https://doi.org/10.3285/eg.16.1.05, 1965a.

Ložek, V.: Problems of analysis of the Quaternary nonmarine molluscan fauna in Europe, Geol. Soc. Am. Spec. Pap., 84, 201–218, 1965b.

Ložek, V.: The loess environment in Central Europe, in: Loess and related eolian deposits of the world, Linc. Univ. Press, 67–80, 1965c.

Pecsi, M.: Loess is not just the accumulation of dust, Quatern. Int., 7/8, 1–21, 1990.

Rousseau, D. D.: Paleoclimatology of the Achenheim Series (Middle and Upper Pleistocene, Alsace, France) – a Malacological Analysis, Palaeogeogr. Palaeoclim, 59, 293–314, 1987.

Rousseau, D. D.: The weight of internal and external constraints on *Pupilla muscorum* L. (Gastropoda: Stylommatophora) during the Quaternary in Europe, in: Past and Future Rapid Environmental Changes: The Spatial and Evolutionary Responses of Terrestrial Biota, edited by: Huntley B, Cramer, W., Morgan, A. V., Prentice, H. C., and Allen, J. R. M., Springer-Verlag, Heidelberg, 47, 303–318, 1997.

Rousseau, D.-D., Ghil, M., Kukla, G., Sima, A., Antoine, P., Fuchs, M., Hatté, C., Lagroix, F., Debret, M., and Moine, O.: Major dust events in Europe during marine isotope stage 5 (130–74 ka): a climatic interpretation of the "markers", Clim. Past, 9, 2213–2230, https://doi.org/10.5194/cp-9-2213-2013, 2013.

Rousseau, D.-D., Chauvel, C., Sima, A., Hatte, C., Lagroix, F., Antoine, P., Balkanski, Y., Fuchs, M., Mellett, C., Kageyama, M., Ramstein, G., and Lang, A.: European glacial dust deposits: Geochemical constraints on atmospheric dust cycle modeling, Geophys. Res. Lett., 41, 7666–7674, https://doi.org/10.1002/2014gl061382, 2014.

Sima, A., Kageyama, M., Rousseau, D.-D., Ramstein, G., Balkanski, Y., Antoine, P., and Hatté, C.: Modeling dust emission response to North Atlantic millennial-scale climate variations from the perspective of East European MIS 3 loess deposits, Clim. Past, 9, 1385–1402, https://doi.org/10.5194/cp-9-1385-2013, 2013.

Smalley, I. J., Jefferson, I. F., Dijkstra, T. A., and Derbyshire, E.: Some major events in the development of the scientific study of loess, Earth-Sci. Rev., 54, 5–18, 2001.

E&G Quaternary Sci. J., 70, 235–237, 2021
https://doi.org/10.5194/egqsj-70-235-2021

Open Access E&G Quaternary Science Journal

Retrospective

A tribute to Schwarzbach (1968): Recent ice age hypotheses

Jürgen Ehlers

Hellberg 2a, 21514 Witzeeze, Germany

Correspondence: Jürgen Ehlers (jehlersqua@outlook.de)

Relevant dates: Received: 1 August 2021 – Revised: 20 August 2021 – Accepted: 5 November 2021 – Published: 17 December 2021

How to cite: Ehlers, J.: A tribute to Schwarzbach (1968): Recent ice age hypotheses, E&G Quaternary Sci. J., 70, 235–237, https://doi.org/10.5194/egqsj-70-235-2021, 2021.

Special issue statement. This article is part of a special issue published on the occasion of the 70th anniversary of *E&G Quaternary Science Journal (EGQSJ)*. The special issue celebrates the journal's notable contribution to Quaternary research by revisiting selected milestone articles published in the long history of *EGQSJ*. The German Quaternary Association (DEUQUA) presents translations of the originals and critical appraisals of their impact in tandem anniversary issues of *DEUQUASP* and *EGQSJ*, respectively.

Original article: https://doi.org/10.3285/eg.19.1.21

Translation: https://doi.org/10.5194/deuquasp-3-79-2021

In Germany, Martin Schwarzbach is often regarded as the "father of palaeoclimatology". He published the results of his work in his book *Das Klima der Vorzeit* (*Climate of the past*). This standard work, which has gone through several editions, was first published in 1950. A Russian edition followed after 5 years, and a few years later the book was also translated into English. Schwarzbach dealt with the entire field of palaeoclimatology, and a large part of his work was devoted to the identification of the numerous climate indicators in the rocks of the Earth. His paper in *Eiszeitalter und Gegenwart* deals with only one aspect of his research, the ice ages, and specifically with the more recent ice age hypotheses.

Today, one can hardly imagine the technical difficulties Schwarzbach had to contend with at that time in order to work on a global scale. There were no computers and, importantly, there was no internet to gather new scientific information from all over the world. Schwarzbach nevertheless succeeded in gaining an overview of the palaeoclimatic development of the Earth and presenting it in an easily accessible way.

In 1968, there was no doubt that major ice ages had occurred repeatedly in the course of Earth's history. What was missing was a generally accepted timescale for the ice ages and also a comprehensive explanation for their causes. It was well known that there had been long-, medium-, and short-term climate fluctuations in the course of Earth's history. But only the traces of the more recent fluctuations within the last 600 million years were accessible for investigation. Not much was known about what had happened in the preceding six-sevenths of Earth's history, in the Precambrian. Nevertheless, the number of ice age hypotheses grew.

The article of Schwarzbach (1968) is a critical discussion of the then current hypotheses. The idea that the continents had changed their position in the course of Earth's history had been brought into play by Alfred Wegener long before, but as his theory had been rejected by his influential opponents Hans Cloos and Hans Stille, hardly anyone in Germany believed in it anymore (Hallam, 1975). Schwarzbach brings this theory back into the discussion. He points out that the shifting of the continents in the course of Earth's history is hardly doubted by geoscientists in Australia and in North and South America.

He briefly discusses the expansion of the Earth, which the physicist Pascual Jordan had postulated. At first glance, it seemed like an interesting idea that might explain, for example, the drifting apart of the continents. But this hypothesis contradicted geological findings.

Schwarzbach calls the idea put forward by geologist Johann Steiner as a possible cause for the formation of the ice ages "quite a funny hypothesis". According to Steiner, it takes 280 million years for our solar system to circle once around the centre of our Milky Way. The last three great ice ages were also separated from each other by roughly 280 million years. But that might still be coincidence. The assumed change in the gravitational constant in the course of this cycle was too small to trigger the ice ages.

Also, the importance of volcanic dust for climate fluctuations was considered rather small. Schwarzbach cites the Krakatau eruption of 1895 as evidence. And even the Tambora eruption of 1815, which was followed a year later by the so-called "year without a summer", did not result in any longer-lasting climatic consequences. And the alleged catastrophic volcanic eruption on the sub-Antarctic Thompson Island, with which the climatologist Lamb (1967) explained a series of cool years in New Zealand and southern Chile in 1967, was unproven. Today, we know that not only did the eruption never happen but also the island never existed (Dreyer-Eimbcke, 1990).

Schwarzbach knew that if one wanted to understand the ice age, one needed reliable age data. Milankovitch's radiation curve had offered a first possibility. But the fluctuations of Earth's orbital elements had existed at all times, even when there were no glaciers on Earth. Radiometric age determinations now provided a method to check at least the youngest part of the curve. At first it looked as if the results of the dating could be reconciled with the radiation curve. But the last glaciation maximum, for which a radiometric age of 18 000 years had been determined in the USA, seemed to be 7000 years younger than predicted by Milankovitch. In addition, the age known at that time of the last interglacial, the Eemian, of 70 kyr (Flint and Rubin, 1955) was 50 kyr younger than analysed shortly afterwards (Shackleton, 1969).

Apart from that, there was another problem. The continental stratigraphical sequences were too short and included too many gaps. But there were other, more complete sediment series provided by deep-sea drillings. Emiliani (1955) was able to publish a rough temperature curve for the most recent parts of the Pleistocene (Imbrie and Palmer Imbrie, 1979).

It was only the realisation that the sea floor was moving and thus driving plate tectonics (sea floor spreading) that brought continental drift back to the fore (Dietz, 1961; Vine, 1966). But in 1968 this realisation had not yet reached Germany. Very soon it would become clear that the study of drill cores from the Atlantic and the Pacific opened up the possibility of establishing a new basic framework for the climatic history of the Quaternary. But that was after 1968. Isotope stratigraphy based on deep-sea drillings was still in its infancy at the time.

However, Earth scientists had already begun to look for traces of past climate fluctuations in the ice itself. The first deep borehole in an ice sheet was drilled at Camp Century, an American military base on Greenland, in 1966. Low-resolution uncertainties about dating and lack of knowledge about the ice flow behaviour at the site of the drilling limited the value of the results. However, the borehole reached deep enough to yield an important first result. In the deepest samples from the borehole, ice was found that had been formed during the last interglacial. This proved that the Greenland ice sheet had not completely melted during the Eemian warm stage (Langway, 1967). And the borehole had shown the potential of studying ice cores (Dansgaard et al., 1969).

The first deep borehole in Antarctic ice was drilled at the American Byrd Station in 1968. When the results were compared with those from Camp Century, it became apparent that there was a strong correspondence between the cores from Antarctica and the Greenland cores. Our current understanding of the chronology of at least the Pleistocene dramatically improved with the first ice core drillings in Greenland in 1966 and in Antarctica in 1968, which showed the potential of studying these high-resolution archives (Dansgaard et al., 1969).

Together with the results of drill cores in the North Atlantic, short-term Dansgaard–Oeschger (D–O) cycles of 1000–2000 years with temperature jumps of 12 °C (Rahmstorf, 2003) and enormous instabilities of ice shields, so-called Heinrich events, linked to some of the D–O events are part of the high-resolution event stratigraphy of the last 100 kyr (INTIMATE). Antarctic ice cores ranging down to 800 ka (Wolff, 2008) provide data on the former greenhouse gas concentrations (CO_2, CH_4) in relation to temperature change, allowing researchers to establish better climate models with supercomputers.

This was far beyond Schwarzbach's knowledge. However, with his considerations on a "multilateral ice age formation" he emphasised the unsatisfactory conclusions of many of the then modern ice age hypotheses. As the sun's radiant force must have remained roughly constant over 600 million years, with the exception of minor fluctuations, the climate course must have been influenced by other factors according to Schwarzbach: "the profound geographical changes in the distribution of land and sea and in the relief, i.e. the constantly changing face of the Earth, changes in the CO_2 and water vapour content of the atmosphere, periodic changes in the elements of Earth's orbit, and dark clouds in space, but also continental drift and many other factors". The interaction of all these factors was seen by Schwarzbach as the cause of the small and large climate fluctuations in Earth's history in the sense of a multilateral ice age development. Moreover, Schwarzbach regarded continental drift as a main factor beside primary variations in solar radiation. Thus, he already had a deep understanding of the complexity of the climate system that is quite similar to our modern one, where the effects of plate tectonics and weathering processes (Raymo and Rudddiman, 1992) together with changes in Earth's orbit elements (Hays et al., 1976) provide reasonable explanations of the general pace of climate change (Ruddiman, 2014). Schwarzbach had already emphasised positive feedbacks when he regarded that "the initial formation of larger ice masses in the polar region certainly plays a decisive role due to the secondary cooling 'self-reinforcing' effects that are automatically coupled with it". Schwarzbach was open-minded when he did not even exclude the possibility of autocyclic processes and the "possibility that long-term and medium-term climate fluctuations may occur relatively independently of each other".

In 1968, Schwarzbach had not given up hope that a single, all-encompassing explanation for the phenomenon of the ice ages might be found. However, this has not yet been achieved (Ehlers et al., 2016).

Acknowledgements. I thank Phil Gibbard for his help with the translation. The anonymous reviewer made valuable suggestions.

Financial support. The article processing charge was funded by the Quaternary scientific community, as represented by the host institution of *EGQSJ*, the German Quaternary Association (DEUQUA).

Review statement. This paper was edited by Frank Preusser and reviewed by one anonymous referee.

References

Dansgaard, W., Johnsen, S., Møller, J., and Langway, C.: One Thousand Centuries of Climatic Record from Camp Century on the Greenland Ice Sheet, Science, 166, 377–381, 1969.

Dietz, R. S.: Continent and ocean basin evolution by spreading of the sea floor, Nature, 190, 854–857, https://doi.org/10.1038/190854a0, 1961.

Dreyer-Eimbcke, O.: Mythische und imaginäre Inseln des Atlantiks im Kartenbild, Mitteilungen der Geographischen Gesellschaft in Hamburg, 80, 651–681, 1990.

Ehlers, J., Hughes, P., and Gibbard, P. L.: The Ice Age, Wiley, Blackwell, Chichester, 548 pp., 2016.

Emiliani, C.: Pleistocene temperatures, J. Geol., 63, 538–578, available at: https://www.jstor.org/stable/30080906 (last access: last access: 6 December 2021), 1955.

Flint, R. F. and Rubin, M.: Radiocarbon dates of pre-Mankato events in eastern and central North America, Science, 121, 649–658, 1955.

Hallam, A.: Alfred Wegener and the Hypothesis of Continental Drift, Sci. Am., 232, 88–97, available at: https://www.jstor.org/stable/24949733 (last access: 6 December 2021), 1975.

Hays, J. D., Imbrie, J., and Shackleton, N.: Variation in the Earth's orbit: Pacemaker of the Ice Ages, Science, 194, 1121–1132, https://doi.org/10.1126/science.194.4270.1121, 1976.

Imbrie, J. and Palmer Imbrie, K.: Ice Ages – Solving the mystery, Harvard University Press, 224 pp., 1979.

Lamb, H. H.: The Problem of Thompson Island, Brit. Antarct. Surv. B., 13, 85–88, 1967.

Langway, C. C.: Stratigraphic analysis of a deep ice core from Greenland, CRREL Research Report 77, 185 pp., 1967.

Rahmstorf, S.: Timing of abrupt climate change: A precise clock, Geophys. Res. Lett., 30, 1510, https://doi.org/10.1029/2003GL017115, 2003.

Raymo, M. E. and Ruddiman, W. F.: Tectonic forcing of late Cenozoic climate, Nature, 359, 117–122, 1992.

Ruddiman W. F.: Earth's Climate: Past and Future, W.H. Freeman and Sons, New York, 445 pp., 2014.

Schwarzbach, M.: Das Klima der Vorzeit, Enke, Stuttgart, 211 pp., 1950.

Shackleton, N. J.: The last interglacial in the marine and terrestrial records, P. R. Soc. Lond. B-Bio., 174, 135–154, https://doi.org/10.1098/rspb.1969.0085, 1969.

Vine, F. J.: Spreading of the Ocean Floor: New Evidence: Magnetic anomalies may record histories of the ocean basins and Earth's magnetic field for 2×10^8 years, Science, 154, 1405–1415, https://doi.org/10.1126/science.154.3755.1405, 1966.

Wolff, E. W.: The past 800 ka viewed through Antarctic ice cores, Episodes, 31, 219–221, https://doi.org/10.18814/epiiugs/2008/v31i2/005, 2008.

E&G Quaternary Sci. J., 70, 239–242, 2021
https://doi.org/10.5194/egqsj-70-239-2021

Open Access E&G Quaternary Science Journal

Retrospective

A tribute to Menke (1970): Results of pollen analysis on the Pleistocene stratigraphy and the Pliocene–Pleistocene boundary in Schleswig-Holstein

Roberta Pini

CNR – Institute of Environmental Geology and Geoengineering (IGAG), Research Group on Vegetation, Climate and Human Stratigraphy, Laboratory of Palynology and Palaeoecology, Piazza della Scienza 1, 20126 Milan, Italy

Correspondence: Roberta Pini (roberta.pini@igag.cnr.it)

Relevant dates: Received: 28 June 2021 – Revised: 1 September 2021 – Accepted: 30 October 2021 – Published: 17 December 2021

How to cite: Pini, R.: A tribute to Menke (1970): Results of pollen analysis on the Pleistocene stratigraphy and the Pliocene–Pleistocene boundary in Schleswig-Holstein, E&G Quaternary Sci. J., 70, 239–242, https://doi.org/10.5194/egqsj-70-239-2021, 2021.

Special issue statement. This article is part of a special issue published on the occasion of the 70th anniversary of *E&G Quaternary Science Journal (EGQSJ)*. The special issue celebrates the journal's notable contribution to Quaternary research by revisiting selected milestone articles published in the long history of *EGQSJ*. The German Quaternary Association (DEUQUA) presents translations of the originals and critical appraisals of their impact in tandem anniversary issues of *DEUQUASP* and *EGQSJ*, respectively.

Original article: https://doi.org/10.3285/eg.21.1.01

Translation: https://doi.org/10.5194/deuquasp-3-87-2021

1 Introduction

The Quaternary history of Europe has been strongly influenced by the waxing and waning of ice masses and sea level oscillations. Climate change drove the behaviour of both ice sheets and sea levels and shaped terrestrial environments as far as land morphology, plant cover, fauna occurrence and diversity, and human migrations and survival were concerned. A major effort undertaken in the 20th century dealt with the assessment and the critical inventory of Quaternary stratigraphic units. Scientists paid great attention to the way in which environments have changed through time and how this topic can be investigated in stratigraphic records using a proxy-based approach. Among proxies, a robust descriptor of past terrestrial environments and climate is pollen. Pollen is almost ubiquitous in the vast majority of marine and terrestrial stratigraphic archives; it has huge fossilization potential due to its tough outer layer (exine) and can often be identified to a high taxonomic level of detail. In Europe pollen analytical investigations have been largely used to recognize warm and cold phases; biostratigraphical (pollen) data have then been used as a basis for time–stratigraphic subdivision and correlations of Quaternary sequences (i.e. Zagwijn, 1985).

Burchard Menke was a prominent German palynologist based at the Geological Survey of Schleswig-Holstein (in German, Geologisches Landesamt Schleswig-Holstein). Trusting in the robustness of the palynological approach, he explored German deposits of the Pliocene to Holocene, to obtain their hidden environmental and climatic message. In Menke's (1970) paper, the author provided a significant overview of the Pleistocene stratigraphy of Schleswig-Holstein and of the issues concerned. He published later papers adding more insights into the stratigraphic and the palaeoenvironmental context of the area during Pliocene and Quaternary times (Menke, 1975, 1976a; Stephan and

Menke, 1993), but research has continued since. Revisiting Menke's (1970) paper after more than 50 years implies having a closer look at the current state of the art of the pollen stratigraphical frame of Schleswig-Holstein to check how far his statements are still valid or instead need a substantial reappraisal.

2 Plio-Pleistocene pollen stratigraphy of Schleswig-Holstein – where are we after Menke's (1970) critical inventory?

Research published in the past decades provides new elements of further knowledge on the Quaternary palaeogeographic and palaeoenvironmental history of Schleswig-Holstein. I hereafter recall four of the issues raised in Menke's (1970) paper, aiming to put them in an up-to-date context.

1. "Only little information is available from Schleswig-Holstein about the course of the Weichselian Pleniglacial. It seems that there are hardly any deposits suitable for radiocarbon dating" (Menke, 1970, page 9).

   The application of luminescence dating techniques to sediments beyond the radiocarbon limit laid the foundation of the chronological frame of the Weichselian Pleniglacial in Schleswig-Holstein, the attribution of sedimentary bodies to distinct glacial advances and their correlation with adjacent areas. Evidence of an early Middle Weichselian glaciation, named the "Ellund Phase", were TL dated to between 59.4 ± 8.9 and 52.5 ± 7.9 ka (Marks et al., 1995) and later referred to OSL ages between 92 ± 24 and 61 ± 16 ka (Preusser, 1999). These ages, obtained in the early times of luminescence dating techniques and possibly in need of a revision with improved methodologies, are in agreement with those of the "Ristinge Glaciation" in Denmark (Houmark-Nielsen, 2007). The Ellund Phase was followed by a period of ca. 30 kyr of persisting cold climate with some minor milder breaks. During the Upper Weichselian several glacial advances are testified to in the area (Brandenburg, Frankfurt, Pomeranian and Mecklenburg phases; Litt et al., 2007), related to the development of Baltic ice streams covering northern Mecklenburg and part of Schleswig-Holstein (Stephan, 2014). Issues concerning the reliability of early luminescence ages (Frank Preusser, personal communication, 2021) and the nature and extent of Upper Weichselian glacial advances (Stephan, 2014) require further analysis.

2. "In Eemian deposits the oldest zones are generally only weakly represented" (Menke, 1970, page 6).

   Menke and Tynni (1984) investigated a 32 m thick lacustrine sequence from Rederstall (western Holstein) documenting the interval from the early Eemian to the second post-Eemian interstadial (Odderade). According to the authors, pollen spectra obtained from the basal centimetres of the core are dominated by *Pinus* and *Betula*, along with some reworked pre-Quaternary palynomorphs. As suggested by biostratigraphic data, a hiatus occurs immediately above these sediments, as highlighted by the lack of the beginning of the *Corylus* and *Quercus* curves, displaying in zone E IVa percent values of around 20 %–30 % and 10 %–20 %, respectively. A continuous sequence then follows, documenting the complete remaining interglacial succession and the Early Weichselian stadials and interstadials.

3. "We are still poorly informed about the Pre-Elsterian Pleistocene in Central Europe" (Menke, 1970, page 11).

   Stephan (2014) mentions the scarcity of Elsterian deposits in eastern Germany due to the fact that in most areas they were eroded by subsequent glacial advances and only limited bodies were preserved in depressions. According to Vinxs et al. (1997), besides an older till at the base of the Lieth sequence, glacial deposits had not yet reliably been attributed to pre-Elsterian time. Authors do not, however, exclude the possibility that northern Germany was reached by older glaciations, as actually testified to north of the Danish–German border by deposits attributed to an early Middle Pleistocene advance (Stephan, 2011).

4. What is the state of the art of correlation between the northern Germany and Dutch Early Pleistocene?

   The Early Pleistocene Lieth sequence, recovered from a limestone pit, was investigated by Menke (1970, 1975) and correlated first with the Quaternary series of the Netherlands elaborated by Zagwijn (1960) and then with the Lower Rhine sequence by Urban (1978) (Stephan and Menke, 1993). In revising the stratigraphical terms adopted for glaciated areas in northern Germany, Litt et al. (2007) recall the monumental work done by Menke on cores and sections and recognize that the criteria for palaeoclimatic subdivision into cold and warm stages largely relies on palynology. According to these authors, most of the correlations proposed by Menke between northern Germany and the Dutch Early Pleistocene are valid. Moreover, the pollen records elaborated by Menke and colleagues during the late 1960s–1970s later provided some Early Pleistocene stratotypes, such as the Kaltenhörn-Kaltzeit (Kaltenhörn Cold Stage), the Ekholt-Kaltzeit (Ekholt Cold Stage) and the Nordende-Warmzeit (Nordende Warm Stage).

According to Stephan (2014), the correlation of the Lieth sequence with the Dutch series is questionable in some parts. The main issues refer to the lack of a clear chronostratigraphic framework at Lieth (magnetostratigraphy failed because of a weak signal of magnetic grains in sands between organic beds) and to the limited continuity of the Dutch series, not yet found in complete superposition. Further elements of concern were addressed by Menke (1975) and later on recalled by Kemna and Westerhoff (2007); according to these authors, facies-related features of sedimentation hamper any robust correlation among the series.

3 Final remarks

Generations of students and scholars dealing with the Pleistocene pollen stratigraphy of northern Germany have undoubtedly come across Menke's (1970) paper. The paper presented a clear overview of the state of the art for Schleswig-Holstein: most of the statements provided by the original author are still valid. Substantial reappraisals mostly depend on the following:

- The development and application of new dating techniques, not yet in use in the late 1960s–early 1970s, are now available. As mentioned by Wintle (2008), OSL dating techniques were developed in 1985; 1999 was a year of further development, with the set-up of procedures for fast bleaching of single aliquots of quartz and instrumental improvements. The application of OSL methods to Weichselian stratigraphies allowed for setting them into a chronological frame, well beyond the limits of the radiocarbon method in use at that time. However, many of the sections mentioned by Menke (1970) and following authors still deserve proper attention as far as their age attribution by OSL is concerned.

- The increased number of investigated sequences has improved the quantity and quality of the available information, essential for a robust reconstruction of the complex stratigraphic and palaeoenvironmental history of Schleswig-Holstein. Other sites will hopefully be investigated in the future, and they will undoubtedly increase the level of knowledge that has been reached up to the present day.

Finally, as a palynologist who was initially trained on the Early Pleistocene sequence of Leffe (northern Italy), let me express sincere, although posthumous, thanks to Menke for the compilation of an important photographic atlas (Menke, 1976b). This book contains almost 1000 microphotographs of pollen grains and spores that he identified in Pliocene to Early Pleistocene deposits. Palynologists often face difficulties in finding appropriate iconographic documentation of palynomorphs of that age; Menke's atlas is of great help in this regard, and it is highly recommended in all pollen labs.

Acknowledgements. Thanks are due to Frank Preusser and to Philipp Stojakowits for suggestions.

Financial support. The article processing charge was funded by the Quaternary scientific community, as represented by the host institution of *EGQSJ*, the German Quaternary Association (DEUQUA).

Review statement. This paper was edited by Frank Preusser and reviewed by Philipp Stojakowits.

References

Houmark-Nielsen, M.: Extent and age of Middle and Late Pleistocene glaciations and periglacial episodes in southern Jylland, Denmark, B. Geol. Soc. Denmark, 50, 9–35, https://doi.org/10.37570/bgsd-2007-55-02, 2007.

Kemna, H. A. and Westerhoff, W. E.: Remarks on the palynology-based chronostratigraphical subdivision of Pliocene terrestrial deposits in NW-Europe, Quatern. Int., 164–165, 184–196, https://doi.org/10.1016/j.quaint.2006.10.017, 2007.

Litt, T., Behre, K.-E., Meyer, K.-D., Stephan, H.-J., and Wansa, S.: Stratigraphische Begriffe für das Quartär des norddeutschen Vereisungsgebiete, E&G Quaternary Sci. J., 56, 7–65, https://doi.org/10.23689/fidgeo-1278, 2007.

Marks, C., Piotrowski, J. A., Stephan, H.-J., Fedorowicz, S., and Byìutrym, J.: Thermoluminescence indications of the Middle Weichselian (Vistulian) Glaciation in northwest Germany, Meyniana, 18, 35–42, 1995.

Menke, B.: Ergebnisse der Pollenanalyse zur Pleistozän-Stratigraphie und zur Pliozän-Pleistozän-Grenze in Schleswig-Holstein, E&G Quaternary Sci. J., 21, 5–21, https://doi.org/10.3285/eg.21.1.01, 1970.

Menke, B.: Vegetationsgeschichte und Florenstratigraphie Nordwestdeutschlands im Pliozän und Frühquartär mit einem Beitrag zur Biostratigraphie des Weichselfrühglazials, Geol. Jb. Hannover, A26, 3–151, 1975.

Menke, B.: Neue Ergebnisse zur Stratigraphie und Landschaftsentwicklung im Jungpleistozän Westholsteins, E&G Quaternary Sci. J. (formerly Eiszeitalter und Gegenwart), 27, 53–68, https://doi.org/10.23689/fidgeo-1666, 1976a.

Menke, B.: Pliozäne und ältestquartäre Sporen- und Pollenflora von Schleswig-Holstein, Geol. Jb., Hannover, A32, 3–127, 1976b.

Menke, B. and Tynni, R.: Das Eeminterglazial und das Weichselfrühglazial von Rederstall/Dithmarschen und ihre Bedeutung für die mitteleuropäische Jungpleistozän-Gliederung, Geol. Jb., Hannover, A76, 3–120, 1984.

Preusser, F.: Lumineszenzdatierung fluviatiler Sedimente; Fallbeispiele aus der Schweiz und Norddeutschland, Kölner Forum für Geologie und Paläontologie, 3, 1–62, 1999.

Stephan, H.-J.: Geschiebestratigraphische Untersuchungen im Bereich der Stauchmoräne Kisdorfer Wohld, Südholstein und in ihrem Hinterland, Geschiebekunde aktuell. Sonderh., 9, 113–124, 2011.

Stephan, H.-J.: Climato-stratigraphic subdivision of the Pleistocene in Schleswig-Holstein, Germany and adjoining areas, E&G Quaternary Sci. J., 63, 3–18, https://doi.org/10.3285/eg.63.1.01, 2014.

Stephan, H.-J. and Menke, B.: Das Pleistozän in Schleswig-Holstein, Geologisches Landesamt Schleswig-Holstein, 3, 19–62, 1993.

Urban, B.: Vegetationsgeschichtliche Untersuchungen zur Gliederung des Altquartär der Niederrheinischen Bucht, Sonderveröffentlichungen des geologischen Instituts der Universität Köln, Köln, 34, 1–165,, 1978.

Vinxs, R., Grube, A. T., and Grube, F.: Lithologie, Geschiebeführung, und Geochemie eines Prä-Elster I-Tills von Lieth bei Elmshorn, Leipziger Geowissenschaften, Leipzig, 5, 83–103, 1997.

Wintle, A. G.: Fifty years of luminescence dating, Archaeometry, 50, 276–312, https://doi.org/10.1111/j.1475-4754.2008.00392.x, 2008.

Zagwijn, W. H.: Aspects of the Pliocene and early Pleistocene vegetation in the Netherlands, Mededelingen van de Geologische Stichting, Ser. C-III-1, 1–78, 1960.

Zagwijn W. H.: An outline of the Quaternary stratigraphy of the Netherlands, Geol. Mijnbouw, 64, 17–24, 1985.

E&G Quaternary Sci. J., 70, 243–246, 2021
https://doi.org/10.5194/egqsj-70-243-2021

Open Access E&G Quaternary Science Journal

Retrospective

A tribute to Rohdenburg (1970): Morphodynamic activity and stability phases instead of pluvial and interpluvial times

Dominik Faust[1] **and Markus Fuchs**[2]

[1]Institute of Geography, TUD, Dresden, 01062, Germany
[2]Department of Geography, Justus Liebig University, Giessen, 35390, Germany

Correspondence: Dominik Faust (dominik.faust@tu-dresden.de)

Relevant dates: Received: 21 May 2021 – Revised: 2 July 2021 – Accepted: 30 October 2021 – Published: 17 December 2021

How to cite: Faust, D. and Fuchs, M.: A tribute to Rohdenburg (1970): Morphodynamic activity and stability phases instead of pluvial and interpluvial times, E&G Quaternary Sci. J., 70, 243–246, https://doi.org/10.5194/egqsj-70-243-2021, 2021.

Special issue statement. This article is part of a special issue published on the occasion of the 70th anniversary of *E&G Quaternary Science Journal (EGQSJ)*. The special issue celebrates the journal's notable contribution to Quaternary research by revisiting selected milestone articles published in the long history of *EGQSJ*. The German Quaternary Association (DEUQUA) presents translations of the originals and critical appraisals of their impact in tandem anniversary issues of *DEUQUASP* and *EGQSJ*, respectively.

Original article: https://doi.org/10.3285/eg.21.1.07

Translation: https://doi.org/10.5194/deuquasp-3-101-2021

1 Scientific background

In 1970 Heinrich Rohdenburg (Rohdenburg, 1970) published an article entitled "Morphodynamic activity and stability times instead of pluvial and interpluvial times", which had a lasting influence on the disciplines of Quaternary geology and geomorphology up to the present day. At that time, Quaternary geologists and geomorphologists had hardly any reliable data on palaeoclimatic conditions and effects of the subtropical and tropical zones. For this reason, Rohdenburg's publication is based primarily on hypothetical considerations and conceptual models that he developed against the background of the state of research at that time. It was assumed that during the Quaternary period, and especially during the last cold period in Central Europe, the climate was characterized by cyclical changes. This finding was the basis for the division of the glacial periods into stadials and interstadials. However, he observed that the glacial climate fluctuations, as assumed for Central Europe, could not be transferred to tropical and subtropical zones due to a lack of detailed stratigraphic evidence from these zones. With his publication, based on his own observations, Rohdenburg was one of the first to postulate effective morphodynamic Quaternary climate fluctuations for the subtropics and tropics.

In his early years Heinrich Rohdenburg was considered to be an admirer of Julius Büdel's theses. With the inclusion of relevant scientific disciplines, he was able to significantly deepen Büdel's basic idea of climatic geomorphology and present this new concept in his textbook *Introduction into climate-genetic geomorphology* (*Einführung in die klimagenetische Geomorphologie*; Rohdenburg, 1971, reprint in 2006). In doing so, he partially refuted Büdel's theses. In contrast to Büdel, who attributed the relief of the tropics to processes operating up to 100 million years and who assigned older processes of landform development mainly to epirogenic deformation (Büdel, 1981, p. 198), Rohdenburg proposed that climate and climate change were the most important factors controlling landform development. He recognized that in the mid-latitudes, the glacial periods, with powerful thermal fluctuations, resulted in landform change during periglacial conditions. In particular, he recognized that recent studies of loess–palaeosol sequences from Central Europe revealed multiple climatic changes over the last glacial period. Rohdenburg assumed – correct according to current understanding – that changes in morphodynamics in the tropics and subtropics were not likely to be controlled by such processes but instead mainly by precipitation changes. However, according to the concepts prevailing at that time, it was still assumed that erosion in the lower latitudes was continuous and that changes in geomorphological activity were mainly triggered by tectonic impulses (e.g. uplifted marine terraces).

Rohdenburg was able to comprehensibly refute this thesis by using the evidence from calcareous crusts in subtropical arid regions. As a result of intensive scientific discussion with colleagues working on soil formation, Rohdenburg proposed a new concept for the origin of calcareous crusts in subtropical drylands, for which he regarded alternations of climate as a basic condition for their development. According to the state of knowledge at that time, it was still assumed that $CaCO_3$ crusts in drylands were formed by ascending soil water, in which $CaCO_3$ is dissolved in the subsoil and transported to, and precipitated at, the surface by rising soil water movement. Rohdenburg, on the other hand, inferred that the $CaCO_3$ crusts were formed under more humid conditions by percolating water (p. 84) decalcifying the soil parent material. He then proposed that subsequent aridity would result in a thinner vegetation cover, leading to erosion of the topsoil, and the $CaCO_3$ horizon would be exposed and subsequently hardened by overland flow. Based on subsequent detailed studies of calcareous crust formation in the subtropical zones, this finding has become widely accepted, although incomprehensibly, many still assume that most of the calcareous crusts in arid regions are the result of ascending groundwater.

2 Climate fluctuations and morphodynamic effects

Climatic geomorphology (Rohdenburg, 2006) refers exclusively to the relief formed by fluvial processes (*fluviale Abtragungsrelief*). Mensching (1955) introduced this concept and assumed that climate induced changes in relief in the subtropics based on the presence of "very old" slope debris covers, which were considered to have been deposited in a pluvial period. This concept of pluvial periods originates from the idea that during glacial periods the climatic zones shifted southwards so that, for instance, the Mediterranean region was characterized by a climate like that of Central Europe today. Rohdenburg strongly doubted and rejected this assumption because he predicted that climate fluctuations would also occur in the Mediterranean region within a "pluvial period" – analogous to stadials and interstadials in Central Europe. He concluded that geomorphological activity, and in particular rates of slope formation, is a response to climate change. From this basic reasoning Rohdenburg developed the concept of times of morphodynamic activity and stability. The "morphodynamic active phase" is characterized by pronounced denudation, erosion and surface runoff under semi-arid conditions, while a "morphodynamic stable phase" is characterized by soil formation and linear incision of the fluvial system with a more humid climatic regime.

According to Rohdenburg, there is no actualistic counterpart for morphodynamic activity. He assumed more accentuated precipitation for this morphodynamic active phase, with high surface runoff and strong soil erosion, especially during heavy rainfall events. He postulates that these conditions do not occur anywhere at present largely because he had no access to numerical dating that could have provided a time span for the "event-related arid morphodynamics" and an estimation of the duration of their total forming power.

3 Originality from today's perspective

The topicality of Rohdenburg's publication, which was both innovative and groundbreaking for its time, is not only demonstrated by the concept of alternating, climatically induced, morphodynamic "activity and stability phases" but also by the many suggestions which today stimulate scientific discussion, something that could not be perceived at the time. Examples of this are as follows:

- He made clear in his article that a multidisciplinary approach has many advantages (p. 84), the approach that underpins modern research in geosciences.
- The "tipping over" of the ecological system anticipates the term "threshold" and the recently much-cited term "tipping point" (p. 87, Lenton et al., 2019).
- Rohdenburg attributes the "overturning" of the system to self-reinforcing processes within the geomorphodynamic system which are in particular climatically induced.
- The so-called "pluvial period" north and south of the Sahara, but also in the Mediterranean region, was characterized by significantly higher aridity (pp. 92 and 94) with high annual variation in precipitation and morphodynamically effective heavy rainfall events. Rohdenburg subsequently rejected the term "pluvial period".
- Climate change and morphodynamic changes are asynchronous. However, morphodynamic activity becomes out of phase with climate forcing because vegetation cover can delay the response of the geomorphological system (see also Vicente-Serrano et al., 2013). With respect to the effects of vegetation cover Rohdenburg used the expressions "with its exceedingly effective capacity" (p. 88) and great "fighting power" (p. 93). The idea

of a time lag between climate change and system change is highly relevant today.

- Rohdenburg stressed the importance of vegetation as a central controlling factor for geomorphological systems, and today, numerous research projects are focused on the role of biology in earth surface processes. This importance is also reflected in the increasing importance of biogeomorphology.

- The so-called geomorphological partial activity (*Teilaktivität*) marks a spatial and/or temporal system transition, a topic that determined the scientific debate as the motto of the DEUQUA conference in Dresden in 2016.

The list stresses that Rohdenburg always endeavoured to integrate aspects of soil science, vegetation science and climatology into his understanding of morphodynamics. This reflects his contacts with highly regarded scientists such as Ernst Schönhals from Giessen and Brunk Meyer from Göttingen, who mainly worked on soil formation, as well as with the geobotanist Heinz Ellenberg from Göttingen, Quaternary geologist Arno Semmel from Frankfurt and, last but not least, with the well-known climatologist Hermann Flohn from Bonn. Heinrich Rohdenburg emphatically stressed how much he benefited from neighbouring disciplines and called for active interdisciplinary cooperation in order to strengthen the disciplines of landscape ecology and geomorphology in general.

4 Critical points

Heinrich Rohdenburg repeatedly pointed out that there was a lack of quantitative analyses to distinguish, for example, morphodynamically active phases in the dry subtropics and dry tropics from those of the semi-humid and inner tropics and the Mediterranean subtropics. The relationship between erosion rates and the mean annual precipitation had already been demonstrated quantitatively by Langbein and Schumm (1958). Rohdenburg refers to this in Fig. 1 of his article and states that in desert margins, mean annual precipitation would have to increase to generate morphodynamic activity, whereas in the (semi-)humid tropics of the tree savannas it would have to decrease to allow comparable processes to take place. The validity of this statement is readily apparent from the diagram in Langbein and Schumm (1958, Fig. 2). Thus, without doubt, the decrease and increase in the mean annual precipitation can lead to the same geomorphological effects depending on the climate of the reference point. Rohdenburg's thoughts remain open as to whether the climatic conditions for activity times during the Quaternary were synchronous in the corresponding climatic zones, for instance in the course of the shift of the climatic zones.

Although Rohdenburg had extensive international contacts, these were primarily with his colleagues in geomorphology and Quaternary geology. For this reason, the concepts of "rhexistasia" and "biostasia", which Erhart (1955) published in a remarkable essay, were unnoticed by Rohdenburg. Erhart (1955) anticipates Rohdenburg's considerations and states that under favourable climatic conditions soil formation takes place under a stable vegetation cover ("biostasy"), whereas more arid conditions result in thinning of the vegetation and increased soil erosion ("rhexistasia"). Since there was little contact with French soil scientists and biologists, Rohdenburg had no knowledge of this essay.

The lack of numerical dating at that time meant that Rohdenburg was unable to grasp the significance of duration for a morphodynamic process, and duration was therefore neglected in Rohdenburg's hypothetical discussions or was viewed from a strongly actualistic perspective. Ultimately, the lack of quantitative analyses and the lack of reliable data made a continuation and verification of Rohdenburg's conceptual model – as he himself noted – impossible at the time.

5 Implications for today's geosciences

The concept of alternation between phases of morphodynamic activity and those of morphodynamic stability is nowadays widely accepted as an indispensable part of geomorphological knowledge. Rohdenburg was mainly interested in the geomorphological process with respect to an alternating climate and less with the dating of the morphodynamic phases. Today, the dating and timing of morphodynamic phases has become possible due to significantly improved methodology. Climate archives, which are available with very good chronological resolution (e.g. Svensson et al., 2008), provide a reference. This has shifted the scientific focus to a comparison with well-dated sedimentary sequences, particularly with respect to the synchronicity of measurable geochemical or geophysical features that show similar cyclic patterns in the respective archives. These relationships are often uncritically interpreted as synchronous events, even though the archives are located in different climatic zones. Rohdenburg addresses this problem in his paper in a prescient way, suggesting that climate change can generate different morphodynamic processes in different climatic zones ("divergence phenomenon" according to Schumm, 1991). Using the example of soil water balance, he shows that climate change can lead to an improvement in soil water balance with associated soil formation in one climatic zone and to increased erosion with unfavourable soil water conditions in an adjacent climatic zone (p. 81), thus resulting in contrary morphodynamic processes. Furthermore, Rohdenburg assumes that the morphodynamic system changes in the tropics and subtropics caused by Quaternary climate change may not have occurred simultaneously.

Rohdenburg's concept is nowadays cited not only in the context of longer climatic cycles but also with respect to short-term climatic fluctuations in the Holocene (Faust and Wolf, 2017). The idea of alternating morphodynamic phases is as ingenious as it is timeless, and Rohdenburg's concept explains the change in geomorphological processes through time within a climatic zone and in relation to a certain geomorphological form (e.g. glacis). Basically, Rohdenburg developed his ideas on the basis of his own observations and fieldwork. It is due to his scientific creativity and his holistic perspective that we today have several groundbreaking conceptual essays (cf. Rohdenburg, 1983). Likewise, hypothetical discussions and the development of concepts published in large numbers in the German Quaternary journal *Eiszeitalter und Gegenwart* (*E&G*; today *EGQSJ*) have stimulated long-lasting scientific progress.

Acknowledgements. We would like to express our sincere thanks to Jim Rose and Ludwig Zoeller for improving our manuscript.

Financial support. The article processing charge was funded by the Quaternary scientific community, as represented by the host institution of *EGQSJ*, the German Quaternary Association (DEUQUA).

Review statement. This paper was edited by Frank Preusser and reviewed by Ludwig Zoeller.

References

Büdel, J.: Klima-Geomorphologie, 2. Auflage, Gebrüder Borntraeger, Berlin – Stuttgart, 304 pp., 1981.

Erhart, H.: "Biostasie" et "rhexistasie": esquisse d'une theorie sur le rôle de la pedogenese en tant que phenomene geologique, C. R. Acad. Sci., 241, 1218–1220, 1955.

Faust, D. and Wolf, D.: Interpreting drivers of change in fluvial archives of the Western Mediterranean – A critical view, Earth Sci. Rev., 174, 53–83, 2017.

Langbein, W. B. and Schumm, S. A.: Yield of Sediment in Relation to Mean Annual Precipitation, Am. Geophys. Union Trans., 39, 1076–1084, 1958.

Lenton, T. M., Rockström, J., Gaffney, O., Rahmstorf, S., Richardson, K., Steffen, W., Schellnhuber, H. J.: Climate tipping points – too risky to bet against, Nature, 575, 592–595, 2019.

Mensching, H.: Karst und Terra Rossa auf Mallorca, Erdkunde, 9, 188–196, 1955.

Rohdenburg, H.: Morphodynamische Aktivitäts- und Stabilitätszeiten statt Pluvial- und Interpluvialzeiten, E&G Quaternary Sci. J., 21, 81–96, https://doi.org/10.3285/eg.21.1.07, 1970.

Rohdenburg, H.: Beiträge zur allgemeinen Geomorphologie der Tropen und Subtropen. Geomorphodynamik und Vegetation – Klimazyklische Sedimentation – Panplain/Pediplain-Pediment-Terrassentreppen, Catena, 10, 393–438, 1983.

Rohdenburg, H.: Einführung in die Klimagenetische Geomorphologie, 3. Auflage, Catena-Verlag, Stuttgart, ISBN 978-3-923381-53-1, 352 pp., 2006 (reprint from 1971).

Schumm, S. A.: To interpret the Earth – Ten ways to be wrong, Cambridge University press, Cambridge, 0-521-39507-0, 133 pp., 1991.

Svensson, A., Andersen, K. K., Bigler, M., Clausen, H. B., Dahl-Jensen, D., Davies, S. M., Johnsen, S. J., Muscheler, R., Parrenin, F., Rasmussen, S. O., Röthlisberger, R., Seierstad, I., Steffensen, J. P., and Vinther, B. M.: A 60 000 year Greenland stratigraphic ice core chronology, Clim. Past, 4, 47–57, https://doi.org/10.5194/cp-4-47-2008, 2008.

Vicente-Serrano, S. M., Gouveia, C., Camarero, J. J., Beguerìa, S., Trigo, R., Loìpez-Moreno, J. I., Azoriìn-Molina, C., Pasho, E., Lorenzo-Lacruz, J., Revuelto, J., Moraìn-Tejeda, E., and Sanchez-Lorenzo, A.: Response of vegetation to drought timescales across global land biomes, P. Natl. Acad. Sci. USA, 110, 52–57, https://doi.org/10.1073/pnas.1207068110, 2013.

E&G Quaternary Sci. J., 70, 247–250, 2021
https://doi.org/10.5194/egqsj-70-247-2021

Open Access E&G Quaternary Science Journal

Retrospective

A tribute to Smolíková (1971): Principles of soil development in the Quaternary

Lenka Lisá[1] **and Aleš Bajer**[2]

[1]Institute of Geology, Czech Academy of Sciences, Rozvojová 269, Prague 6, 165 00, Czech Republic
[2]Department of Geology and Soil Science, Faculty of Forestry and Wood Technology, Mendel University in Brno, Brno, 613 00, Czech Republic

Correspondence: Lenka Lisá (lisa@gli.cas.cz)

Relevant dates: Received: 1 June 2021 – Revised: 8 November 2021 – Accepted: 12 November 2021 – Published: 17 December 2021

How to cite: Lisá, L. and Bajer, A.: A tribute to Smolíková (1971): Principles of soil development in the Quaternary, E&G Quaternary Sci. J., 70, 247–250, https://doi.org/10.5194/egqsj-70-247-2021, 2021.

Special issue statement. This article is part of a special issue published on the occasion of the 70th anniversary of *E&G Quaternary Science Journal (EGQSJ)*. The special issue celebrates the journal's notable contribution to Quaternary research by revisiting selected milestone articles published in the long history of *EGQSJ*. The German Quaternary Association (DEUQUA) presents translations of the originals and critical appraisals of their impact in tandem anniversary issues of *DEUQUASP* and *EGQSJ*, respectively.

Original article: https://doi.org/10.3285/eg.22.1.12

Translation: https://doi.org/10.5194/deuquasp-3-111-2021

1 Soils in the context of Quaternary studies of Czechoslovakia at the end of the last century

To better understand Libuse Smolíková's background and study, one needs to understand the beginnings of cooperation between soil science, Quaternary geologists and archeologists in the former Czechoslovakia. The concept of soil study in the former Czechoslovakia followed the "Russian school". It focused mainly on the genesis of soils, in contrast to the American one, which was directed more economically, i.e., to assess soil fertility. Thanks to this, it was possible at that time to better connect pedological sciences with the study of Quaternary sediments related to climatic changes. One important work on combining soil research and Quaternary studies was from Musil et al. (1955); in this study osteologist, archeologists and soil scientists worked together, mapping the occurrence of paleosols in loess formations in southern and central Moravia and discussing their significance for Quaternary climate cycle dating (Musil et al., 1955). The soil scientist in this study, Pelíšek, used classical pedological methods for the time; i.e., in the field he distinguished macroscopic properties of soil horizons, and in the laboratory he then determined the content of organic matter, carbonates, pH and grain size composition. Thick loess formations with buried paleosol served as one of the best-studied environmental archives, and its stratigraphical record was assigned to the then valid stratigraphy of the last Quaternary climate cycle. Very detailed study of the sedimentary archives helped to divide more precisely the stratigraphy of the Vistula ("Würm" – see Alpine chronostratigraphy) glacial in the early 1950s. Its division was generally accepted by two fluctuations, which were referred to as "Würm 1/2" and "Würm 2/3" (respectively LGl 1/2 and LGl 2/3) and which included the soils "Göttweig" (W 1/2) and "Paudorf" (W 2/3) or "Oberfellabrunn" (according to the outcrop in the brickyard in Lower Austria) and "Paudorf" (Brandtner, 1956) or "Stillfried A" and "Stillfried B" (according to the outcrop in Stillfried). Such a division of the last glacial was also applied in Czech literature under the term "Soergel-Zeuner system" (Valoch, 2012). Much later, Valoch (2012) published an important study, in which he tried to compare the terminology of the stratigraphic classification of soils of the last glacial cycle used at the time with that corresponding to current knowledge. The reason was that the climatic stratigraphy of the last Quaternary cycle is crucial for the classification of finds of the Middle and Upper Paleolithic and that the important archeological works from the 1960s were based on the stratigraphical terminology valid at that time.

2 The main messages of Smolíková's work

Smolíková was one of the first pedologists who pointed out that paleosol horizons in Quaternary paleosol–sediment successions are often described by Quaternary geologists who are not trained in pedology and that it may increase the problems with the interpretations. As a result, many existing descriptions of paleosols in the literature were hardly pedologically interpreted in terms of the kind of pedogenic processes and the environmental conditions that they are indicative of. She pointed out that the description and interpretation of paleosols must be linked to a profound taxonomy of soils, including all kinds of soil formation in all possible stages of development. Smolíková (1971) further highlighted the importance of the position of the soil profile in the landscape and that the influence of relief has to be considered. If possible, soil horizons should be observed along some distance in order to recognize reworking, disturbance and accumulation of soil sediments.

Her seminal paper discussed here is an outstanding example of how the views of geologists, environmentalists and archeologists on pedocomplexes can be united. The concept of Quaternary climatic division was followed by Smolíková in her micromorphological description of pedocomplexes (Němeček et al., 1990), and its link to the soil genesis and environmental conditions under which pedocomplexes developed represent the main message of her work. The problems of this "early" paleopedological work was the non-stable soil terminology. Smolíková often described the micromorphological properties and linked them to the types of soils which are, however, recently not used any more. Later, when the pedological system changed, Smolíková did not adapt her terminology to it. Therefore, it is complicated to use the terminology and interpretation from the time when she investigated the old localities (Adameková et al., 2021). Another problem with the application of her terminology applied to the pedocomplexes is due to the increasing knowledge of climatic changes. Since the publication of Smolíková's work, i.e., over the last 50 years, the understanding of the situation of the climatic development of the last glacial cycle in Central Europe, as well as the understanding of the situation of the Paleolithic, has changed significantly. The system of pedocomplexes, which document the so-called warm phases (interglacials or interstadials), is only suitable for a more general division of the entire Pleistocene. On a detailed scale, however, they are often unsatisfactory.

3 Pedocomplexes and paleopedological provinces in the light of Smolíková's work

An example of the unsatisfactory basic division is the last glacial, in which Smolíková separated two pedocomplexes called PKI and PKII. However, later research revealed that there had developed another paleosol between these two pedocomplexes, the preservation of which is simultaneously affected by erosion processes. This pedocomplex is the so-called Bohunice soil after its eponymous locality, Bohunice in Brno. From the point of view of Paleolithic research, this pedocomplex is crucial because industry from the turn of the Middle and Upper Paleolithic (early Upper Paleolithic: Bohunician, Szeletian, Aurignacian) is tied to it. Later, Smolíková, as a co-author in the first comprehensive monograph on pedology and paleopedology published in Czechoslovakia (Němeček et al., 1990), significantly expanded the paleopedological and paleogeographic concepts published in her article commented upon herein concerning the use of pedological data in the Quaternary. There, she described in detail the importance of paleopedology for the understanding of paleoclimate and paleogeography during the Quaternary in Central Europe. It clearly defined the patterns of soil development in the Quaternary cycle and emphasized the importance of soils as part of Quaternary geology. Probably the most important contributions to the study of Quaternary paleosols are specific micromorphological descriptions of these soils and a description of the genesis of these soils on individual soil-forming substrates preserved in a whole range of Quaternary sediments, especially in loess.

To connect pedology with Quaternary research, Smolíková used a basic methodological tool, namely the microstructure of soils, i.e., the so-called soil micromorphology. In addition to the microstructure itself, the type and degree of preservation of organic and organomineral soil components can be described, as well as the pedofeatures related to soil development; further, post-sedimentary processes can be detected. This can be quite complex and might reflect the changing climatic conditions of the site.

The study of soil microstructure was introduced into the literature in the 1930s by Kubiëna (exact year unknown). Smolíková was a student of Kubiëna and took over his terminology, which she began to apply to the study of paleosols in the Central European context in the 1960s. In the 1960s, Brewer (1964) proposed a more systematic, morphological approach to the description of soil samples, followed by a number of other authors. The efforts of the 3rd International Meeting on Soil Micromorphology in Wroclaw (Poland) in 1969 resulted in a long-term accepted terminology and a standard way to describe thin sections (Bullock et al., 1985).

This terminology is widely used up today, but most of the researchers combine that terminology with the more systematic terminology of Stoops (2003).

At the time when Smolíková published her annotated article, interest in the importance of paleosols was not only in the context of archeology (Lisá et al, 2015), but it intensified especially in the 1970s when Kukla suggested to the president of the United States the importance of studying paleosols in the context of future climate change (i.e., global cooling versus global warming). On this account, Kukla created the above-mentioned concept of pedocomplexes, which Smolíková elaborated in terms of soil micromorphology (Němeček et al., 1990). The principles on the basis of which pedocomplexes were determined are described in great detail in her 1971 article. Smolíková's (1971) article, and the way in which it used soil micromorphology, was therefore completely original for its time. In our opinion, it has become a building stone for further studies of a similar type. Since then, a number of studies have been published in which soil micromorphology has played a crucial role in recognizing soil processes that reflect the relatively complex conditions of a changing climate.

Further, Smolíková (1971) showed one very important aspect when interpreting the differences in soil development. In her work, she strongly refers to zonal concepts that have also become outdated. Recent and subrecent soil cover that developed on loess substrate over the Holocene in Central and Western Europe differs according to the continental gradient and as a result of orographic influences (e.g., rain shadow effect). Such effects controlled the spatial differences in pedogenesis in loess also under past climatic conditions. Smolíková (1971) also pointed out the importance of comparing pedological characteristics of paleosols with their modern analogs, which allows for the reconstruction of the climatic conditions that prevailed during their formation. In this respect, she highlights the use of micromorphology, together with pollen, kernels of fruits, phytoliths, rhizoliths, and mollusk shells, for a detailed characterization of the pedogenic features that can be identified in a paleosol. Her recommendations were crucial for understanding the importance of the identification of the environmental conditions when interpreting buried paleosols.

4 Current state of knowledge, perspectives and trends

Soil micromorphology has undergone relatively fundamental changes in the terminology and possibilities of instrumentation since Smolíková (1971) used it – or, better, introduced it – in her article. While its importance for the study of recent soils has declined, it has become an integral part of paleopedological research and at the same time an innovative tool for anthropogenic sediment research. Unfortunately, the conditions in Czechoslovakia did not allow Smolíková (1971) to innovate the ways of studying soil excavations in the direction they went in Western Europe. Therefore, its descriptions and terminology published after 2000 use more or less the original terminology and are thus often deprived of the context that can be obtained by using new terminology and methodological approaches. Examples are the size of the samples used for the study, the use of an electron microscope or a UV microscope, or the detection of pedofeatures, which have not been given the deserved recognition in the past. For example, Fitzpatrick's ingenious work can be a parallel. His system and comparative collection, very innovative for its time, are currently basically unusable. As was the case with Fitzpatrick, the importance of soil micromorphology in Quaternary studies gradually disappears after Smolíková stopped her active work. Smolíková's micromorphological terminology (1971) used to distinguish pedocomplexes is not only due in her time to the style of marking pedofeatures but is also interpretatively linked to the pedological system of that time. Today, there is basically nothing like a conversion table between soils described and interpreted on the basis of soil micromorphology by Smolíková and the current pedological system. Therefore, any comparison of recent terminology with older works is very difficult and nearly impossible in some cases (Adameková et al., 2021). Firstly, this is because soil traits are mostly tied to regional conditions (Hošek et al., 2017; Lisá et al., 2015), so within soil catena, different looking pedocomplexes may form during one climatic cycle (e.g., Adameková et al., 2021). The second reason is that buried soil horizons are often complex and strongly affected by soil erosion. Another and probably the most important factor that fundamentally complicates the inclusion of soil pedocomplexes in the current pedological system is that if the soils were not covered with loess or colluvial sediments, new soils began to form under the new climatic conditions but from the substrate of older soils. In such a case, soil micromorphology is an invaluable tool for detecting not so much the inclusion of soil in the system but rather the processes that lead to pedogenesis. It is evident that soil micromorphology is a key tool for detecting climate change. Today, much more sophisticated methods are preferred for climate studies, such as isotope studies and comparisons of regional records with, for example, marine or glacier climate archives. Studies that have over-generalized and underestimated the importance of soils have unnecessarily led, for example, to the creation of pseudo-terms such as "Podhradem interstadial". Such dogmas are then very difficult to overcome, but new methodological approaches combined with soil micromorphology can help to solve such problems (Lisá et al., 2018). Today, soil micromorphology is not the preferred method to study paleosols or soils. It is often replaced by chemical methods, and although soil geochemistry is highly suitable, it can never replace a direct view of the internal structure of the soil. Soil micromorphology should therefore remain a necessary reference of processes and an integral part of environmental Quaternary research.

Financial support. The article processing charge was funded by the Quaternary scientific community, as represented by the host institution of *EGQSJ*, the German Quaternary Association (DEUQUA).

Review statement. This paper was edited by Christine Thiel and reviewed by one anonymous referee.

References

Adameková, K., Lisá, L., Neruda, P., Petřík, J., Doláková, N., Novák, J., and Volánek, J.: Pedosedimentary record of MIS 5 as an interplay of climatic trends and local conditions: Multi-proxy evidence from the Palaeolithic site of Moravský Krumlov IV (Moravia, Czech Republic), Catena, 200, 105174, https://doi.org/10.1016/j.catena.2021.105174, 2021.

Brandtner, F.: Lößstratigraphie und paläolithische Kulturabfolge in Niederösterreich und den angrenzenden Gebieten (Zugleich ein Beitrag zur Frage der Würmgliederung), E&G Quaternary Sci. J., 7, 127–175, https://doi.org/10.3285/eg.07.1.13, 1956.

Brewer, R.: Fabric and mineral analysis of soils, John Wiley & Sons, New York, USA, 1964.

Bullock, P., Fedoroff, N., Jorgerius, A., Stoops, G., Tursina, T., and Babel, U.: Handbook for soil thin section description, Waine Research Publications, Wolverhampton, UK, 1985.

Hošek, J., Lisá, L., Hambach, U., Petr, L., Vejrostová, L., Bajer, A., Matys Grygar, T., Moska, P., Gottvald, Z., and Horsák, M.: Middle Pleniglacial pedogenesis on the northwestern edge of the Carpathian basin: A multidisciplinary investigation of the Bíňa pedo-sedimentary section, SW Slovakia, Palaeogeogr. Palaeocl., 487, 321–339, 2017.

Lisá, L., Hošek, J., Bajer, A., Matys Grygar, T., and Vandenberghe, D.: Geoarchaeology of Upper Palaeolithic loess sites located within a transect through Moravian valleys, Czech Republic, Quatern. Int., 351, 25–37, 2015.

Lisá, L., Neruda, P., Nerudová, Z., and Nejman, L.: Podhradem Interstadial. A critical review of the middle and late MIS 3 (Denekamp, Hengelo) in Moravia, Czech Republic, Quaternary Sci. Rev., 182, 191–201, 2018.

Musil, R., Valoch, K., and Nečesaný, V.: Pleistocénní sedimenty okolí Brna. – Sbor. geol. Věd, Anthropozoikum, 4, 107–168, 1955.

Němeček, J., Kutílek, M., and Smolíková, L.: Pedologie a Paleopedologie, Academia, Prague, Czech Republic, 546 pp., 1990.

Smolíkovaá, L.: Gesetzmäßigkeiten der Bodenentwicklung im Quartär, E&G Quaternary Sci. J., 22, 156–177, https://doi.org/10.3285/eg.22.1.12, 1971.

Stoops, G.: Guidelines for Analysis and Description of Soil and Regolith Thin Sections, Soil Science Society of America, Madison, WI, USA, 2003.

Valoch, K.: K historii členění würmského/viselského glaciálu v českých zemích, Archeologické rozhledy, LXIV, 129–135, 2012.

E&G Quaternary Sci. J., 70, 251–255, 2021
https://doi.org/10.5194/egqsj-70-251-2021

Open Access E&G Quaternary Science Journal

Retrospective

A tribute to Boenigk (1978): The fluvial development of the Lower Rhine Basin during the late Tertiary and early Quaternary

Philip L. Gibbard

Scott Polar Research Institute, University of Cambridge, Lensfield Road, Cambridge CB2 1ER, UK

Correspondence: Philip L. Gibbard (plg1@cam.ac.uk)

Relevant dates: Received: 15 May 2021 – Revised: 27 June 2021 – Accepted: 30 October 2021 – Published: 17 December 2021

How to cite: Gibbard, P. L.: A tribute to Boenigk (1978): The fluvial development of the Lower Rhine Basin during the late Tertiary and early Quaternary, E&G Quaternary Sci. J., 70, 251–255, https://doi.org/10.5194/egqsj-70-251-2021, 2021.

Special issue statement. This article is part of a special issue published on the occasion of the 70th anniversary of *E&G Quaternary Science Journal (EGQSJ)*. The special issue celebrates the journal's notable contribution to Quaternary research by revisiting selected milestone articles published in the long history of *EGQSJ*. The German Quaternary Association (DEUQUA) presents translations of the originals and critical appraisals of their impact in tandem anniversary issues of *DEUQUASP* and *EGQSJ*, respectively.

Original article: https://doi.org/10.3285/eg.28.1.01

Translation: https://doi.org/10.5194/deuquasp-3-125-2021

1 Introduction

The Lower Rhine Embayment (LRE, or Lower Rhine Basin) has been an area of subsidence since early in the Tertiary. It therefore preserves one of the most complete records of Neogene and Quaternary terrigenous and shallow marine deposits in western Europe. Throughout this period the region's evolution has been controlled by its being underlain by a complex network of tectonically active south-east- to north-west-orientated faults which give rise to horst, graben, and tilted block structures which have imposed a distinctive control on the subsidence history. The south-eastern part of the Netherlands forms the continuation of the LRE which effectively represents the maximum south-easterly extension of the North Sea basin. To the south the LRE is bounded by the Palaeozoic rocks of the Rhenish Massif, the area forming part of the continent-wide European Rift System (e.g. Ziegler, 1994; Van Balen et al., 2005).

For over a century the exploitation of clay in the Netherlands–Germany border area in the west to north-western part of the basin and extensive open-cast brown-coal mining in the southern part of the region since the mid-20th century (e.g. Boenigk, 1978; Schäfer et al., 2004, 2005) have provided substantial, often spectacular exposures that have been, and continue to be, the focus of extensive research. Boenigk's (1978) article presents a significant milestone summary of thorough investigations in this basin, based on extensive field work and "sedimentological and sedimentary-petrographical" (i.e. gravel petrographical and heavy mineralogical) analyses, supported by palynological research and palaeomagnetism. His results provide a concise systematic summary of the state of knowledge of the geological history of the region through the late Cenozoic in the late 1970s. The general results of this paper have stood the test of time, having been modified only marginally due to more recent investigations. Despite being based upon what some might consider to be a "standard" systematic approach to regional geological and palaeogeographical reconstruction, it is fundamentally central to the understanding of evidence, and moreover, it remains the foundation upon which modern geological investigations continue to be based.

Seen from the perspective of 40 years later, Boenigk's (1978) article is still a significant contribution which laid the foundation for all subsequent investigations in the LRE, but inevitably research has continued since. Indeed, Boenigk himself published later summaries that further refined and elaborated his own 1978 framework (e.g. Boenigk, 2002; Boenigk and Frechen, 2006), although latterly it has fallen to others to build on his foundations. In particular the extensive work of Westerhoff (2009) and Westerhoff et al. (2008) in the border area and the north-western extension of the LRE to the Roer Valley Graben (RVG) structure beneath the southern Netherlands, together with Kemna (2005, 2008) and Schäfer et al. (2004) among others, has provided further insights into the chronology and evolution of the Rhine system in this critical region.

2 The Rhine sequence in the Lower Rhine Embayment (LRE)

In principle, the sequence described in Boenigk's (1978) classic paper outlines the development of the region from the latest Oligocene to the Middle Pleistocene, a period characterized by the complex interplay of tectonic activity, climatic variations, marine transgression–regression cycles, and the resulting depositional and erosional responses, each of which operated at different rates. As he says, following the high sea level of the Oligocene when the LRE was flooded by the North Sea, the early Miocene saw the sea regress towards the west and north-west, it being replaced by fluviolacustrine deposition. The latter resulted from local drainage flowing from bounding upland areas, especially the Rhenish Massif to the south and south-west and latterly from the Belgian area to the west. This deltaic sedimentation, favoured by local subsidence, broadly represents an alternating sequence of lignite which interdigitated with fluvial sands, in part derived from the Upper Rhine Graben. These freshwater and marine deposits reflect short-term oscillating sea level superimposed on long-term basinal subsidence. Climatic changes during this interval also alternated from semi-arid early in the Miocene to subtropical and tropical, the latter during the formation of the main lignite. Episodically, the Rhine river drained an area extending southwards into the Upper Rhine Graben (URG) during this time slice.

The Rhine developed in a preliminary form in the Middle Miocene so that by the Pliocene it had already evolved considerably. According to Boenigk (1978), the early Pliocene Rhine deposited large quantities of coarse clastics in the Lower Rhine, the materials originating from a pre-weathered provenance area, comprising highly stable minerals and rounded pebbles, mainly of quartz and quartzite being derived predominantly from the Moselle area. These "Hauptkies" or Waubach Gravel sediments are included in the Kieseloolite Formation. At this time, the Rhine was only a local stream in the Rhenish Massif area.

Reinvestigation of the complex sedimentary sequence of the Lower Rhine Embayment area between Köln (Cologne) in Germany and Venlo in the Netherlands, particularly in the application of modern concepts of sedimentation, has refined, but not revised, the reconstructions. The sediment fill of the LRE consists of thick marine strata in the deepest part that were deposited during the Oligocene, Miocene, and Pliocene (Schäfer et al., 2004). Up to 100 m thick brown coal or lignite seams occur in the southern part of the LRE (Zagwijn and Hager, 1987) as Boenigk (1978) also acknowledged. They interdigitate with the marine deposits. The upper part of the sediment fill consists of fluvial deposits that started to develop on top of the lignite as a result of increased uplift of the surrounding Rhenish Massif. The onset of the fluvial deposition is thought to be of Late Miocene age (Boenigk, 1978; Schäfer et al., 2004), the river environments gradually prograding north-westwards, reaching the southern part of the Netherlands in the course of the Pliocene, following the shifting coastline (Zagwijn, 1974). This process continued into the Early Pleistocene and eventually resulted in a shift of the marine realm far into the present North Sea.

The subsurface tectonic framework of the southern North Sea basin, including the LRE, strongly controlled the deposition during the Quaternary. The Pliocene and Pleistocene saw the fluvial systems in the LRE typified by a low ratio between accommodation space and sediment supply (Schäfer et al., 2004) leading to fluvial sequences adopting a wide, relatively shallow valley form. Establishment of this "braided" fluvial pattern was facilitated by the deteriorated climatic conditions prevailing at the time. Sediment delivery exceeded the available regional accommodation space of the LRE and RVG, causing the majority of the fluvially transported sediment to bypass these areas and to be deposited further northwards in the main marine depocentre of the North Sea basin (Westerhoff et al., 2008; Westerhoff, 2009). Whilst the RVG provided an important sediment trap, at the basin scale it functioned simply as a regional depocentre where gradual lowering of local base-level increased the preservation potential of Lower Pleistocene deposits.

The subsurface structure of the LRE being determined by the predominantly south-east- to north-west-orientated fault pattern, the faults define individual tectonic blocks of which the subsidence rate can vary considerably. The complexity of this block tectonic pattern of subsidence is highlighted by the fact that the easternmost tectonic block on the LRE, the "Köln–Krefelder Scholle", was tilted along a south-west–north-east trending axis located near the northern margin of the LRE, around the town of Emmerich (Boenigk and Frechen, 2006). This particular tectonic movement has led to the relative uplift of the southern part of the Köln–Krefelder Scholle, causing incision by the Rhine river and related establishment of a terrace staircase over the course of the Pleistocene until the present day there. This terrace flight can be correlated with that of the Middle Rhine Valley within the Rhenish Massif (Boenigk and Frechen, 2006). The hinge line of the basin is situated to the south-east in the LRE. The pattern of the hinge line has been identified in regional subsidence models of the Quaternary. Its position possibly shifted basinwards through the last few million years, but it is assumed that the overall pattern can be compared to the present-day situation (Westerhoff et al., 2008).

Within the RVG and Rurscholle the thickness of the preserved depositional sequences increases from south-east to north-west, this implying that subsidence rates increase in the same direction (Van Balen et al., 2005; Westerhoff et al., 2008). The thicknesses of the various lithostratigraphical units in the Rurscholle in Germany and the RVG in the Netherlands have remained generally constant during Pliocene and Early Pleistocene times, while a minor increase has been recognized during the Middle and Late Pleistocene (Van Balen et al., 2005).

A thorough review, based on standard lithostratigraphy, supported by heavy-mineral analyses from key exposures, has demonstrated that the classic Plio-Pleistocene sequence proposed by previous authors, particularly by Zagwijn (1960) and others, required modification (Westerhoff et al., 2008). This modification has become apparent partially as a result of the reassessment of the Netherlands' lithostratigraphical scheme in which two new formations were recently proposed to replace existing terms. The marked change in provenance of the Late Pliocene Rhine (Boenigk, 2002) has indicated a distinction between a pre-Rhine (Kieseloolite Formation) and the Alpine-connected Rhine system (Waalre Formation). Deposits of the north- and north-eastward-draining Belgian rivers (Stramproy Formation) can also be well-recognized before their confluence with the Rhine fluvial system sequences.

Some time before the beginning of the Middle Pleistocene, climatic deterioration combined with increased uplift of the Rhenish Massif (Meyer and Stets, 2002) accounted for deposition of the so-called "Hauptterrassen" or main terrace sequence in the LRE (Boenigk and Frechen, 2006). These cold-climatic, mainly coarse deposits are found throughout the entire LRE. Downstream, in the Netherlands, the Sterksel Formation of the Dutch lithostratigraphy is correlated with the main terrace deposits.

The question of chronology on the LRE sequences is of central importance. At Boenigk's (1978) time, apart from the independent palaeontological and heavy-mineral evidence, there were only two main marker horizons in the record of Late Pliocene and Early Pleistocene fluvial deposits that provide some time control. The lowermost marker horizon represents the first occurrence of Alpine material in the region, expressed by the substantial increase in unstable heavy minerals at the base of the Oebel Beds (Waalre Formation: Boenigk, 2002; Boenigk and Frechen, 2006; Westerhoff et al., 2008). This change was due to the extension of the Rhine's drainage area to the southern URG, with an antecedent course through the Rhenish Massif. Palaeomagnetic measurements from both the Oebel Beds and the underlying Kieseloolite Formation Reuver Clay demonstrate that these deposits, being normally magnetized, fall within the Gauss Epoch (Kemna, 2005, 2008). They are therefore of Late Pliocene age, a conclusion that corresponds with the available palaeontological evidence (e.g. Zagwijn, 1960, 1974, 1989; Boenigk and Frechen, 2006). The second time control, at the beginning of the Middle Pleistocene, is represented by the Brunhes–Matuyama magnetic reversal that was identified in the deposits "towards the end of the Hauptterrassen phase" (HT III), as Boenigk (1978) mentions.

3 Implications

The marked increase in sedimentation that occurred in the latest Cenozoic (e.g. Boenigk, 1978; Westerhoff et al., 2008) reflects the substantial climatic deterioration that characterized the later Pliocene and the beginning of the Quaternary, with glaciation extending to sea level and periglacial frost-dominated climates becoming established across Europe. As already mentioned, the LRE preserves the longest and oldest of the fluvial sequences and terrace flights in Europe. Initial deposition of the Kieseloolite Formation in the middle to late Pliocene represents the first of three major depositional events in the LRE. This represents a "mega-fan"-like accumulation of material derived from pre-weathered quartz regolith that resulted from the initial response to climatic deterioration to cold conditions, combined with uplift of the Rhenish Massif. The quartz regolith inherited from the humid Neogene climates phases formed by chemical weathering under dense vegetation cover.

This is followed at the beginning of the Quaternary by deposition of the Waalre Formation, a sequence of relatively fine-grained deposits, laid down under varied climates by the rivers flowing under a predominantly meandering/anastomosing regime. Like the Kieseloolite Formation, these deposits occupy a wide, shallow valley topography, related to the subdued relief. The warm-climate events are of interglacial character with diverse forest vegetation, whilst the colder phases include evidence for frost-dominated periglacial conditions (e.g. Zagwijn, 1960).

The third broad division, as Boenigk (1978) notes, is the late Early-Middle Pleistocene main terraces (Hauptterrassen), which represent a second mega-fan-like accumulation, aided by increased rate of tectonic uplift (Meyer and Stets, 2002). The downstream equivalent of the later Hauptterrassen and earliest middle terraces comprise coarse sands and gravels of the Sterksel Formation and have a mixed Rhine and Meuse provenance (Van Balen et al., 2005). Upstream of the confluence of these rivers, and to the west of the LRE, pure Meuse deposits are found ("East-Maas"), which Boenigk and Frechen (2006) referred to as the "Holzweiler Formation". Deposits which can be assigned to the East-Maas according to their sediment-petrography have been identified within the south-western LRE from the Pliocene to late Early Pleistocene (Boenigk, 1978; Westerhoff et al., 2008). Although downstream of the confluence the Hauptterrassen do contain some rare Meuse-derived pebbles, this material is potentially reworked from the Holzweiler deposits. The Hauptterrassen are certainly cold-climate accumulations that were deposited by the river adopting a braided pattern. They broadly relate to the late Early Pleistocene to early Middle Pleistocene.

By the time of the formation of the Middle Pleistocene Mittelterrassen (middle terraces), Boenigk (1978) notes that the Rhine had left the western part of the LRE as a consequence of local tectonic movement, migrating to the east of the Ville Block, the move being accompanied by the markedly increased incision of the river's valley. This incision has continued to the present day.

From the Middle Pleistocene, the somewhat better-dated sequences preserved in the LRE overwhelmingly comprise sediments of gravel and sand of braided river, cold-climate origin that began with the Hauptterrassen. This contrast with the Neogene strongly suggests that enhanced fluvial activity was a result of the occurrence of cold climates and the supply of abundant fresh materials by periglacial slope processes, intensified during the Middle Pleistocene transition (1.2–0.8 Ma).

Whilst the processes of valley incision are complex and affected by such factors as flow regime, bed material load, gradient and bedrock exposure, and erodibility, these were also positively affected during cold-climate episodes after this transition. Apparently, climate was at least as significant as tectonic uplift (in the Rhenish Massif), and complex, block-tectonic movement (in the LRE) acted as a primary driver of fluvial incision in the Pleistocene Rhine system (cf. Gibbard and Lewin, 2008). These authors have shown that the evidence corresponds to that of low-relief land surfaces that dominated much of Europe until the Pleistocene. However, in contrast, the younger Middle and Late Pleistocene middle and lower terraces of the Rhine system occur as narrow deposit spreads within a deeply incised valley (e.g. Meyer and Stets, 2002) that was determined by the interplay of "fluvial activity" and tectonics. The change from shallow to deep incision is also reflected in the calibre of the sediment in transport which increases dramatically during the Middle Pleistocene and broadly corresponds to the Middle Pleistocene Transition.

Finally, what is striking to the modern reader is that Boenigk's (1978) review was compiled before the widespread adoption of the marine (oxygen) isotope chronology by terrestrial workers to provide a stratigraphical framework. Despite this it is evident that Boenigk was fully aware of the implications of climate cyclicity to the LRE sequences and the Rhine drainage evolution. Until the recognition of the implications of the marine isotope succession in the early 1970s, terrestrial evidence formed the foundation for the division of Quaternary time. Today the contrast could not be greater, with many abandoning the firmly founded terrestrial chronostratigraphical classification in favour of the less-precisely defined ocean-floor isotope stratigraphy to provide a foundation for the division of events. Whilst undoubtedly the isotope and ice-core sequences offer a reliable framework, it is important to emphasize that these sequences, especially those in the ocean-bottom sediments, record global-scale changes. This contrasts substantially with terrestrial or shallow marine sequences which preserve locally dominated successions, reflecting local events. Such events are not necessarily represented in the global patterns because the local responses to changes will inevitably lead to modifications to any all-encompassing pattern. For this reason, direct correlation of terrestrial sediment sequences with those in the oceans is a serious matter which should not be undertaken uncritically, and assumed equivalence should be considered critically. Lessons from the past have repeatedly shown that simplistic or mechanistic correlation when examined in detail is unsustainable, Boenigk's (1978) classic article being indisputably a case in point. In essence, Boenigk (1978 and subsequent articles) integrated all his knowledge into a comprehensive picture of the palaeogeographical development and fluvial drainage patterns over time.

Acknowledgements. I thank Frank Preusser for kindly inviting me to prepare this appraisal, and I express my gratitude to Hans Axel Kemna for his generous review and constructive comments that improved the text.

Financial support. The article processing charge was funded by the Quaternary scientific community, as represented by the host institution of *EGQSJ*, the German Quaternary Association (DEUQUA).

Review statement. This paper was edited by Frank Preusser and reviewed by Hans Axel Kemna.

References

Boenigk, W.: Die flußgeschichtliche Entwicklung der Niederrheinischen Bucht im Jungtertiär und Altquartär., E&G Quaternary Sci. J., 28, 1–9, https://doi.org/10.3285/eg.28.1.01, 1978.

Boenigk, W.: The Pleistocene drainage pattern in the Lower Rhine Basin, Neth. J. Geosci., 81, 201–209, 2002.

Boenigk, W. and Frechen, M.: The Pliocene and Quaternary Fluvial Archives of the Rhine System, Quaternary Sci. Rev., 25, 550–574, 2006.

Gibbard, P. L. and Lewin, J.: River incision and terrace formation in the late Cenozoic of Europe, Tectonophysics, 474, 41–55, https://doi.org/10.1016/j.tecto.2008.11.017, 2008.

Kemna, H. A.: Pliocene and Lower Pleistocene stratigraphy in the Lower Rhine Embayment, Germany, Kölner Forum, 14, 1–121, 2005.

Kemna, H. A.: A revised stratigraphy for the Pliocene and Lower Pleistocene deposits of the Lower Rhine Embayment, Neth. J. Geosci., 87-1, 91–106, 2008.

Meyer, W. and Stets, J.: Pleistocene to recent tectonics in the Rhenish Massif, Neth. J. Geosci., 81, 217–221, 2002.

Schäfer, A., Utescher, T., and Mörs, T.: Stratigraphy of the Cenozoic Lower Rhine Basin, northwestern Germany, Newsl. Stratigraphy, 40, 73–110, 2004.

Schäfer, A., Utescher, T., Klett, M., and Valdivia-Manchego, M.: The Cenozoic Lower Rhine Basin – rifting, sedimentation, and cyclic stratigraphy, Int. J. Earth Sci. (Geol. Rundsch.), 94, 621–639, https://doi.org/10.1007/s00531-005-0499-7, 2005.

Van Balen, R. T., Houtgast, R. F., and Cloetingh, S. A. P. L.: Neotectonics of The Netherlands: a review, Quaternary Sci. Rev., 24, 439–454, 2005.

Westerhoff, W.: Stratigraphy and sedimentary evolution. The lower Rhine-Meuse system during the Late Pliocene and Early Pleistocene (southern North Sea Basin), Dissertation, Vrije Universiteit Amsterdam, Amsterdam, the Netherlands, 168 pp., 2009.

Westerhoff, W. E., Kemna, H., and Boenigk, W.: The confluence area of Rhine, Meuse, and Belgian rivers: Late Pliocene and Early Pleistocene fluvial history of the northern Lower Rhine Embayment, Neth. J. Geosci., 87-1, 107–126, 2008.

Zagwijn, W. H.: Aspects of the Pliocene and Early Pleistocene vegetation in the Netherlands, Mededelingen Geologisch Stichting, C3, 78 pp, 1960.

Zagwijn, W. H.: Bemerkungen zur stratigraphischen Gliederung der plio-pleistozänen Schichten des niederländischen-deutschen Grenzgebietes zwischen Venlo und Brüggen, Zeitschrift der Deutschen Geologischen Gesellschaft, 125, 11–16, 1974.

Zagwijn, W. H.: The Netherlands during the Tertiary and Quaternary. A case history of coastal lowland evolution, Geol. Mijnbouw, 68, 107–120, 1989.

Zagwijn, W. H. and Hager, H.: Correlations of continental and marine Neogene deposits in the south eastern Netherlands and the Lower Rhine district. Mededelingen Werkgroep Tertiaire and Kwartaire, Geologie, 24, 59–78, 1987.

Ziegler, P. A.: Cenozoic rift system of western and central Europe. An overview, Geol. Mijnbouw, 73, 99–127, 1994.

continued from back cover

https://www.eg-quaternary-science-journal.net/ ISSN 0424-7116

CONTENTS

continued on the inside cover

https://www.eg-quaternary-science-journal.net/

ISSN 0424-7116